Rhenium(I) Complexes of *N*-Heterocyclic Carbene for Medicinal Applications

Nuchareenat Wiratpruk

A thesis submitted in total fulfilment of

the requirement for the degree of

Doctor of Philosophy

Department of Chemistry and Physics

School of Molecular Sciences

College of Science, Health and Engineering

La Trobe University

Victoria, Australia

September 2021

Statement of Authorship

This thesis includes work by the author that has been published or accepted for publication as described in the text. Except where reference is made in the text of the thesis, this thesis contains no other material published elsewhere or extracted in whole or in part from a thesis accepted for the award of any other degree of diploma. No other person's work had been used without due acknowledgement in the main text of the thesis. This thesis has been submitted for the award of any degree or diploma in any other tertiary institution.

Nuchareenat Wiratpruk, PhD Candidate

Date: 27th September 2021

Statement of Candidate Contribution

Chapter 2 contains work that has been published and details of the publication with an estimate of the percentage contribution of each author is indicated:

N. Wiratpruk, A. Noor, C. A. McLean, P. S. Donnelly and P. J. Barnard, *Dalton Transactions*, 2020, **49**, 4559-4569.

N. Wiratpruk (65%) was responsible for preparing the manuscript, synthesised and characterised the compounds in addition to completing the logP and photophysical studies. A. Noor (10%) and P. S. Donnelly (5%) carried out the biological studies (ThT assay and Epi-fluorescence microscopy studies). C. A. McLean (5%) provided the clinically diagnosed Alzheimer's disease patient's brain tissue. P. J. Barnard (15%) has carried out the X-ray crystallography and editing the manuscript.

We hereby declare that the individual authors, or the corresponding author, have granted permission to the candidate (Nuchareenat Wiratpruk) to use the results presented in the manuscript above in this thesis.

	Supervisor	PhD Candidate
	Dr Peter Barnard	Nuchareenat Wiratpruk
Date:	27th September 2021	27th September 2021

Acknowledgement

The road to Doctor of Philosophy to me is like riding on a gigantic roller coaster. I could see the twists and turns together with the ups and downs. Knowing what I had to experience throughout this long journey, I still decided to ride this roller coaster. There is no doubt that I faced numerous difficulties and solved countless problems along the way, but the price at the finish line is worth it. I definitely would not have reached the end of the road without the push and pull from my supervisor, Dr Peter Barnard. Thank you so much for all your help during my PhD journey and for allowing me to be a part of your laboratory. I would not have been able to reach the finished line without your support. I also would like to thank my co-supervisor, Prof. Adam Mechler and my chair Prof. Conor Hogan for their time over the past four years. I would like to express my appreciation to La Trobe University for providing me with the opportunity to study as a PhD candidate. This work was supported by a La Trobe University Postgraduate Research Scholarship and a La Trobe Full Fee Research Scholarship.

My collaboration within the chemistry department and other fields significantly enhanced my knowledge and research skills. I would like to thank Prof. Paul Donnelly and Dr Asif Noor from Bio21 Institute, and Prof. Catriona Maclean from the Florey Institute of Neuroscience and Mental Health, University of Melbourne, for their precious time and for carrying out the biological experiments and providing the amyloid plaques brain tissue that I required for the second chapter of my thesis, respectively. I would like to express my gratitude to Prof. Mark Hulett from the Department of Biochemistry and Genetics, La Trobe University, for allowing me to conduct the biological studies for Chapter 3 in his laboratory. A special thanks to Ms Guneet Bindra for all her help with the cell cultures and MTT experiments. I would also like to thank Dr Alex Hamilton from Sheffield Hallam University, who prepared the computational calculations for Chapter 3.

Family is a significant component of my life that helped me achieve and be who I am today. Words cannot describe how thankful I am to my mum, Mrs Buakaew Tree and my grandmother Giang Yathilert, who always supported me with their unconditional love. I am grateful for having my family, including Mr Antony Tree, Mr Grisgorn Tree, Ms Apitchaya Tree and my relatives in Australia and Thailand by my side throughout my study. I would like to devote wholehearted gratitude to my grandparents Robert and Audine Tree and my aunt Debra Duncan for inspiring me to continue my research in the hope that one day we will find the cure for Parkinson, Motor Neuron Disease and cancer.

As a PhD student, my time would have been dulled without my chemistry friends. Therefore, I would like to thank the past and present members of the Barnard group for all the enjoyable times in the laboratory. A special thanks to Dr Linh Quan for her advice and encouragement since the first day I started my postgraduate study. I would like to thank Dr Zili Li for ensuring that I was safe in the laboratory and Mr Dat Duong for proofreading my thesis. Thank you, Dr Rebecca Christoff, Dr Rebecca Karmis and Ms Pria Ramkissoon, for our countless chemistry discussions.

It is no surprise that undertaking a PhD can stray one away from their social life. I would like to express my great appreciation to my Thai friends, Dr Chantanee Mungkhetklang, Dr Kanlaya Jongcherdchootrakul, Dr Wanchana Tongkhampao, Dr Sirakul Suwinthawong, Dr Boonlom Thavornyutikarn, Dr Arissara Phosanam, Dr Chirayu Ruengrungsom and Dr Thiti Osatakul, for setting great examples on how a PhD student should balance their work and social life. I would like to thank my best friend, Ms Eliza Johnson, for our endless dinners and dessert times. Finally, I would like to express my thankfulness to Ms Angie Woo and Ms Kim Trang Vu for keeping me socially active throughout my study and continuously checking that I was alright.

Abstract

Two tridentate ligand systems bearing *N*-heterocyclic carbene (NHC), amine and carboxylate donor groups coupled to either benzothiazole- or stilbene-based amyloid binding moieties were synthesised. The reaction of these pro-ligands with $Re(CO)_5Cl$ yielded the corresponding rhenium(I) metal complexes, which were characterised by NMR, and X-ray crystallography. These ligands are of interest for the potential preparation of technetium-99m imaging agents for Alzheimer's disease, and the capacity of these Re(I) complexes to bind to amyloid fibrils and amyloid plaques in human frontal cortex brain tissue was evaluated using ThT assay and confocal fluorescence microscopy. These studies showed that the complexes bound efficiently to amyloid-β fibrils and some evidence of binding to amyloid-β plaques.

A series of rhenium(I) complexes bearing pyridyl-imidazolylidene or *bis*-imidazolylidene ligand and *N*-acetyl amino acid derivatives including glycine, isoleucine and proline have been synthesised and characterised by NMR and HRMS. These complexes are of interest as potential anticancer agents, and as Re(I) complexes are known to have a similar mechanism of action to that of cisplatin, ^{1}H NMR time-course experiments were used to evaluate the aquation rates for Re(I) complexes of the *bis*-imidazolylidene ligand (k_1 = ~ 6.22×10^{-5} s^{-1}) and the pyridyl-imidazolylidene ligand (k_1 = ~3.00×10^{-5} s^{-1}). The related cytotoxicity studies against three cancer cell lines (MDA-MB-231, PC3 and HEPG2) showed that Re(I) complexes of the *bis*-imidazolylidene ligand were significantly more toxic than cisplatin against PC3 cell line (IC_{50} = ~7 μM).

Numerous examples of polynuclear platinum(II) and rhenium(I) complexes have been shown to exhibit excellent anticancer properties. A series of imidazolium-based NHC pro-ligands bearing either pentyl or *bis*-α-chloroamide linkages, which were designed to form dinuclear Re(I) complexes, were prepared. The aquation rates of the Re(I)

complexes prepared from these ligands were determined using ^{1}H NMR time-course experiments, and the results showed that Re(I) complex of the pyridyl-imidazolylidene ligand ($k_1 = 6.60 \times 10^{-5}$ s^{-1}) has a relatively slower aquation rate compared to that of the *bis*-imidazolylidene ligand ($k_1 = 1.57 \times 10^{-4}$ s^{-1}).

Increased cellular uptake of glucose is associated with the overexpression of glucose transporters (GLUTs) in many cancers; therefore, targeting GLUTs by glucose-based metal complex can enhance the delivery of anticancer agents to tumour cells. A series of Re(I) complexes of pyridyl-imidazolylidene ligand coupled with benzyl protected glucosamine or acetyl protected glucose have been synthesised to target GLUTs. However, the protecting groups could not be efficiently removed when using classical deprotecting reagents. To circumvent this problem, a PEG linker group was incorporated into the structure of Re(I) complex of the pyridyl-imidazolylidene ligand coupled to a glucose unit. This complex was prepared by a one-pot Re(I) complex synthesis and deacetylation procedure, and NMR and HRMS analysis confirmed the formation of this complex.

Table of Contents

Statement of Authorship ..... **I**

Statement of Candidate Contribution ..... **II**

Acknowledgement ..... **III**

Abstract ..... **V**

Table of Contents ..... **VII**

List of Compounds ..... **X**

Abbreviations ..... **XVIII**

Chapter 1 : Introduction **1**

1.1. Radiopharmaceuticals 1

1.1.1 Technetium 3

1.1.2 Rhenium 5

1.2. Carbenes 7

1.2.1. *N*-Heterocyclic Carbenes 8

1.2.2. Technetium and Rhenium Complexes of *N*-Heterocyclic Carbene Ligands 10

1.3. Technetium and Rhenium in Molecular Imaging and Radiotherapy 12

1.3.1. Alzheimer's Disease (AD) 12

1.3.2. Cancer 20

1.4. Thesis Overview 33

1.5. References 35

Chapter 2 : Charge Neutral Rhenium Tricarbonyl Complexes of Tridentate *N*-Heterocyclic Carbene Ligands that Bind to Amyloid Plaques of Alzheimer's Disease 43

2.1. Introduction 43

2.2. Results and Discussion 46

2.2.1. Ligand Synthesis 46

2.2.2. Rhenium Complex Synthesis 48

2.2.3. X-ray Structural Studies 51

2.2.4. Octanol-Water Partition Coefficient 52

2.2.5. Interaction of 2.17 and 2.18 with Amyloid-β(1-40) and Amyloid-Plaques 53

2.3. Conclusion 55

2.4. Experimental Details 57

2.4.1. X-ray Crystallography 57

2.4.2. ThT Fluorescence Aβ Binding Assays 57
2.4.3. Staining of Human AD Brain Tissues 58
2.4.4. Partition Coefficient (LogP) Studies 59
2.4.5. Synthesis 59
2.5. References 68
Chapter 3 : Anticancer properties of Rhenium(I) Tricarbonyl Complexes of *N*-Heterocyclic Carbene Ligands **72**
3.1. Introduction 72
3.2. Results and Discussion 75
3.2.1. Complex synthesis 75
3.2.2. Ligand Exchange Studies 82
3.2.3. Theoretical Studies 87
3.2.4. Photophysical Studies 90
3.2.5. Cytotoxicity Studies 93
3.3. Conclusion 96
3.4. Experimental Details 98
3.4.1. Synthesis 98
3.4.2. Theoretical Studies 106
3.4.3. Cell Culture 106
3.4.4. MTT Assay 106
3.5. Reference 107
Chapter 4 : Synthesis and Studies of Dinuclear Re(I) Complexes and Re(I) Carbohydrate Conjugates **111**
4.1. Introduction 111
4.2. Polynuclear Re(I) NHC Complexes 116
4.2.1. Synthesis of Polynuclear Re(I) Complexes of NHC Ligands 116
4.2.2. Ligand Exchange Studies 120
4.2.3. Photophysical Studies 126
4.3. Re(I) Carbohydrate Complexes 128
4.3.1. Synthesis of Re(I) Complex of a Glucosamine Functionalised NHC Ligand 128
4.3.2. Synthesis of a Re(I) Complex of a Glucose Functionalised NHC Ligand 131
4.3.3. Synthesis of a Re(I) Complex of a Glucose Functionalised NHC Ligand with an Extended PEG Linker 139
4.4. Conclusion 142

4.5. Experimental Details 144
4.6. Reference 158
Chapter 5 : Thesis Conclusion and Future Directions **161**
5.1. Thesis Conclusion 161
5.2. References 168
Appendix 1 : General Procedure **169**
1.1. General Procedure 169
Appendix 2 : For Chapter 2 ..... **170**
2.1. NMR Spectra 170
2.2. FT-IR Spectra 188
2.3. X-ray Crystallography 189
2.4. Partition Coefficient (LogP) Studies 190
2.5. Photophysical Studies 195
Appendix 3 : For Chapter 3 ..... **198**
3.1. IR Spectra 198
3.2. NMR Spectra 201
3.3. High-Resolution Mass Spectra 221
3.4. Computational Studies 230
3.5. Ligand Exchange Studies 232
3.6. Photophysical Studies 237
Appendix 4 : For Chapter 4 ..... **238**
4.1. Ligand Exchange Studies 238
4.2. Photophysical Studies 243
4.3. NMR Spectra 244
4.4. Mass Spectrum 267

List of Compounds

Chapter 2	
Compound Number	**Structure**
2.5	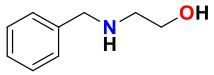
2.6	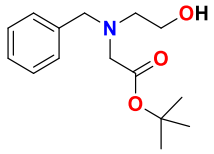
2.7	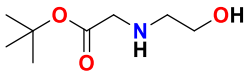
2.8	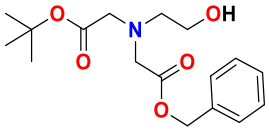
2.9	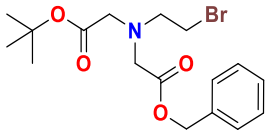
2.10	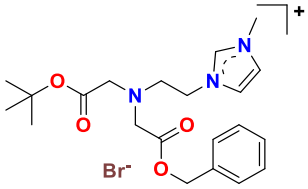
2.11	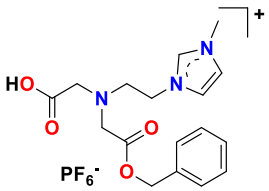

2.12	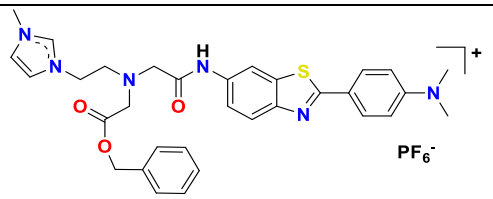
2.13	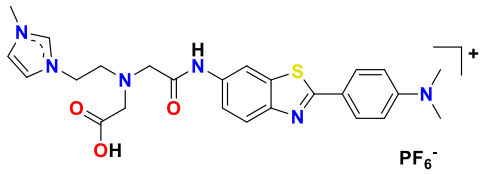
2.14	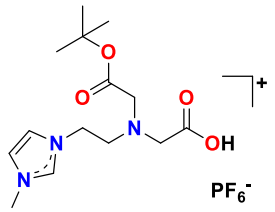
2.15	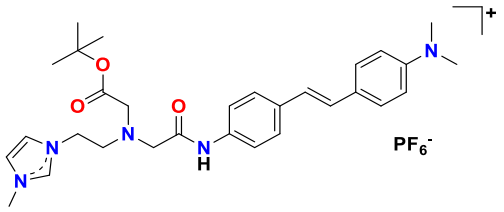
2.16	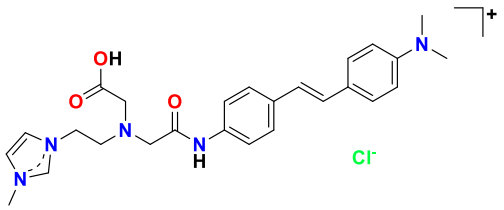
2.17	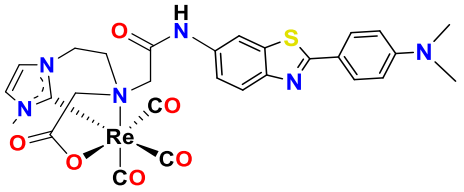
2.18	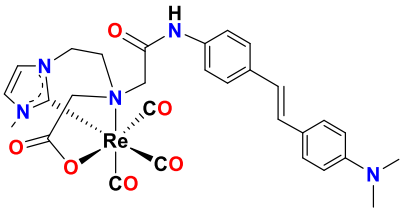
6-amino-2-(4-*N*,*N*-dimethylaminophenyl)benzothiazole	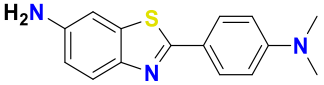

4-amino-4'-(*N*,*N*-dimethylamino)stilbene	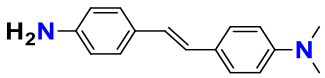

Chapter 3

Compound Number	Structure
***N*-acetyl-glycine**	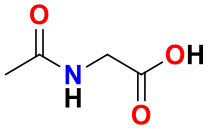
***N*-acetyl-L-isoleucine**	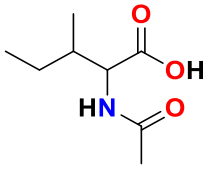
***N*-acetyl-L-proline**	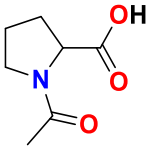
3.1	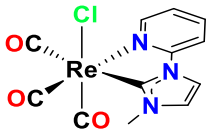
3.2	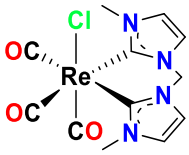
3.4	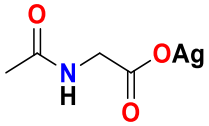

3.5	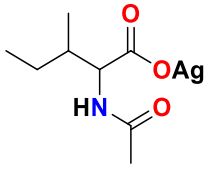
3.6	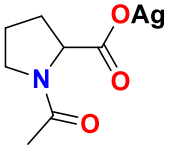
3.7	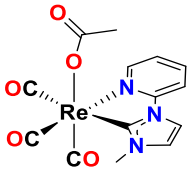
3.8	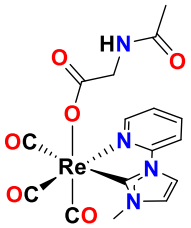
3.9	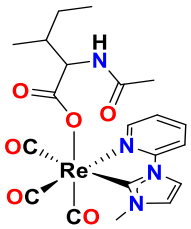
3.10	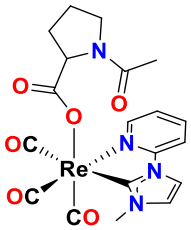
3.11	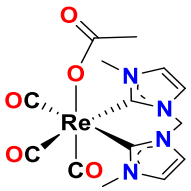

3.12	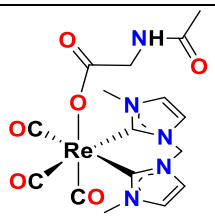
3.13	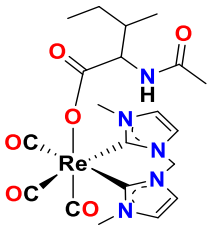
3.14	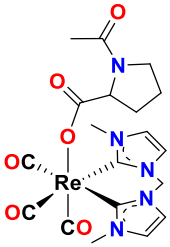

Chapter 4

Compound Number	Structure
4.25	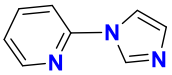
4.26	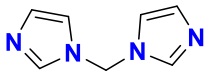
4.27	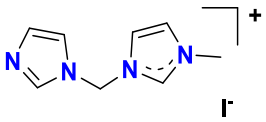
4.28	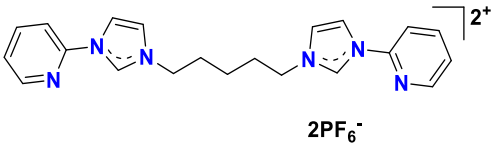

4.29	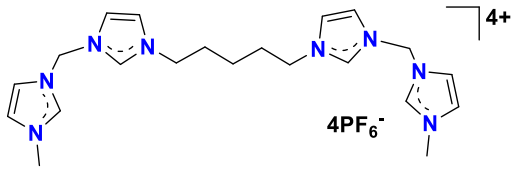
4.30	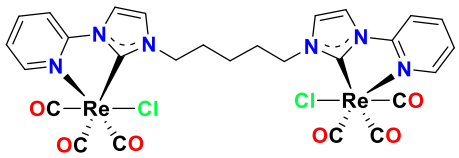
4.31	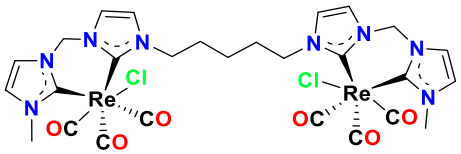
4.32	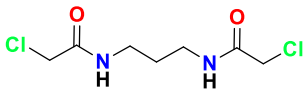
4.33	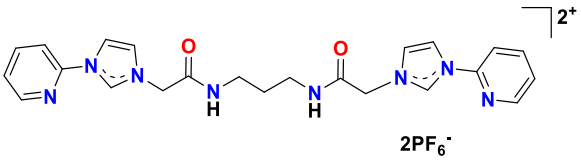
4.34	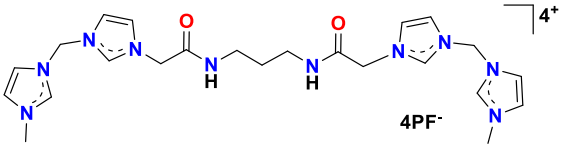
4.35	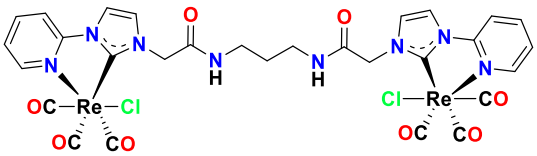
4.36	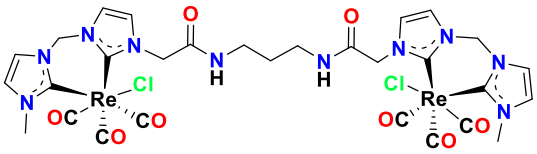

4.43	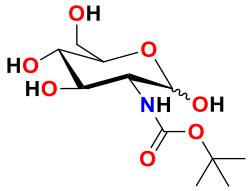
4.44	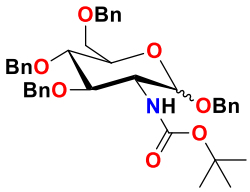
4.45	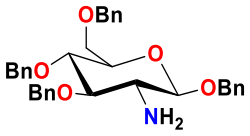
4.46	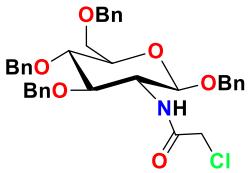
4.47	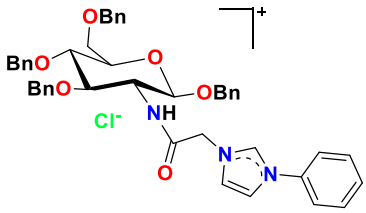
4.50	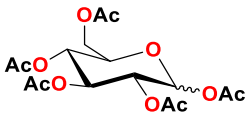
4.51	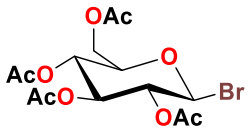
4.52	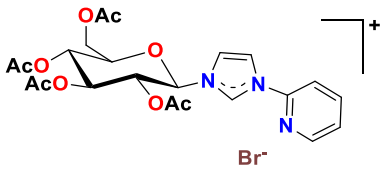

4.54	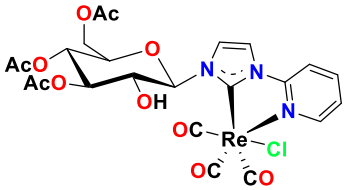
4.60	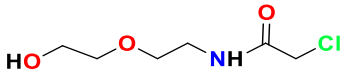
4.61	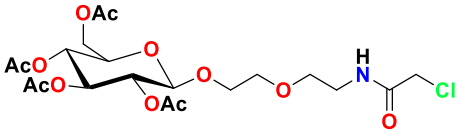
4.62	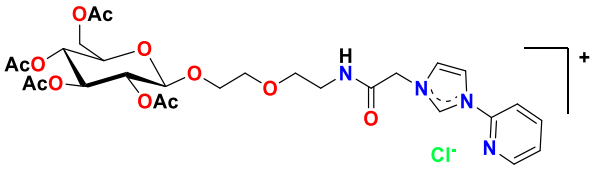
4.63	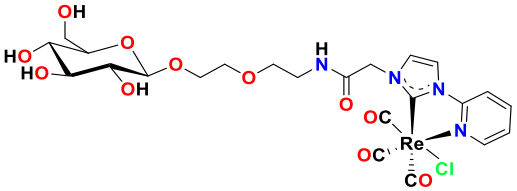

Abbreviations

A549	Cisplatin-resistance cancer cell line
AD	Alzheimer's disease
AHDF	Adult human dermal fibroblast cell line
AIF	Apoptosis-inducing factor
Ar	Aromatic
ASPC1	Pancreatic cancer cell line
BBB	Blood brain barrier
BDE	Bond dissociation free energy
bpy	2,2'-bipyridine
br	Broad
Bn	Benzyl
BOC	*tert*-butyloxycarbonyl
Calcd	Calculated
cat.	Catalyst
d	Doublet (in NMR)
DFT	Density functional theory
DMF	*N*,*N*-Dimethylformamide
DMSO	Dimethyl sulfoxide
eq.	Equivalent
em	Emission
ESI	Electrospray ion
ex	Excitation
FDG	^{18}F-fluorodeoxyglucose
h	Hour

HeLa	Henrietta Lacks cancer cell line
HEPG2	Human hepatocellular carcinoma cell line
HRMS	High-resolution mass spectrometer
GLUT	Glucose transporter
IC_{50}	50% growth inhibitory concentration
'In vitro'	Latin phrase meaning 'in glass'
'In vivo'	Latin phrase meaning 'within the living'
imi	Imidazole
m	Multiplet
MCF-7	Human breast adenocarcinoma
MDA-MB-231	Human metastatic breast cancer cell line
MLCT	Metal-to-ligand charge transfer
MTT	(3-(4,5-dimethylthiazol-2-yl)-2,5-diphenyltetrazolium bromide
NHC	*N*-heterocyclic carbene
NMR	Nuclear magnetic resonance
OAc	Acetate
K_i	Binding affinity
k_1	Forward reaction rate constant
k_{-1}	Reverse reaction rate constant
PBS	Phosphate buffer saline
PEG	Polyethylene glycol
PET	Positron emission tomography
PC3	Human prostate cancer cell line
Ph	Phenyl
ppt	Precipitate

PyBop	Benzotriazol-1-yloxytripyrrolidinophosphonium hexafluorophosphate
q	Quartet (in NMR)
s	Singlet (in NMR)
SAR	Structure-activity relationship
SPECT	Single photon emission computed tomography
t	Triplet (in NMR)
$t_{1/2}$	Half-life
TBABr	Tetrabutylammonium bromide
TBACl	Tetrabutylammonium chloride
TFA	Trifluroacetic acid
ThT	Thioflavin-T
RDG	Reduced density gradient
rt	Room temperature
UV-Vis	Ultraviolet-visible

Chapter 1 : Introduction

1.1. Radiopharmaceuticals

Radiopharmaceuticals are drugs containing a radioactive atom or a radionuclide. The radiation emitted from the radionuclide can be used for the diagnosis or for the therapy of various diseases.[1] The selection of an appropriate radionuclide primarily depends on its physical and chemical properties, availability, production and medical applications.[2-3] Radiopharmaceuticals for medical applications can be divided into two classes based on their applications, and these are either for therapy or diagnosis. Therapeutic radiopharmaceuticals utilise electrically charged particles such as alpha (α) particles, beta (β^-) particles or Auger electrons to damage the target cells, which results in cell death, disease control or pain palliation.[4-5] Diagnostic radiopharmaceuticals are mainly used to analyse disease progression or to monitor the effects of treatment.[2-3,6] Radionuclides used in diagnostic imaging emit gamma (γ) or positron (β^+) radiation, which can be detected in the imaging techniques of Single Photon Emission Computed Tomography (SPECT) or Positron Emission Tomography (PET), respectively.[7]

The PET and SPECT imaging techniques are non-invasive and routinely used for disease diagnosis and medical imaging. Although PET provides higher resolution images, it is a more costly technique compared to SPECT and is not readily available in all hospitals. For this reason, SPECT is still widespread and commonly used as there is no requirement for an on-site cyclotron, and the SPECT isotopes such as ^{99m}Tc ($t_{1/2}$ = 6.06 hours) and ^{123}I ($t_{1/2}$ = 13.2 hours) have a longer half-life than many PET isotopes, e.g. ^{18}F ($t_{1/2}$ = 109.8 mins), and ^{68}Ga ($t_{1/2}$ = 1.13 hours).[8] Imaging agents used in SPECT are generally attached to a ligand designed to target specific organs or tissues.[2,9-10] Numerous SPECT imaging radionuclides attached to neurotransmitter analogues have been approved for brain

imaging.[11] For examples, the ^{123}I labelled amphetamine analogue (Iofetamine **1.1**[12-13]) is commonly used for cerebral blood perfusion imaging, while the ^{123}I labelled cocaine analogue (Ioflupane **1.2**) has been approved for the diagnosis of Parkinson's disease (Figure 1.1).[14-16]

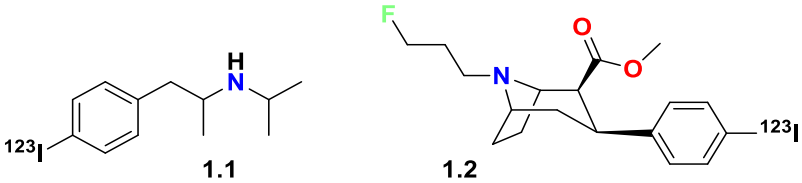

Figure 1.1. SPECT imaging agents: Iofetamine **1.1** and Ioflupane **1.2**, both of which are labelled with ^{123}I.

Many modern radiopharmaceuticals based on metallic radionuclides are designed based on a bifunctional strategy, where the imaging agent is comprised of (i) a suitable biomolecule that targets the radiopharmaceutical to a site of interest in the body, (ii) a bifunctional chelate that forms a link between a biomolecule and a radiometal and (iii) an appropriate metallic radionuclide (Figure 1.2).[17] The bifunctional strategy is widely used as a range of biomolecules are highly selective for specific target tissues. Commonly used targeting biomolecules are small molecules, e.g. sugars, peptides, and macromolecules such as proteins and antibodies.[3,5] A bifunctional chelate is required to form a stable linkage between the metallic radionuclide and the biomolecule. A linker group is generally used to separate the radionuclide from the biomolecule to prevent possible interference with the biomolecule receptor binding site.[3,5]

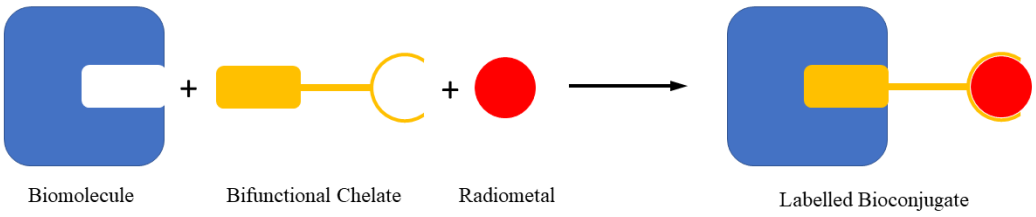

Figure 1.2. Schematic representation of bifunctional strategy for radiopharmaceutical design.[17]

The integrated strategy is another approach that is used in radiopharmaceutical design. For this approach, the radionuclide is incorporated into the radiopharmaceutical in such a way as to mimic the high-affinity receptor structure with minimal changes in size, conformation, and binding affinity.[3,17] However, this approach is synthetically challenging and can result in molecules with lowered binding affinity for the target and also changes the lipophilicity of the ligand.[3] Examples of the integrated approach using the metal rhenium are shown in Figure 1.3. In these examples, Re(V) (**1.3** and **1.4**) was used to develop imaging agents for the estrogen receptor **1.5**, which is overexpressed in several types of cancers.

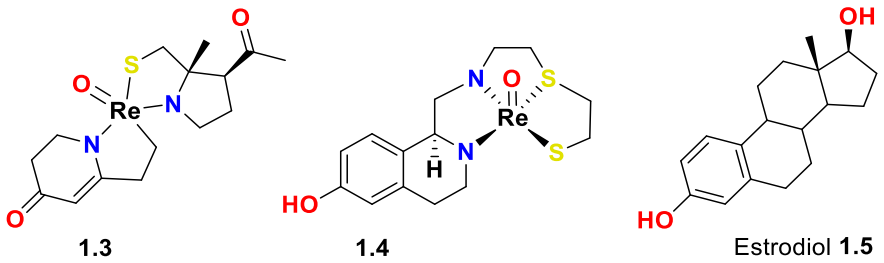

Figure 1.3. Examples of integrated approach strategy for the formation of Re complexes **1.3** and **1.4** that designed to mimic estrodiol **1.5**.

1.1.1 Technetium

Technetium is the 43rd element, which is located in group 7 of the periodic table.[18-20] It has a $4d^5 5s^2$ valence electron configuration, and technetium complexes can have

coordination numbers ranging from 4 to 9 as well as oxidation states ranging from -1 to +7. Furthermore, there are numerous isotopes of technetium in a range of ^{85}Tc to ^{120}Tc, and all isotopes of technetium are radioactive.[18] Technetium is widely used in diagnostic imaging applications due to its nuclear and chemical properties.[19] In particular, the half-life of ^{99m}Tc is ideal for diagnostic imaging as it provides a reasonable time for preparation, transportation, administration of radiopharmaceuticals and imaging the patients.[19,21] Furthermore, the energy of the gamma radiation (140 keV) emitted by ^{99m}Tc is sufficient to penetrate human tissue without resulting in a large radiation dose.[18,20] These features of ^{99m}Tc have made its one of the most important radionuclides in molecular imaging, and more than 80% of SPECT imaging agents are ^{99m}Tc-based radiotracers.[20,22]

Technetium-99m is widely available for clinical application because of the ^{99}Mo/^{99m}Tc generator.[23] The preparation of ^{99m}Tc starts with the absorption of ^{99}Mo in an alumina column as ^{99}Mo-molybdate or $[^{99}MoO_4]^{2-}$. The ^{99}Mo decays to produce ^{99m}Tc in the form of pertechnetate $[^{99m}TcO_4]^-$, which can be eluted from the column with a saline solution (Figure 1.4).[23]

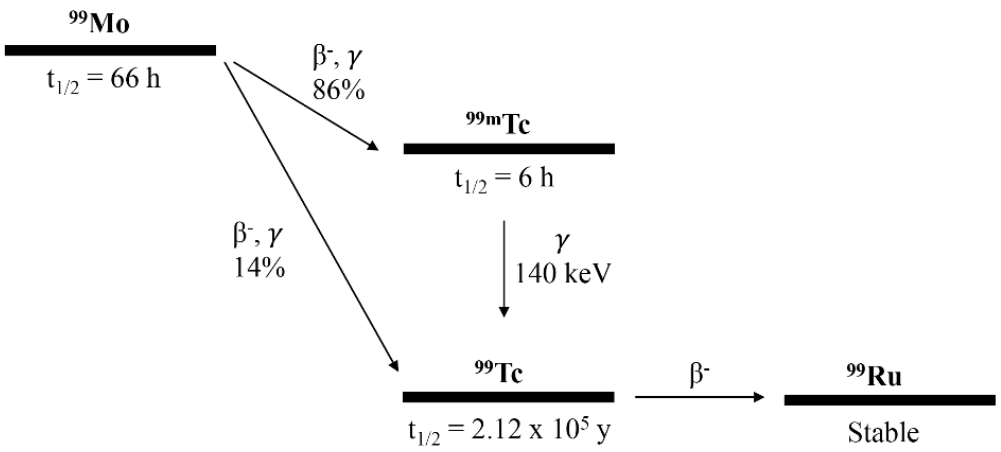

Figure 1.4. ^{99m}Tc production in the ^{99}Mo/^{99m}Tc generator.[23]

When synthesising ^{99m}Tc complexes, three components need to be considered, including the use of pertechnetate as the starting material, the nature of the reducing agent and the coordinating ligands.[18,20] The nature of the reducing agent is essential to reduce $^{99m}TcO_4^-$ to a lower oxidation state that allows the ligand to coordinate and form the ^{99m}Tc complex.[20] A large number of ^{99m}Tc imaging agents are available such as Tetrofosmin **1.6** and ^{99m}Tc-MIBI (Sestamibi) **1.7** (Figure 1.5), which are used for cardiac imaging.[24] Additionally, ^{99m}Tc-apcitide **1.8**, a radiolabelled polypeptide, was developed to target glycoprotein IIb/IIIa receptors involved in acute thrombosis.[25-26] It is currently in phase III clinical trials for imaging acute deep venous thrombosis (DVT).[26]

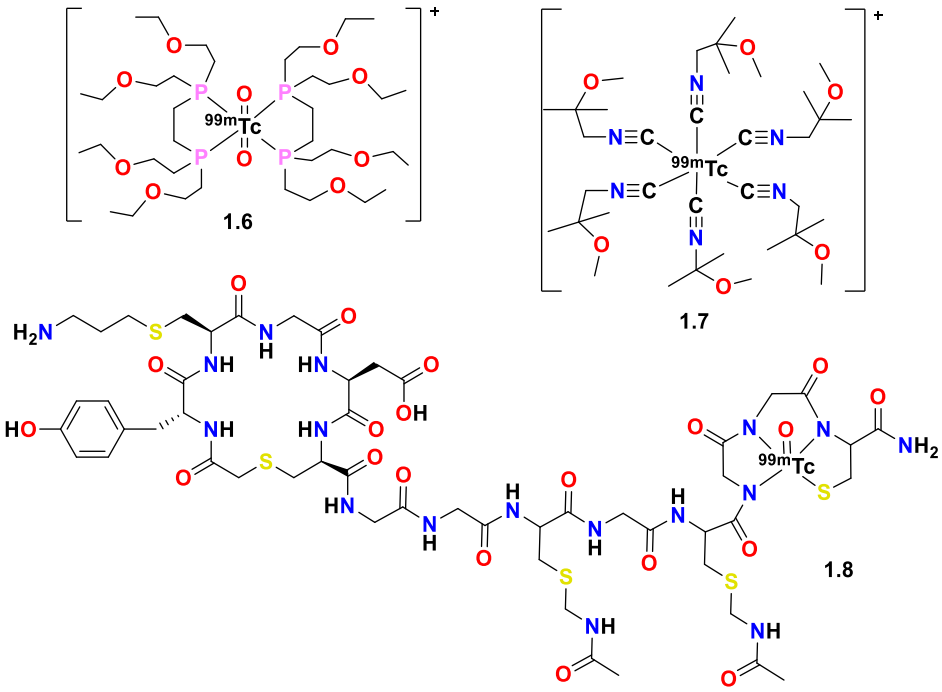

Figure 1.5. SPECT imaging agents radiolabelling with ^{99m}Tc: Tetrofosmin **1.6**, Sestamibi **1.7** and ^{99m}Tc radiopeptide-apcitide **1.8**.

1.1.2 Rhenium

Rhenium is the 75th element in the periodic table (below technetium in group 7) and is said to be a congener (similar properties) of Tc due to the lanthanide contraction.[18,27] The lanthanide contraction results from the poorly shielded 4f orbitals, which cause the

element in the 5th and 6th periods of the periodic table to have similar atomic radii.[20] As is the case for Tc, Re complexes also have oxidation states ranging from -1 to +7 and coordination numbers up to nine.[27] As all isotopes of Tc are radioactive; Re is commonly used to prepare non-radioactive analogues of ^{99m}Tc imaging agents for the purpose of chemistry development and other studies.[28] There are two radioisotopes of rhenium that are used in radiotherapy, and these are ^{186}Re and ^{188}Re.[29] In the case of ^{186}Re, it can be produced via neutron capture by the parent radionuclide ^{185}Re (Figure 1.6a). In contrast, ^{188}Re can be produced in a nuclear reactor based method, which involves the production of ^{188}Re as perrhenate Na[^{188}ReO$_4$] via a ^{188}W/^{188}Re isotope generator similar to that of ^{99m}Tc generator (Figure 1.6b). [21, 30-31]

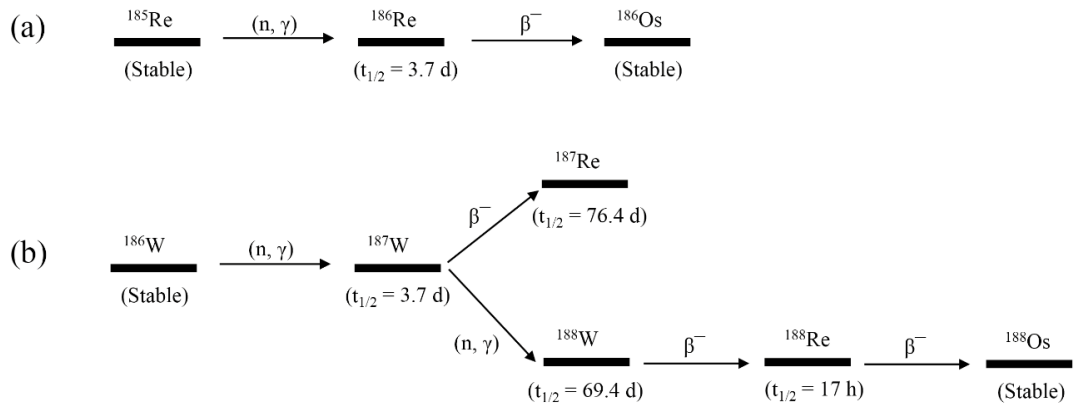

Figure 1.6. Nuclear pathways for the preparation of ^{186}Re and ^{188}Re.[21,31]

Rhenium has gained significant attention in radiochemistry as it can coordinate to many different ligand types, and there are two available rhenium isotopes that can be produced in the hospital setting for radiotherapeutic purposes.[32-33] One of the available rhenium isotopes is a ^{186}Re that emits β^- radiation (β^- maximum energy of 1.07 MeV) with a half-life of 3.7 days, while ^{188}Re is also a β^- emitter (β^- maximum energy of 2.12 MeV) with a shorter half-life of 16.9 h. The lower energy emission of ^{186}Re has a tissue penetration range of 4.5 mm, which is more suitable for treating small to medium-sized tumours.[31,34,

[27] Additionally, the longer half-life of ^{186}Re provides the potential for labelling antibodies and peptides. For example, the hydroxyethylidine diphosphonate (HEDP) peptides labelled with ^{186}Re **1.9** are clinically used for the treatment of bone metastases from prostatic cancer[35] or breast cancer[36] (Figure 1.7).[34] In contrast, ^{188}Re has a longer penetration range of 11 mm, which is more appropriate for targeting large tumours.[27,31] Several biomolecules labelled with ^{188}Re are currently being investigated in clinical trials.[27] For example, ^{188}Re coupled to 4-hexadecyl-1, 2, 9, 9-tetramethyl-4. 7-diaza-1, 10-decanethiol or HDD (**1.10**) has been evaluated in clinical trials for the treatment of hepatocellular carcinoma, a primary liver cancer with a poor prognosis (Figure 1.7).[27,29] In the second example, the small molecule meso-2,3-dimercaptosuccinic acid (DMSA) labelled with ^{188}Re (**1.11**) targets medullary carcinoma (Figure 1.7).[27]

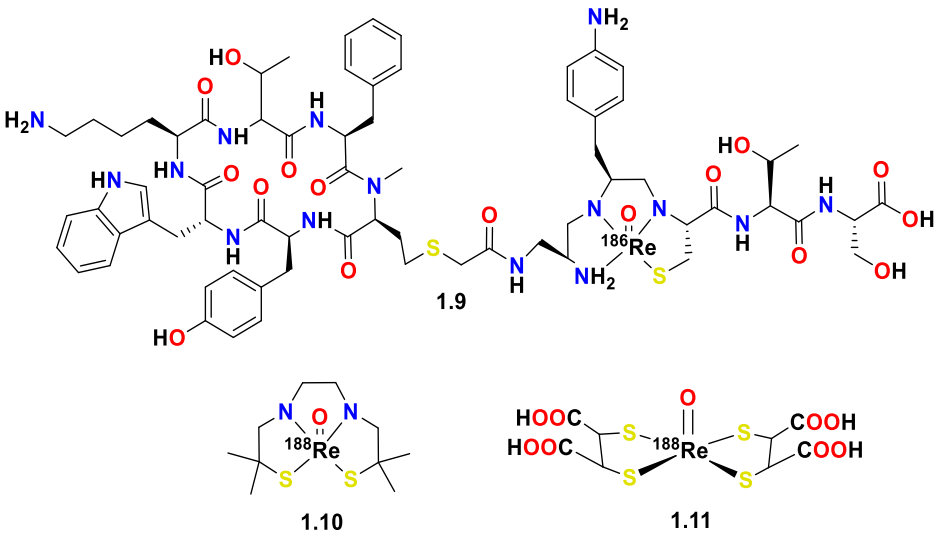

Figure 1.7. Clinically use radiotherapeutic agents based on ^{186}Re and ^{188}Re.

1.2. Carbenes

A carbene is a compound containing a neutral divalent carbon atom and two unshared electrons, where the geometry at the carbene carbon can be either linear or bent.[37] The linear geometry occurs when the carbene carbon is *sp*-hybridised with both non-bonding electrons occupy the degenerated *p* orbitals, thus giving a triplet carbene (**I**, Figure 1.8).[37-

[38] However, this is not a common geometry for carbenes as most carbenes have the sp^2-hybridised carbon that gives rise to a bent geometry.[37] The bent geometry can occur when each of the non-bonding electrons occupies two empty orbitals that result in a triplet state (**II**, Figure 1.8).[37-38] The singlet carbene can form when two electrons are placed in the sp^2-hybridised orbitals with an antiparallel spin orientation (**III**, Figure 1.8).[37]

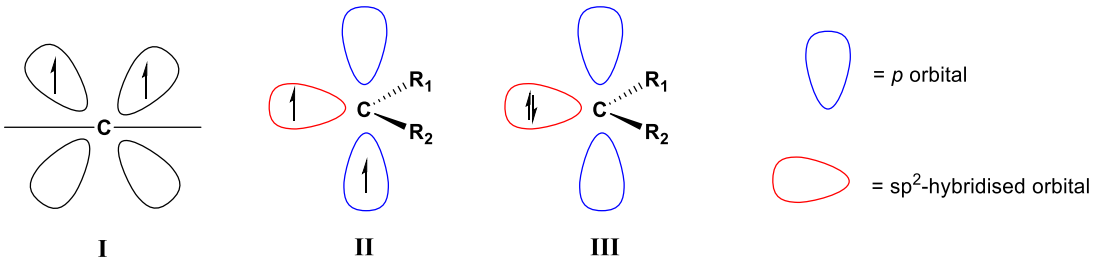

Figure 1.8. Electronic structures of carbenes.[37-38]

1.2.1. *N*-Heterocyclic Carbenes

N-heterocyclic carbenes (NHCs) are a class of carbene containing molecules with at least one nitrogen atom in the heterocyclic ring structure.[39] NHCs have a singlet ground state electronic configuration with an electron lone pair in the sp^2-hybridised orbital and an unoccupied *p*-orbital at the carbene carbon, stabilising by mesomeric and inductive effects from the flanking nitrogen atoms.[39] The presence of nitrogen atoms in the ring structure is an important feature for NHCs as the σ-electron-withdrawing property of nitrogen atoms can stabilise the carbene centre by lowering the energy of the occupied σ-orbital. Additionally, the π-electron-donating property of the flanking nitrogen atoms can donate electron density into the empty *p*-orbital (Figure 1.9), thereby resulting in stabilisation of the singlet carbene.[39]

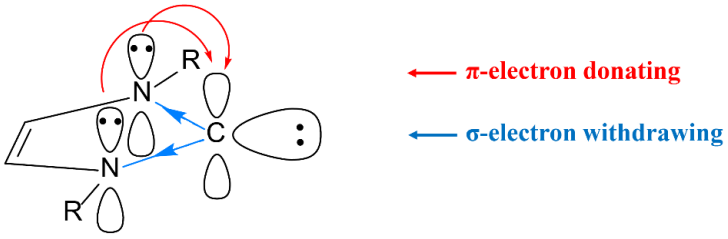

Figure 1.9. The electronic structure of imidazole-2-ylidenes showing "push-pull" electronic effects.[39]

The first isolation of a free NHC was compound **1.13** (Figure 1.10), which was reported by Arduengo and co-workers in 1991.[40] The compound was synthesised by the deprotonation of imidazolium precursor **1.12** with sodium hydride and catalytic dimethyl sulfoxide (Figure 1.10). Furthermore, an X-ray crystal structure was obtained for this compound.[40]

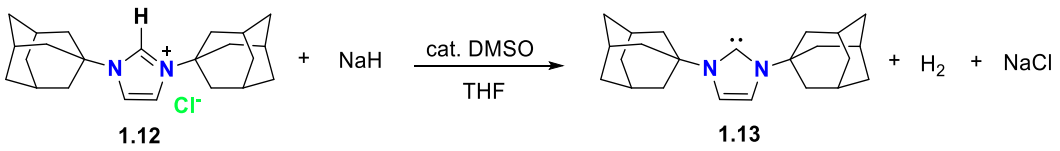

Figure 1.10. Synthetic route for the preparation of the first crystalline NHC **1.13**.

Since the isolation of the first free NHC, interest in the chemistry of NHC ligands has dramatically increased.[41] Numerous NHC scaffolds (**1.14-1.18**, Figure 1.11) have been synthesised for various applications, including organocatalysts and for potential medical applications.[39,41-43]

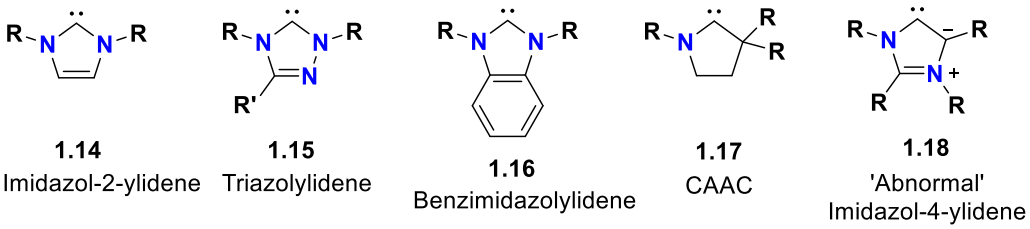

Figure 1.11. The structures of common classes of NHCs.

1.2.2. Technetium and Rhenium Complexes of *N*-Heterocyclic Carbene Ligands

N-heterocyclic carbenes (NHCs) have been extensively used in the development of transition metal complexes due to their strong σ-donor character[44-46], and the s*p*^{2}-hybridised lone pair of NHCs can donate into a σ-accepting orbital of a transition metal.[39,47] The first metal-NHC complexes were prepared independently by Wanzlick[48] and Öfele[49] in 1968, where they reported the Hg(II) **1.19** and Cr(II)-NHC **1.20** complexes (Figure 1.12).

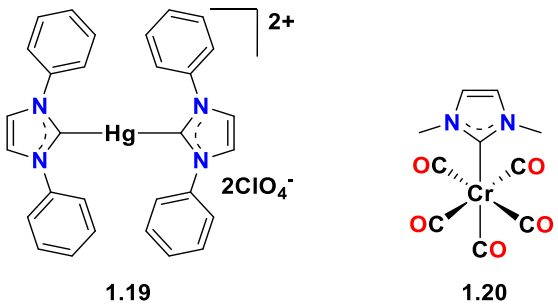

Figure 1.12. The first metal complexes of NHC ligands, **1.19** and **1.20**.

Despite the excellent catalytic activity of NHC-metal complexes, inadequate research has focused on the use of NHCs as ligands in molecular imaging and radiotherapeutic applications. Youngs and co-workers have shown that Ag(I)-NHC complexes can be used to transfer NHC ligands to ^{105}Rh(III) that have potential for use in radiotherapy.[50-51]

Abram and co-workers reported the first synthesis of a ^{99}Tc-NHC complex **1.21** (Figure 1.13).[52-54] This group has also extensively studied the chemistry of the $[Tc(CO)_3]^+$ core with NHC ligands.[55-56] They demonstrated that NHC complexes of the $[Tc(CO)_3]^+$ core are chemically robust and resistant to oxidation. The same group also demonstrated that reaction between $[Tc(CO)_3(H_2O)_3]^+$ and acetylcyclopentadiene produced neutral cyclopentadienyl complex, $[Tc(CO)_3(C_5H_4COCH_3)]$. [55-56]

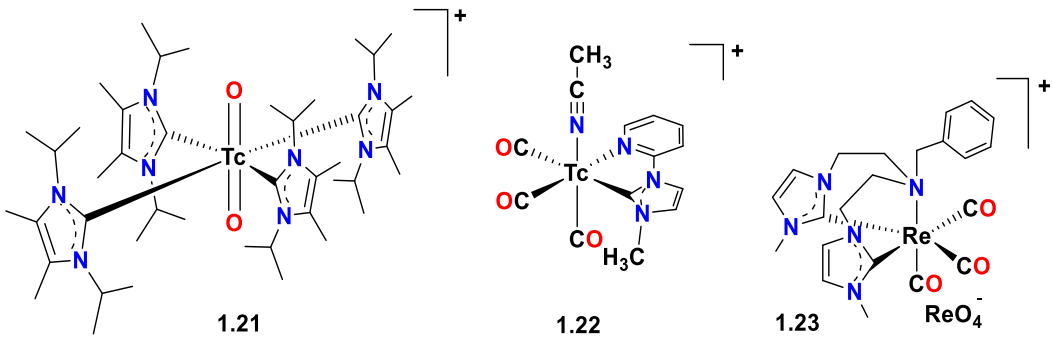

Figure 1.13. The first ^{99}Tc-NHC complex **1.21**; the first ^{99m}Tc-NHC complex **1.22**; and a tridentate *bis*-NHC-amine ligand **1.23** bound to the $[Re(CO)_3]^+$ core.

The radiolabelling of an NHC ligand with the $^{99m}[Tc(CO)_3]^+$ core was first reported by Barnard and co-workers.[57] In this research, the carboxylic acid functionalised azolium salts was coupled to glycine benzyl ester, and the stability of the $[Re(CO)_3]^+$ complexes corresponding to these NHC ligands were evaluated. The results from radio-HPLC and ESI-mass spectrometry experiments showed that the NHC ligand (1-(2-pyridyl)-3-methylimidazolylidene) could be labelled with ^{99}Tc and ^{99m}Tc (**1.22**, Figure 1.13). However, this complex was found to be unsuitable for use in imaging applications due to the labile nature of the monodentate acetonitrile ligand.

The same research group later prepared a series of bidentate, *bis*-bidentate and tridentate Re(I)-NHC complexes via Ag(I) transmetalation protocols.[57] The stability of the Re(I)-NHC complexes was investigated using challenge experiments with the metal-binding amino acids L-histidine or L-cysteine. The results of these studies suggested that the tridentate, *bis*(NHC)-amine ligand bound to the $[Re(CO)_3]^+$ core (**1.23**, Figure 1.13) produced kinetically stable complexes suitable for *in vivo* studies. Thus, the *bis*(NHC)-amine ligand offers the potential formation of a SPECT imaging agent for Alzheimer's disease.

1.3. Technetium and Rhenium in Molecular Imaging and Radiotherapy

1.3.1. Alzheimer's Disease (AD)

Alzheimer's disease (AD) is a progressive neurodegenerative disorder that causes dementia.[58] The clinical characteristics of this disease include memory loss, cognitive impairment and behavioural changes that eventually lead to death.[59] The hippocampus plays a key role in maintaining new memories; therefore, neuronal death in this area of the brain is responsible for the disease symptoms.[60]

The underlying causes of Alzheimer's disease are currently unknown. However, research in this area suggests that the process of the disease could involve the formation of amyloid β plaques in the brain.[61] The amyloid precursor protein (APP) is a transmembrane protein with a small cytoplasmic region and long extracellular tail. There are two proteolytic pathways for the cleavage of the amyloid precursor protein.[61] In the amyloidogenic pathway, APP is cleaved by β- and γ-secretases to release the neurotoxic Aβ peptide into the extracellular space.[62] The Aβ peptide is composed of 40 amino acid residues ($A\beta_{1-40}$) or 42 amino acid residues ($A\beta_{1-42}$).[62] The association of the Aβ peptide molecules results in fibrils consist of ~9:1 ($A\beta_{1-40}$:$A\beta_{1-42}$) that eventually leads to the deposition of insoluble Aβ plaques.[61] In the non-amyloidogenic pathway, α-secretase cleaves within the Aβ domain and thus inhibit the formation of Aβ plaques.[61]

Currently, there are no medical treatments for AD, but there are treatments available to relieve the symptoms of this disease.[63] Diagnosing AD in its early stages is very difficult because the symptoms are generally not yet apparent.[63] Intellectual functioning assessments and characterising neuropsychological features are often used as diagnostic tools.[64] However, the results from intellectual and neuropsychological tests can be misinterpreted, as the symptoms of early stages of AD are similar to the typical signs of

aging.[65] The development of new diagnostic tools for Alzheimer's disease in its early stages are required to allow the current and new treatments to be most effective.

1.3.1.1. PET Radiotracers for Alzheimer's Disease

The required properties for Aβ plaques imaging agents are: (i) good penetration through the blood-brain barrier (BBB), (ii) relatively small size and (iii) selective binding to Aβ plaques.[66-67] A number of imaging agents have been developed for PET imaging of AD, with Pittsburgh Compound B (PiB **1.24**, Figure 1.14) being one of the first Aβ probes.[68] PiB was designed based on the structure of compounds such as Congo Red (CR) and Thioflavin-T (ThT **1.25**, Figure 1.14), which are histological dyes that bind to amyloid plaques with high affinity.[69-70] Therefore, the modification of CR or ThT continues to be the key strategy for the development of PET imaging agents.[71]

The common features of PET imaging agents for AD include a rigid scaffold and aromatic groups. The compound STB-8 (**1.26**, Figure 1.14) was synthesised based on the structure of CR. [71] It is reported that STB-8 has the capacity to pass through BBB as well as the ability to bind to amyloid β plaques selectively. Additionally, AD imaging agents labelled with ^{18}F such as Flutemetamol **1.27**[72], Florbetapir **1.28**[73], and Florbetaben **1.29**[74] have gained approval from the US Food and Drug Administration (FDA) to determine the amyloid plaques load in humans (Figure 1.14).[75]

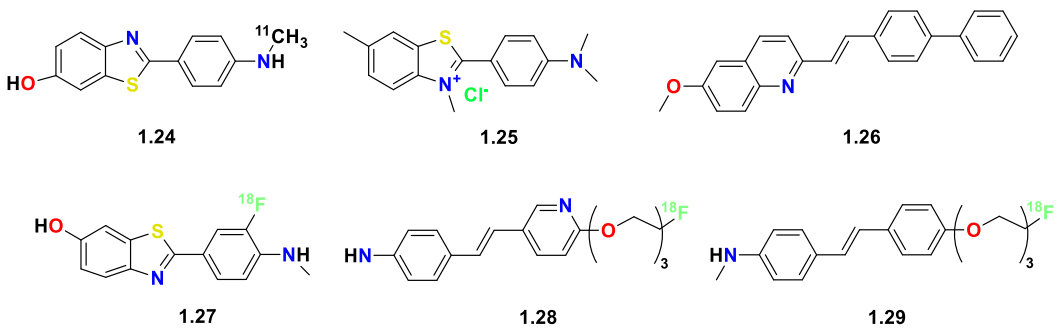

Figure 1.14. Structures of Pittsburgh Compound B **1.24**; the histological dye Thioflavin-T **1.25**; STB-8 **1.26**; and imaging agents for AD labelled with ^{18}F: Flutemetamol **1.27**, Florbetapir **1.28**, Florbetaben **1.29**.

Theoretical studies have been used to investigate the interaction between STB-8 (**1.26**, Figure 1.14) and amyloid fibrils.[76] The results suggested that **1.26** can bind to the end, side, top, or bottom face of the amyloid fibril, and the orientation of the ligand can be on the long axis of the fibril or parallel to the peptide strands.[76] Molecular dynamics simulation results showed that **1.26** bound parallel to the long axis of the top face and bottom face of the fibril. These results are expected as the side chains of the amino acid form hydrophobic pockets where π-π interaction occur between the aromatic group of the ligand and the phenyl rings of the amino acid side chains.[76]

In recent years, inorganic radionuclides such as ^{68}Ga and ^{64}Cu have been studied for the development of PET imaging agents for the early diagnosis of AD.[77] A common bifunctional chelator of ^{68}Ga(III) is 1,4,7,10-tetraazacyclododecane-1,4,7,10-tetraacetic acid (DOTA).[77] However, the reaction of ^{68}Ga(III) with DOTA often required harsh conditions such as high temperature and long reaction times that could damage or deactivate sensitive proteins or biomolecules.[77] Therefore, hexadentate chelators such as 1,4,7-triazacyclononane-1,4,7-triacetic acid (NOTA), diethylenetriaminepentaccetic acid (DTPA), and *N*,*N*-Bis[2-hydroxy-5-(carboxyethyl)benzyl]ethylenediamine-*N*,*N*-diacetic acid (HBED) are often used as alternative ligands.[77] For example, a series of ^{68}Ga

complexes of bivalent styrylpyridines coupling to the HBED ligand (**1.30**, Figure 1.15) were prepared, and the ability of these ^{68}Ga complexes to bind to the Aβ plaques aggregate in blood vessel walls was investigated.[78] An *in vitro* competitive binding assay to Aβ aggregate using [^{125}I]IMPY showed that the bivalent complexes **1.30** had higher binding affinities towards Aβ aggregates (K_i = 6.70-30.6 nM) compared to a monovalent complex **1.31** (K_i = 185 nM).[78] The binding ability of ^{68}Ga complexes coupling with styrylpyridinyl amyloid binding moiety to Aβ aggregates was further confirmed using *in vitro* autoradiography in post-mortem AD brain sections.[78]

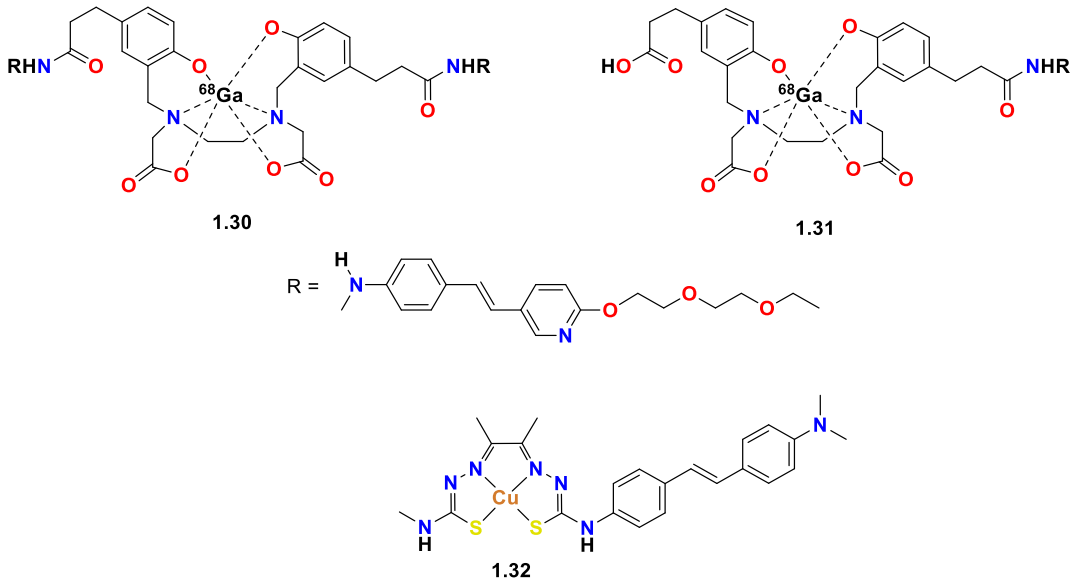

Figure 1.15. Chemical structures of bivalent ^{68}Ga(III) complex **1.30**; the monovalent ^{68}Ga complex **1.31**; and a ^{64}Cu *bis*(thiosemicarbazonato)-stilbenyl **1.32**.

The complex CuATSM or diacetyl*bis*(*N*(4)-methylthiosemicarbazonato)copper(II) has been investigated as a PET imaging agent for hypoxia in humans, as it has a low molecular weight, high lipophilicity and is uncharged allowing it to pass through the BBB.[79-80] Recently, ^{64}CuATSM coupled to a stilbene functional group (**1.32**, Figure 1.15) has been reported.[81] This complex was found to bind to Aβ plaques in post-mortem human frontal cortex brain tissue from a clinically diagnosed AD patient and **1.32** (2.2 ± 0.6% ID/g)

also displayed similar brain uptake to that of ^{64}CuATSM (0.9 ± 0.4% ID/g) in wild-type mice.[81] Further studies are required to investigate the uptake and retention of **1.32** *in vivo* and evaluate its affinity for Aβ plaques.

1.3.1.2. SPECT Radiotracers for Alzheimer's Disease

There has been significant interest in the development of ^{99m}Tc based SPECT imaging agents for AD. To this end, a range of bifunctional ligands for ^{99m}Tc coupled to amyloid binding moieties has been developed. Ligands that have been investigated include *bis*(aminoethanethiol) (BAT) and monoamine-monoamide dithiol (MAMA),[61] which provide an N_2S_2 donor group that forms neutral complexes with the Re(V)=O or Tc(V)=O cores.[61] Several derivatives of benzothiazole[82] (**1.33**, Figure 1.16), chalcone[83], flavone and aurone[84], benzoxazole[85], dibenzylideneacetone[86], phenylbenzoxazole (**1.34**, Figure 1.16)[8] conjugating with BAT and MAMA have been reported. However, *in vitro* studies showed that these complexes either had a low affinity for amyloid plaques or failed to cross the BBB.[8,82-86]

Ligands with N_2S_2 donor groups are air-sensitive and are prone to oxidation. To combat this problem, a chelator called the thiol-free hydroxamamide (Ham) had been explored for the development of ^{99m}Tc based SPECT imaging agents.[77] Ham can be radiolabelled with ^{99m}Tc under mild conditions, and the bidentate chelator properties of Ham may enhance the binding affinity of these complexes towards Aβ plaques.[77] A series of ^{99m}Tc-Ham complexes conjugated to the Aβ binding moieties 2-phenylbenzothiazole (**1.35**, Figure 1.16), stilbene (**1.36**, Figure 1.16) and dimethylaminobenzene (**1.37**, Figure 1.16) has been reported.[87] The binding affinity to Aβ plaques of complexes **1.35-1.37** was confirmed by the *in vitro* inhibition assay and *in vitro* autoradiography studies using brain tissue sections from Tg2575 mice. Additionally, a biodistribution study for **1.35** was performed in normal mice, and the result indicated that this compound had a poor brain

uptake (0.28% ID/g), which suggests that the complex crosses the BBB at low levels. However, ^{99m}Tc-Ham complexes may be useful for the development of cerebral amyloid angiopathy (CAA) imaging agents to differentiate CAA from AD.[88]

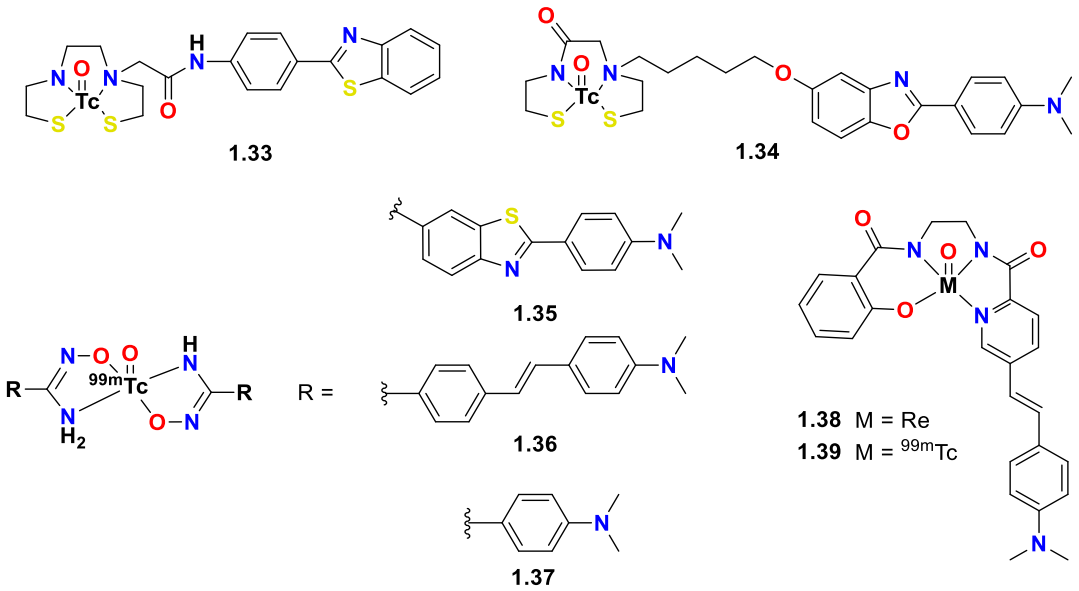

Figure 1.16. Examples of technetium-99m complexes of the MAMA ligand conjugated to a benzothiazole derivative **1.33** and the BAT ligand conjugated to a phenyl benzoxazole derivative **1.34**; ^{99m}Tc-Ham complexes coupled to amyloid binding moieties **1.35-1.37**; structure of ^{99m}Tc/Re-labelled styrylpyridyl **1.38** and **1.39**.

In a related study, a tetradentate N_3O ligand conjugated to styrylpyridyl was designed to form a charge neutral complex with oxorhenium(V) **1.38** and oxotechnetium(V) **1.39** (Figure 1.16).[89] Despite the low binding affinity of **1.38** to $A\beta_{1-42}$ fibrils (K_i = 855 nM), the complex showed clear localisation to the Aβ plaques of human brain tissue from a clinically diagnosed AD patient.

A series of bifunctional single amino acid chelate ligands (SAAC) that can be linked to small peptides for targeting specific receptors *in vivo* has been reported.[56,90-91] One of these chelators conjugated to the fMLF peptide **1.40** (which specifically binds to neutrophil receptors) was complexed with the $[Re(CO)_3]^+$ core (Figure 1.17).[90-91] The

affinity of this probe was evaluated by flow cytometry, and these studies showed that the Re(I) complex had a similar receptor affinity to the parent peptide.[90]

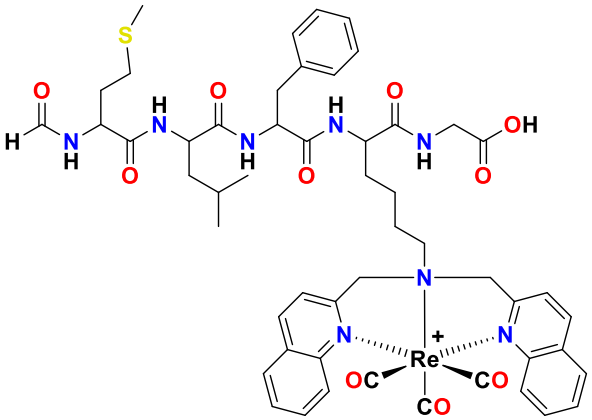

1.40

Figure 1.17. Structure of fMLF[Re(CO)$_3$]-SAACQ]G **1.40**.

To expand the scope of potential SPECT imaging agents for AD, Barnard *et al.* have designed a bifunctional macrocyclic *bis*(NHC)-amine ligand, allowing the attachment of biologically active groups such as the amyloid binding moieties benzothiazole **1.41** or stilbene **1.42** (Figure 1.18).[92] The [Re(CO)$_3$]$^+$ complexes of these ligands were synthesised using an Ag_2O transmetalation process, and the ability of these Re(I)-NHC complexes to bind to amyloid fibrils was assessed using a Thioflavin T (ThT) competitive assay. ThT is a cationic benzothiazole dye that has a high affinity for amyloid fibrils. Thus, it has been extensively used in various applications associated with assessing the capacity of molecules to bind to amyloid fibrils.[93] The fluorescence intensity of ThT in the presence of amyloid fibrils was significantly reduced upon the addition of complexes **1.41** and **1.42**, suggesting that these molecules competitively bind to amyloid fibrils.[92] Additionally, epi-fluorescence microscopy studies showed that **1.42** bound selectively to the amyloid plaques in the brain tissue from a patient diagnosed with Alzheimer's disease.[92]

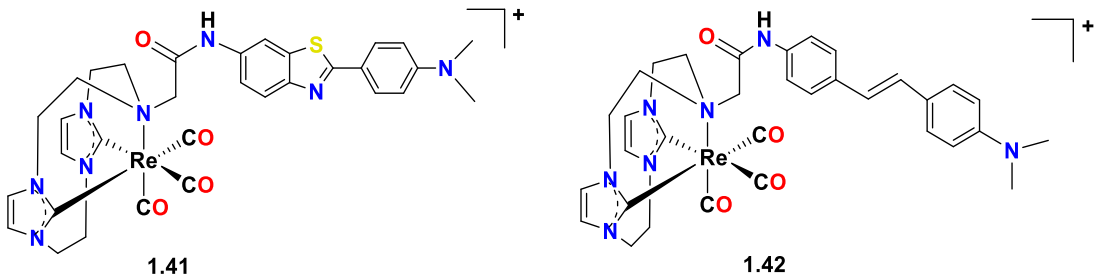

Figure 1.18. Structure of complexes **1.41** and **1.42**.

Cyclopentadienyl tricarbonyl complexes ([CpM(CO_3)], M = Re, ^{99m}Tc) provide an integrated approach to potential SPECT imaging agents for AD.[94] This class of complexes generally displays low molecular weight, neutral charge, good lipophilicity, and high stability, which favours their ability to cross the BBB.[94] A series of CpRe/Cp^{99m}Tc complexes coupled to 2-phenyl benzothiazole and pyridylbenzothiazoles via ester linkages have been reported (**1.43** and **1.44**, Figure 1.19).[94] *In vitro* autoradiography on Tg mice and AD patient brain sections indicated that complex **1.44** had a high binding affinity to Aβ plaques. However, these complexes showed moderate to low brain uptake (1.06%-0.54% ID/g at 2 min), suggesting that they have lower efficiency in penetrating the BBB compared to other ^{99m}Tc-labelled central nervous system probes.[94] The integrated approach was also explored by synthesising ^{99m}Tc complexes of 2-phenylbenzothiazole **1.45**, benzimidazole **1.47**, *N*-methylbenzimidazole **1.49** and their corresponding Re complexes **1.46**, **1.48**, **1.50** (Figure 1.19). *In vitro* competition binding assays indicated that **1.48** (K_i = 7.0 nM) and **1.50** (K_i = 5.7 nM) had strong affinity for Aβ aggregates and these are the lowest value reported for potential Aβ SPECT imaging agents bearing the [CpM(CO_3)] (M = Re, ^{99m}Tc) core. In addition, these [Cp^{99m}Tc(CO_3)] complexes displayed excellent brain uptake with the values ranging between 7.94-3.99% ID/g at 2 min in mice.

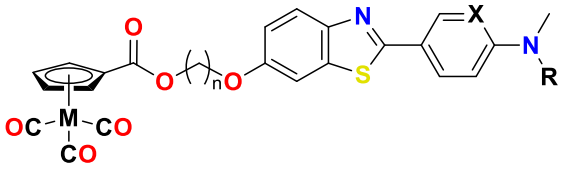

1.43 n = 5, R = CH_3, X = N, M = Re **1.44** n = 5, R = CH_3, X = N, M = ^{99m}Tc

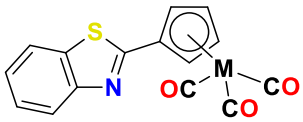

1.45 M = ^{99m}Tc
1.46 M = Re

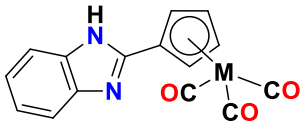

1.47 M = ^{99m}Tc
1.48 M = Re

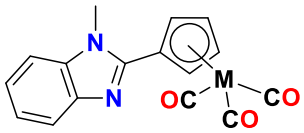

1.49 M = ^{99m}Tc
1.50 M = Re

Figure 1.19. Structures of 2-arylbenzothiazole derivatives of the [CpRe(CO_3)] core **1.43** and the [Cp^{99m}Tc(CO_3)] core **1.44**, and structures of Re/^{99m}Tc complexes substituted with 2-phenylbenzothiazole **1.45-1.46**, benzimidazole **1.47-1.48**, and *N*-methylbenzimidazole **1.49-1.50**.

1.3.2. Cancer

Cancer is one of the leading causes of death and continues to be a major concern in public health due to the high incidence of the disease and the high mortality rate.[95] Research over the past century has revealed that cancer is associated with genetic mutations, causing abnormal cells to proliferate into tumours.[96] These abnormal cells can escape from the original location via blood or lymph and repeat the same process in different organs (also called metastasis).[96]

There are over 200 different types of cancer that can occur in the human body.[97] It is now accepted that specific mutated genes are responsible for cancer.[97] For example, BRCA1 and BRCA2 are genes inherited in both males and females.[98] When one of these genes is mutated either as a result of genetics or DNA damage due to external carcinogens, it will lead to prostate cancer in males and breast cancer in females. Currently, prostate cancer is the most common cancer in males, while breast cancer is the most common for

females.[95] Since the pathogenesis of cancer occurs at the molecular level, precise diagnosis and optimal treatment are still a major challenge.

The techniques used for diagnosis differ depending on the type of cancer. For common cancers, for example, breast cancer, mammography screening at a certain age has become a widespread program.[99] In contrast, prostate cancer is diagnosed using prostate tissue obtained from a needle biopsy, and biomarker tests (e.g., prostate cancer antigen 3 test) are often used to avoid false-negative results.[100] Several types of cancer (e.g. pancreatic cancer) are often only detected at the invasive or metastasis stage, and detection at this late stage often leads to poor five-year survival rates for patients.[101] Molecular imaging is an alternative non-invasive technique that also provides reliable information on the cancer microenvironment.[102] However, accurate methods for the detection and diagnosis of several cancers are still limited, which drives the ongoing need for new molecular imaging agents in order to diagnose cancer in its early stage.[102-103]

The common cancer treatments are surgery, radiotherapy, chemotherapy, combination therapy and laser therapy.[104] The way cancer is treated depends on the stage at diagnosis and is based on the size and extension of the tumour, regional lymph node involvement, and the presence of distant metastases.[105] For example, the treatment for an early stage of cancer often involves surgery to remove the cancerous tumour, whereas chemotherapy is more common for the later stage of cancer.[105] Among anticancer agents used, platinum-based drugs including cisplatin, carboplatin, and oxaliplatin are frontline anticancer agents used in chemotherapy, but patients treated with these drugs commonly suffer from severe side-effects due to poor specificity and severe systemic toxicities.[106] Therefore, a new class of anticancer agents with less side effects is required for cancer treatment.

1.3.2.1. Platinum-Based Anticancer Agents

The platinum-based anticancer drug cisplatin **1.51** was discovered in the 1960s by Rosenberg,[107-108] and this compound gained approval for treating testicular and ovarian cancer in 1978 (Figure 1.20).[107]

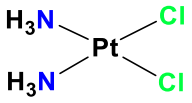

1.51

Figure 1.20. The first platinum-based anticancer agent is called *cis*-diamminedichloroplatinum(II) or cisplatin **1.51**.

Cisplatin is a neutral complex of platinum(II) with a square-planar geometry containing two *cis* amine and two *cis* chloride ligands (Figure 1.20).[109] The amine ligands are non-leaving groups as they remain bound to the platinum throughout the intracellular processes. Once cisplatin enters the cell, the chloride ligands are exchanged for water molecules producing a cationic aqua complex **1.53** (Figure 1.21).[110] Aquation occurs successively and the monaqua complex **1.52** is most important in binding to biomolecules (Figure 1.21).[110-111] However, experimental results suggest that cisplatin binds preferentially to DNA at the N7 atoms of guanosine and adenosine groups, which are exposed in the major groove of DNA.[110,112] The square-planar geometry of cisplatin facilitates the interaction between cisplatin and DNA, resulting in three types of adducts, including mono-adducts, intra-strand crosslinks, and inter-strand crosslinks. This DNA damage activates genes that are involved in transcription processes resulting in cell death.[112]

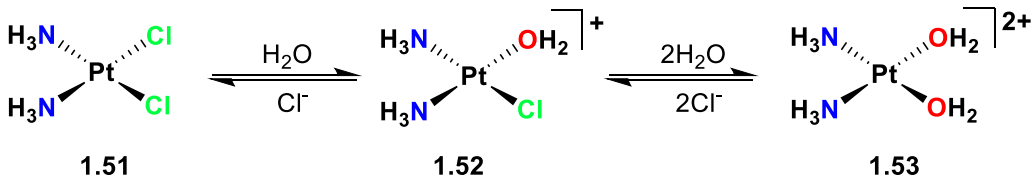

Figure 1.21. The exchange of the chloride ligands of cisplatin **1.51** for water molecules to give the monoaqua complex **1.52** and diaqua complex **1.53**.

Despite the success of cisplatin in cancer treatment, there are several disadvantages associated with this drug, including severe toxicities such as nephrotoxicity, neurotoxicity, ototoxicity and emetogenesis.[110,113] Additionally, the resistance of various cancers towards cisplatin often limits its efficacy.[114] The disadvantages of cisplatin provide a strong impetus for the development of new anticancer drugs with reduced toxicity, decreased side effects and higher efficacy.

Several platinum-based drugs have been approved for clinical use, including carboplatin **1.54** and oxaliplatin **1.55** (Figure 1.22).[110] Carboplatin **1.54** acts with a similar mechanism to cisplatin with reduced side effects, and it has become a commonly used treatment for ovarian and lung cancers.[112-113] Despite the reduced side effects, the problem of both intrinsic and acquired resistance still remains.[112] To overcome these limitations associated with carboplatin **1.54**, oxaliplatin **1.55** was developed and introduced as a treatment for colorectal cancer.[110] It has a similar mechanism of action to cisplatin and acts as an alkylating agent on DNA with the formation of intra-strand crosslink.[110,115] However, the bulkier side chain and increased hydrophobic property of oxaliplatin cause it to be more effective in inhibiting DNA synthesis, and this drug is more cytotoxic than cisplatin.[115,113,116-117] Recently, studies have shown that oxaliplatin can inhibit the function of ribosome biogenesis, in addition to inducing DNA damage, which is likely to be responsible for the increased cytotoxic of oxaliplatin compared to cisplatin.[118]

The fourth generation of anticancer agents, satraplatin (JM-216) **1.56**, is the first platinum-based drug that can be orally administrated, and this compound is currently undergoing phase III clinical trials for the treatment of prostate cancer (Figure 1.22).[110,112,119] Satraplatin is a Pt(IV) agent that has been shown to have a similar antitumor activity to cisplatin and carboplatin.[112] Furthermore, studies of satraplatin in selected cisplatin-resistant cell lines also showed that it has the potential to treat cisplatin-resistant tumours.[112,119]

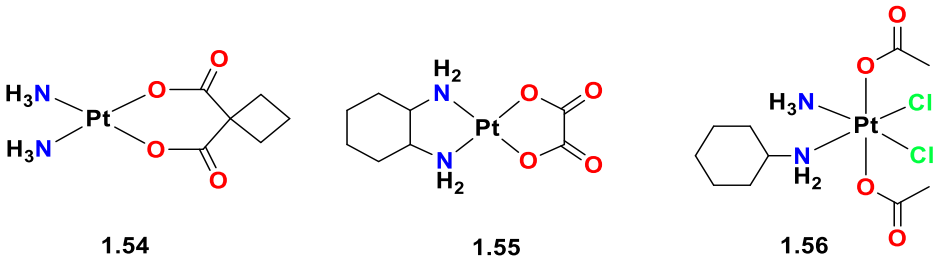

Figure 1.22. Structures of carboplatin **1.54**, oxaliplatin **1.55** and satraplatin **1.56**.

The sugar glucose is an important precursor for the generation of adenosine triphosphate (ATP) through the glycolysis pathway.[120] Glucose is transported through the hydrophobic cell membrane into the cytosol via glucose transporters (GLUTs).[120] In the early 1900s, Otto Warburg reported that cancer cells consumed high levels of glucose and produced lactate via the glycolytic pathway even under aerobic conditions, and cancer cells are known to express a higher level of GLUTs than normal cells. [165,121-122]

A significant amount of work has taken advantage of the increased requirement for glucose displayed by cancer cells to promote the active uptake of inorganic drug candidates.[123] A glucose conjugated platinum drug **1.57** has been prepared, and interestingly it exhibited high levels of cytotoxicity toward cancer cells (Figure 1.23).[124] The complex was designed by maintaining the *cis* arrangement of the amine donors in combination with a malonate ligand attached to the glucose molecule at the sixth position

of the ring. *In vitro* studies conducted on complex **1.57** showed that it has activity against cancer cells with low toxicity in healthy cells.[124] They also observed that increasing the linker length between glucose and Pt(II) metal centre reduced the ability of Pt-glucose complexes to enter the GLUT1 transporter. This event could be caused by the steric hindrance of longer linkers that blocked the GLUT1 transporter, thus reducing its ability to uptake Pt-glucose complexes.

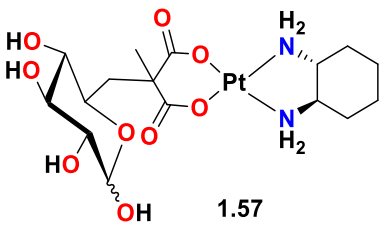

Figure 1.23. Structure of Pt anticancer drug glucose conjugate **1.57**.

1.3.2.2. Rhenium-Based Anticancer Agents

The limitation associated with platinum-based anticancer agents has stimulated studies into the use of alternative metals for anticancer applications,[125] and rhenium is one of the transition metals that has been recently explored for its anticancer properties. Several studies have been shown that complexes incorporating the $[Re(CO)_3]^+$ core are cytotoxic and may act via a similar mechanism of action to cisplatin. The first Re(I) nucleobase complex **1.58** was reported in 1995 (Figure 1.24)[126], and the X-ray crystal structure of **1.58** showed that the Re(I) metal centre was bound to the N7 position of the guanine unit, as is the case for cisplatin. The interaction of the *fac*-$[M(CO)_3]^+$ core (M = ^{99m}Tc, ^{188}Re) with several nucleotides including 9-methylguanine, guanosine and 2-deoxyguanosine has been investigated, and in this study, the technetium and rhenium complexes **1.59** bound to two guanine ligands (Figure 1.24) were reported.[127] No evidence of Re(I) coordinating to carbonyl oxygen, ribose or direct binding to the amine ($-NH_2$) was observed. These results also suggested that steric hindrance associated with the sugar

group prevented binding of the Re(I) complex to position N3 of the guanine ring.[127] NMR studies showed that the rate constant for the Re(I) complex binding to the N7 position of guanine was similar in magnitude to cisplatin, indicating the potential of $[Re(CO)_3]^+$ complexes for the development of chemotherapeutic agents.[127-128]

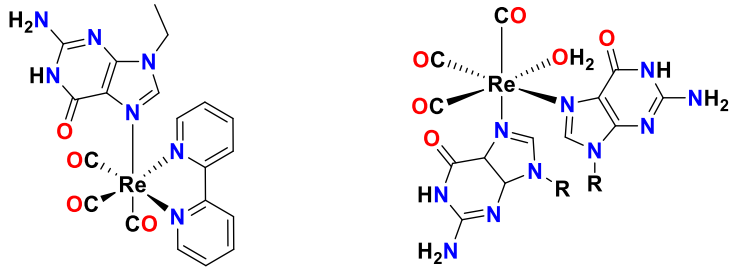

1.58 1.59

Figure 1.24. Structures of the Re(I) complexes **1.58** and **1.59**.

In the development of new Re(I)-based anticancer drugs, the labile aqua ligands of $[Re(H_2O)_3(CO)_3]^+$ were replaced by more strongly bound amino acid ligands. Amino acids were chosen for this purpose as they can form stable complexes, are naturally occurring and can be recycled via biochemical pathways, hence decreasing toxic side effects.[129] Complex **1.60** (Figure 1.25) represents the first macrocyclic trimers of Re atoms coupled to amino acid ligands.[129] Analysis using HPLC-MS and X-ray crystallography showed that the trimer **1.60** reacted with 9-methylguanine to form mononuclear Re(I) bound to 9-methylguanine **1.61**.[128-129] Interestingly, studies using plasmid DNA in gel mobility shift assays showed that the *N*,*N*-dimethylglycine could be replaced by the guanine.[129] These studies also suggested that the Re(I) complexes were less potent than cisplatin, but they can be used as lead structures for further metal complexes design.[129]

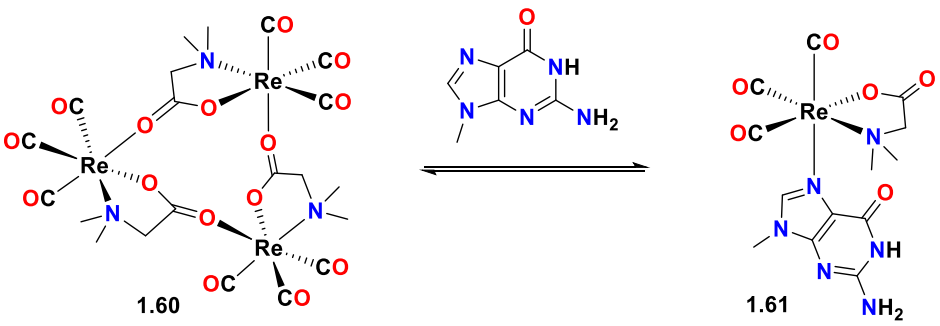

Figure 1.25. The interaction of the macrocyclic trimer Re(I)-*N*,*N*-dimethylglycine **1.60** with guanine, forming Re(I) guanine complex **1.61**.

One of the advantages of Re(I) complexes over cisplatin is the rich spectroscopic properties observed for these compounds, which provides opportunities for cell imaging and microscopy studies. The luminescence often observed for complexes of the $[Re(CO)_3]^+$ core allows them to be used in fluorescent microscopy cell imaging studies and the unique stretching frequencies of carbonyl moieties enable imaging by vibrational spectroscopy.[130-131] Cell imaging can provide insights into drug distribution in cancer cells, which is useful during preclinical drug development and to monitor the drug uptake, biodistribution and toxicity.[132] Therefore, a series of Re(I) complexes of polypyridyl ligands (**1.62-1.65**, Figure 1.26) was prepared, and the confocal fluorescence microscopy studies of these complexes in HeLa cells showed that complex **1.64** was localised throughout the cytosol.[133] As Re is the congener of Tc, similar chemistry between these two metals allows the use of ^{99m}Tc analogues of these rhenium compounds as diagnostic tools for luminescence-based biodistribution studies.[130-132] *In vivo* biodistribution studies of the ^{99m}Tc analogue of **1.64** indicated that this compound has reliable biodistribution profiles with hepatic and renal excretion.[133] Additionally, the anticancer properties of these complexes were evaluated against ovarian and lung cancer cell lines, and also the cisplatin-resistant cervical cancer cell lines KB3-1 and KBCP20.[128] These studies showed that complex **1.64** was the most potent compound out of seven evaluated.[128]

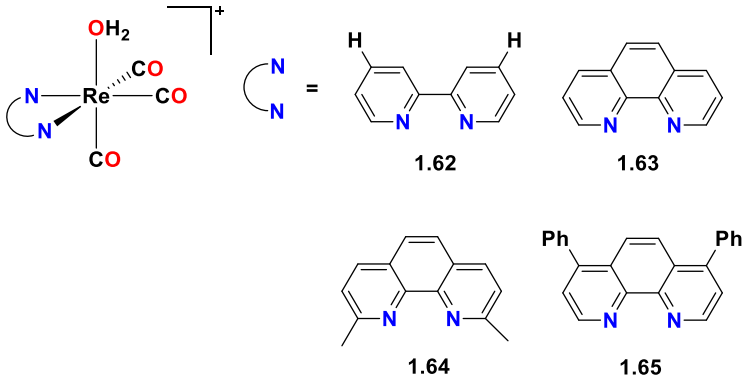

Figure 1.26. Structure of $[Re(CO)_3H_2O]^+$ complexes with four different polypyridyl ligands **1.62-1.65**.

Acquired resistance to chemotherapeutic drugs is one of the major problems in cancer therapy.[134] Therefore, a greater understanding of the pathways leading to resistance can significantly benefit the development of anticancer drugs. The anticancer properties of complex **1.66** were evaluated in ovarian cancer, and it was found to be active by inducing ER stress resulting in cell apoptosis, which is a different pathway from that of platinum-based drugs.[134] In recent research, the cell line (A2780TR), resistant to **1.66**, was developed from the ovarian cancer cell line A2780 cells[135]. A series of Re(I) polypyridyl complexes (**1.67** and **1.68**, Figure 1.27) in combination with several known anticancer drugs such as cisplatin, oxaliplatin and taxol were studied in the A2780TR cell line. These results suggested that the mechanism by which A2780TR cells become resistant towards **1.66** and taxol is similar, and minor structural modification could overcome the rhenium-based anticancer agents' resistance problem.[135] Further gene analysis showed that the ATP-binding cassette transporter P-glycoprotein (an efflux transporter responsible for detoxifying taxol) was overexpressed in A2780TR cells.[135] In addition, ovarian cancer cells resistance mechanism towards rhenium-based anticancer drugs is different from conventional platinum-based anticancer drugs, suggesting that Re(I) anticancer drugs may have the potential to treat platinum-resistant ovarian cancer.

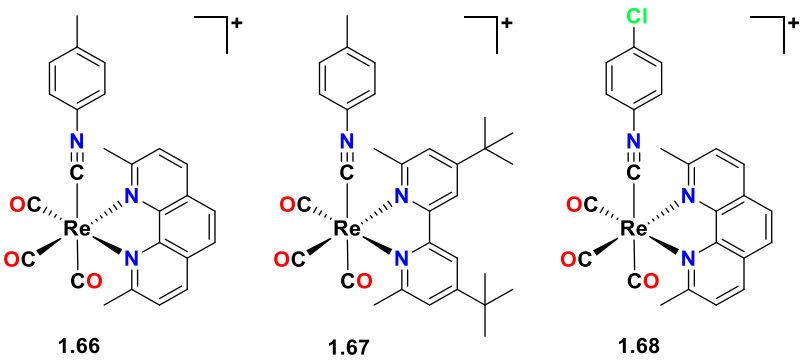

Figure 1.27. Structures of $[Re(CO)_3]^+$ isonitrile polypyridyl complex **1.66**, metylphenyl isonitrile *tert*-butyl bipyridine complex **1.67** and the *para*-chlorophenyl isonitrile polypyridyl complex **1.68**.

The anticancer properties of two $[Re(CO)_3]^+$ complexes with β-carboline ligands (**1.69** and **1.70**, Figure 1.28) were evaluated.[136] *In vitro* studies on these compounds showed that they were highly cytotoxic against human lung carcinoma cells A549 while less active against non-cancerous human lung fibroblasts (HLF).[136] The mechanism of action of **1.69** was further explored, and it was found that this compound can induce autophagy by destroying lysosomal enzymatic activity. This compound is the first example of a Re(I) complex association with autophagy induction.[136] Additionally, *in vivo* studies of **1.69** in mice bearing A549 tumours showed that this compound could inhibit tumour cell proliferation.

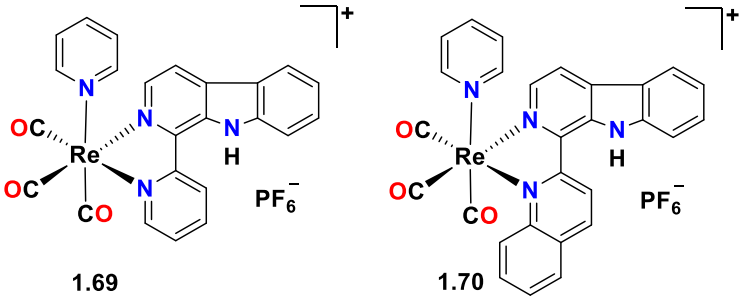

Figure 1.28. Structures of Re(I) complexes of two β-carboline ligands **1.69** and **1.70**.

The first Re(I) complexes of NHC ligands with anticancer properties were reported by Massi *et al.* in 2017.[106] A range of Re(I)-NHC complexes were synthesised and evaluated, including **1.71** and **1.72**, where the NHC ligand is conjugated to indomethacin **1.72**, a non-steroidal anti-inflammatory derivative (Figure 1.29).[106] The cytotoxicity of both complexes was studied in human pancreatic cancer cell lines, including HPAF-II, ASPC1, and CFPAC and healthy human embryonic kidney 293T cells (HEK293T).[106] Interestingly, both complexes were found to inhibit pancreatic cancer cell proliferation at concentrations below 10 µM, but they were less cytotoxic towards the HEK293T cells, suggesting that they have some selectivity towards pancreatic cancer cells. Further cell cycle analysis and the use of three-dimensional soft agar colony formation assays indicated that the mechanism of action for **1.71** was inhibition of the phosphorylation of Aurora-A kinase, an enzyme overexpressed in pancreatic cancer cells. In addition, the structure-activity relationship (SAR) demonstrated that the labile ancillary ligand of complexes **1.71** and **1.72** was responsible for their anticancer properties.[106]

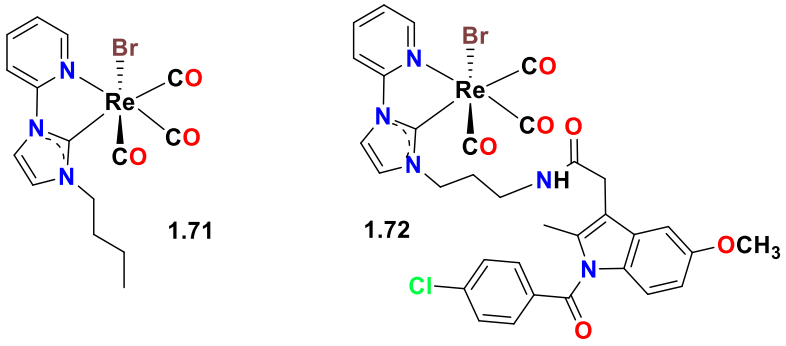

Figure 1.29. Structures of Re(I) *N*-heterocyclic carbene complexes **1.71** and **1.72**.

As mentioned in the previous section, it is well known that tumour cells exhibit high levels of glucose uptake, and the transporter proteins GLUTs provide a promising pathway to target cancer cells for therapeutic purposes.[120-122] A series of Re(I) complexes coupled to carbohydrates were synthesised as the potential anticancer agents.[137-139] *N*-functionalised glucosamine coupled to salicylaldehyde was bound to the Re(I) precursor

yielding complex **1.73** (Figure 1.30). The ligand was also radiolabelled with ^{99m}Tc **1.74** and ^{186}Re **1.75**, and the stability of complex **1.74** was further analysed using cysteine/histidine challenge experiments. Unfortunately, the complex **1.74** displayed only moderate stability in the cysteine and histidine challenges, with decomposition occurring within four hours.[137] In an effort to improve the stability of the Re(I) complex, the ligand structure was modified to a tridentate ligand with a *bis*-pyridine amine core.[138] The ligand was used to prepare complex **1.76**, and the corresponding ^{99m}Tc **1.77** and ^{186}Re **1.78** complexes were also synthesised (Figure 1.30). The stability of complex **1.77** was again evaluated in cysteine/histidine challenge experiments, and as expected, the tridentate ligand formed a stable complex with ^{99m}Tc and resisted ligand exchange processes for 24 hours.[138] Similar compounds have been reported for carbohydrate-pyridinone ligands coupled to Re, ^{99m}Tc and ^{186}Re (**1.79-1.93**, Figure 1.30). The stability of radiolabelled compounds with ^{99m}Tc was evaluated using cysteine and histidine challenge experiments, and at 24 hours, some decomposition was observed due to the displacement of the ligands by the metal-binding amino acids.[139]

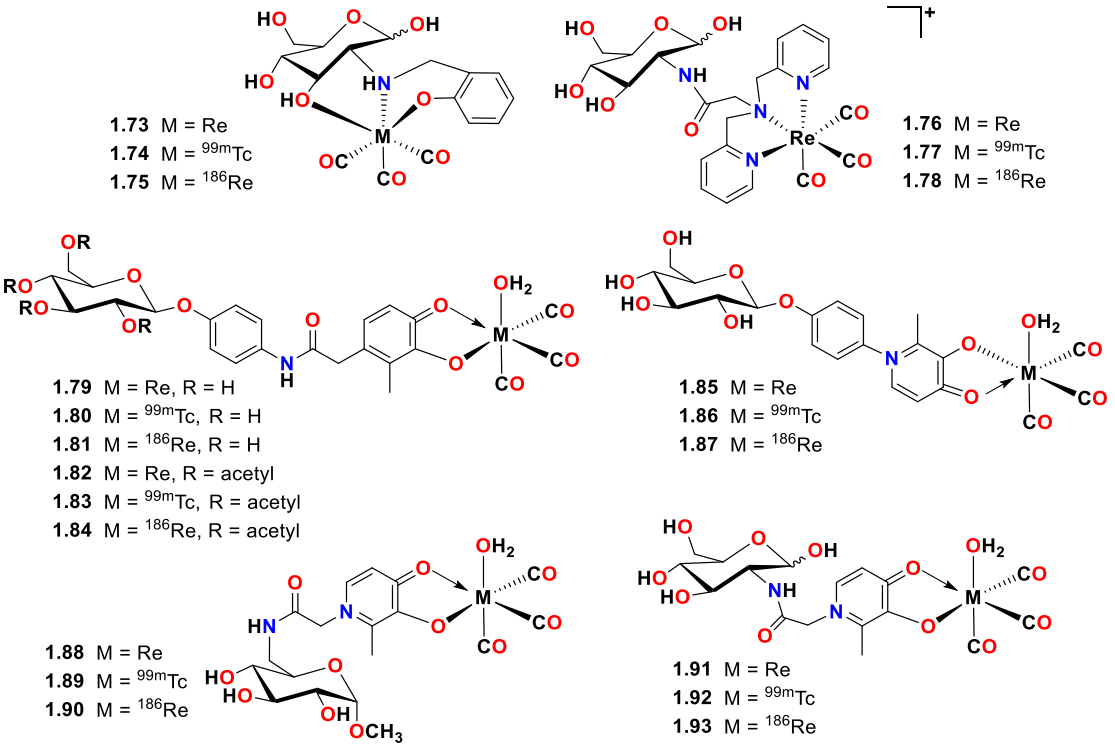

Figure 1.30. Structures of a series of Re and Tc complexes of ligands coupled to carbohydrates, Re(I) **1.73**, ^{99m}Tc **1.74** and ^{186}Re **1.75**; Re(I) **1.76**, ^{99m}Tc **1.77** and ^{186}Re **1.78**; Re(I), ^{99m}Tc and ^{186}Re complexes with carbohydrate pyridinone ligands **1.79-1.93**.

The synthesis of a series of neutral dinuclear Re(I) glycoconjugates **1.94-1.99** (Figure 1.31) as bio-conjugated luminophores were reported. These complexes were studied as bio-imaging dyes in living HeLa cells, and the results showed that they have high cell permeability, organelle selectivity and low cytotoxicity.[140] The same group also reported dinuclear Re(I) complex coupled to three equivalents of glucose **1.97**, mannose **1.98** and galactose **1.99** (Figure 1.31).[141] In the presence of sodium dodecyl sulfate (SDS), a membrane-mimicking agent, the luminescence emission of these compounds was significantly enhanced. Additionally, the studies of complexes **1.97-1.99** with lectins demonstrated the ability of these compounds to interact with lectins, hence suggesting the possibility for their use as lectin sensors.

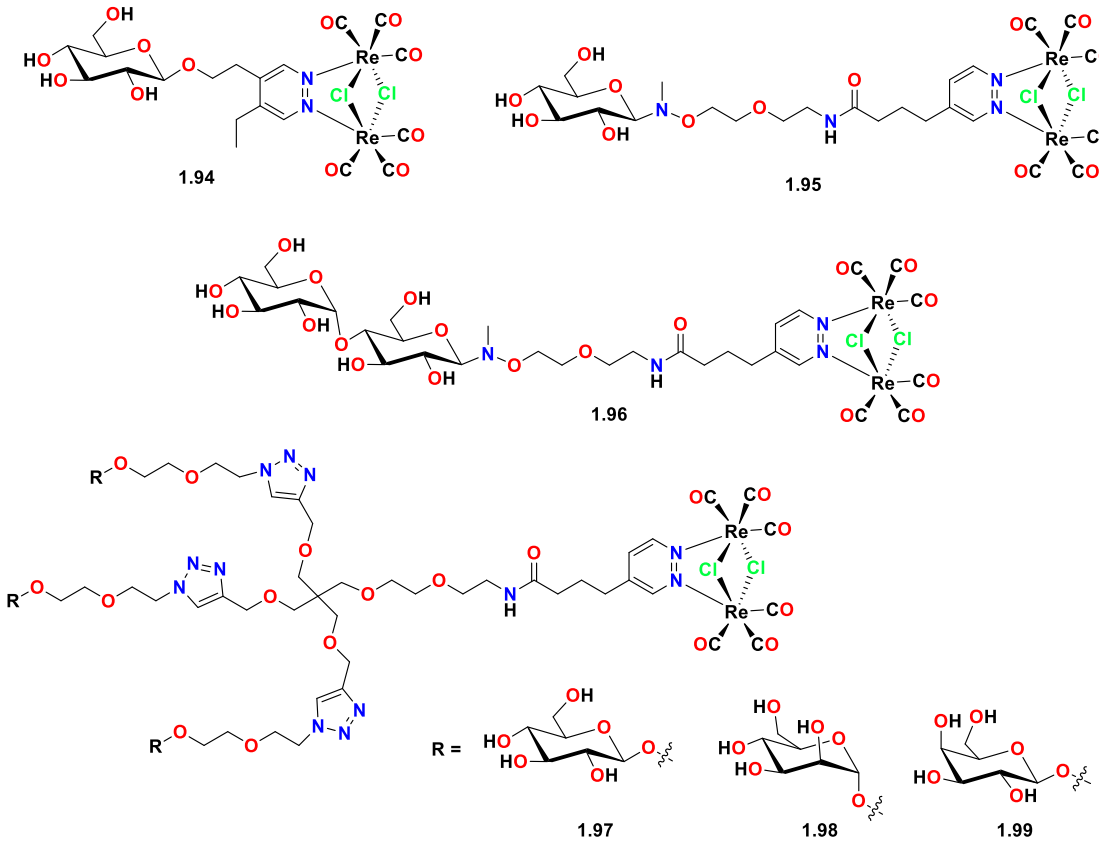

Figure 1.31. Structures of multivalent rhenium complex glycoconjugates **1.94-1.96**, β-D-glycopyranosidic **1.97**, α-D-mannopyranosidic **1.98** or β-D-galactopyranosidic **1.99**.

1.4. Thesis Overview

Despite the excellent σ-donating properties and stable complexes formed by NHC ligands, very few examples of Re(I)-NHC complexes have been reported for molecular imaging and therapeutic applications. Therefore, there is a need to expand the scope of Re(I) complexes of NHC ligands due to their attractive photoluminescent properties and their potential for the development of radiopharmaceutical agents.[33] This thesis reports the preparation and evaluation of Re(I) complexes of NHC ligands as analogues of potential ^{99m}Tc molecular imaging probes for Alzheimer's disease and the potential rhenium-based anticancer agents.

In chapter 2, the synthesis and studies of two charge neutral Re(I) complexes of tridentate NHC ligands bearing imidazolylidene, amine and carboxylate donor groups coupled to amyloid binding moieties (stilbene or benzothiazole) are reported. Both Re(I) complexes were prepared as analogues of potential ^{99m}Tc imaging agents. The capacity of these Re(I) complexes to bind to amyloid fibrils was evaluated using the ThT fluorescence assay. Additionally, the interaction between the prepared Re(I) complexes and amyloid plaques in brain tissues from clinically diagnosed Alzheimer's disease patients was evaluated.

Chapter 3 reports a series of Re(I) complexes of *bis*-imidazolium and pyridyl-imidazolium ligands coordinating to an *N*-acetyl amino acid glycine, isoleucine and proline that have been designed and synthesised as potential anticancer drugs. Anticancer Re(I) complexes have been previously shown to have a similar mechanism of action to cisplatin. Therefore, the aquation of the synthesised complexes, where the labile amino acid ligand is replaced by water in an aqueous solution, was evaluated using ^{1}H NMR studies. In addition, the cytotoxic properties of these Re(I) complexes were evaluated in both the cancer cells and primary cell lines.

Chapter 4 reports a series of studies designed to expand the research field of Re(I) complexes of NHC ligands as anticancer agents, a series of dinuclear Re(I) complexes of *bis*-imidazolium and pyridyl-imidazolium ligands featuring either alkyl or diamide linkage were synthesised. The aquation rate of two selected Re(I) complexes was estimated using ^{1}H NMR studies, and the photophysical properties of these dinuclear Re(I) complexes were also evaluated. The second part of chapter 4 investigated the synthetic strategy for Re(I) complexes of pyridyl-imidazolium ligands bearing benzyl or acetyl protected glucose ligand.

Chapter 5 provides an overall conclusion to the studies conducted in this thesis and potential future work.

1.5. References

1. Liu, S.; Edwards, D. S., *Chem. Rev.* **1999,** *99* (9), 2235-2268.
2. Bhattacharyya, S.; Dixit, M., *Dalton Trans.* **2011,** *40* (23), 6112-6128.
3. Liu, S., *Chem. Soc. Rev.* **2004,** *33* (7), 445-461.
4. Orsini, F.; Guidoccio, F.; Mariani, G., In *Nuclear Medicine Textbook: Methodology and Clinical Applications*, Volterrani, D.; Erba, P. A.; Carrió, I.; Strauss, H. W.; Mariani, G., Eds. Springer International Publishing: Cham, 2019; pp 99-116.
5. Vermeulen, K.; Vandamme, M.; Bormans, G.; Cleeren, F., *Semin. Nucl. Med.* **2019,** *49* (5), 339-356.
6. Martini, P.; Pasquali, M.; Boschi, A.; Uccelli, L.; Giganti, M.; Duatti, A., *Molecules* **2018,** *23* (8), 2039.
7. Feng, Y.; Phelps, T. E.; Carroll, V.; Gallazzi, F.; Sieckman, G.; Hoffman, T. J.; Barnes, C. L.; Ketring, A. R.; Hennkens, H. M.; Jurisson, S. S., *Dalton Trans.* **2017,** *46* (42), 14677-14690.
8. Wang, X.; Cui, M.; Yu, P.; Li, Z.; Yang, Y.; Jia, H.; Liu, B., *Bioorg. Med. Chem. Lett.* **2012,** *22* (13), 4327-31.
9. Biswal, B. K.; Cherney, M. M.; Wang, M.; Garen, C.; James, M. N. G., *Acta Crystallogr. D: Struct. Biol.* **2005,** *61* (11), 1492-1499.
10. Kung, M.-P.; Hou, C.; Zhuang, Z.-P.; Skovronsky, D.; Kung, H. F., *Brain Res.* **2004,** *1025* (1–2), 98-105.
11. Pimlott, S. L.; Sutherland, A., *Chem. Soc. Rev.* **2011,** *40* (1), 149-162.
12. Johnson, K. A.; Mueller, S. T.; Walshe, T. M.; English, R. J.; Holman, B. L., *Arch. Neurol.* **1987,** *44* (2), 165-168.
13. Johnson, K. A.; Holman, B. L.; Rosen, T. J.; Nagel, J. S.; English, R. J.; Growdon, J. H., *Arch. Intern. Med.* **1990,** *150* (4), 752-756.
14. Bajaj, N.; Hauser, R. A.; Grachev, I. D., *J. Neurol. Neurosurg. Psychiatr.* **2013,** *84* (11), 1288-1295.
15. Catafau, A. M.; Tolosa, E., *Mov. Disord.* **2004,** *19* (10), 1175-1182.
16. Djang, D. S. W.; Janssen, M. J. R.; Bohnen, N.; Booij, J.; Henderson, T. A.; Herholz, K.; Minoshima, S.; Rowe, C. C.; Sabri, O.; Seibyl, J.; Van Berckel, B. N. M.; Wanner, M., *J. Nucl. Med.* **2012,** *53* (1), 154-163.
17. Bartholomä, M. D.; Louie, A. S.; Valliant, J. F.; Zubieta, J., *Chem. Rev.* **2010,** *110* (5), 2903-2920.

18. Rathmann, S. M.; Ahmad, Z.; Slikboer, S.; Bilton, H. A.; Snider, D. P.; Valliant, J. F., In *Radiopharmaceutical Chemistry*, Lewis, J. S.; Windhorst, A. D.; Zeglis, B. M., Eds. Springer International Publishing: Cham, 2019; pp 311-333.

19. Papagiannopoulou, D., *J. Labelled Comp. Radiopharm.* **2017,** *60* (11), 502-520.

20. Costa, B.; Ilem-Özdemir, D.; Santos-Oliveira, R., *J. Coord. Chem.* **2019,** *72* (11), 1759-1784.

21. Mindt, T.; Struthers, H.; Garcia-Garayoa, E.; Desbouis, D.; Schibli, R., *Chimia.* **2007,** *61* (11), 725-731.

22. Ehrlich, D. J.; Walker, R. H., *J. Mov. Disord.* **2017,** *4* (1), 8.

23. Jürgens, S.; Herrmann, W. A.; Kühn, F. E., *J. Organomet. Chem.* **2014,** *751*, 83-89.

24. Yeh, R.; Miloushev, V. Z.; Ichise, M., In *Handbook of Neuro-Oncology Neuroimaging (Second Edition)*, Newton, H. B., Ed. Academic Press: San Diego, 2016; pp 359-370.

25. Dunzinger, A.; Hafner, F.; Schaffler, G.; Piswanger-Soelkner, J.-C.; Brodmann, M.; Lipp, R. W., *Eur. J. Nucl. Med. Mol. Imaging* **2008,** *35* (11), 2082-2087.

26. Taillefer, R.; Edell, S.; Innes, G.; Lister-James, J., *J. Nucl. Med.* **2000,** *41* (7), 1214-1223.

27. Lepareur, N.; Lacœuille, F.; Bouvry, C.; Hindré, F.; Garcion, E.; Chérel, M.; Noiret, N.; Garin, E.; Knapp, F. F. R., *Front. Med.* **2019,** *6* (132).

28. R. Dilworth, J.; J. Parrott, S., *Chem. Soc. Rev.* **1998,** *27* (1), 43-55.

29. F. F.(Russ) Knapp, J., *Cancer Biother. Radiopharm.* **2009,** *13* (5), 337-349.

30. Argyrou, M.; Valassi, A.; Andreou, M.; Lyra, M., *ISRN Mol. Imaging* **2013,** *2013*, 124603.

31. Moustapha, M. E.; Ehrhardt, G. J.; Smith, C. J.; Szajek, L. P.; Eckelman, W. C.; Jurisson, S. S., *Nucl. Med. Biol.* **2006,** *33* (1), 81-89.

32. Kuninobu, Y.; Takai, K., *Chem. Rev.* **2011,** *111* (3), 1938-1953.

33. Hille, C.; Kuhn, F. E., *Dalton Trans.* **2016,** *45* (1), 15-31.

34. Ali, S. K. I.; Khandaker, M. U.; Kassim, H. A., *Appl. Radiat. Isot.* **2018,** *135*, 239-250.

35. Maxon Iii, H. R.; Thomas, S. R.; Hertzberg, V. S.; Schroder, L. E.; Englaro, E. E.; Samaratunga, R.; Scher, H. I.; Moulton, J. S.; Deutsch, E. A.; Deutsch, K. F.; Schneider, H. J.; Williams, C. C.; Ehrhardt, G. J., *Semin. Nucl. Med.* **1992,** *22* (1), 33-40.

36. Lam, M. G. E. H.; De Klerk, J. M. H.; Van Rijk, P. P., *Eur. J. Nucl. Med. Mol. Imaging* **2004,** *31* (SUPPL. 1), S162-S170.

37. Hahn, F. E.; Jahnke, M. C., *Angew. Chem. Int. Ed. Engl.* **2008,** *47* (17), 3122-3172.

38. Kühl, O., *Chem. Soc. Rev.* **2007,** *36* (4), 592-607.

39. Hopkinson, M. N.; Richter, C.; Schedler, M.; Glorius, F., *Nature* **2014,** *510* (7506), 485-496.

40. Arduengo, A. J.; Harlow, R. L.; Kline, M., *J. Am. Chem. Soc.* **1991,** *113* (1), 361-363.

41. Hindi, K. M.; Panzner, M. J.; Tessier, C. A.; Cannon, C. L.; Youngs, W. J., *Chem. Rev.* **2009,** *109* (8), 3859-3884.

42. Marion, N.; Díez-González, S.; Nolan, S. P., *Angew. Chem. Int. Ed. Engl.* **2007,** *46* (17), 2988-3000.

43. Peris, E.; Crabtree, R. H., *Coord. Chem. Rev.* **2004,** *248* (21), 2239-2246.

44. Clavier, H.; Coutable, L.; Guillemin, J.-C.; Mauduit, M., *Tetrahedron Asymmetry* **2005,** *16* (5), 921-924.

45. Siemeling, U.; Memczak, H.; Bruhn, C.; Vogel, F.; Trager, F.; Baio, J. E.; Weidner, T., *Dalton Trans.* **2012,** *41* (10), 2986-94.

46. Chen, J.; Huang, Y., *Nat. Commun.* **2014,** *5*, 3437.

47. Herrmann, W. A., *Angew. Chem. Int. Ed. Engl.* **2002,** *41* (8), 1290-1309.

48. Wanzlick, H.-W.; Schönherr, H.-J., *Angew. Chem. Int. Ed. Engl.* **1968,** *7* (2), 141-142.

49. Öfele, K., *J. Organomet. Chem.* **1968,** *12* (3), P42-P43.

50. Quezada, C. A.; Garrison, J. C.; Panzner, M. J.; Tessier, C. A.; Youngs, W. J., *Organomet.* **2004,** *23* (21), 4846-4848.

51. Garrison, J. C.; Tessier, C. A.; Youngs, W. J., *J. Organomet. Chem.* **2005,** *690* (24–25), 6008-6020.

52. Oehlke, E.; Kong, S.; Arciszewski, P.; Wiebalck, S.; Abram, U., *J. Am. Chem. Soc.* **2012,** *134* (22), 9118-9121.

53. Wagner, T.; Zeglis, B. M.; Groveman, S.; Hille, C.; Pöthig, A.; Francesconi, L. C.; Herrmann, W. A.; Kühn, F. E.; Reiner, T., *J. Labelled Comp. Radiopharm.* **2014,** *57* (7), 441-447.

54. Braband, H.; Zahn, T. I.; Abram, U., *Inorg. Chem.* **2003,** *42* (20), 6160-6162.

55. Alberto, R., *J. Organomet. Chem.* **2007,** *692* (6), 1179-1186.

56. Bartholoma, M.; Valliant, J.; Maresca, K. P.; Babich, J.; Zubieta, J., *ChemComm.* **2009,** (5), 493-512.

57. Chan, C. Y.; Pellegrini, P. A.; Greguric, I.; Barnard, P. J., *Inorg. Chem.* **2014,** *53* (20), 10862-10873.

58. Brookmeyer, R.; Johnson, E.; Ziegler-Graham, K.; Arrighi, H. M., *Alzheimers Dement.* **2007,** *3* (3), 186-191.

59. Almeida, O. P., *Neuroradiol. J.* **2006,** *19* (4), 433-440.

60. Burgess, N.; Maguire, E. A.; O'Keefe, J., *Neuron* **2002,** *35* (4), 625-641.

61. Hayne, D. J.; Lim, S.; Donnelly, P. S., *Chem. Soc. Rev.* **2014,** *43* (19), 6701-6715.

62. Cappai, R.; White, A. R., *Int. J. Biochem.* **1999,** *31* (9), 885-889.

63. Villemagne, V. L.; Rowe, C. C., *Int. Psychogeriatr.* **2011,** *23* (SupplementS2), S41-S49.

64. McKhann, G.; Drachman, D.; Folstein, M.; Katzman, R.; Price, D.; Stadlan, E. M., *Neurology* **1984,** *34* (7), 939-44.

65. McKhann, G. M.; Knopman, D. S.; Chertkow, H.; Hyman, B. T.; Jack Jr, C. R.; Kawas, C. H.; Klunk, W. E.; Koroshetz, W. J.; Manly, J. J.; Mayeux, R.; Mohs, R. C.; Morris, J. C.; Rossor, M. N.; Scheltens, P.; Carrillo, M. C.; Thies, B.; Weintraub, S.; Phelps, C. H., *Alzheimers Dement.* **2011,** *7* (3), 263-269.

66. Ono, M.; Saji, H., *Int. J. Mol. Sci.* **2011,** *2011*, 543267.

67. Zhen, W.; Han, H.; Anguiano, M.; Lemere, C. A.; Cho, C. G.; Lansbury, P. T., Jr., *J. Med. Chem.* **1999,** *42* (15), 2805-15.

68. Klunk, W. E.; Engler, H.; Nordberg, A.; Wang, Y.; Blomqvist, G.; Holt, D. P.; Bergström, M.; Savitcheva, I.; Huang, G.-F.; Estrada, S.; Ausén, B.; Debnath, M. L.; Barletta, J.; Price, J. C.; Sandell, J.; Lopresti, B. J.; Wall, A.; Koivisto, P.; Antoni, G.; Mathis, C. A.; Långström, B., *Ann. Neurol.* **2004,** *55* (3), 306-319.

69. Klunk, W. E.; Wang, Y.; Huang, G.-f.; Debnath, M. L.; Holt, D. P.; Mathis, C. A., *Life Sci.* **2001,** *69* (13), 1471-1484.

70. Klunk, W. E.; Bacskai, B. J.; Mathis, C. A.; Kajdasz, S. T.; McLellan, M. E.; Frosch, M. P.; Debnath, M. L.; Holt, D. P.; Wang, Y.; Hyman, B. T., *J. Neuropathol.* **2002,** *61* (9), 797-805.

71. Li, Q.; Min, J.; Ahn, Y. H.; Namm, J.; Kim, E. M.; Lui, R.; Kim, H. Y.; Ji, Y.; Wu, H.; Wisniewski, T.; Chang, Y. T., *Chembiochem.* **2007,** *8* (14), 1679-87.

72. Serdons, K.; Terwinghe, C.; Vermaelen, P.; Van Laere, K.; Kung, H.; Mortelmans, L.; Bormans, G.; Verbruggen, A., *J. Med. Chem.* **2009,** *52* (5), 1428-1437.

73. Zhang, W.; Oya, S.; Kung, M.-P.; Hou, C.; Maier, D. L.; Kung, H. F., *Nucl. Med. Biol.* **2005,** *32* (8), 799-809.

74. Zhang, W.; Oya, S.; Kung, M.-P.; Hou, C.; Maier, D. L.; Kung, H. F., *J. Med. Chem.* **2005,** *48* (19), 5980-5988.

75. Adlard, P. A.; Tran, B. A.; Finkelstein, D. I.; Desmond, P. M.; Johnston, L. A.; Bush, A. I.; Egan, G. F., *Front. Neurosci.* **2014,** *8*, 327.

76. Skeby, K. K.; Sorensen, J.; Schiott, B., *J. Am. Chem. Soc.* **2013,** *135* (40), 15114-28.

77. Chen, K.; Cui, M., *MedChemComm* **2017,** *8* (7), 1393-1407.

78. Zha, Z.; Song, J.; Choi, S. R.; Wu, Z.; Ploessl, K.; Smith, M.; Kung, H., *Bioconjugate Chem.* **2016,** *27* (5), 1314-1323.

79. Donnelly, P. S.; Liddell, J. R.; Lim, S.; Paterson, B. M.; Cater, M. A.; Savva, M. S.; Mot, A. I.; James, J. L.; Trounce, I. A.; White, A. R.; Crouch, P. J., *Proc. Natl. Acad. Sci. U.S.A.* **2012,** *109* (1), 47-52.

80. Tsuchiya, J.; Yoneyama, T.; Ohtake, M.; Tateishi, K.; Bae, H.; Kishino, M.; Tateishi, U., *Nucl. Med. Commun.* **2020,** *41* (6), 567-574.

81. Noor, A.; Hayne, D. J.; Lim, S.; Van Zuylekom, J. K.; Cullinane, C.; Roselt, P. D.; McLean, C. A.; White, J. M.; Donnelly, P. S., *Inorg. Chem.* **2020,** *59* (16), 11658-11669.

82. Serdons, K.; Verduyckt, T.; Cleynhens, J.; Terwinghe, C.; Mortelmans, L.; Bormans, G.; Verbruggen, A., *Bioorg. Med. Chem. Lett.* **2007,** *17* (22), 6086-6090.

83. Ono, M.; Ikeoka, R.; Watanabe, H.; Kimura, H.; Fuchigami, T.; Haratake, M.; Saji, H.; Nakayama, M., *ACS Chem. Neurosci.* **2010,** *1* (9), 598-607.

84. Ono, M.; Ikeoka, R.; Watanabe, H.; Kimura, H.; Fuchigami, T.; Haratake, M.; Saji, H.; Nakayama, M., *Bioorg. Med. Chem. Lett.* **2010,** *20* (19), 5743-8.

85. Hausner, S. H.; Alagille, D.; Koren, A. O.; Amici, L.; Staley, J. K.; Cosgrove, K. P.; Baldwin, R. M.; Tamagnan, G. D., *Bioorg. Med. Chem. Lett.* **2009,** *19* (2), 543-5.

86. Yang, Y.; Cui, M.; Jin, B.; Wang, X.; Li, Z.; Yu, P.; Jia, J.; Fu, H.; Jia, H.; Liu, B., *Eur. J. Med. Chem.* **2013,** *64*, 90-8.

87. Iikuni, S.; Ono, M.; Watanabe, H.; Matsumura, K.; Yoshimura, M.; Harada, N.; Kimura, H.; Nakayama, M.; Saji, H., *Mol. Pharm.* **2014,** *11* (4), 1132-1139.

88. Iikuni, S.; Ono, M.; Watanabe, H.; Matsumura, K.; Yoshimura, M.; Kimura, H.; Ishibashi-Ueda, H.; Okamoto, Y.; Ihara, M.; Saji, H., *Sci. Rep.* **2016,** *6* (1), 25990.

89. Hayne, D. J.; White, J. M.; McLean, C. A.; Villemagne, V. L.; Barnham, K. J.; Donnelly, P. S., *Inorg. Chem.* **2016,** *55* (16), 7944-7953.

90. Stephenson, K. A.; Banerjee, S. R.; Besanger, T.; Sogbein, O. O.; Levadala, M. K.; McFarlane, N.; Lemon, J. A.; Boreham, D. R.; Maresca, K. P.; Brennan, J. D.; Babich, J. W.; Zubieta, J.; Valliant, J. F., *J. Am. Chem. Soc.* **2004,** *126* (28), 8598-8599.

91. Wei, L.; Babich, J. W.; Ouellette, W.; Zubieta, J., *Inorg. Chem.* **2006,** *45* (7), 3057-3066.

92. Chan, C. Y. La Trobe University, 2016.

93. Khurana, R.; Coleman, C.; Ionescu-Zanetti, C.; Carter, S. A.; Krishna, V.; Grover, R. K.; Roy, R.; Singh, S., *J. Struct. Biol.* **2005,** *151* (3), 229-238.

94. Jia, J.; Zhou, K.; Dai, J.; Liu, B.; Cui, M., *Eur. J. Med. Chem.* **2016,** *124*, 763-772.

95. Siegel, R. L.; Miller, K. D.; Jemal, A., *CA-Cancer J. Clin.* **2017,** *67* (1), 7-30.

96. Hanahan, D.; Weinberg, R. A., *Cell* **2000,** *100* (1), 57-70.

97. Hassanpour, S. H.; Dehghani, M., *J. Cancer Res. Pract.* **2017,** *4* (4), 127-129.

98. Fong , P. C.; Boss , D. S.; Yap , T. A.; Tutt , A.; Wu , P.; Mergui-Roelvink , M.; Mortimer , P.; Swaisland , H.; Lau , A.; O'Connor , M. J.; Ashworth , A.; Carmichael , J.; Kaye , S. B.; Schellens , J. H. M.; de Bono , J. S., *N. Engl. J. Med.* **2009,** *361* (2), 123-134.

99. Waks, A. G.; Winer, E. P., *JAMA* **2019,** *321* (3), 288-300.

100. Litwin, M. S.; Tan, H.-J., *JAMA* **2017,** *317* (24), 2532-2542.

101. McGuigan, A.; Kelly, P.; Turkington, R. C.; Jones, C.; Coleman, H. G.; McCain, R. S., *World J. Gastroenterol.* **2018,** *24* (43), 4846-4861.

102. Seaman, M. E.; Contino, G.; Bardeesy, N.; Kelly, K. A., *Expert Rev. Mol. Med.* **2010,** *12*, e20-e20.

103. Monteiro, L. O. F.; Fernandes, R. S.; Castro, L. C.; Cardoso, V. N.; Oliveira, M. C.; Townsend, D. M.; Ferretti, A.; Rubello, D.; Leite, E. A.; de Barros, A. L. B., *Biomed. Pharmacother.* **2017,** *89*, 146-151.

104. Mansoori, B.; Mohammadi, A.; Davudian, S.; Shirjang, S.; Baradaran, B., *Adv. Pharm. Bull.* **2017,** *7* (3), 339-348.

105. Miller, K. D.; Siegel, R. L.; Lin, C. C.; Mariotto, A. B.; Kramer, J. L.; Rowland, J. H.; Stein, K. D.; Alteri, R.; Jemal, A., *CA-Cancer J. Clin.* **2016,** *66* (4), 271-289.

106. Simpson, P. V.; Casari, I.; Paternoster, S.; Skelton, B. W.; Falasca, M.; Massi, M., *Chem. Eur. J.* **2017,** *23* (27), 6518-6521.

107. Wong, E.; Giandomenico, C. M., *Chem. Rev.* **1999,** *99* (9), 2451-2466.

108. Rosenberg, B.; Van Camp, L.; Grimley, E. B.; Thomson, A. J., *J. Biol. Chem.* **1967,** *242* (6), 1347-52.

109. Johnstone, T. C.; Suntharalingam, K.; Lippard, S. J., *Chem. Rev.* **2016,** *116* (5), 3436-3486.

110. Rabik, C. A.; Dolan, M. E., *Cancer Treat.* **2007,** *33* (1), 9-23.

111. Davies, M. S.; Berners-Price, S. J.; Hambley, T. W., *Inorg. Chem.* **2000,** *39* (25), 5603-5613.

112. Ho, Y. P.; Au-Yeung, S. C. F.; To, K. K. W., *Med. Res. Rev.* **2003,** *23* (5), 633-655.

113. McWhinney, S. R.; Goldberg, R. M.; McLeod, H. L., *Mol. Cancer Ther.* **2009,** *8* (1), 10-6.

114. Wang, X.; Guo, Z., *Chem. Soc. Rev.* **2013,** *42* (1), 202-224.

115. Misset, J. L.; Bleiberg, H.; Sutherland, W.; Bekradda, M.; Cvitkovic, E., *Crit. Rev. Oncol. Hematol.* **2000,** *35* (2), 75-93.

116. Cavaletti, G.; Tredici, G.; Petruccioli, M. G.; Donde, E.; Tredici, P.; Marmiroli, P.; Minoia, C.; Ronchi, A.; Bayssas, M.; Etienne, G. G., *Eur. J. Cancer Care (Engl)* **2001,** *37* (18), 2457-63.

117. Krishnan, A. V.; Goldstein, D.; Friedlander, M.; Kiernan, M. C., *Muscle Nerve* **2005,** *32* (1), 51-60.

118. Bruno, P. M.; Liu, Y.; Park, G. Y.; Murai, J.; Koch, C. E.; Eisen, T. J.; Pritchard, J. R.; Pommier, Y.; Lippard, S. J.; Hemann, M. T., *Nat. Med.* **2017,** *23* (4), 461-471.

119. Yamano, Y.; Shiiba, M.; Negoro, K.; Nakatani, K.; Kasamatsu, A.; Yamatoji, M.; Sakuma, K.; Ogoshi, K.; Iyoda, M.; Shinozuka, K.; Yokoe, H.; Wada, T.; Fujita, S.; Iwasawa, S.; Takiguchi, Y.; Tanzawa, H.; Uzawa, K., *Head Neck* **2011,** *33* (3), 309-17.

120. Adekola, K.; Rosen, S. T.; Shanmugam, M., *Curr. Opin. Oncol.* **2012,** *24* (6), 650-654.

121. Ancey, P.-B.; Contat, C.; Meylan, E., *FEBS J.* **2018,** *285* (16), 2926-2943.

122. Barbosa, A. M.; Martel, F., *Cancers* **2020,** *12* (1), 154.

123. Mikata, Y., In *Encyclopedia of Inorganic and Bioinorganic Chemistry*, pp 1-19.

124. Patra, M.; Johnstone, T. C.; Suntharalingam, K.; Lippard, S. J., *Angew. Chem. Int. Ed. Engl.* **2016,** *55* (7), 2550-2554.

125. Ott, I.; Gust, R., *Arch. Pharm.* **2007,** *340* (3), 117-126.

126. Oriskovich, T. A.; White, P. S.; Thorp, H. H., *Inorg. Chem.* **1995,** *34* (7), 1629-1631.

127. Zobi, F.; Spingler, B.; Fox, T.; Alberto, R., *Inorg. Chem.* **2003,** *42* (9), 2818-2820.

128. Zobi, F.; Blacque, O.; Sigel, R. K. O.; Alberto, R., *Inorg. Chem.* **2007,** *46* (25), 10458-10460.

129. Zobi, F.; Spingler, B.; Alberto, R., *Chembiochem.* **2005,** *6* (8), 1397-1405.

130. Lo, K. K.-W., *Acc. Chem. Res* **2015,** *48* (12), 2985-2995.

131. Clède, S.; Policar, C., *Chem. Eur. J.* **2015,** *21* (3), 942-958.

132. Cheff, D. M.; Hall, M. D., *J. Med. Chem.* **2017,** *60* (11), 4517-4532.

133. Knopf, K. M.; Murphy, B. L.; MacMillan, S. N.; Baskin, J. M.; Barr, M. P.; Boros, E.; Wilson, J. J., *J. Am. Chem. Soc.* **2017,** *139* (40), 14302-14314.

134. King, A. P.; Marker, S. C.; Swanda, R. V.; Woods, J. J.; Qian, S.-B.; Wilson, J. J., *Chem. Eur. J.* **2019,** *25* (39), 9206-9210.

135. Marker, S. C.; King, A. P.; Swanda, R. V.; Vaughn, B.; Boros, E.; Qian, S.-B.; Wilson, J. J., *Angew. Chem. Int. Ed. Engl.* **2020,** *59* (32), 13391-13400.

136. He, L.; Pan, Z.-Y.; Qin, W.-W.; Li, Y.; Tan, C.-P.; Mao, Z.-W., *Dalton Trans.* **2019,** *48* (13), 4398-4404.

137. Bayly, S. R.; Fisher, C. L.; Storr, T.; Adam, M. J.; Orvig, C., *Bioconjugate Chem.* **2004,** *15* (4), 923-926.

138. Storr, T.; Fisher, C. L.; Mikata, Y.; Yano, S.; Adam, M. J.; Orvig, C., *Dalton Trans.* **2005,** (4), 654-655.

139. Ferreira, C. L.; Bayly, S. R.; Green, D. E.; Storr, T.; Barta, C. A.; Steele, J.; Adam, M. J.; Orvig, C., *Bioconjugate Chem.* **2006,** *17* (5), 1321-1329.

140. Palmioli, A.; Aliprandi, A.; Septiadi, D.; Mauro, M.; Bernardi, A.; De Cola, L.; Panigati, M., *Org. Biomol. Chem.* **2017,** *15* (7), 1686-1699.

141. Palmioli, A.; Panigati, M.; Bernardi, A., *Org. Biomol. Chem.* **2018,** *16* (37), 8413-8419.

Chapter 2 : Charge Neutral Rhenium Tricarbonyl Complexes of Tridentate *N*-Heterocyclic Carbene Ligands that Bind to Amyloid Plaques of Alzheimer's Disease

2.1. Introduction

The work in this chapter was published in 2020.[1a] Alzheimer's disease (AD) is a progressive neurodegenerative disease characterised by severe memory loss and disturbances in cognitive and behavioural functions.[2] The pathological mechanism of AD remains unknown, however the formation of insoluble plaques in the brain composed of the amyloid-β peptide are believed to play an important role in the progression of this disease.[3] Therefore, evaluation and quantification of the amyloid-β plaque load using targeted radiopharmaceutical diagnostic agents offer the potential for the early diagnosis of AD.[4]

Positron emission tomography (PET) and single photon emission computed tomography (SPECT) are the two most common nuclear imaging techniques that use radioactive tracers to diagnose diseases.[5] These techniques allow for the non-invasive visualisation of disease progression at various levels ranging from molecular to whole organ.[6] PET radiotracers require positron emitting radionuclides such as ^{11}C ($t_{1/2}$ = 20.3 mins) and ^{18}F ($t_{1/2}$ = 109.8 mins), whereas SPECT radiotracers require gamma emitting radionuclides such as ^{99m}Tc ($t_{1/2}$ = 6.06 hours) and ^{123}I ($t_{1/2}$ = 13.2 hours).[7-8] Even though SPECT has a lower sensitivity and resolution compared to PET, it is widely available in many hospitals and for the commonly used isotope ^{99m}Tc there is no requirement for an onsite cyclotron.[9-

[a] N. Wiratpruk (65%) was responsible for preparing the manuscript, synthesised and characterised the compounds in addition to completing the logP and photophysical studies. A. Noor (10%) and P. S. Donnelly (5%) carried out the biological studies (ThT assay and Epi-fluorescence microscopy studies). C. A. McLean (5%) provided the clinically diagnosed Alzheimer's disease patient's brain tissue. P. J. Barnard (15%) has carried out the X-ray crystallography and editing the manuscript.

[10] Therefore, the development of SPECT radiotracers labelled with ^{99m}Tc for the diagnosis AD offers the potential for an easily accessible and affordable nuclear medicine technique for the early detection of this disease.[11-13]

Metal complexes of *N*-heterocyclic carbene (NHC) ligands have been extensively studied for a range of applications, including as homogeneous chemical catalysts,[14] luminescent and electroluminescent materials[15] and as potential medicinal agents.[16] Despite their outstanding properties as ligands, less work has been directed towards the use of NHCs for the development of diagnostic imaging agents based on metallic radionuclide. The Barnard group is interested in the preparation of new NHC ligands for radiopharmaceutical applications and previously the same group has reported the first example of labelling an NHC ligand with the ^{99m}Tc (in the form of $[^{99m}Tc(CO)_3]^+$).[17] As part of this research, the chemistry of the $[Re(CO)_3]^+$ core with bidentate and tridentate NHC ligands has been studied.[17-18] Che and co-workers reported early examples of Re(I) complexes of NHC ligands e.g. **2.1**,[19] while more recently, Re(I) complexes with bidentate pyridyl-, quinolinyl- and pyrimidyl-functionalized NHC ligands e.g. **2.2**, and **2.3** and **2.4** have been described (Figure 2.1).[20-21]

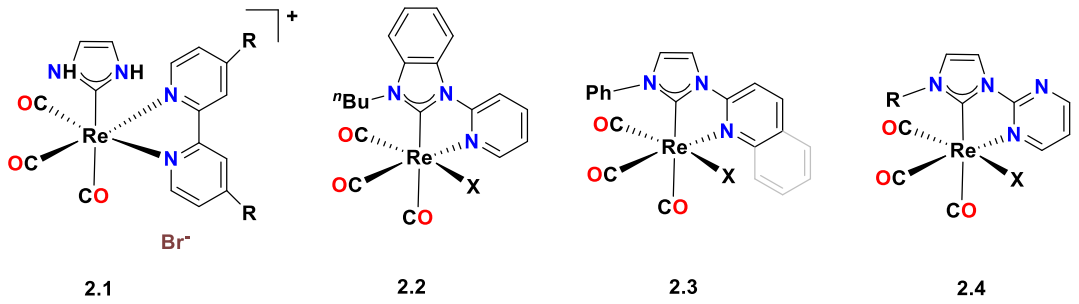

Figure 2.1. Examples of $Re(CO)_3$ complexes with *N*-heterocyclic carbene ligands.

Previously Barnard group reported a series of Re(I) complexes of bifunctional *bis*(NHC)-amine ligands coupled to benzothiazole- **1.41** and stilbene-based **1.42** amyloid binding moieties (Figure 2.2).[22] These complexes were highly stable in ligand challenge

experiments with histidine and cysteine and bound to amyloid fibrils composed of the amyloid-β peptide. In addition, epi-fluorescence microscopy studies showed that **1.42** bound selectively to amyloid plaques in human Alzheimer's disease brain tissue.[22] Despite these promising results, complexes of this type are unlikely to be useful for radiopharmaceutical applications as the cationic charge associated with complex **1.42** is likely to impede its passage through the blood brain barrier.[23]

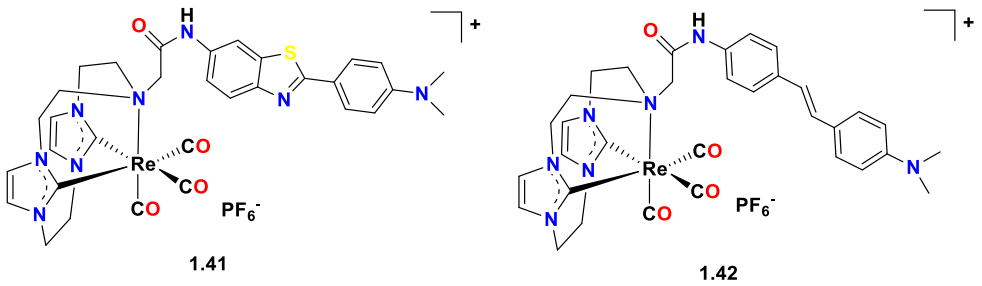

Figure 2.2. Structures of Re complexes of cyclic *bis*(NHC)-amine ligands coupled to benzothiazole- **1.41** and (b) stilbene-based **1.42** amyloid binding moieties.

In an effort to improve the potential application of *N*-heterocyclic carbene ligand of the $[Re(CO)_3]^+/[Tc(CO)_3]^+$ core for radiopharmaceutical applications, this chapter reports the synthesis of a new series of tridentate ligands that combine a NHC unit with amine and carboxylate donors to produce neutral complexes with the $[M(CO)_3]^+$ core. These ligands have been coupled to benzothiazole- and stilbene-based amyloid binding moieties and the capacity of the Re(I) complexes to bind to amyloid fibrils and amyloid plaques in human frontal cortex brain tissue are evaluated.

2.2. Results and Discussion

2.2.1. Ligand Synthesis

A key goal of this work was the development of bifunctional tridentate *N*-heterocyclic carbene pro-ligands that would form neutral complexes of the $[Re(CO)_3]^+$ core. To this end, the closely related pro-ligands **2.11** (Scheme 2.1) and **2.14** (Scheme 2.3) were prepared. The synthetic pathway for the formation of pro-ligand **2.11** began with the reductive amination of benzaldehyde with ethanolamine using sodium borohydride ($NaBH_4$) to produce **2.5** (Scheme 2.1). Compound **2.5** was then *N*-alkylated with *t*-butyl bromoacetate to form **2.6** followed by removal of the amine benzyl-protecting group via catalytic hydrogenolysis, yielding compound **2.7**. The deprotected secondary amine of **2.7** was then *N*-alkylated with benzyl bromoacetate to form **2.8**, thereby introducing orthogonal *t*-butyl ester and benzyl ester carboxylic acid protecting groups. The orthogonal protecting groups were introduced to allow selective deprotection using either trifluroacetic acid (TFA) or via catalytic hydrogenolysis. The primary alcohol unit of **2.8** was then converted to an alkyl bromide using triphenylphosphine and *N*-bromosuccinimide to produce compound **2.9** and the alkylation of 1-methylimidazole with **2.9** produced the imidazolium salt **2.10** (Scheme 2.1). Removal of the *t*-butyl ester group of **2.10** with TFA yielded compound **2.11** with a free carboxylic acid group. Difficulties were encountered in the purification of **2.11** as the bromide salt and to overcome this issue, a metathesis reaction was performed to convert the bromide anion to hexaflorophosphate. Thus, **2.11** was isolated in its pure form as the hexaflorophosphate salt, which displayed appropriate solubility in organic solvents for the coupling reaction (amide bond formation) to introduce the amyloid binding moiety.

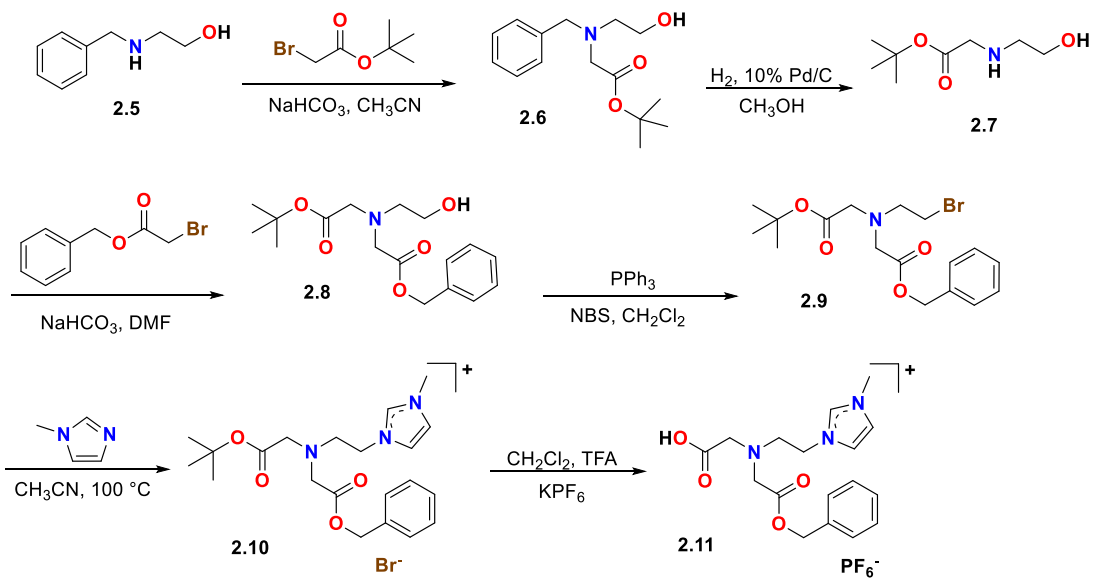

Scheme 2.1. Synthesis of pro-ligand **2.11** using the orthogonal protecting group strategy.

The coupling reagent PyBop ((benzotriazol-1-yloxy)tripyrrolidinophosphonium hexafluorophosphate) was used to couple the carboxylic acid group of the pro-ligand **2.11** and the amine unit of the amyloid binding moiety 6-amino-2-(4-*N*,*N*-dimethylaminophenyl)benzothiazole (Scheme 2.2). PyBop was chosen for this reaction as the by-product phosphonium salt could be readily removed from the product **2.12**, by washing with diethyl ether and the final ligand **2.13** was obtained as a bright yellow solid after catalytic hydrogenolysis to remove the benzyl ester protecting group (Scheme 2.2).

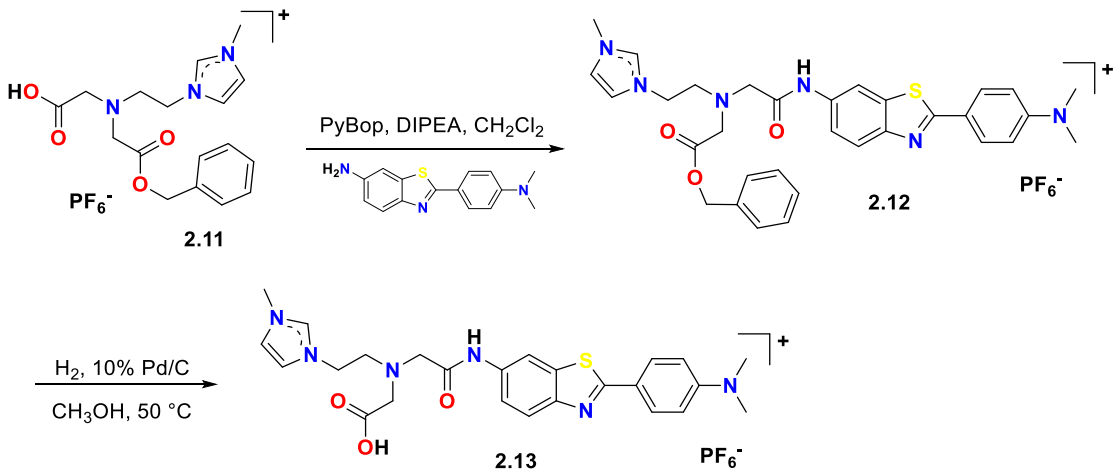

Scheme 2.2. Synthetic scheme for the formation of **2.13**.

In the case of pro-ligand **2.16**, coupled to the stilbene-based amyloid binding moiety 4-amino-4'-(*N*,*N*-dimethylamino)stilbene (Scheme 2.3), catalytic hydrogenolysis was not suitable for unmasking the final carboxylic acid group due to the potential for simultaneous reduction of the alkene group of the stilbene unit. Therefore, the benzyl ester protecting group of **2.10** was first deprotected via catalytic hydrogenolysis to generate **2.14** and the formed carboxylic acid group was then coupled to 4-amino-4'-(*N*,*N*-dimethylamino)stilbene using PyBop yielding **2.15** (Scheme 2.3). The *t*-butyl ester group was then removed in the final step using TFA, producing pro-ligand **2.16**.

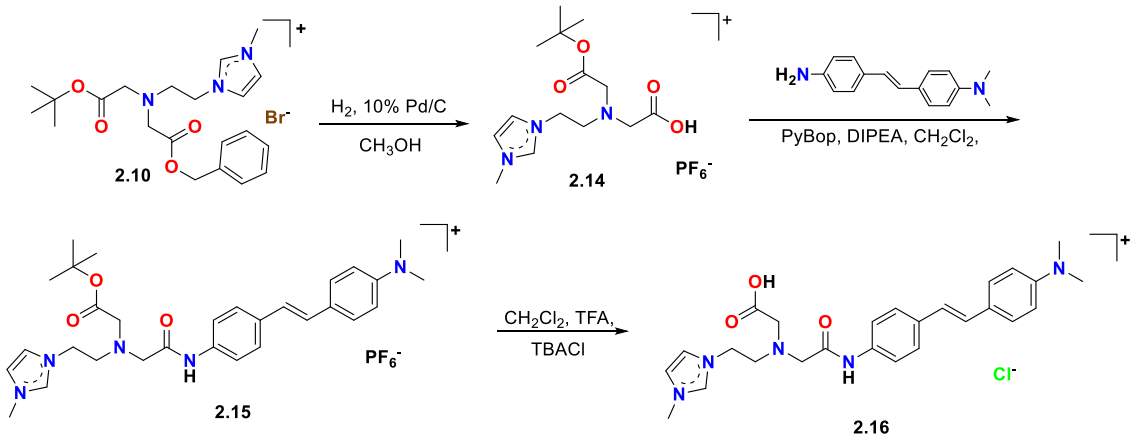

Scheme 2.3. Synthetic pathway for the formation of the stilbene derivative **2.16**.

2.2.2. Rhenium Complex Synthesis

A silver transmetalation protocol was utilised for the synthesis of rhenium tricarbonyl complexes **2.17** and **2.18** from ligands **2.13** and **2.16** respectively (Scheme 2.4). The silver transmetalation methodology utilising Ag_2O has been commonly employed for the formation of metal complexes of NHC ligands from precursor imidazolium salts,[24-25] and the Barnard group has previously described the synthesis of a range of NHC complexes of the $[Re(CO)_3]^+$ core using this approach.[17-18,22] In the present work, complex **2.17** was prepared by stirring a suspension of **2.13** and Ag_2O in acetonitrile for 24 h to allow the Ag-NHC complex to form and then $Re(CO)_5Cl$ was added and the reaction mixture was

stirred for a further 24 h at 60 °C. After completion of the reaction, the desired complex was purified by column chromatography on alumina and complex **2.17** was obtained as an orange solid (Scheme 2.4).

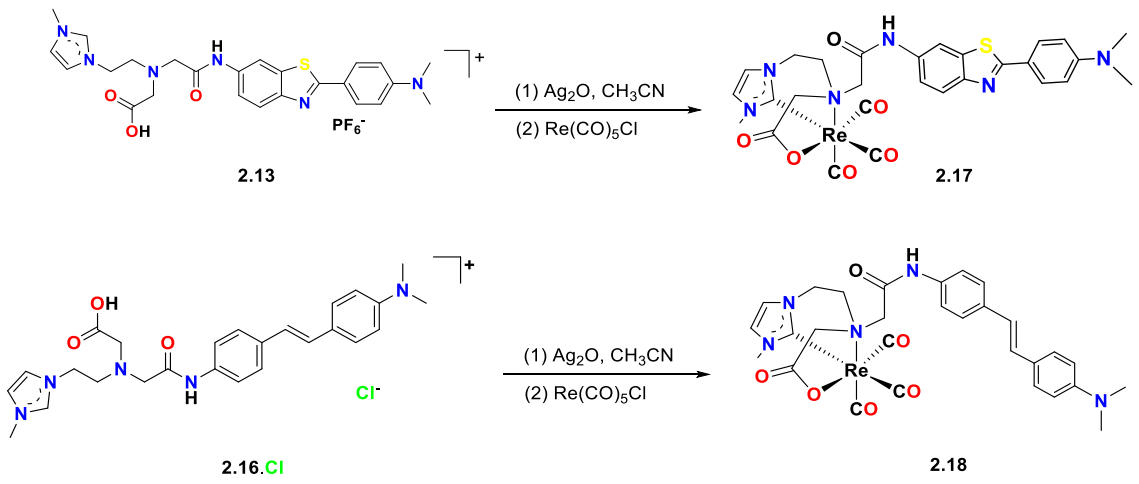

Scheme 2.4. Synthetic pathway for the formation of the Re complexes **2.17** and **2.18**.

For the synthesis of the Re complex of pro-ligand **2.16**, the same procedure as that described for the preparation of **2.18** was initially investigated, however the desired compound could not be isolated under these conditions, possibly due to slow formation of the intermediate Ag complex. To facilitate formation of the Ag complex, a metathesis reaction was used to exchange the counterion of **2.16** from hexafluorophosphate to chloride yielding compound **2.16**·Cl which allowed for the successful synthesis of the desired Re complex **2.18** (Scheme 2.4).

As expected, no signals corresponding to the carboxylic acid or the imidazolium C2 protons of the pro-ligands were apparent in the ^{1}H NMR spectra of complexes **2.17** and **2.18**, indicating that these groups are deprotonated and coordinated to the Re metal centre. The amide N-H signals resonate as downfield shifted singlets at 10.5 ppm and 10.3 ppm for **2.17** and **2.18**, respectively (Figures A2.17 and A2.18, Appendix 2). The ^{1}H NMR spectrum for **2.17** is shown in Figure 2.3. As the facially coordinated tridentate ligands

have three different donor groups (amine, carboxylate, and carbene) the Re metal is a chiral centre for complexes **2.17** and **2.18**, and the non-superimposable mirror image forms of core structure for these complexes are shown in Figure 2.4. As a result of this chirality, the methylene protons of the acetamide linker group (shown in red on Figure 2.3) are diastereotopic and resonate as an AB pattern (highlighted in red in Figure 2.3). The ^{13}C NMR spectra of complexes **2.17** and **2.18** show the expected number of peaks for the respective complexes (Figures A2.17 and A2.18, Appendix 2). For each complex, three individual signals corresponding to the carbonyl ligands are evident in the region of 198-196 ppm consistent with this group being *trans* to the three different donor groups of the tridentate ligand.

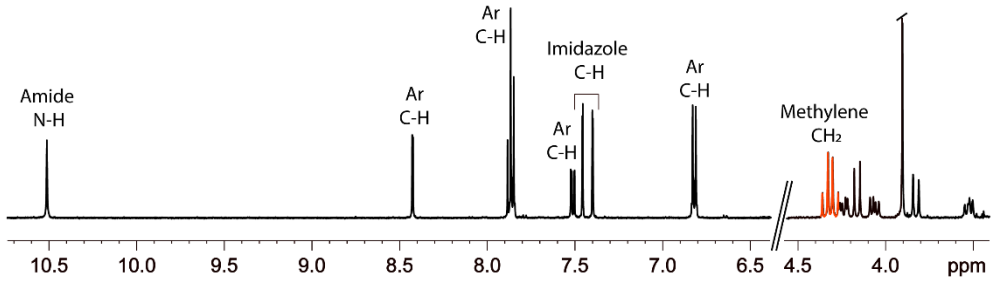

Figure 2.3. ^{1}H NMR spectrum of complex **2.17** (DMSO-d_6) The signal corresponding to the methylene group protons of the acetamide linker is highlighted in red.

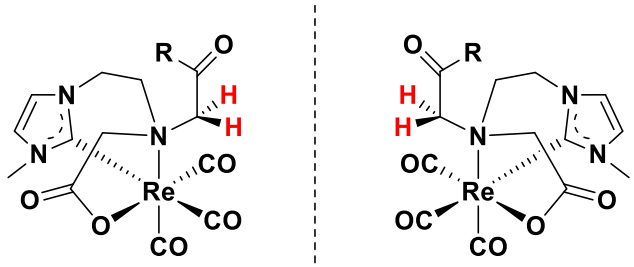

Figure 2.4. Diagram showing the non-superimposable forms of the chiral complexes **2.17** and **2.18** (R = amyloid binding moiety).

To explore the influence of the different donor groups of the tridentate ligand on the carbonyl ligands, the solid-state IR spectra for complexes **2.17** and **2.18** (Figures A2.19 and A2.20, Appendix 2) were recorded. In each case, strong and distinct CO stretching signals were observed at 2017 cm^{-1} and 2015 cm^{-1}, while broad (apparently overlapping as a result of solid-state effects[26-28]) signals were observed at 1890 cm^{-1} and 1886 cm^{-1} for complexes **2.17** and **2.18**. These results are consistent with the expected three individual signals for each of the carbonyl ligands which are either *trans* to the amine, carboxylate or carbene donor groups. It is well known that the strong σ-donor properties of NHCs causes the signal for carbonyl ligand *trans* to these groups to be shifted to higher wavenumbers and as such the signals observed at 2017 cm^{-1} and 2015 cm^{-1} for **2.17** and **2.18**, respectively can be assigned to the carbonyl ligand *trans* to the NHC donor.[29]

2.2.3. X-ray Structural Studies

The X-ray crystal structure for complexes **2.17** and **2.18** are shown in Figure 2.5. The X-ray crystallographic data for these compounds are given in Table A2.1 (Appendix 2). In each case, the X-ray crystal structures confirm that the ligands are coordinated to the Re metal centres as *facial* tridentates via the NHC, tertiary amine and carboxylate groups, with the additional three coordination sited being occupied by carbonyl ligands. For compounds **2.17** and **2.18**, respectively, the benzothiazole- and stilbene-based amyloid binding moieties are linked to the tertiary amine donor atom via an acetamide linkage. The $Re{-}C_{carbene}$, $Re{-}N_{amine}$ and $Re{-}O_{carboxylate}$ bond lengths (Figure 2.5 caption) are similar for each complex and the $Re\text{-}C_{carbonyl}$ bond lengths lie within typical ranges (1.90-2.10 Å).[19,28,30] As mentioned in the previous section, NHC ligands are strong σ-donors and are well known to exert a strong *trans* influence. In the case of compound **2.17** and **2.18**, the *trans* influence exerted by the NHC ligand is apparent and the Re-carbonyl bond length (Re-C(2) = 1.963(10) and 1.962(7) Å for **2.17** and **2.18**, respectively) is

significantly longer than those for the two other carbonyl ligands (Re-C(3) = 1.916(9) and 1.928(8) Å and Re-C(4) = 1.887(10) and 1.916(8) Å for **2.17** and **2.18**, respectively).

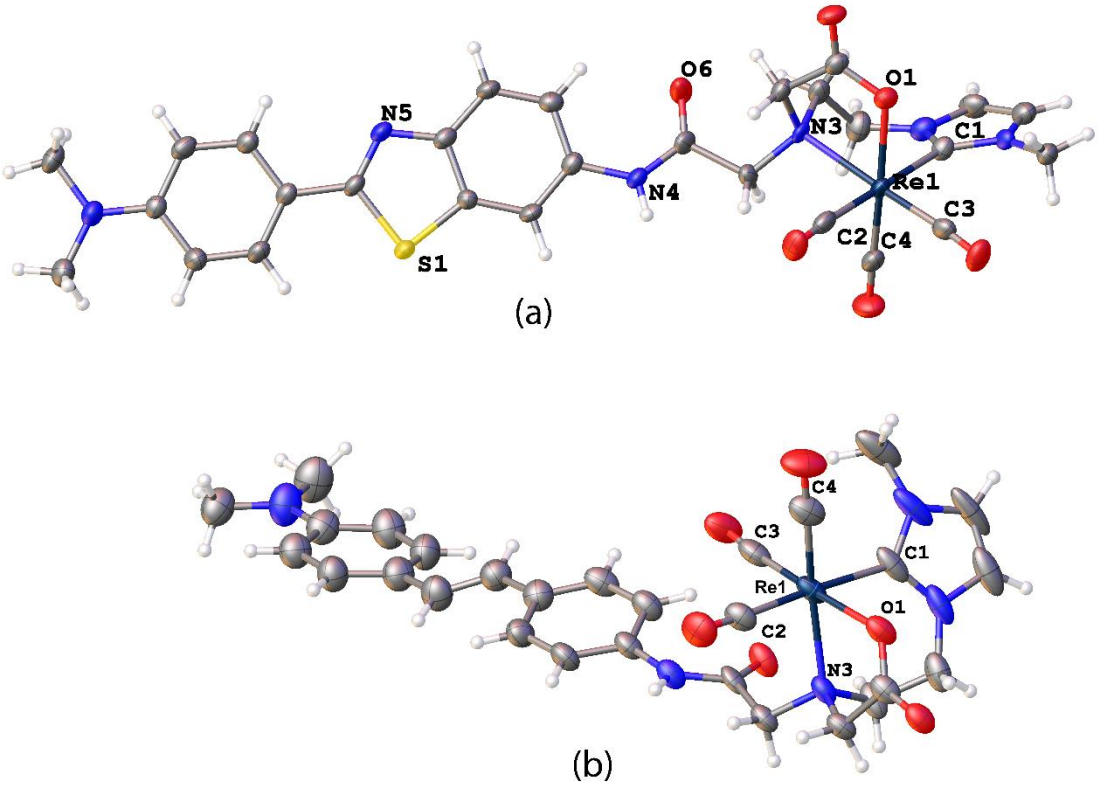

Figure 2.5. X-ray crystal structures of the Re complexes (a) **2.17** and (b) **2.18**. Ellipsoids are shown 40% probability. Selected bond lengths: **2.17** Re-O(1) = 2.142(6) Å, Re-N(3)= 2.287(6) Å, Re-C(1) = 2.179(9) Å, Re-C(2)= 1.963(10) Å, Re-C(3) = 1.916(9) Å, Re-C(4)= 1.887(10) Å and **2.18** Re-O(1) = 2.156(4) Å, Re-N(3) = 2.273(5) Å, Re-C(1) = 2.164(7) Å, Re-C(2) = 1.962(7) Å, Re-C(3) = 1.928(8) Å, Re-C(4) = 1.916(8) Å.

2.2.4. Octanol-Water Partition Coefficient

The NHC ligands reported here were designed for the generation of neutral complexes with either the $[Re(CO)_3]^+$ or $[Tc(CO)_3]^+$ cores for potential radiopharmaceutical applications. As neuroimaging applications are of interest, neutral complexes were desired to achieve sufficient lipophilicity to modulate the blood brain barrier (BBB) permeability. Molecules are known to cross the blood-brain barrier (BBB) by several

mechanisms, including passive diffusion or active transport. Passive diffusion is the most common mechanism for drugs to cross the BBB and relies upon a moderate to high degree of lipid solubility.[31] To evaluate the lipid solubility of the Re complexes **2.17** and **2.18**, the log*P* values were estimated using octanol-water partition coefficient experiments, conducted using the slow stirring method.[32] The results of these studies show that complex **2.17** has log*P* value of 0.15 ± 0.01, while complex **2.18** has a higher log*P* value of 0.39 ± 0.01. These log*P* values of both are somewhat lower than the optimum range required for good BBB permeability, for example Hansch and Leo found that BBB penetration is optimal when the log*P* values are in the range of 1.5-2.7.[33] However, with the development of this new synthetic approach for the preparation of tridentate NHC pro-ligands, the introduction of more lipophilic groups (for example extended alkyl chains on the NHC units) will be straightforward and allow for the ready modulation of log*P* values for the resulting complexes.

2.2.5. Interaction of 2.17 and 2.18 with Amyloid-β(1-40) and Amyloid-Plaques

The formation of amyloid-β (Aβ) fibrils from the $A\beta_{(1-40)}$ peptide *in vitro* can be monitored using thioflavin-T (ThT) as the interaction between ThT and Aβ fibrils results in strong fluorescence emission at 480 nm.[34-39] The interaction between the Re complexes **2.17** and **2.18** and amyloid was studied using a ThT-based fluorescence assay. The fluorescence emission at λ_{em} = 480 nm for a freshly prepared solution of $A\beta_{1-40}$ (4 μM) and ThT (4 μM) at 37 °C in the presence of each of the complexes **2.17** and **2.18** was monitored over a period of 66 h but no change was observed after 10 h (Figure 2.6). The control sample, where no complex was added, confirmed the formation of Aβ fibrils as indicated by the increased fluorescence intensity for fibril bound ThT at λ_{em} = 480 nm. The addition of either complex **2.17** or **2.18** resulted in a significantly reduced

fluorescence, suggesting that Re complexes **2.17** and **2.18** either bind competitively with ThT to $A\beta_{(1-40)}$ fibrils or that the complexes inhibit the formation of $A\beta_{(1-40)}$ fibrils.

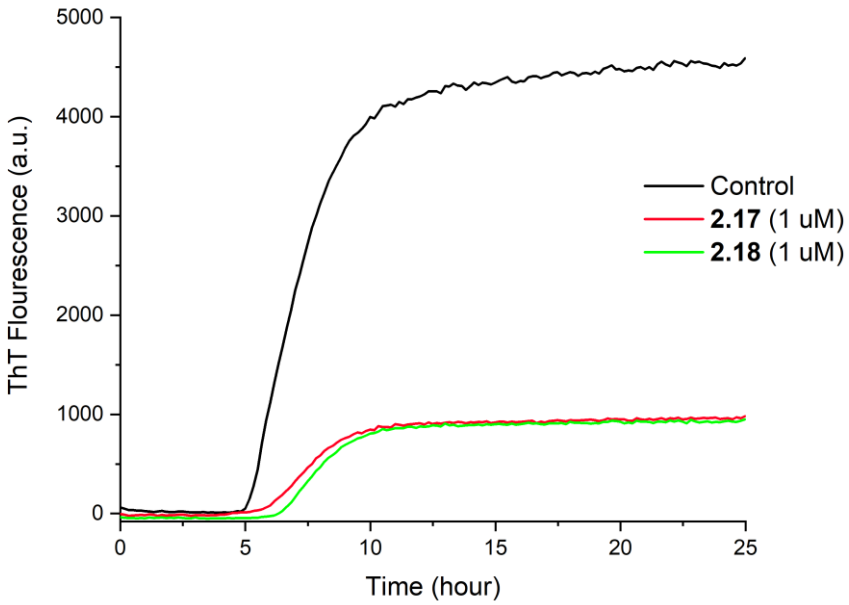

Figure 2.6. Thioflavin T (ThT) fluorescence assay over a period of 25 h for solutions of ThT (4 µM) and $A\beta_{1-40}$ (4 µM) at 37 °C in the presence of: no addition (control, black), **2.17** (red) and **2.18** (green) (1 µM in each case).

The capacities of the complexes to bind to amyloid plaques in human brain tissue were investigated using epi-fluorescence microscopy. To facilitate these studies the electronic absorption and emission spectra for the metal complexes **2.17** and **2.18** (together with the pro-ligands **2.13** and **2.16**) were recorded (Figures A2.23-A2.26, Appendix 2) and for the complexes, the emission maxima occurred at λ ~ 420 nm and λ ~ 457 nm, respectively. Frontal cortex brain tissue (7 µm sections) collected from post-mortem subjects with clinically diagnosed AD was compared to tissue from an age-matched healthy control following treatment with complex **2.17** or complex **2.18**. The treated tissues were examined by epi-fluorescence microscopy and then compared to contiguous sections that were immuno-stained with an anti-amyloid-$\beta_{(1-42)}$ antibody (1E8) to identify Aβ plaques

(Figure 2.7). The results of these human brain staining studies showed evidence for moderate levels of co-localisation of complexes **2.17** and **2.18** with the amyloid-β plaques (Figure 2.7b and Figure 2.7f). However, the epi-fluorescent images for the age-matched controls showed no evidence of non-specific binding for both complexes. Although the cause of the relatively low levels of co-localisation for these complexes with the amyloid plaques is not known, it may be due to the relatively short linker group between the amyloid binding moiety and the relatively large octahedral Re metal complexes.

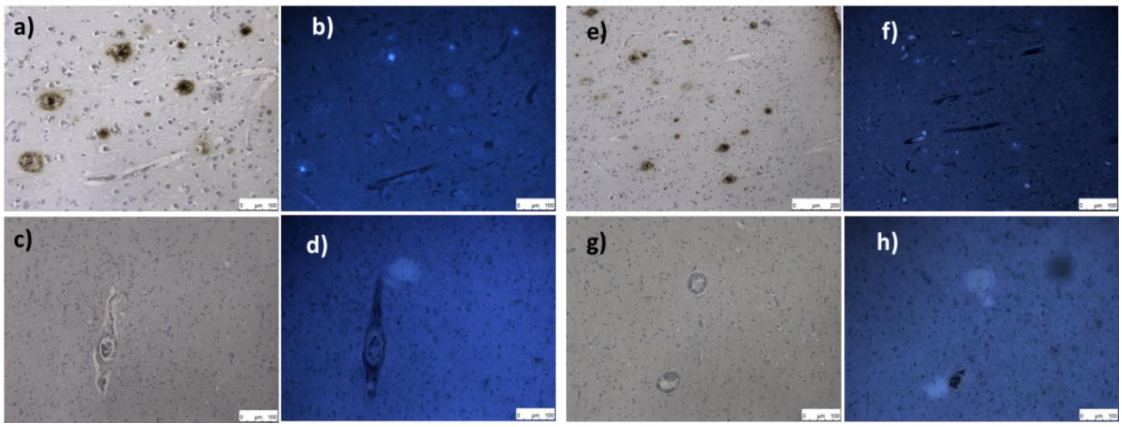

Figure 2.7. Epi-fluorescence microscopy images of frontal cortex brain tissue from AD patient treated (a, b, e & f) and from healthy age-matched control (c, d, g & h). Images a, e, c & g were stained with amyloid specific antibody (1E8) and visualised under brightfield. Images b & d were stained with **2.17** and f & h were stained with **2.18** and visualised using epi-fluorescence microscopy (λ_{ex} = 405 nm, λ_{em} = 460 nm)

2.3. Conclusion

In this chapter, the synthesis of two tridentate *N*-heterocyclic carbene pro-ligands bearing imidazolium, amine and carboxylate donor groups coupled to either a benzothiazole- or a stilbene-based amyloid binding moiety is described. These pro-ligands were used to prepare two neutral NHC complexes of the $[Re(CO)_3]^+$ core (**2.17** and **2.18**) and the log*P* values for these compounds were determined to be 0.15 ± 0.01 and 0.39 ± 0.01,

respectively. Studies using the histological dye Thioflavin-T showed that these complexes bound to fibrils formed from the amyloid-$\beta_{(1-40)}$ peptide. Epi-fluorescence microscopy co-localisation studies for compounds **2.17** and **2.18** and the amyloid specific antibody 1E8 in frontal cortex brain tissue from AD patient were consistent with the complexes binding to amyloid-β plaques at moderate to low levels. It is possible that the presence of the octahedral metal complex and the relatively low lipophilicity of **2.17** and **2.18** reduced their ability to bind to amyloid plaques. Previous study has shown that the related cationic Re-NHC cationic complexes [22] exhibited better binding profiles compared to the compounds explored in this chapter, suggesting that the properties of cationic complexes should also be investigated in future studies. Additional studies on these complexes should include quantum yield measurements to allow a comparison of the emission intensity between the neutral and the cationic Re(I)-NHC complexes. The log*P* values for the Re complexes (**2.17** and **2.18**) are not within the optimum range for CNS penetration, however the structures of the synthesised pro-ligands offer the potential to be modified to increase the lipophilicity. For example, the NHC unit has a methyl substituent, and this could be modified to a more lipophilic component e.g., *tert*-butyl or cyclohexyl in a relatively straightforward manner. The new ligand systems reported here are promising for the development of NHC based imaging agents as they form neutral and stable complexes with the $[Re(CO)_3]^+$ core. For future studies, the stability of the Re(I) complexes could be evaluated using ligand challenge experiments in the metal binding amino acids such as L-histidine and L-cysteine.[22] Additionally, the interaction of the Re(I) complexes with amyloid fibrils could be evaluated using transmission electron microscopy (TEM) to observe the morphology of amyloid fibrils after being treated with Re(I) complexes.[44] Additionally, it is of interest to prepare the corresponding $[^{99m}Tc(CO)_3]^+$ complexes of these ligands to allow for a comparison with these $[Re(CO)_3]^+$ complexes

2.4. Experimental Details

2.4.1. X-ray Crystallography

Single crystals of complexes **2.17** and **2.18** suitable for X-ray diffraction studies were grown by slow evaporation in dichloromethane solutions of these complexes. Crystallographic data for all structures determined are given in Table A2.1 (Appendix 2). For all samples, crystals were removed from the crystallisation vial and immediately coated with Paratone oil on a glass slide. A suitable crystal was mounted in Paratone oil on a glass fiber and cooled rapidly to 150 K (**2.17**) or 136 K (**2.18**) in a stream of cold N_2 using an Oxford low-temperature device. Diffraction data were measured using an Oxford Gemini diffractometer mounted with Mo-Kα λ = 0.71073 Å and Cu-Kα λ = 1.54184 Å. Data were reduced and corrected for absorption using the CrysAlis Pro program.[41] The SHELXL2013-2[42] program was used to solve the structures with Direct Methods, with refinement by the Full-Matrix Least-Squares refinement techniques on F^2. The non-hydrogen atoms were refined anisotropically and hydrogen atoms were placed geometrically and refined using the riding model. Coordinates and anisotropic thermal parameters of all non-hydrogen atoms were refined. All calculations were carried out using the program Olex^2.[43] Further XRD details are provided in the Electronic Supplementary Information. CCDC 1969630-1969631 contains the supplementary crystallographic data for this paper. These data can be obtained free of charge from The Cambridge Crystallographic Data Centre via https://www.ccdc.cam.ac.uk/structures/

2.4.2. ThT Fluorescence Aβ Binding Assays

Synthetic $A\beta_{1-40}$ (500 μg, Bachem, 4014442) was dissolved in HFIP (500 μL) then incubated on ice for 1 hour. The solution was then allowed to evaporate overnight followed by drying by high speed vacuum centrifugation to remove residual HFIP and

moisture. The peptide was dissolved in 60 mM NaOH (100 μL) and incubated for 3 min at room temperature then MilliQ water (350 μL) was added and the solution was vortexed briefly followed by ultrasoniacation for 5 minutes on ice. 10 × PBS (pH 7.4, 50 μL) was added to the solution then vortexed briefly and centrifuged for 5 min. Supernatant was transferred to a fresh tube and kept on ice. The concentration of the $A\beta_{1-40}$ solution was determined by its absorbance at 214 nm (ε = 94526 M^{-1} cm^{-1}) and found to be 148 μM. Stock solutions of ThT (1 mM in PBS), complexes **2.17** and **2.18** (1 mM in DMSO) were prepared freshly and final samples were prepared on ice by mixing $A\beta_{1-40}$ (final concentration: 4 μM), ThT (final concentration, 4 μM) and the chosen Re complex (final concentration: 1 μM), and the control consisting of $A\beta_{1-40}$ (final concentration: 4 μM) and ThT (final concentration: 4 μM). All samples were prepared in triplicates and the ThT fluorescence intensity of each sample was recorded every 10 min at 37 °C using a FLUOstar Omega filter-based multi-mode microplate reader with 440/480 nm excitation/emission filters over a period of 66 h with orbital shaking before each cycle.

2.4.3. Staining of Human AD Brain Tissues

The Health Sciences Human Ethics Sub-committee, The University of Melbourne, approved all experiments using human brain tissue (Ethics Approval No. 1341145). Brain tissue was collected at autopsy. Brain tissue from the frontal cortex was preserved by formalin fixation and paraffin embedding. AD pathology was confirmed according to standard National Institute of Aging and Reagan Institute Working Group on Diagnostic Criteria for the Neuropathological Assessment of Alzheimer's Disease (1997) criteria. The brain tissue samples of age-matched Human controls (HC) were subject to the above criteria. The AD and HC brain tissue sections (7 μm) were first deparaffined (xylene, 3 × 2 min) followed by rehydration (soaking for 2 min in a series of 100%, 90%, 70%, and 0% v/v ethanol/water). The hydrated tissue sections were washed in phosphate buffer

saline (PBS, 5 min). Autofluorescence of the tissue was quenched using potassium permanganate ($KMnO_4$) (0.25% in PBS, 20 min) and the sections were further washed with PBS (2 × 2 min) to remove the excess $KMnO_4$. The brown-coloured sections were washed with potassium metabisulfite and oxalic acid (1% in PBS) until the brown colour was removed followed by washing with PBS (3 × 2 min). The sections were blocked with bovine serum albumin (2% BSA in PBS, pH 7.0, 10 min) and covered with a solution of the chosen Re complex (10 μM in 15% v/v DMSO/PBS, 10 min). The sections were treated with BSA again (4 min) to remove any Re complex non-specifically bound to the tissue. Finally, the sections were washed with PBS (3 × 2 min), DI water, and mounted with a DAKO fluorescence mounting medium Fluorescence images were visualized using a Leica DM IL LED microscope.

2.4.4. Partition Coefficient (LogP) Studies

1-Octanol/water partition coefficients for complexes **2.17** and **2.18** were determined using the slow-stirring method as described by Pereiro and co-workers.[32] The 1-octanol and Mili-Q water were saturated prior their use and the starting concentration of complexes **2.17** and **2.18** in the 1-octanol phase was 80 μM. Approximately 5 mL of the pre-saturated water and 1-octanol were added to a glass vial containing a magnetic stir bar. The vials were slowly stirred and maintained at 25 °C for two days. The metal complex concentration in the 1-octanol phase was then analysed using an Agilent Technologies Cary 300 UV-visible spectrophotometer in a quartz cuvette (1 cm). A calibration curve for each complex was prepared at its λ_{max} value (365 nm for **2.17** and 360 nm for **2.18**).

2.4.5. Synthesis

6-nitro-2-(4-*N*,*N*-dimethylaminophenyl)benzothiazole. This compound was synthesised as reported by Racane[44] from 2-amino-5-nitrothiophenol (0.85 g, 5.00 mmol), 4-(dimethylamino)benzaldehyde (0.75 g, 5.00 mmol) in pyridine (10 mL). The product

was obtained as an orange solid. (Yield: 0.72g, 48%). ^{1}H NMR (400 MHz, $CDCl_3$): δ (ppm) 3.11 (s, 6H, CH_3), 6.76 (d, 2H, $^{3}J_{H\text{-}H}$ = 9.04 Hz, H_{Ar}), 7.98-8.00 (m, 3H, H_{Ar}), 8.30-8.33 (dd, 1H, $^{2}J_{H\text{-}H}$ = 2.32, $^{3}J_{H\text{-}H}$ = 8.96 Hz, H_{Ar}), 8.76 (d, 1H, $^{3}J_{H\text{-}H}$ = 2.28 Hz, H_{Ar}). ^{13}C NMR (100 MHz, $CDCl_3$): δ (ppm) 40.1 (CH$_3$), 111.6 (CH$_{Ar}$), 117.9 (CH$_{Ar}$), 120.3 (C_q), 121.9 (CH$_{Ar}$), 121.9 (CH$_{Ar}$), 129.5 (CH$_{Ar}$), 134.8 (C_q), 144.0 (C_q), 153.0 (C_q), 158.6 (C_q), 174.5 (C_q).

6-amino-2-(4-*N,N*-dimethylaminophenyl)benzothiazole. This compound was synthesised as reported by Racane[44] from anhydrous tin(II) chloride (2.17 g, 9.62 mmol), 6-nitro-2-(4-N,N-dimethylaminophenyl)benzothiazole (0.72 g, 2.41 mmol), conc. HCl (4.5 mL) and methanol (4.5 mL). The product was obtained as a brown solid. (Yield: 0.094 g, 15%). ^{1}H NMR (400 MHz, DMSO-d_6): δ (ppm) 2.90 (s, 6H, 2CH_3), 5.18 (s, 2H, NH_2), 6.53 (d, 2H, $^{3}J_{H\text{-}H}$ = 8.44 Hz, H_{Ar}), 6.69 (d, 2H, $^{3}J_{H\text{-}H}$ = 8.44 Hz, H_{Ar}), 6.78 (s, 2H, HC=CH), 7.29 (d, 2H, $^{3}J_{H\text{-}H}$ = 8.48 Hz, H_{Ar}), 7.32 (d, 2H, $^{3}J_{H\text{-}H}$ = 8.84 Hz, H_{Ar}). ^{13}C NMR (100 MHz, DMSO-d_6): δ (ppm) 39.5-40.5 (CH$_3$), 104.5 (CH$_{Ar}$), 112.4 (CH$_{Ar}$), 115.1 (CH$_{Ar}$), 121.5 (C_q),121.6 (C_q), 122.7 (CH$_{Ar}$), 128.1 (CH$_{Ar}$), 135.7 (C_q), 145.9 (C_q), 147.1 (C_q), 152.0 (C_q), 162.0 (C_q).

***p*-nitro-*p'*-*N,N*-dimethylaminostilbene.** This compound was synthesised as described by Gao[45] from *p*-nitro-phenylacetic acid (5.00 g, 30 mmol), *p*-dimethylaminobenzaldehyde (6.18 g, 41 mmol), and piperidine (10 mL). The product was obtained as a bright orange solid. (Yield: 2.96 g, 42%). ^{1}H NMR (500 MHz, $CDCl_3$): δ (ppm) 3.03 (s, 6H, CH_3), 6.72 (d, 2H, H_{Ar}), 6.94 (d, 1H, $^{3}J_{H\text{-}H}$ = 16.2 Hz, HC=CH), 7.22 (d, 1H, $^{3}J_{H\text{-}H}$ = 16.3 Hz, HC=CH), 7.45 (d, 2H, $^{3}J_{H\text{-}H}$ = 8.70 Hz, H_{Ar}), 7.57 (d, 2H, $^{3}J_{H\text{-}H}$ = 8.70 Hz, H_{Ar}), 8.19 (d, 2H, $^{3}J_{H\text{-}H}$ = 8.85 Hz, H_{Ar}). ^{13}C NMR (125 MHz, $CDCl_3$): δ (ppm) 40.3 (CH$_3$), 112.2 (CH$_{Ar}$), 121.6 (C=C), 124.2 (CH$_{Ar}$), 126.1 (CH$_{Ar}$), 128.4 (CH$_{Ar}$), 133.4 (C=C), 145.0 (C_q), 150.9 (C_q).

***p*-amino-*p'N,N*-dimethylaminostilbene.** This compound was prepared using the same procedure as described by Gao[45] from *p*-nitro-*p'*-*N,N*-dimethylaminostilbene (0.91 g, 3.54 mmol), anhydrous tin(II) chloride (3.20 g, 14.2 mmol), conc. HCl (10 mL) and methanol (10 mL). The product was obtained as a yellow solid. (Yield: 0.10 g, 12%). ^{1}H NMR (500 MHz, DMSO-d_6): δ (ppm) 2.99 (s, 6H, 2CH_3), 5.33 (s, 2H, NH_2), 6.72-6.74 (dd, 1H, H_{Ar}), 6.79 (d, 2H, $^{3}J_{H\text{-}H}$ = 8.85, H_{Ar}). ^{13}C NMR (125 MHz, DMSO-d_6): δ (ppm) 112.9 (CH$_{Ar}$), 114.4 (CH$_{Ar}$), 123.7 (C_q), 125.1 (HC=CH), 126.1 (CH$_{Ar}$), 126.6 (CH$_{Ar}$), 127.4 (CH$_{Ar}$), 148.4 (C_q), 149.8 (C_q).

2.5. This compound was synthesised as described by Hemelaere[46] from ethanolamine (5.00 g, 81.9 mmol), $MgSO_4$ (19.7 g, 164 mmol) and benzylaldehyde (8.69 g, 81.9 mmol) in methanol (150 mL). The product was obtained as a yellow oil. (Yield: 9.85 g, 79%). ^{1}H NMR (400 MHz, $CDCl_3$): δ (ppm) 2.76 (t, 2H, $^{3}J_{H\text{-}H}$ = 5.20 Hz, CH_2CH$_2$), 2.94 (s, 2H, NH_2), 3.64 (t, 2H, $^{3}J_{H\text{-}H}$ = 5.12 Hz, CH$_2$CH_2), 3.78 (s, 2H, CH_2OH), 7.24-7.32 (m, 5H, H_{Ar}). ^{13}C NMR (100 MHz, $CDCl_3$): δ (ppm) 50.6 (CH$_2$CH$_2$), 53.5 (CH$_2$$CH_2$), 60.7 ($CH_2$N), 127.2 ($CH_{Ar}$), 128.3 ($CH_{Ar}$), 128.5 ($CH_{Ar}$).

2.6. To a stirred solution of **2.5** (0.5 g, 3.31 mmol) in acetonitrile (30 mL), $NaHCO_3$ (0.42 g, 4.95 mmol) was added. The mixture was cooled to 0 °C before a solution of *t*-butyl bromoacetate (0.65 g, 3.31 mmol) in acetonitrile (5 mL) was added dropwise, and the resultant mixture was stirred at room temperature for 2 h and the solvent was then removed on a rotatory evaporator. The crude product was redissolved in dichloromethane, washed with water (3 × 10 mL), dried with $MgSO_4$ and the solvent was evaporated to dryness on a rotatory evaporator. The crude product was purified on silica with methanol (3%) and dichloromethane (97%) as the eluent. The product was obtained as a yellow oil. (Yield: 0.37 g, 42%). ^{1}H NMR (400 MHz, $CDCl_3$): δ (ppm) 1.46 (s, 9H, 3CH_3), 2.85 (t, 2H, $^{3}J_{H\text{-}H}$ = 5.20 Hz, CH_2CH$_2$), 3.23 (s, 2H, CH_2COO), 3.59 (t, 2H, $^{3}J_{H\text{-}H}$ = 5.08 Hz,

CH_2CH_2), 3.82 (s, 2H, CH_2N), 7.28-7.34 (m, 5H, H_{Ar}). ^{13}C NMR (100 MHz, $CDCl_3$): δ (ppm) 27.8 (CH_3), 55.5 (CH_2COO), 56.6 (CH_2CH_2), 58.6 (CH_2CH_2), 59.0 (CH_2N), 81.3 (C_q), 127. 3 (CH_{Ar}), 128.4 (CH_{Ar}), 128.9 (CH_{Ar}), 138.5 (C_q), 171.2 (C_q).

2.7. To a solution of **2.6** in methanol (2.71 g, 10.2 mmol), was added 10% Pd/C (0.50 g) and the mixture was stirred overnight under a hydrogen atmosphere. The solution was filtered through a plug of Celite, evaporated to dryness on a rotatory evaporator and purified on silica with dichloromethane (2%) and methanol (98%) as the eluent. The pure compound was obtained as a yellow oil (Yield: 1.53 g, 85%). ^1H NMR (400 MHz, $CDCl_3$): δ (ppm) 1.44 (s, 9H, $3CH_3$), 2.60 (s_{br}, 1H, NH), 2.74 (t, 2H, $^3J_{H-H}$ = 5.20 Hz, CH_2), 3.28 (s, 2H, $OCCH_2$), 3.59 (t, 2H, $^3J_{H-H}$ = 5.12 Hz, CH_2). ^{13}C NMR (100 MHz, $CDCl_3$): δ (ppm) 28.0 (CH_3), 51.1 (OCN), 51.2 (CH_2), 60.9 (CH_2), 81.4 (C_q), 171.9 (C_q).

2.8. To a solution of **2.7** (0.50 g, 2.85 mmol) in anhydrous DMF (5 mL) was added $NaHCO_3$ (0.29 g, 3.42 mmol). The mixture was cooled to 0 °C and a solution of benzyl bromoacetate (0.72 g, 3.14 mmol) in anhydrous DMF (2 mL) was added dropwise. The mixture was stirred at 0 °C for 1 h, allowed to warm to room temperature then stirred for another 12 h. The solution was filtered, and the solvent was removed on a rotatory evaporator. The crude product was purified on silica with ethyl acetate (40%) and hexane (60%) as the eluent. The pure compound was obtained as a yellow oil. (Yield: 0.74g, 81%). ^1H NMR (400 MHz, $CDCl_3$): δ (ppm) 1.46 (s, 9H, CH_3), 2.90 (t, 2H, $^3J_{H-H}$ = 4.12 Hz, CH_2), 3.46 (s, 2H, NCH_2), 3.54 (t, 2H, $^3J_{H-H}$ = 2.12 Hz, CH_2), 3.61 (s, 2H, NCH_2), 5.16 (s, 2H, CH_2), 7.34-7.37 (m, 5H, H_{Ar}). ^{13}C NMR (100 MHz, $CDCl_3$): δ (ppm) 28.1 (CH_3), 55.8 (NCH_2), 56.5 (NCH_2), 57.1 (OCH_2), 59.3 (NCH_2), 66.6 (O-CH_2-Ar), 81.6 (C_q), 128.3 (CH_{Ar}), 128.4 (CH_{Ar}), 128.6 (CH_{Ar}), 135.5 (C_q), 171.3 (C_q), 171.9 (C_q).

2.9. A mixture of **2.8** (2.57 g, 7.95 mmol) and triphenylphosphine (2.09 g, 7.95 mmol) was dissolved in anhydrous DCM (20 mL) and cooled to 0 °C under a nitrogen

atmosphere. *N*-bromosuccinimide (1.42 g, 7.95 mmol) was added portion-wise and the mixture was stirred for 2.5 h at 0 °C.[45] A pale orange crystalline solid was obtained after the solvent was removed on a rotatory evaporator. The crude product was washed with ether (2 × 20 mL) and then purified on silica with hexane (40%) and ethyl acetate (60%) as the eluent. The pure compound was obtained as a yellow oil. (Yield: 1.87 g, 43%). ^{1}H NMR (400 MHz, $CDCl_3$): δ (ppm) 1.46 (s, 9H, CH_3), 3.17 (t, 2H, $^{3}J_{H\text{-}H}$ = 7.68 Hz, CH_2), 3.43 (s, 2H, CH_2), 3.66 (s, 2H, CH_2), 5.16 (s, 2H, CH_2), 7.35-7.39 (m, 5H, H_{Ar}). ^{13}C NMR (100 MHz, $CDCl_3$): δ (ppm) 28.1 (CH$_3$), 30.2 (CH$_2$Br), 55.6 (NCH$_2$), 56.4 (NCH$_2$), 56.7 (NCH$_2$), 66.5 (O-CH$_2$-Ar), 81.4 (C_q), 128.3 (CH$_{Ar}$), 128.4 (CH$_{Ar}$), 128.6 (CH$_{Ar}$), 135.6 (C_q), 170.4 (C_q), 171.1 (C_q).

2.10. A solution of 1-methylimidazole (0.12 g, 1.51 mmol) in acetonitrile (10 mL) was added dropwise to a solution of **2.9** (0.58 g, 1.51 mmol) in acetonitrile (40 mL) and the mixture was refluxed at 100 °C overnight. After removal of solvent on a rotatory evaporator, the crude product was purified on silica with methanol (2%) and dichloromethane (98%) as the eluent and the pure product was obtained as a yellow oil. (Yield: 0.47 g, 81%). ^{1}H NMR (400 MHz) ($CDCl_3$): δ (ppm) 1.42 (s, 9H, CH_3), 3.18 (m, 2H, CH_2), 3.39 (s, 2H, CH_2), 3.56 (s, 2H, CH_2), 3.99 (s, 3H, CH_{3imi}), 4.43 (m, 2H, CH_2), 7.26 (t, 1H, $^{3}J_{H\text{-}H}$ = 1.76 Hz, H_{imi}), 7.31-7.36 (m, 5H, H_{Ar}), 7.88 (t, 1H, $^{3}J_{H\text{-}H}$ = 1.72 Hz, H_{imi}), 10.0 (s, 1H, NCHN). ^{13}C NMR (100 MHz, $CDCl_3$): δ (ppm) 36.5 CH$_{3imi}$, 48.2 CH$_2$, 50.6 C_q, 55.0 NCH$_2$, 56.1 NCH$_2$, 56.7 NCH$_2$, 66.7 O CH$_2$-Ar, 81.9 C_q, 122.0 C_{imi}, 123.6 C_{imi}, 128.3 C_{Ar}, 128.5 C_{Ar} 128.7 C_{Ar}, 135.3 C_q, 138.0 C_{imi}, 170.3 C_q, 171.1 C_q. HRESI-MS$^+$ (CH_3OH): $[C_{21}H_{30}N_3O_4]^+$ *m/z* = 388.2257, calcd = 388.2236.

2.11. To a stirred solution of **2.10** (0.40 g, 1.03 mmol) in dichloromethane (15 mL) at 0 ºC was added dropwise a solution of trifluroacetic acid (2.55 g, 22.3 mmol) in dichloromethane (5 mL). The mixture was then stirred at room temperature overnight.

After removal of the solvent on a rotatory evaporator, a yellow oil was obtained, which was dissolved in water (20 mL) and a saturated solution of KPF_6 (1.33 g, 7.22 mmol) in water (20 mL) was added dropwise resulting in the formation of a white precipitate. The mixture was extracted with dichloromethane (3 × 20 mL) and the combined organic extracts were dried with $MgSO_4$. The solvent was removed on a rotatory evaporator yielding the pure compound as a colourless oil. (Yield: 0.47 g, 44%). ^{1}H NMR (500 MHz, DMSO-d_6): δ (ppm) 3.05 (t, 2H, $^3J_{H\text{-}H}$ = 5.48 Hz, CH_2), 3.45 (s, 2H, NCH_2), 3.61 (s, 2H, NCH_2), 3.81 (s, 3H, CH_3), 4.21 (t, 2H, CH_2), 5.10 (s, 2H, C$H_{2benzyl}$), 7.34-7.39 (m, 5H, H_{Ar}), 7.63 (t, 1H, $^3J_{H\text{-}H}$ = 1.64 Hz, H_{imi}), 7.71 (t, 1H, $^3J_{H\text{-}H}$ = 1.68 Hz, H_{imi}), 9.05 (s, 1H, NCHN$_{imi}$). ^{13}C NMR (125 MHz, DMSO-d_6): δ (ppm) 36.1 CH$_3$, 47.6 CH$_2$, 53.9 CH$_2$, 54.0 NCH$_2$, 55.0 NCH$_2$, 66.1 O-CH$_2$-Ar, 123.2 C_{imi}, 123.3 C_{imi}, 128.5 C_{Ar}, 128.6 C_{Ar}, 128.9 C_{Ar}, 136.4 C_q, 137.5 C_{imi}, 171.4 C=O, 172.9 C=O. HRESI-MS$^+$ (CH_3OH): $[C_{17}H_{22}N_3O_4]^+$ m/z = 332.1607, calcd = 332.1610.

2.12. A mixture of **2.11** (0.32 g, 0.67 mmol), DIPEA (0.24 g, 1.83 mmol), PyBop (0.32 g, 0.670 mmol) and 6-amino-2-(4-*N*,*N*-dimethylaminophenyl)benzothiazole (0.16 g, 0.670 mmol) in dichloromethane (20 mL) was stirred at room temperature overnight. The solvent was removed using a rotary evaporator and the crude product was washed with diethyl ether (3 × 10 mL) and a minimal amount of dichloromethane to yield the pure product as a yellow solid. (Yield: 0.26 g, 40%). ^{1}H NMR (400 MHz, DMSO-d_6): δ (ppm) 3.02 (s, 6H, CH_3), 3.17 (t, 2H, $^3J_{H\text{-}H}$ = 5.16 Hz, CH_2), 3.57 (s, 2H, NCH_2O), 3.72 (s, 2H, NCH_2), 3.76 (s, 3H, CH_{3imi}), 4.28 (t, 2H, $^3J_{H\text{-}H}$ = 5.28 Hz, CH_2), 5.15 (s, 2H, CH_2), 6.82 (d, 2H, $^3J_{H\text{-}H}$ = 9.00 Hz, H_{Ar}), 7.34-7.39 (m, 5H, H_{Ar}), 7.61 (s, 1H, H_{Ar}), 7.78 (d, 1H, $^3J_{H\text{-}H}$ = 1.56 Hz, H_{imi}), 7.84 -7.87 (m, 3H, H_{Ar}), 8.36 (d, 1H, $^3J_{H\text{-}H}$ = 1.92 Hz, H_{imi}), 9.12 (s, 1H, H_{imi}), 9.91 (s, 1H, NH). ^{13}C NMR (100 MHz, DMSO-d_6): δ (ppm) 36.1 CH$_{3imi}$, 39.5-40.5 CH$_3$, 47.6 CH$_2$, 54.4 CH$_2$, 55.5 NCH$_2$, 58.3 NCH$_2$, 66.2 O-CH$_2$-Ar, 111.9 C_{imi}, 112.3 C_{Ar}, 119.0 C_q,120.7 C_{Ar}, 122.3 C_{Ar}, 123.2 C_{imi}, 123.5 C_{Ar}, 128.5-128.9 $C_{benzothiazole}$, 134.8

C_q, 135.9 C_q, 136.3 C_q, 137.5 C_{imi}, 150.6 C_q, 152.6 C_q, 167.1 C_q, 169.6 C_q, 171.8 C_q. HRESI-MS$^+$ (*CH₃OH*): $[C_{32}H_{35}N_6O_3S]^+$ *m/z* = 583.2516, calcd = 583.2491.

2.13. To a solution of **2.12** (0.21 g, 0.30 mmol) in hot methanol (50 mL) was added 10% Pd/C (0.05 g) and the mixture was heated at 40 °C under an atmosphere of hydrogen for 5 h. The reaction mixture was filtrated through a plug of Celite, and after removal of the solvent on a rotatory evaporator the product was obtained as a bright yellow solid. (Yield: 0.18 g, 82%). ^{1}H NMR (400 MHz, DMSO-d_6): δ (ppm) 3.02 (s, 6H, CH_3), 3.16 (t, 2H, $^3J_{H\text{-}H}$ = 5.48, NCH_2), 3.54 (s, 2H, NCH_2), 3.54 (s, 2H, NCH_2), 3.77 (s, 3H, NCH_3), 4.26 (t, 2H, $^3J_{H\text{-}H}$ = 5.36, CH_2), 6.82 (d, 2H, $^3J_{H\text{-}H}$ = 8.92, H_{Ar}), 7.45-7.47 (m, 1H, H_{Ar}), 7.62 (s, 1H, H_{Ar}), 7.79 (s, 1H, H_{imi}), 7.85 (d, 2H, H_{Ar}), 7.87 (d, 1H, H_{Ar}), 8.37 (d, 1H, $^3J_{H\text{-}H}$ = 1.80 Hz, H_{imi}), 9.14 (s, 1H, H_{imi}). ^{13}C NMR (100 MHz, DMSO-d_6): δ (ppm) 36.1 CH_{3imi}, 39.5-40.5 CH_3, 47.6 CH_2, 55.7 NCH_2, 58.6 NCH_2, 111.8 C_{imi}, 112.3 C_{Ar}, 118.9 C_{Ar}, 120.7 C_q, 122.3 C_{Ar}, 123.2 C_{imi}, 123.5 C_{Ar}, 128.7 C_{Ar}, 134.9 C_q, 135.9 C_q, 137.5 C_{imi}, 150.5 C_q, 152.6 C_q, 167.1 C_q, 169.9 C_q, 173.7 C_q. HRESI-MS$^+$ (*CH₃OH*): $[C_{25}H_{29}N_6O_3S]^+$ *m/z* = 493.1995, calcd = 493.2022.

2.14. To a stirred solution of **2.10** (5.50 g, 11.7 mmol) in methanol (70 mL), 10% Pd/C (0.50 g) was added and the reaction was stirred under an atmosphere of hydrogen overnight. The mixture was filtered through a plug of Celite and the solvent was removed on a rotatory evaporator yielding a yellow oil. The yellow oil was dissolved in water (10 mL) and a solution of KPF_6 (1.01 g, 5.51 mmol) in water (10 mL) was added dropwise, resulting in the formation of a white precipitate. The mixture was extracted with dichloromethane (3 × 10 mL) and the combined organic extracts were dried with $MgSO_4$ and the solvent was removed on a rotatory evaporator yielding the pure compound as yellow oil. (Yield: 0.45 g, 38%). ^{1}H NMR (400 MHz, DMSO-d_6): δ (ppm) 1.40 (s, 9H, CH_3), 3.03 (t, 2H, $^3J_{H\text{-}H}$ = 5.64 Hz, CH_2), 3.41 (s, 2H, NCH_2), 3.43 (s, 2H, NCH_2), 4.21

(t, 2H, $^3J_{H-H}$ = 5.36 Hz, CH_2), 7.67 (s, 1H, H_{imi}), 7.75 (s, 1H, H_{imi}), 9.08 (s, 1H, H_{imi}). ^{13}C NMR (100 MHz, DMSO-d_6): δ (ppm) 28.3 CH_3, 36.1 CH_{3imi}, 47.6 CH_2, 54.0 CH_2, 55.0 NCH_2, 55.8 NCH_2, 80.9 C_q, 123.2 C_{imi}, 123.2 C_{imi}, 137.5 C_{imi}, 170.7 C=O, 172.9 C=O. HRESI-MS$^+$ (CH_3OH): $[C_{14}H_{24}N_3O_4]^+$ m/z = 298.1766, calcd = 298.1767.

2.15. The compound was prepared as described for **2.12** from **2.14** (0.20 g, 0.43 mmol), DIPEA (0.17 g, 1.30 mmol), PyBop (0.23 g, 0.43 mmol), 4-amino-4'-(*N*,*N*-dimethylamino)stilbene (0.10 g, 0.42 mmol). (Yield: 0.05 g, 17%). ^{1}H NMR (400 MHz, DMSO-d_6): δ (ppm) 1.43 (s, 9H, C$H_{3t\text{-}butyl}$), 2.93 (s, 6H, C$H_{3stilbene}$), 3.13 (t, 2H, $^3J_{H-H}$ = 5.75 Hz, CH_2), 3.48 (s, 4H, NCH_2), 3.78 (s, 3H, CH_{3imi}), 4.25 (t, 2H, $^3J_{H-H}$ = 5.70 Hz, CH_2), 6.71 (d, 2H, $^3J_{H-H}$ = 8.85 Hz, H_{Ar}), 6.91 (d, 1H, $^3J_{H-H}$ = 16.4 Hz, CH=CH), 7.03 (d, 1H, $^3J_{H-H}$ = 16.5 Hz, CH=CH), 7.40 (d, 2H, $^3J_{H-H}$ = 8.80 Hz, H_{Ar}), 7.47 (d, 2H, $^3J_{H-H}$ = 8.70 Hz, H_{Ar}), 7.52 (d, 2H, $^3J_{H-H}$ = 8.60 Hz, H_{Ar}), 7.64 (s, 1H, H_{imi}), 7.78 (s, 1H, H_{imi}), 9.10 (s, 1H, H_{imi}), 9.72 (s, 1H, NH). ^{13}C NMR (100 MHz, DMSO-d_6): δ (ppm) 28.3 $CH_{3t\text{-}butyl}$, 36.1 CH_{3imi}, 39.5 $CH_{3stilbene}$, 47.6 CH_2, 54.5 CH_2, 56.4 NCH_2, 58.3 NCH_2, 81.3 $C_{t\text{-}butyl}$, 112.8 C_{Ar}, 119.6 C_{Ar}, 123.2 C_{imi}, 123.5 C_{imi}, 123.6 C_{Ar}, 125.6 C_{Ar}, 126.7 C_{Ar}, 127.8 C_{Ar}, 128.0 C_q, 133.6 C_q, 137.5 C_{imi}, 137.7 C_q, 150.3 C_q, 169.5 C=O, 171.2 C=O. HRESI-MS$^+$ (CH_3OH): $[C_{30}H_{40}N_5O_3]^+$ m/z = 518.3162, calcd = 518.310.

2.16. To a stirred solution of **2.15** (0.28 g, 0.42 mmol) in dichloromethane (15 mL) at 0 °C was added dropwise a solution of trifluroacetic acid (2.37 g, 20.8 mmol) in dichloromethane (5 mL) and the mixture was stirred at room temperature overnight. The solvent was removed on a rotatory evaporator yielding a yellow solid, which was dissolved in water (20 mL), the pH was then adjusted to 12 with 1M NaOH and the solution washed with dichloromethane (3 × 10 mL). The pH of the solution was then adjusted to pH 7 using concentrated hydrochloric acid and the water was removed using rotatory evaporator to obtain a yellow solid. The yellow solid (0.44 g) was redissolved in

acetonitrile and a solution of TBACl (0.26 g, 0.95 mmol) in acetonitrile was added dropwise and the yellow precipitate was collected via centrifugation. The solvent was removed on a rotatory evaporator yielding the pure compound as a yellow solid. (Yield: 0.21 g, 57%). ^{1}H NMR (500 MHz, DMSO-d_6): δ (ppm) 2.92 (s, 6H, C$H_{3stilbene}$), 3.11 (t, 2H, $^{3}J_{H-H}$ = 5.50 Hz, CH_2), 3.16 (s, 4H, CH_2), 3.65 (s, 3H, CH_{3imi}), 4.21 (s, 2H, CH_2), 6.70 (d, 2H, $^{3}J_{H-H}$ = 9.15 Hz, H_{Ar}), 6.90 (d, 1H, $^{3}J_{H-H}$ = 16.4 Hz, CH=CH), 7.01 (d, 1H, $^{3}J_{H-H}$ = 16.4 Hz, CH=CH), 7.39 (d, 2H, $^{3}J_{H-H}$ = 8.80 Hz, H_{Ar}), 7.44 (d, 2H, $^{3}J_{H-H}$ = 8.60 Hz, H_{Ar}), 7.54 (s, 1H, H_{imi}), 7.65 (d, 2H, $^{3}J_{H-H}$ = 8.40 Hz, H_{Ar}), 7.83 (s, 1H, H_{imi}), 9.83 (s, 1H, H_{imi}). ^{13}C NMR (125 MHz, DMSO-d_6): δ (ppm) 35.9 CH$_{3imi}$, 39.5 CH$_{3stilbene}$, 47.8 CH$_2$, 56.4 CH$_2$, 58.1 CH$_2$, 61.7 CH$_2$, 65.4 C_q, 112.8 C_{Ar},119.6 C_{Ar}, 123.0 C_{imi}, 123.4 C_{imi}, 123.9 CH=CH, 125.7 C_q, 126.5 C_{Ar}, 127.6 C_q, 127.7 C_{Ar}, 133.1 C_q, 138.0 C_{imi}, 150.3 C_q, 171.3 C_q. HRESI-MS$^+$ (CH_3OH): $[C_{26}H_{32}N_5O_3]^+$ m/z = 462.2512, calcd = 462.2505.

2.17. A mixture of **2.13** (0.043 g, 0.069 mmol) and Ag_2O (0.032 g, 0.14 mmol) in acetonitrile (25 mL) was stirred at 60 °C for 24 h. $Re(CO)_5Cl$ (0.025 g, 0.069 mmol) was then added and the mixture was stirred at 60 °C for a further 24 h. The mixture was filtered through Celite and the solvent was removed from the filtrate on a rotatory evaporator yielding a yellow/brown solid. The yellow/brown solid was dissolved in minimal amount of acetonitrile and purified on alumina using methanol (5%) and dicholoromethane (95%) as the eluent. The product was obtained as yellow solid. (Yield: 0.020 g, 32%). ^{1}H NMR (500 MHz, DMSO-d_6): δ (ppm) 3.02 (s, 6H, CH_3), 3.32-3.33 (m, 1H, CH_2), 3.50-3.55 (m, 1H, CH_2), 3.83 (d, 1H, $^{3}J_{H-H}$ = 16.4 Hz, CH_2COO), 3.90 (s, 3H, CH_{3imi}), 4.04-4.09 (m, 1H, CH_2), 4.16 (d, 1H, $^{3}J_{H-H}$ = 16.3 Hz, CH_2COO), 4.22-4.26 (m, 1H, CH_2), 4.31 (d, 2H, A$^{3}J_{H-H}$ = 15.8 Hz, B$^{3}J_{H-H}$ = 15.8 Hz, CH_2CONH), 6.82 (d, 2H, $^{3}J_{H-H}$ = 9.15 Hz, H_{Ar}), 7.40 (d, 1H, $^{3}J_{H-H}$ = 1.75 Hz, H_{imi}), 7.46 (d, 1H, $^{3}J_{H-H}$ = 1.80 Hz, H_{imi}), 7.51 (dd, 1H, $^{3}J_{H-H}$ = 2.15, 6.65 Hz, H_{Ar}), 7.84-7.88 (m, 3H, H_{Ar}), 8.43 (d, 1H, $^{3}J_{H-H}$ = 2.05, H_{Ar}), 10.5 (s, 1H, NH). ^{13}C NMR (125 MHz, DMSO-d_6): δ (ppm) 39.0 CH$_{3imi}$, 39.5-40.5 CH$_3$, 47.1 CH$_2$,

59.8 CH_2, 65.1 CH_2, 69.4 CH_2, 112.3 C_{imi}, 119.4 C_{Ar}, 122.4 C_{Ar}, 123.1 C_{Ar}, 123.2 C_{imi}, 128.8 C_{Ar}, 134.9 C_q, 135.6 C_q, 150.8 C_q, 152.6 C_q, 162.8 C_q, 166.8 C_q, 167.4 C_q, 178.5 C_q, 180.1 C_q, 196.2 Re-*C*O, 197.4 Re-*C*O, 197.7 Re-*C*O. HRESI-MS$^+$ (*CH_3OH*): $[C_{28}H_{28}N_6O_6ReSNa]^+$ *m/z* = 785.1170, calcd = 785.1168.

2.18. The compound was prepared as described for **2.17** from **2.16** (0.043 g, 0.069 mmol), Ag_2O (0.032 g, 0.14 mmol) and $Re(CO)_5Cl$ (0.025 g, 0.069 mmol) in 1:9 dichloromethane and methanol (25 mL). The product was obtained as yellow solid. (Yield: 0.030 g, 38%). ^{1}H NMR (500 MHz, DMSO-*d*$_6$): δ (ppm) 2.93 (s, 6H, $CH_{3stilbene}$), 3.32-3.33 (m, 1H, CH_2), 3.46-3.51 (m, 1H, CH_2), 3.80 (d, 1H, $^3J_{H-H}$ = 16.5 Hz, CH_2COO), 3.90 (s, 3H, CH_{3imi}), 4.03-4.08 (m, 1H, CH_2), 4.14 (d, 1H, $^3J_{H-H}$ = 16.0 Hz, CH_2COO), 4.21-4.24 (m, 1H, CH_2), 4.25-4.31 (m, 2H, CH_2CONH), 6.72 (d, 2H, $^3J_{H-H}$ = 8.50 Hz, H_{Ar}), 6.92 (d, 1H, $^3J_{H-H}$ = 16.0 Hz, CH=C*H*), 7.05 (d, 1H, $^3J_{H-H}$ = 16.0 Hz, C*H*=CH), 7.39-7.41 (m, 3H, H_{Ar}), 7.43 (d, 1H, $^3J_{H-H}$ = 1.50 Hz, H_{imi}), 7.49 (d, 2H, $^3J_{H-H}$ = 9.00 Hz, H_{Ar}), 7.57 (d, 2H, $^3J_{H-H}$ = 8.50 Hz, H_{Ar}), 10.3 (s, 1H, N*H*). ^{13}C NMR (125 MHz, DMSO-*d*$_6$): δ (ppm) 39.0 CH_{3imi}, 39.5-40.5 $CH_{3stilbene}$, 47.1 CH_2CH_2, 59.8 CH_2CH_2, 65.1 CH_2COO, 69.4 CH_2COO, 112.7 C_{Ar}, 120.1 C_{Ar}, 123.1 C_{imi}, 123.2 C_{imi}, 123.6 *C*H=CH, 125.6 C_{Arq}, 126.7 C_{Ar}, 127.8 C_{Ar}, 128.2 CH=*C*H, 134.0 C_q, 137.4 C_q, 150.4 C_q, 166.5 *C*ONH, 178.5 *C*OO, 180.2 N*C*N, 196.2 Re-*C*O, 197.4 Re-*C*O, 197.7 Re-*C*O. HRESI-MS$^+$ (*CH_3OH*): $[C_{29}H_{31}N_5O_6ReNa]^+$ *m/z* = 754.1590, calcd = 754.1651.

2.5. References

1. Wiratpruk, N.; Noor, A.; McLean, C. A.; Donnelly, P. S.; Barnard, P. J., *Dalton Trans.* **2020,** *49* (14), 4559-4569.
2. Moya-Alvarado, G.; Gershoni-Emek, N.; Perlson, E.; Bronfman, F. C., *Mol. Cell. Proteom.* **2016,** *15* (2), 409-425.
3. Mattson, M. P., *Nature* **2004,** *430*, 631.

4. Brier, M. R.; Gordon, B.; Friedrichsen, K.; McCarthy, J.; Stern, A.; Christensen, J.; Owen, C.; Aldea, P.; Su, Y.; Hassenstab, J.; Cairns, N. J.; Holtzman, D. M.; Fagan, A. M.; Morris, J. C.; Benzinger, T. L. S.; Ances, B. M., *Sci. Transl. Med.* **2016,** *8* (338), 338ra66-338ra66.

5. Pimlott, S. L.; Sutherland, A., *Chem. Soc. Rev.* **2011,** *40* (1), 149-162.

6. Wadas, T. J.; Wong, E. H.; Weisman, G. R.; Anderson, C. J., *Chem. Rev.* **2010,** *110* (5), 2858-2902.

7. Arora, A.; Bhagat, N., *Int. J. Biomed. Imaging* **2016,** *2016*, 7462014.

8. Kung, M. P.; Hou, C.; Zhuang, Z. P.; Skovronsky, D.; Kung, H. F., *Brain Res.* **2004,** *1025* (1-2), 98-105.

9. Wang, X.; Cui, M.; Yu, P.; Li, Z.; Yang, Y.; Jia, H.; Liu, B., *Bioorg. Med. Chem. Lett.* **2012,** *22* (13), 4327-4331.

10. Bartholomä, M. D.; Louie, A. S.; Valliant, J. F.; Zubieta, J., *Chem. Rev.* **2010,** *110* (5), 2903-2920.

11. Kiritsis, C.; Mavroidi, B.; Shegani, A.; Palamaris, L.; Loudos, G.; Sagnou, M.; Pirmettis, I.; Papadopoulos, M.; Pelecanou, M., *ACS Med. Chem. Lett.* **2017,** *8* (10), 1089-1092.

12. Chen, C. J.; Bando, K.; Ashino, H.; Taguchi, K.; Shiraishi, H.; Shima, K.; Fujimoto, O.; Kitamura, C.; Matsushima, S.; Uchida, K.; Nakahara, Y.; Kasahara, H.; Minamizawa, T.; Jiang, C.; Zhang, M. R.; Ono, M.; Tokunaga, M.; Suhara, T.; Higuchi, M.; Yamada, K.; Ji, B., *J. Nucl. Med* **2015,** *56* (1), 120-6.

13. Ono, M.; Saji, H., *MedChemComm* **2015,** *6* (3), 391-402.

14. Díez-González, S.; Marion, N.; Nolan, S. P., *Chem. Rev.* **2009,** *109* (8), 3612-3676.

15. Visbal, R.; Gimeno, M. C., *Chem. Soc. Rev.* **2014,** *43* (10), 3551-3574.

16. Mercs, L.; Albrecht, M., *Chem. Soc. Rev.* **2010,** *39* (6), 1903-1912.

17. Chan, C. Y.; Pellegrini, P. A.; Greguric, I.; Barnard, P. J., *Inorg. Chem.* **2014,** *53* (20), 10862-10873.

18. Chan, C. Y.; Barnard, P. J., *Dalton Trans.* **2015,** *44* (44), 19126-19140.

19. Xue, W.-M.; Chan, M. C.-W.; Su, Z.-M.; Cheung, K.-K.; Liu, S.-T.; Che, C.-M., *Organomet.* **1998,** *17* (8), 1622-1630.

20. Li, X.-W.; Li, H.-Y.; Wang, G.-F.; Chen, F.; Li, Y.-Z.; Chen, X.-T.; Zheng, Y.-X.; Xue, Z.-L., *Organomet.* **2012,** *31* (10), 3829-3835.

21. Wang, G.-F.; Liu, Y.-Z.; Chen, X.-T.; Zheng, Y.-X.; Xue, Z.-L., *Inorg. Chim. Acta* **2013,** *394* (Supplement C), 488-493.

22. Chan, C. Y.; Noor, A.; McLean, C. A.; Donnelly, P. S.; Barnard, P. J., *Chem. Commun.* **2017,** *53* (15), 2311-2314.

23. Chow, B. W.; Gu, C., *Trends Neurosci.* **2015,** *38* (10), 598-608.

24. Wang, H. M. J.; Lin, I. J. B., *Organomet.* **1998,** *17* (5), 972-975.

25. Lin, I. J. B.; Vasam, C. S., *Comments Inorg. Chem.* **2004,** *25* (3-4), 75-129.

26. Simpson, P. V.; Skelton, B. W.; Raiteri, P.; Massi, M., *New J. Chem.* **2016,** *40* (7), 5797-5807.

27. Chen, C.-h.; Liu, Y.-h.; Peng, S.-m.; Chen, J.-t.; Liu, S.-t., *Dalton Trans.* **2012,** *41* (9), 2747-2754.

28. Canella, D.; Hock, S. J.; Hiltner, O.; Herdtweck, E.; Herrmann, W. A.; Kühn, F. E., *Dalton Trans.* **2012,** *41* (7), 2110-2121.

29. Hiltner, O.; Boch, F. J.; Brewitz, L.; Härter, P.; Drees, M.; Herdtweck, E.; Herrmann, W. A.; Kühn, F. E., *Eur. J. Inorg. Chem.* **2010,** (33), 5284-5293.

30. Liu, C.-Y.; Chen, D.-Y.; Lee, G.-H.; Peng, S.-M.; Liu, S.-T., *Organomet.* **1996,** *15* (3), 1055-1061.

31. Banks, W. A., *BMC Neurol.* **2009,** *9* (1), S3.

32. Vieira, N. S. M.; Bastos, J. C.; Rebelo, L. P. N.; Matias, A.; Araújo, J. M. M.; Pereiro, A. B., *Chemosphere* **2019,** *216*, 576-586.

33. Hansch, C.; Björkroth, J. P.; Leo, A., *J. Pharm. Sci.* **1987,** *76* (9), 663-687.

34. Klunk, W. E.; Wang, Y.; Huang, G.-f.; Debnath, M. L.; Holt, D. P.; Mathis, C. A., *Life Sci.* **2001,** *69* (13), 1471-1484.

35. Klunk, W. E.; Bacskai, B. J.; Mathis, C. A.; Kajdasz, S. T.; McLellan, M. E.; Frosch, M. P.; Debnath, M. L.; Holt, D. P.; Wang, Y.; Hyman, B. T., *J. Neuropathol. Exp. Neurol.* **2002,** *61* (9), 797-805.

36. Skeby, K. K.; Sørensen, J.; Schiøtt, B., *J. Am. Chem. Soc.* **2013,** *135* (40), 15114-15128.

37. Li, Q.; Min, J.; Ahn, Y.-H.; Namm, J.; Kim, E. M.; Lui, R.; Kim, H. Y.; Ji, Y.; Wu, H.; Wisniewski, T.; Chang, Y.-T., *ChemBioChem* **2007,** *8* (14), 1679-1687.

38. Hudson, S. A.; Ecroyd, H.; Kee, T. W.; Carver, J. A., *FEBS J.* **2009,** *276* (20), 5960-5972.

39. Xue, C.; Lin, T. Y.; Chang, D.; Guo, Z., *R. Soc. Open Sci.* **2017,** *4* (1), 160696-160696.

40. Noor, A.; Hayne, D. J.; Lim, S.; Van Zuylekom, J. K.; Cullinane, C.; Roselt, P. D.; McLean, C. A.; White, J. M.; Donnelly, P. S., *Inorg. Chem.* **2020,** *59* (16), 11658-11669.

41. Dolomanov, O. V.; Bourhis, L. J.; Gildea, R. J.; Howard, J. A. K.; Puschmann, H., *J. Appl. Crystallogr.* **2009,** *42* (2), 339-341.

42. Sheldrick, G., *Acta Crystallogr., Sect. A: Found. Crystallogr.* **2008,** *64* (1), 112-122.

43. Liu, B.; Liu, X.; Chen, C.; Chen, C.; Chen, W., *Organomet.* **2011,** *31* (1), 282-288.

44. Racane, L.; Stojkovic, R.; Tralic-Kulenovic, V.; Karminski-Zamola, G., *Molecules* **2006,** *11* (5), 325.

45. Gao, F.; Zhong, X.; Wang, Q.; Li, H.; Zhang, S., *Chin. J. Chem.* **2010,** *28* (7), 1057-1068.

46. Hemelaere, R.; Desroches, J.; Paquin, J.-F., *Org. Lett.* **2015,** *17* (7), 1770-1773.

47. INC., M. 2001.

Chapter 3 : Anticancer properties of Rhenium(I) Tricarbonyl Complexes of *N*-Heterocyclic Carbene Ligands

3.1. Introduction

Since their discovery, platinum-based medicines including cisplatin, carboplatin, and oxaliplatin continue to be frontline anticancer agents used in chemotherapy. Unfortunately, patients treated with platinum-based drugs commonly suffer from severe side-effects resulting from poor specificity and systemic toxicities associated with these compounds.[1] Due to the limitation of platinum anticancer drugs, much recent attention has focussed on the discovery of alternative metal-based anticancer compounds[2] and a range of metals have been explored including ruthenium,[3-4] silver,[5-6] gold,[7-8] and rhenium.[9-10]

Several studies have demonstrated the promising anticancer properties of complexes based on the $[Re(CO)_3]^+$ core and these compounds have been shown to operate via a similar mechanism to cisplatin.[11-13] For example, a Re(I) complex of the nucleobase guanine **1.57** (Figure 3.1) was prepared and the metal centre was bound to position N7 of the guanine molecule in a similar manner to the adduct formed when cisplatin binds to DNA.[11] The electronic properties of complex **1.57** were evaluated and these data showed that guanine displayed good π-donating properties, which contributed to the formation of a stable bond with the π-accepting $[Re(CO)_3]^+$ core.[11] In a related study, Alberto and co-workers investigated the chemistry of the *fac*-$[M(CO)_3]^+$ moiety (M = Re, ^{99m}Tc) with several nucleotides including 9-methylguanine, guanosine and 2-deoxyguanosine,[12,14] and they found that the metal bound to the N7 position of two guanines ligands e.g. **1.58** (Figure 3.1).[12,15] The rate constants for the formation of the Re(I) guanine nucleobase complexes were measured using ^{1}H NMR studies and were found to be similar in

magnitude to cisplatin, suggesting the potential of Re(I) and ^{99m}Tc(I)- based complexes to act as potential chemotherapeutic and radiotherapeutic agents.[12,16]

Rhenium is routinely used as a non-radioactive congener of Tc, and on this basis ^{99m}Tc analogue of Re-based chemotherapeutic agents can be prepared for single photon emission computed tomography (SPECT) imaging studies.[17-18] Imaging can be used to monitor drug uptake, clearance rates and side effects, which can be very useful during preclinical drug development studies.[19] A series of Re(I) polypyridyl complexes with an labile axial aqua ligand were prepared (e.g. **1.63**, Figure 3.1) and evaluated as anticancer compounds.[20] Complex **1.63** was the most potent compound out of seven complexes synthesised and this molecule was active against the cisplatin resistant cancer cell line KBCP20. In addition, *in vitro* assays showed that **1.63** induced cell death without producing reactive oxygen species and imaging studies using the ^{99m}Tc analogue in mice indicated that the compound was excreted via hepatic and renal pathways.[20]

N-heterocyclic carbene (NHC) ligands have gained much attention in metallodrug design because of their strong σ-donor properties, high chemical and thermal stability of the metal complexes that these ligands often produce.[21] Rhenium complexes of NHC ligands have been the focus of several recent studies as potential anticancer agents. Massi and co-workers have evaluated the cytotoxicity of a range of Re(I) complexes of NHC ligands, (e.g. **1.70** and **1.71**, Figure 3.1),[22] and structure-activity relationships (SAR) derived from this work has demonstrated that the cytotoxic activity was correlated with the nature of the labile monodentate ancillary ligand.[22] The Barnard group has also previously reported the synthesis and studies of Re(I) complexes of bidentate NHC ligands and measured the rate constants for exchanging of the labile axial chloride ligand with acetonitrile using ^{1}H NMR spectroscopic studies.[23-24] Interestingly, the same group has also shown that the $[Re(CO)_3]^+$ core forms relatively stable complexes with monodentate oxygen donor ligands such as benzoate and toluenesulfonate in combination with NHC ligands.[23-24]

More recently, tridentate NHC-based acyclic and macrocyclic ligand systems have been prepared that form highly stable complexes with the $[Re(CO)_3]^+$ core.[23,25]

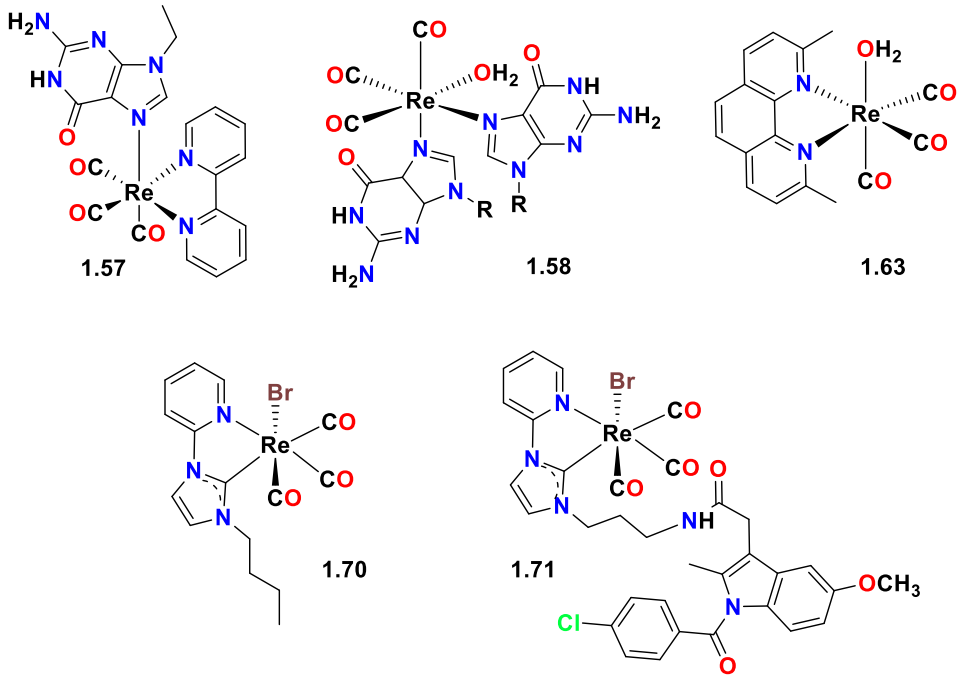

Figure 3.1. Selected examples of medically important $[Re(CO)_3]^+$ complexes **1.57**, Re(I) *bis*-guanine complex **1.58**, Re(I) tricarbonyl aqua complex **1.63**, Re-NHC complex **1.70** and Re-NHC complex coupled to indomethacin **1.71**.

Given the recent interest in the anticancer properties of $[Re(CO)_3]^+$ complexes of NHC ligands, this chapter reports the synthesis and characterisation for a series of Re(I) complexes of pyridyl-imidazolylidene and *bis*-imidazolylidene ligands coordinating to labile *N*-acetyl amino acids. Additionally, the ligand exchange rates, together with the computational studies, photophysical properties and cytotoxicity activities of these Re(I) complexes, have been investigated.

3.2. Results and Discussion

3.2.1. Complex synthesis

The *N*-acetyl amino acid substituted complexes **3.7-3.14** (Scheme 3.1) were prepared by treating complexes **3.1** and **3.2** with either silver acetate (**3.3)** or the silver salts of the *N*-acetylated amino acids glycine, isoleucine and proline (**3.4-3.6)**. The precursor complexes **3.1** and **3.2** (Scheme 3.1) were prepared as previously described using a silver trans-metalation reaction between $Re(CO)_5Cl$ and the imidazolium salt NHC ligand precursors,[24] while the silver salts of the deprotonated *N*-acetyl amino acids were prepared by treating the *N*-acetyl amino acids with silver oxide in acetonitrile.

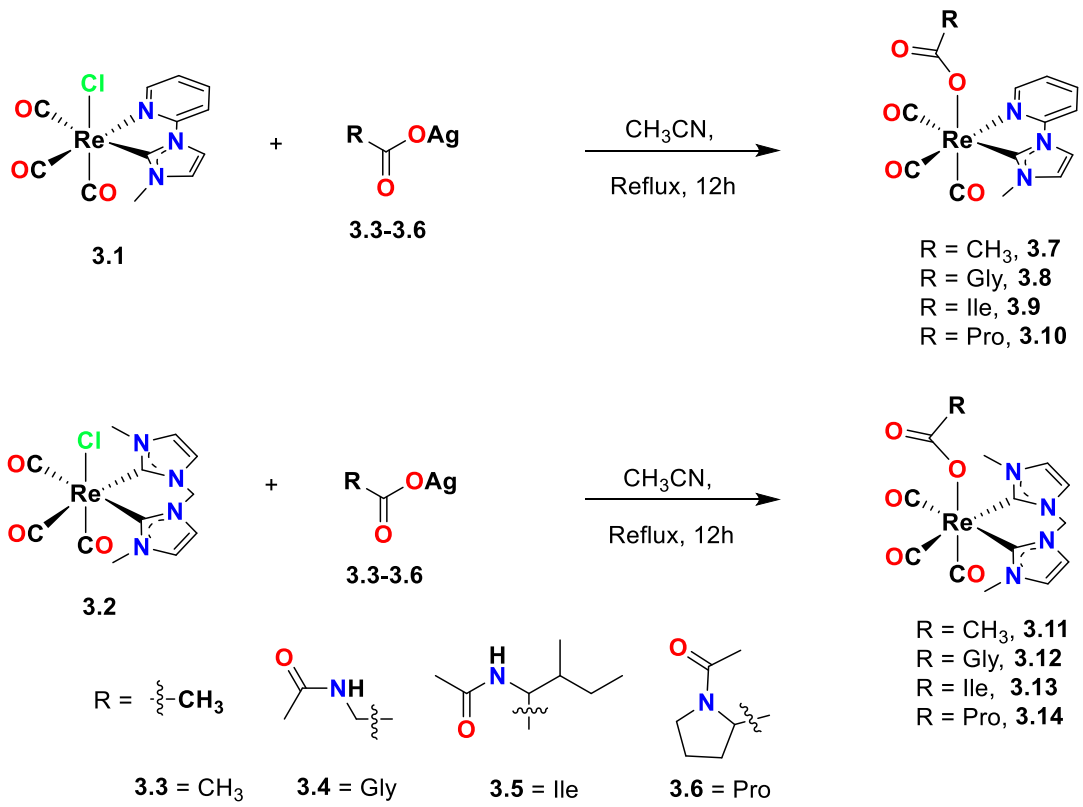

Scheme 3.1. Synthesis of Re(I) complexes **3.7-3.14** of the *N*-acetyl amino acids glycine, isoleucine and proline.

Complexes **3.8-3.10** and **3.12-3.14** were purified via column chromatography on silica and obtained in moderate to good yields, while complexes **3.7** and **3.11** were purified by

recrystallisation in methanol. The compounds were characterised by IR, ^{1}H and ^{13}C NMR spectroscopy, and high-resolution mass spectrometry (HRMS). In each case, the IR spectra for complexes **3.8**-**3.10** and **3.12**-**3.14** show three sharp carbonyl stretching absorption bands, with the frequencies (Table 3.1) being consistent with those reported previously for related compounds.[26] These results are consistent with the CO ligands being coordinated to the Re(I) metal centre in a facial arrangement, where two CO ligands are bound *trans* to the NHC, pyridine and carboxylate ligands for compounds **3.8**-**3.10**, while for **3.12**-**3.14** the CO ligands are *trans* to the *bis*-imidazolylidene ligand, and the last CO ligand is occupying the site *trans* to the carboxylate group of the amino acid.

Table 3.1. The CO stretching frequencies (cm^{-1}) for complexes **3.8**-**3.10** and **3.12**-**3.14**.

Complex	Frequencies (cm^{-1})
3.8	2012 vs, 1907 s, 1859 s
3.9	2019 vs, 1923 s, 1890 s
3.10	2021 vs, 1925 s, 1892 s
3.12	2010 vs, 1909 s, 1863 s
3.13	2006 vs, 1906 s, 1865 s
3.14	2007 vs, 1907 s, 1869 s

*Solution in chloroform

The ^{13}C NMR spectra of the Re(I) amino acid complexes (**3.8**-**3.14**) show characteristic downfield shifted ^{13}C signals in the region of 199-200 ppm for the carbonyl ligands in addition to a signal for the coordinated carbene group, which resonated within the range of 174-179 ppm. The complexes of the achiral amino acid, *N*-acetyl glycine (**3.8** and **3.12**) gave relatively simple ^{1}H and ^{13}C NMR spectra. In contrast, the complexes of the chiral amino acids (L-isoleucine and L-proline) **3.9**-**3.10** and **3.13**-**3.14** have three or two chiral centres, respectively and can exist in multiple stereoisomeric forms, as a result of this, the ^{1}H and ^{13}C NMR spectra for these compounds are considerably more complex.

A schematic example of two possible stereoisomeric forms of complex **3.9** is shown in Figure 3.2. For this compound L-*N*-acetyl isoleucine is coordinated as the axial ligand, and this amino acid contains two stereocenters (α-carbon and chiral sidechain). As only naturally occurring L-isoleucine was used, only one diastereomeric form of this ligand is present with the configuration (2S,3S). In contrast, a racemic mixture of the precursor complex **3.1** was used, where the Re(I) metal is also a stereogenic centre, (here the three facial carbonyl ligands can be considered to be one unit, giving rises to a pseudo-tetrahedral geometry). As such, two isomeric forms of complex **3.9** are possible (Figure 3.2).

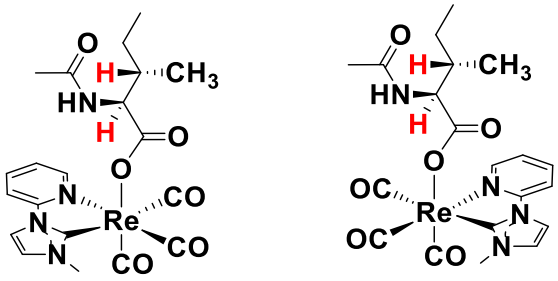

Figure 3.2. Diagram showing the diastereomeric forms of the chiral complex **3.9**.

^{1}H NMR analysis shows that the Re(I) complex of the achiral *N*-acetyl glycine ligand (**3.8**, Figure 3.3a) exhibits a relatively simple spectrum, with only one signal observed for each aromatic proton as well as the wingtip group of the pyridyl-imidazolylidene unit. In contrast, the ^{1}H NMR spectra of Re(I) complex of the chiral amino acids, *N*-acetyl L-isoleucine and *N*-acetyl L-proline **3.9** and **3.10**, show two distinctive peaks for each magnetically inequivalent proton in the complex. This result is consistent with NMR results for previously reported transition metal complexes with amino acid derivatives.[27-29] For complex **3.9**, two peaks at 8.82 ppm and 8.89 ppm (Figure 3.3b) represent a pyridyl proton of the pyridyl-imidazolylidene ligand, confirming the presence of diastereomers. The ratio of two diastereomers can be calculated from the integration of two signals for this proton, and the ratios were found to be 54:45 and 87:13 for complex **3.9** and **3.10**,

respectively. A plausible explanation for the unequal populations of two diastereomers is that one of the diastereomeric forms is formed more readily than the other during the synthetic reaction. Although not elucidated at this stage, the different amounts of each diastereomeric form may be the result of kinetic and/or thermodynamic factors. It is apparent that there is a significantly larger difference between the quantities of the diastereomeric form of complex **3.9** compared to complex **3.10**. This result suggests that the cyclic ring of *N*-acetyl proline results in a stronger preference for one diastereomeric form, in contrast to diastereomer *N*-acetyl isoleucine, which appears to have a much smaller impact on the ratio between two diastereomers formed by complex **3.9**.

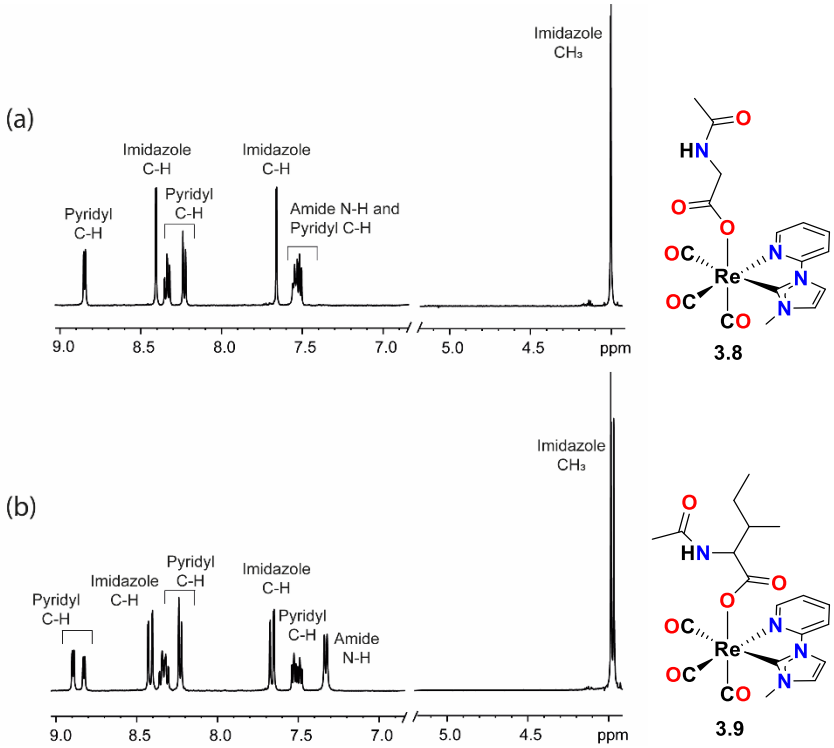

Figure 3.3. ^{1}H NMR spectrum of Re(I) complexes (a) **3.8** and (b) **3.9** in DMSO-d_6.

In the case of Re(I) complexes of *bis*-imidazolylidene ligand (**3.12-3.14**) ligand, re-orientation of the bridging methylene unit between the NHC rings gives rise to conformational isomers once the carbenic carbons are coordinated to the Re(I) centre.[30-31] For these complexes, the bridging methylene group can adopt two different orientations with respect to the equatorial plane, giving rise to two conformational isomeric forms of

these complexes when the axial ligands are different (Figure 3.4).[26] On this basis, the ^{1}H NMR spectrum of Re(I) complex of the achiral amino acid *N*-acetyl glycine **3.12** (Figure 3.5a), shows two doublet signals for the inequivalent protons of the bridging methylene group of the *bis*-imidazolylidene ligand at 6.01 ppm and 6.48 ppm. This result is consistent with the ring-flip exchange process between the isomers being fast on the NMR timescale.

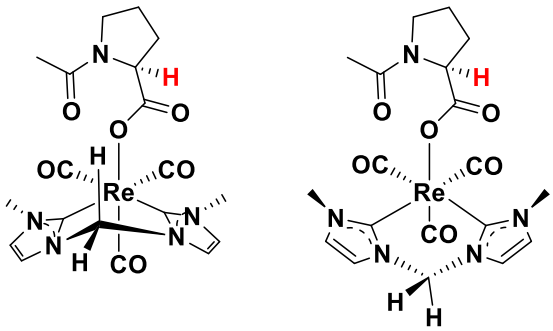

Figure 3.4. The diagram showing the two forms of chiral complex **3.14**.

As was the case for complexes **3.8** and **3.9**, the ^{1}H NMR spectra for the Re(I) complexes of the *bis*-imidazolylidene ligand, in combination with the chiral amino acids *N*-acetyl L-isoleucine and *N*-acetyl L-proline (**3.13** and **3.14**), are significantly more complicated than that obtained for the achiral *N*-acetyl glycine ligand. It is apparent that the chirality of the amino acid ligand, when coordinated to the Re(I) metal centre, gives rise to diastereomeric forms of the complex. For example, the ^{1}H NMR spectrum of Re(I) complex of the chiral *N*-acetyl proline amino acid **3.14** (**Figure 3.5**b) shows two distinct sets of doublet signals for the methylene group protons, 6.04 ppm and 6.49 ppm for a major product and 5.81 ppm and 6.26 ppm for a minor product. This result is consistent with the methylene group protons of the *bis*-imidazolylidene ligand for complexes **3.13** and **3.14** being diastereotopic due to the two possible geometric isomeric forms of the Re(I) complex in combination with the chiral centres of the amino acid ligand. The ratio

of two diastereomers can be calculated from the integration of two signals for this proton, and the ratios were found to be 88:12 and 61:39 for complex **3.13** and **3.14**, respectively.

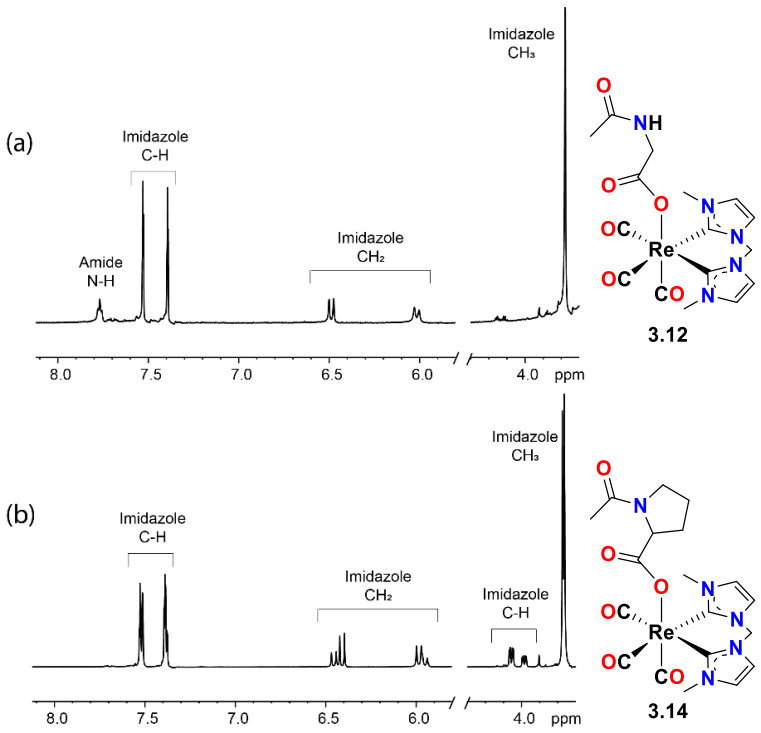

Figure 3.5.^{1}H NMR spectrum of Re(I) complexes of *bis*-imidazolylidene ligand; (a) complex **3.12** and (b) complex **3.14** in DMSO-d_6.

All of the Re(I) complexes with *N*-acetyl amino acid ligand were subjected to HRMS analysis, and in all cases, the positive ion HRMS spectra recorded for these complexes (Figure A3.27-A3.31, Appendix 3) show a peak corresponding to their expected masses. The positive ion HRMS spectrum recorded for complex **3.12** shows four intense signals at 447.0462, 586.0712, 1008.1255, and 1147.1499 (Figure 3.6a). The base peak (*m/z* = 586.0712) corresponds to the sodium adduct of the neutral complex **3.12** (Figure 3.6b, zoom scan and simulated isotopic distribution). The peak at 1008.1255 corresponds to a dimer composed of intact complex **3.12** and its fragment, where *N*-acetyl glycine ligand had been lost (Figure 3.6c, zoom scan and isotopic distribution). Finally, the peak at 1147.1499 corresponds to the sodium of a dimer of two molecules of **3.12** (Figure 3.6d, zoom scan and isotopic distribution).

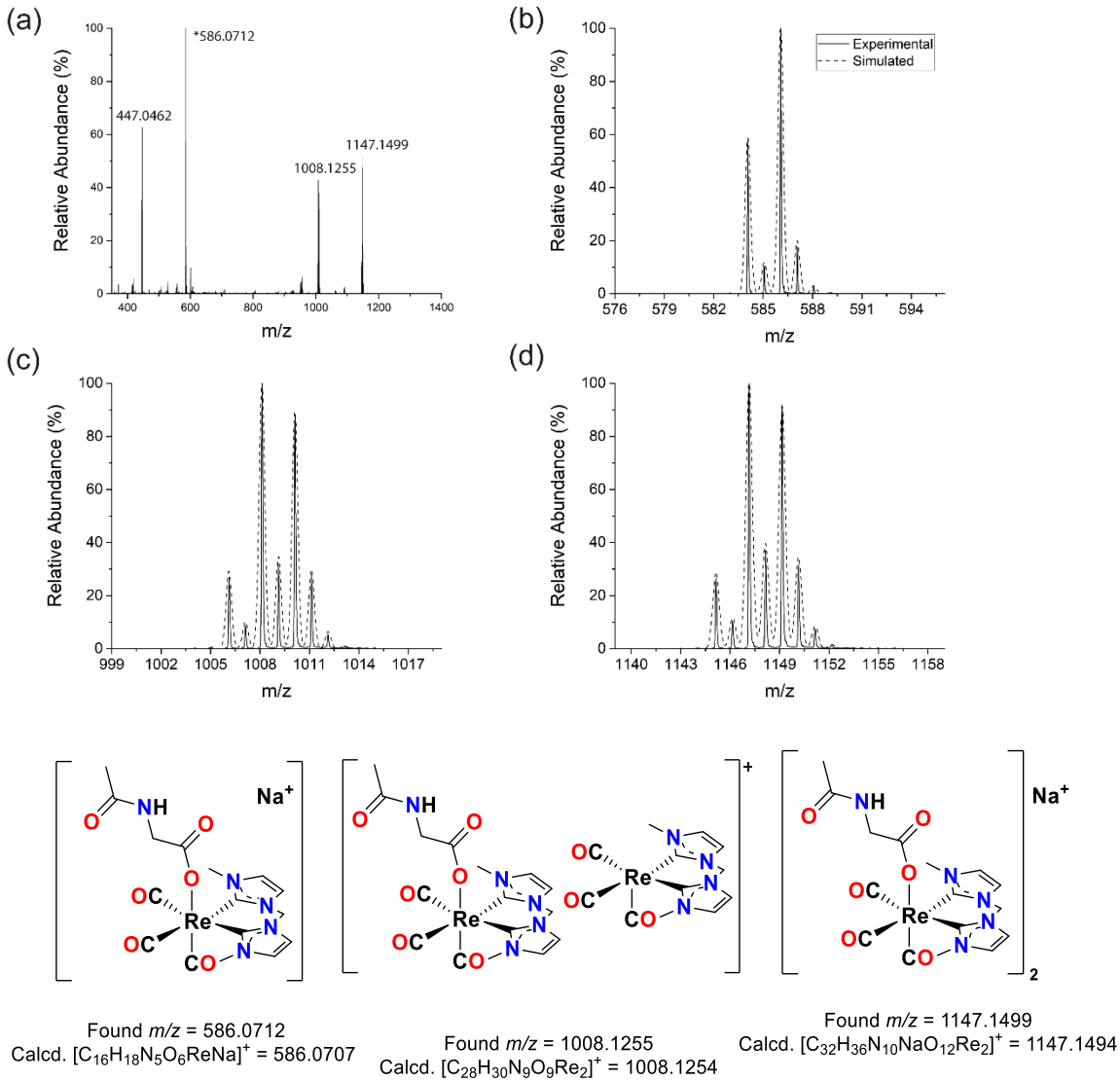

Figure 3.6. (a) HRMS spectrum of a freshly prepared solution of **3.12** in methanol. Each of the main signals from the HRMS spectrum is plotted together with the simulated isotopic distribution: (b) expanded signals at 586.0712, (c) expanded signals at 1008.1255, and (d) expanded signals at 1147.1499. Lower panel, proposed structures of cations corresponding to these masses.

3.2.2. Ligand Exchange Studies

These amino acid substituted complexes are of interest for their potential anticancer properties because it is envisaged that the cytotoxicity mechanism would involve ligand exchange between the labile amino acid ligand and a water molecule, similarly to the chloride exchange process of cisplatin. For the drug cisplatin, the aquation rate (replacement of chloride ligands with water molecules yielding a cationic complex) is known to be critical to its anticancer properties, and it was therefore of interest to determine the aquation rate for the compounds prepared in this chapter.

The ligand exchange rates for a series of Re(I) complexes of NHC ligands have previously determined by Barnard group, where the axial chloride ligand was exchanged with acetonitrile using ^{1}H NMR spectroscopy.[23] In the present study, the reaction of complex **3.12** with water was monitored using ^{1}H NMR spectroscopy (WATERGATE) over a period of 24 h. In this study, the ^{1}H NMR sample was prepared in a mixture of mili Q water (76%), deuterated dimethyl sulfoxide/DMSO-d_6 (20%), and deuterium oxide/D_2O (4%). It is important to note that the nature of co-solvent, including the structure, ionic strength, basicity, and dielectric constant has an influence on the aquation rate.[32] The effect of DMSO as a co-solvent on the aquation rate of $[Co(NH_3)_5Br]^{2+}$ has been previously studied.[33] The results from this study suggested that the aquation rate decreases as the proportion of DMSO in water increases, due to a slight difference in the dielectric constant that stabilised the dissociation of halide ion.[33-34] However, the solvent composition of the co-solvent and water did not significantly change the thermodynamic parameters for the aquation of $[Co(NH_3)_5Br]^{2+}$, indicating that increasing the composition of DMSO has little effect on the transition state of the complex.[33-34] Due to solubility problems, in the present studies, the Re(I) complexes were dissolved in 76% H_2O, 20% DMSO-d_6, and 4% D_2O. Therefore, the aquation rate estimated in this study may have been lower (due to the effect of DMSO), than those in pure water.

The aquation of complexes **3.9**, **3.10** and **3.12-3.14** to give the aqua complexes **3.15** and **3.16** is shown in Scheme 3.2.

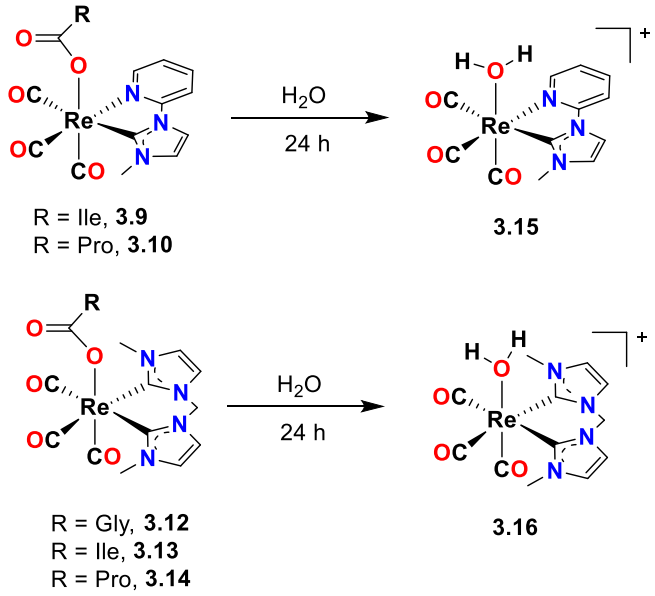

Scheme 3.2. Aquation of complexes **3.9**, **3.10** and **3.12-3.14** to give the aqua complexes **3.15** and **3.16**.

A series of stacked ^{1}H NMR spectra recorded for **3.12** in this time-course experiment are shown in Figure 3.7. The first recorded ^{1}H NMR spectrum (t = 0.25 h) shows an intense set of signals, which corresponds to complex **3.12**, where an *N*-acetyl glycine is bound in the axial position to the Re(I) metal centre (blue asterisks). In the same spectrum, a second weak set of signals is also apparent, which corresponds to the cationic Re(I) complex (**3.16**), where the amino acid ligand has been exchanged with water. As the time-course experiments proceed, the signals corresponding to **3.16** increase in intensity, while the intensity of the signals corresponding to the starting complex **3.12** decreases. After 24 h, the complex **3.16** is the dominant species in solution (red asterisks).

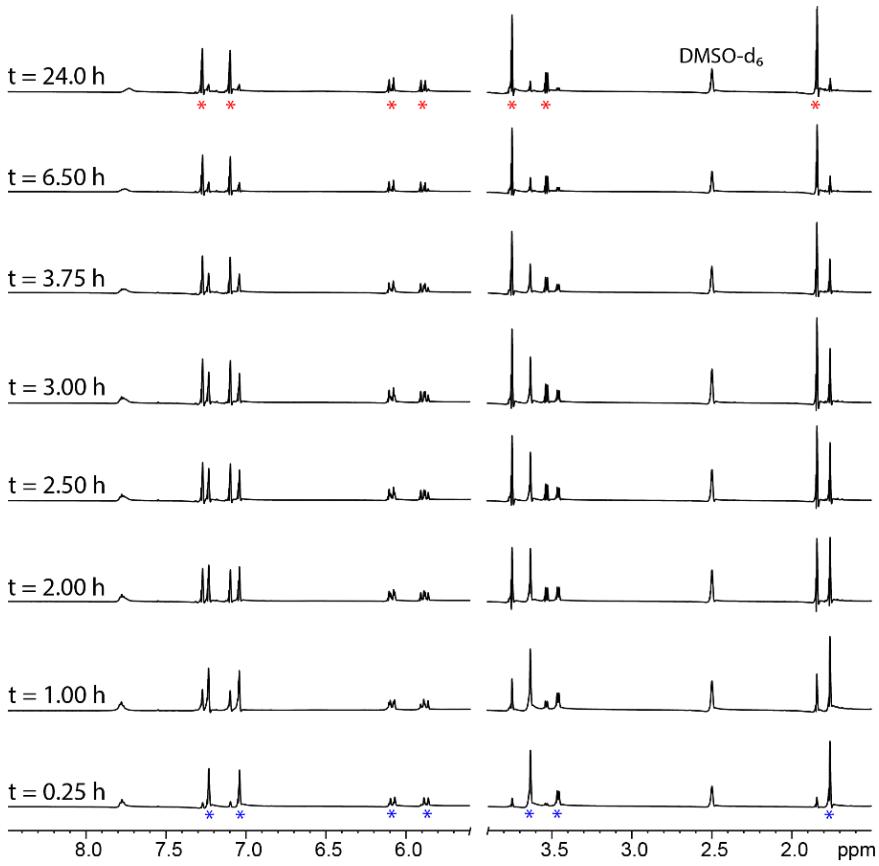

Figure 3.7. ^{1}H NMR spectra (500.13 MHz) recorded for a solution of **3.12** in water over a period of 24 h at 25.0 ± 0.1 °C. The spectra show exchange of the *N*-acetyl glycine ligand for a water molecule.

The sample used in the ^{1}H NMR WATERGATE kinetics study was subsequently subjected to HRMS analysis, and the spectrum is shown in Figure 3.8a. The base peak in this spectrum (*m/z* = 447.0464) corresponds to the cationic 5-coordinate Re(I) complex **3.18** (Figure 3.8). The expected cationic Re(I) aqua adduct was not detected in the mass spectrum, most likely as a result of the water molecule being bound weakly to the 5-coordinate complex **3.18**, leading to fragmentation. Computational studies examining the nature of the bond formed between the water molecule and the $[Re(CO)_3]^+$ core are reported in section 3.2.3. Although the aqua complex was not observed, a peak at 909.0938 corresponds to a dimeric hydroxyl-bridged Re(I) complex (Figure 3.8c) and a weak signal at 927.1024 is corresponded to a dimeric structure (Figure 3.8d), that may

have been formed from a precursor aqua complex, were seen. Taken together, these mass spectral results are consistent with the amino acid ligand being replaced by water in the NMR time course study.

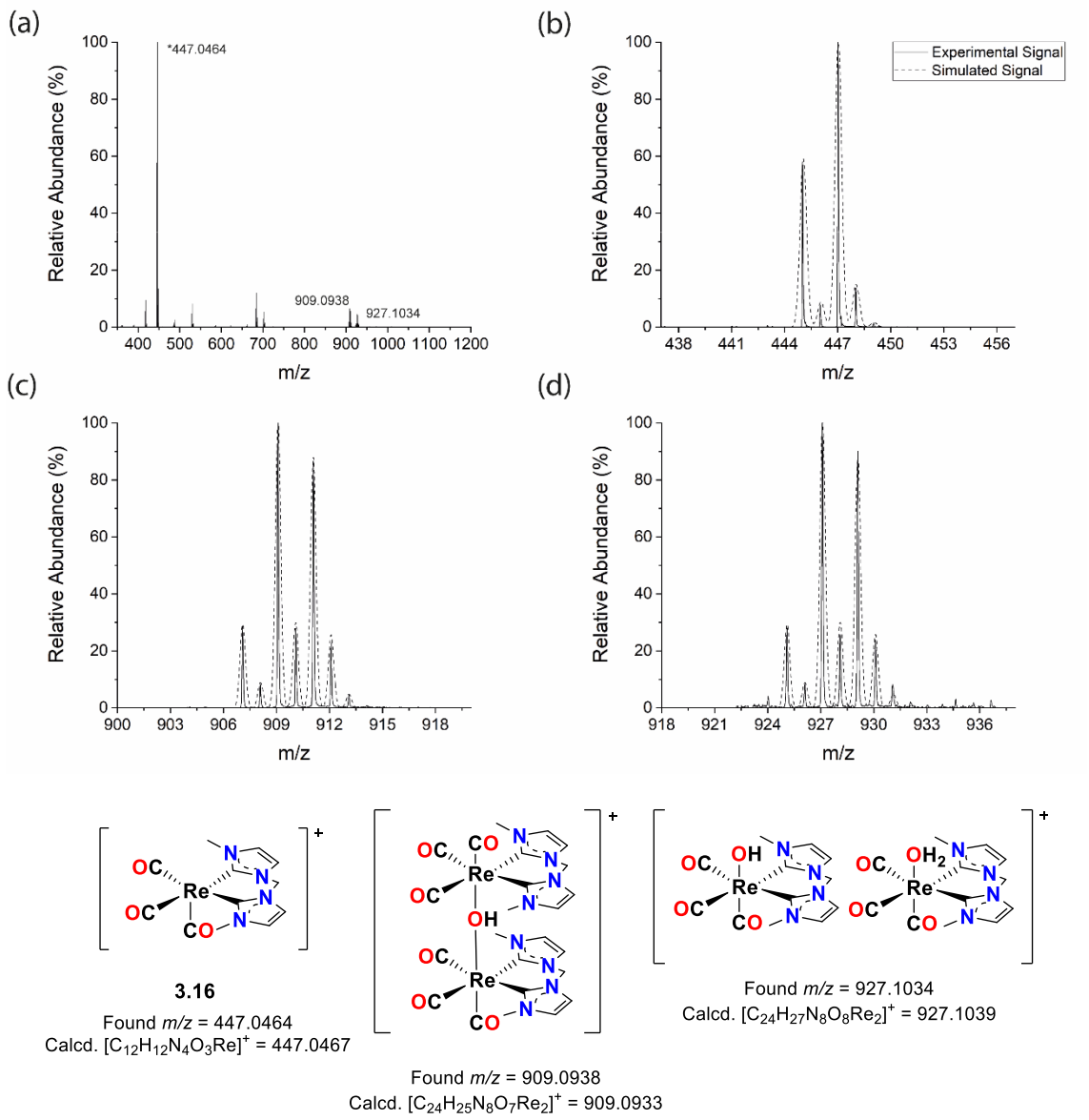

Figure 3.8. (a) High-resolution mass spectrum of compound **3.12** after being subjected to the ^{1}H NMR time course study for 24 h at 25.0 ± 0.1 °C. Zoom scans of the main signals at (b) 447.0464, (c) 909.0938 and (d) 927.1034 are plotted together with the simulated spectra for the formulas $[C_{12}H_{12}N_4O_3Re]^+$ (**3.18**), $[C_{24}H_{25}N_8O_7Re_2]^+$, $[C_{24}H_{27}N_8O_8Re_2]^+$, respectively. The structures of the compounds corresponding to these formulae are shown in the lower panel.

The aquation rate for complex **3.12** was determined by fitting the ^{1}H NMR data to the pseudo-first-order (H_2O in large excess) kinetic model shows in Equation 1.

$$\text{Re-}N\text{-acetyl amino acid} + H_2O \underset{k_{-1}}{\overset{k_1}{\rightleftharpoons}} [\text{Re-}H_2O]^+ + N\text{-acetyl amino acid}^- \quad (H_2O \text{ in large excess}) \tag{1}$$

The estimated forward and reverse rate constants for the aquation of complexes **3.9**-**3.10** and **3.12**-**3.14** are summarised on Table 3.2. These studies show that the aquation rates for Re(I) complexes of the *bis*-imidazolylidene ligand (**3.12-3.14**) are faster compared to the complexes of the pyridyl-imidazolylidene ligands (**3.9-3.10**), and it is apparent that the *cis*-effect influences the aquation rates of these complexes. The classical *cis*-effect is defined as the labilisation of carbonyl (CO) group in the *cis* position of the octahedral complex $M(CO)_5X$, where M is a transition metal and X is the *cis*-CO labilising ligand.[35-37] Additionally, previous studies have shown that the rate constant and bond length for the substitution reaction of CO in the *cis* position largely depends on the nature of electronic and steric properties of the co-ligand.[35-37] In this study, the *N*-acetyl amino acid occupies a *cis*-axial position relative to the mono- or *bis*-carbene ligand, indicating that the electronic (and steric) properties of the carbene ligand influence the aquation rates of these complexes via a *cis* effect. In addition, carbenes such as the NHCs in these complexes are well known for their strong σ-donating properties that enhance the electron density at the metal centre and the strong *trans*-effect they exert.[38-41] Therefore, it is likely that the stronger electron-donating properties of the *bis*-imidazolylidene carbene ligand contribute to a longer Re-O bond length (Table 3.3), thereby influencing the faster substitution of *N*-acetyl amino acid by water molecule for complexes **3.12-3.14** compared to the pyridyl-imidazolylidene ligand **3.9-3.10**.

Table 3.2. Aquation rate constants for the Re(I) amino acid complexes at 25 °C. The error was estimated by Scientist® Version 3.0 program.

Compound	Rate constant	
	k_1 (s^{-1})	k_{-1} (M^{-1} s^{-1})
Cisplatin	$2.37 \times 10^{-5} \pm 0.04$	$4.50 \times 10^{-3} \pm 1.2^{*}$
3.9	$3.50 \times 10^{-5} \pm 0.004$	$7.48 \times 10^{-5} \pm 0.004$
3.10	$2.59 \times 10^{-5} \pm 0.003$	$4.11 \times 10^{-6} \pm 0.003$
3.12	$7.76 \times 10^{-5} \pm 0.044$	$8.85 \times 10^{-6} \pm 0.044$
3.13	$5.96 \times 10^{-5} \pm 0.007$	$9.03 \times 10^{-6} \pm 0.007$
3.14	$4.95 \times 10^{-5} \pm 0.027$	$4.32 \times 10^{-6} \pm 0.027$

*For cisplatin data obtained from reference[42]

3.2.3. Theoretical Studies

In order to gain a deeper understanding of the structures and properties of the Re(I) complexes prepared in this chapter, density functional theory (DFT) calculated structures were obtained at the PBE0-D3BJ/def2-TZVP level of theory, using the Orca 4.2 software package. The theoretical studies in this section were performed by Dr Alex Hamilton from Sheffield Hallam University. The calculated structures of complexes **3.7-3.14** are shown in Figure 3.9, and the bond dissociation energies and the bond length for the Re-O (carboxylate) bonds of these complexes are listed in Table 3.3. The results in Figure 3.9 show that all Re(I) complexes have distorted octahedral geometries, where the three carbonyl groups are bound to the metal centre in a *facial* arrangement. For complexes **3.7-3.10**, the pyridyl-imidazolylidene ligand adopts a relatively planar structure in the equatorial position, and the amino acid derivative is bound to the Re(I) centre in the axial position. Complexes **3.11-3.14** may adopt two possible configurational isomers due to the orientation of the methylene linker of the *bis*-imidazolylidene ligand. The two configurations are shown in structures **3.11-3.14** and **3.11i-3.14i** (Figure 3.9).[30-31] In the case of **3.11-3.14**, the methylene linker is oriented 'up' towards the amino acid ligands,

while for **3.11i-3.14i** the methylene group is oriented in the opposite 'down' direction. These results are consistent with the ^{1}H NMR results described in the section 3.2.1.

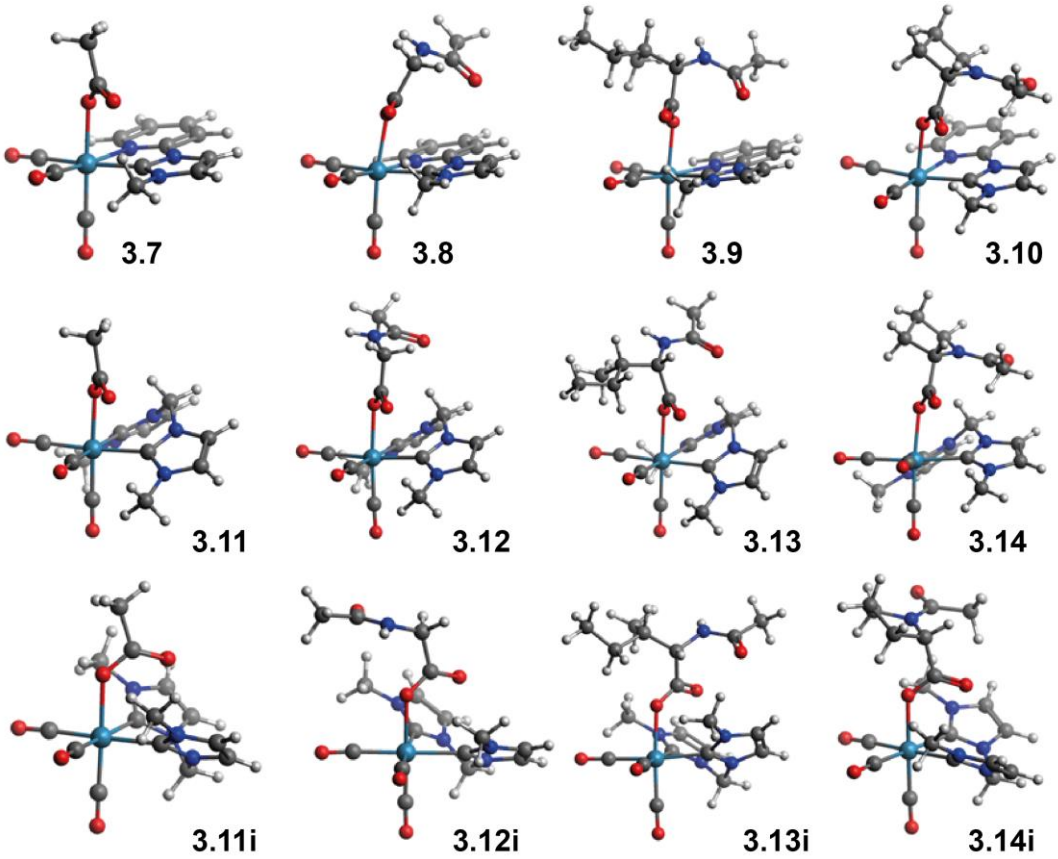

Figure 3.9. Calculated structures for complexes **3.7-3.10, 3.11-3.14** and **3.11i-3.14i**.

The bond dissociation energy (BDE) and bond distance between the amino acid carboxylate group and a Re(I) metal centre are useful parameters for predicting the aquation rate of the Re(I) compounds. As previously discussed in section 3.2.2, the aqua ligand is weakly bound, and this complex is expected to be more reactive with biomolecules, e.g., DNA. The relationship between BDE and bond distance has been extensively studied, and BDE is generally inversely proportional to the bond length.[43] The calculated BDE and bond length for complexes **3.7-3.14** are consistent with this relationship as shown in Table 3.3, where the calculated BDE for complexes **3.7-3.10** is generally higher, and their bond length is shorter than those for complexes **3.11-3.14**.

Table 3.3. Re-O bond dissociation energies (kJ mol^{-1}) and Re-O bond length (Å) for complexes **3.7**-**3.14**.

Complex	BDE (ΔG^{298K}_{solv})	Bond Length
3.7	108.4	2.138
3.8	94.6	2.163
3.9	96.2	2.139
3.10	113.4	2.144
3.11	95.8	2.161
3.12	82.4	2.176
3.13	84.1	2.173
3.14	101.3	2.178
3.11i	91.6	2.163
3.12i	78.2	2.184
3.13i	74.5	2.172
3.14i	100.8	2.176

The possible structures of cationic Re(I) complex **3.15** (Figure A3.32, Appendix 3) and **3.16** (Figure 3.8) identified in the mass spectrometric studies were investigated using density functional theory (DFT) studies. These complexes are 5-coordinate with a vacant site where the amino acid was bound, and the results from DFT studies suggest that they are the most stable structure for both of the Re(I) complexes of pyridyl-imidazolylidene (**3.17**) ligand and *bis*-imidazolylidene (**3.18**) with a relative energy of 0.00 kJ mol^{-1} (Figure 3.10). The diastereomeric forms of the Re(I) *bis*-imidazolylidene ligand (**3.18** and **3.18i**) have a relative energy difference of 0.75 kJ mol^{-1}, where **3.18** is the most stable form. This result is consistent with the gas phase BDE because Re(I) complex where the methylene linker is oriented "up" towards the water ligand (**3.16**) is more favourable with the BDE of 62.8 kJ mol^{-1}, while the structure where the methylene linker is oriented "down" towards the axial carbonyl ligand (**3.16i**) has a lower BDE value (53.6 kJ mol^{-1}). Additionally, the gas phase BDE for **3.15** is 67.4 kJ mol^{-1}, which is similar to the result

for the Re(I) complex **3.16**. These results suggest that the coordinate bond between Re(I) metal centre and a water molecule is relatively weak compared to other metals. For example, the calculated bond dissociations of the water molecule for Pt(II) and Pd(II) metal centre are 82.1 and 72.5 kJ mol^{-1}, respectively.[44]

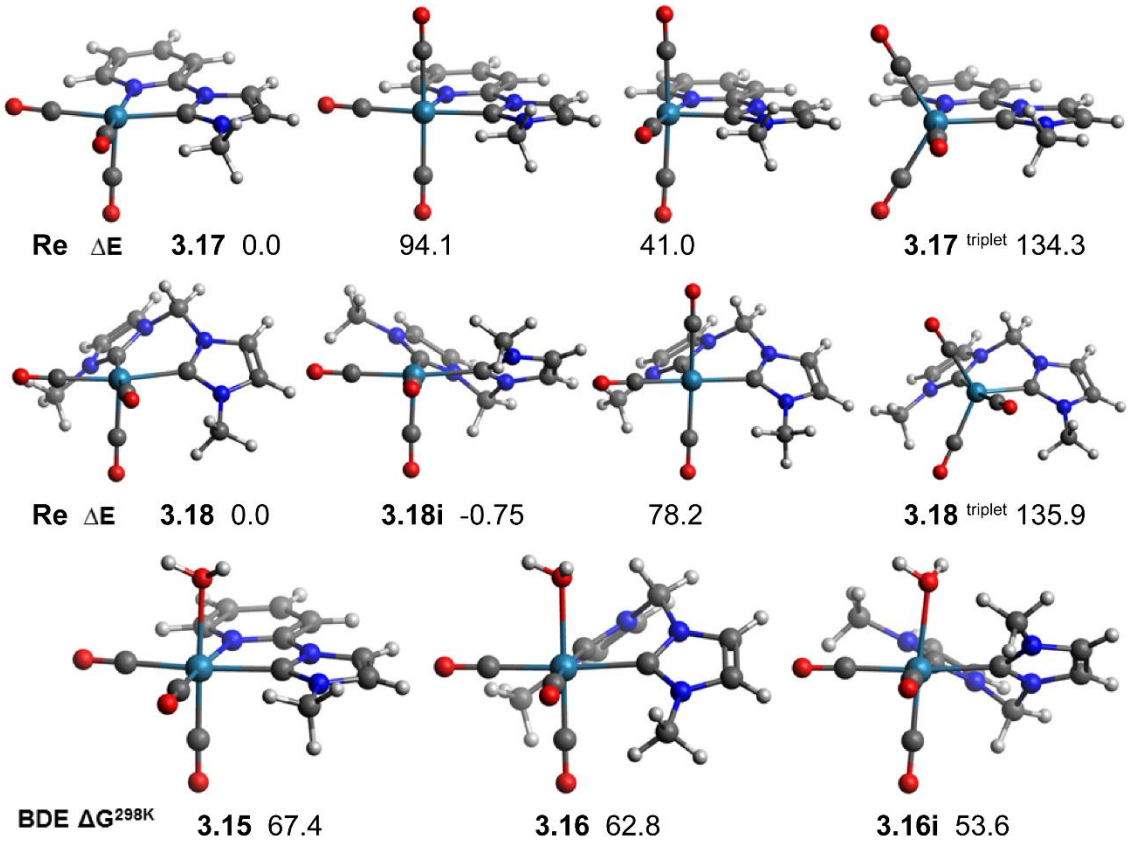

Figure 3.10. DFT calculated geometries, relative energies (Re ΔE kJ mol^{-1}) and gas phase bond dissociation free energies (BDE ΔG^{298K} kJ mol^{-1}) for the cationic complexes **3.15** and **3.16**.

3.2.4. Photophysical Studies

Due to the well-known luminescence properties of Re(I) complexes of NHC ligands, the photophysical properties of Re(I) complexes prepared here were investigated.[45-47] The UV-Vis spectra for the precursor complexes **3.1** and **3.2**, the Re(I) pyridyl-imidazolylidene complexes **3.9** and **3.10** and Re(I) *bis*-imidazolylidene **3.13** and **3.14** are

shown in (Figure 3.11). For Re(I) pyridyl-imidazolylidene complexes (**3.1**, **3.9** and **3.10**), strong absorption bands are observed at ~275 nm and ~340 nm. These results are similar to the data previously reported for related compounds, where the low energy absorption band (320-460 nm) has been assigned to the metal-to-ligand charge transfer (^{1}MLCT) transitions (dπ(Re) → π* (pyridyl-imidazolium ligand)).[45,47-49] The absorption band at higher energy (250-320 nm) corresponds to intraligand π → π* transitions (pyridyl-imidazolium ligand).[45,47-49] In comparison, the Re(I) *bis*-imidazolylidene complexes (**3.2**, **3.13** and **3.14**) display an intense absorption band at ~320 nm, which may be tentatively assigned to dπ(Re) → π* transitions. These complexes also display a weak shoulder at ~350 nm.

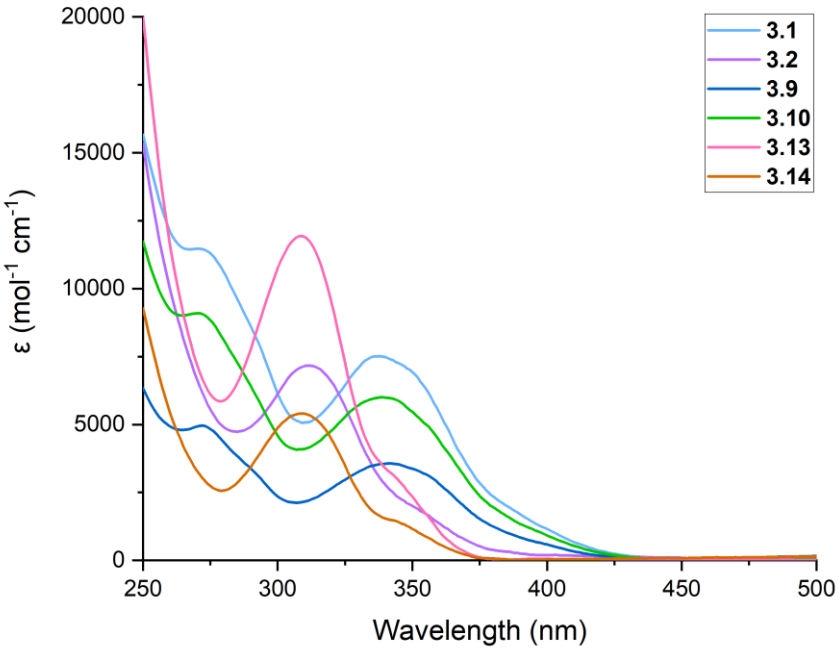

Figure 3.11. UV-Vis spectra of Re(I) complexes **3.1** (blue), **3.2** (purple), **3.9** (indigo), **3.10** (green), **3.13** (pink) and **3.14** (orange). All spectra were recorded at the concentration of 10 µM in methanol solutions.

All of the evaluated Re(I) complexes were luminescent and the emission spectra of Re(I) starting materials (**3.1**-**3.2**, Figure 3.12) and the Re(I) complexes of the pyridyl-

imidazolylidene ligands (**3.9** and **3.10**, Figure 3.13**)** and the *bis*-imidazolylidene ligands (**3.13** and **3.14**, Figure 3.12) were recorded.

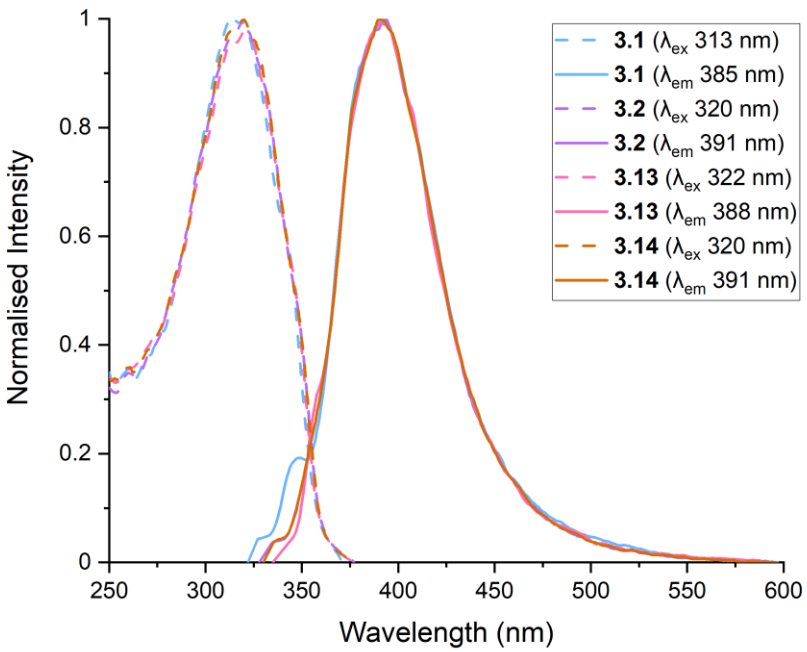

Figure 3.12. Emission spectra for complexes **3.1**, **3.2**, **3.13** and **3.14**. The complexes were recorded at 10 µM in methanol solution.

When using the excitation wavelengths between 313-320 nm, complexes **3.1**, **3.2**, **3.13** and **3.14** gave the emission between 380-390 nm (Figure 3.12). Interestingly, complex **3.9** and **3.10** display dual emission bands at ~390 nm and ~500 nm and the intensity of these bands are dependent on the excitation wavelength used (Figure 3.13). For example, complex **3.10** has a strong emission at 393 nm when excited at 316 nm; however, when the complex is excited at 339 nm, a weaker emission at 500 nm is observed. The dual emission properties of Re(I) complexes of pyridyl-imidazolylidene ligands have been previously reported, and the emission at ~380 nm wavelength has been assigned to a singlet ^{1}MLCT (dπ(Re) → π* (pyridyl-imidazolium ligand) transition.[46,49-50] Additionally, a small band at ~500 nm is typical of a long-lived ^{3}MLCT (dπ(Re) → π*

(pyridyl-imidazolium ligand)) transition.[50] Rhenium is a heavy atom, and the presence of this metal can increase the spin-orbit coupling that can lead to the intersystem crossing.[50] Once the pyridyl-imidazolium ligand is bound to the Re(I) centre, and it promotes the population of a ^{3}MLCT (dπ(Re) → π* (pyridyl-imidazolium ligand) from the emissive ^{1}MLCT (dπ(Re) → π* (pyridyl-imidazolium ligand) excited state. As a result, a small band corresponds to the ^{3}MLCT phosphorescence can be observed at ~500 nm.[50]

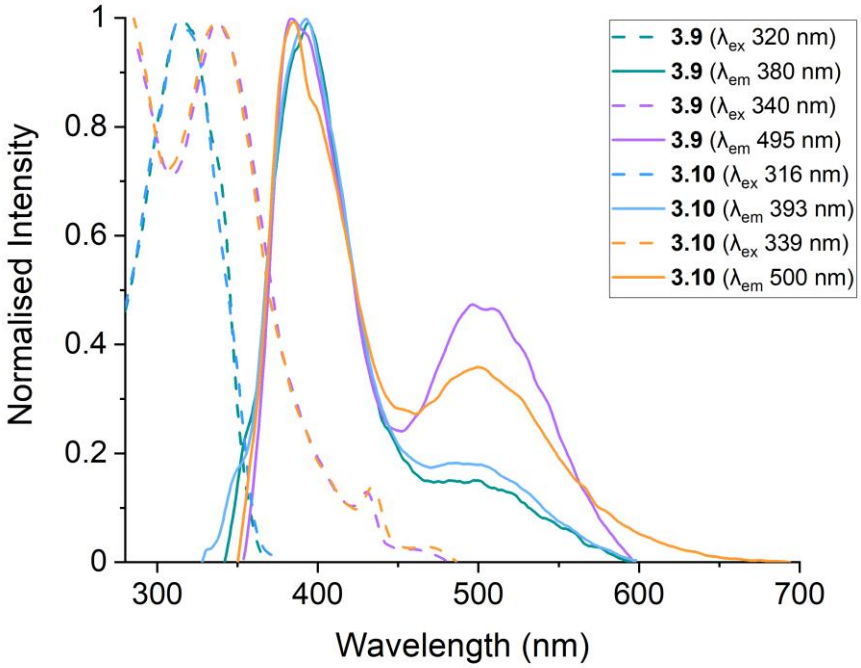

Figure 3.13. Excitation and emission spectra for complexes **3.9** and **3.10**. The complexes were recorded at 10 µM in methanol solution.

3.2.5. Cytotoxicity Studies

The cytotoxic properties of the Re(I) complexes against selected cancer cell lines were investigated using the MTT assay. Re(I) complexes **3.9**, **3.10**, **3.13** and **3. 14** were chosen for cell viability assay because they have moderate solubility in water. Each complex was studied in three different cancer cell lines, including MDA-MB-231 (human metastatic breast cancer cell line), PC3 (human prostate cancer cell line) and HEPG2 (human

hepatocellular carcinoma), and also a noncancerous cell line AHDF (adult human dermal fibroblast). As the Re(I) complexes displayed moderate solubility in water, the stock solutions were prepared in methanol, and these were then further diluted with the relative growth media solution to ensure that the final methanol concentration was below 1%. Vehicle control was performed for each cell line to ensure that the effect on the cancer cells was due to the Re(I)-NHC complex. The results from vehicle control on all cancer cell lines suggested that methanol did not have any activity against cancer or the primary cell lines.

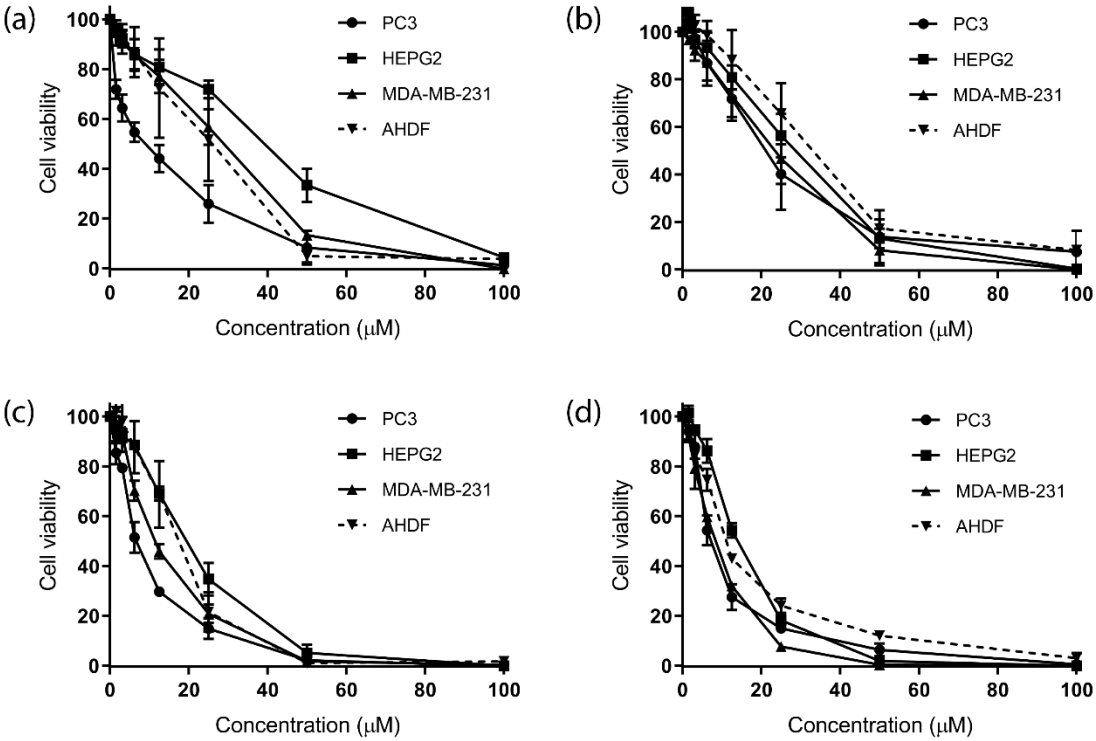

Figure 3.14. Cell viability assay of (a) complex **3.9**, (b) complex **3.10**, (c) complex **3.13** and (d) complex **3.14** against cancer cell lines, including MDA-MB-231 (human metastatic breast cancer cell line), PC3 (human prostate cancer cell line), HEPG2 (human hepatocellular carcinoma) and also the noncancerous cell line AHDF (adult human dermal fibroblast).

The *in vitro* cytotoxicity studies show that the Re(I) complexes of the *bis*-imidazolylidene ligand (**3.13** and **3.14**) were more toxic than the complexes of the pyridyl-imidazolylidene ligand (**3.9** and **3.10**) (Figure 3.14). The 50% growth inhibitory concentration (IC_{50}) values for these compounds are given in Table 3.4. Notably, the IC_{50} values show that complex **3.14** has the same cytotoxicity within error in the prostate cancer PC3 and breast cancer MDA-MB-231 cell lines (IC_{50} = ~7 μM), while complex **3.13** is significantly more toxic toward the PC3 cell line (IC_{50} = ~7 μM) compared to the HEPG2 and MDA-MB-231 cell lines. In addition, the IC_{50} values for **3.13** and **3.14** in the PC3 cell line are considerably lower than those previously reported for cisplatin (25.1 ± 2.2 μM). In contrast, complexes **3.9** and **3.10** are less active in the evaluated cancer cell lines, and the IC_{50} values for these compounds are above 20 μM in all cases, which suggests they do not display selectivity towards a particular cancer cell line. Complexes **3.9**, **3.10**, **3.13** and **3.14** were further evaluated in a primary cell line of a noncancerous adult human dermal fibroblast AHDF. Unfortunately, the data from this study shows that the Re(I)-NHC complexes have similar activity against this noncancerous primary cell line, indicating that these compounds do not display selective toxicity towards cancer cells over healthy cells.

A plausible mechanism for the increased cytotoxicity of the Re(I) complexes of the *bis*-imidazolylidene ligand (**3.13** and **3.14)** compared to the Re(I) complexes of the pyridyl-imidazolylidene ligand (**3.9** and **3.10**) is the increased reactivity of these compounds in exchange reactions of the amino acid ligand, as demonstrated in the aquation kinetic studies reported earlier in this chapter. It is well known for anticancer drugs such as cisplatin that the aquation rate plays a key role in the activity of the compounds, as the exchange of one chloride ligand with a water molecule gives the reactive cationic monoaqua complex that is necessary for DNA binding *in vivo*.[42] As described in section 3.2.2, the *bis*-imidazolylidene ligand measurably increases the aquation rate for these

complexes, potentially as a result of the strong σ-donor ability of the *bis*-carbene ligand compared to the single carbene donor group of the pyridyl-imidazolylidene.

Table 3.4. IC_{50} for cisplatin and Re(I) amino acid complexes.

Compound	IC_{50} (μM)			
	PC3	HEPG2	MDA-MB-231	ADHF
Cisplatin	25.1 ± 2.2[51]	37.1 ± 4.6[52]	22.4 ± 1.6[53]	N/A
3.9	30.1 ± 2.3	74.8 ± 1.7	31.0 ± 1.1	24.9 ± 1.2
3.10	19.2 ± 1.1	28.3 ±1.1	24.8 ± 1.1	27.2 ± 1.1
3.13	7.35 ± 1.1	19.8 ± 1.0	11.7 ± 1.1	16.3 ± 1.1
3.14	7.05 ± 1.1	13.6 ± 1.0	8.16 ±1.1	11.2 ± 1.1

3.3. Conclusion

The search for non-platinum anticancer drugs remains a research area of great interest. In this chapter, a novel series of Re(I) complexes bearing *N*-heterocyclic carbene (NHC) ligand and *N*-acetyl amino acids have been synthesised and studied. These complexes were developed as potential anticancer agents where the oxygen bound amino acid ligand is labile allowing the potential for DNA binding. The mechanism of action for anticancer agents such as cisplatin is mediated by exchanging halide ligands for water molecules, which promotes DNA binding and ultimately cell apoptosis.[1] Previously investigated Re(I) complexes with potential anticancer properties have reported the aquation rate of a leaving halide ligand to be in the rage of $6.3 \times 10^{-3} – 14.0 \times 10^{-4}$ s^{-1}.[54-58] To provide a comparison of the aquation rate to the well-known anticancer drug cisplatin and other Re(I) complexes that exhibit anticancer properties, the aquation rates for complexes **3.9**, **3.10**, **3.12** and **3.14** were measured using ^{1}H NMR time-course studies. The results showed that the *N*-acetyl amino acid ancillary ligand was labile and could be exchanged with water to give cationic Re(I) aqua complexes. In addition, the results also indicated that the aquation rates of Re(I) complexes of the *bis*-imidazolylidene ligand were relatively faster compared to Re(I) complexes of the pyridyl-imidazolylidene ligand. The

increased rates measured for the Re(I) complexes of the *bis*-imidazolylidene ligand were likely due to the *cis*-effect influenced by the strong σ-donor properties of the *bis*-imidazolylidene ligand.[54-57] In addition, the Re(I) *bis*-imidazolylidene complexes have aquation rates that were similar or slightly faster aquation rates to that of cisplatin, and other reported of Re(I) complexes.

The cytotoxicity properties of the Re(I)-NHC complexes, **3.9**, **3.10**, **3.13** and **3.14**, were studied in three cancer cell lines MDA-MB-231, PC3 and HEPG2. These studies showed that complex **3.14** was the most potent compound evaluated, with selective and low micromolar range activity against PC3 cells, indicating that this complex has moderate efficacy in blocking the proliferation of prostate cancer cells. These complexes were also evaluated in the noncancerous adult human dermal fibroblast primary cell line AHDF. Unfortunately, this study did not have clear evidence for selectivity towards the cancer cells, and the cytotoxicity against the primary cell line was also relatively high. However, the results obtained in this work were similar to those reported previously for related Re(I)-NHC complexes. For example, the cytotoxicity of Re(I)-NHC complexes with ancillary halide ligand has been studied in the pancreatic cancer cell line ASPC1, and healthy human embryonic kidney 293T cells, where the IC_{50} values were in the range of 4-10 µM for cancer cells and the IC_{50} values for healthy cells were in the rage of 8-14 µM.[22] In the present studies, the Re(I)-NHC complexes, particularly complexes of *bis*-imidazolylidene ligands **3.13** and **3.14** have IC_{50} values of approximately 7 µM and the IC_{50} for healthy AHDF were in the range of 11-16 µM, indicating that both **3.13** and **3.14** exhibited similar anticancer properties to the previously reported Re(I)-NHC complexes. The cytotoxicity profile of **3.14** reported in this chapter suggests that it is a promising anticancer candidate and further investigation should be made on this compound. In future studies, the cellular localization of this compound could be examined to observe if it can enter the cell and if so, which organelle it localizes in.[59-62] The DNA binding properties

of **3.14** could also be evaluated using calf thymus DNA (CT-DNA) and monitoring the interaction using UV-vis and luminescence titration studies.[59-62] Additionally, the mechanism of action of **3.14** could be further investigated by identifying protein targets using Western blot analysis of whole-cell lysates.[59-62]

3.4. Experimental Details

3.4.1. Synthesis

Preparation of *N*-acetyl amino acid

The acetylation reaction was performed using a known procedure described by Schreiner and co-workers.[63] A solution of selected amino acid and acetic anhydride in methanol was refluxed for 6 h. The crude product was dried and triturated with ethyl acetate to yield the pure product as white crystalline solid.

***N*-acetyl-glycine.** L-glycine (1.00 g, 1.12 mmol), acetic anhydride (1.72 g, 1.68 mmol) in methanol. The product was obtained as white crystalline solid. (Yield: 1.04 g, 55 %). ^{1}H NMR (500 MHz, DMSO-d_6): δ (ppm) 1.84 (s, 3H, CH_3), 3.71 (d, 2H, CH_2), 8.15 (s, 1H, N*H*). ^{13}C NMR (125 MHz, DMSO-d_6): δ (ppm) 22.8 (CH$_3$), 41.1 (CH$_2$), 170.0 (COOH), 171.9 (COCH$_3$).

***N*-acetyl-L-isoleucine.** L-isoleucine (2.00 g, 1.52 mmol) and acetic anhydride (4.05 g, 3.96 mmol) in methanol. The product was obtained as white crystalline solid. (Yield: 1.18 g, 50 %). ^{1}H NMR (500 MHz, DMSO-d_6): δ (ppm) 0.083-0.86 (m, 6H, CH_3), 1.13-1.22 (m, 1H, CH_2), 1.36-1.44 (m, 1H, CH_2), 1.70-1.78 (m, 1H, C*H*NH), 1.86 (s, 3H, OCH_3), 4.15-4.18 (dd, 1H, $^{3}J_{H\text{-}H}$ = 2.40 Hz, $^{3}J_{H\text{-}H}$ = 6.05 Hz, C*H*CH$_3$), 7.96-7.97 (d, 1H, N*H*, $^{3}J_{H\text{-}H}$ = 8.40 Hz), 12.5 (s, 1H, COO*H*). ^{13}C NMR (125 MHz, DMSO-d_6): δ (ppm) 11.7 (CH$_3$), 16.0 (CH$_3$), 22.8 (OCH$_3$), 25.2 (CH$_2$), 36.8 (CHNH), 56.7 (CHCH$_3$), 169.8 (COCH$_3$),

173.6 (*C*OOH). HRESI-MS$^+$ (*CH$_3$OH*): [$C_8H_{15}NO_3Na$]$^+$ *m/z* = 196.0949, calcd = 196.0945.

***N*-acetyl-L-proline.** L-proline (2.00 g, 1.74 mmol) and acetic acid (4.61 g, 4.52 mmol) in methanol. The product was obtained as white crystalline solid. (Yield: 1.08 g, 41%). ^{1}H NMR (500 MHz, DMSO-*d$_6$*): δ (ppm) *cis-isomer* 1.81-1.86 (m, 1H, C*H*$_2$CH), 1.86-1.92 (m, 2H, CH$_2$C*H*$_2$CH$_2$), 1.96 (s, 3H, C*H*3), 2.09-2.16 (m, 1H, C*H*$_2$CH), 3.45-3.54 (m, 2H, C*H*$_2$N), 4.17-4.19 (dd, 1H, $^3J_{H-H}$ = 3.95 Hz, $^3J_{H-H}$ = 4.95 Hz, C*H*) *trans-isomer* 1.67-1.77 (m, 1H, CH$_2$C*H*$_2$CH$_2$), 1.77-1.86 (m, 1H, CH$_2$C*H*$_2$CH$_2$), 1.85 (s, 3H, C*H*$_3$), 2.00-2.06 (m, 1H, C*H*$_2$CH), 2.17-2.25 (m, 1H, C*H*$_2$CH), 3.33-3.36 (m, 2H, C*H*$_2$N), 4.44-4.46 (dd, 1H, $^3J_{H-H}$ = 2.50 Hz, $^3J_{H-H}$ = 6.20 Hz, C*H*). ^{13}C NMR (125 MHz, DMSO-*d$_6$*): δ (ppm) *cis-isomer* 22.6 (*C*H$_3$), 24.8 (CH$_2$*C*H$_2$CH$_2$), 29.5 (*C*H$_2$CH), 47.7 (*C*H$_2$N), 58.6 (*C*H), 168.7 (*C*OCH$_3$), 174.0 (*C*OOH) *trans-isomer* 22.5 (*C*H$_3$), 22.9 (CH$_2$*C*H$_2$CH$_2$), 31.3 (*C*H$_2$CH), 46.2 (*C*H$_2$N), 59.8 (*C*H), 168.9 (*C*OCH$_3$), 174.3 (*C*OOH). HRESI-MS$^+$ (*CH$_3$OH*): [$C_7H_{11}NO_3Na$]$^+$ *m/z* = 180.0635, calcd = 180.0632.

3.1. This compound was prepared as described by Barnard and co-workers[24] from Re(CO)$_5$Cl (0.13 g, 0.35 mmol), 1-(2pyridyl)-3-methylimidazolium iodide (0.10 g, 0.35 mmol), and Ag$_2$O (0.16 g, 0.70 mmol) in dichloromethane (60 mL). The product was obtained as yellow crystalline solid. (Yield: 0.06 g, 36%). ^{1}H NMR (500 MHz, CDCl$_3$): δ (ppm) 4.05 (s, 3H, C*H*$_3$), 7.07 (d, 1H, $^3J_{H-H}$ = 2.15 Hz, *H*$_{imi}$), 7.32-7.35 (m, 1H, *H*$_{Ar}$), 7.53-7.54 m, 1H, overlapped *H*$_{Ar}$), 7.55 (d, 1H, $^3J_{H-H}$ = 3.75 Hz, *H*$_{imi}$), 8.02-8.06 (m, 1H, *H*$_{Ar}$), 8.91 (dd, 1H, $^2J_{H-H}$ = 1.90 Hz, $^3J_{H-H}$ = 3.65 Hz, *H*$_{Ar}$). ^{13}C NMR (125 MHz, CDCl$_3$): δ (ppm) 39.2 (*C*H$_3$), 111.4 (*C*H$_{py}$), 115.8 (*C*H$_{imi}$), 123.4 (*C*$_{py}$), 124.1 (*C*H$_{imi}$), 140.8 (*C*$_q$), 150.8 (N*C*N), 153.8 (*C*H$_{py}$). HRESI-MS$^+$ (*CH$_3$OH*): [$C_{14}H_{12}N_3O_5ReNa$]$^+$ *m/z* = 430.0195, calcd = 430.0201.

3.2. This compound was prepared as described by Barnard and co-workers[64] from $Re(CO)_5Cl$ (0.08 g, 0.35 mmol), *bis*(3-methyl-2,3-dihydro-1H-imidazol-1-yl)methane (0.10 g, 0.35 mmol), and Ag_2O (0.16 g, 0.70 mmol) in mixture of 1:4 methanol and dichloromethane (30 mL). The product was obtained as white crystalline solid. (Yield: 0.03 g, 31%). ^{1}H NMR (500 MHz, DMSO-d_6): δ (ppm) 3.90 (s, 6H, 2CH_3), 5.88 (d, 1H, $^2J_{H\text{-}H}$ = 13.00 Hz, H_{imi}), 6.57 (d, 1H, $^2J_{H\text{-}H}$ = 12.95 Hz, CH_2), 7.41 (d, 1H, $^3J_{H\text{-}H}$ = 1.70 Hz, CH_2), 7.52 (d, 1H, $^3J_{H\text{-}H}$ = 1.75 Hz, H_{imi}). ^{13}C NMR (125 MHz, DMSO-d_6): δ (ppm) 43.0 (2CH$_3$), 67.9 (CH$_2$), 126.3 (CH$_{imi}$), 127.8 (CH$_{imi}$), 181.9 (NCN), 202.6 (Re-CO). HRESI-MS$^+$ (CH_3OH): $[C_{14}H_{12}N_3O_5ReNa]^+$ *m/z* = 447.0470, calcd = 447.0467.

<u>Preparation of silver salts of amino acid ligands</u>

The silver salt was synthesised using a known procedure described by Milstein and co-workers[65] as well as Grubbs and co-workers[66]. An *N*-acetyl amino acid and silver oxide were stirred in acetonitrile for 24 h, filtered and washed with acetonitrile and ether. The product was dried under vacuum to yield a solid residue that was shielded from light.

3.4. *N*-acetyl-glycine (0.20 g, 0.17 mmol), silver oxide (0.20 g, 0.085 mmol) in acetonitrile. The product was obtained as off-white solid. (Yield: 0.17 g, 89%). ^{1}H NMR (500 MHz, DMSO-d_6): δ (ppm) 1.81 (s, 3H, CH_3), 3.56 (d, 2H, $^2J_{H\text{-}H}$ = 5.45 Hz, CH_2), 7.72 (s, 1H, NH). ^{13}C NMR (125 MHz, DMSO-d_6): δ (ppm) 23.1 (CH$_3$), 43.5 (CH$_2$), 169.1 (COCH$_3$), 173.4 (COAg). HRESI-MS$^+$ (CH_3OH): $[C_4H_6NO_3AgNa]^+$ *m/z* = 245.9291, calcd = 245.9291.

3.5. L-*N*-acetyl-isoleucine (0.50 g, 0.29 mmol), silver oxide (0.33 g, 0.14 mmol) in acetonitrile. The product was obtained as off-white solid. (Yield: 0.25 g, 62%).^{1}H NMR (500 MHz, DMSO- d_6): δ (ppm) 0.79-0.84 (m, 6H, CH_3), 1.08-1.17 (m, 1H, CH_2), 1.39-1.47 (m, 1H, CH_2), 1.68-1.75 (m, 1H, CHCH$_3$), 1.83 (s, 3H, OCH_3), 4.12-4.15 (dd, 1H, $^3J_{H\text{-}H}$ = 3.45 Hz, $^3J_{H\text{-}H}$ = 5.30 Hz, CHNH), 7.48 (d, 1H, $^3J_{H\text{-}H}$ = 8.75, NH). ^{13}C NMR (125

MHz, DMSO-d_6): δ (ppm) 12.2 (CH_3), 16.4 (CH_3), 23.3 (OCH_3), 25.4 (CH_2), 38.1 ($CHCH_3$), 58.6 (*C*HNH), 168.8 ($COCH_3$), 175.2 (*C*OOAg). HRESI-MS$^+$ (*CH₃OH*): $[C_8H_{14}NO_3AgNa]^+$ *m/z* = 301.9922, calcd = 301.9917.

3.6. L-*N*-acetyl-proline (0.10 g, 0.065 mmol), silver oxide (0.076 g, 0.033 mmol) in acetonitrile. The product was obtained as off-white solid. (Yield: 0.04 g, 46%). ^{1}H NMR (500 MHz, DMSO-d_6): δ (ppm) *cis-isomer* 1.70-1.77 (m, 2H, $CH_2CH_2CH_2$), 1.97-2.04 (m, 1H, CH_2CH), 2.07-2.15 (m, 1H, CH_2CH), 3.27-3.32 (m, 2H, CH_2N), 4.20-4.23 (m, 1H, C*H*) *trans-isomer* 1.80-1.82 (m, 2H, $CH_2CH_2CH_2$ and CH_2CH), 1.91 (s, 3H, $CH_2CH_2CH_2$ and CH_3), 1.97-2.04 (m, 1H, CH_2CH), 3.41-3.51 (m, 2H, CH_2N), 4.23-4.25 (m, 1H, C*H*). ^{13}C NMR (125 MHz, DMSO-d_6): δ (ppm) *cis-isomer* 22.7 (CH_3), 23.1 ($CH_2CH_2CH_2$), 32.0 (CH_2CH), 46.2 (CH_2N), 62.4 (*C*H), 168.9 ($COCH_3$), 176.1 (*C*OOAg) *trans-isomer* 22.9 (CH_3), 24.7 ($CH_2CH_2CH_2$), 30.3 (CH_2CH), 47.7 (CH_2N), 60.8 (*C*H), 167.9 ($COCH_3$), 176.4 (*C*OOAg). HRESI-MS$^+$ (*CH₃OH*): $[C_7H_{10}NO_3AgNa]^+$ *m/z* = 285.9605, calcd = 285.9604.

3.7. A mixture of **1** (0.050 g, 0.011 mmol) and AgOAc (0.018 g, 0.011 mmol) in acetonitrile was heated at 90 °C overnight. The reaction mixture was filtered through a plug of Celite and the solvent was evaporated on a rotary evaporator. The crude product was recrystallised from methanol yielding the pure product as yellow solid. (Yield: 0.045 g, 86%). ^{1}H NMR (500 MHz) (DMSO-d_6): δ (ppm) 1.43 (s, 3H, $COOCH_3$), 3.97 (s, 3H, CH_{3imi}), 7.48–7.51 (m, 1H, CH_{py}), 7.64 (d, 1H, $^3J_{H-H}$ = 2.05 Hz, CH_{imi}), 8.21 (d, 1H, $^3J_{H-H}$ = 8.30 Hz, CH_{py}), 8.29-8.32 (m, 1H, CH_{py}), 8.39 (d, 1H, $^3J_{H-H}$ = 2.10 Hz, CH_{imi}), 8.84–8.85 (m, 1H, CH_{py}). ^{13}C NMR (DMSO-d_6): δ (ppm) 23.4 $COCH_3$, 38.9 CH_{3imi}, 113.0 CH_{py}, 117.6 CH_{imi}, 124.2 CH_{py}, 125.4 CH_{imi}, 142.9 CH_{py}, 153.25 C_{py}, 154.1 CH_{py}, 174.6 $COCH_3$, 192.0 NCN_{imi}, 199.8 Re-*C*O, 200.1 Re-*C*O, 200.5 Re-*C*O. HRESI-MS$^+$ (*CH₃OH*): $[C_{14}H_{12}N_3O_5ReNa]^+$ *m/z* = 512.0227, calcd = 512.0227.

3.8. A mixture of **1** (0.025 g, 0.054 mmol) and **4** (0.012 g, 0.054 mmol) in acetonitrile was heated at 90 °C overnight. The reaction mixture was filtered through a plug of Celite and the solvent was evaporated on a rotary evaporator. The crude product was purified via silica column chromatography using methanol (2%) and dichloromethane (98%) as eluent to yield the pure product as yellow solid. (Yield: 0.011 g, 37%). ^{1}H-NMR (500 MHz) (DMSO-*d*$_6$): δ (ppm): 1.50 (s, 3H, C*H*$_{3gly}$), 3.13-3.17 (m, 2H, C*H*$_2$NH), 3.97 (s, 3H, C*H*$_{3imi}$), 7.49-7.54 (m, 2H, C*H*$_{py}$ and N*H* overlapped), 7.64 (d, 1H, $^{3}J_{H-H}$ = 2.10 Hz, C*H*$_{imi}$), 8.21 (d, 1H, $^{3}J_{H-H}$ = 8.30 Hz, C*H*$_{py}$), 8.30–8.34 (m, 1H, C*H*$_{py}$), 8.39 (d, 1H, $^{3}J_{H-H}$ = 2.15 Hz, C*H*$_{imi}$), 8.82–8.83 (m, 1H, C*H*$_{py}$). ^{13}C-NMR (DMSO-*d*$_6$): δ (ppm) 22.77 *C*H$_{3gly}$, 38.92 *C*H$_{3imi}$, 42.20 *C*H$_2$NH, 113.1 *C*H$_{py}$, 117.7 *C*H$_{imi}$, 124.3 *C*H$_{py}$, 125.4 *C*H$_{imi}$, 142.9 *C*H$_{py}$, 153.3 *C*$_{py}$, 153.9 *C*H$_{py}$, 168.9 *C*OCH$_3$, 173.4 *C*OCH, 190.7 N*C*N$_{imi}$, 199.6 Re-*C*O, 199.9 Re-*C*O, 200.0 Re-*C*O. HRESI-MS$^+$ (*CH$_3$OH*): [$C_{16}H_{15}N_4O_6ReNa$]$^+$ *m/z* = 569.0445, calcd = 569.0442.

3.9. This compound was prepared as described for **8** from **1** (0.050 g, 0.11 mmol) and **5** (0.030 g, 0.11 mmol). The product was obtained as yellow solid. (Yield: 0.057 g, 92%). ^{1}H NMR (500 MHz) (DMSO-*d*$_6$): δ (ppm) *major product* 0.34 (d, 3H, $^{3}J_{H-H}$ = 6.85 Hz, CHC*H*$_3$), 0.47–0.50 (m, 3H, CH$_2$C*H*$_3$), 0.59–0.67 (m, 1H, C*H*$_2$CH$_3$), 1.10–1.23 (m, 2H, C*H*$_2$CH$_3$ and C*H*CH$_3$ overlapped), 1.73 (s, 3H, OC*H*$_3$), 3.80–3.84 (m, 1H, HNC*H*), 3.98 (s, 3H, C*H*$_{3imi}$), 7.33 (s, 1H, N*H*), 7.51–7.54 (m, 1H, C*H*$_{py}$), 7.67 (d, 1H, $^{3}J_{H-H}$ = 2.05 Hz, C*H*$_{imi}$), 8.22 (s, 1H, C*H*$_{py}$), 8.30–8.36 (m, 1H, C*H*$_{py}$), 8.42 (d, 1H, $^{3}J_{H-H}$ = 2.05 Hz, C*H*$_{imi}$), 8.89 (d, 1H, $^{3}J_{H-H}$ = 5.50 Hz, C*H*$_{py}$). *Minor product* 0.29 (d, 3H, $^{3}J_{H-H}$ = 6.85 Hz, CHC*H*$_3$), 0.42–0.45 (m, 3H, CH$_2$C*H*$_3$), 0.59–0.67 (m, 2H, C*H*$_2$CH$_3$), 1.10–1.23 (m, 2H, C*H*$_2$CH$_3$ and C*H*CH$_3$ overlapped), 3.80–3.84 (m, 1H, HNC*H*), 3.97 (s, 3H, C*H*$_{3imi}$), 7.32 (s, 1H, N*H*), 7.48–7.50 (m, 1H, C*H*$_{py}$), 7.65 (d, 1H, $^{3}J_{H-H}$ = 2.05 Hz, C*H*$_{imi}$), 8.23 (s, 1H, C*H*$_{py}$), 8.30–8.36 (m, 1H, C*H*$_{py}$), 8.40 (d, 1H, $^{3}J_{H-H}$ = 2.05 Hz, C*H*$_{imi}$), 8.83 (d, 1H, $^{3}J_{H-H}$ = 5.50 Hz, C*H*$_{py}$). ^{13}C NMR (DMSO-*d*$_6$): δ (ppm) *major product* 12.3 CH$_2$*C*H$_3$, 15.1 CH*C*H$_3$,

23.1 O*C*H$_3$, 25.3 *C*H$_2$CH$_3$, 38.1 *C*HCH$_3$, 39.0 *C*H$_{3imi}$, 56.9 HN*C*H, 113.0 *C*H$_{py}$, 117.4 *C*H$_{imi}$, 124.5 *C*H$_{py}$, 125.5 *C*H$_{imi}$, 143.0 *C*H$_{py}$, 153.4 *C*$_{py}$, 154.1 *C*H$_{py}$, 168.7 *C*OCH$_3$, 174.6 *C*OCH, 191.8 N*C*N$_{imi}$, 193.6 Re-*C*O, 193.7 Re-*C*O. *Minor product* 12.2 CH$_2$*C*H$_3$, 15.4 CH*C*H$_3$, 23.1 O*C*H$_3$, 25.2 *C*H$_2$CH$_3$, 37.9 *C*HCH$_3$, 38.9 *C*H$_{3imi}$, 56.7 HN*C*H, 112.0 *C*H$_{py}$, 117.7 *C*H$_{imi}$, 124.1 *C*H$_{py}$, 125.4 *C*H$_{imi}$, 143.1 *C*H$_{py}$, 153.5 *C*$_{py}$, 154.0 *C*H$_{py}$, 167.9 *C*OCH$_3$, 174.5 *C*OCH, 191.9 N*C*N$_{imi}$. HRESI-MS$^+$ (*CH$_3$OH*): $[C_{20}H_{23}N_4O_6ReNa]^+$ *m/z* = 625.1065, calcd = 625.1068.

3.10. This compound was prepared as described for **8** from **1** (0.036 g, 0.077 mmol) and **6** (0.020 g, 0.077 mmol). The product was obtained as yellow solid. (Yield: 0.038 g, 74%). ^{1}H NMR (500 MHz) (DMSO-*d$_6$*): δ (ppm) *major product* 1.09–1.18 (m, 2H, C*H*$_{2pro}$), 1.37 (d, 3H, $^3J_{H-H}$ = 2.90 Hz, OC*H*$_3$), 1.44–1.49 (m, 1H, C*H*$_{2pro}$), 1.69–1.76 (m, 1H, C*H*$_{2pro}$), 2.76–2.85 (m, 1H, C*H*$_{2pro}$), 2.92–3.01 (m, 1H, C*H*$_{2pro}$), 3.82–3.86 (m, 1H, C*H*), 3.95 (d, 3H, $^3J_{H-H}$ = 1.51 Hz, C*H*$_{3imi}$), 7.49–7.51 (m, 1H, C*H*$_{py}$), 7.65–7.66 (m, 1H, C*H*$_{imi}$), 8.21–8.23 (m, 1H, C*H*$_{py}$), 8.31–8.35 (m, 1H, C*H*$_{py}$), 8.38–8.44 (m, 1H, C*H*$_{imi}$), 8.81–8.85 (m, 1H, C*H*$_{py}$). *Minor product* 0.96-1.04 (m, 1H, C*H*$_{2pro}$), 1.52-1.57 (m, 3H, C*H*$_{2pro}$), 1.60 (s, 3H, OC*H*$_3$), 2.92-3.01 (m, 1H, C*H*$_{2pro}$), 3.12-3.17 (m, 1H, C*H*), 3.93 (s, 3H, C*H*$_{3imi}$), 7.63 (d, 1H, $^3J_{H-H}$ = 2.00 Hz, C*H*$_{imi}$), 8.77 (d, 1H, $^3J_{H-H}$ = 4.60 Hz, C*H*$_{py}$). ^{13}C NMR (DMSO-*d$_6$*): δ (ppm) *major product* 21.5 O*C*H$_3$, 22.5 *C*H$_{2pro}$, 31.6 *C*H$_{2pro}$, 38.9 *C*H$_{3imi}$, 45.7 *C*H$_{2pro}$, 61.4 *C*H$_{pro}$, 113.1 *C*H$_{py}$, 117.8 *C*H$_{imi}$, 124.3 *C*H$_{py}$, 125.4 *C*H$_{imi}$, 143.1 *C*H$_{py}$, 153.3 *C*$_{py}$, 153.8 *C*H$_{py}$, 168.4 *C*OCH$_3$, 175.8 *C*OCH, 191.6 N*C*N$_{imi}$, 193.8 Re-*C*O, 199.5 Re-*C*O, 199.8 Re-*C*O. *Minor product* 22.5 O*C*H$_3$, 23.8 *C*H$_{2pro}$, 23.9 *C*H$_{2pro}$, 29.9 *C*H$_{2pro}$, 38.9 *C*H$_{3imi}$, 47.1 *C*H$_{2pro}$, 59.6 *C*H, 125.3 *C*H$_{imi}$, 153.3 *C*$_{py}$, 153.4 *C*H$_{py}$, 167.4 *C*OCH$_3$, 175.7 *C*OCH, 191.8 N*C*N$_{imi}$, 193.8 Re-*C*O, 199.6 Re-*C*O. HRESI-MS$^+$ (*CH$_3$OH*): $[C_{19}H_{19}N_4O_6ReNa]^+$ *m/z* = 609.0753, calcd = 609.0755.

3.11. This compound was prepared as described for **7** from **2** (0.050 g, 0.010 mmol) and AgOAc (0.017 g, 0.010 mmol). The pure product was obtained as off-white solid. (Yield: 0.045 g, 84%). ^{1}H NMR (500 MHz) (DMSO-d_6): δ (ppm) 1.66 (s, 3H, COCH_3), 3.75 (s, 6H, CH_{3imi}), 5.98 (d, 1H, CH_2), 6.45 (d, 1H, CH_2), 7.37 (d, 2H, CH_{imi}), 7.52 (d, 2H, CH_{imi}). ^{13}C NMR (DMSO-d_6): δ (ppm) 23.1 COCH$_3$, 38.1 CH$_{3imi}$, 121.8 CH$_{imi}$, 122.7 CH$_{imi}$, 174.8 CO, 179.3 NCN, 196.9 Re-CO, 197.1 Re-CO, 199.2 Re-CO. HRESI-MS$^+$ (CH_3OH): $[C_{14}H_{15}N_4O_5ReNa]^+$ *m/z* = 529.0493, calcd = 529.0493.

3.12. This compound was prepared as described for **8** from **2** (0.032 g, 0.033 mmol) and **4** (0.016 g, 0.033 mmol). The product was obtained as off-white solid. (Yield: 0.014 g, 38%).^{1}H NMR (500 MHz) (DMSO-d_6): δ (ppm) 1.76 (s, 3H, CH_{3gly}), 3.42 (d, 2H, $^{3}J_{H-H}$ = 5.70 Hz, CH_2NH) 3.76 (s, 6H, CH_{3imi}), 6.01 (d, 1H, $^{3}J_{H-H}$ = 12.8 Hz, CH_{2imi}), 6.48 (d, 1H, $^{3}J_{H-H}$ = 12.9 Hz, CH_{2imi}), 7.39 (d, 2H, $^{3}J_{H-H}$ = 1.75 Hz, CH_{imi}), 7.53 (d, 2H, $^{3}J_{H-H}$ = 1.50 Hz, CH_{imi}), 7.76 (t, 1H, $^{3}J_{H-H}$ = 5.35, $^{3}J_{H-H}$ = 10.9 Hz, NH). ^{13}C NMR (DMSO-d_6): δ (ppm) 23.0 CH$_{3gly}$, 38.2 CH$_{3imi}$, 42.0 CH$_{2gly}$, 62.3 CH$_{2imi}$, 121.9 CH$_{imi}$, 122.8 CH$_{imi}$, 169.1 COCH$_3$, 173.6 COCH, 179.1 NCN$_{imi}$, 197.7 Re-CO, 199.1 Re-CO 199.8 Re-CO. HRESI-MS$^+$ (CH_3OH): $[C_{16}H_{18}N_5O_6ReNa]^+$ *m/z* = 586.0712, calcd = 586.0707.

3.13. This compound was prepared as described for **8** from **2** (0.058 g, 0.12 mmol) and **5** (0.034 g, 0.12 mmol). The product was obtained as off-white solid. (Yield: 0.033 g, 44%). ^{1}H NMR (500 MHz) (DMSO-d_6): δ (ppm) *major product* 0.64 (d, 3H, $^{3}J_{H-H}$ = 6.11 Hz, CHCH_3), 0.67 (t, 3H, $^{3}J_{H-H}$ = 7.35 Hz, CH$_2$CH_3), 0.86–0.92 (m, 1H, CH_2CH$_3$), 1.13–1.18 (m, 1H, CH_2CH$_3$), 1.46–1.51 (m, 1H, CHCH$_3$), 1.77 (s, 3H, COCH_3), 3.77 (s, 3H, CH_{3imi}), 3.79 (s, 3H, CH_{3imi}), 3.93–3.96 (m, 1H, HNCH), 6.04 (d, 1H, $^{2}J_{H-H}$ = 12.8 Hz, CH_{2imi}), 6.49 (d, 1H, $^{2}J_{H-H}$ = 12.8 Hz, CH_{2imi}), 7.40–7.41 (m, 2H, CH_{imi}), 7.51 (d, 2H, $^{3}J_{H-H}$ = 1.80 Hz, CH_{imi} and NH overlapped), 7.55 (d, 1H, $^{3}J_{H-H}$ = 1.85 Hz, CH_{imi}). *Minor product* 0.73 (d, 3H, $^{3}J_{H-H}$ = 6.90 Hz, CHCH_3), 0.79 (t, 3H, $^{3}J_{H-H}$ = 7.35 Hz, CH$_2$CH_3), 1.05–1.10 (m,

2H, CH_2CH$_3$), 1.38–1.44 (m, 1H, CH_2CH$_3$), 1.64–1.69 (m, 1H, C*H*CH$_3$), 1.80 (s, 3H, COCH_3), 3.83 (s, 3H, CH_{3imi}), 3.88 (s, 3H, CH_{3imi}), 5.81 (d, 1H, $^3J_{H-H}$ = 13.9 Hz, CH_{2imi}), 6.26 (d, 1H, $^3J_{H-H}$ = 14.1 Hz, CH_{2imi}), 7.49 (s, 1H, N*H*), 7.55 (d, 2H, $^3J_{H-H}$ = 1.85 Hz, CH_{imi}), 7.60 (d, 2H, $^3J_{H-H}$ = 1.60 Hz, CH_{imi}). ^{13}C NMR (DMSO-d_6): δ (ppm) *major product* 11.9 CHCH$_{3Ile}$, 16.1 CH$_2C$H$_{3Ile}$, 23.1 COCH$_3$, 25.2 CH$_{2Ile}$, 37.8 CHCH$_3$, 38.3 CH$_{3imi}$, 38.4 CH$_{3imi}$, 57.7 HNCH, 62.6 CH$_{2imi}$, 121.8 CH$_{imi}$, 122.7 CH$_{imi}$, 168.9 COCH$_3$, 175.6 COCH, 179.1 NCN$_{imi}$, 199.0 Re-CO, 199.1 Re-CO, 199.2 Re-CO. *Minor product* 12.6 CHCH$_{3Ile}$, 16.4 CH$_2C$H$_{3Ile}$, 23.6 COCH$_3$, 25.6 CH$_{2Ile}$, 38.2 CHCH$_3$, 38.8 CH$_{3imi}$, 38.9 CH$_{3imi}$, 121.8 CH$_{imi}$, 122.9 CH$_{imi}$. HRESI-MS$^+$ (*CH$_3$OH*): [C$_{20}$H$_{26}$N$_5$O$_6$ReNa]$^+$ *m/z* = 642.1335, calcd = 642.1333.

3.14. This compound was prepared as described for **8** from **2** (0.060 g, 0.12 mmol) and **6** (0.033 g, 0.12 mmol). The product was obtained as off-white solid. (Yield: 0.041 g, 54%). ^{1}H NMR (500 MHz) (DMSO-d_6): δ (ppm) *major product* 1.54 (s, 3H, COCH_3), 1.59–1.66 (m, 1H, CH_{2Pro}), 1.71–1.77 (m, 2H, CH_{2Pro}), 1.95–2.02 (m, 1H, CH_{2Pro}), 3.18–3.25 (m, 2H, CH_{2Pro}), 3.76 (s, 3H, CH_{3imi}), 3.77 (s, 3H, CH_{3imi}), 4.06 (dd, 2H, $^3J_{H-H}$ = 3.05, $^3J_{H-H}$ = 11.5 Hz, C*H*), 5.98 (d, 1H, $^3J_{H-H}$ = 13.0 Hz, CH_{2imi}), 6.41 (d, 1H, $^3J_{H-H}$ = 13.0 Hz, CH_{2imi}), 7.38–7.41 (m, 2H, CH_{imi}), 7.52–7.54 (m, 2H, CH_{imi}). *Minor product* 1.59–1.66 (m, 2H, CH_{2Pro}), 1.71–1.76 (m, 1H, CH_{2Pro}), 1.81–1.84 (m, 1H, CH_{2Pro}), 1.86 (s, 3H, COCH_3), 3.31–3.35 (m, 2H, CH_{2Pro}), 3.76 (s, 3H, CH_{3imi}),), 3.77 (s, 3H, CH_{3imi}), 3.99 (dd, 1H, $^3J_{H-H}$ = 3.15, $^3J_{H-H}$ = 11.7 Hz, C*H*), 5.95 (d, 1H, $^3J_{H-H}$ = 13.0 Hz, CH_{2imi}), 6.46 (d, 1H, $^3J_{H-H}$ = 13.0 Hz, CH_{2imi}), 7.38–7.41 (m, 2H, CH_{imi}), 7.52–7.54 (m, 2H, CH_{imi}). ^{13}C NMR (DMSO-d_6): δ (ppm) *major product* 22.0 COCH$_3$, 23.1 CH$_{2pro}$, 31.8 CH$_{2pro}$, 38.2 CH$_{3imi}$, 38.0 CH$_{3imi}$, 46.2 CH$_{2pro}$, 61.2 CH, 62.7 CH$_{2imi}$, 121.8 CH$_{imi}$, 121.9 CH$_{imi}$, 122.7 CH$_{imi}$, 122.8 CH$_{imi}$, 168.2 COCH$_3$, 176.3 COCH, 179.1 NCN$_{imi}$, 196.9 Re-CO, 198.9 Re-CO, 199.0 Re-CO. *Minor product* 22.8 COCH$_3$, 24.6 CH$_{2pro}$, 30.1 CH$_{2pro}$, 38.3 CH$_{3imi}$, 47.5 CH$_{2pro}$, 59.6 CHN, 121.6 CH$_{imi}$, 121.7 CH$_{imi}$, 122.6 CH$_{imi}$, 167.7 COCH$_3$, 176.5

*C*ONH, 179.4 N*C*N. HRESI-MS$^+$ (*CH$_3$OH*): [$C_{19}H_{22}N_5O_6ReNa$]$^+$ *m/z* = 626.1015, calcd = 626.1020.

3.4.2. Theoretical Studies

All complexes were optimised with the PBE0/def2-TZVP level of theory in the ORCA version 4.2.1 software package. Integration grids were set to 'grid4 finalgrid5' to ensure smooth optimisation. Analytical frequency calculations were undertaken to confirm all structure were minima and to calculate the thermal and entropic contributions to the free energy terms. Single point energy solvation calculations were performed on the optimised structures, with the CPCM method and parameters for water. QTAIM analysis was carried out with Multiwfn version 3.5 software.

3.4.3. Cell Culture

MDA-MB-231, PC3 and HepG2 cells were cultured in DMEM (Dulbecco's Modified Eagle Medium, RMPI 1640 (Roswell Park Memorial Institute) or MEME (Minimal Essential Medium) mediums, respectively, supplemented with 10% fetal calf serum and 1% penicillin-streptomycin.

3.4.4. MTT Assay

Cell viability was determined using an MTT assay. In brief, cells were washed with 1 × PBS, harvested using 0.05% trypsin with 3 × volume media added to inactivate the trypsin, followed by centrifugation at 300 g for 5 minutes. The cells were counted using a haemocytometer and diluted in culture media to obtain 1×10^5 cells/ml in 50 µl per well of a 96 well plate. Plates were placed in a 37 °C and 5% CO_2 incubator for 24 h. Following overnight incubation, cells were subjected to complexes at varying concentrations (0-100 µM) for 48 h, followed by addition of 1 mg/ml MTT reagent to the cells in 1:1 volumetric ratio and incubation for a further 3 h. The medium was then removed and 100 µl of

dimethyl sulfoxide was used to solubilise the MTT crystals. The plates were analysed using a microplate reader at a wavelength of 570 nm.

3.5. Reference

1. Jia, P. P.; Ouyang, R. Z.; Cao, P. H.; Tong, X.; Zhou, X.; Lei, T.; Zhao, Y. F.; Guo, N.; Chang, H. Z.; Miao, Y. Q.; Zhou, S., *J. Coord. Chem.* **2017,** *70* (13), 2175-2201.
2. Ott, I.; Gust, R., *Arch. Pharm. (Weinheim)* **2007,** *340* (3), 117-26.
3. Zeng, L.; Gupta, P.; Chen, Y.; Wang, E.; Ji, L.; Chao, H.; Chen, Z. S., *Chem. Soc. Rev.* **2017,** *46* (19), 5771-5804.
4. Alessio, E.; Messori, L., *Molecules* **2019,** *24* (10), 1995.
5. Allison, S. J.; Sadiq, M.; Baronou, E.; Cooper, P. A.; Dunnill, C.; Georgopoulos, N. T.; Latif, A.; Shepherd, S.; Shnyder, S. D.; Stratford, I. J.; Wheelhouse, R. T.; Willans, C. E.; Phillips, R. M., *Cancer Lett.* **2017,** *403*, 98-107.
6. Liang, X.; Luan, S.; Yin, Z.; He, M.; He, C.; Yin, L.; Zou, Y.; Yuan, Z.; Li, L.; Song, X.; Lv, C.; Zhang, W., *Eur. J. Med. Chem.* **2018,** *157*, 62-80.
7. Mora, M.; Gimeno, M. C.; Visbal, R., *Chem. Soc. Rev.* **2019,** *48* (2), 447-462.
8. Porchia, M.; Pellei, M.; Marinelli, M.; Tisato, F.; Del Bello, F.; Santini, C., *Eur. J. Med. Chem.* **2018,** *146*, 709-746.
9. Konkankit, C. C.; Marker, S. C.; Knopf, K. M.; Wilson, J. J., *Dalton Trans.* **2018,** *47* (30), 9934-9974.
10. Lee, L. C.-C.; Leung, K.-K.; Lo, K. K.-W., *Dalton Trans.* **2017,** *46* (47), 16357-16380.
11. Oriskovich, T. A.; White, P. S.; Thorp, H. H., *Inorg. Chem.* **1995,** *34* (7), 1629-1631.
12. Zobi, F.; Spingler, B.; Fox, T.; Alberto, R., *Inorg. Chem.* **2003,** *42* (9), 2818-2820.
13. Zobi, F.; Spingler, B.; Alberto, R., *ChemBioChem* **2005,** *6* (8), 1397-1405.
14. Zobi, F.; Blacque, O.; Schmalle, H. W.; Spingler, B.; Alberto, R., *Inorg. Chem.* **2004,** *43* (6), 2087-96.
15. Zobi, F.; Spingler, B.; Alberto, R., *Chembiochem* **2005,** *6* (8), 1397-405.
16. Zobi, F.; Blacque, O.; Sigel, R. K. O.; Alberto, R., *Inorg. Chem.* **2007,** *46* (25), 10458-10460.
17. Lo, K. K.-W., *Acc. Chem. Res.* **2015,** *48* (12), 2985-2995.
18. Clède, S.; Policar, C., *Chem. Eur. J.* **2015,** *21* (3), 942-958.
19. Cheff, D. M.; Hall, M. D., *J. Med. Chem.* **2017,** *60* (11), 4517-4532.

20. Knopf, K. M.; Murphy, B. L.; MacMillan, S. N.; Baskin, J. M.; Barr, M. P.; Boros, E.; Wilson, J. J., *J. Am. Chem. Soc.* **2017,** *139* (40), 14302-14314.

21. Liu, W. K.; Gust, R., *Coord. Chem. Rev.* **2016,** *329*, 191-213.

22. Simpson, P. V.; Casari, I.; Paternoster, S.; Skelton, B. W.; Falasca, M.; Massi, M., *Chem. Eur. J.* **2017,** *23* (27), 6518-6521.

23. Chan, C. Y.; Barnard, P. J., *Dalton Trans.* **2015,** *44* (44), 19126-40.

24. Chan, C. Y.; Pellegrini, P. A.; Greguric, I.; Barnard, P. J., *Inorg. Chem.* **2014,** *53* (20), 10862-73.

25. Chan, C. Y.; Barnard, P. J.; Noor, A.; Donnelly, P. S.; McLean, C. A., *Chem. Commun. (Camb.)* **2017,** *53* (15), 2311-2314.

26. Hiltner, O.; Boch, F. J.; Brewitz, L.; Harter, P.; Drees, M.; Herdtweck, E.; Herrmann, W. A.; Kuhn, F. E., *Eur. J. Inorg. Chem.* **2010,** *2010* (33), 5284-5293.

27. Herrick, R. S.; Houde, K. L.; McDowell, J. S.; Kiczek, L. P.; Bonavia, G., *J. Organomet. Chem.* **1999,** *589* (1), 29-37.

28. Herrick, R. S.; Ziegler, C. J.; Bohan, H.; Corey, M.; Eskander, M.; Giguere, J.; McMicken, N.; Wrona, I. E., *J. Organomet. Chem.* **2003,** *687* (1), 178-184.

29. Herrick, R. S.; Wrona, I.; McMicken, N.; Jones, G.; Ziegler, C. J.; Shaw, J., *J. Organomet. Chem.* **2004,** *689* (25), 4848-4855.

30. Aznarez, F.; Iglesias, M.; Hepp, A.; Veit, B.; Miguel, P. J. S.; Oro, L. A.; Jin, G. X.; Hahn, F. E., *Eur. J. Inorg. Chem.* **2016,** *2016* (28), 4598-4603.

31. Saha, S.; Ghatak, T.; Saha, B.; Doucet, H.; Bera, J. K., *Organometallics* **2012,** *31* (15), 5500-5505.

32. El-Subruiti, G. M.; Chehata, A. K.; Massoud, S. S., *Int. J. Chem. Kinet.* **2002,** *34* (1), 1-6.

33. El-Subruiti, G. M.; Younes, G. O.; Zeitouni, F. S.; Amira, M. F., *Int. J. Chem. Kinet.* **2004,** *36* (9), 494-499.

34. Ashley, K. R.; Hamm, R. E., *Inorg. Chem.* **1966,** *5* (10), 1645-1649.

35. Asali, K. J.; Al Janaydeh, H., *Transit. Met. Chem.* **2003,** *28* (2), 193-198.

36. Atwood, J. D.; Brown, T. L., *J. Am. Chem. Soc.* **2002,** *98* (11), 3160-3166.

37. Kovacs, A.; Frenking, G., *Organometallics* **2001,** *20* (12), 2510-2524.

38. Janssen-Muller, D.; Schlepphorst, C.; Glorius, F., *Chem. Soc. Rev.* **2017,** *46* (16), 4845-4854.

39. Zou, T.; Lok, C. N.; Wan, P. K.; Zhang, Z. F.; Fung, S. K.; Che, C. M., *Curr Opin. Chem. Biol.* **2018,** *43*, 30-36.

40. Mercs, L.; Albrecht, M., *Chem. Soc. Rev.* **2010,** *39* (6), 1903-1912.

41. Hopkinson, M. N.; Richter, C.; Schedler, M.; Glorius, F., *Nature* **2014,** *510* (7506), 485-96.

42. Davies, M. S.; Berners-Price, S. J.; Hambley, T. W., *Inorg. Chem.* **2000,** *39* (25), 5603-13.

43. Zavitsas, A. A., *J. Phys. Chem.* **2003,** *107* (6), 897-898.

44. Sajith, P. K.; Suresh, C. H., *J. Organomet. Chem.* **2011,** *696* (10), 2086-2092.

45. Gabr, M. T.; Pigge, F. C., *Dalton Trans.* **2017,** *46* (43), 15040-15047.

46. Fernández-Moreira, V.; Ortego, M. L.; Williams, C. F.; Coogan, M. P.; Villacampa, M. D.; Gimeno, M. C., *Organometallics* **2012,** *31* (16), 5950-5957.

47. Ramos, L. D.; de Macedo, L. H.; Gobo, N. R. S.; de Oliveira, K. T.; Cerchiaro, G.; Morelli Frin, K. P., *Dalton Trans.* **2020,** *49* (45), 16154-16165.

48. Pan, Z. Y.; Cai, D. H.; He, L., *Dalton Trans.* **2020,** *49* (33), 11583-11590.

49. Choi, A. W.; Louie, M. W.; Li, S. P.; Liu, H. W.; Chan, B. T.; Lam, T. C.; Lin, A. C.; Cheng, S. H.; Lo, K. K., *Inorg. Chem.* **2012,** *51* (24), 13289-302.

50. Salassa, L.; Garino, C.; Albertino, A.; Volpi, G.; Nervi, C.; Gobetto, R.; Hardcastle, K. I., *Organometallics* **2008,** *27* (7), 1427-1435.

51. Wu, X. W.; Zheng, Y.; Wang, F. X.; Cao, J. J.; Zhang, H.; Zhang, D. Y.; Tan, C. P.; Ji, L. N.; Mao, Z. W., *Chem.* **2019,** *25* (28), 7012-7022.

52. Takano, M.; Otani, Y.; Tanda, M.; Kawami, M.; Nagai, J.; Yumoto, R., *Drug Metab. Pharmacokinet.* **2009,** *24* (5), 418-27.

53. Koh, S. Y.; Moon, J. Y.; Unno, T.; Cho, S. K., *Nutrients* **2019,** *11* (3), 624.

54. Schutte-Smith, M.; Marker, S. C.; Wilson, J. J.; Visser, H. G., *Inorg. Chem.* **2020,** *59* (21), 15888-15897.

55. Malaza, S.; Govender, P.; Schutte-Smith, M.; Visser, H. G.; Smith, G. S., *Eur. J. Inorg. Chem.* **2017,** *2017* (33), 3919-3927.

56. Schutte, M.; Kemp, G.; Visser, H. G.; Roodt, A., *Inorg. Chem.* **2011,** *50* (24), 12486-98.

57. Salignac, B.; Grundler, P. V.; Cayemittes, S.; Frey, U.; Scopelliti, R.; Merbach, A. E.; Hedinger, R.; Hegetschweiler, K.; Alberto, R.; Prinz, U.; Raabe, G.; Kolle, U.; Hall, S., *Inorg. Chem.* **2003,** *42* (11), 3516-26.

58. Grundler, P. V.; Helm, L.; Alberto, R.; Merbach, A. E., *Inorg. Chem.* **2006,** *45* (25), 10378-90.

59. Chauhan, M.; Banerjee, K.; Arjmand, F., *Inorg. Chem.* **2007,** *46* (8), 3072-3082.

60. Katoh, I.; Tomimori, Y.; Ikawa, Y.; Kurata, S.-i., *J. Biol. Chem.* **2004,** *279* (15), 15515-15523.

61. Nehru, S.; Veeralakshmi, S.; Kalaiselvam, S.; Subin David, S. P.; Sandhya, J.; Arunachalam, S., *J. Biomol. Struct. Dyn.* **2021,** *39* (6), 2242-2256.

62. Wäster, P. K.; Öllinger, K. M., *J. Invest. Dermatol.* **2009,** *129* (7), 1769-1781.

63. Wende, R. C.; Seitz, A.; Niedek, D.; Schuler, S. M. M.; Hofmann, C.; Becker, J.; Schreiner, P. R., *Angew. Chem., Int. Ed.* **2016,** *55* (8), 2719-2723.

64. Chan, C. Y.; Barnard, P. J., *Dalton Trans.* **2015,** *44* (44), 19126-19140.

65. Dorta, R.; Shimon, L.; Milstein, D., *J. Organomet. Chem.* **2004,** *689* (4), 751-758.

66. Hartung, J.; Dornan, P. K.; Grubbs, R. H., *J. Am. Chem. Soc.* **2014,** *136* (37), 13029-13037.

Chapter 4: Synthesis and Studies of Dinuclear Re(I) Complexes and Re(I) Carbohydrate Conjugates

4.1. Introduction

The mechanism of action and the clinical applications of cisplatin are well understood. However, this frontline anticancer agent is currently experiencing resistance problems, which limits its activities against many common cancers.[1] For this reason, there has been significant interest in the exploration of new structurally different compounds with distinct DNA binding mechanisms.[1] For example, polynuclear platinum complexes consisting of two or more platinum cores that are linked by bridging aliphatic groups have been shown to form long-distance intra- and inter-strand crosslinks with DNA.[2] A number of complexes of this type have been reported in recent years,[1,3] and among these, BBR 3464 (**4.1**) was selected for preclinical studies as a novel anticancer agent (Figure 4.1).[3] The results from the preclinical studies showed that **4.1** was extremely potent against cisplatin-resistant cancers.[3] Unfortunately, the results from phase II clinical trials did not support compound **4.1** to proceed as an anticancer agent due to the lack of significant responses from a group of patients with relapsed small-cell lung cancer.[4]

Other examples of polynuclear platinum anticancer compounds include a series of dual-functional complexes, where arene-based ligands allowed the complexes to bind to DNA via an intercalative mechanism, and at the same time, the Pt(II) metal core could coordinate directly to a DNA base (**4.2**, Figure 4.1).[5] In a second example, a series of dual-functional dinuclear Pt(II) complexes with a linker composed of 7-10 methylene groups (**4.3**-**4.6**, Figure 4.1) was reported.[6] The results of DNA binding and theoretical studies indicated that complexes with an appropriate alkyl chain length (in this case, nine carbons **4.5**) could form stable inter-strand cross-links between the Pt(II) centres and

DNA.[6] The field of polynuclear Pt(II) complexes was further expanded with the development of a series of dinuclear Pt(II) complexes with NHC ligands (**4.7**-**4.13**, Figure 4.1).[7] These complexes induced cell death via a mechanism involving apoptosis-inducing factor (AIF) and caspase 12 translocation, which is different to the action of cisplatin.[7] On this basis, Pt complexes of NHC ligands may offer the potential for new anticancer agents in the treatment of cisplatin-resistance tumours.

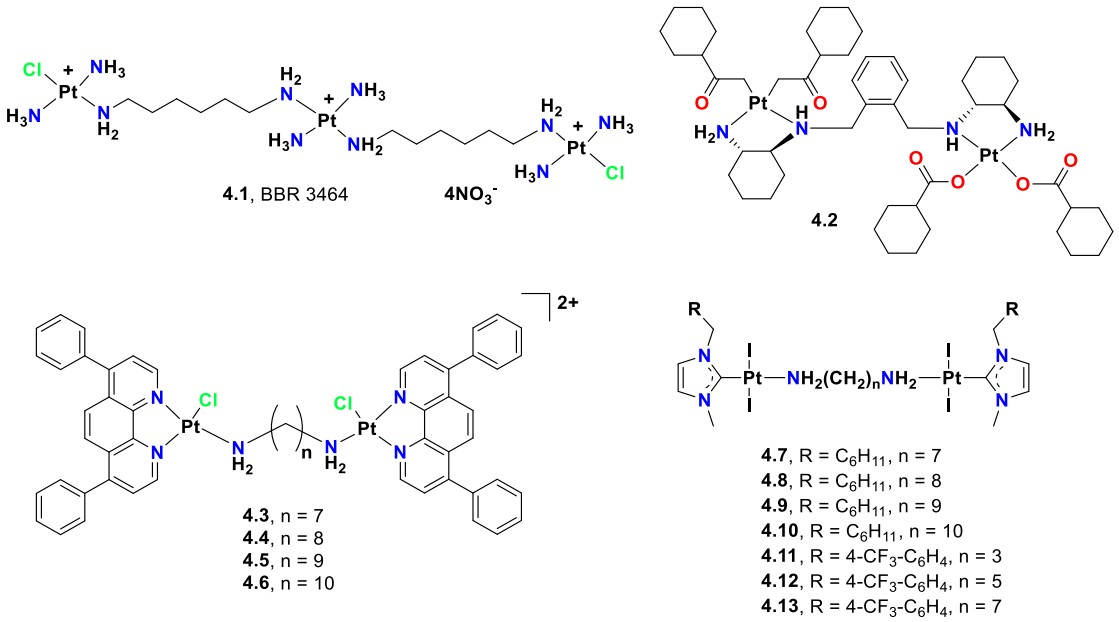

Figure 4.1. Examples of polynuclear Pt(II) complexes with different bridging groups **4.1**-**4.13**.

The emergence of cancers resistant to cisplatin has drawn the attention from numerous researchers to investigate a range of other metals as alternatives to platinum.[8] A number of rhenium(I) tricarbonyl complexes have shown promising properties for the development of new anticancer agents.[9-11] Several clinical agents containing the rhenium radioisotopes ^{188}Re and ^{186}Re are in current used, and radiopharmaceuticals of this type can be used in combination with ^{99m}Tc as potential radiodiagnostic and radiotherapeutic agents.[8] Complexes **4.14** and **4.15**, (Figure 4.2) were designed to induce cell death via lysosomal pathways,[12] and interestingly **4.15** was found to function as an $^1O_2$ sensitiser

and also displayed high phototoxicity against the cisplatin-resistance cancer cell line A549.[12] Furthermore, polynuclear Re(I) complexes have also been investigated as anticancer agents. For example, complexes **4.16-4.19** (Figure 4.2) were prepared,[13] and *in vitro* cytotoxicity studies showed that compound **4.18** and **4.19** have comparable anticancer activity to cisplatin.[13]

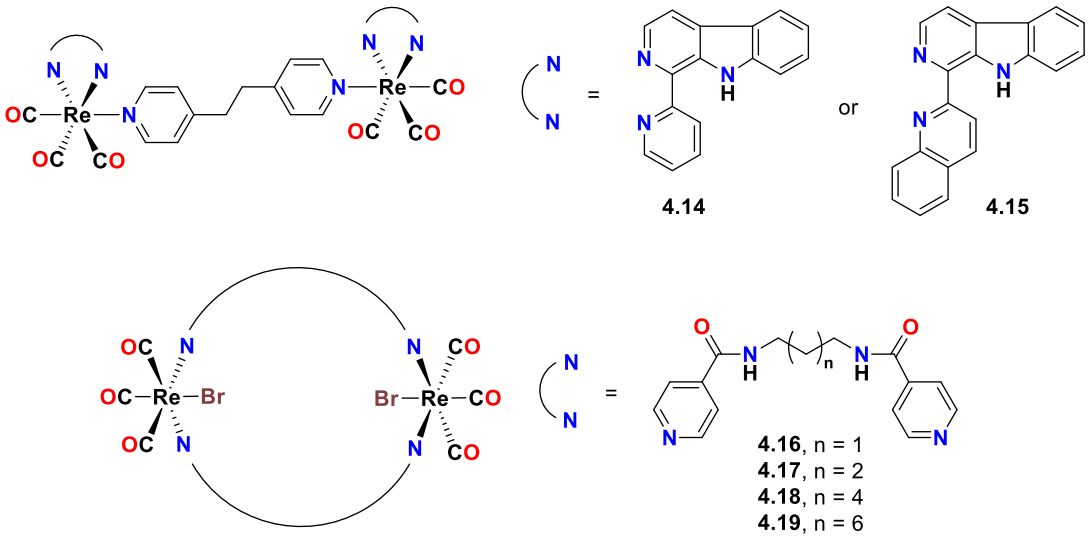

Figure 4.2. Examples of polynuclear Re(I) complexes: dinuclear Re(I) with aromatic ring linkage (**4.14-4.15**) and dinuclear Re(I) with amide linkage (**4.16-4.19**).

Cancer patients require accurate and non-invasive detection and evaluation of tumours for optimum treatment strategies.[14] To allow accurate diagnosis and treatment, the radiopharmaceutical agent should specifically target the tumour site to avoid undesired side effects.[14] Glucose is a fundamental energy source for living organisms that is commonly produced from ingested carbohydrates.[15] The hydrophilic nature of glucose requires specific glucose transporter proteins (GLUTs) to facilitate cellular uptake.[14-15] Tumour cells have high glucose consumption, and as a result, GLUT transporters are generally overexpressed by 20-30 fold in cancer cells compared to noncancerous cells to increase glucose uptake.[14-15] Therefore, a strategy to target cancer cells could involve coupling of glucose group to the anticancer agent.

One of the frontline cancer imaging agents is 2-deoxy-2-[^{18}F]fluoro-D-glucose (**4.20**, Figure 4.3), and this compound is monitored in the body using positron emission tomography (PET).[14] The structure of compound **4.20** is very similar to that of D-glucose, and it is transported across various tissues by glucose transporters (particularly GLUT1 and GLUT4).[15-16] Once inside the cell, **4.20** enters the glycolysis pathway and is phosphorylated and trapped, particularly in tumour cells where its uptake is upregulated, allowing tumours to be identified via PET imaging.[15-16] Numerous examples have been reported of novel anticancer agents incorporating carbohydrate motifs to allow cancer targeting. For example, the 3,6-di-*O*-acetyl-2-deoxy-D-glucose (**4.21**, Figure 4.3) is a promising anticancer agent candidate.[15] Compound **4.21** (an analogue of **4.20**) is designed to undergo deacetylation by esterases and acts as a competitive inhibitor of hexokinase, thereby inhibiting the glycolytic pathway. Moreover, **4.21** can cross the BBB by passive diffusion, which makes it an excellent candidate for treating brain cancers, and this compound is currently in clinically trial for glioblastoma and other highly glycolytic tumours.[17]

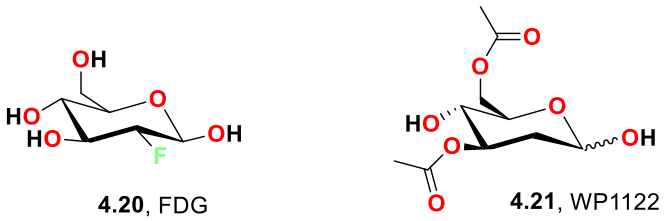

Figure 4.3. Chemical structures of 2-deoxy-2-[^{18}F]fluoro-D-glucose (FDG) **4.20** and 3,6-di-O-acetyl-2-deoxy-D-glucose (WP1122) **4.21**.

Despite the growing interest in preparing Re(I) complexes as potential anticancer drugs and therapeutic agents, there are very limited examples of Re(I) glucose derivatives.[18] Three Re(I) polypyridine glucose complexes **4.22**-**4.24** (Figure 4.4) have been reported as biomolecule probes for cancer cells.[18] *In vitro* cytotoxicity studies of these complexes showed that they are less toxic than cisplatin.[18] However, compound **4.24** displayed high

cellular uptake in cancer cell lines (HeLa and human breast adenocarcinoma MCF-7 cells) that overexpress the GLUT transporter.[18] Since GLUTs have an essential role in the cellular uptake of this complex, these results indicated that Re(I) conjugated to glucose derivatives could enter cells via GLUTs.[18]

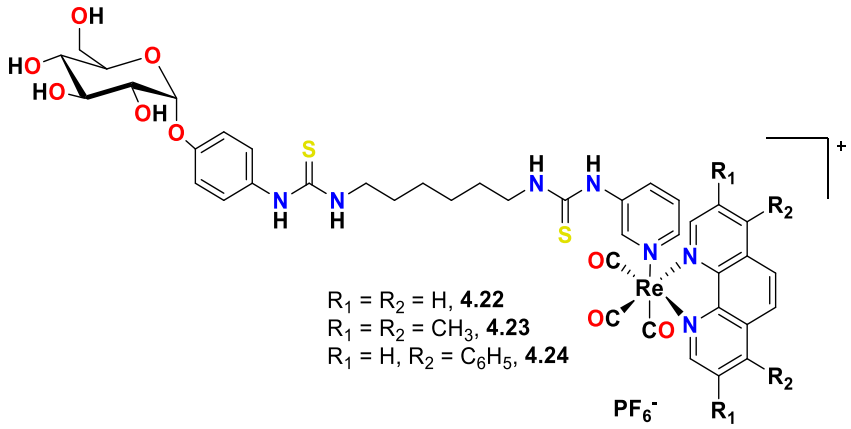

Figure 4.4. Structures of Re(I) polypyridine glucose complexes with three ligand derivates, including 1,10-phenanthroline **4.22**, 3,4,7,8-tetramethyl-1,10-phenanthroline **4.23**, and 4,7-diphenyl-1,10-phenanthroline **4.24**.

The promising results for Re(I) complexes of *N*-acetyl amino acid ligands described in Chapter 3 have led us to further explore the anticancer properties of Re(I) complexes. The first part of this chapter describes the synthesis of a series of polynuclear Re(I) complexes of pyridyl-imidazolylidene and *bis*-imidazolylidene ligands with either alkyl or diamide linkages. Additionally, kinetic studies of the aquation of these complexes and their photophysical properties were also investigated. The second part of this chapter describes the synthesis of Re(I)-NHC complexes conjugated to glucose derivatives.

4.2. Polynuclear Re(I) NHC Complexes

4.2.1. Synthesis of Polynuclear Re(I) Complexes of NHC Ligands

The Re(I) complexes described in this chapter required the initial synthesis of compounds **4.25** and **4.27** (Scheme 4.1).[19-20] Here, compound **4.25** was synthesised by the reaction of imidazole and 2-bromopyridine in the presence of copper(I) iodide using an Ullmann-type coupling procedure (Scheme 4.1).[19] For compound **4.27**, two equivalents of imidazole were reacted with dibromomethane yielding **4.26**, which was mono-alkylated with iodomethane (Scheme 4.1).

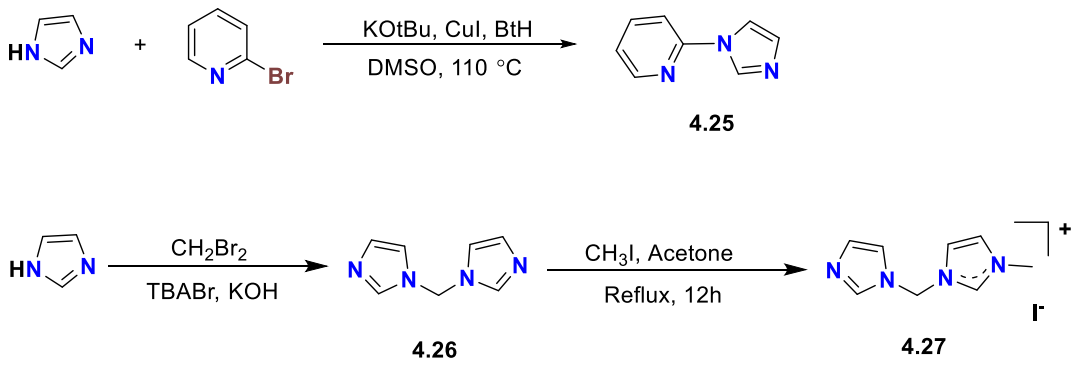

Scheme 4.1. Synthesis route for the preparation of compounds **4.25** and **4.27**.

The pyridyl-imidazolium pro-ligand **4.28** was prepared by a reaction of 1,5-dibromopentane with two equivalents of **4.25** in an acetonitrile solution (Scheme 4.2). A similar procedure was used to prepare the *tetra*-imidazolium pro-ligand **4.29** from 1,5-dibromopentane and **4.27** (Scheme 4.2). In both cases, the imidazolium crude products were obtained as precipitate from the reaction mixtures. Following the reactions, the bromide counterions of these products were exchanged for hexafluorophosphate by metathesis with a saturated aqueous solution of KPF_6. This procedure was essential to obtain pure products, particularly for compound **4.29** as the reaction product is expected to have a mixture of bromide and iodide anions. The ^{1}H NMR spectra of both pro-ligands **4.28** and **4.29** show that the pre-carbenic (NC*H*N) protons resonate significantly

downfield at 10.1 ppm for **4.28**, and 9.47 ppm and 9.61 ppm for **4.29**. In addition, the protons on the methylene linker between the imidazolium units of **4.29** give a singlet at 6.71 ppm.

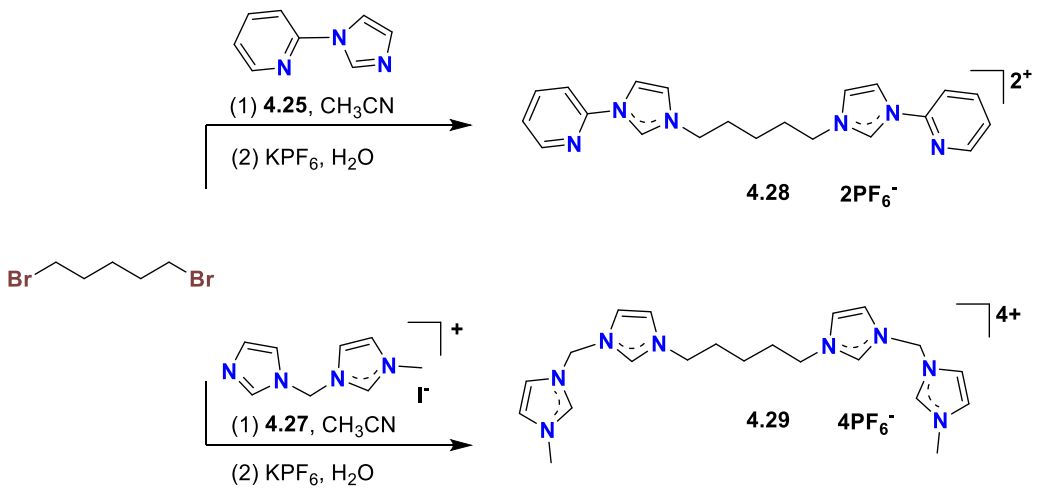

Scheme 4.2. Synthesis of the alkyl linkage of pyridyl-imidazolium salt (**4.28**) and *bis*-imidazolium salt (**4.29**) via the alkylation of 1,5-dibromopentane with **4.25** and **4.27**, respectively.

The dinuclear Re(I) complexes **4.30** and **4.31** were synthesised by a reaction of $Re(CO)_5Cl$ and pro-ligand (either **4.28** or **4.29**) in the presence of silver(I) oxide (Scheme 4.3). The pro-ligands **4.28** and **4.29** have low solubility in the solvent dichloromethane due to the di- or tetra-positive charge of these salts. As a result, a small amount of methanol was added to the reaction mixture in the Re(I) complex synthesis reactions to improve the solubility of these pro-ligands. The ^{1}H NMR spectra for complexes **4.30** and **4.31** no longer show a signal for the imidazolium C2 proton, suggesting the carbene was deprotonated and coordinated to the metal. The ^{13}C NMR spectra of these complexes also show a significant downfield shift of the C2 carbon in both cases (**4.30** = 189.6 ppm, **4.31** = 177.0 ppm), consistent with the carbene formation. In addition, the characteristic downfield signals for carbonyl carbon bound to Re(I) metal centre were observed in the range between 190-200 ppm. These results indicate that the Re(I)-NHC complexes **4.30**

and **4.31** were successfully formed. Interestingly, the protons of the linker unit between the coordinated NHC groups of **4.31** resonate as two doublet signals, suggesting that these protons are inequivalent and the interconversion between the two environments is fast with respect to the NMR time scale.[20]

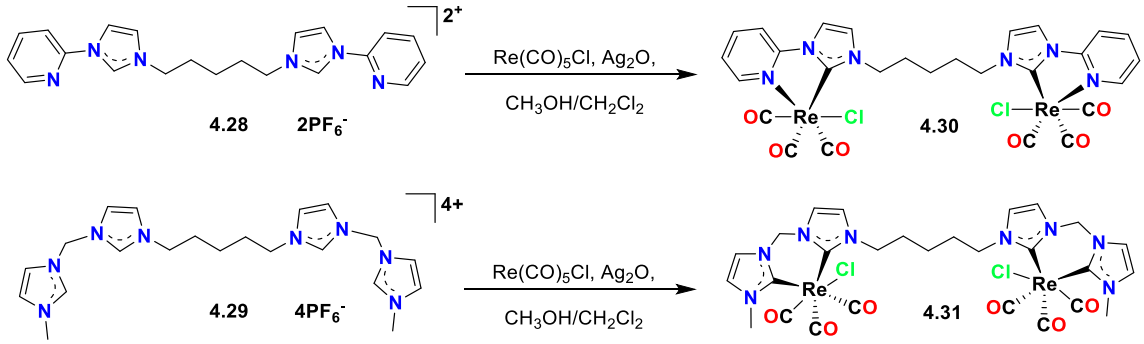

Scheme 4.3. Synthesis of Re(I) complexes **4.30** and **4.31**.

The dinuclear Re(I) complexes with pentyl linkage (**4.30** and **4.31)** had relatively low solubility in aqueous solution and could only be dissolved in a mixture of water and DMSO (60% water:40% dimethyl sulfoxide). In an effort to improve the solubility, a second set of imidazolium pro-ligands **4.32** and **4.33** with a diamide linker group were prepared (Scheme 4.4). Initially, compound **4.32** was synthesised by the reaction of 1,3-diaminopropane with two equivalents of 2-chloroacetyl chloride. Compound **4.32** was then reacted with either two equivalents of **4.25** or **4.27** in a solution of acetonitrile, yielding compounds **4.33** and **4.34**, respectively (Scheme 4.4). In both cases, the crude products precipitated from the reaction mixtures, and these compounds were isolated as hexafluorophosphate salts, which were purified using a similar procedure described for **4.28** and **4.29** to convert chloride counterions to hexafluorophosphate. Due to the symmetrical structure of pro-ligands **4.33** and **4.34**, the ^{1}H NMR spectra of these compounds are relatively simple with the expected downfield shifted signal for the pre-carbenic (NC*H*N) proton at 10.0 ppm for **4.33**, and 9.34 ppm and 9.35 ppm for **4.34**. The amide protons for both pro-ligands resonate as a triplet at 8.48 ppm for **4.33** and 8.54 ppm

for **4.34**, as they are coupled to the adjacent methylene group protons of the alkyl linkage. In addition, the methylene protons between the imidazolium units of **4.34** resonate as a singlet signal at 6.67 ppm in a similar manner to compound **4.29**.

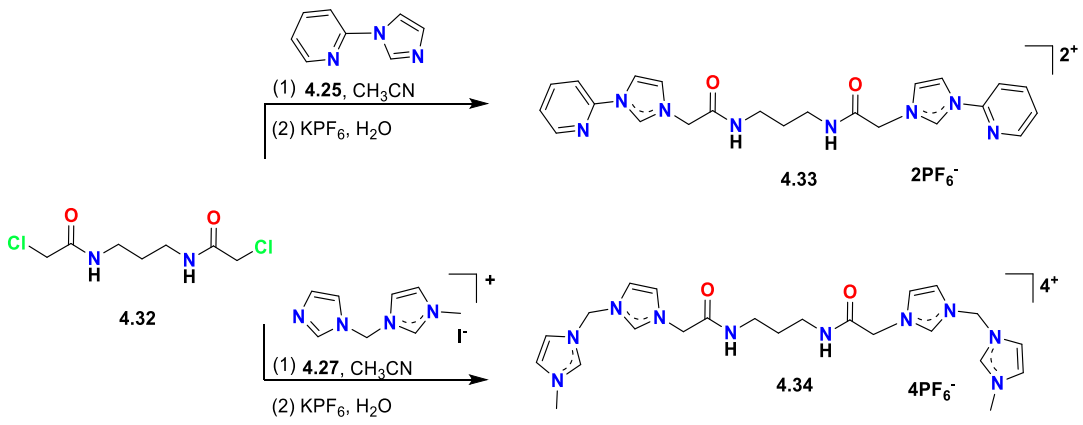

Scheme 4.4. Synthesis of the imidazolium salt pro-ligands **4.33** and **4.34** via the reaction of **4.32** with **4.25** and **4.27**, respectively.

The Re(I) complexes **4.35** and **4.36** were synthesised using a similar method to that described for **4.30** and **4.31** from the pro-ligand (either **4.33** or **4.34**), $Re(CO)_5Cl$ and silver oxide in a mixture of methanol and dichloromethane (Scheme 4.5). The ^{1}H NMR spectra for Re(I) complexes **4.35** and **4.36** did not show a signal for the imidazolium C2-H proton, suggesting that the C2 carbon of the imidazolium pro-ligands had been successfully deprotonated and coordinated to the Re(I) metal centre as a carbene. Additionally, the ^{1}H NMR spectrum for complex **4.35** shows a multiplet signal in a range of 8.11-8.14 ppm that corresponds to the amide N-H protons. Furthermore, sets of doublet signals were also observed, which correspond to the protons of the methylene group located between the NHC units of complex **4.36**. This pattern is consistent with these protons being inequivalent due to the presence of conformational isomers, in a similar manner to that described previously for **4.31**.[20] The ^{13}C NMR spectrum of complex **4.35** also shows the characteristic downfield shifted signals for the carbonyl carbon bound to Re(I) metal centre in the range of 192-199 ppm, while the C2 carbon is resonated at 189.0

ppm. The dinuclear Re(I) complexes with diamide linker groups were prepared to improve the aqueous solubility of these dinuclear Re(I) complexes. However, the solubility of these complexes was not significantly improved as the same ratio of water and DMSO (60% water:40% dimethyl sulfoxide) was required to dissolve the dinuclear Re(I) complexes.

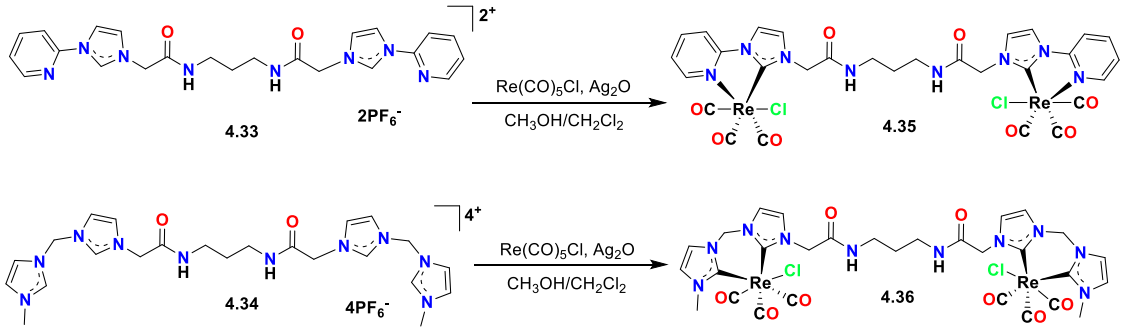

Scheme 4.5. Synthesis of Re(I) complexes **4.35** and **4.36** via a Ag_2O transmetalation reaction.

4.2.2. Ligand Exchange Studies

As the dinuclear Re(I) complexes were synthesised as potential anticancer agents, it is important to investigate the kinetics of the aquation process where the chloride ligands are replaced by water molecules.[21-22] The ligand exchange process between the chloride ligands and water for complexes **4.30** and **4.31** was investigated in an aqueous solution using WATERGATE ^{1}H NMR spectroscopy. In this process, the anionic chloride ligands are replaced by water molecules to give cationic Re(I) complexes. Both complexes **4.30** and **4.31** were dissolved in a mixture of water (56%), DMSO-d_6 (40%), and D_2O (4%) and the WATERGATE ^{1}H NMR spectra were recorded at specific time points over the course of 48 h.

A stacked plot of the ^{1}H NMR spectra (aromatic region) for compound **4.30** recorded over a 24 h period is shown in Figure 4.5, with the first ^{1}H NMR spectrum being recorded at

0.25 h. The peaks (blue asterisks) observed in the first recorded spectrum correspond to complex **4.30**, where the chloride ligands are still bound to the Re(I) metal centres. After 1 h, a new set of signals begins to appear, and these peaks correspond to the cationic complex **4.37** with water molecules bound in the place of the chloride ligands (the peaks for this complex are labelled with red asterisks). Over the course of the experiment, the intensity of the new set of signals increases, while the intensity of the signals for the original complex decreases. After 24 h, the signals for the original neutral complex have reached very low intensity.

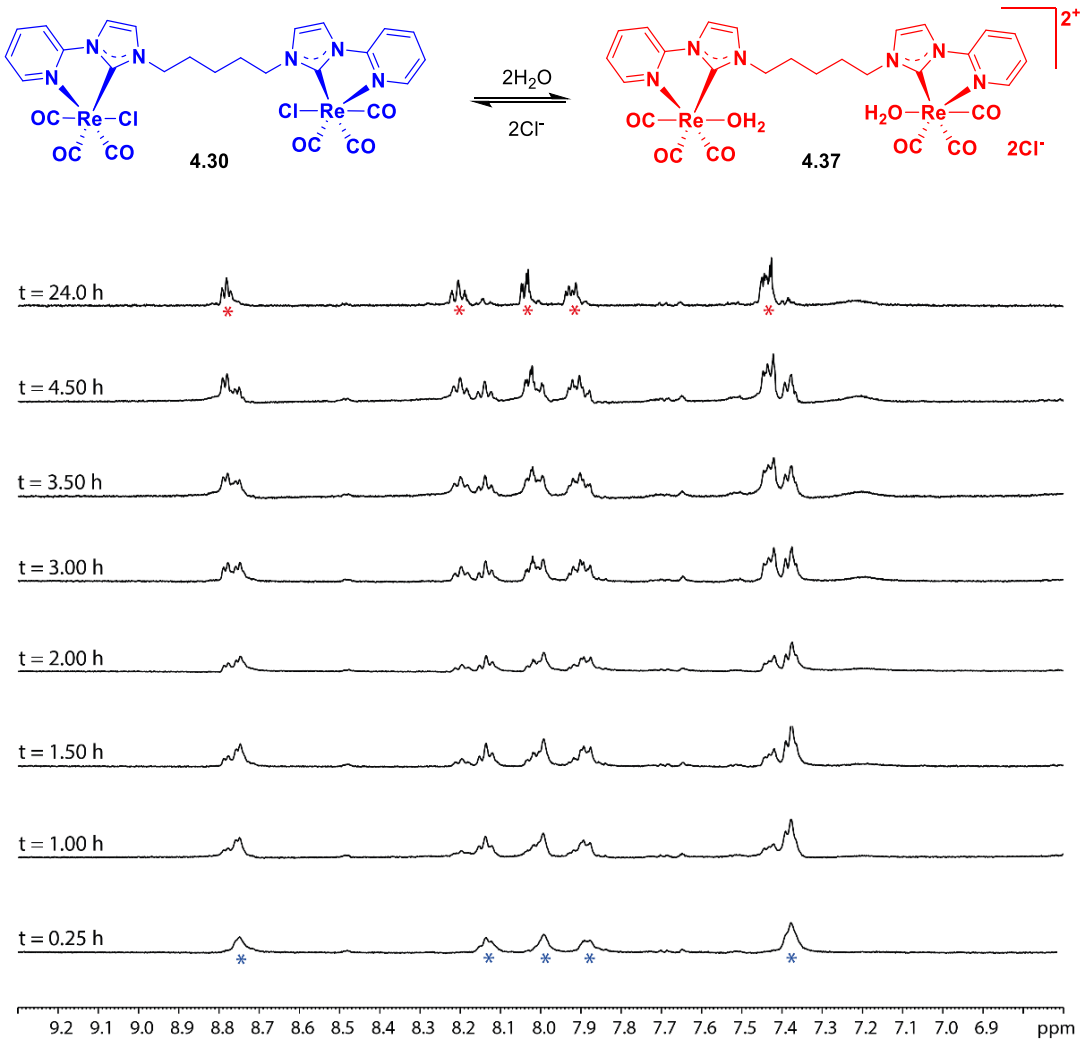

Figure 4.5. Stacked ^{1}H NMR (500.13 MHz) spectra (aromatic region) recorded for **4.30** in aqueous solution over a period of 24 h at 25.0 ± 0.1 °C.

Complex **4.30** is dinuclear and it is expected that an intermediate form of the complex, where one Re(I) centre is coordinated to water, while the other is bound to a chloride ligand may be formed. Interestingly, however, this asymmetric structure was not observed in the time-course NMR spectra (where the concentration of water is much higher than that of the complex). This observation is likely to be due to the extended linker group between the Re(I) centres, which results in no electronic or other interactions between the metals in the dinuclear complexes. The positive ion high-resolution mass spectrum (Figure 4.6a) was recorded from the kinetic experimental solution after 48 h. Each of the Re(I) signals obtained from the HRMS spectrum (solid line) is plotted against the simulated signal for the assigned structure (dashed line) in Figure 4.6. The peak at *m/z* = 933.0820 is consistent with the chemical formula $[C_{27}H_{25}N_6O_8Re_2]^+$, where one Re(I) centre is bound to a water molecule, while the other metal centre is bound to a hydroxyl group **4.39** (Figure 4.6c). Additionally, the peak at *m/z* = 915.0711 corresponds to the chemical formula $[C_{27}H_{23}N_6O_7Re_2]^+$, where only one of the Re(I) centres is coordinating to one hydroxyl group **4.38** (Figure 4.6b).

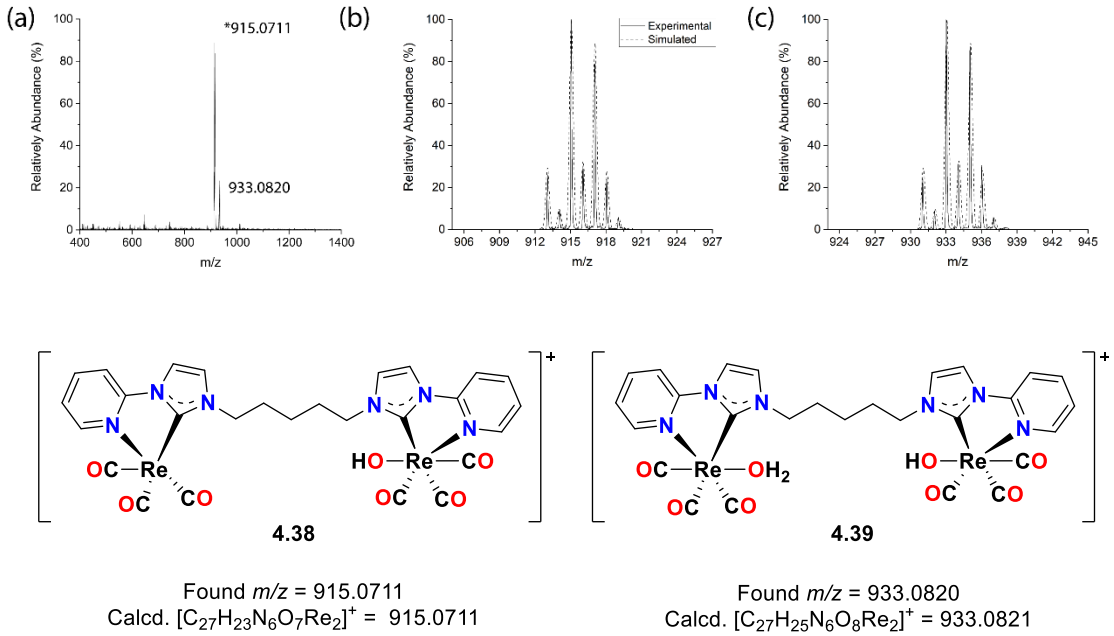

Figure 4.6. (a) High-resolution mass spectrum of compound **4.30** after being subjected to the ^{1}H NMR time course study for 24 h at 25.0 ± 0.1 °C. Zoom scans of the main signals at (b) *m/z* = 915.0711, (c) *m/z* = 933.0820 are plotted together with the simulated spectra for the formulas $[C_{27}H_{23}N_6O_7Re_2]^+$ (**4.38**), and $[C_{27}H_{25}N_6O_8Re_2]^+$ (**4.39**), respectively. The structures of the compounds (**4.38** and **4.39**) corresponding to these formulae are shown in the lower panel.

Kinetic analysis of the collected ^{1}H NMR data for **4.30** was performed using the computer program Scientist® Version 3.0 (see Figure A4.3 and Figure A4.4, Appendix 4). Because a pseudo-first-order (water in large excess) condition was used, the simple kinetic model shown in Equation (1) was employed to calculate the rate constant for complex **4.30**.

$$\mathbf{4.30}Cl_2 + 2H_2O \underset{k_{-1}}{\overset{k_1}{\rightleftharpoons}} [\mathbf{4.30}(H_2O)_2]^{2+} + 2Cl^- \quad (H_2O \text{ in large excess}) \tag{1}$$

To ensure that the rate constant calculated remains consistent, one of the imidazolylidene group protons and one of the pyridyl group protons were used to estimate the rate constant. The estimated forward and reverse rate constants calculated based on the

imidazolylidene proton were k_1 = 6.60 × 10^{-5} s^{-1} (± 0.004) and k_{-1} = 8.05 × 10^{-5} s^{-1} (± 0.004), while the estimated forward and reverse rate constants for a pyridyl proton were k_1 = 5.96 × 10^{-5} s^{-1} (± 0.001) and k_{-1}= 7.80 × 10^{-5} s^{-1} (± 0.001), respectively.

The same ligand exchange experiment described for complex **4.30** was performed on complex **4.31**. The stacked ^{1}H NMR spectra (aromatic region) for complex **4.31** are shown in Figure 4.7. Similar changes were observed for the time-course ^{1}H NMR experiment for complex **4.31**, as were seen for **4.30**, the chloride ligands are exchanged for water molecules. The peaks corresponding to the starting complex **4.31** are labelled with blue asterisks, while those for the cationic aqua complex **4.40** are labelled with red asterisks.

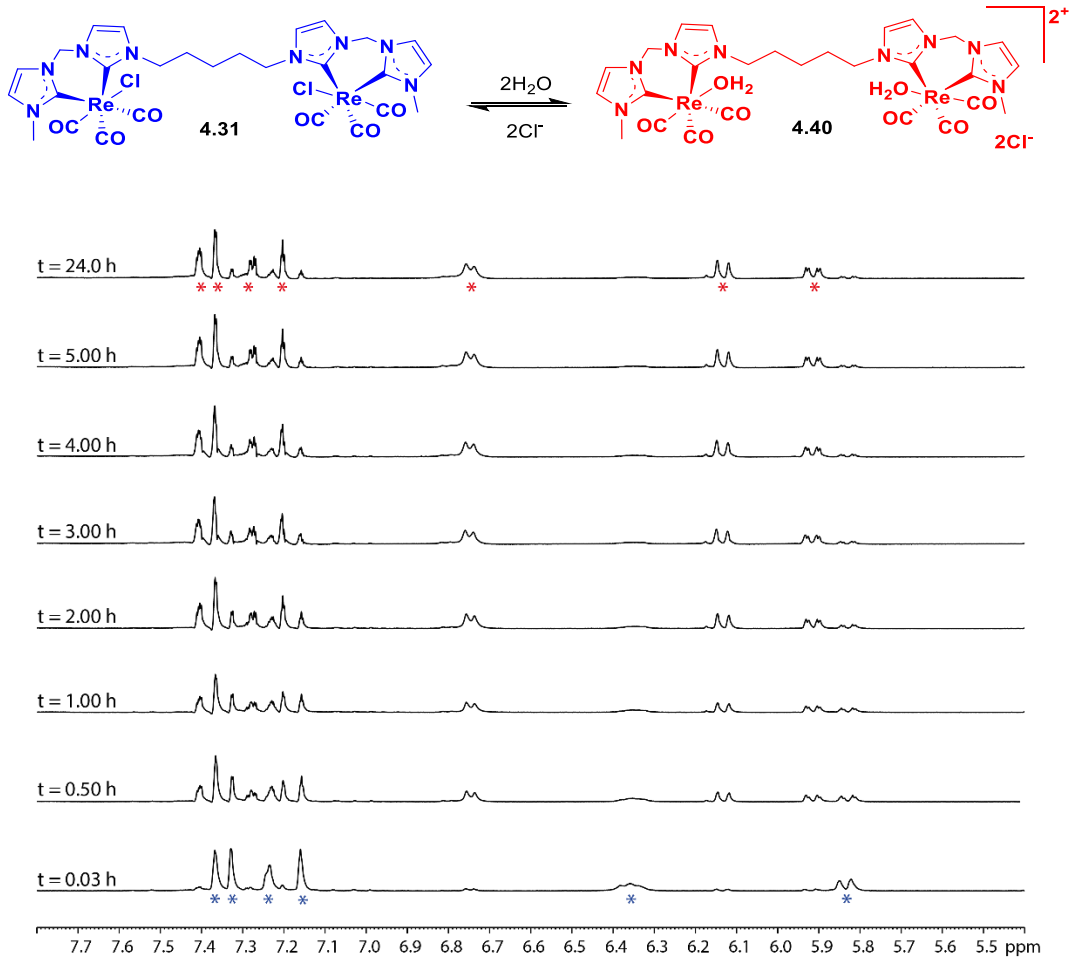

Figure 4.7. Stacked ^{1}H NMR (500.13 MHz) spectra (aromatic region) recorded for **4.31** in aqueous solution over a period of 24 h at 25.0 ± 0.1 °C.

The positive ion high-resolution mass spectrum was recorded from the NMR solution of **4.31** after 48 h. Each of the Re(I) signals obtained from the HRMS spectrum (solid lines) was plotted against the simulated signal for the assigned structures (dashed line) (Figure 4.8a). The peak at *m/z* = 967.1352 is consistent with the chemical formula of $[C_{27}H_{31}N_8O_8Re_2]^+$, where one Re(I) centre is bound to a water molecule, while the other Re(I) centre is bound to a hydroxyl group (Figure 4.8c). Additionally, the peak at *m/z* = 949.1246 corresponds to the chemical formula $[C_{27}H_{29}N_8O_7Re_2]^+$, where only one of the Re(I) centres is coordinating to one hydroxyl group (Figure 4.8b).

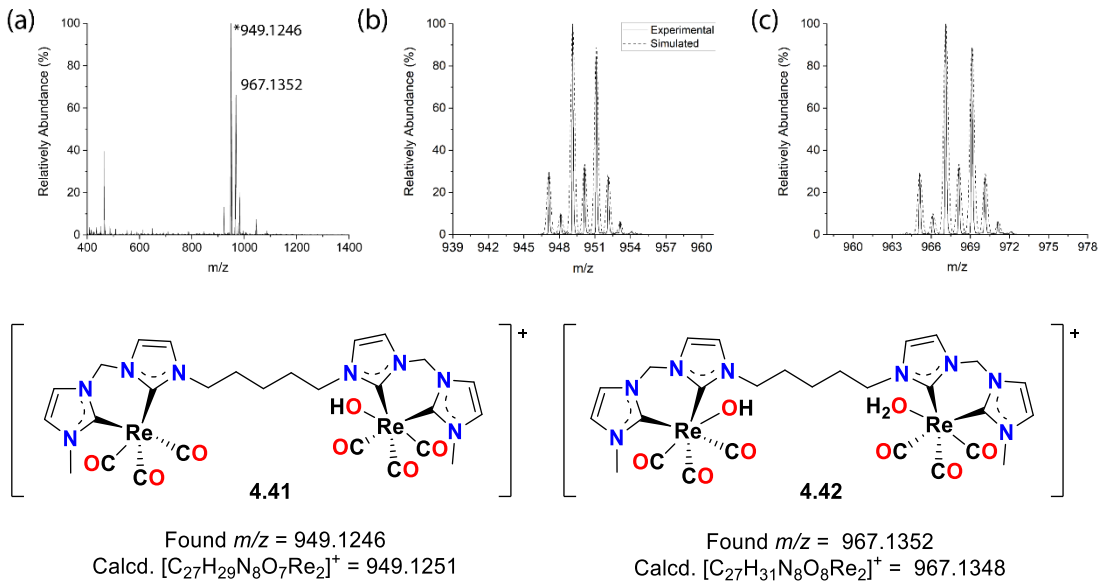

Figure 4.8. (a) High-resolution mass spectrum of compound **4.31** after being subjected to the ^{1}H NMR time-course study for 24 h at 25.0 ± 0.1 °C. Zoom scans of the main signals at (b) *m/z* = 949.1246, (c) *m/z* = 967.1352 are plotted together with the simulated spectra for the formulas $[C_{27}H_{29}N_8O_7Re_2]^+$ (**4.41**), and $[C_{27}H_{31}N_8O_8Re_2]^+$ (**4.42**), respectively. The structures of the compounds (**4.41** and **4.42**) corresponding to these formulae are shown in the lower panel.

Kinetic analysis of the collected ^{1}H NMR data for **4.31** was performed using the same method as that described for **4.30** (see Figure A4.5 and Figure A4.6, Appendix 4). Since

a pseudo-first-order (water in large excess) condition was used, the simple kinetic model shown in Equation (2) was employed to calculate the rate constant for complex **4.31**.

$$\mathbf{4.31}Cl_2 + 2H_2O \underset{k_{-1}}{\overset{k_1}{\rightleftharpoons}} [\mathbf{4.31}(H_2O)_2]^{2+} + 2Cl^- \quad (H_2O \text{ in large excess}) \tag{2}$$

To ensure that the rate constant calculated remains consistent, one of the methyl group protons and one of the methylene protons between *bis*-imidazolylidene groups were used to estimate the rate constant. The estimated forward and reverse rate constants were calculated based on the methyl protons were $k_1 = 1.57 \times 10^{-4}$ s^{-1} (± 0.004) and $k_{-1} = 3.12 \times 10^{-5}$ s^{-1} (± 0.004), while estimated forward and reverse rate constants for a methylene proton were $k_1 = 1.58 \times 10^{-4}$ s^{-1} (± 0.002) and $k_{-1} = 3.30 \times 10^{-5}$ s^{-1} (± 0.002), respectively.

The results from ^{1}H NMR kinetics experiments suggested that the rate of aquation for the Re(I) *bis*-imidazolium complex **4.31** is significantly faster compared to complex **4.30**. This result is expected on the basis of a *cis* effect influences by the increased electron donating properties of the NHC donors.[23-27] The effect of the different donor properties of the pyridyl-imidazolylidene and *bis*-imidazolylidene ligands on the aquation rate of Re(I) complexes was discussed in Chapter 3.

4.2.3. Photophysical Studies

The photophysical properties of polynuclear Re(I) complexes were investigated. The electronic absorption spectra of complexes **4.30**, **4.31**, **4.35** and **4.36** are shown in Figure 4.9. Due to the solubility issue, all polynuclear Re(I) complex solutions were prepared in 10% DMSO and 90% methanol. The spectra show that complexes **4.30** and **4.35** absorb strongly at 334 nm and 340 nm, respectively. For complex **4.31** and **4.36**, an intense absorption band is observed at 312 nm and 309 nm, respectively. When compared to previously reported results for related compounds, the low energy absorption band

between 320-460 nm may be assigned to ^{1}MLCT transitions.[12,21,28] In addition, the high energy absorption band between 250-320 nm can be assigned to the intraligand $\pi \rightarrow \pi^*$ transitions.[12,21,28]

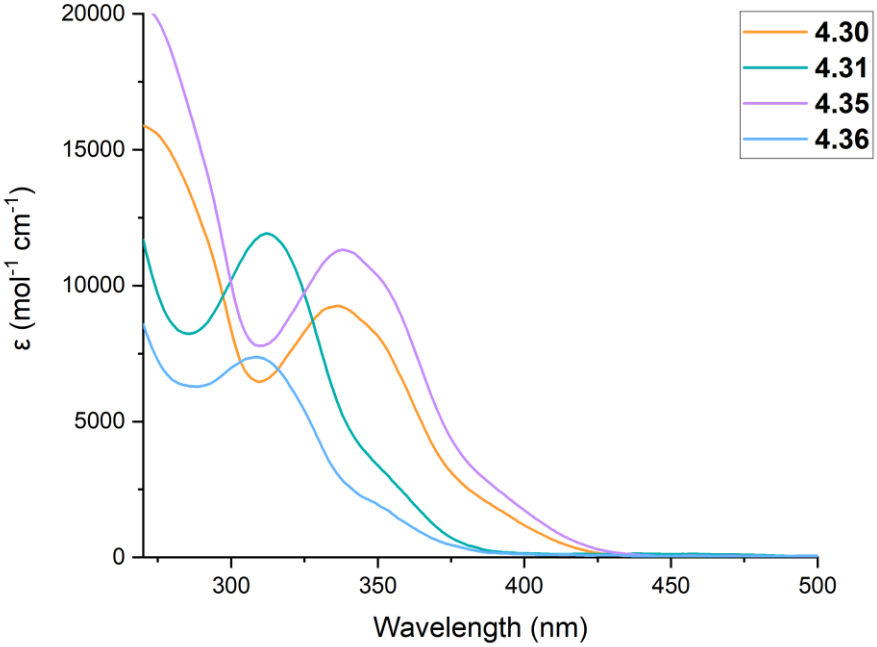

Figure 4.9. UV-visible spectra for complex **4.30** (orange), **4.31** (green), **4.35** (purple) and **4.36** (blue) in 10% DMSO and 90% methanol solutions (10 µM).

The luminescence emission spectra for complexes **4.30**, **4.31** and **4.35** are shown in Figure 4.10, and it is apparent that the emission profiles are similar for **4.30** (λ_{em} = 383 nm), **4.31** (λ_{em} = 393 nm), and **4.35** (λ_{em} = 391 nm). Complex **4.36** did not produce detectable emission, which may be due to the low extinction coefficients for this compound.

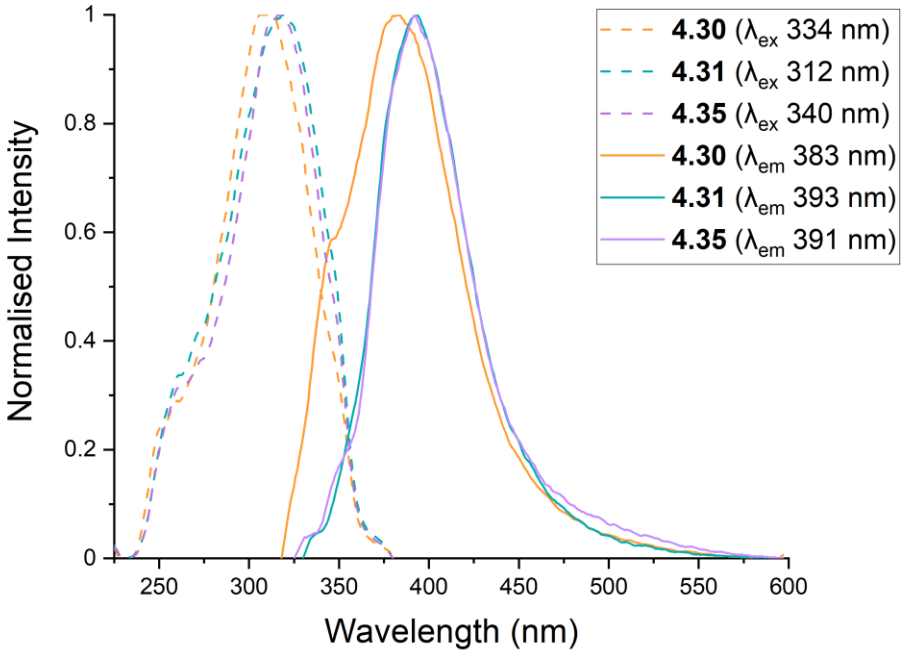

Figure 4.10. Emission spectra for complex **4.30** (orange), **4.31** (green) and **4.35** (purple) recorded from 10 µM solutions in 10% DMSO and 90% methanol.

4.3. Re(I) Carbohydrate Complexes

4.3.1. Synthesis of Re(I) Complex of a Glucosamine Functionalised NHC Ligand

Due to the high glucose demand of tumours and the overexpression of GLUT transporters by cancer cells, it was of interest to conjugate potential anticancer Re(I)-NHC complexes to glucose derivatives. The first synthetic approach to developing compounds of this type is shown in Scheme 4.6. In this synthetic scheme, the hydrochloride salt of glucosamine was reacted with di-*tert*-butyl dicarbonate to form the *tert*-butyloxycarbonyl (BOC) protected glucosamine **4.43** (Scheme 4.6).[29] Compound **4.43** was then benzylated with benzyl bromide in the presence of excess sodium hydride as a strong base in anhydrous dimethylformamide to afford compound **4.44**.[29] This compound was then reacted with trifluoroacetic acid (TFA) to remove the *tert*-butoxylcarbonyl group and yielded compound **4.45**.[29] Compound **4.45** was obtained as the β anomer, which was purified

using column chromatography on silica gel, and it was converted to the α-chloroamide **4.46** by a reaction with one equivalent of 2-chloroacetyl chloride. The final pro-ligand **4.47** was prepared by reacting an equimolar mixture of **4.46** and **4.25** in acetonitrile at reflux. The reaction was monitored by TLC, and this showed that increased reaction times resulted in an improved yield of the desired product (18%).

The ^{1}H NMR spectrum of **4.47** shows a downfield signal for the NC*H*N (pre-carbenic) proton at 10.98 ppm, and the formation of the glucose conjugated product was indicated by a doublet signal at 9.76 ppm corresponding to the amide N-H proton. Here, the amide N-H proton appeared as a doublet because it is coupled to the H2 proton of the glucose moiety. The ^{13}C NMR spectrum shows a downfield signal for the imidazolium carbon at 164.1 ppm, suggesting that the imidazole ring was successfully alkylated.

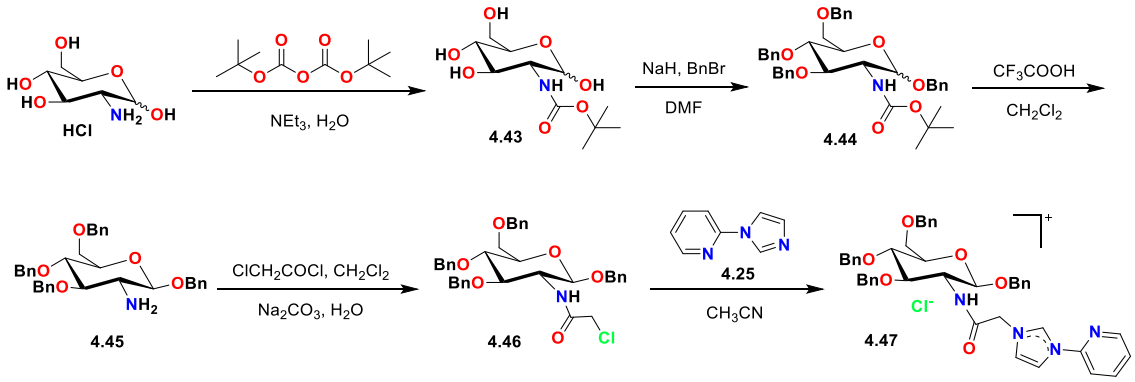

Scheme 4.6. Synthesis of *N*-heterocyclic carbene pro-ligand conjugated to benzylated glucosamine (**4.47**).

The Re(I) tricarbonyl complex of pro-ligand **4.48** was synthesised via a one-pot silver transmetalation procedure as shown in Scheme 4.7. The crude product was purified using column chromatography on silica gel to obtain the pure product as a yellow solid. The results from NMR studies indicate the formation of the expected Re(I) complex **4.48**. For example, the ^{1}H NMR spectrum of **4.48** exhibits no pre-carbenic proton signal, suggesting the deprotonation of the C2 position of the imidazole ring and its coordination to the

$[Re(CO)_3]^+$ core. In addition, the ^{13}C NMR spectrum also shows a downfield shifted signal of the C2 carbene carbon at 187.8 ppm, confirming the coordination of the carbene to the Re(I) metal centre. Furthermore, the characteristic carbonyl signals resonate in the range of 193-196 ppm are corresponded to the carbonyl groups bound to $[Re(CO)_3]^+$ core.

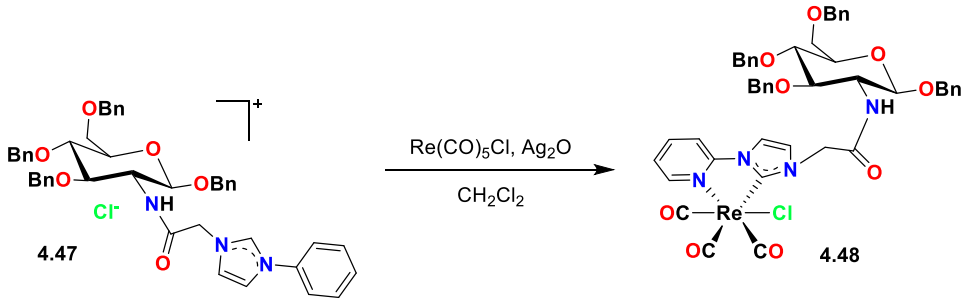

Scheme 4.7. Synthesis of the Re(I) complex **4.48** via a Ag(I) transmetalation reaction.

In the effort to remove the benzyl protecting groups, complex **4.48** was subjected to a hydrogenolysis reaction over a 10% Pd/C catalyst (Scheme 4.8). The reaction mixture was monitored using TLC; however, this showed that the benzyl groups were not removed using this synthetic approach. In an effort to obtain the desired complex **4.49**, a range of other reaction conditions were explored. For example, the reaction time was increased (up to seven days), or the solution was heated at 50 °C and finally, the catalyst $Pd(OH)_2$ was also investigated. Despite these attempts, the benzyl protecting could not be removed from complex **4.48**.

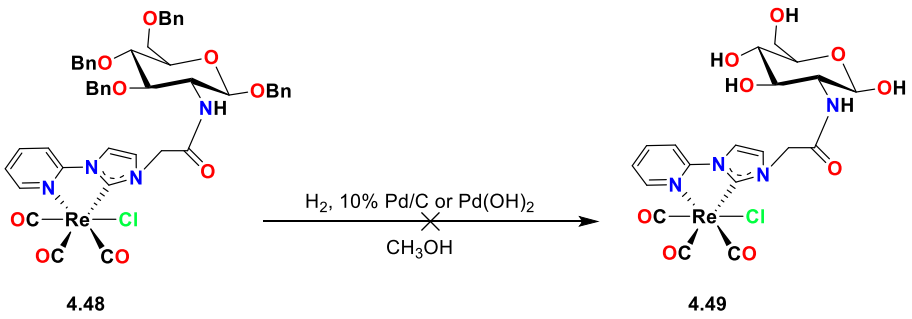

Scheme 4.8. Unsuccessful attempts for the removal of the benzyl protecting groups of **4.48**.

4.3.2. Synthesis of a Re(I) Complex of a Glucose Functionalised NHC Ligand

The second approach investigated for the synthesis of an imidazolium pro-ligand coupled to glucose began by preparing the pentaacetyl protected glucose **4.50** according to a previously reported procedure.[30-31] This compound was brominated using a solution of 33% HBr in glacial acetic acid yielding **4.51**[30-31] (Scheme 4.9), and it was subsequently used to alkylate compound **4.25** in an S_N2 reaction to give the pro-ligand **4.52**. For the synthesis of complex **4.53**, the pro-ligand **4.52** was reacted with $Re(CO)_5Cl$ using a silver transmetalation reaction (Scheme 4.9). Interestingly, rather than the expected Re(I) complex with fully protected acetyl groups **4.53**, one of the acetyl group was cleaved during the complex synthesis reaction to give complex **4.54** (Scheme 4.9). The purification of the crude product was attempted by column chromatography using a mixture of methanol and dichloromethane as the eluents. Although complex **4.54** was purified via column chromatography, a minor impurity was still be observed in the ^{1}H NMR and mass spectra (Figure A4.25, Appendix 4). It is important to note that complex **4.54** is a product of nucleophilic acetyl substitution; therefore, the reaction will favour secondary substituted alcohol (e.g. C2-OH, C3-OH and C4-OH) compared to the primary substituted alcohol (C6-OH).[32-34] Previous studies have shown that C2-OH is the most reactive hydroxyl group for D-glucose while C4-OH is the least reactive.[32-34] Therefore, one of the acetyl groups would likely to be cleaved on the C2 position of glucose.

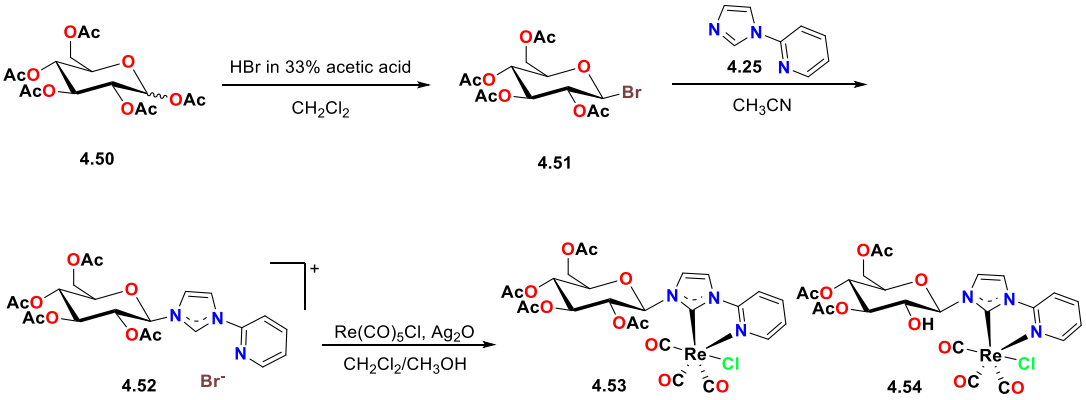

Scheme 4.9. Synthetic route for preparing pro-ligand conjugated to tetraacetylglucose (**4.52**) and the Re(I) complexes (**4.53** and **4.54**).

Removal of the acetyl protecting groups of glucose is generally carried out using a hydrolysis reaction with a strong base such as NaOMe and NaOH or using an organic base such as Et_3N.[35] In the effort to remove the acetyl groups, complex **4.54** was subjected to a reaction with K_2CO_3 in a mixture of methanol and water solution (Scheme 4.10).[36] The reaction mixture was monitored using ^{1}H NMR; however, this showed that the acetyl groups were not removed using this synthetic approach. In order to prepare the desired complex **4.55**, various attempts including using different bases (e.g. Cs_2CO_3[37] or Et_3N[35]), elevated temperature, addition of the catalyst TBABr were investigated. However, these attempts were unsuccessful, and the acetyl protecting groups could not be removed from complex **4.54**.

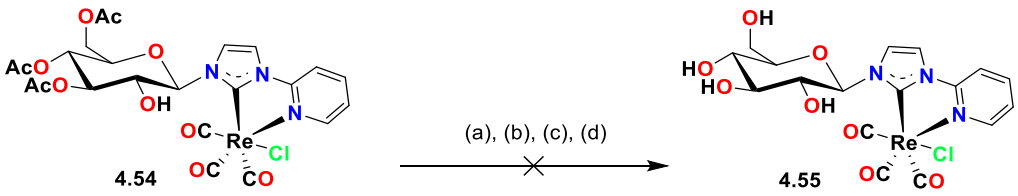

Scheme 4.10. Unsuccessful attempts for the removal of the acetyl protecting groups of **4.54**; (a) K_2CO_3, CH_3OH/H_2O, (b) Cs_2CO_3, CH_3CN, (c), Et_3N, CH_3OH, (d) Na_2CO_3, TBABr.

The unexpected formation of complex **4.54** was confirmed by ^{1}H NMR and mass spectroscopy analysis. For the ^{1}H NMR spectrum of this complex, the characteristic deshielded pre-carbenic proton (NC*H*N) was absent, indicating deprotonation of the carbene and coordination of pyridyl-imidazolylidene ligand to the Re(I) metal centre (Figure 4.11a). The chemical shifts for the aromatic protons and the protons of glucose for complex **4.54** were shifted when compared to the pro-ligand **4.52** (Figure 4.11b). When the signals corresponding to the acetyl groups of complex **4.54** were integrated, only nine protons (rather than the expected twelve) could be assigned to these peaks. In addition, some small peaks are visible that correspond to a second reaction product (**4.57**, Figure 4.11), the structure of this compound was identified by HRMS analysis (Figure 4.12).

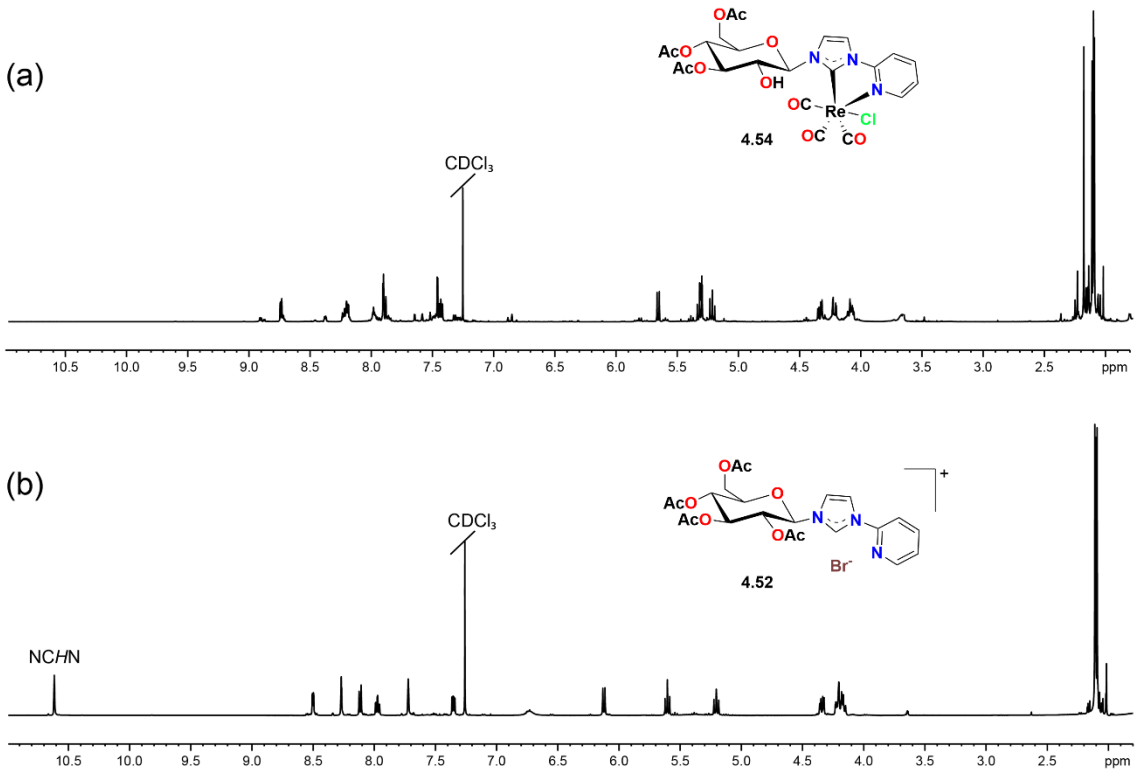

Figure 4.11. ^{1}H NMR spectrum of (a) complex **4.54** and (b) pro-ligand **4.52** recorded from $CDCl_3$ solutions.

The positive ion high-resolution mass spectrum was recorded for complex **4.54**, and the results were in agreement with the ^{1}H NMR spectrum. The full mass spectrum is plotted in Figure 4.12 (a), and each of the Re(I) containing peaks is plotted against the simulated peak (dashed line) for the assigned formula (Figure 4.12b-d). The peak at *m/z* = 704.0893 is consistent with the chemical formula $[C_{23}H_{23}N_3O_{11}Re]^+$, where one acetyl glucose protecting group had been cleaved, and the chloride ligand was dissociated, yielding a cationic compound **4.54** (Figure 4.12b). The base peak at *m/z* = 745.1152 corresponds to the chemical formula $[C_{25}H_{26}N_4O_{11}Re]^+$, where one acetyl group was cleaved, and the Re(I) complex had undergone a ligand exchange reaction, while the chloride ligand was replaced with a acetonitrile molecule **4.56** (Figure 4.12c). Interestingly, a peak was observed at *m/z* = 849.1535, and this peak is consistent with the chemical formula of $[C_{31}H_{30}N_6O_{11}Re]^+$ (complex **4.57**), where one of the acetyl groups was cleaved, and in addition, the chloride ligand was exchanged for compound **4.25** (Figure 4.12d). This result is consistent with complex **4.57** being the impurity that is apparent in the ^{1}H NMR spectrum. In addition, the formation of complex **4.54** differed in each synthetic reaction, with the quantities produced ranging from 0-50%. These results indicate that an unexpected acetyl group cleavage reaction was occurring during the silver transmetalation reaction to form the Re(I) complex.

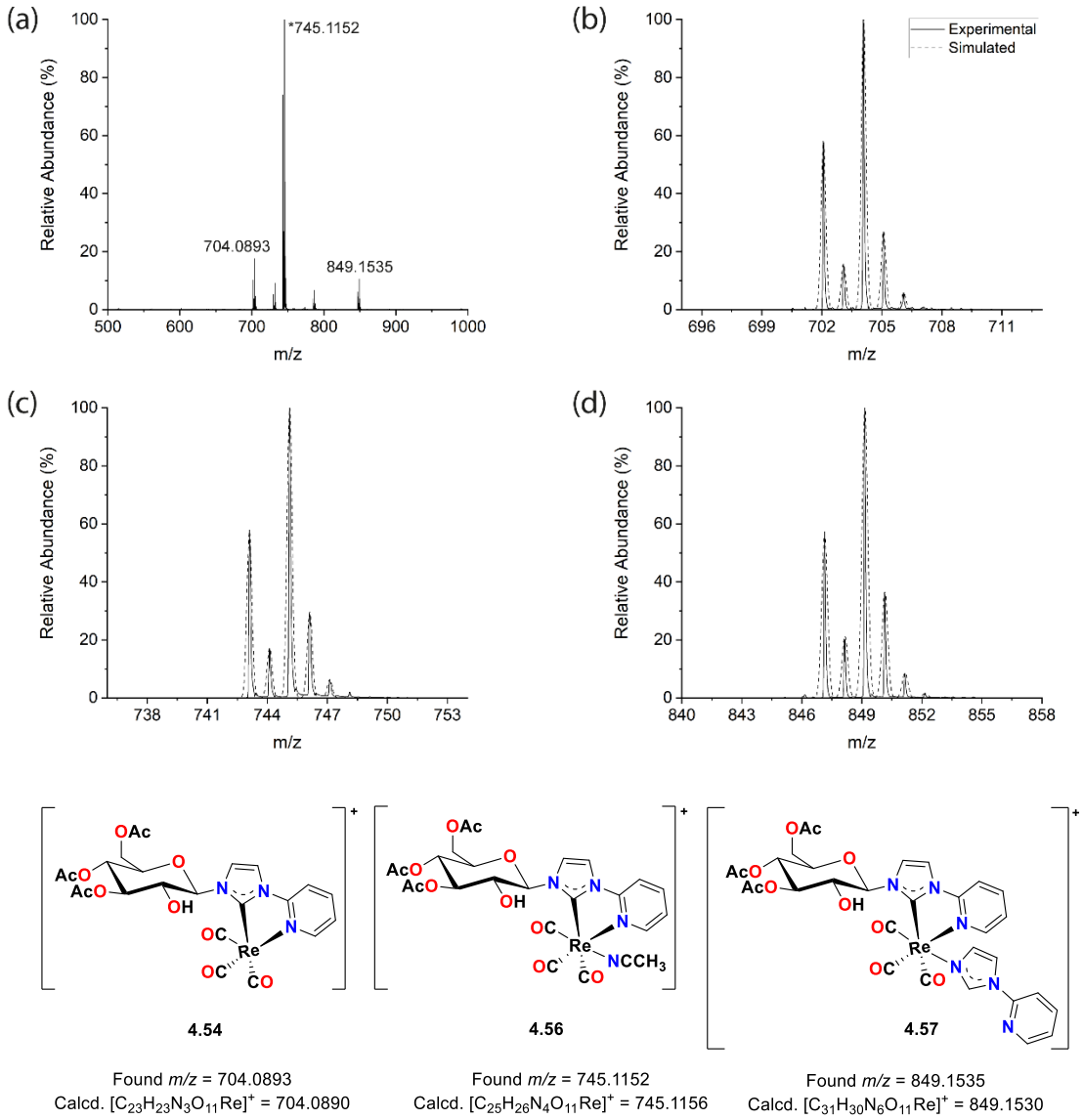

Figure 4.12. (a) HRMS spectrum of a freshly prepared solution of **4.54** in acetonitrile. Zoom scans of the main signals at (b) *m/z* = 704.0893, (c) *m/z* = 745.1152 and (d) *m/z* = 849.1535 are plotted together with the simulated spectra for the formulas $[C_{23}H_{23}N_3O_{11}Re]^+$ (**4.54**), $[C_{25}H_{26}N_4O_{11}Re]^+$ (**4.56**), $[C_{31}H_{30}N_6O_{11}Re]^+$ (**4.57**), respectively. The structures of the compounds (**4.54** – **4.57**) corresponding to these formulae are shown in the lower panel.

These results show that the acetyl protecting groups of **4.52** were cleaved during the silver oxide transmetalation reaction to form **4.55**. To evaluate if it was silver oxide that was causing this hydrolysis reaction, the equivalents of silver oxide added to the reaction

mixture to form complex **4.55** were increased to five and the mixture was stirred for seven days (Scheme 4.11).

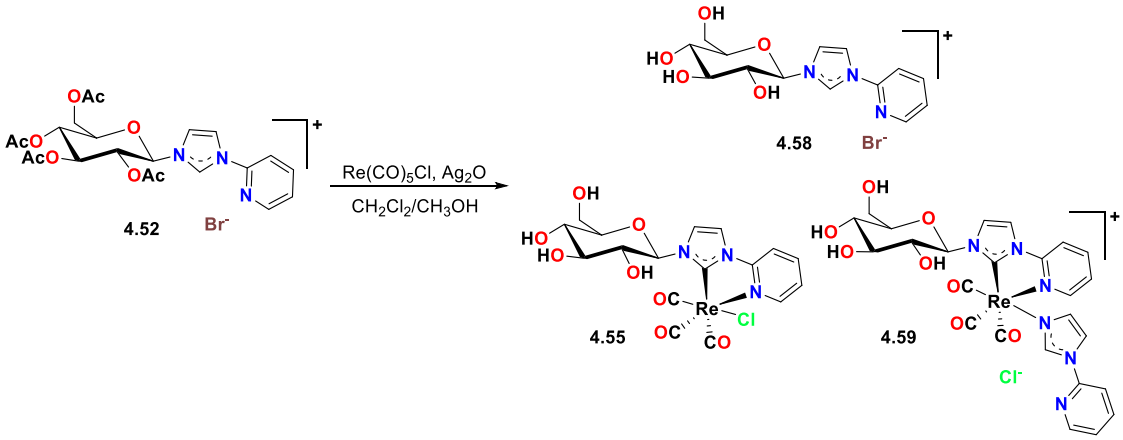

Scheme 4.11. Synthetic route for the synthesis of the Re(I) complex of pro-ligand **4.52**, where five equivalents of silver oxide and a reaction time of seven days were used.

After seven days, the positive ion high-resolution mass spectrum was recorded for the isolated complex (Figure 4.13a). In this spectrum, a peak was observed at *m/z* = 308.1243, and this is consistent with the chemical formula $[C_{14}H_{18}N_3O_5]^+$, which corresponds to the fully deprotected glucose pro-ligand **4.58** (Figure 4.13b). The base peak of the spectrum is observed at *m/z* = 578.0574 and corresponds to the chemical formula $[C_{17}H_{17}N_3O_8Re]^+$. This formula is consistent with removal of all four of the acetyl protecting groups to produce a cation **4.55** (Figure 4.13c). The peak observed at *m/z* = 723.1208 is consistent with the chemical formula $[C_{25}H_{24}N_6O_8Re]^+$, where the acetyl protecting groups were cleaved, and also ligand **4.25** was coordinated to the Re metal (**4.59**, Figure 4.13d). These results suggest that the acetyl groups were removed in the presence of silver oxide, and when higher concentrations of this reagent were used in combination with increased reaction times, a greater level of cleavage was observed. Despite several attempts, the deprotected NHC-glucose pro-ligand **4.58** and the Re(I)-NHC complex (**4.55** and **4.59**) could not be separated.

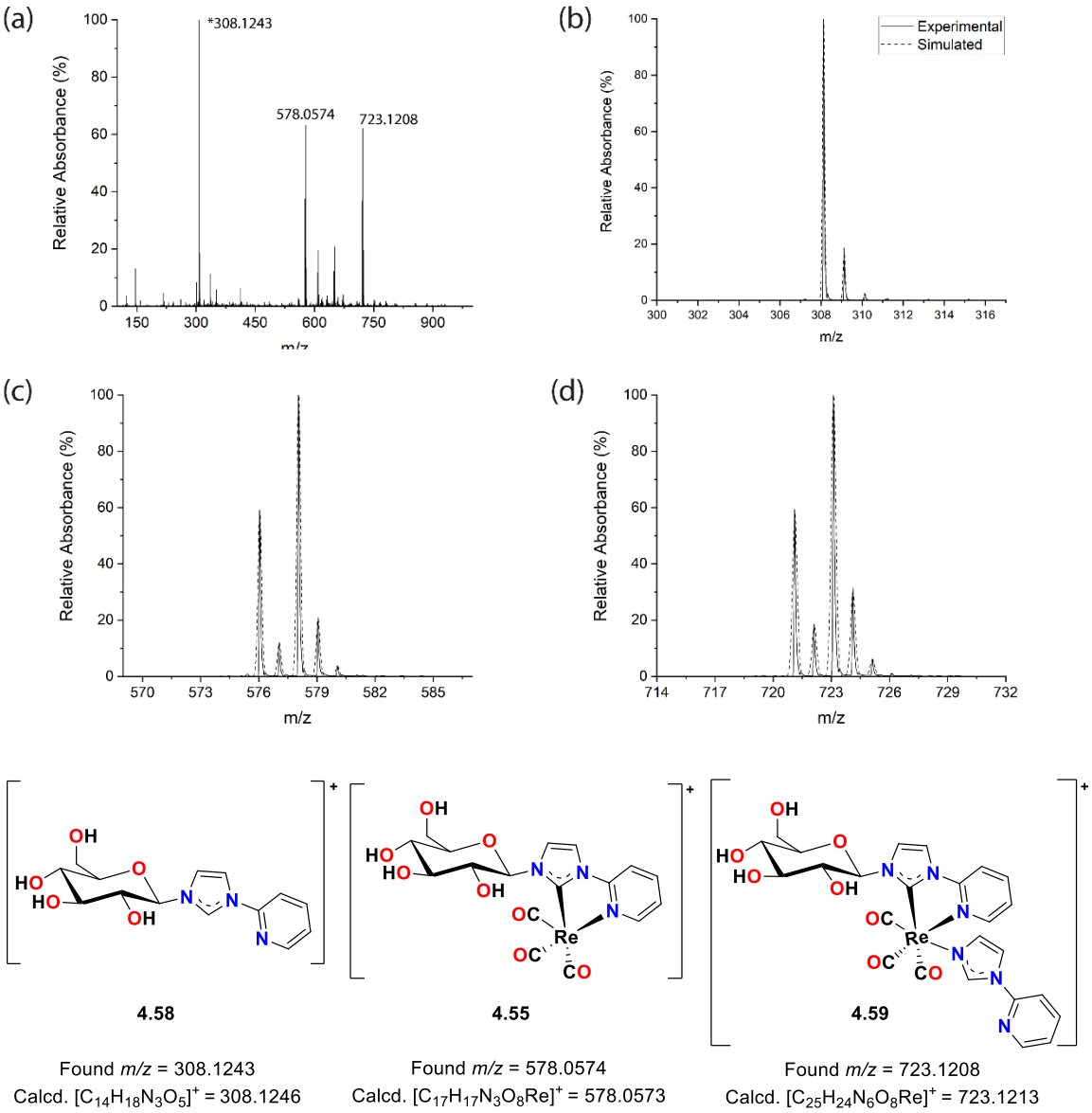

Figure 4.13. (a) HRMS spectrum of a freshly prepared solution of **4.55** in methanol. Zoom scans of the main signals at (b) *m/z* = 308.1243, (c) *m/z* = 578.0574 and (d) *m/z* = 723.1208 are plotted together with the simulated spectra for the formulas $[C_{14}H_{18}N_3O_5]^+$ (**4.58**), $[C_{17}H_{17}N_3O_8Re]^+$ (**4.55**), and $[C_{25}H_{24}N_6O_8Re]^+$ (**4.59**), respectively. The structures of the compounds (**4.55**, **4.58** and **4.59**) corresponding to these formulae are shown in the lower panel.

Based on the HRMS results for the reaction of pro-ligand **4.52** with $Re(CO)_5Cl$], it is apparent that in addition to cleavage of the acetyl protecting groups of the glucose moiety, compound **4.25** was also cleaved from the anomeric carbon (or C1) position of the glucose

molecule. The mass spectrometric results show that the cleaved **4.25** coordinates to the Re(I) metal centre (via ligand exchange with the chloride ligand) during the complex synthesis reaction, yielding the cationic product **4.59** (Figure 4.13). Although the exact mechanism of this process remains unknown, a similar reaction pathway has been observed for the glycosidic bond cleavage in DNA purine nucleosides.[38-39] During the deglycosylation reaction, nucleophiles such as water can facilitate the cleavage of the C-N bond that connects the C1 position of deoxyribose to the nucleobase.[38-39] For example, Scheme 4.12a shows the attack of water on the anomeric carbon of guanosine and cleavage of sugar from the nucleobase.[38-39] It seems likely that a similar mechanism is occurring in the cleavage of **4.25** from the glucose moiety of pro-ligand **4.58**, where the glycosidic bond cleavage is facilitated by an oxygen-based nucleophiles such as a water molecule or a hydroxide ion formed from silver(I) oxide to give a molecule of **4.25** and the glucose unit (Scheme 4.12b).

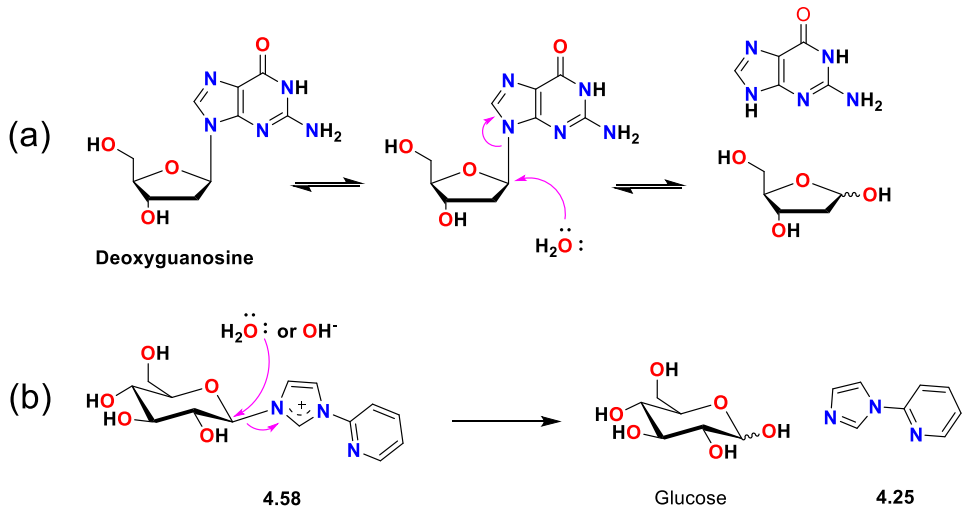

Scheme 4.12. Proposed mechanistic pathways for the pathway of the glycosidic bond cleavage in (a) deoxyguanosine and (b) the pro-ligand **4.58**.

Deacetylation is the reaction where an acetyl group is cleaved from a chemical compound.[40-41] In the case of pro-ligand **4.52**, the acetyl groups were cleaved from the glucose molecule during the synthesis of the Re(I) complex **4.53** via a silver

transmetalation reaction. It is likely that the silver oxide used in this reaction was the source of the base that facilitated the acetyl group hydrolysis reaction. Here, silver(I) oxide dissociates in solution to give two equivalents of silver cations and one equivalent of the oxide anion, which in turn reacts with a water molecule to give two equivalents of hydroxide (Figure 4.14). These hydroxide groups then react at the carbonyl group leading to the deacetylation reaction.[41]

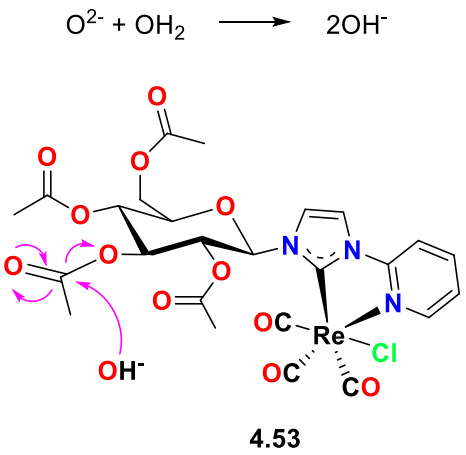

Figure 4.14. Proposed mechanism for the deacetylation process observed in the synthesis of the Re(I) complex **4.53**.

4.3.3. Synthesis of a Re(I) Complex of a Glucose Functionalised NHC Ligand with an Extended PEG Linker

To circumvent the problems encountered with pro-ligand **4.52** (i.e. the cleavage of the sugar), a modified pro-ligand was prepared with a polyethylene glycol (PEG) linker between the metal-binding group and the sugar. The synthetic scheme for the preparation of the chelator is shown in Scheme 4.13. In the first step, a mixture of compounds **4.51** and **4.60** was stirred in the presence of iodine to give compound **4.61**.[42-43] Compound **4.61** was then treated with one equivalent of **4.25** to give **4.62**. The Re(I) complex **4.63** was synthesised via a silver transmetalation reaction (Scheme 4.13). Similar reaction conditions to those used to prepare complex **4.55** were used to synthesise complex **4.63**.

Here, five equivalents of silver(I) oxide were added, and the mixture was stirred for seven days. The crude product was purified using a cation exchange resin CM-Sephadex C-25 and the product was eluted with water. Since CM-Sephadex C-25 is a cation-exchange resin, cationic compounds will be retained on the column until a suitable cation source, e.g., a NaCl solution, is added. Therefore, the uncharged complex **4.63** was eluted with water, and a positively charged pro-ligand was retained in the Sephadex column.

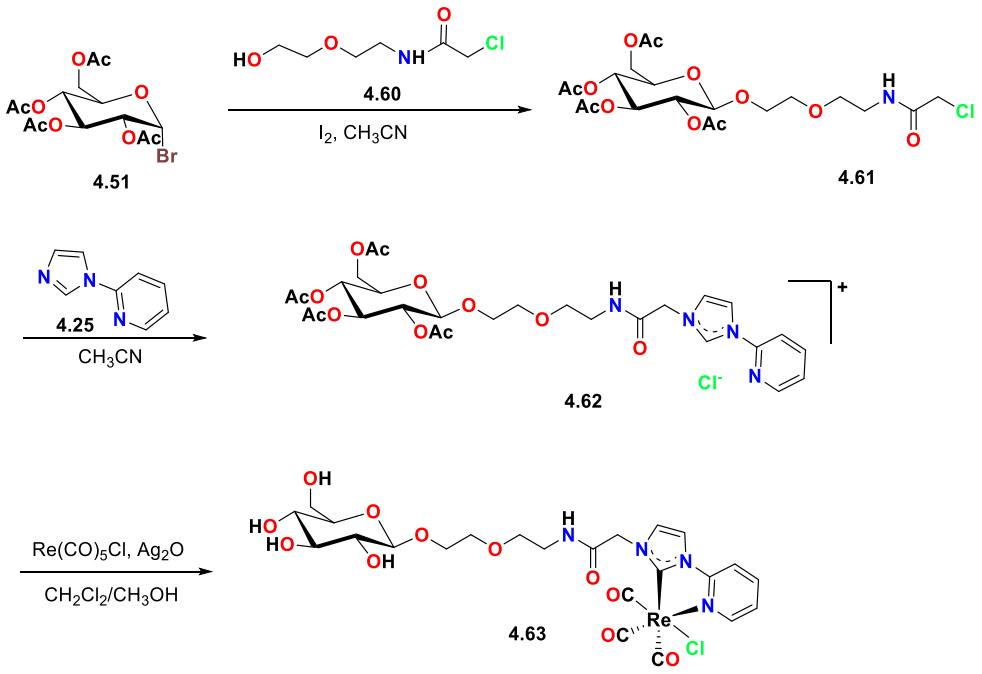

Scheme 4.13. Synthesis of pro-ligand **4.62** and the Re(I) complex **4.63**.

The structure of the isolated complex **4.63** was characterised by ^{1}H NMR spectroscopy. Figure 4.15 shows the stacked plot of complex **4.63** (Figure 4.15a) and the pro-ligand **4.62** (Figure 4.15b). For pro-ligand **4.62**, the characteristic deshielded pro-carbenic proton and the amide proton were not seen because the polar-protic solvent deuterated methanol was used, and the pro-carbenic and amide protons were exchanged with the deuterium. The ^{1}H NMR spectrum for complex **4.63** was relatively simple, and the absence of the signals for methyl groups around 2.00 ppm indicates that the acetyl groups were fully removed in the complex synthesis reaction. In addition, the ^{13}C NMR spectrum of complex **4.63** shows the carbonyl signals in the range of 197-198 ppm.

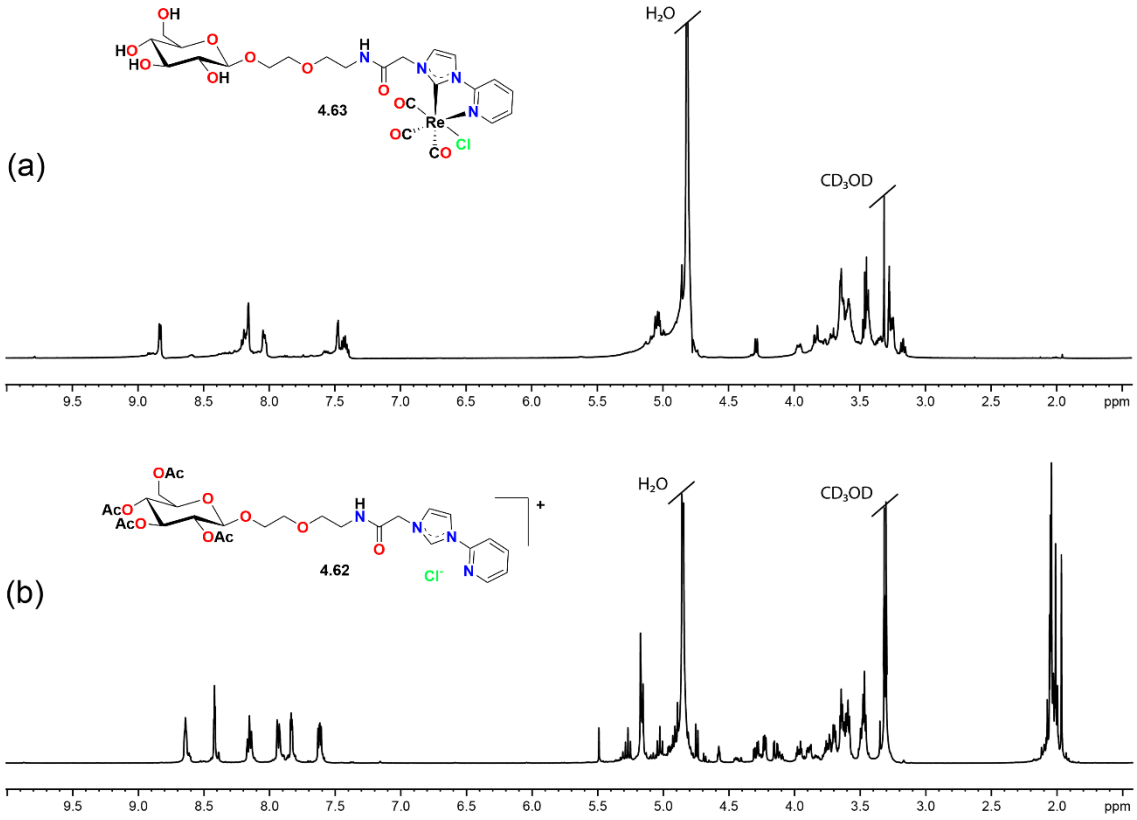

Figure 4.15. ^{1}H NMR spectrum of (a) complex **4.63** and (b) pro-ligand **4.62**.

To support the ^{1}H and ^{13}C NMR analytical results, the positive ion high-resolution mass spectrum was recorded for complex **4.63** (Figure 4.16a). In this spectrum, a base peak was observed at *m/z* = 723.1317, which corresponds to the chemical formula $[C_{23}H_{28}N_4O_{11}Re]^+$, and it is consistent to the fully deprotected complex **4.63** without the chloride ligand (Figure 4.16b). It is also apparent that the fully deprotected pro-ligand peak with the exact mass of *m/z* = 453.1985 is not present in the mass spectrum shown in Figure 4.16a. Therefore, the HRMS result suggests that the acetyl protecting groups on glucose moiety were fully cleaved, and the Re(I) complex of PEG linker coordinating to sugar moiety was isolated.

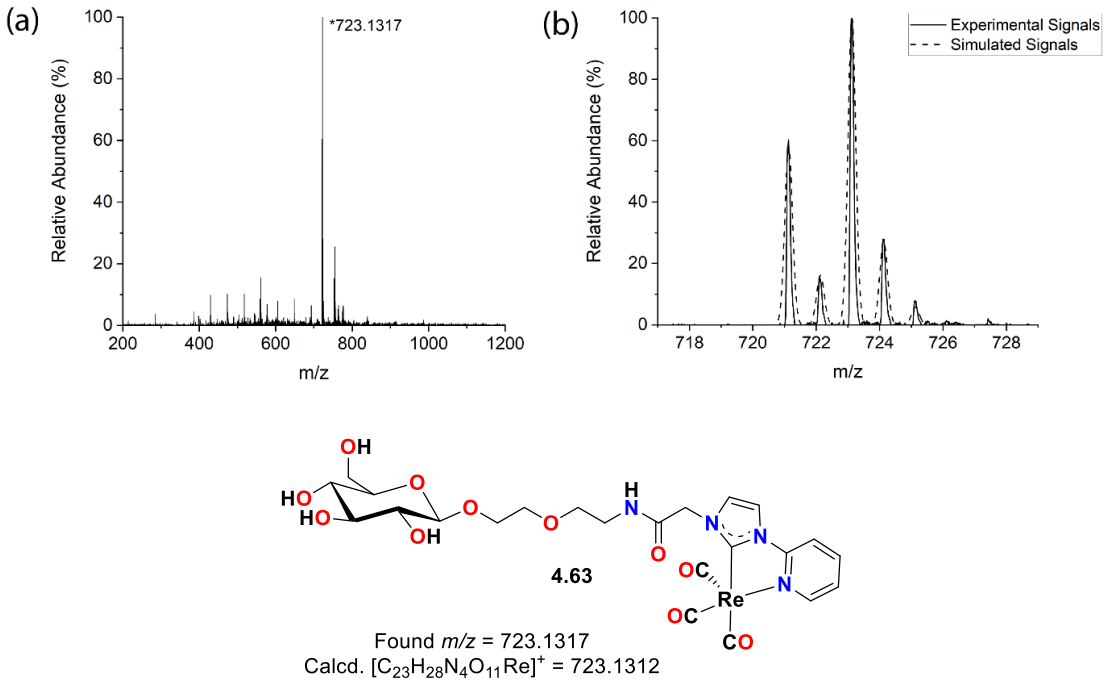

Figure 4.16. (a) HRMS spectrum of a freshly prepared solution of **4.63** in methanol. Zoom scan of the main signal at *m/z* = 723.1317 (solid line) is plotted together with the simulated spectrum (b) for the formula $[C_{23}H_{28}N_4O_{11}Re]^+$ (dashed line). The structure of compound **4.63** corresponding to this formula is shown in the lower panel.

The NMR and HRMS analytical results suggest that complex **4.63** was formed and isolated. As expected, the incorporation of PEG linkage in the structure of Re(I) complex prevents the cleavage of the glucose moiety at the C1 position of the sugar.

4.4. Conclusion

The first part of this chapter described the synthesis of new NHC pro-ligands designed to form dinuclear Re(I) complexes with alkyl or diamide linkage between the metal-binding groups. The dinuclear Re(I) tricarbonyl complexes were prepared from these ligands using silver transmetalation reactions. Both classes of the dinuclear Re(I)-NHC complexes prepared (**4.30** and **4.31**) had labile chloride ligands, and the aquation of these molecules was investigated using ^{1}H NMR time-course experiments. These studies showed that the aquation rate of each complex depended on the nature of the NHC ligand,

where the Re(I) complex of the *bis*-imidazolylidene ligand had a significantly faster aquation rate (**4.31**, k_1 = 1.57 x 10^{-4} s^{-1}) compared to the Re(I) complex of the pyridyl-imidazolylidene ligand (**4.30**, k_1 = 6.60 x 10^{-5} s^{-1}). These aquation rates are essential to understand the pharmacologic behaviour of Re(I) complexes as potential treatments for cancer. When comparing the aquation rates of these dinuclear Re(I) complexes to the well-known anticancer agent cisplatin (k_1= 2.38 x 10^{-5} s^{-1})[43], it is evident that the Re(I) *bis*-imidazolylidene ligand has a faster aquation rate than cisplatin. In contrast, the aquation rate for the Re(I) complex of the pyridyl-imidazolylidene ligand has a similar aquation rate value to that of cisplatin. Determining the aquation rates for these compounds is an important first step in evaluating the anticancer properties of these complexes; however, further biological studies are required. The photophysical properties of dinuclear Re(I)-NHC complexes were also evaluated, and these studies show that complexes **4.30**, **4.31**, and **4.35** were luminescence at approximately 390 nm.

In the second part of this chapter, a series of NHC pro-ligands was prepared, where a bidentate NHC based donor has coupled to benzyl protected glucosamine or acetyl protected glucose. Full protection of the glucose alcohol groups was undertaken to allow activation of the anomeric carbon and subsequent alkylation of the 1-(2-pyridinyl)-1H-imidazole or PEG linker group. The $[Re(CO)_3]^+$ complex of the benzyl protected glucosamine ligand (**4.48**) was synthesised using the silver(I) transmetalation process. However, the removal of benzyl protecting groups was unsuccessful when the hydrogenolysis reaction was undertaken using common catalysts such as Pd/C and $Pd(OH)_2$. Acetyl protecting groups were then explored as an alternative to the benzyl groups for protecting the alcohol units. The $[Re(CO)_3]^+$ complex of the acetyl protected glucose ligand (**4.54**) was then synthesised. The traditional deprotection methods using bases such as Cs_2CO_3, K_2CO_3 or Et_3N were unsuccessful, and the acetyl groups were not removed under these conditions. Significantly, however, a new one-pot Re(I) complex

synthesis and deacetylation method was discovered for the synthesis of Re(I) complexes of these NHC-glucose ligands. In this procedure, an excess of silver(I) oxide was added to the mixture to induce both formations of the Re(I)-NHC complex and the removal of the acetyl protecting groups. In this reaction, it was apparent that the pyridyl-imidazolylidene ligand was also cleaved at the C1 position of the glucose, which resulted in the formation of Re(I) complex **4.59**. To circumvent this problem, a PEG derivative has been designed and incorporated into a novel Re(I) sugar complex **4.63**. Further biological studies of complex **4.63** are required to determine the potential anticancer property of this complex.

4.5. Experimental Details

4.25. This compound was synthesised as described previously from imidazole (1.00 g, 14.7 mmol), 1-bromopyridine (2.32 g, 14.7 mmol), KOtBu (2.31 g, 20.6 mmol), CuI (0.14 g, 0.74 mmol), BtH (0.18 g, 1.47 mmol).[19] The product was obtained as a yellow oil. (Yield: 4.24 g, 40%). ^{1}H NMR (500 MHz, DMSO-d_6): δ (ppm) 7.13 (t, 1H, $^{3}J_{H\text{-}H}$ = 1.05 Hz, H_{imi}), 7.36-7.39 (m, 1H, H_{py}), 7.82 (d, 1H, $^{3}J_{H\text{-}H}$ = 8.25 Hz, H_{py}), 7.99-8.02 (m, 1H, H_{imi}), 8.49-8.51 (m, 1H, H_{py}), 8.54 (t, $^{3}J_{H\text{-}H}$ = 1.05 Hz, NC*H*N). ^{13}C NMR (125 MHz, DMSO-d_6): δ (ppm) 113.2 (CH$_{py}$), 117.0 (CH$_{imi}$), 122.8 (CH$_{py}$), 130.6 (CH$_{imi}$), 135.4 (NCHN), 140.2 (CH$_{py}$), 149.1 (C_{py}), 149.3 (CH$_{py}$). HRESI-MS^{+} (CH_3OH): $[C_8H_7N_3]^{+}$ *m/z* = , calcd = 145.0640.

4.26. This compound was synthesised as described previously from imidazole (1.00 g, 14.7 mmol), TBABr (0.095 g, 0.29 mmol), KOH (1.64 g, 29.4 mmol), CH_2Br_2 (1.28 g, 7.35 mmol).[20] The product was obtained as a white crystallised solid. (Yield: 1.09 g, 50%). ^{1}H NMR (500 MHz, DMSO-d_6): δ (ppm) 6.21 (s, 2H, CH_2), 6.90 (t, 2H, $^{3}J_{H\text{-}H}$ = 1.05 Hz, H_{imi}), 7.39 (t, 2H, $^{3}J_{H\text{-}H}$ = 1.25 Hz, H_{imi}), 7.92 (s, 2H, NC*H*N). ^{13}C NMR (125

MHz, DMSO-d_6): δ (ppm) 55.3 (CH$_2$), 119.6 (CH$_{imi}$), 129.6 (CH$_{imi}$), 137.8 (NCN). HRESI-MS$^+$ (CH_3OH): $[C_7H_8N_4]^+$ *m/z* = , calcd = 148.0749.

4.27. This compound was synthesised as described previously from **4.26** (0.42 g, 2.84 mmol) and CH_3I (0.41 g, 2.84 mmol).[20] The product was obtained as an off-white solid. (Yield: 0.23 g, 27%). ^{1}H NMR (500 MHz, DMSO-d_6): δ (ppm) 3.87 (s, 3H, CH_3), 6.46 (s, 2H, CH_2), 6.99 (s, 1H, H_{imi}), 7.47 (t, 1H, $^3J_{H-H}$ = 1.25 Hz, H_{imi}), 7.73 (t, 1H, $^3J_{H-H}$ = 1.75 Hz, H_{imi}), 7.93 (t, 1H, $^3J_{H-H}$ = 1.80 Hz, H_{imi}), 8.01 (s, 1H, NCHN), 9.32 (s, 1H, NCHN). ^{13}C NMR (125 MHz, DMSO-d_6): δ (ppm) 39.6 (CH$_3$), 57.3 (CH$_2$), 119.8 (CH$_{imi}$), 122.1 (CH$_{imi}$), 124.8 (CH$_{imi}$), 130.1 (CH$_{imi}$), 137.5 (NCHN), 138.3 (NCHN). HRESI-MS$^+$ (CH_3OH): $[C_8H_{11}N_4]^+$ *m/z* = , calcd = 163.0984.

4.28. A solution of **4.25** (1.00 g, 6.79 mmol) and 1,5-dibromopentane (0.78 g, 3.40 mmol) in acetonitrile (30 mL) was heated at 100 °C for 24 h. The crude product was collected, and the residue was dissolved in water (2 mL) followed by addition of a saturation solution of KPF_6 in water (5 mL). The precipitate was collected and washed with water and diethyl ether to obtain the pure product as an off-white solid. (Yield: 0.84 g, 47%). ^{1}H NMR (500 MHz, DMSO-d_6): δ (ppm) 1.31-1.37 (m, 2H, CH$_2$CH$_2$CH_2CH$_2$CH$_2$), 1.95-1.98 (m, 4H, CH$_2$CH_2CH$_2$CH_2CH$_2$), 4.32 (t, 4H, $^3J_{H-H}$ = 7.10 Hz, CH_2CH$_2$CH$_2$CH$_2$CH_2), 7.64-7.67 (m, 2H, H_{py}), 8.04 (d, 2H, $^3J_{H-H}$ = 8.25 Hz, H_{py}), 8.08 (d, 2H, $^3J_{H-H}$ = 1.60 Hz, H_{imi}), 8.21-8.24 (m, 2H, H_{py}), 8.55 (s, 2H, H_{imi}), 8.65-8.66 (m, 2H, H_{py}), 10.1 (s, 2H, NCHN). ^{13}C NMR (125 MHz, DMSO-d_6): δ (ppm) 22.5 (CH$_2$CH$_2$$CH_2CH_2CH_2$), 28.9 (CH$_2$$CH_2CH_2$$CH_2CH_2$), 49.6 ($CH_2CH_2CH_2CH_2$$CH_2$), 114.7 ($CH_{py}$), 119.8 ($CH_{imi}$), 124.1 ($CH_{py}$), 125.7 ($CH_{imi}$), 135.5 (N$C$HN), 141.1 ($CH_{py}$), 146.9 ($C_{(q)py}$), 149.7 ($CH_{py}$). HRESI-MS$^+$ (CH_3OH): $[C_{21}H_{24}N_6]^+$ *m/z* = 180.1031, calcd = 180.1031.

4.29. This compound was prepared using the same procedure as described for **4.28** from **4.27** (0.23 g, 0.80 mmol) and 1,5-dibromopentane (0.092 g, 0.40 mmol) in acetonitrile.

The pure product as an off-white solid. (Yield: 0.18 g, 47%). ^{1}H NMR (500 MHz, DMSO-d_6): δ (ppm) 1.33 (t, 2H, $^{3}J_{H-H}$ = 7.05 Hz, $CH_2CH_2CH_2CH_2CH_2$), 1.84-1.90 (m, 4H, $CH_2CH_2CH_2CH_2CH_2$), 3.92 (s, 6H, CH_3), 4.25 (t, 4H, $^{3}J_{H-H}$ = 7.30 Hz, $CH_2CH_2CH_2CH_2CH_2$), 6.71 (s, 4H, CH_{2imi}), 7.81 (s, 2H, H_{imi}), 7.94 (s, 2H, H_{imi}), 8.04 (s, 2H, H_{imi}), 8.05 (s, 2H, H_{imi}), 9.47 (s, 2H, NC*H*N), 9.61 (s, 2H, NC*H*N). ^{13}C NMR (125 MHz, DMSO-d_6): δ (ppm) 22.6 ($CH_2CH_2CH_2CH_2CH_2$), 28.9 ($CH_2CH_2CH_2CH_2CH_2$), 36.8 (CH_3), 49.4 ($CH_2CH_2CH_2CH_2CH_2$), 58.6 (CH_{2imi}), 122.4 (CH_{imi}), 122.6 (CH_{imi}), 123.6 (CH_{imi}), 124.9 (CH_{imi}), 138.0 (N*C*HN), 138.6 (N*C*HN). HRESI-MS^{+} (CH_3CN): $[C_{22}H_{26}N_3O_9]^{+}$ *m/z* = 476.1666, calcd = 476.1669.

4.30. A mixture of **4.28** (0.062 g, 0.12 mmol), Ag_2O (0.055 g, 0.24 mmol), and $Re(CO)_5Cl$ (0.086 g, 0.24 mmol) in methanol (5 mL) and dichloromethane (15 mL) was heated at 60 °C for 24 h. The mixture was filtered through Celite and the solvent was removed from the filtrate on a rotatory evaporator. The crude product recrystallised from ethanol to obtain the pure product as a yellow solid. (Yield: 0.019 g, 16%). ^{1}H NMR (500 MHz, DMSO-d_6): δ (ppm) 1.42-1.52 (m, 2H, $CH_2CH_2CH_2CH_2CH_2$), 1.92-1.96 (m, 4H, $CH_2CH_2CH_2CH_2CH_2$), 4.23 (t, 4H, $^{3}J_{H-H}$ = 7.30 Hz, $CH_2CH_2CH_2CH_2CH_2$), 7.50-7.52 (m, 2H, H_{py}), 7.73 (d, 2H, $^{3}J_{H-H}$ = 2.05 Hz, H_{imi}), 8.26 (d, 2H, $^{3}J_{H-H}$ = 8.35 Hz, H_{py}), 8.31-8.34 (m, 2H, H_{py}), 8.46 (d, 2H, $^{3}J_{H-H}$ = 1.20 Hz, H_{imi}), 8.84 (d, 2H, $^{3}J_{H-H}$ = 3.40 Hz, H_{py}). ^{13}C NMR (125 MHz, DMSO-d_6): δ (ppm) 23.3 ($CH_2CH_2CH_2CH_2CH_2$), 30.8 ($CH_2CH_2CH_2CH_2CH_2$), 51.5 ($CH_2CH_2CH_2CH_2CH_2$), 113.2 (CH_{py}), 118.0 (CH_{imi}), 124.5 (CH_{py} and CH_{imi}), 142.8 (CH_{py}), 153.0 ($C_{(q)py}$), 153.7 (CH_{py}), 189.6 (N*C*N), 190.6 (Re-*C*O), 198.5 (Re-*C*O), 199.3 (Re-*C*O). HRESI-MS^{+} (CH_3OH): $[C_{27}H_{22}ClN_6O_6Re_2]^{+}$ *m/z* = 935.0404, calcd = 935.0404.

4.31. This compound was prepared using the same procedure as described for **4.30** from **4.29** (0.050 g, 0.051 mmol), Ag_2O (0.030 g, 0.13 mmol), and $Re(CO)_5Cl$ (0.037 g, 0.10

mmol). The crude product recrystallised in methanol yielding the pure product as an off-white solid. (Yield: 0.015 g, 30%). ^{1}H NMR (500 MHz, DMSO-d_6): δ (ppm) 1.44-1.50 (m, 2H, $CH_2CH_2CH_2CH_2CH_2$), 1.83-1.89 (m, 4H, $CH_2CH_2CH_2CH_2CH_2$), 3.90 (s, 6H, CH_3), 4.09-4.16 (m, 2H, $CH_2CH_2CH_2CH_2CH_2$), 4.36-4.43 (m, 2H, $CH_2CH_2CH_2CH_2CH_2$), 5.89 (d, 2H, $^{3}J_{H-H}$ = 13.1 Hz, CH_{2imi}), 6.57 (d, 2H, $^{3}J_{H-H}$ = 12.1 Hz, CH_{2imi}), 7.40 (d, 2H, $^{3}J_{H-H}$ = 1.80 Hz, H_{imi}), 7.49 (d, 2H, $^{3}J_{H-H}$ = 1.95 Hz, H_{imi}), 7.52 (d, 2H, $^{3}J_{H-H}$ = 1.85 Hz, H_{imi}), 7.55 (d, 2H, $^{3}J_{H-H}$ = 1.75 Hz, H_{imi}). ^{13}C NMR (125 MHz, DMSO-d_6): δ (ppm) 23.7 ($CH_2CH_2CH_2CH_2CH_2$), 31.1 ($CH_2CH_2CH_2CH_2CH_2$), 38.3 (CH_3), 50.5 ($CH_2CH_2CH_2CH_2CH_2$), 63.2 (CH_{2imi}), 121.3 (CH_{imi}), 121.5 (CH_{imi}), 122.3 (CH_{imi}), 123.1 (CH_{imi}), 177.0 (NCN), 192.5 (Re-CO), 197.6 (Re-CO), 197.7 (Re-CO). HRESI-MS^{+} (CH_3OH): $[C_{27}H_{28}ClN_8O_6Re_2]^{+}$ *m/z* = 969.0933, calcd = 969.0935.

4.32. This compound was synthesised as described previously[44] from 1,3-diaminopropane (2.00 g, 27.0 mmol) and 2-chloroacetyl chloride (6.09 g, 54.0 mmol) and 1 M NaOH (50 mL). The product was obtained as a white crystallised solid. (Yield: 1.80 g, 29%). ^{1}H NMR (500 MHz, DMSO-d_6): δ (ppm) 1.71-1.76 (m, 2H, CH_2CH_2), 3.37 (q, 4H, CH_2CH_2), 4.07 (s, 4H, CH_2Cl), 7.14 (s, 2H, N*H*). ^{13}C NMR (125 MHz, DMSO-d_6): δ (ppm) 29.4 (CH_2CH_2), 36.4 (CH_2CH_2), 42.6 ($CH_2C{=}O$), 166.8 (C=O). HRESI-MS^{+} (CH_3OH): $[C_7H_{12}Cl_2N_2O_2Na]^{+}$ *m/z* = 249.0166, calcd = 249.0168.

4.33. This compound was prepared using the same procedure as described for **4.28** from **4.25** (0.75 g, 5.17 mmol) and **4.32** (0.59 g, 2.59 mmol). The product was obtained as an off-white solid. (Yield: 0.36 g, 52%). ^{1}H NMR (500 MHz, DMSO-d_6): δ (ppm) 1.62-1.69, (m, 2H, $CH_2CH_2CH_2$), 3.19-3.23 (m, 4H, $CH_2CH_2CH_2$), 5.08 (s, 4H, $CH_2C{=}O$), 7.64-7.67 (m, 2H, H_{py}), 7.94 (t, 2H, $^{3}J_{H-H}$ = 1.75 Hz, H_{imi}), 8.02 (d, 2H, $^{3}J_{H-H}$ = 8.25 Hz, H_{py}), 8.20-8.24 (m, 2H, H_{py}), 8.48 (t, 2H, $^{3}J_{H-H}$ = 5.40 Hz, N*H*), 8.52 (t, 2H, $^{3}J_{H-H}$ = 1.80 Hz, H_{imi}), 8.64-8.66 (m, 2H, H_{py}), 10.0 (s, 2H, NC*H*N). ^{13}C NMR (125 MHz, DMSO-

d₆): δ (ppm) 29.2 ($CH_2CH_2CH_2$), 37.2 ($CH_2CH_2CH_2$), 51.6 ($CH_2C{=}O$), 114.7 (CH_{py}), 119.2 (CH_{imi}), 125.6 (CH_{py}), 125.9 (CH_{imi}), 136.42 (N*C*HN), 141.1 (CH_{py}), 146.71 ($C_{q(py)}$), 149.8 (CH_{py}), 165.0 (*C*=O). HRESI-MS$^+$ (CH_3CN): $[C_{23}H_{26}N_8O_2]^+$ *m/z* = 223.1083, calcd = 223.1084.

4.34. This compound was prepared using the same procedure as described for **4.29** from **4.27** (0.45 g, 1.56 mmol) and **4.32** (0.18 g, 0.78 mmol). The product was obtained as an off-white solid. (Yield: 0.23 g, 46 %). ^{1}H NMR (500 MHz, DMSO-*d₆*): δ (ppm) 1.62, (t, 2H, $^3J_{H\text{-}H}$ = 7.00 Hz, $CH_2CH_2CH_2$), 3.14-3.18 (m, 4H, $CH_2CH_2CH_2$), 3.91 (s, 6H, CH_{3imi}), 5.02 (s, 4H, $CH_2C{=}O$), 6.67 (s, 4H, CH_{2imi}), 7.76 (t, 2H, $^3J_{H\text{-}H}$ = 1.65 Hz, H_{imi}), 7.79 (t, 2H, $^3J_{H\text{-}H}$ = 1.65 Hz, H_{imi}), 7.93 (t, 2H, $^3J_{H\text{-}H}$ = 1.60 Hz, H_{imi}), 7.93 (t, 2H, $^3J_{H\text{-}H}$ = 1.80 Hz, H_{imi}), 7.96 (t, 2H, $^3J_{H\text{-}H}$ = 1.80 Hz, H_{imi}), 8.45 (t, 2H, $^3J_{H\text{-}H}$ = 5.30 Hz, N*H*), 9.34 (s, 2H, NC*H*N), 9.38 (s, 2H, NC*H*N). ^{13}C NMR (125 MHz, DMSO-*d₆*): δ (ppm) .27.1 ($CH_2CH_2CH_2$), 34.6 (CH_{3imi}), 35.3 1 ($CH_2CH_2CH_2$), 49.2 ($CH_2C{=}O$), 56.7 (CH_{2imi}), 119.78 (CH_{imi}), 119.86 (CH_{imi}), 122.94 (CH_{imi}), 123.05 (CH_{imi}), 136.42 (N*C*HN), 136.97 (N*C*HN), 167.76 (*C*=O). HRESI-MS$^+$ (CH_3CN): $[C_{22}H_{26}N_3O_9]^+$ *m/z* = 476.1666, calcd = 476.1669.

4.35. This compound was prepared using the same procedure as described for **4.30** from **4.33** (0.072 g, 0.098 mmol), Ag_2O (0.046 g, 1.97 mmol), and $Re(CO)_5Cl$ (0.071 g, 1.97 mmol). The crude product recrystallised in methanol. The product was obtained as a yellow solid. (Yield: 0.022 g, 21%). ^{1}H NMR (500 MHz, DMSO-*d₆*): δ (ppm) 1.61-1.64 (m, 2H, $CH_2CH_2CH_2$), 3.10-3.24 (m, 4H, $CH_2CH_2CH_2$), 4.87 (d, 2H, $^3J_{H\text{-}H}$ = 16.7 Hz, $CH_2C{=}O$), 5.00 (d, 2H, $^3J_{H\text{-}H}$ = 16.7 Hz, $CH_2C{=}O$), 7.52 (t, 2H, $^3J_{H\text{-}H}$ = 6.45 Hz, H_{py}), 7.63 (d, 2H, $^3J_{H\text{-}H}$ = 2.05 Hz, H_{imi}), 8.11-8.14 (m, 2H, N*H*), 8.26-8.29 (m, 2H, H_{py}), 8.31-8.35 (m, 2H, H_{py}), 8.44 (d, 2H, $^3J_{H\text{-}H}$ = 1.85 Hz, H_{imi}), 8.83 (d, 2H, $^3J_{H\text{-}H}$ = 4.95 Hz, H_{py}). ^{13}C NMR (125 MHz, DMSO-*d₆*): δ (ppm) 29.5 ($CHCH_2CH_2$), 37.2 ($CH_2CH_2CH_2$), 53.6

(CH_2C=O), 113.4 (CH_{py}), 117.7 (CH_{imi}), 124.5 (CH_{py}), 125.8 (CH_{imi}), 142.8 (CH_{py}), 153.2 ($C_{q(py)}$), 153.7 (CH_{py}), 165.9 (NH*C*O), 189.0 (N*C*N), 192.9 (Re-*C*O), 198.6 (Re-*C*O), 198.8 (Re-*C*O). HRESI-MS$^+$ (*CH_3OH*): $[C_{29}H_{24}ClN_8O_8Re_2]^+$ *m/z* = 1021.0519, calcd = 1021.0521.

4.36. This compound was prepared using the same procedure as described for **4.35** from **4.34** (0.060 g, 0.0098 mmol), Ag_2O (0.055 g, 0.024 mmol), and $Re(CO)_5Cl$ (0.069 g, 0.019 mmol). The crude product was recrystallised in methanol. The product was obtained as a white solid. However, the quantity of this isolated complex was too low to obtain its yield, and only ^{1}H NMR and HRMS analytical data for this compound was obtained. ^{1}H NMR (500 MHz, CH_3OD): δ (ppm) 1.67-1.76 (m, 4H, CH_2), 3.99 (s, 6H, CH_3), 5.43 (q, 2H, $^3J_{H-H}$ = 9.70 Hz, CH_2), 5.99 (dd, 2H, $^2J_{H-H}$ = 4.10 Hz, $^3J_{H-H}$ = 9.15 Hz, CH_2), 6.40-6.45 (m, 2H, CH_2), 7.20 (d, 2H, $^3J_{H-H}$ =1.40 Hz, H_{imi}), 7.23 (q, 2H, $^3J_{H-H}$ =1.90 Hz, H_{imi}), 7.38 (t, 2H, $^3J_{H-H}$ = 1.95 Hz, H_{imi}), 7.41 (dd, 2H, $^2J_{H-H}$ = 1.90 Hz, $^3J_{H-H}$ = 4.45 Hz, H_{imi}). HRESI-MS$^+$ (*CH_3OH*): $[C_{29}H_{30}ClN_{10}O_8Re_2]^+$ *m/z* = 1055.1048, calcd = 1055.1052.

4.43. This compound was synthesised as described previously from glucosamine hydrochloride (0.50 g, 2.32 mmol), Boc anhydride (0.51 g, 2.32 mmol) and Et_3N (0.24 g, 2.32 mmol).[29] The product was obtained as a white crystallised solid. (Yield: 0.47, 64%). ^{1}H NMR (500 MHz, DMSO-d_6): δ (ppm) 1.38 (s, 9H, OCH_3), 3.06-3.11 (m, 1H, *H*-4), 3.19-3.25 (m, 1H, *H*-1), 3.41-3.45 (m, 1H, *H*-3), 3.46-3.48 (m, 1H, *H*-6), 3.53-3.57 (m, 1H, *H*-5), 3.58-3.62 (m, 1H, *H*-6), 4.40 (t, 1H, $^3J_{H-H}$ = 5.49 Hz, O*H*-6), 4.60 (d, 1H, $^3J_{H-H}$ = 5.20 Hz, O*H*-3), 4.86 (d, 1H, $^3J_{H-H}$ = 5.00 Hz, O*H*-4), 4.93 (t, 1H, $^3J_{H-H}$ = 3.90 Hz, *H*-2), 6.21 (d, 1H, $^3J_{H-H}$ = 7.80 Hz, O*H*-1), 6.33 (d, 1H, $^3J_{H-H}$ = 3.55 Hz, N*H*). ^{13}C NMR (125 MHz, DMSO-d_6): δ (ppm) 28.7 (CH_3), 56.3 (*C*H-3), 61.6 (*C*H-6), 70.7 (*C*H-1), 71.5

(*C*H-4), 72.5 (*C*H-5), 78.1 (C_q), 91.2 (*C*H-2), 155.9 (*C*O). HRESI-MS$^+$ (*CH$_3$OH*): $[C_{11}H_{21}NO_7Na]^+$ *m/z* = 302.1214, calcd = 302.1210.

4.44. This compound was synthesised as described previously from **4.43** (1.06 g, 3.78 mmol), NaH (0.50 g, 20.7 mmol) and BnBr (2.84 g, 16.6 mmol).[29] The product was obtained as an off-white solid. (Yield: 1.14 g, 46%). ^{1}H NMR (500 MHz, DMSO-*d$_6$*): δ (ppm) 1.44 (s, 9H, C*H*$_3$), 3.40 (s$_{br}$, 1H, C*H*), 3.53 (sbr, 1H, C*H*), 3.62-3.66 (m, 2H, C*H*$_2$), 3.94 (s$_{br}$, 1H, C*H*), 4.55 (d, 1H, $^3J_{H-H}$ = 7.80 Hz, C*H*$_{2Ar}$), 4.58 (d, 1H, $^3J_{H-H}$ = 6.80 Hz, C*H*$_{2Ar}$), 4.61 (d, 1H, $^3J_{H-H}$ = 7.005 Hz, C*H*$_{2Ar}$), 4.64 (d, 1H, $^3J_{H-H}$ = 7.10 Hz, C*H*$_{2Ar}$), 4.72 (d, 2H, $^3J_{H-H}$ = 11.05 Hz, C*H*$_{2Ar}$), 4.79 (d, 1H, $^3J_{H-H}$ = 6.28 Hz, C*H*$_{2Ar}$), 4.81 (d, 1H, $^3J_{H-H}$ = 6.35 Hz, C*H*$_{2Ar}$), 4.91 (d, 1H, $^3J_{H-H}$ = 12.2 Hz, C*H*$_{2Ar}$), 7.19 (dd, 2H, $^2J_{H-H}$ = 1.85 Hz, $^3J_{H-H}$ = 6.00 Hz, *H*$_{Ar}$), 7.27-7.34 (m, 18H, *H*$_{Ar}$). ^{13}C NMR (125 MHz, DMSO-*d$_6$*): δ (ppm) 28.4 (*C*H$_3$), 57.4 (*C*H), 69.0 (*C*H$_2$), 70.6 (*C*H$_2$), 73.5 (*C*H$_2$), 74.6 (*C*H$_2$), 74.9 (*C*H), 78.5 (*C*H), 79.6 (C_q), 81.4 (*C*H), 99.7 (*C*H), 127.5 (*C*H$_{Ar}$), 127.6 (*C*H$_{Ar}$), 127.7 (*C*H$_{Ar}$), 127.8 (*C*H$_{Ar}$), 127.9 (*C*H$_{Ar}$), 128.0 (*C*H$_{Ar}$), 128.3 (*C*H$_{Ar}$), 128.35 (*C*H$_{Ar}$), 128.38 (*C*H$_{Ar}$), 128.4 (*C*H$_{Ar}$), 137.6 (C_q), 138.1 (C_q), 138.2 (C_q), 138.3 (C_q), 155.3 (*C*O). HRESI-MS$^+$ (*CH$_3$OH*): $[C_{39}H_{45}NO_7Na]^+$ *m/z* = 662.3088, calcd = 662.3088.

4.45. This compound was synthesised as described previously from **4.44** (0.58 g, 0.90 mmol) and CF_3COOH (1.03 g, 9.02 mmol). The product was obtained as a yellow oil. (Yield: 0.18 g, 36%).[29] ^{1}H NMR (500 MHz, DMSO-*d$_6$*): δ (ppm) 2.95 (dd, 1H, $^2J_{H-H}$ = 1.85 Hz, $^3J_{H-H}$ = 7.90 Hz, *H*-2), 3.44 (t, 1H, $^3J_{H-H}$ = 9.55 Hz, *H*-3), 3.49-3.52 (m, 1H, *H*-5), 3.68 (t, 1H, $^3J_{H-H}$ = 9.30 Hz, *H*-4), 3.76-3.77 (m, 2H, *H*-6), 4.31 (d, 1H, $^3J_{H-H}$ = 7.90 Hz, *H*-1), 4.57-4.61 (m, 3H, C*H*$_{2Ar}$), 4.66 (d, 1H, $^3J_{H-H}$ = 12.3 Hz, C*H*$_{2Ar}$), 4.71 (d, 1H, $^3J_{H-H}$ = 11.3 Hz, C*H*$_{2Ar}$), 4.80 (d, 1H, $^3J_{H-H}$ = 10.8 Hz, C*H*$_{2Ar}$), 4.93 (d, 1H, $^3J_{H-H}$ = 9.35 Hz, C*H*$_{2Ar}$), 4.95 (d, 1H, $^3J_{H-H}$ = 9.05 Hz, C*H*$_{2Ar}$), 7.19-7.21 (m, 2H, *H*$_{Ar}$), 7.27-7.38 (m, 18H, *H*$_{Ar}$). ^{13}C NMR (125 MHz, DMSO-*d$_6$*): δ (ppm) 57.0 (*C*H-2), 68.9 (*C*H-6), 71.1 (*C*H$_2$), 73.6 (*C*H$_2$), 74.8 (*C*H$_2$), 75.3 (*C*H$_2$), 75.4 (*C*H-5), 78.6 (*C*H-4), 85.2 (*C*H-3), 103.1

(*C*H-1), 127.6 (*C*H_{2Ar}), 127.8 (*C*H_{2Ar}), 127.87 (*C*H_{2Ar}), 127.9 (*C*H_{2Ar}), 128.1 (*C*H_{2Ar}), 128.44 (*C*H_{2Ar}), 128.47 (*C*H_{2Ar}), 128.49 (*C*H_{2Ar}), 128.57 (*C*H_{2Ar}), 137.4 (C_q), 137.9 (C_q), 138.2 (C_q), 138.4 (C_q). HRESI-MS$^+$ (*CH₃OH*): $[C_{34}H_{38}NO_5]^+$ *m/z* = 540.2746, calcd = 540.2744.

4.46. To a mixture of **4.45** (0.076 g, 0.14 mmol) in dichloromethane (2 mL) and Na_2CO_3 (0.060 g, 0.56 mmol) in water (2 mL) at 0 °C, a solution of 2-chloroacetyl chloride (0.018 g, 0.16 mmol) in dichloromethane (2 mL) was added. The mixture was stirred at room temperature for 1 h. The organic layer was washed with water (3 × 5 mL) and brine (3 × 5 mL) then dried with $MgSO_4$.The solvent was removed on a rotatory evaporator to obtain the pure compound as an off-white solid. (Yield: 0.062 g, 71%). ^{1}H NMR (500 MHz, $CDCl_3$): δ (ppm) 3.56-3.59 (m, 1H, *H*5), 3.67-3.72 (m, 2H, *H*2 and *H*3), 3.76-3.78 (m, 2H, *H*6), 3.80 (d, $^3J_{H\text{-}H}$ = 2.35 Hz, 2H, C*H*$_2$Cl), 3.95-3.98 (m, 1H, *H*4), 4.56 (d, $^3J_{H\text{-}H}$ = 12.3 Hz, 1H, C*H*$_{2Ar}$), 4.59 (d, $^3J_{H\text{-}H}$ = 4.65 Hz, 1H, C*H*$_{2Ar}$), 4.61 (d, $^3J_{H\text{-}H}$ = 5.00 Hz, 2H, C*H*$_{2Ar}$), 4.64 (d, $^3J_{H\text{-}H}$ = 4.40 Hz, 1H, C*H*$_{2Ar}$), 4.77-4.80 (m, 3H, C*H*$_{2Ar}$ and *H*1), 4.88 (d, $^3J_{H\text{-}H}$ = 12.2 Hz, 1H, C*H*$_{2Ar}$), 6.54 (d, $^3J_{H\text{-}H}$ = 8.20 Hz, 1H, N*H*), 7.20-7.22 (dd, $^2J_{H\text{-}H}$ = 1.9 Hz, $^3J_{H\text{-}H}$ 9.25 Hz, *H*2, H_{Ar}), 7.25-7.34 (m, 18H, H_{Ar}). ^{13}C NMR (125 MHz, $CDCl_3$): δ (ppm) 42.5 (*C*H$_2$Cl), 56.6 (*C*H-2), 68.9 (*C*H-6), 70.6 (*C*H_{2Ar}), 73.1 (*C*H_{2Ar}), 74.6 (*C*H_{2Ar}), 74.7 (*C*H_{2Ar}), 74.9 (*C*H-5), 78.5 (*C*H-3), 80.3 (*C*H-4), 98.7 (*C*H-1), 127.6 (*C*H_{Ar}), 127.7 (*C*H_{Ar}), 127.82 (*C*H_{Ar}), 127.89 (*C*H_{Ar}), 127.9 (*C*H_{Ar}), 128.0 (*C*H_{Ar}), 128.4 (*C*H_{Ar}), 128.41 (*C*H_{Ar}), 128.44 (*C*H_{Ar}), 128.46 (*C*H_{Ar}), 137.4 (C_q), 137.9 (C_q), 138.1 (C_q), 138.3 (C_q), 165.9 (C=O). HRESI-MS$^+$ (*CH₃OH*): $[C_{36}H_{38}ClNO_6]^+$ *m/z* = 638.2284, calcd = 638.2280.

4.47. A solution of **4.46** (0.062 g, 0.10 mmol) and **4.25** (0.015 g, 0.10 mmol) in acetonitrile (10 mL) was heated at 100 °C for 48 h. After removal of the solvent on a rotatory evaporator, the crude product was purified on silica gel column chromatography with methanol (5%) and dichloromethane (95%) as the eluent to obtain the pure product

as a yellow solid. (Yield: 0.014 g, 18%). ^{1}H NMR (500 MHz, $CDCl_3$): δ (ppm) 3.57-3.60 (m, 1H, *H*-4), 3.65-3.69 (m, 2H, *H*-6), 3.73 (d, $^{3}J_{H-H}$ = 3.10 Hz, 2H, CH_2C=O), 3.95 (t, $^{3}J_{H-H}$ = 8.85 Hz, 1H, *H*-5), 4.18 (q, $^{2}J_{H-H}$ = 8.80 Hz, $^{3}J_{H-H}$ = 9.45 Hz, 1H, *H*-2), 4.50-4.54 (m, 2H, CH_{2Ar}), 4.58-4.62 (m, 2H, CH_{2Ar}), 4.73 (d, $^{3}J_{H-H}$ = 11.2 Hz, 1H, CH_{2Ar}), 4.77 (d, $^{3}J_{H-H}$ = 8.40 Hz, 1H, *H*-3), 4.86 (t, $^{3}J_{H-H}$ = 4.00 Hz, 2H, CH_{2Ar}), 4.92 (d, $^{3}J_{H-H}$ = 5.9 Hz, 1H, CH_{2Ar}), 4.95 (d, $^{3}J_{H-H}$ = 5.25 Hz, 1H, CH_{2Ar}), 4.98 (s, 1H, CH_{2Ar}), 5.18 (d, $^{3}J_{H-H}$ = 13.7 Hz, 1H, *H*-1), 6.99-7.01 (m, 1H, H_{Ar}), 7.04-7.10 (m, 5H, H_{Ar}), 7.12-7.17 (m, 5H, H_{Ar}), 7.23-7.25 (m, 4H, H_{Ar}), 7.38 (m, 1H, H_{py}), 7.54 (t, $^{3}J_{H-H}$ = 1.70 Hz, 1H, H_{imi}) 7.63 (d, $^{3}J_{HH}$ = 8.20 Hz, 1H, H_{py}), 7.71 (t, $^{3}J_{H-H}$ = 1.80 Hz, 1H, H_{imi}), 7.88 (dd, $^{2}J_{H-H}$ = 1.80 Hz, $^{3}J_{H-H}$ = 6.37 Hz, 1H, H_{py}), 8.46-8.48 (m, 1H. H_{py}), 9.76 (d, $^{3}J_{H-H}$ = 9.55 Hz, 1H, N*H*), 10.9 (s, 1H, NC*H*N). ^{13}C NMR (125 MHz, $CDCl_3$): δ (ppm) 53.0 (*C*H-1), 55.6 (*C*H-2), 68.8 (*C*H_2Cl), 70.7 (*C*H-6), 73.4 (*C*H_{2Ar}), 74.6 (*C*H_{2Ar}), 74.8 (*C*H_{2Ar}), 75.0 (*C*H-5), 78.3 (*C*H-3), 82.8 (*C*H-4), 101.0 (*C*H_{2Ar}), 113.7 (*C*H_{py}), 117.9 (*C*H_{imi}), 123.3 (*C*H_{imi}), 125.1 (*C*H_{py}), 126.7 (*C*H_{Ar}), 126.9 (*C*H_{Ar}), 127.0 (*C*H_{Ar}), 127.1 (*C*H_{Ar}), 127.5 (*C*H_{Ar}), 127.6 (*C*H_{Ar}), 127.7 (*C*H_{Ar}), 127.9 (*C*H_{Ar}), 128.0 (*C*H_{Ar}), 128.2 (*C*H_{Ar}), 128.3 (*C*H_{Ar}), 134.8 (N*C*HN), 137.9 (C_q), 138.3 (C_q), 139.0 (C_q), 140.2 (*C*H_{py}), 145.4 (C_q), 149.1 (*C*H_{py}), 164.1 (*C*=O). HRESI-MS^{+} (*CH_3OH*): $[C_{22}H_{26}N_3O_9]^{+}$ *m/z* = 476.1666, calcd = 476.1669.

4.48. A mixture of **4.47** (0.043 g, 0.056 mmol), Ag_2O (0.016 g, 0.068 mmol), and $Re(CO)_5Cl$ (0.020 g, 0.056 mmol) in dichloromethane (5 mL) was heated at 45 °C for 24 h. The mixture was filtered through Celite and the solvent was removed from the filtrate on a rotatory evaporator. The crude product was purified on a silica gel column chromatography using methanol (2%) and dichloromethane (98%) as the eluent. The product was obtained as a yellow solid. (Yield: 0.017 g, 29%). ^{1}H NMR (500 MHz, $CDCl_3$): δ (ppm) 3.45-3.49 (m, 1H, H-4), 3.61-3.67 (m, 1H, H-5), 3.67-3.73 (m, 2H, H-6), 3.85 (t, $^{3}J_{H-H}$ = 8.90 Hz, 1H, *H*-3), 4.18-4.22 (m, 2H, CH_{2Ar}), 4.27 (m, 1H, *H*-2), 4.47-4.51 (m, 1H, CH_{2Ar}), 4.52-4.57 (m, 2H, CH_{2Ar}), 4.60-4.66 (m, 2H, CH_{2Ar}), 4.69-4.73 (m,

2H, CH_2C=O), 4.78 (d, $^3J_{H-H}$ = 11.0 Hz, 1H, CH_{2Ar}), 4.85 (t, $^3J_{H-H}$ = 12.0 Hz, 1H, CH_{2Ar}), 4.92 (d, $^3J_{H-H}$ = 11.3 Hz, 1H, CH_{2Ar}), 5.29 (dd, $^2J_{H-H}$ = 6.80 Hz, $^3J_{H-H}$ = 8.40 Hz, 1H, *H*-1), 6.60 (d, $^3J_{H-H}$ = 2.10 Hz, 1H, H_{imi}), 6.76 (d, $^3J_{H-H}$ = 2.15 Hz, 1H, H_{imi}), 6.86 (d, $^3J_{H-H}$ = 2.10 Hz, 1H, H_{imi}), 7.06 (d, $^3J_{H-H}$ = 2.10 Hz, 1H, H_{imi}), 7.07-7.09 (dd, $^2J_{H-H}$ = 5.70 Hz, $^3J_{H-H}$ = 8.60 Hz, 1H, H_{py}), 7.13-7.15 (dd, $^2J_{H-H}$ = 2.00 Hz, $^3J_{H-H}$ = 5.71 Hz, 1H, H_{py}), 7.19-7.21 (m, 2H, H_{Ar}), 7.23-7.45 (m, 2H, H_{Ar}), 8.06-8.11 (m, 1H, H_{py}), 8.91 (d, $^3J_{H-H}$ = 5.55 Hz, 1H, H_{py}). ^{13}C NMR (125 MHz, $CDCl_3$): δ (ppm) 56.4 (*C*H-1), 56.5 (*C*H-2), 70.5 (CH_{2Ar}), 71.2 (CH_{2Ar}), 73.4 (CH_{2Ar}),74.1 (CH_{2Ar}), 75.1 (*C*H-4), 75.4 (CH_{2Ar}), 78.3 (*C*H-5), 82.2 (*C*H-3), 82.8 (*C*H-6), 100.8 (CH_2C=O), 111.7 (CH_{py}), 116.6 (CH_{imi}), 123.1 (CH_{imi}), 126.4 (CH_{Ar}), 127.1 (CH_{Ar}), 127.2 (CH_{Ar}), 127.2 (CH_{Ar}), 127.3 (CH_{Ar}), 127.5 (CH_{Ar}), 127.5 (CH_{Ar}), 127.5 (CH_{Ar}), 127.6 (CH_{py}), 127.7 (CH_{py}), 127.8 (CH_{Ar}), 128.0 (CH_{Ar}), 128.1 (CH_{Ar}), 128.2 (CH_{Ar}), 128.3 (CH_{Ar}), 138.0 (C_q), 138.3 (C_q), 138.4 (C_q), 138.7 (C_q), 144.2 (CH_{py}), 152.8 (C_q), 153.8 (CH_{py}), 165.3 (*C*=O), 187.8 (N*C*N), 193.9 (Re-*C*O), 194.3 (Re-*C*O), 196.9 (Re-*C*O). HRESI-MS$^+$ (*CH_3OH*): $[C_{22}H_{26}N_3O_9]^+$ *m/z* = 476.1666, calcd = 476.1669.

4.50. This compound was synthesised as described previously from DL-glucose (5.00 g, 27.9 mmol), CH_3COONa (4.56 g, 55.6 mmol), and acetic anhydride (28.4 g, 0.28 mol).[30-31] The product was obtained as a white solid. (Yield: 9.17 g, 84%). ^{1}H NMR (500 MHz, DMSO-*d_6*): δ (ppm) 1.94 (s, 3H. CH_3), 1.99-2.01 (m, 9H, CH_3), 2.07 (s, 3H, CH_3), 3.99 (dd, 1H, $^2J_{H-H}$ = 2.00, $^3J_{H-H}$ = 10.3 Hz, *H*-6), 4.16 (dd, 1H, $^3J_{H-H}$ = 4.85, 7.50 Hz, *H*-6), 4.19-4.22 (m, 1H, *H*-4), 4.90-4.98 (m, 2H, H-2, *H*-5), 5.44 (t, 1H, $^3J_{H-H}$ = 9.60 Hz, *H*-3), 5.96 (d, 1H, $^3J_{H-H}$ = 8.30 Hz, *H*-1). ^{13}C NMR (125 MHz, DMSO-*d_6*): δ (ppm) 20.7 (O*C*H_3), 20.8 (O*C*H_3), 20.9 (O*C*H_3), 61.9 (*C*H-6), 68.1 (*C*H-5), 70.6 (*C*H-2), 71.8 (*C*H-4), 72.2 (*C*H-3), 91.3 (*C*H-1). HRESI-MS$^+$ (*CH_3OH*): $[C_{16}H_{22}N_{11}Na]^+$ *m/z* = 413.1050, calcd = 413.1054.

4.51. This compound was synthesised as described previously from **4.50** (0.92 g, 2.37 mmol) and HBr in 33% acetic acid (0.67 g, 8.29 mmol).[30-31] The product was obtained as a yellow oil. (Yield: 0.36 g, 31%). ^{1}H NMR (500 MHz, DMSO-d_6): δ (ppm) 2.04 (s, 3H, CH_3), 2.05 (s, 3H, CH_3), 2.09 (s, 3H, CH_3), 2.10 (s, 3H, CH_3), 4.13 (dd, 1H, $^{2}J_{H\text{-}H}$ = 2.00, $^{3}J_{H\text{-}H}$ = 10.6 Hz, *H*-6), 4.29-4.35 (m, 2H, H5, *H*-6), 4.67 (dd, 1H, $^{2}J_{H\text{-}H}$ = 4.10 Hz, $^{3}J_{H\text{-}H}$ = 5.90 Hz, *H*-2), 5.16 (t, 1H, $^{3}J_{H\text{-}H}$ = 10.1 Hz, *H*-4), 5.56 (t, 1H, $^{3}J_{H\text{-}H}$ = 9.75 Hz, *H*-3), 6.61 (d, 1H, $^{3}J_{H\text{-}H}$ = 4.05 Hz, *H*-1). ^{13}C NMR (125 MHz, DMSO-d_6): δ (ppm) 20.5 (*C*H_3), 20.6 (*C*H_3), 20.65 (*C*H_3), 20.67 (*C*H_3), 60.9 (*C*H-6), 67.2 (*C*H-4), 70.2 (*C*H-3), 70.6 (*C*H-2), 72.1 (*C*H-5), 86.6 (*C*H-1), 169.5 (*C*O), 169.8 (*C*O), 169.9 (*C*O), 170.5 (*C*O). HRESI-MS^{+} (*CH_3OH*): $[C_{14}H_{19}BrO_9Na]^{+}$ *m/z* = 433.0100, calcd = 433.0105.

4.52. A mixture of **4.51** (0.20 g, 0.48 mmol) and **4.25** (0.071 g, 0.48 mmol) in acetonitrile (20 mL) was heated at 100 °C for 12 h. The solvent was removed on a rotatory evaporator and the crude product was purified on silica gel column chromatography with methanol (5%) and dichloromethane (95%) as the eluent and the pure product was obtained as a yellow oil. (Yield: 0.23 g, 59%). ^{1}H NMR (500 MHz, $CDCl_3$): δ (ppm) 2.09 (s, 3H, CH_3), 2.11 (s, 3H, CH_3), 2.12 (s, 3H, CH_3), 4.17-4.22 (m, 3H, *H*6, *H*3, *H*2), 4.34 (dd, $^{2}J_{H\text{-}H}$ = 5.05 Hz, $^{3}J_{H\text{-}H}$ = 7.70 Hz, 1H, *H*6), 5.20 (t, $^{3}J_{H\text{-}H}$ = 9.90 Hz, 1H, *H*5), 5.57 (t, $^{3}J_{H\text{-}H}$ = 9.50 Hz, 1H, *H*4), 6.09 (d, $^{3}J_{H\text{-}H}$ = 9.05 Hz, 1H, *H*1), 6.50 (d, $^{3}J_{H\text{-}H}$ = 7.00 Hz, 1H, O*H*), 7.38-7.40 (m, 1H, H_{py}), 7.68 (t, $^{3}J_{H\text{-}H}$ = 1.80, 1H, H_{imi}), 7.98-8.02 (dt, $^{2}J_{H\text{-}H}$ = 1.80 Hz, $^{3}J_{H\text{-}H}$ = 5.75 Hz, 1H, H_{py}), 8.19 (d, $^{3}J_{H\text{-}H}$ = 8.25 Hz, 1H, H_{py}), 8.26 (t, $^{3}J_{H\text{-}H}$ = 1.85 Hz, 1H, H_{imi}), 8.51-8.53 (m, 1H, H_{py}), 10.7 (s, 1H, NC*H*N). ^{13}C NMR (125 MHz, $CDCl_3$): δ (ppm) 20.5 (*C*H_3), 20.8 (*C*H_3), 21.0 (*C*H_3), 61.7 (*C*H-6), 64.9 (*C*H-5), 71.3 (*C*H-3), 73.8 (*C*H-4), 75.1 (*C*H-2), 87.4 (*C*H-1), 115.0 (CH_{py}), 119.7 (CH_{imi}), 119.9 (CH_{imi}), 125.1 (CH_{py}), 134.0 (N*C*HN), 140.8 (CH_{py}), 145.9 (C_q), 149. 1 (CH_{py}), 169.5 (*C*=O), 170.6 (*C*=O), 170.8 (*C*=O). HRESI-MS^{+} (*CH_3OH*): $[C_{22}H_{26}N_3O_9]^{+}$ *m/z* = 476.1666, calcd = 476.1669.

4.54. This compound was prepared using the same procedure as described for **4.48** from **4.52** (0.050 g, 0.090 mmol), Ag_2O (0.042 g, 0.18 mmol), and $Re(CO)_5Cl$ (0.033 g, 0.090 mmol). The product was obtained as yellow solid. However, the quantity of this complex which was isolated was too low to obtain its yield, and only ^{1}H NMR and HRMS analytical data for this compound was obtained. ^{1}H NMR (500 MHz, $CDCl_3$): δ (ppm) 2.01-2.10 (m, 9H, CH_3), 4.05-4.10 (m, 2H, H_{glu}), 4.21 (dd, 1H, $^2J_{H\text{-}H}$ = 2.05 Hz, $^3J_{H\text{-}H}$ = 10.6 Hz, H_{glu}), 4.33 (dd, 1H, $^2J_{H\text{-}H}$ = 5.05 Hz, $^3J_{H\text{-}H}$ = 7.60 Hz, H_{glu}), 5.21 (t, 1H, $^3J_{H\text{-}H}$ = 9.90 Hz, H_{glu}), 5.32 (t, 1H, $^3J_{H\text{-}H}$ = 9.80 Hz, H_{glu}), 5.66 (d, 1H, $^3J_{H\text{-}H}$ = 9.05 Hz, H_{glu}), 7.43-7.45 (m, 1H, H_{py}), 7.47 (d, 1H, $^3J_{H\text{-}H}$ = 2.35 Hz, H_{imi}), 7.91 (d, 1H, $^3J_{H\text{-}H}$ = 2.50 Hz, H_{imi}), 7.98-8.00 (m, 1H, H_{py}), 8.20-8.25 (m, 1H, H_{py}), 8.75 (dd, 1H, $^2J_{H\text{-}H}$ = 1.05 Hz, $^3J_{H\text{-}H}$ = 4.60 Hz, H_{py}). HRESI-MS$^+$ (*CH_3OH*): $[C_{23}H_{23}N_3O_{11}Re]^+$ *m/z* = 704.0862, calcd = 704.0890.

4.60. This compound was synthesised as described previously from 2-chloroacetyl chloride (2.15 g, 19.0 mmol), 2-(2-aminoethoxy)ethanol (2.00 g, 19.0 mmol) and triethylamine (1.90 g, 19.0 mmol).[45] The product was obtained as yellow oil. ^{1}H NMR (500 MHz, $CDCl_3$): δ (ppm) 3.51-3.54 (m, 2H, CH_2NH), 3.59-3.62 (m, 4H, CH_2), 3.75-3.77 (m, 2H, CH_2OH), 4.06 (s, 2H, CH_2Cl), 7.00 (s, 1H, N*H*). ^{13}C NMR (125 MHz, $CDCl_3$): δ (ppm) 39.6 (CH_2NH), 42.7 (CH_2Cl), 61.8 (CH_2OH), 69.5 (CH_2), 72.3 (CH_2), 166.2 (*C*=O). HRESI-MS$^+$ (*CH_3OH*): $[C_6H_{12}ClNO_3Na]^+$ *m/z* = 204.0395, calcd = 204.0398.

4.61. This compound was synthesised using a modified literature procedure[42-43] from **4.51** (0.40 g, 0.96 mmol), **4.60** (0.044 g, 0.96 mmol) and iodine (0.34 g, 1.35 mmol). The solvent was removed on a rotatory evaporator and the crude product was purified on silica gel column chromatography with methanol (5%) and dichloromethane (95%) as the eluent yielding the product as a yellow oil. (Yield: 0.18 g, 37 %). ^{1}H NMR (500 MHz,

$CDCl_3$): δ (ppm) 2.01-2.02 (m, 3H, OC*H*$_3$), 2.02-2.03 (m, 3H, OC*H*$_3$), 2.07-2.08 (m, 3H, OC*H*$_3$), 2.08-2.09 (m, 3H, OC*H*$_3$), 3.24 (d, $^3J_{H-H}$ = 3.35 Hz, 1H, N*H*), 3.48-3.53 (m, 2H, C*H*$_2$Cl), 3.58-3.60 (m, 1H, *H*-4), 3.67-3.69 (m, 2H, C*H*$_2$CH$_2$NH), 3.87-3.90 (m, 1H, *H*-3), 4.10-4.16 (m, 2H, *H*-6), 4.22-4.25 (m, 4H, CH$_2$C*H*$_2$O, CH$_2$C*H*$_2$NH), 4.88-4.92 (m, 1H, *H*-5), 5.06-5.10 (m, 2H, C*H*$_2$CH$_2$O), 5.46 (t, $^3J_{H-H}$ = 3.50 Hz, 1H, *H*-2), 5.53 (t, $^3J_{H-H}$ = 9.80 Hz, 1H, *H*-1). ^{13}C NMR (125 MHz, $CDCl_3$): δ (ppm) 20.6 (O*C*H$_3$), 20.7 (O*C*H$_3$), 20.7 (O*C*H$_3$), 20.8 (O*C*H$_3$), 39.8 (*C*H$_2$Cl), 61.9 (*C*H-6), 63.3 (CH$_2$*C*H$_2$NH), 67.3 (CH$_2$*C*H$_2$O), 68.5 (*C*H$_2$CH$_2$O), 69.0 (*C*H$_2$CH$_2$NH), 69.3 (*C*H-4), 69.8 (*C*H-1), 71.1 (*C*H-5), 90.2 (*C*H-2), 169.6 (NH*C*=O), 170.1 (*C*=OCH$_3$), 170.8 (*C*=OCH$_3$), 170.9 (*C*=OCH$_3$), 171.0 (*C*=OCH$_3$). HRESI-MS$^+$ (*CH$_3$OH*): $[C_{20}H_{30}ClNO_{12}Na]^+$ *m/z* = 534.1350, calcd = 534.1349.

4.62. This compound was prepared using the same procedure as described for **4.52** from **4.61** (0.22 g, 0.43 mmol) and **4.25** (0.063 g, 0.43 mmol). The crude product was purified on a CM-Sephadex C-25 ion-exchange resin (40-120) column and eluted with water followed by 0.1 M NaCl solution. The NaCl layer was collected, the solvent was evaporated using rotary evaporator and re-dissolved in acetonitrile solution. The acetonitrile solution was dried with $MgSO_4$ and the solvent was evaporated using rotary evaporator. The pure product was obtained as a yellow oil with a chloride counter anion. (Yield: 0.13 g, 45 %). ^{1}H NMR (500 MHz, CH$_3$OD): δ (ppm) 1.97-2.06 (m, 12H, OC*H*3), 3.46-3.50 (m, 2H, C*H*2), 3.58-3.61 (m, 2H, C*H*$_2$), 3.62-3.65 (m, 2H, C*H*$_2$CH$_2$NH), 3.69-3.71 (m, 1H, *H*-5), 3.73-3.77 (m, 1H, C*H*$_2$NH), 3.87-3.91 (m, 1H, *H*-3), 3.95-3.99 (m, 1H, C*H*$_2$NH), 4.14 (dd, 1H, $^2J_{H-H}$ = 2.25 Hz, $^3J_{H-H}$ = 11.6 Hz, *H*-6), 4.23 (t, 1H, $^3J_{H-H}$ = 4.75 Hz, *H*-4), 4.29 (dd, 1H, $^2J_{H-H}$ = 4.70 Hz, $^3J_{H-H}$ = 7.40 Hz, *H*-6), 5.03 (t, 1H, $^3J_{H-H}$ = 9.85 Hz, *H*-2), 5.15-5.17 (m, 2H, C*H*$_2$CO), 5.25-5.31 (m, 1H, *H*-1), 7.61-7.63 (m, 1H, H_{py}), 7.83 (dd, 1H, $^2J_{H-H}$ = 1.90 Hz, $^3J_{H-H}$ = 3.25 Hz, H_{imi}), 7.93 (d, 1H, $^3J_{H-H}$ = 8.15 Hz, H_{py}), 8.15 (t, 1H, $^3J_{H-H}$ = 7.85 Hz, H_{py}), 8.42 (t, 1H, $^3J_{H-H}$ = 2.25 Hz, H_{imi}), 8.63-8.65 (m,

1H, H_{py}). ^{13}C NMR (125 MHz, CH_3OD): δ (ppm) 19.1 (OCH_3), 19.2 (OCH_3), 19.3 (OCH_3), 19.4 (OCH_3), 39.4 (CH_2), 51.0 (CH_2C=O), 61.7 (*C*H-6), 63.2 (*C*H-4), 68.4 (*C*H-2), 68.5 (*C*H-5), 68.9 (CH_2), 69.1 (CH_2NH), 69.7 (CH_2CH_2NH), 71.5 (*C*H-3), 72.8 (*C*H-1), 113.6 (CH_{py}), 118.8 (CH_{imi}), 124.7 (CH_{imi}), 125.2 (CH_{py}), 140.3 (CH_{py}), 146.6 (C_q), 149.4 (CH_{py}), 165.2 (*C*ONH), 169.9 (*C*OCH_3), 170.1 (*C*OCH_3), 170.1 (*C*OCH_3), 170.2 (*C*OCH_3). HRESI-MS$^+$ (*CH_3OH*): $[C_{28}H_{37}N_4O_{12}]^+$ *m/z* = 621.2404, calcd = 621.2408.

4.63. This compound was prepared using the same procedure as described for **4.53** from **4.62** (0.044 g, 0.066 mmol), Ag_2O (0.077 g, 0.33 mmol), and $Re(CO)_5Cl$ (0.024 g, 0.066 mmol) and was stirred at 45 °C for seven days. The crude product was purified as described for compound **4.62**. The water layer was collected, and solvent was evaporated using rotary evaporator. The product was obtained as yellow solid. (Yield: 0.0075 g, 15 %). ^{1}H NMR (500 MHz, CH_3OD): δ (ppm) 3.33-3.37 (m, 1H, C*H*-5), 3.26-3.28 (m, 1H, C*H*-4), 3.15-3.18 (m, 1H, C*H*-2), 3.25 (d, 1H, $^3J_{H\text{-}H}$ = 6.60 Hz, C*H*-3), 3.43-3.47 (m, 2H, CH_2), 3.55-3.60 (m, 2H, CH_2), 3.62-3.64 (m, 2H, CH_2CH_2NH), 3.69-3.73 (m, 1H, C*H*-6), 3.76-3.80 (m, 1H, CH_2NH), 3.82-3.85 (m, 1H, C*H*-6), 3.95-3.98 (m, 1H, CH_2NH), 4.29 (d, 1H, $^3J_{H\text{-}H}$ = 7.80 Hz, C*H*-1), 5.02-5.06 (m, 2H, CH_2CO), 7.40-7.45 (m, 1H, H_{py}), 7.47-7.49 (m, 1H, H_{imi}), 8.03-8.05 (m, 1H, H_{py}), 8.16 (d, 1H, $^3J_{H\text{-}H}$ = 1.45 Hz, H_{imi}), 8.18-8.21 (m, 1H, H_{py}), 8.83 (d, 1H, $^3J_{H\text{-}H}$ = 5.35 Hz, H_{py}). ^{13}C NMR (CH_3OD): δ (ppm) 39.2 (CH_2), 53.4 (CH_2CO), 61.3 (*C*H-6), 68.3 (CH_2NH), 68.9 (CH_2), 69.7 (CH_2), 69.8 (CH_2), 70.2 (*C*H-4), 72.3 (*C*H-5), 73.7 (*C*H-2), 76.6 (*C*H-3), 103.1 (*C*H-1), 112.5 (CH_{py}), 116.9 (CH_{imi}), 123.6 (CH_{py}), 124.8 (CH_{imi}), 141.8 (CH_{py}), 149.4 (C_q), 153.2 (CH_{py}), 167.1 (*C*ONH), 196.9 (Re-*C*O), 197.2 (Re-*C*O), 197.4 (Re-*C*O). HRESI-MS$^+$ (*CH_3CN*): $[C_{23}H_{28}N_4O_{11}Re]^+$ *m/z* = 723.1317, calcd = 723.1312.

4.6. Reference

1. Farrell, N., *Cancer Investig.* **1993,** *11* (5), 578-589.

2. Mangrum, J. B.; Farrell, N. P., *Chem. Commun. (Camb.)* **2010,** *46* (36), 6640-6650.

3. Manzotti, C.; Pratesi, G.; Menta, E.; Di Domenico, R.; Cavalletti, E.; Fiebig, H. H.; Kelland, L. R.; Farrell, N.; Polizzi, D.; Supino, R.; Pezzoni, G.; Zunino, F., *Clin. Cancer Res.* **2000,** *6* (7), 2626-2634.

4. Hensing, T. A.; Hanna, N. H.; Gillenwater, H. H.; Gabriella Camboni, M.; Allievi, C.; Socinski, M. A., *Anticancer Drugs* **2006,** *17* (6), 697-704.

5. Bai, L.; Gao, C.; Cai, L.; Liu, Q.; Qian, Y.; Yang, B., *J. Coord. Chem.* **2017,** *70* (22), 3759-3768.

6. He, L.; Meng, Z.; Xu, D.; Shao, F., *Sci. Rep.* **2018,** *8* (1), 767.

7. Chtchigrovsky, M.; Eloy, L.; Jullien, H.; Saker, L.; Ségal-Bendirdjian, E.; Poupon, J.; Bombard, S.; Cresteil, T.; Retailleau, P.; Marinetti, A., *J. Med. Chem.* **2013,** *56* (5), 2074-2086.

8. Leonidova, A.; Gasser, G., *ACS Chem. Biol.* **2014,** *9* (10), 2180-2193.

9. Giffard, D.; Fischer-Fodor, E.; Vlad, C.; Achimas-Cadariu, P.; Smith, G. S., *Eur. J. Med. Chem.* **2018,** *157*, 773-781.

10. Imstepf, S.; Pierroz, V.; Rubbiani, R.; Felber, M.; Fox, T.; Gasser, G.; Alberto, R., *Angew. Chem. Int. Ed.* **2016,** *55* (8), 2792-2795.

11. Kitanovic, I.; Can, S.; Alborzinia, H.; Kitanovic, A.; Pierroz, V.; Leonidova, A.; Pinto, A.; Spingler, B.; Ferrari, S.; Molteni, R.; Steffen, A.; Metzler-Nolte, N.; Wölfl, S.; Gasser, G., *Chem. Eur. J.* **2014,** *20* (9), 2496-2507.

12. Pan, Z.-Y.; Cai, D.-H.; He, L., *Dalton Trans.* **2020,** *49* (33), 11583-11590.

13. Govindarajan, R.; Nagarajaprakash, R.; Veena, V.; Sakthivel, N.; Manimaran, B., *Polyhedron* **2018,** *139*, 229-236.

14. Tekade, R. K.; Sun, X., *Drug Discov. Today* **2017,** *22* (11), 1637-1653.

15. Pajak, B.; Siwiak, E.; Sołtyka, M.; Priebe, A.; Zieliński, R.; Fokt, I.; Ziemniak, M.; Jaśkiewicz, A.; Borowski, R.; Domoradzki, T.; Priebe, W., *Int. J. Mol. Sci.* **2020,** *21* (1), 234.

16. Petriev, V. M.; Tishchenko, V. K.; Krasikova, R. N., *Pharm. Chem. J.* **2016,** *50* (4), 209-220.

17. Priebe, W.; Zielinski, R.; Fokt, I.; Felix, E.; Radjendirane, V.; Arumugam, J.; Tai Khuong, M.; Krasinski, M.; Skora, S., *Neuro-Oncol.* **2018,** *20* (suppl_6), vi86-vi86.

18. Louie, M.-W.; Liu, H.-W.; Lam, M. H.-C.; Lam, Y.-W.; Lo, K. K.-W., *Chem. Eur. J.* **2011,** *17* (30), 8304-8308.

19. Thenarukandiyil, R.; Dutta, C.; Choudhury, J., *Chem. Eur. J.* **2017,** *23* (61), 15529-15533.

20. Li, Z.; Mackie, E. R. R.; Ramkissoon, P.; Mather, J. C.; Wiratpruk, N.; Soares da Costa, T. P.; Barnard, P. J., *Dalton Trans.* **2020,** *49* (36), 12820-12834.

21. Chan, C. Y.; Pellegrini, P. A.; Greguric, I.; Barnard, P. J., *Inorg. Chem.* **2014,** *53* (20), 10862-10873.

22. Chan, C. Y.; Barnard, P. J., *Dalton Trans.* **2015,** *44* (44), 19126-19140.

23. Grundler, P. V.; Helm, L.; Alberto, R.; Merbach, A. E., *Inorg. Chem.* **2006,** *45* (25), 10378-10390.

24. Malaza, S.; Govender, P.; Schutte-Smith, M.; Visser, H. G.; Smith, G. S., *Eur. J. Inorg. Chem.* **2017,** *2017* (33), 3919-3927.

25. Salignac, B.; Grundler, P. V.; Cayemittes, S.; Frey, U.; Scopelliti, R.; Merbach, A. E.; Hedinger, R.; Hegetschweiler, K.; Alberto, R.; Prinz, U.; Raabe, G.; Kölle, U.; Hall, S., *Inorg. Chem.* **2003,** *42* (11), 3516-3526.

26. Schutte, M.; Kemp, G.; Visser, H. G.; Roodt, A., *Inorg. Chem.* **2011,** *50* (24), 12486-12498.

27. Schutte-Smith, M.; Marker, S. C.; Wilson, J. J.; Visser, H. G., *Inorg. Chem.* **2020,** *59* (21), 15888-15897.

28. Louie, M.-W.; Fong, T. T.-H.; Lo, K. K.-W., *Inorg. Chem.* **2011,** *50* (19), 9465-9471.

29. Agarwal, J.; Peddinti, R. K., *J. Org. Chem.* **2011,** *76* (9), 3502-3505.

30. Esmaeilian, N.; Dabir, B.; Malek, R. M. A.; Arami, M.; Mazaheri, F. M., *J. Mol. Liq.* **2020,** *318*, 114269.

31. Šardzík, R.; Noble, G. T.; Weissenborn, M. J.; Martin, A.; Webb, S. J.; Flitsch, S. L., *Beilstein J. Org. Chem.* **2010,** *6*, 699-703.

32. Garegg, P. J.; Hultberg, H., *Carbohydr. Res.* **1982,** *110* (2), 261-266.

33. Wang, T.; Demchenko, A. V., *Org. Biomol. Chem.* **2019,** *17* (20), 4934-4950.

34. Williams, J. M.; Richardson, A. C., *Tetrahedron* **1967,** *23* (3), 1369-1378.

35. Kimmel, R.; Kafka, S.; Košmrlj, J., *Carbohydr. Res.* **2010,** *345* (6), 768-779.

36. Hipólito, T. M. M.; Bastos, G. T. L.; Barbosa, T. W. L.; de Souza, T. B.; Coelho, L. F. L.; Dias, A. L. T.; Rodríguez, I. C.; dos Santos, M. H.; Dias, D. F.; Franco, L. L.; Carvalho, D. T., *Chem. Biol. Drug Des.* **2018,** *92* (2), 1514-1524.

37. Petrig, J.; Schibli, R.; Dumas, C.; Alberto, R.; Schubiger, P. A., *Chem. Eur. J.* **2001,** *7* (9), 1868-1873.

38. Shim, E. J.; Przybylski, J. L.; Wetmore, S. D., *J. Phys. Chem. B.* **2010,** *114* (6), 2319-2326.

39. Stivers, J. T.; Jiang, Y. L., *Chem. Rev.* **2003,** *103* (7), 2729-2760.

40. Wu, R.; Wang, S.; Zhou, N.; Cao, Z.; Zhang, Y., *J. Am. Chem. Soc.* **2010,** *132* (27), 9471-9479.

41. Ren, B.; Wang, M.; Liu, J.; Ge, J.; Zhang, X.; Dong, H., *Green Chem.* **2015,** *17* (3), 1390-1394.

42. Kartha, K. P. R.; Ballell, L.; Bilke, J.; McNeil, M.; Field, R. A., *J. Chem. Soc. Perkin Trans. I* **2001,** (8), 770-772.

43. Kartha, K. P. R.; Cura, P.; Aloui, M.; Readman, S. K.; Rutherford, T. J.; Field, R. A., *Tetrahedron Asymmetry* **2000,** *11* (2), 581-593.

44. Tan, K. V.; Pellegrini, P. A.; Skelton, B. W.; Hogan, C. F.; Greguric, I.; Barnard, P. J., *Inorg. Chem.* **2014,** *53* (1), 468-477.

45. Morfin, J.-F.; Tripier, R.; Baccon, M. L.; Handel, H., *Polyhedron* **2009,** *28* (17), 3691-3698.

Chapter 5 : Thesis Conclusion and Future Directions

5.1. Thesis Conclusion

Complexes of the transition metal rhenium have a diverse range of potential medical applications, including nuclear medicine as diagnostic imaging and therapeutic agents such as anticancer compounds. The aim of this thesis was to explore the potential for Re(I) complexes of *N*-heterocyclic carbene ligands to be used as imaging agents for Alzheimer's disease or as anticancer therapeutic agents.

The first part of this thesis focused on the development of *N*-heterocyclic carbene complexes of the $[Re(CO)_3]^+$ core as models of potential technetium-99m imaging agents for Alzheimer's disease (AD). Chapter 2 described the synthesis of two tridentate *N*-heterocyclic carbene pro-ligands bearing imidazolium, amine and carboxylate groups coupled to an amyloid binding moiety (either a benzothiazole or a stilbene derivative). Neutral Re(I)-NHC complexes (**2.17** and **2.18**) were prepared from these pro-ligands and using the histological dye Thioflavin-T (ThT), an investigation of the binding properties of the complexes to amyloid-β fibrils was undertaken. The results of this study indicated that both complexes **2.17** or **2.18** can either bind to or inhibit the formation of amyloid-β fibrils. In a second study, epi-fluorescence microscopy was used to investigate the binding of these Re(I) complexes to amyloid plaques in frontal cortex brain tissue, and the complexes were found to have moderate levels binding to amyloid-β plaques. A plausible explanation for lower levels of binding may be the relatively short distance between the octahedral metal complex and the amyloid binding group together with the relatively low lipophilicity of complexes **2.17** and **2.18**, which reduced their ability to bind to amyloid plaques.

The partition coefficient or log*P* is a useful value for estimating the lipophilic properties of compounds and their capacity to pass through the blood-brain barrier (BBB). As these Re(I) complexes were designed to act as imaging agents to detect amyloid plaques in human brain tissues, log*P* experiments were conducted, and the values for complexes **2.17** and **2.18** were determined to be 0.15 ± 0.01 and 0.39 ± 0.01, respectively. These log*P* values are not within the optimum range for BBB penetration, indicating that the structures of NHC pro-ligands must be modified to increase the lipophilicity of the complexes. To increase the lipophilicity of these complexes, the methyl substituent on the NHC unit of the ligand could be modified to either a *tert*-butyl **5.1** or cyclohexyl **5.2** group in a relatively straightforward manner (Figure 5.1). In addition, an extended alkyl linker group could be incorporated into the structure of the pro-ligand to extend the linkage between the $[Re(CO)_3]^+$ core and the amyloid binding moiety **5.3**, thereby increasing the lipophilicity and potentially the amyloid binding properties (Figure 5.1).

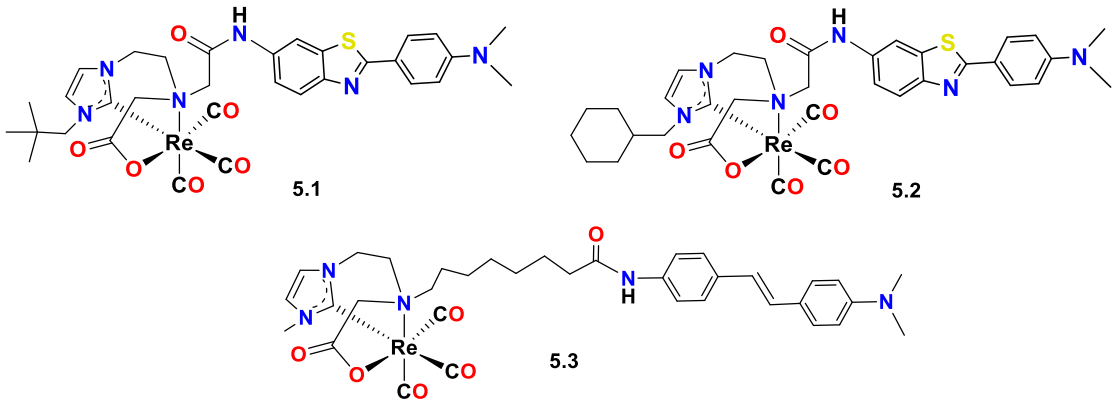

Figure 5.1. Modified structures of Re(I) complexes with tridentate ligands bearing NHC, amine and carboxylate groups with *tert*-butyl **5.1** or cyclohexyl **5.2** substituent on the NHC unit, and the extension of alkyl linkage between the $[Re(CO)_3]^+$ core and stilbene group **5.3**.

The second part of this thesis focused on the development of new anticancer Re(I) complexes of *N*-heterocyclic carbene ligands. In chapter 3, a series of $[Re(CO)_3LCl]$

complexes were prepared, where L represents a pyridyl-imidazolylidene or *bis*-imidazolylidene ligands. The chloride ligand of these complexes was then exchanged for an *N*-acetyl amino acid by treating either **3.1** and **3.2** with the Ag(I) salts of *N*-acetylated amino acids: glycine, isoleucine and proline. The pyridyl-imidazolylidene and *bis*-imidazolylidene carbenes were chosen as ligands to study the effect of one or two carbene donors on the anticancer properties of these complexes.

Previously, studies have shown that certain Re(I) complexes have anticancer properties with a similar mechanism of action to cisplatin, where the cationic aquation product binds covalently to DNA, eventually leading to apoptotic cell death.[1-2] In the present study, the aquation rates of Re(I) complexes of *N*-heterocyclic carbene ligands have been measured using ^{1}H NMR time-course experiments with the WATERGATE NMR routine. The results of these studies in combination with HRMS studies showed that the *N*-acetyl amino acid ancillary ligands were labile and could be exchanged with water to give the cationic Re(I) aqua complexes. The aquation rate for Re(I) complex of the *bis*-imidazolylidene ligand **3.14** ($k_1 = 4.95 \times 10^{-5}\ s^{-1}$) was somewhat faster compared to Re(I) complexes of the pyridyl-imidazolylidene ligand **3.10** ($k_1 = 2.59 \times 10^{-5}\ s^{-1}$). A plausible explanation for the higher aquation rates for Re(I) complexes of the *bis*-imidazolylidene ligand is due to the *cis* effect caused by the strong σ-donor properties of the *bis*-imidazolylidene ligand (i.e. 2 NHC groups). In addition, the aquation rates for Re(I) complexes of the *bis*-imidazolylidene ligand **3.12-3.14** are similar or slightly faster compared to cisplatin ($k_1 = 3.28 \times 10^{-5}\ s^{-1}$) and the second-generation platinum complex carboplatin[3] ($k_1 = 1.25 \times 10^{-5}\ s^{-1}$).[3] The aquation rate is a critical factor in the mechanism of action for cisplatin, as the inactive form of this compound (two chloride ligands) must be converted to an active form (monoaquated species) in order to provide an attractive interaction with the negatively charged phosphate backbone of DNA.[4] The similarity in the aquation rates for Re(I) complexes of the *bis*-imidazolylidene ligands and cisplatin is

a promising result, and further studies are required to determine if these complexes have potential anticancer activity.

In order to gain further insights into the structures and properties of Re(I) complexes with *N*-acetyl amino acid ligands, density functional theory (DFT) calculations on these compounds were performed. The bond dissociation energy (BDE) and the bond length for Re(I) to *N*-acetyl amino acid ligand were calculated, and the results supported the aquation rates measured for the Re(I) complexes. For example, the Re(I) complex of *bis*-imidazolylidene ligand **3.13** has a slightly longer Re-O bond length (2.173 Å) compared to the Re(I) complex of pyridyl-imidazolylidene ligand **3.9** (2.163 Å), suggesting that the *cis* effect exerted by *bis*-imidazolylidene ligand has lengthened this bond length compared to the monocarbene ligand. A longer, weaker bond results in faster substitution of *N*-acetyl amino acid for a water molecule. In addition, the gas phase BDE for both Re(I)-OH_2 bond for the pyridyl-imidazolylidene (67.4 kJ mol^{-1}) and *bis*-imidazolylidene (62.8 kJ mol^{-1} and 53.6 kJ mol^{-1}) ligands indicated that the aqua complex of the *bis*-imidazolylidene ligand would be more reactive than that of the pyridyl-imidazolylidene ligand.

The cytotoxic properties of selected Re(I)-NHC complexes were studied in the cancer cell lines MDA-MB-231, PC3 and HEPG2. The results from these studies showed that complex **3.14** was the most potent compound, especially against PC3 cells (7.05 ± 1.1 μM). The cytotoxicity properties of these Re(I) complexes were also evaluated in the noncancerous adult human dermal fibroblast primary cell line AHDF. Unfortunately, this study did not show strong evidence for selective cytotoxicity towards the cancer cell lines. However, these results are consistent with those reported previously for a related series of Re(I) complexes of NHC ligands. For example, the IC_{50} values for complexes **1.70** and **1.71** with a bromide ancillary ligand in the pancreatic cancer cell line ASPC1 were active

in the range of 4-10 μM.[5] Overall, the results in Chapter 3 have shown that Re(I)-NHC with labile carboxylate ligands have anticancer properties and this approach offers a potential new direction for the development of non-platinum transition metal anticancer agents.

A possible new approach in the development of anticancer Re(I)-NHC complexes of *N*-acetyl amino acids could be incorporating a component that selectively targets specific cancers. Numerous platinum-based anticancer agents have been coupled with peptides or organic molecular fragments that can target specific cancers.[6-7] For example, folic acid receptor (FR) glycoproteins are known to be overexpressed in numerous cancers.[6] Thus, the introduction of folate moiety into Re(I) *bis*-imidazolylidene complex **5.4** could target cancer that overexpresses folic acid receptors (Figure 5.2).

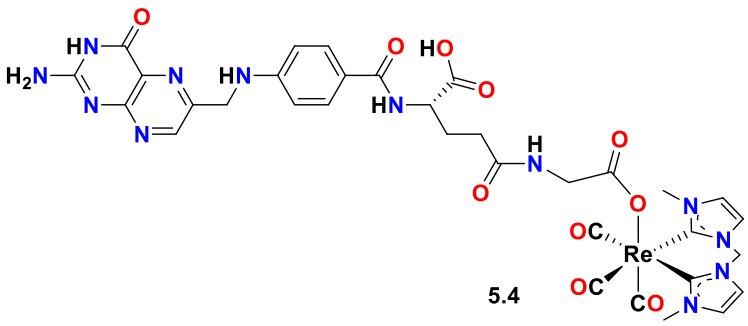

Figure 5.2. Re(I) complex incorporated a folate moiety **5.4** for future studies.

The emergence of cisplatin-resistant cancers has led to much research being devoted to investigating molecules with alternative mechanisms of action to this important anticancer drug. Dinuclear Pt(II) complexes have shown significant promise due to the distinct DNA binding profiles of these compounds.[8] In chapter 4 of this thesis, the preparation and evaluation of a series of dinuclear Re(I) complexes were described. The complexes were prepared with either alkyl or diamide linkage between the bidentate metal-binding groups.

As these dinuclear Re(I) complexes were prepared as potential anticancer agents, it was important to determine the aquation rates of these complexes to provide insights into their potential pharmacological properties. The dinuclear Re(I) complexes of the alkyl linker group (**4.30** and **4.31**) have two labile chloride ligands, and the aquation rates were investigated by ^{1}H NMR time-course experiments. The results from these studies indicated that the aquation rate for the dinuclear Re(I) complex of the *bis*-imidazolylidene ligand **4.31** (k_1 = 1.57 × 10^{-4} s^{-1}) was significantly faster compared to the corresponding Re(I) complex of the pyridyl-imidazolylidene ligand **4.30** (k_1 = 6.60 × 10^{-5} s^{-1}). These results showed that the chloride ligands of complex **4.31** exchanged with water molecules faster than **4.30**, which is likely to be due to the *cis* effect resulting from the strong σ electron-donating properties of the *bis*-imidazolylidene ligand.

These kinetic studies also showed that aquation rates for mononuclear Re(I) complexes with carboxylate leaving group (reported in Chapter 3) had slower aquation rates than the chloride ligand of the dinuclear Re(I) complexes prepared in Chapter 4. For example, the mononuclear Re(I) of the *bis*-imidazolylidene ligand (**3.14**) had a rate constant of k_1 = 4.95 × 10^{-5} s^{-1}, which is significantly slower compared to the aquation rate of dinuclear Re(I) complexes of the same ligand (**4.31**) (k_1 = 1.57 × 10^{-4} s^{-1}). In future work, the aquation rate of Re(I) *bis*-imidazolylidene ligand **4.31** may be tuned by replacing the chloride ligands with *N*-acetyl glycine **5.5** (Figure 5.3). Alternatively, a different NHC ligand, for example, the benzimidazylidene ligand of complex **5.6** (Figure 5.3), could be used to investigate the *cis* effect of different NHC ligands on the aquation rate. Finally, the lipophilic property of this complex could be tuned by adding a PEG-based linker group (**5.6**, Figure 5.3). Moreover, cytotoxicity studies are required to gain further understanding of the anticancer properties of these dinuclear Re(I) complexes.

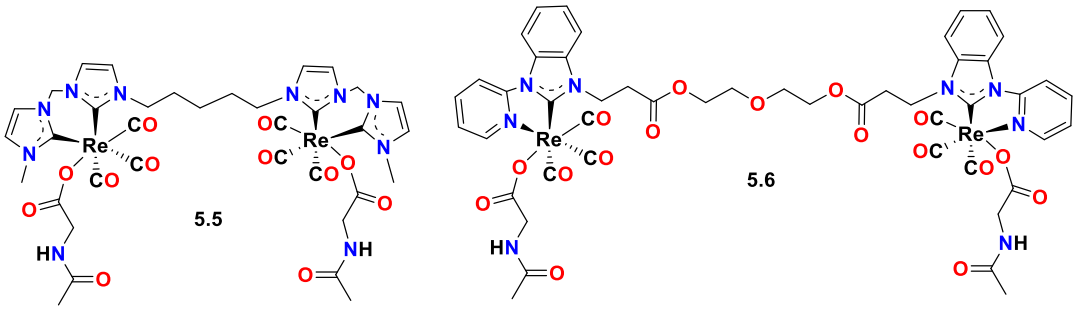

Figure 5.3. Dinuclear Re(I) complex with a labile *N*-acetyl glycine ligand **5.5** and **5.6**.

Due to the overexpression of the glucose transporter (GLUT) by many cancers, targeting GLUTs can provide a means of directing anticancer agents to tumours. The second part of Chapter 4 described the preparation of a series of pro-ligands coupled to benzyl protected glucosamine, or acetyl protected glucose groups. The benzyl protected glucosamine pro-ligand was used to synthesise Re(I)-NHC complex **4.47** via a silver(I) transmetalation reaction. Unfortunately, the benzyl protecting groups could not be removed using hydrogenolysis once the Re(I) complex was formed. Therefore, the Re(I) complex **4.54** was prepared with alternative acetyl protected glucose coupled to the NHC ligand. Again, the protecting groups could not be removed using common deacetylation reagents (e.g. Cs_2CO_3, K_2CO_3 and Et_3N). Interestingly, a one-pot Re(I)-NHC complex synthesis and deacetylation method using several equivalents of silver(I) oxide was discovered. However, in this reaction, ^{1}H NMR and mass spectrometry analysis suggested that the pyridyl-imidazolylidene moiety was cleaved from the C1 position of glucose, resulting in the formation of the unwanted complex **4.59**. To overcome this problem, a PEG derivative ligand was prepared, and this successfully yielded the desired Re(I) sugar complex **4.63**. Both the NMR and HRMS analysis confirmed the formation of complex **4.63**. These results showed that the incorporation of PEG linkage in the structure of the Re(I) complex had prevented the cleavage of the glucose moiety at the C1 position of the sugar. However, further biological studies are required to gain further knowledge of the anticancer properties of this glucose Re(I) complex.

5.2. References

1. Zobi, F.; Spingler, B.; Fox, T.; Alberto, R., *Inorg. Chem.* **2003,** *42* (9), 2818-20.
2. Zobi, F.; Spingler, B.; Alberto, R., *ChemBioChem* **2005,** *6* (8), 1397-405.
3. Hann, S.; Stefanka, Z.; Lenz, K.; Stingeder, G., *Anal. Bioanal. Chem.* **2005,** *381* (2), 405-12.
4. Dasari, S.; Tchounwou, P. B., *Eur. J. Pharmacol.* **2014,** *740*, 364-78.
5. Simpson, P. V.; Casari, I.; Paternoster, S.; Skelton, B. W.; Falasca, M.; Massi, M., *Chem. Eur. J.* **2017,** *23* (27), 6518-6521.
6. Colombo, G.; Curnis, F.; De Mori, G. M.; Gasparri, A.; Longoni, C.; Sacchi, A.; Longhi, R.; Corti, A., *J. Biol. Chem.* **2002,** *277* (49), 47891-7.
7. Wisnovsky, S. P.; Wilson, J. J.; Radford, R. J.; Pereira, M. P.; Chan, M. R.; Laposa, R. R.; Lippard, S. J.; Kelley, S. O., *Chem. Biol.* **2013,** *20* (11), 1323-8.
8. Wang, J.; Li, X.; Yuan, C.; Su, F.; Wu, Y. B.; Lu, L.; Zhu, M.; Xing, S.; Fu, X., *Dalton Trans.* **2021,** *50* (13), 4527-4538.

Appendix 1 : General Procedure

1.1. General Procedure

All reagents were purchased from Sigma Aldrich or Alfa Aesar and were used without further purification unless otherwise stated. NMR spectra were recorded on either a Bruker Avance ARX-400 (400.13 MHz for ^{1}H, 100.61 MHz for ^{13}C), or a Bruker Avance ARX-500 (500.13 MHz for ^{1}H, 125.77 MHz for ^{13}C) spectrometer and were internally referenced to solvent resonances. High resolution mass spectra were obtained using an Agilent 6530 QTOF LC/MS mass spectrometer fitted with an Agilent electrospray ion (ESI) source. The experiments were performed with spray solvent methanol or water (after WATERGATE studies) at a flow rate of 5 µL/min and the capillary voltage was set at 40 kV. UV-visible spectra were recorded using an Agilent Technologies Cary 300 UV-visible spectrophotometer using quartz cuvettes (1 cm). Fluorescence spectra were recorded on a Varian Cary Eclipse spectrofluorimeter (5 nm bandpass, 1 nm data interval, PMT voltage: 600 V) using quartz cuvettes (1 cm). Infra-red spectra were recorded using an Agilent Cary 660 FT-IR spectrophotometer in ATR mode.

Appendix 2 : For Chapter 2

2.1. NMR Spectra

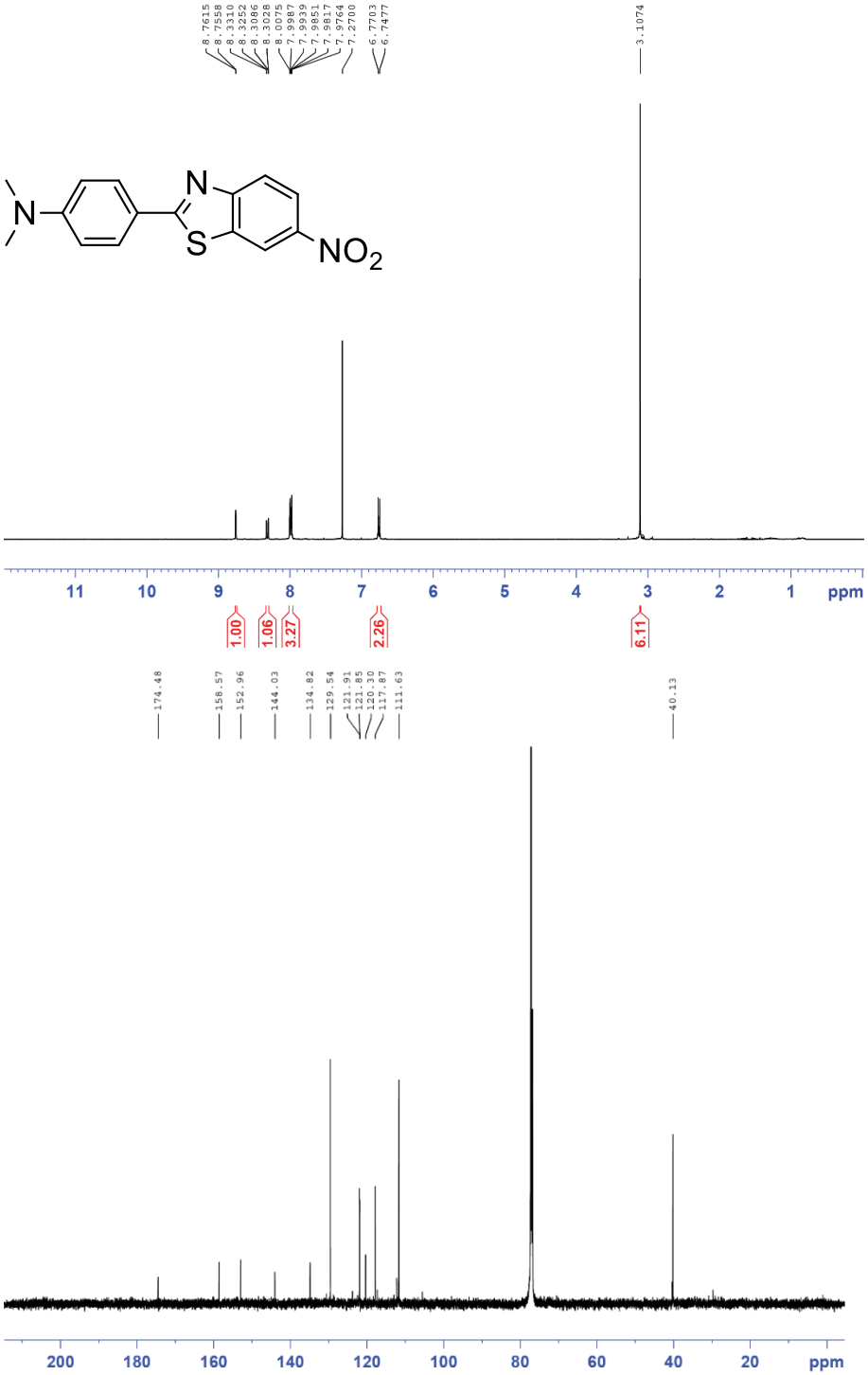

Figure A2.1. ^{1}H and ^{13}C NMR spectra for 6-nitro-2-(4-N,N-dimethylaminophenyl)benzothiazole.

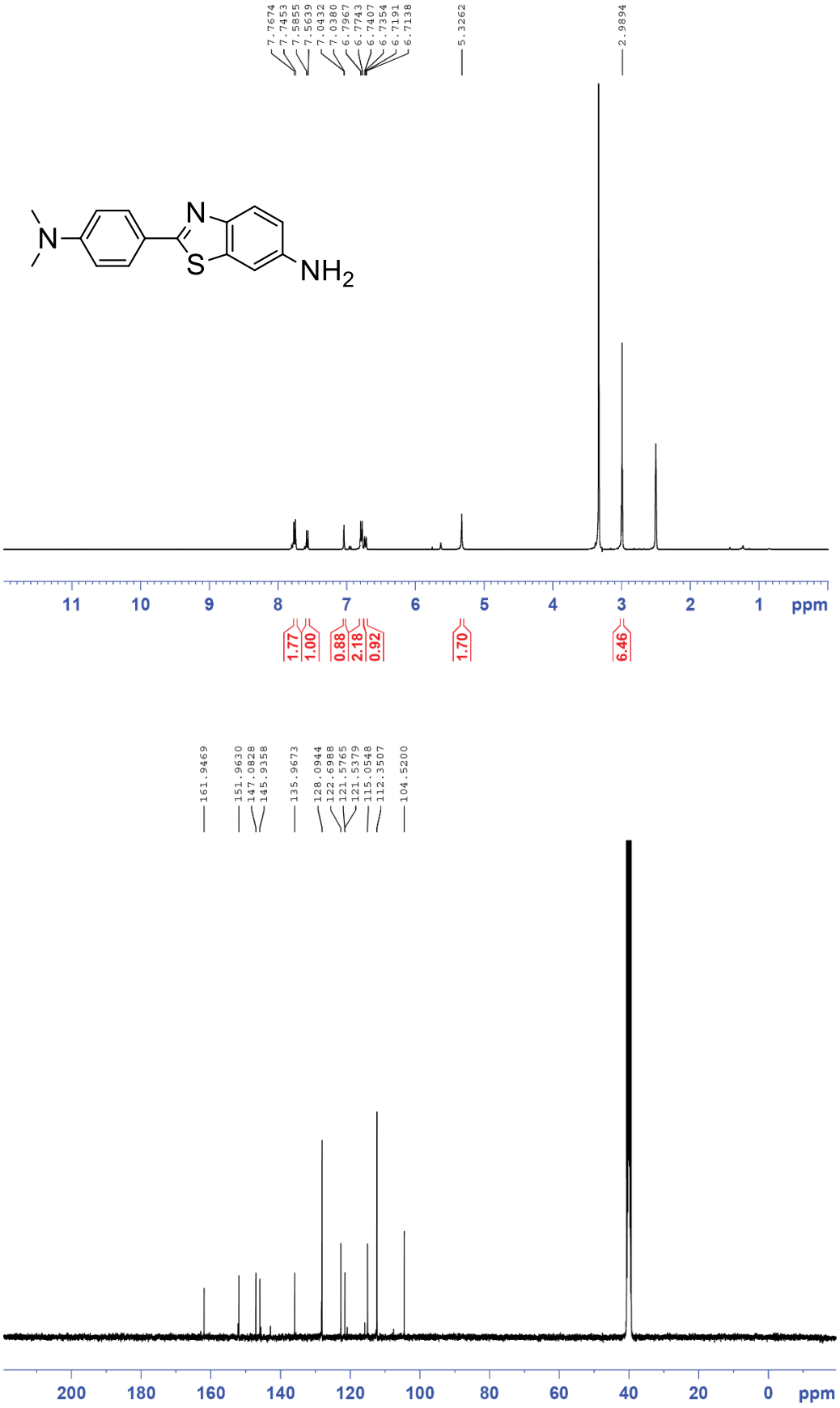

Figure A2.2. ^{1}H and ^{13}C NMR spectra for 6-amino-2-(4-N,N-dimethylaminophenyl)benzothiazole.

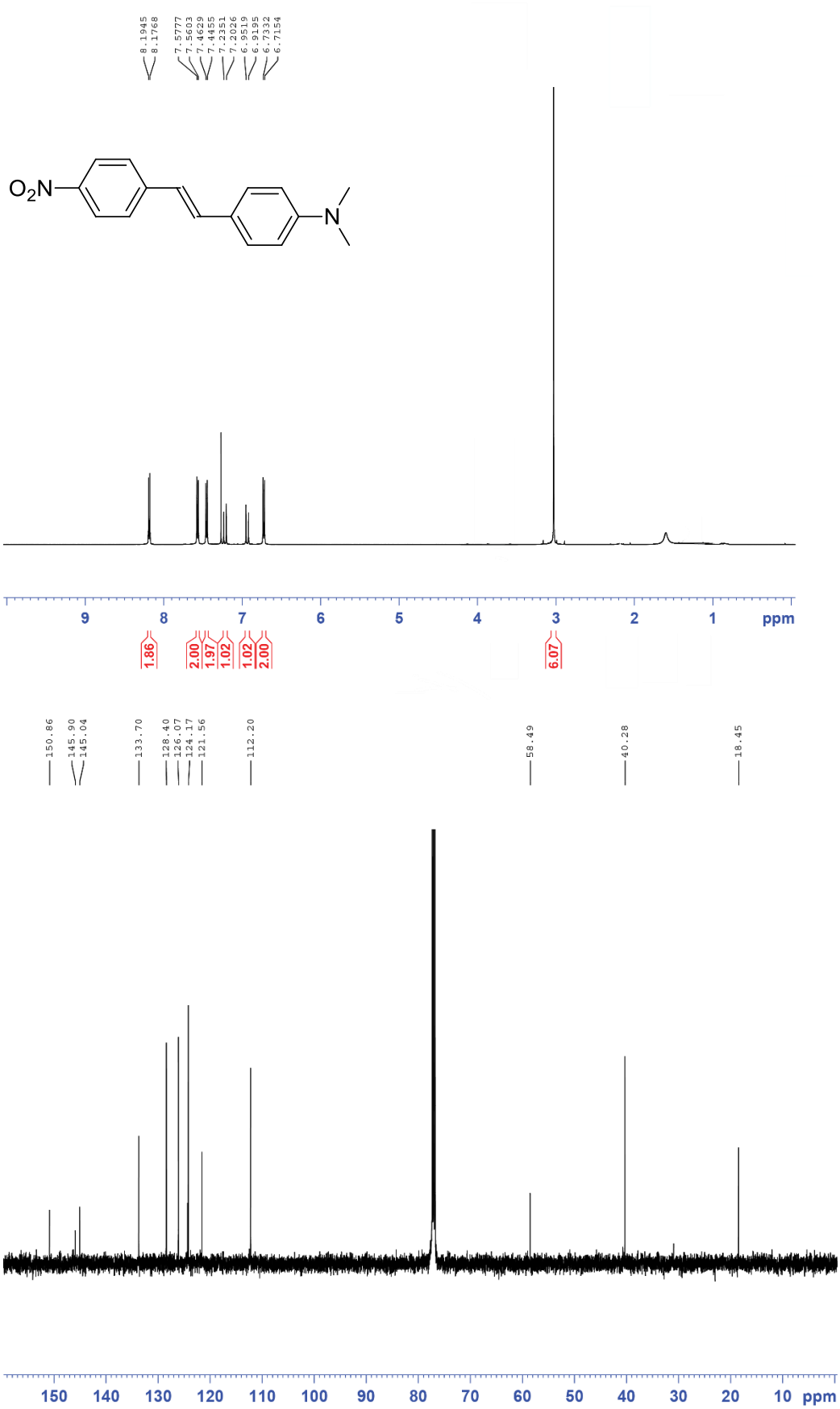

Figure A2.3. ^{1}H and ^{13}C NMR spectra for p-nitro-p'-N,N-dimethylaminostilbene.

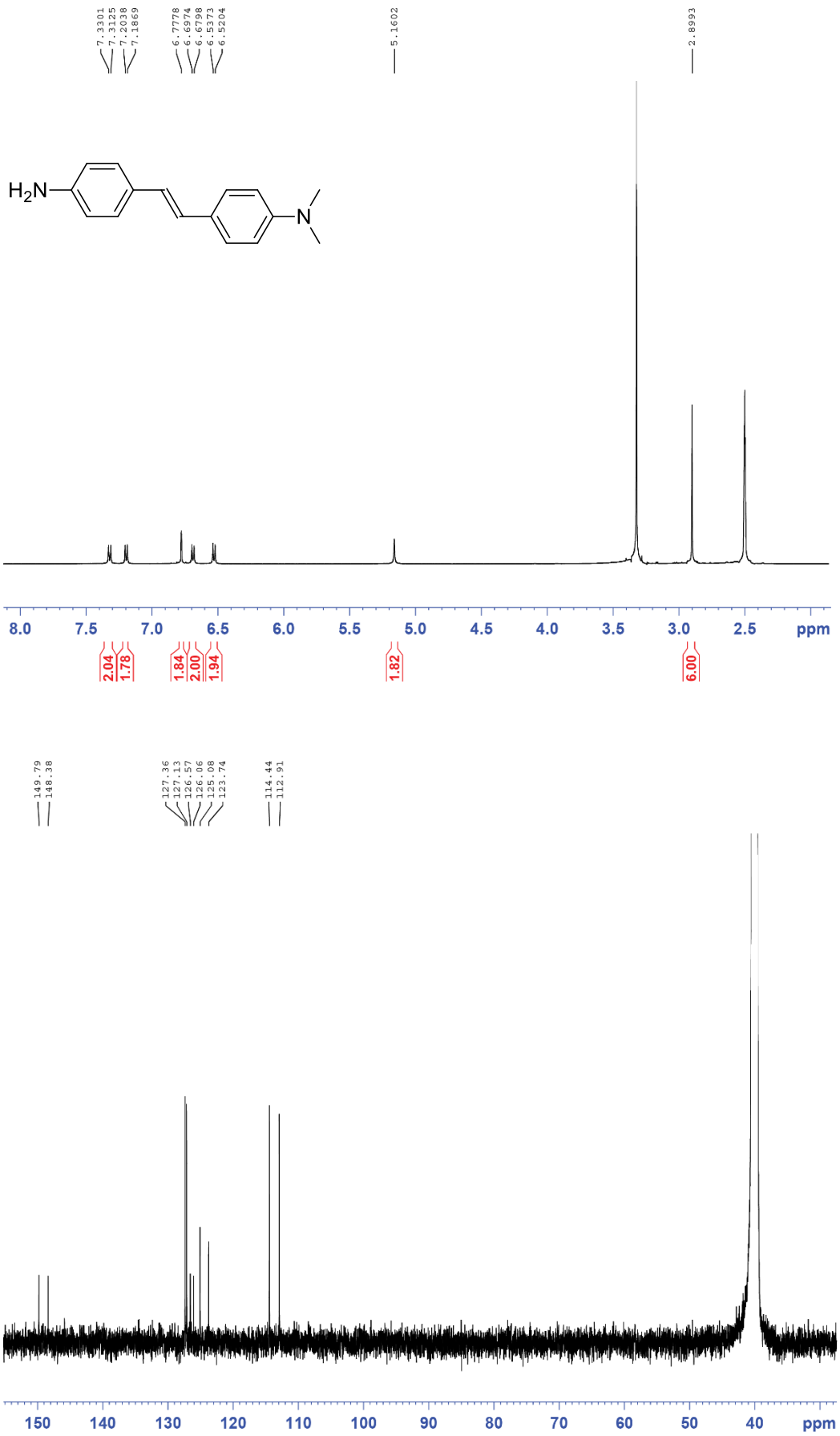

Figure A2.4. ^{1}H and ^{13}C NMR spectra for p-amino-p'N,N-dimethylaminostilbene.

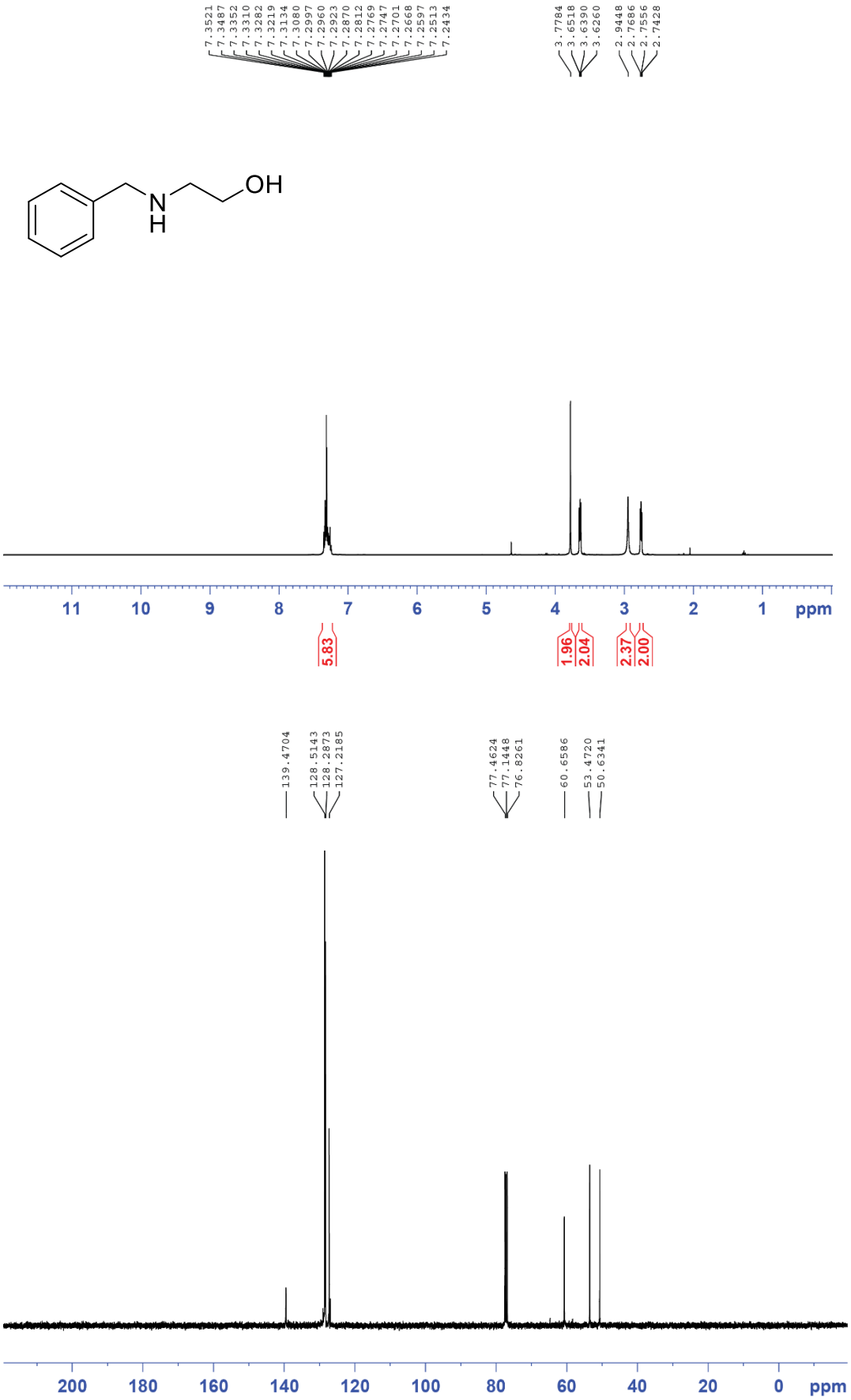

Figure A2.5. ^{1}H and ^{13}C NMR spectra for compound **2.5**.

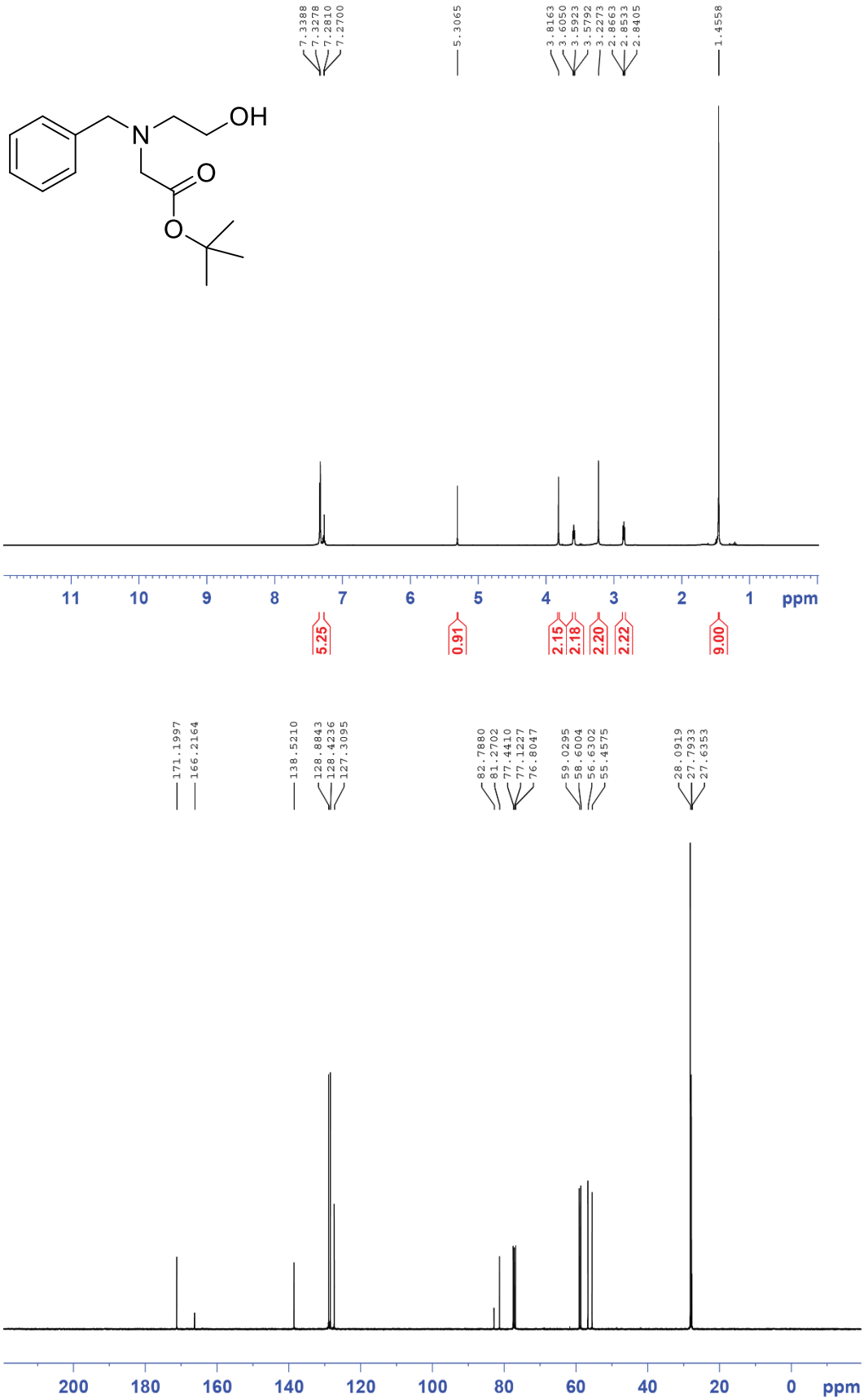

Figure A2.6. ^{1}H and ^{13}C NMR spectra for compound **2.6**.

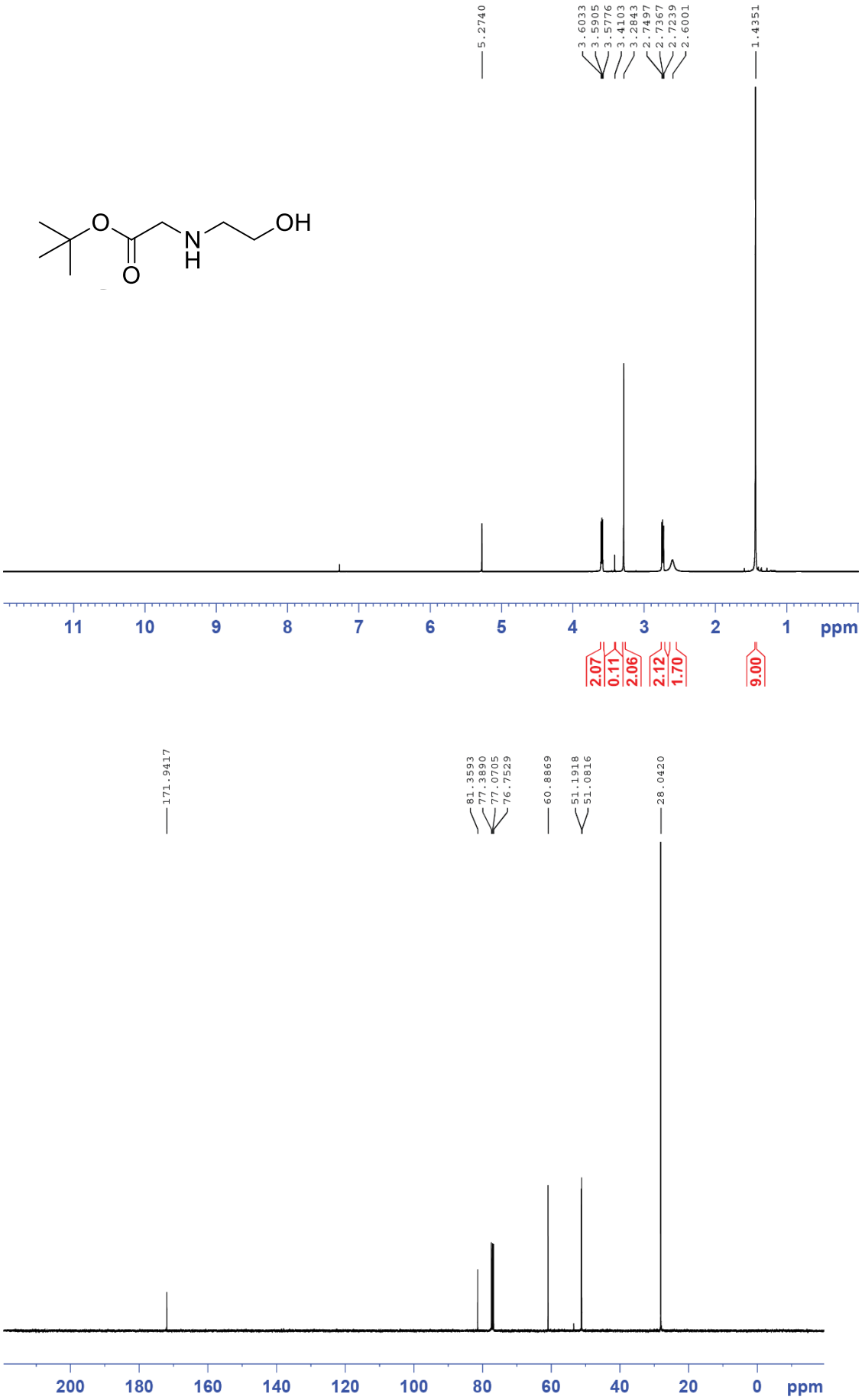

Figure A2.7. ^{1}H and ^{13}C NMR spectra for compound **2.7**.

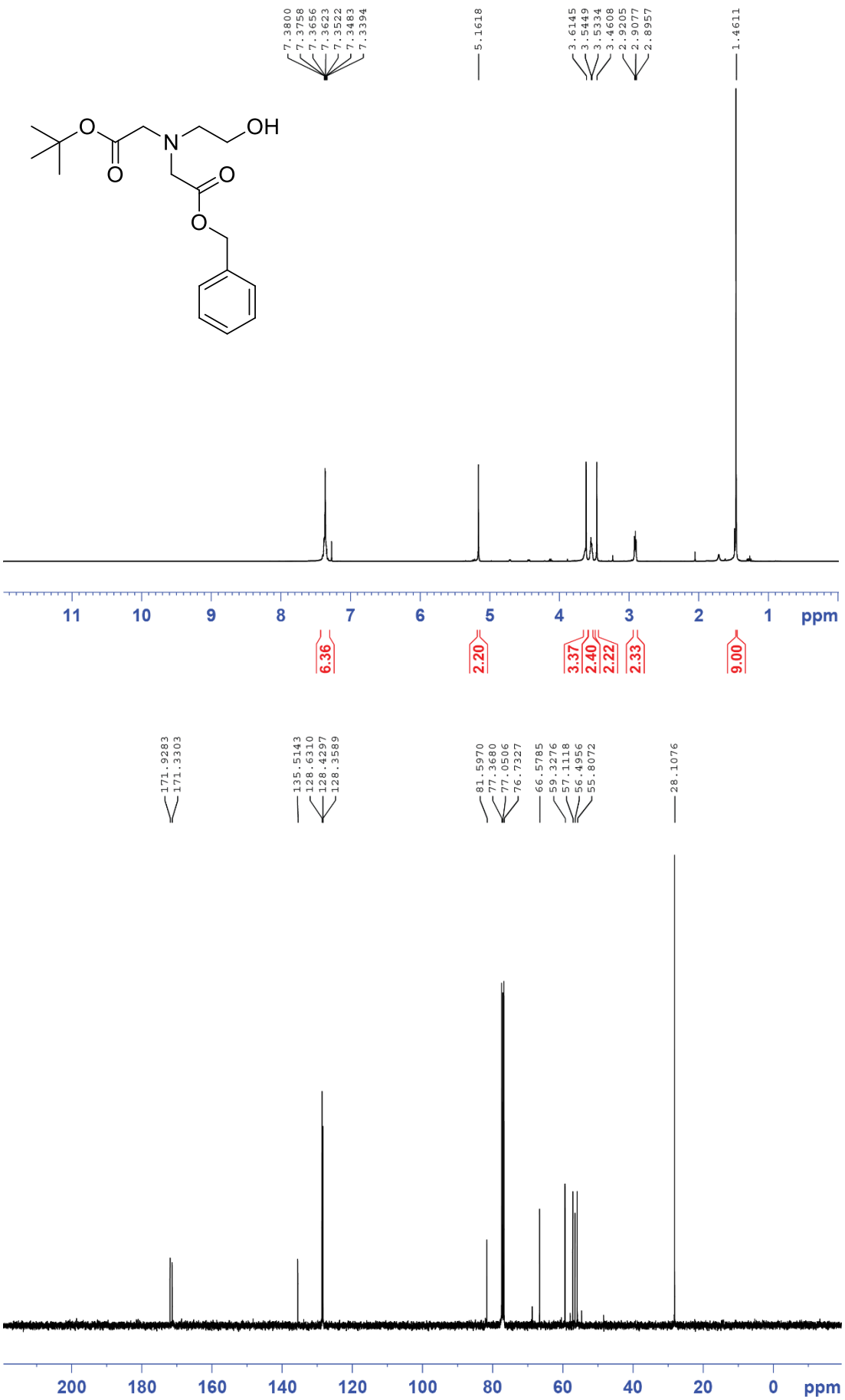

Figure A2.8. ^{1}H and ^{13}C NMR spectra for compound **2.8**.

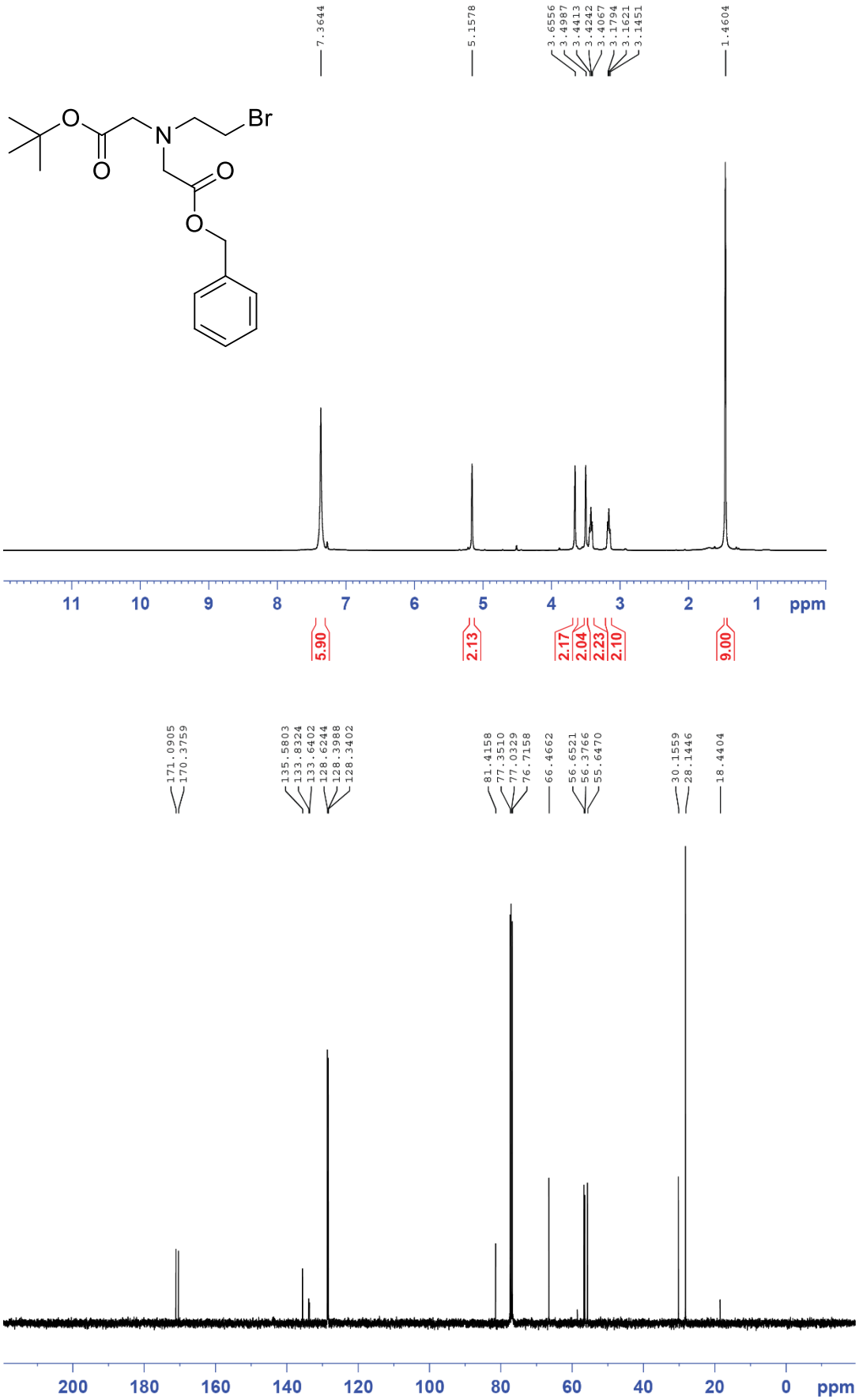

Figure A2.9. ^{1}H and ^{13}C NMR spectra for compound **2.9**.

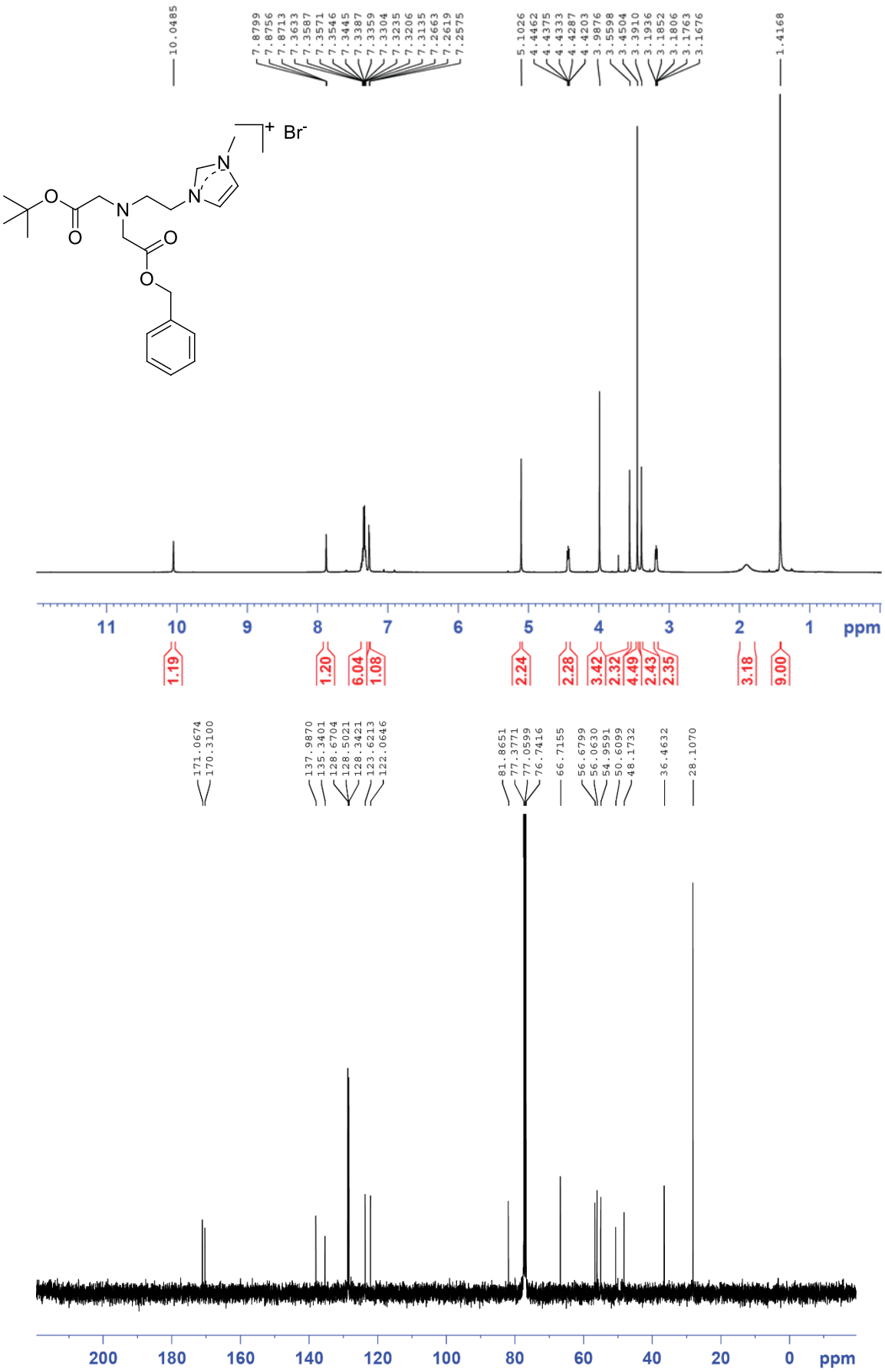

Figure A2.10. ^{1}H and ^{13}C NMR spectra for compound **2.10**

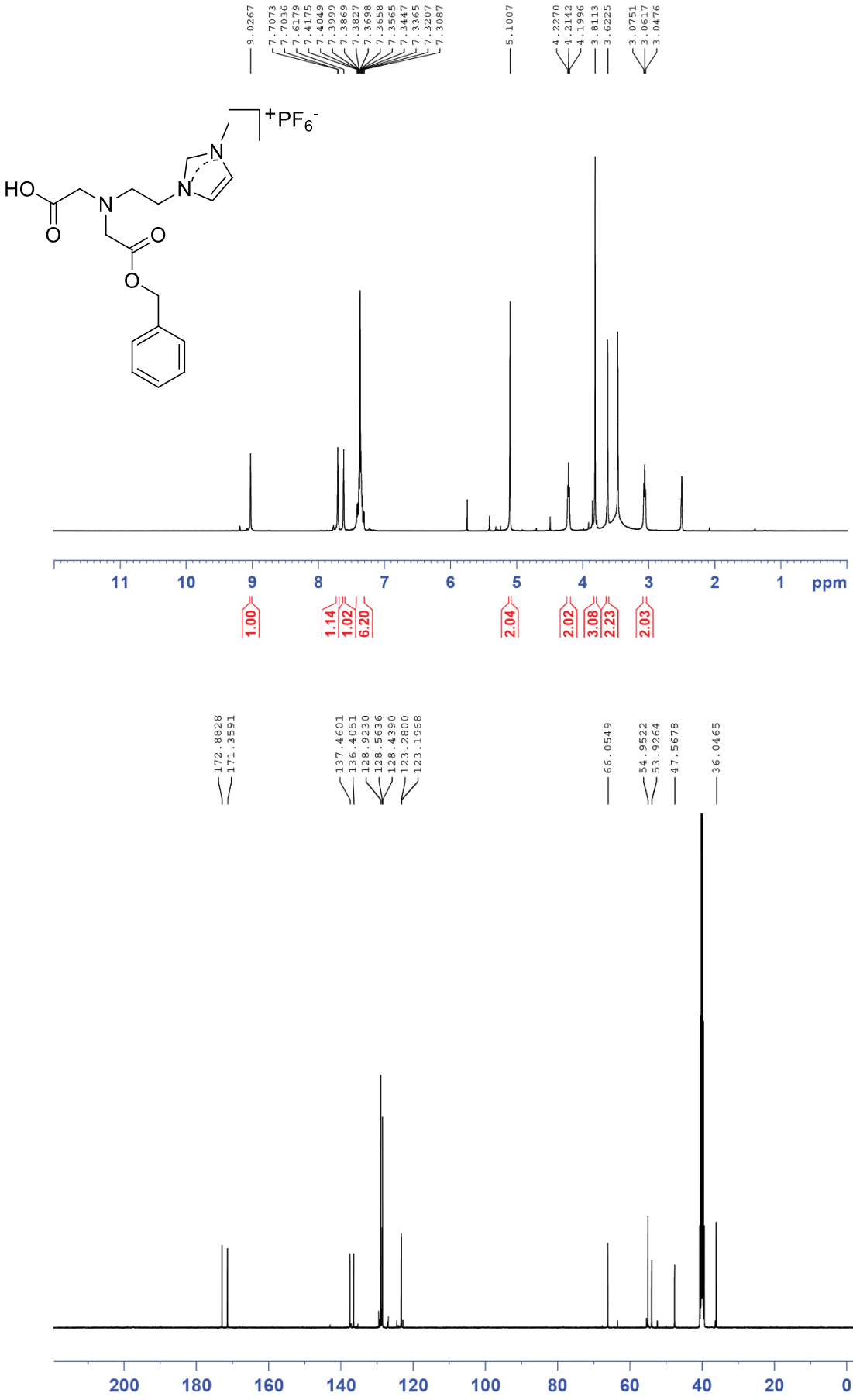

Figure A2.11. ^{1}H and ^{13}C NMR spectra for compound **2.11**.

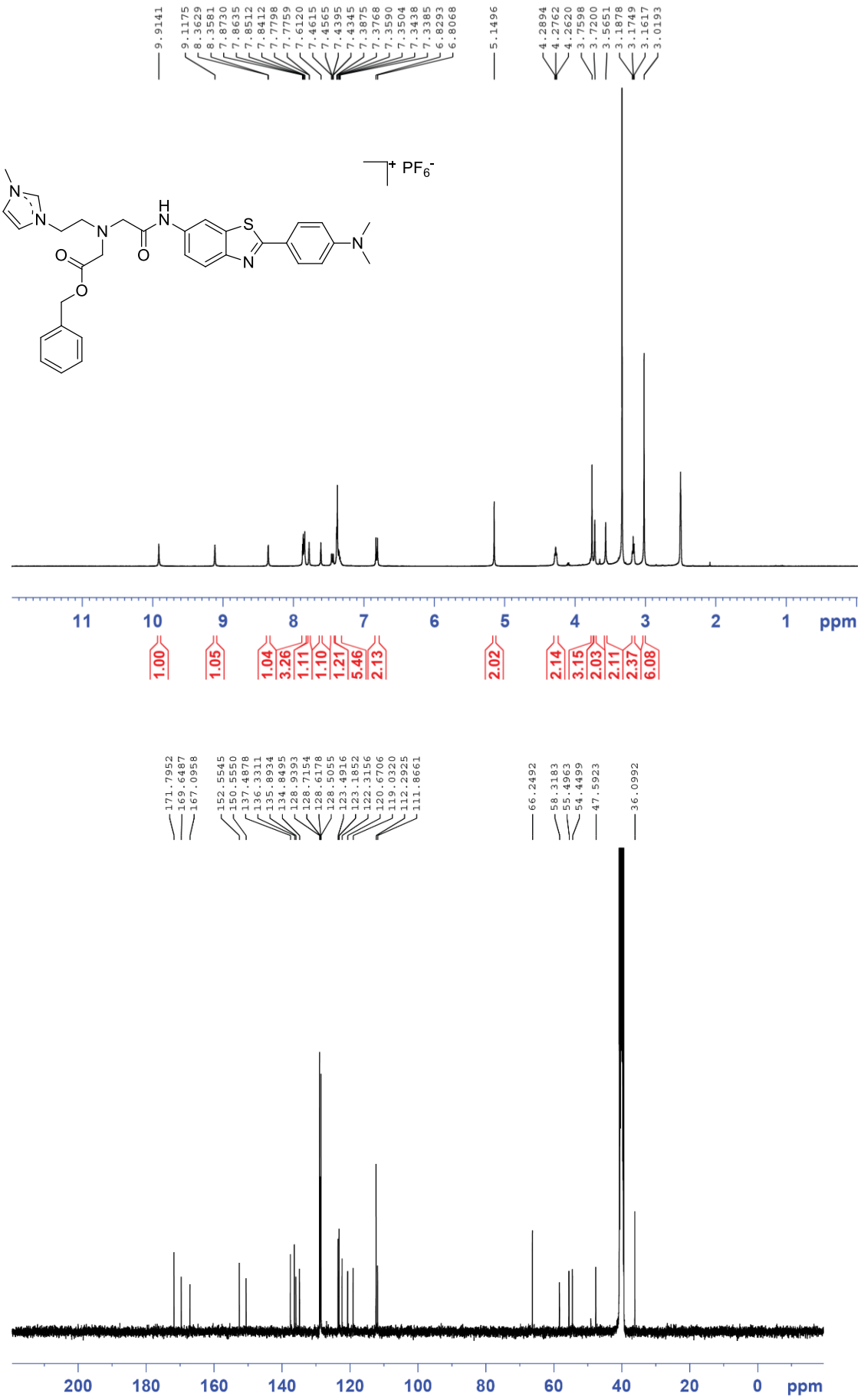

Figure A2.12. ^{1}H and ^{13}C NMR spectra for compound **2.12**.

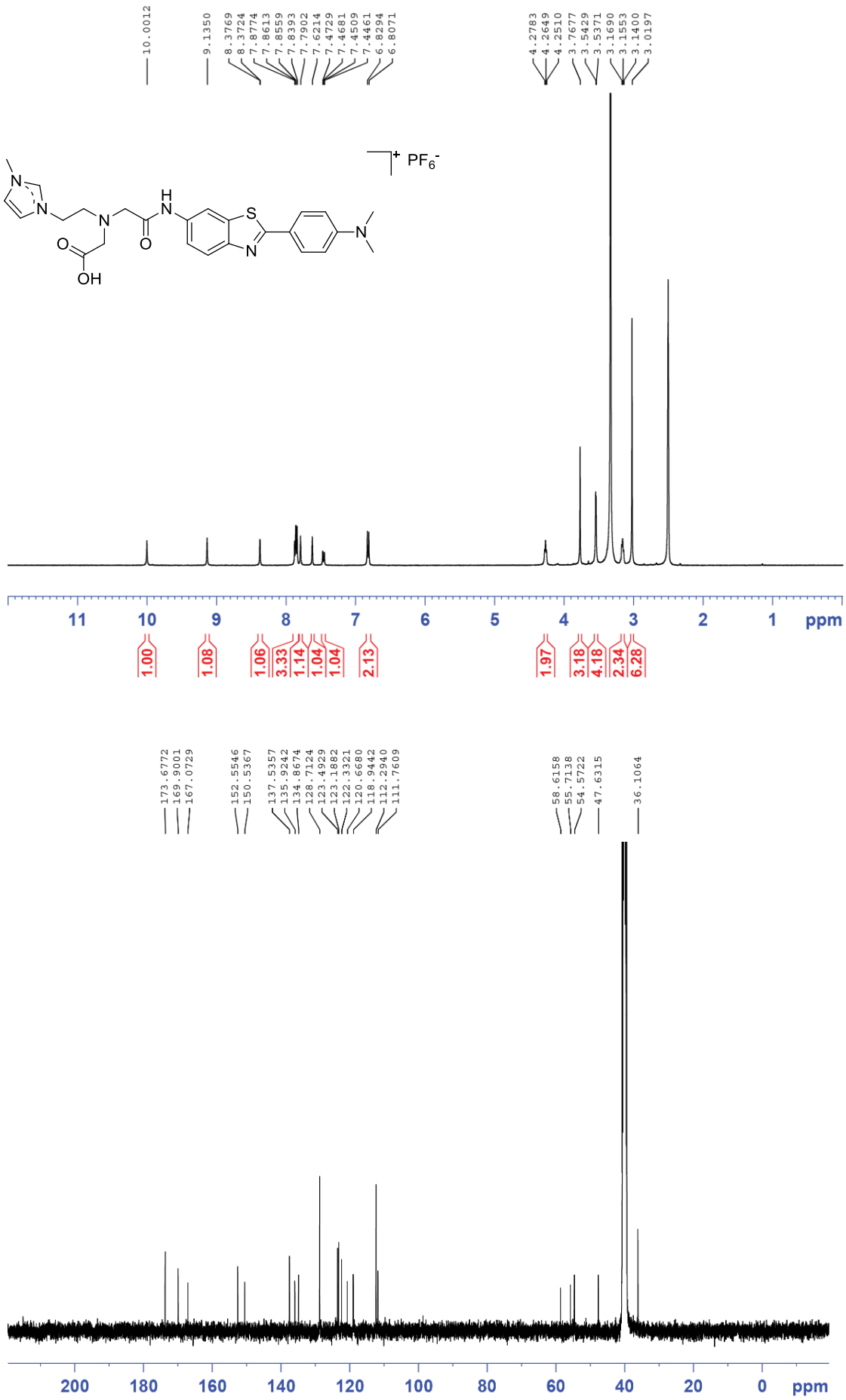

Figure A2.13. ^{1}H and ^{13}C NMR spectra for compound **2.13**.

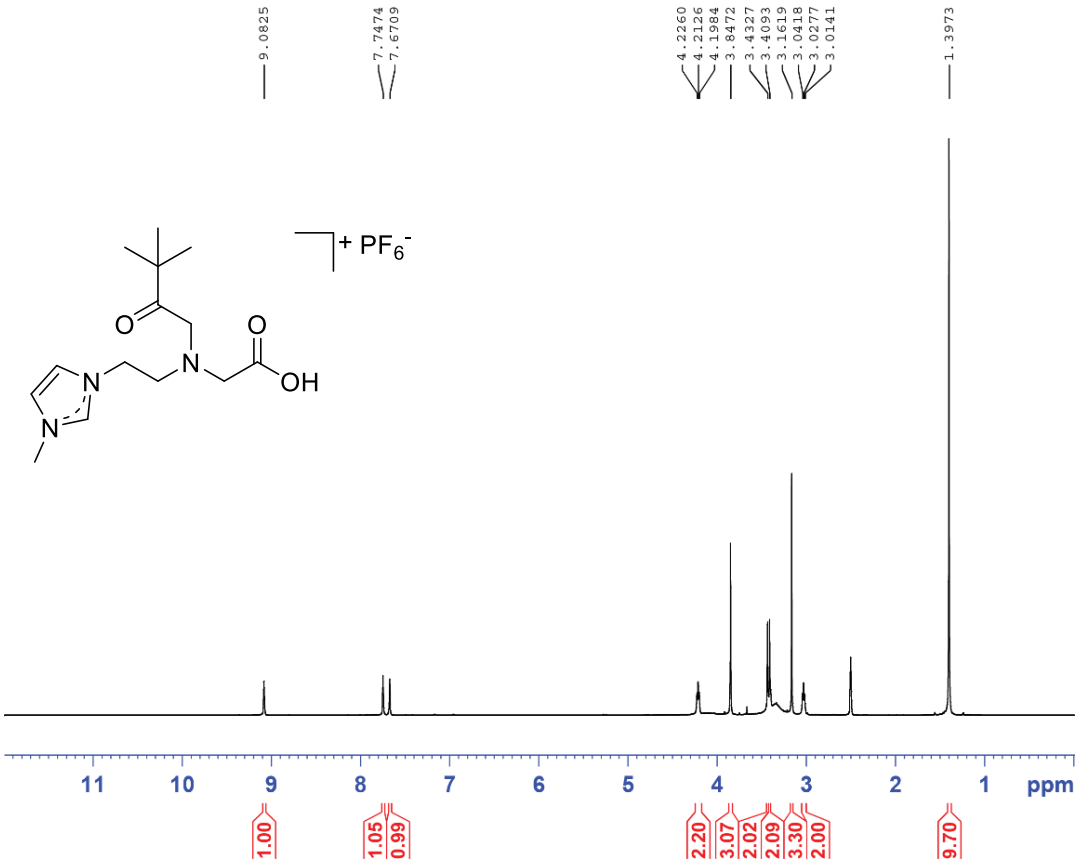

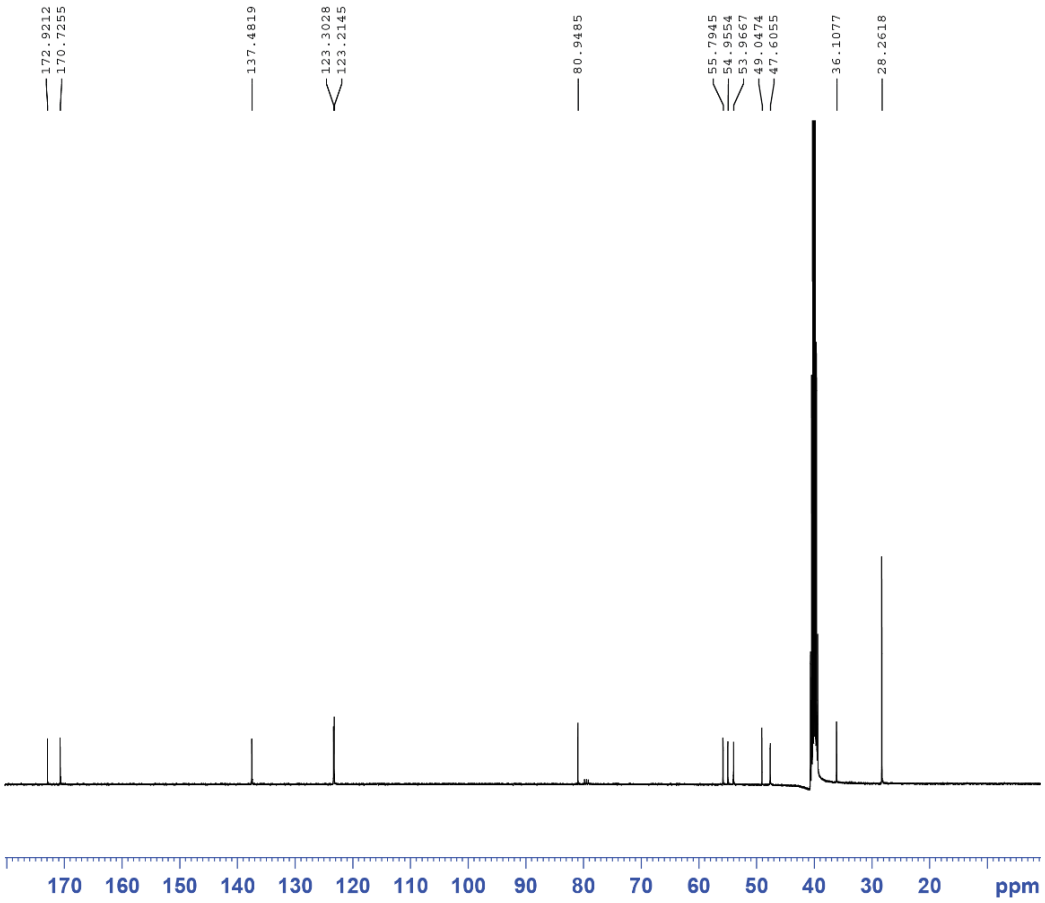

Figure A2.14. ^{1}H and ^{13}C NMR spectra for compound **2.14**.

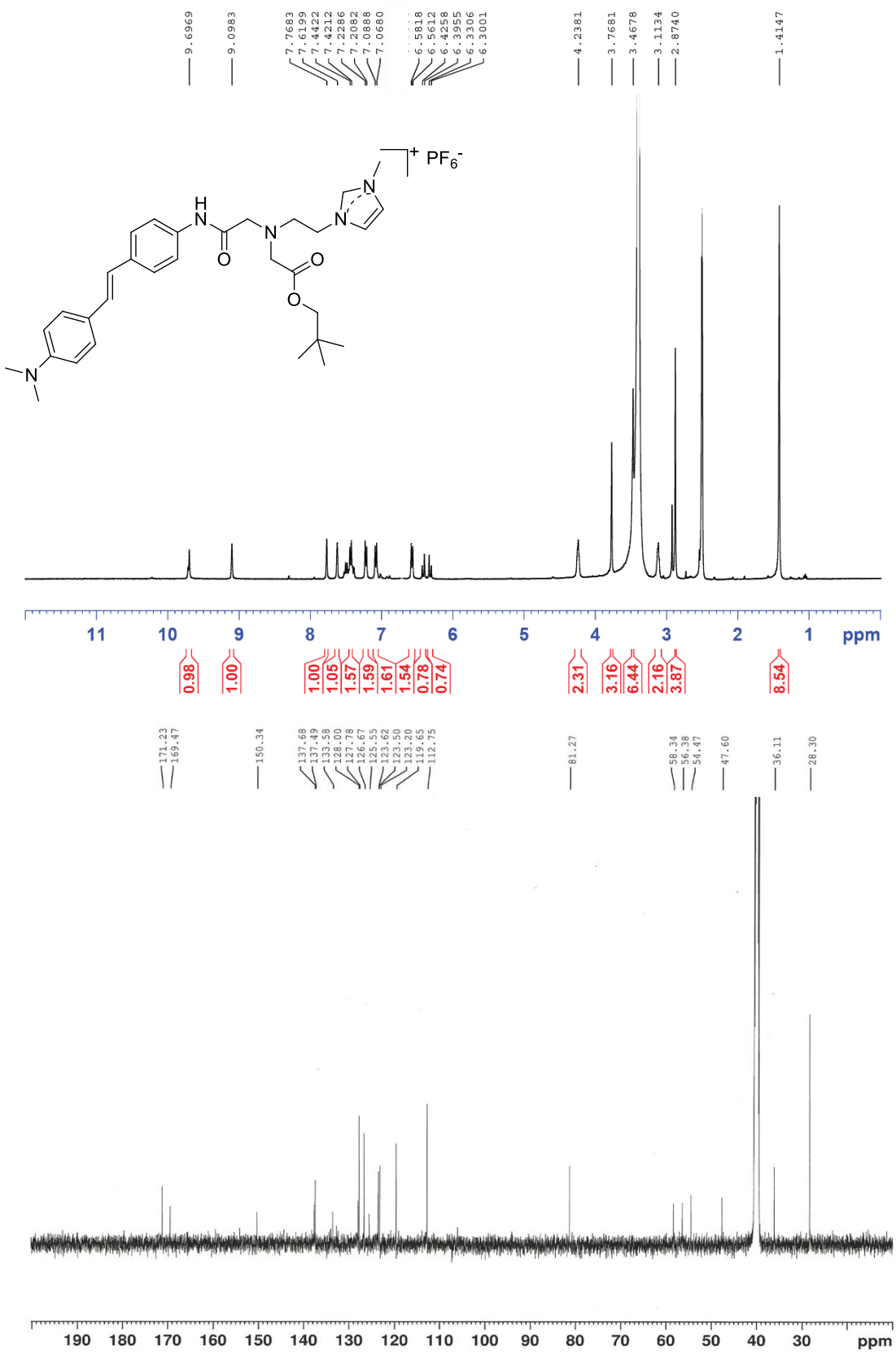

Figure A2.15. ^{1}H and ^{13}C NMR spectra for compound **2.15**.

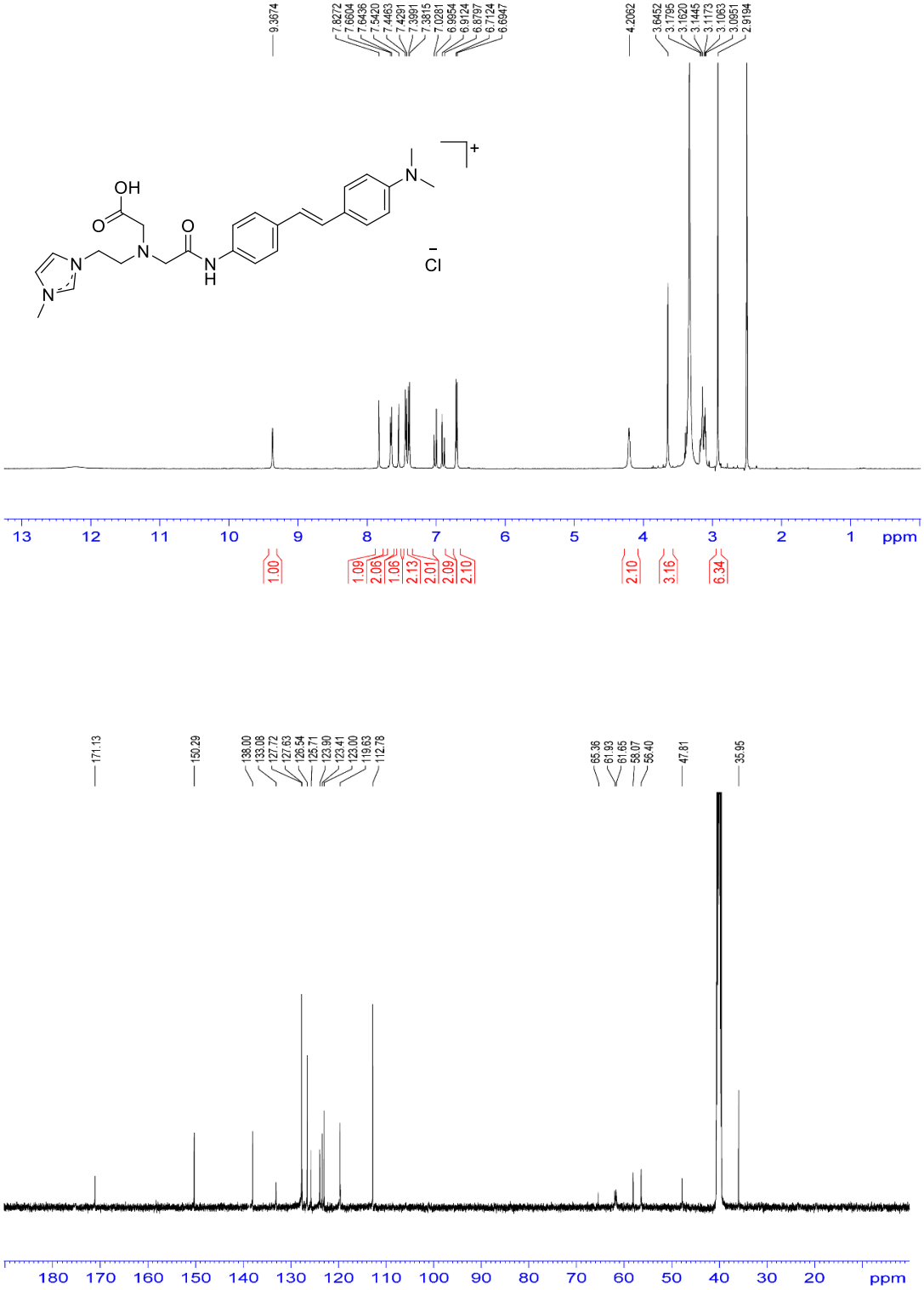

Figure A2.16. ^{1}H and ^{13}C NMR spectra for compound **2.16**.

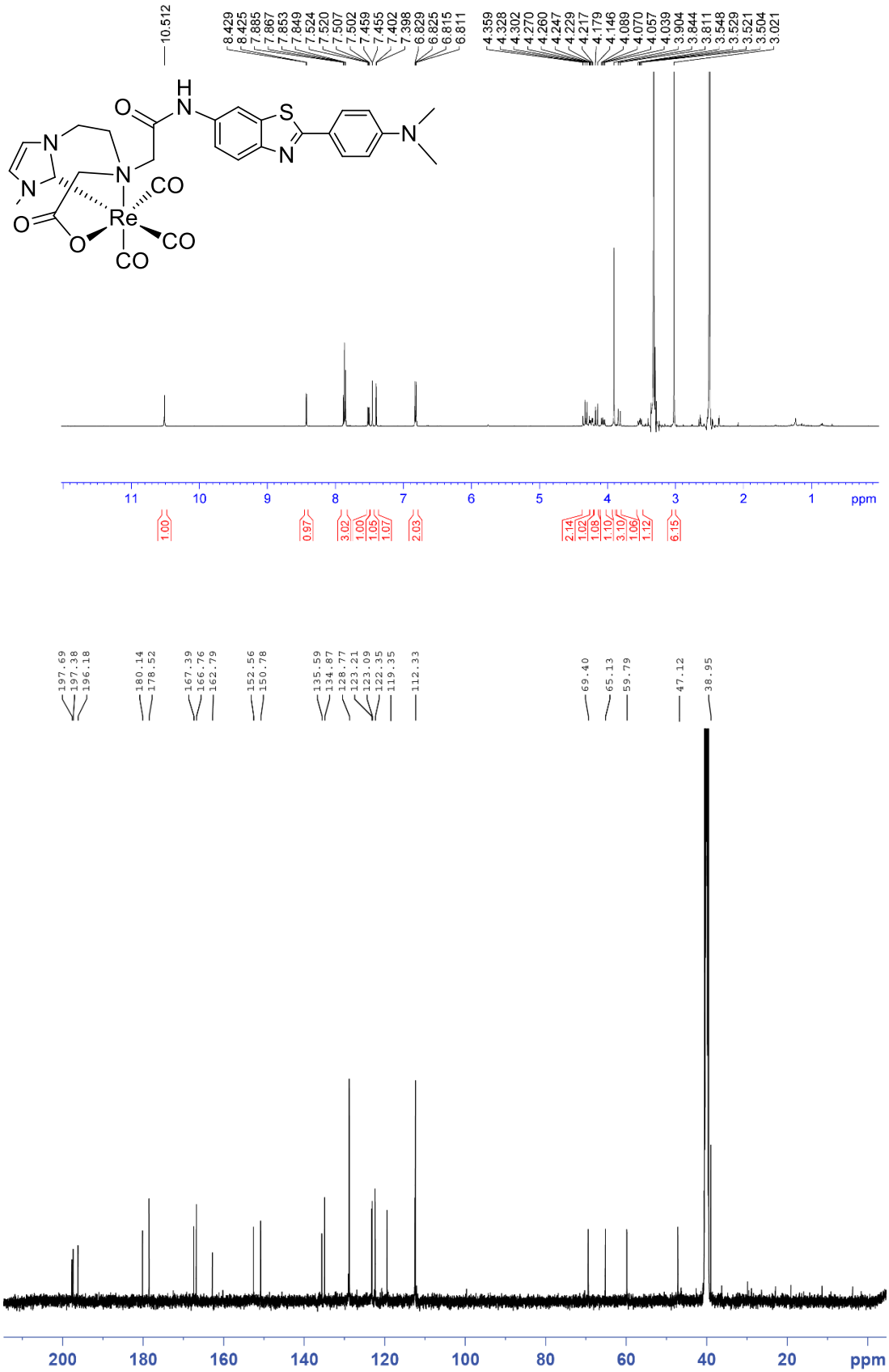

Figure A2.17. ^{1}H and ^{13}C NMR spectra for complex **2.17**.

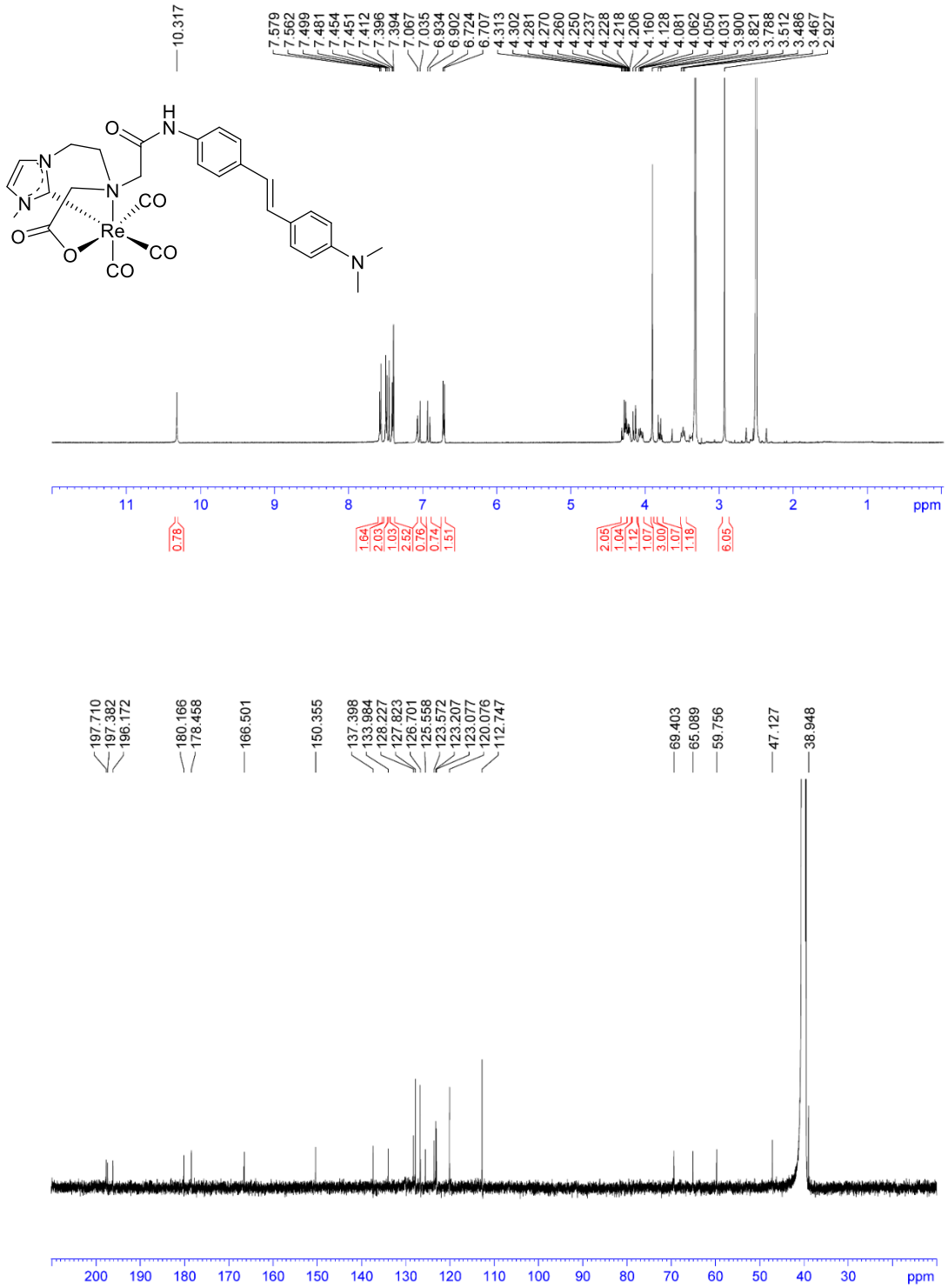

Figure A2.18. ^{1}H and ^{13}C NMR spectra for complex **2.18**.

2.2. FT-IR Spectra

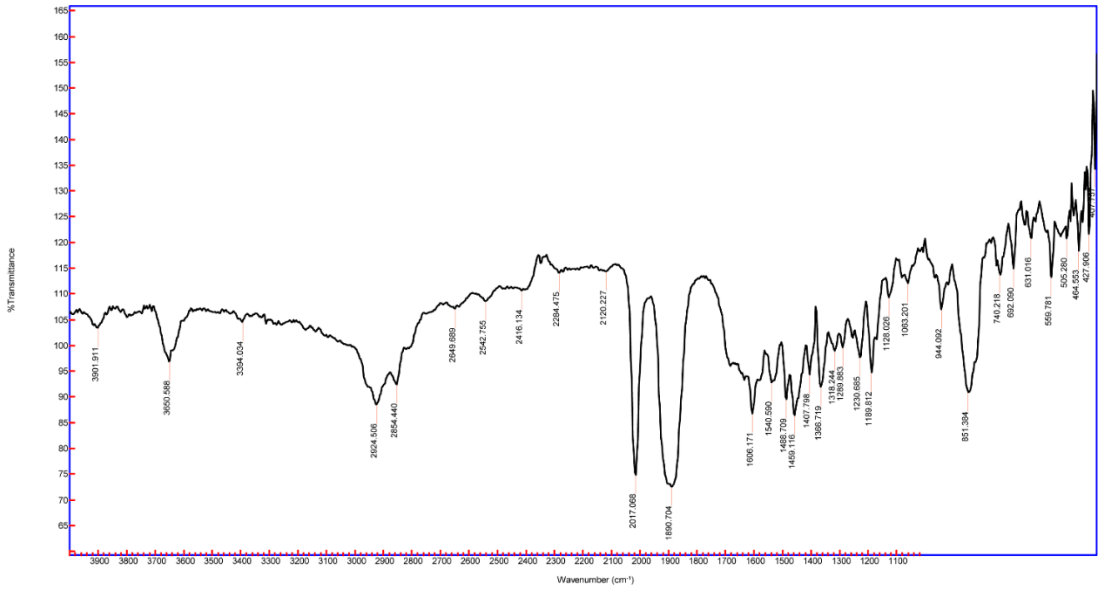

Figure A2.19. FT-IR spectrum for complex **2.17**.

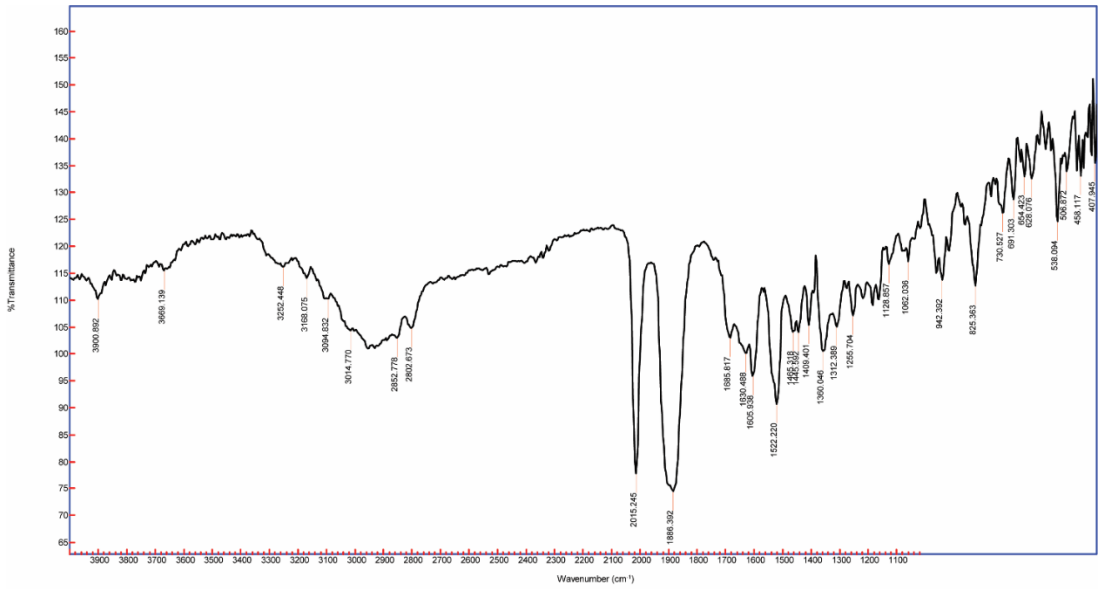

Figure A2.20. FT-IR spectrum for complex **2.18**.

2.3. X-ray Crystallography

Table A2.1. X-ray crystallographic data for compounds **2.17** and **2.18**.

Identification code	**2.17**	**2.18**
Empirical formula	$C_{28}H_{27}N_6O_6ReS$	$C_{30}H_{32}Cl_2N_5O_6Re$
Formula weight	761.81	815.7
Temperature/K	150.00(10)	136(5)
Crystal system	triclinic	monoclinic
Space group	P-1	$P2_1/c$
a/Å	7.20011(12)	15.6976(11)
b/Å	7.20961(14)	11.3209(5)
c/Å	27.7581(7)	19.2779(10)
α/°	91.5713(19)	90
β/°	93.4633(18)	109.671(7)
γ/°	108.3622(16)	90
Volume/Å^3	1363.42(5)	3226.0(3)
Z	2	4
ρ_{calc}g/cm^3	1.856	1.68
μ/mm^{-1}	9.911	9.31
F(000)	752	1616
Crystal size/mm^3	0.04 × 0.03 × 0.03	0.05 × 0.03 × 0.03
Radiation	CuKα (λ = 1.54184)	CuKα (λ = 1.54184)
2Θ range for data collection/°	9.588 to 130.172	9.206 to 149.004
Index ranges	$-8 \leq h \leq 8$, $-8 \leq k \leq 8$, $-32 \leq l \leq 32$	$-19 \leq h \leq 19$, $-14 \leq k \leq 13$, $-23 \leq l \leq 24$
Reflections collected	8184	17006
Independent reflections	8184 [Rsigma = 0.0179]	6591 [R_{int} = 0.0409, R_{sigma} = 0.0472]
Data/restraints/parameters	8184/0/383	6591/0/400
Goodness-of-fit on F^2	1.04	1.049
Final R indexes [I>=2σ (I)]	R1 = 0.0452, wR2 = 0.1233	R_1 = 0.0506, wR_2 = 0.1275
Final R indexes [all data]	R1 = 0.0460, wR2 = 0.1246	R_1 = 0.0630, wR_2 = 0.1394
Largest diff. peak/hole / e Å^{-3}	3.11/-0.83	3.35/-1.42

2.17 Solved in the triclinic space group *P*-1. The structure is twinned, and Crysalis Twin Data Reduction was carried out. Hklf4 and hklf5 files were generated and final refinement on the hklf5 lowered R1 to 4.52%

2.18 Solved in the monoclinic space group $P2_1/c$. The cifcheck report lists 1 level B alert.

(1) PLAT971_ALERT_2_B Check Calcd Resid. Dens. 0.95A From Re01 3.18 eA-3

It is apparent that this residual electron density is associated with the heavy Re metal centre and no attempts were made to model this density.

2.4. Partition Coefficient (LogP) Studies

1-Octanol/water partition coefficients for complexes **2.17** and **2.18** were determined using the slow-stirring method as described by Pereiro and co-workers.[5] The 1-octanol and Mili-Q water were saturated prior their use and the starting concentration of complexes **2.17** and **2.18** in the 1-octanol phase was 80 µM. Approximately 5 mL of the pre-saturated water and 1-octanol were added to a glass vial containing a magnetic stir bar. The vials were slowly stirred and maintained at 25 °C for two days. The metal complex concentration in the 1-octanol phase was then analysed using an Agilent Technologies Cary 300 UV-visible spectrophotometer in a quartz cuvette (1 cm). A calibration curve for each complex was prepared at its λ_{max} value (365 nm for **2.17** and 360 nm for **2.18**).

Complex **2.17**

Table A2.2. Standard samples of **2.17** with its corresponding absorbance.

Concentration (μM)	Absorbance
1	0.046748
2	0.070164
5	0.227143
10	0.419519
20	1.040334
50	2.499851

Max wavelength = 365 nm

Extinction coefficient = 0.0507 μmol^{-1} L cm^{-1}= 50700 mol^{-1} L cm^{-1}

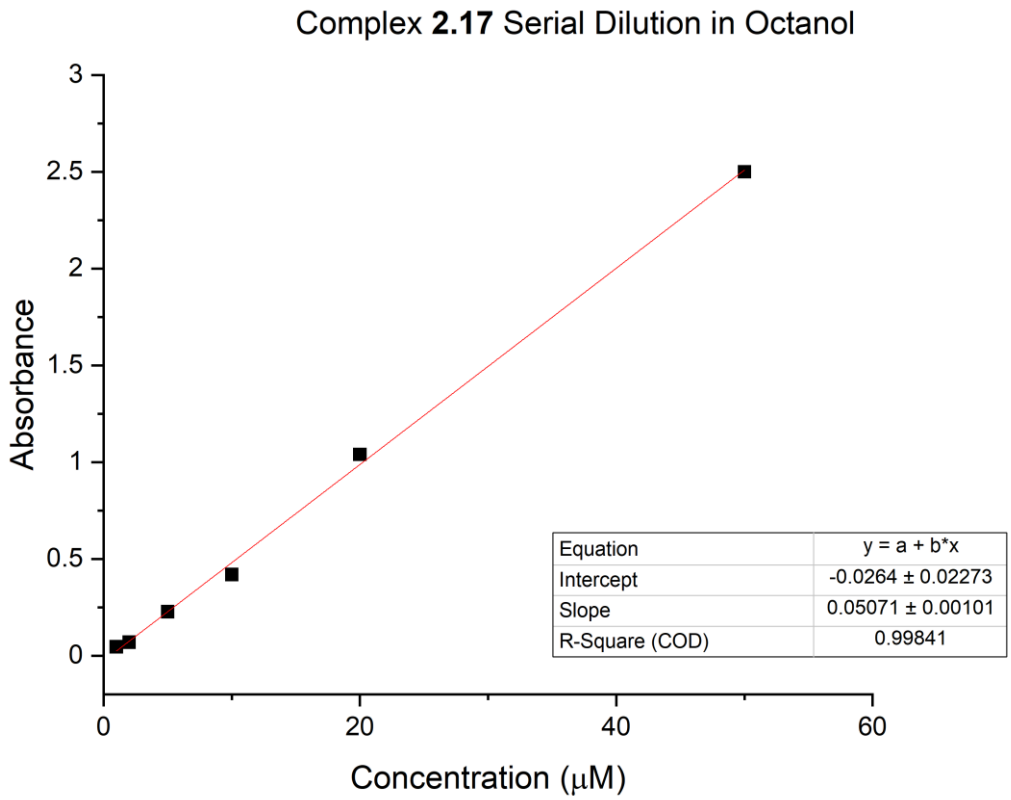

Figure A2.21. Calibration curve for complex **2.17** in 1-octanol.

Replicate 1: λ_{max} = 365 nm, A = 2.39

Concentration in octanol = A/εl = 2.39/(50700 × 1) = 4.71 × 10^{-5} M = 47.1 μM

Total concentration of **2.17** added for partition between water and octanol = 80 μM

Concentration in octanol = 47.1 μM and concentration in water = 32.9 μM

Log P = log $\left(\frac{[2.17]octanol}{[2.17]water}\right)$ = log $\left(\frac{47.1}{32.9}\right)$ = 0.156

Replicate 2: λ_{max} = 365 nm, A = 2.35

Concentration in octanol = A/εl = 2.35/(50700 × 1) = 4.64 × 10^{-5} M = 46.4 μM

Total concentration of **2.17** added for partition between water and octanol = 80 μM

Concentration in octanol = 46.4 μM and concentration in water = 33.6 μM

Log P = log $\left(\frac{[2.17]octanol}{[2.17]water}\right)$ = log $\left(\frac{46.4}{33.6}\right)$ = 0.140

Replicate 3: λ_{max} = 365 nm, A = 2.37

Concentration in octanol = A/εl = 2.37/(50700 × 1) = 4.67 × 10^{-5} M = 46.7 μM

Total concentration of **2.17** added for partition between water and octanol = 80 μM

Concentration in octanol = 46.7 μM and concentration in water = 33.3 μM

Log P = log $\left(\frac{[2.17]octanol}{[2.17]water}\right)$ = log $\left(\frac{46.7}{33.3}\right)$ = 0.147

Complex **2.17**, average log P = 0.15 ± 0.01

Complex **2.18**

Table A2.3. Standard samples of **2.18** with its corresponding absorbance.

Concentration (μM)	Absorbance
1	0.010805
2	0.02689
5	0.08842
10	0.199834
20	0.459253
50	1.223777

Max wavelength = 360 nm

Molar extinction coefficient = 0.0236 μmol^{-1} L cm^{-1}= 23600 mol^{-1} L cm^{-1}

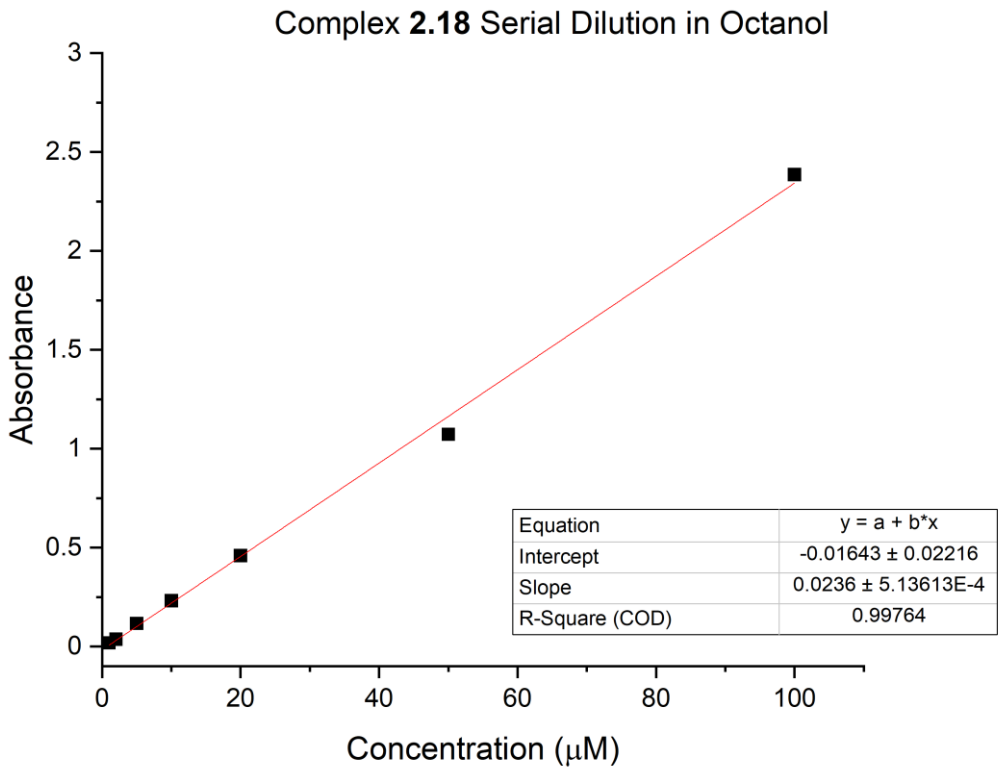

Figure A2.22. Calibration curve for complex **2.18** in 1-octanol.

Replicate 1: λ_{max} = 360 nm, A = 1.34

Concentration in octanol = A/εl = 1.34/(23600 × 1) = 5.68 × 10^{-5} M = 56.8 μM

Total concentration of **2.18** added for partition between water and octanol = 80 μM

Concentration in octanol = 56.8 μM and concentration in water = 23.2 μM.

Log P = log $\left(\frac{[2.18]octanol}{[2.18]water}\right)$ = log $\left(\frac{56.8}{23.2}\right)$ = 0.389

Replicate 2: λ_{max} = 360 nm, A = 1.33

Concentration in octanol = A/εl = 1.33/(23600 × 1) = 5.64 × 10^{-5} M = 56.4 μM

Total concentration of **2.18** added for partition between water and octanol = 80 μM

Concentration in octanol = 56.4 μM and concentration in water = 23.6 μM.

Log P = log $\left(\frac{[2.18]octanol}{[2.18]water}\right)$ = log $\left(\frac{56.4}{23.6}\right)$ = 0.378

Replicate 3: λ_{max} = 360 nm, A = 1.34

Concentration in octanol = A/εl = 1.34/(23600 × 1) = 5.68 × 10^{-5} M = 56.8 μM

Total concentration of **2.18** added for partition between water and octanol = 80 μM

Concentration in octanol = 56.8 μM and concentration in water = 23.2 μM.

Log P = log $\left(\frac{[2.18]octanol}{[2.18]water}\right)$ = log $\left(\frac{56.8}{23.2}\right)$ = 0.389

Complex **2.18**, average log P log P = 0.39 ± 0.01

2.5. Photophysical Studies

Table A2.4. UV-visible absorption and fluorescence spectroscopic data for compounds: benzothiazole ligand, Re(I)-benzothiazole, stilbene ligand and Re(I)-stilbene.

Compound (Solvent)	λ_{max}/nm (ε/$M^{-1}cm^{-1}$)	Photoluminescence λ_{max}/nm
2.13[a]	365 (41500)	424
2.16[a]	357 (34800)	454
2.17[b]	369 (27900)	417
2.18[b]	357 (20400)	457

[a]1 μM in acetonitrile, [b]10 μM in acetonitrile

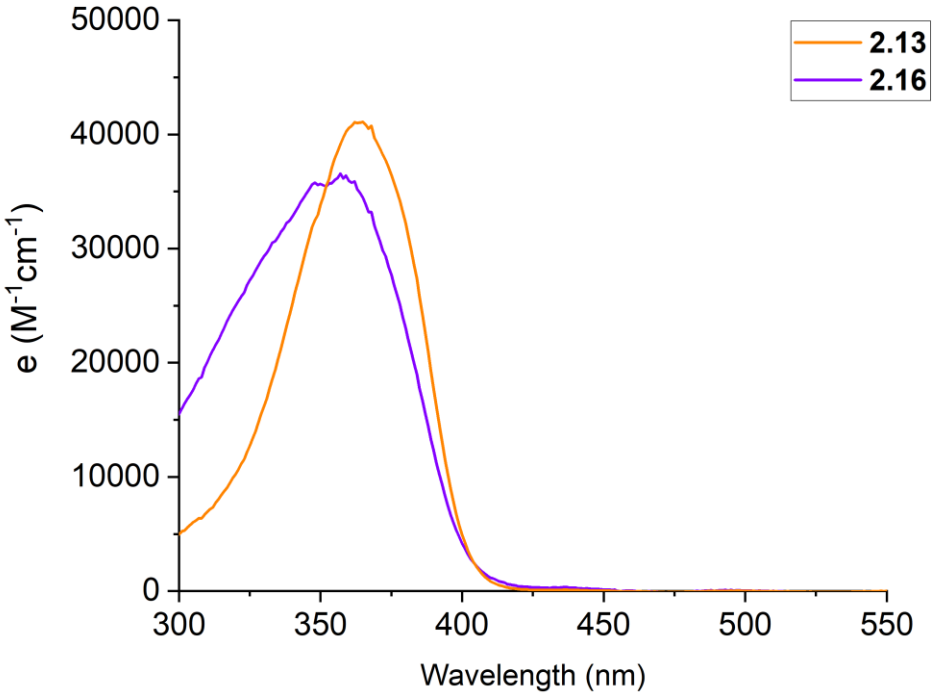

Figure A2.23. UV-vis spectra of **2.13** and **2.16** (1 μM in acetonitrile).

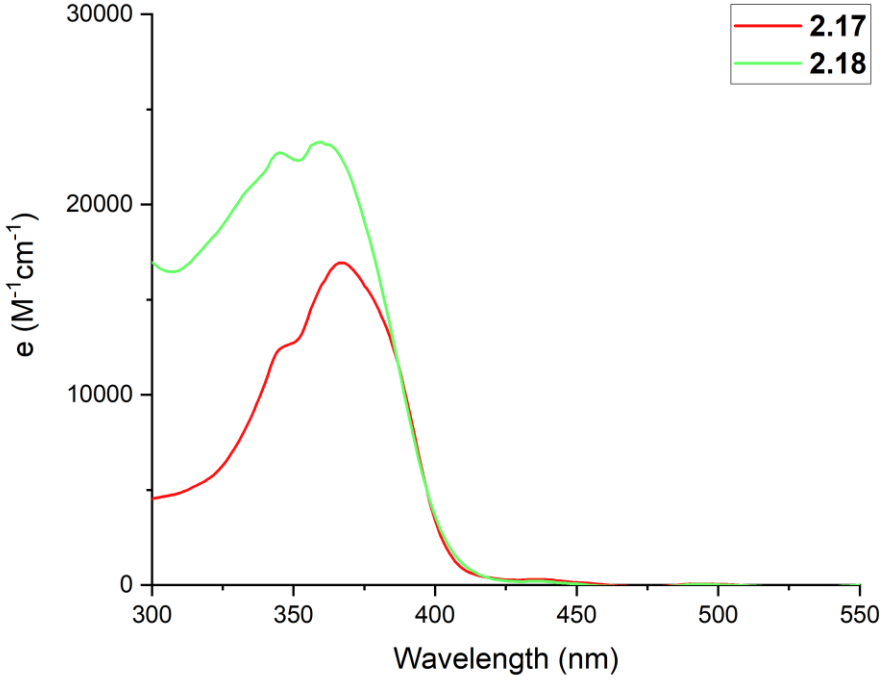

Figure A2.24. UV-vis spectra of **2.17** and **2.18** (10 µM in acetonitrile).

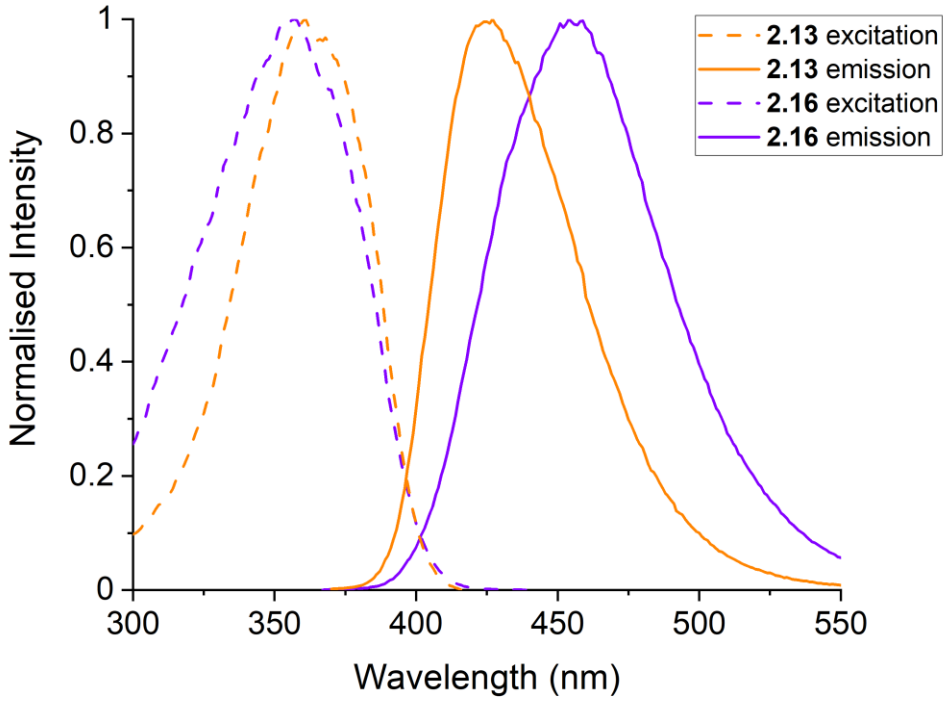

Figure A2.25. Excitation and emission spectra for compounds **2.13** and **2.16** (1 µM in acetonitrile).

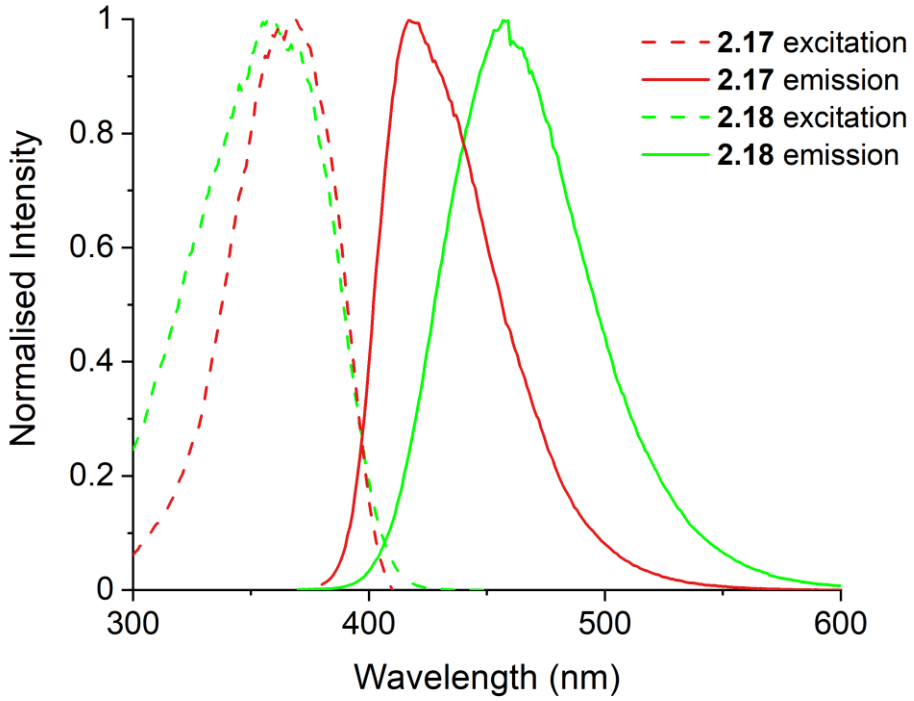

Figure A2.26. Excitation and emission spectra for compounds **2.17** and **2.18** (10 µM in acetonitrile).

Appendix 3 : For Chapter 3

3.1. IR Spectra

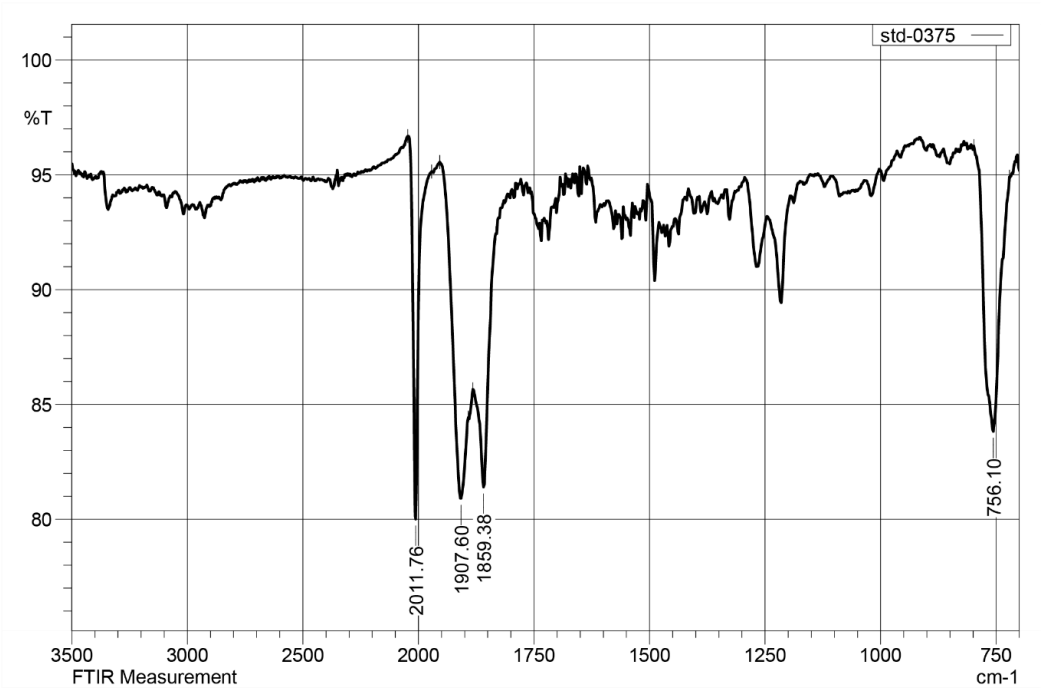

Figure A3.1. FT-IR spectrum for complex **3.8**.

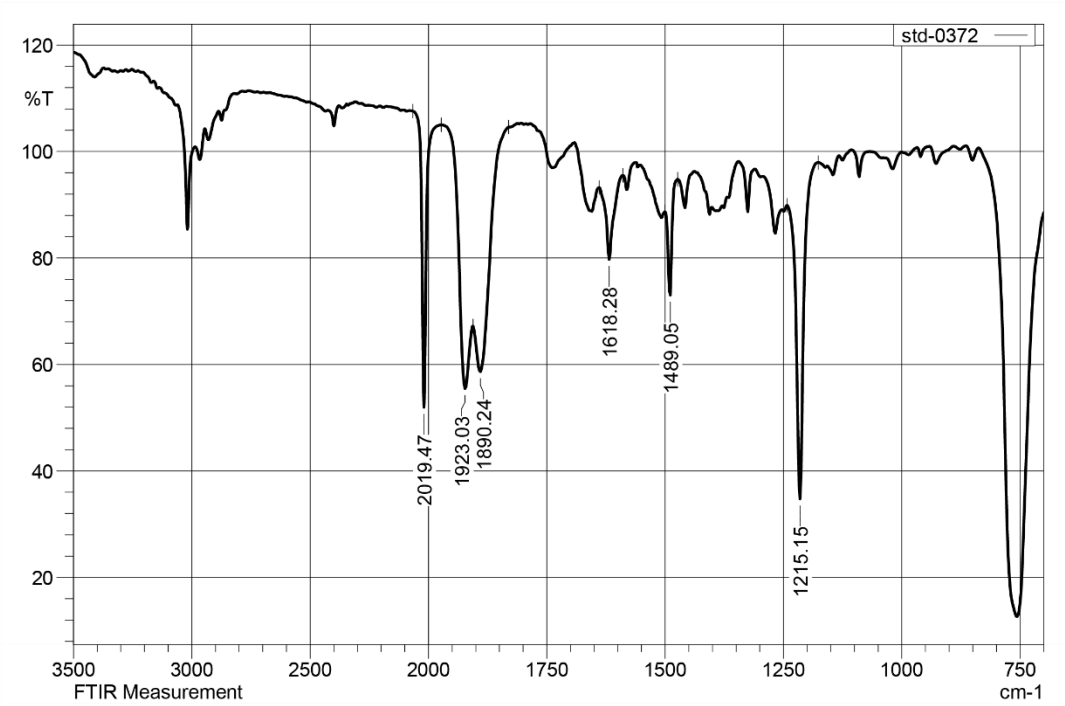

Figure A3.2. FT-IR spectrum for complex **3.9**.

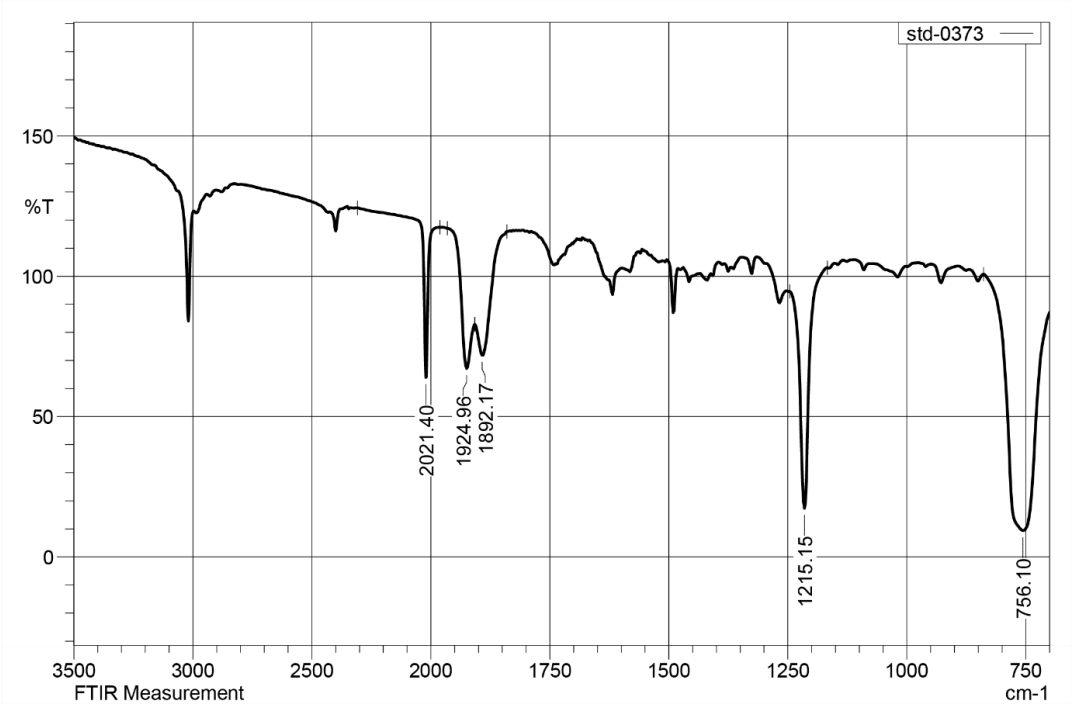

Figure A3.3. FT-IR spectrum for complex **3.10**.

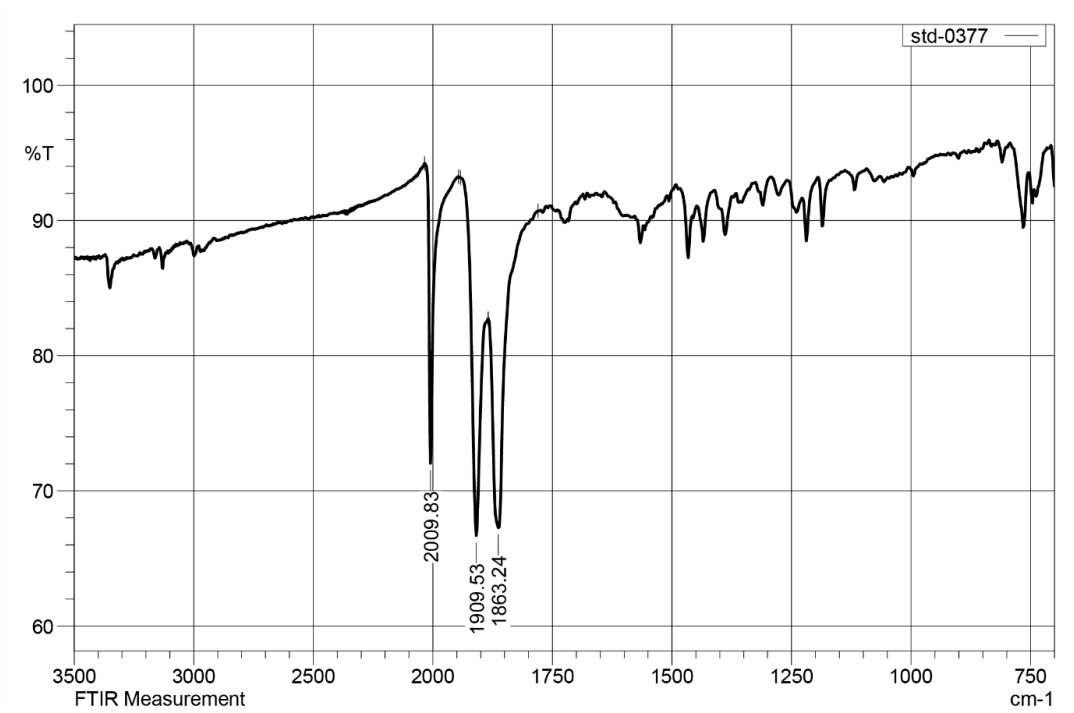

Figure A3.4. FT-IR spectrum for complex **3.12**.

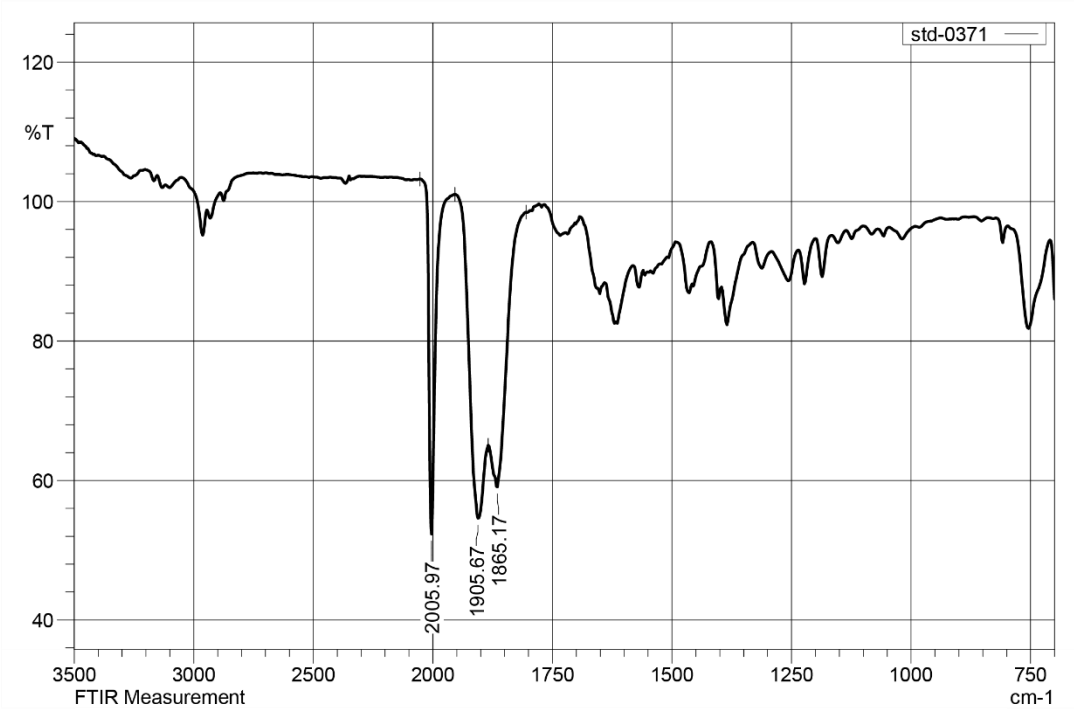

Figure A3.5. FT-IR spectrum for complex **3.13**.

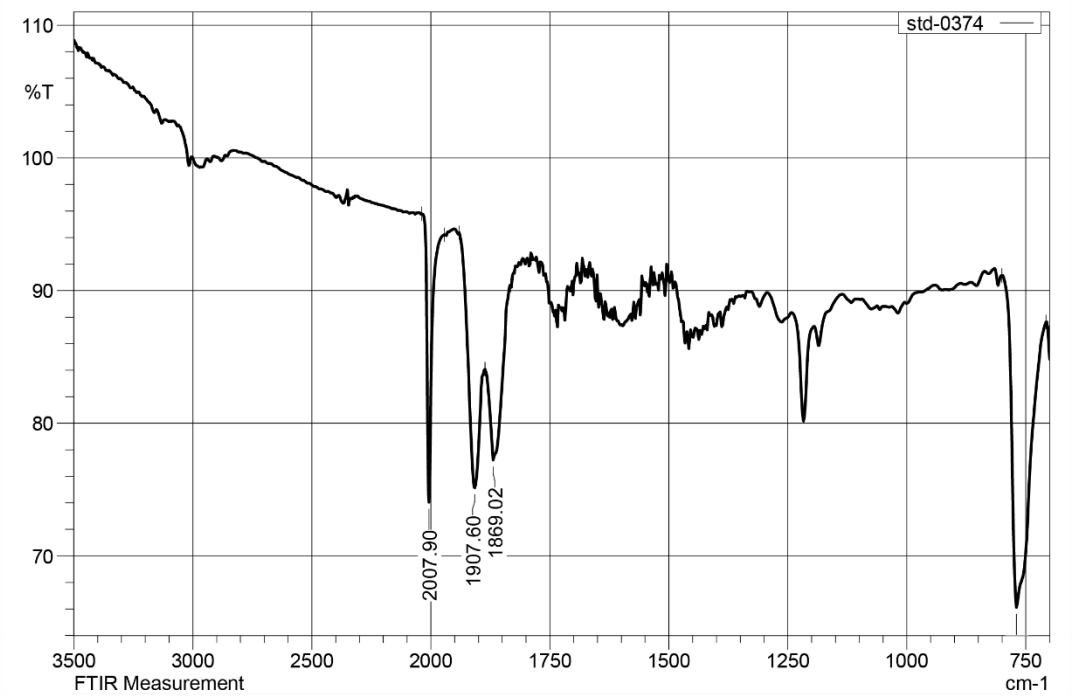

Figure A3.6. FT-IR spectrum for complex **3.14**.

3.2. NMR Spectra

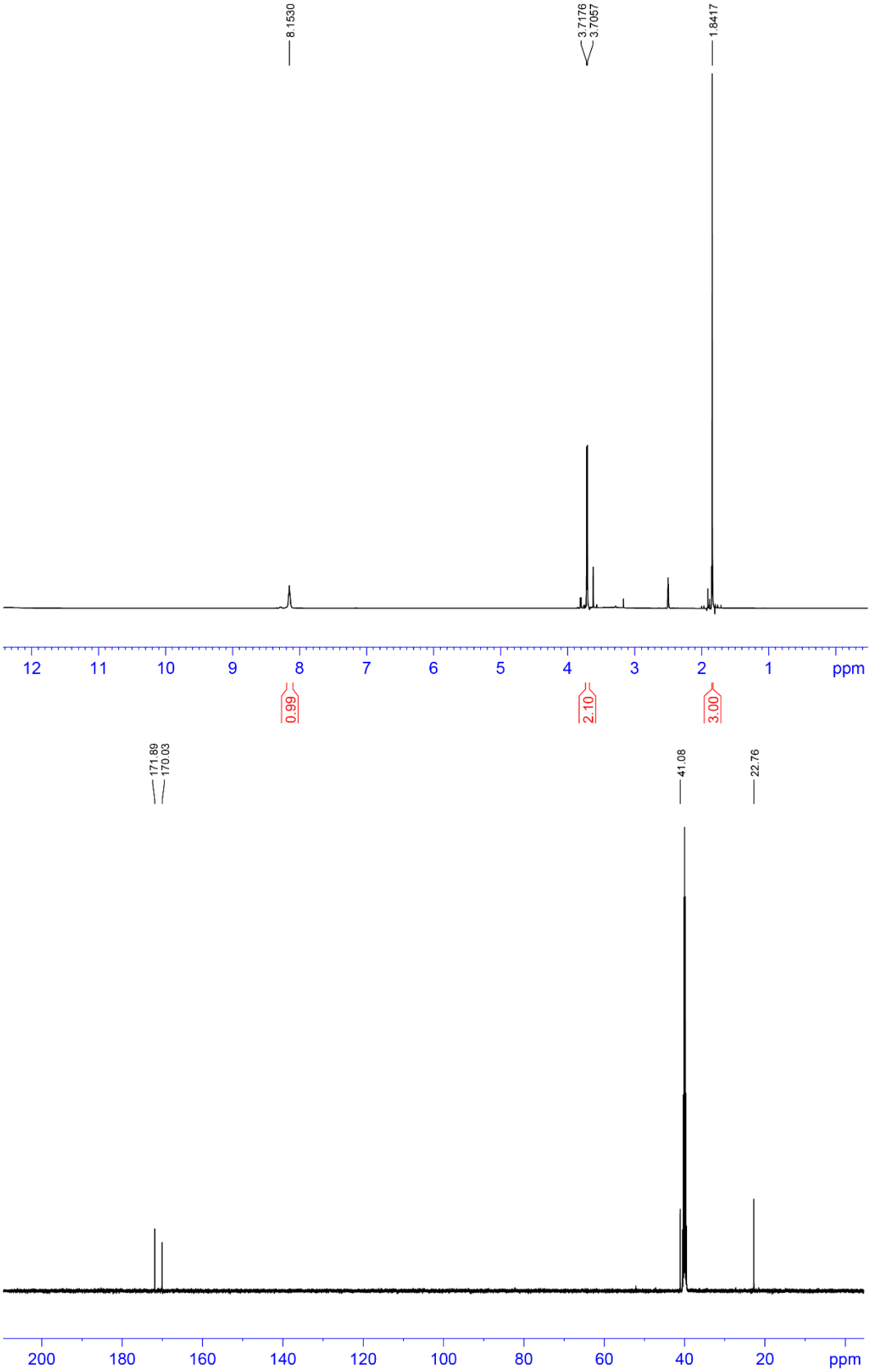

Figure A3.7. ^{1}H and ^{13}C NMR spectra for *N*-acetyl glycine.

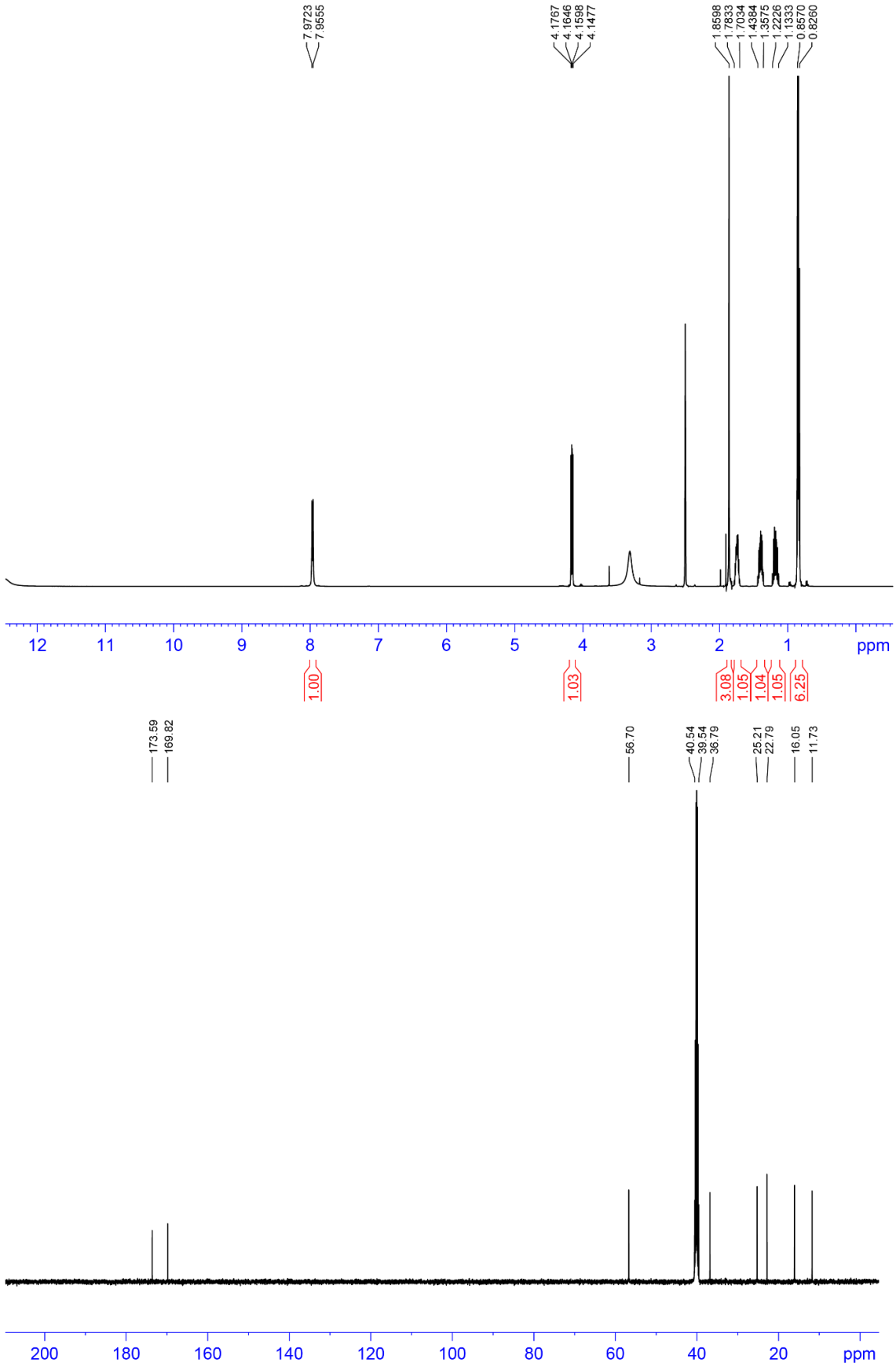

Figure A3.8. ^{1}H and ^{13}C NMR spectra for *N*-acetyl isoleucine.

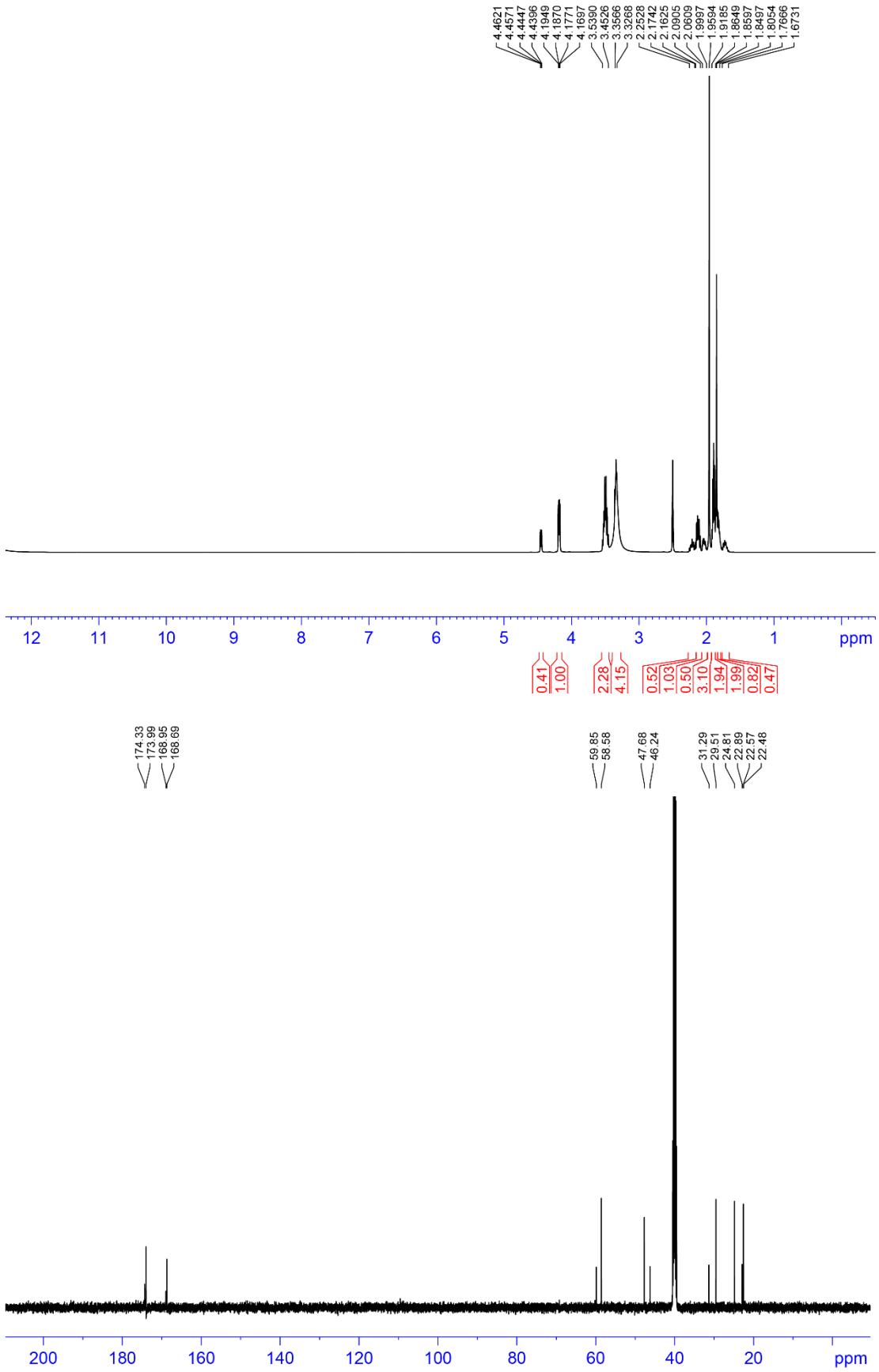

Figure A3.9. ^{1}H and ^{13}C NMR spectra for *N*-acetyl proline.

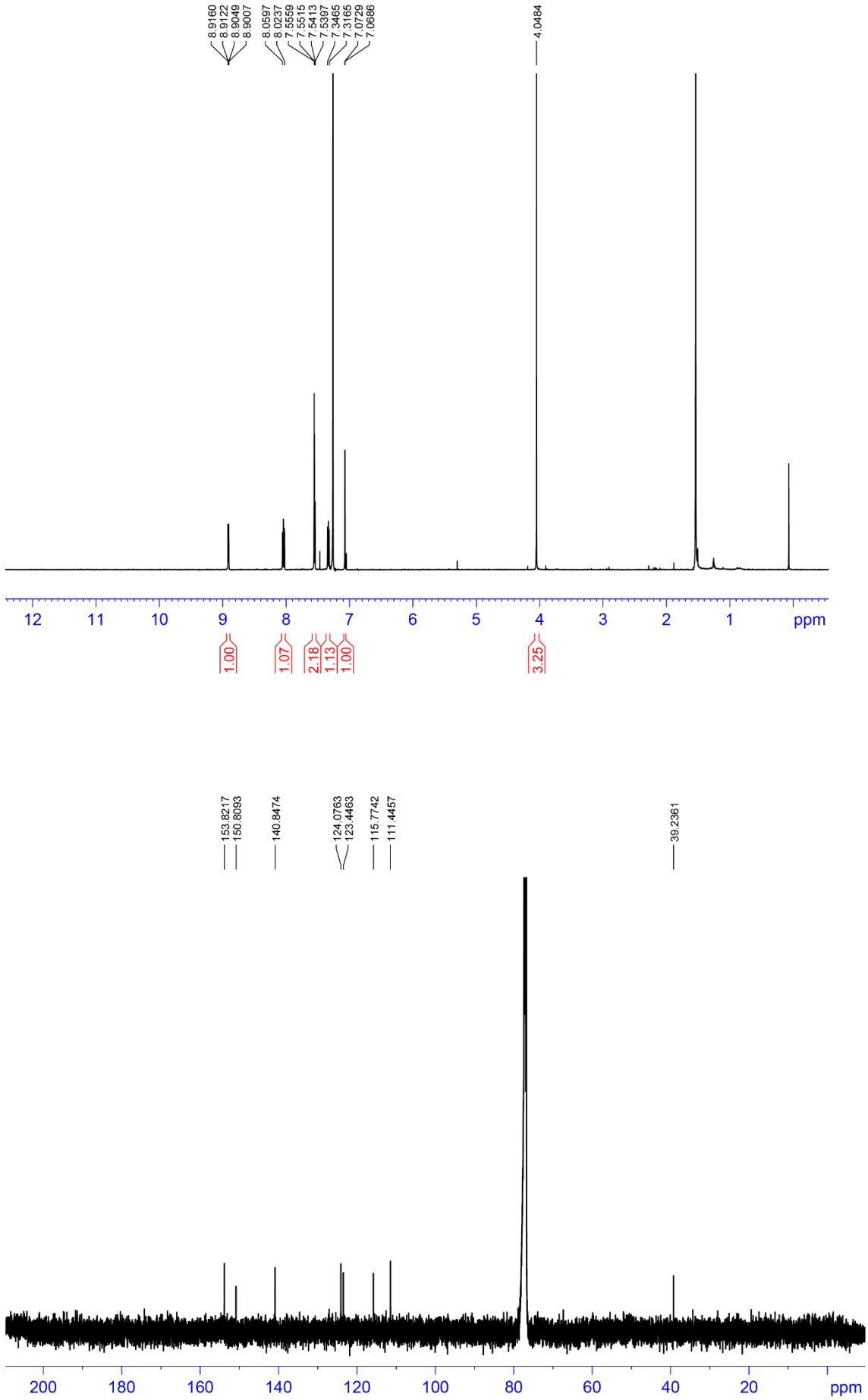

Figure A3.10. ^{1}H and ^{13}C NMR spectra for **3.1**.

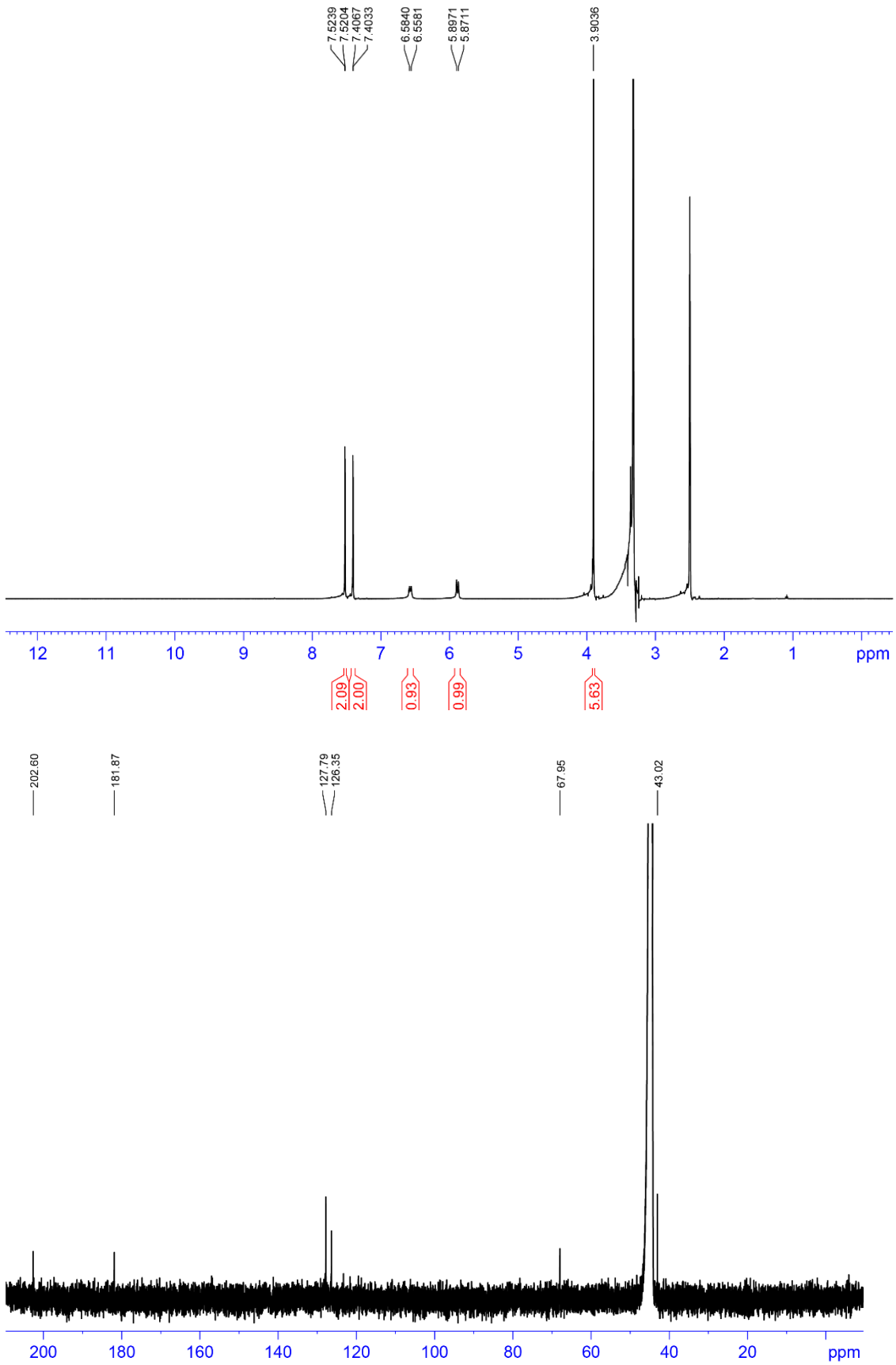

Figure A3.11. ^{1}H and ^{13}C NMR spectra for **3.2**.

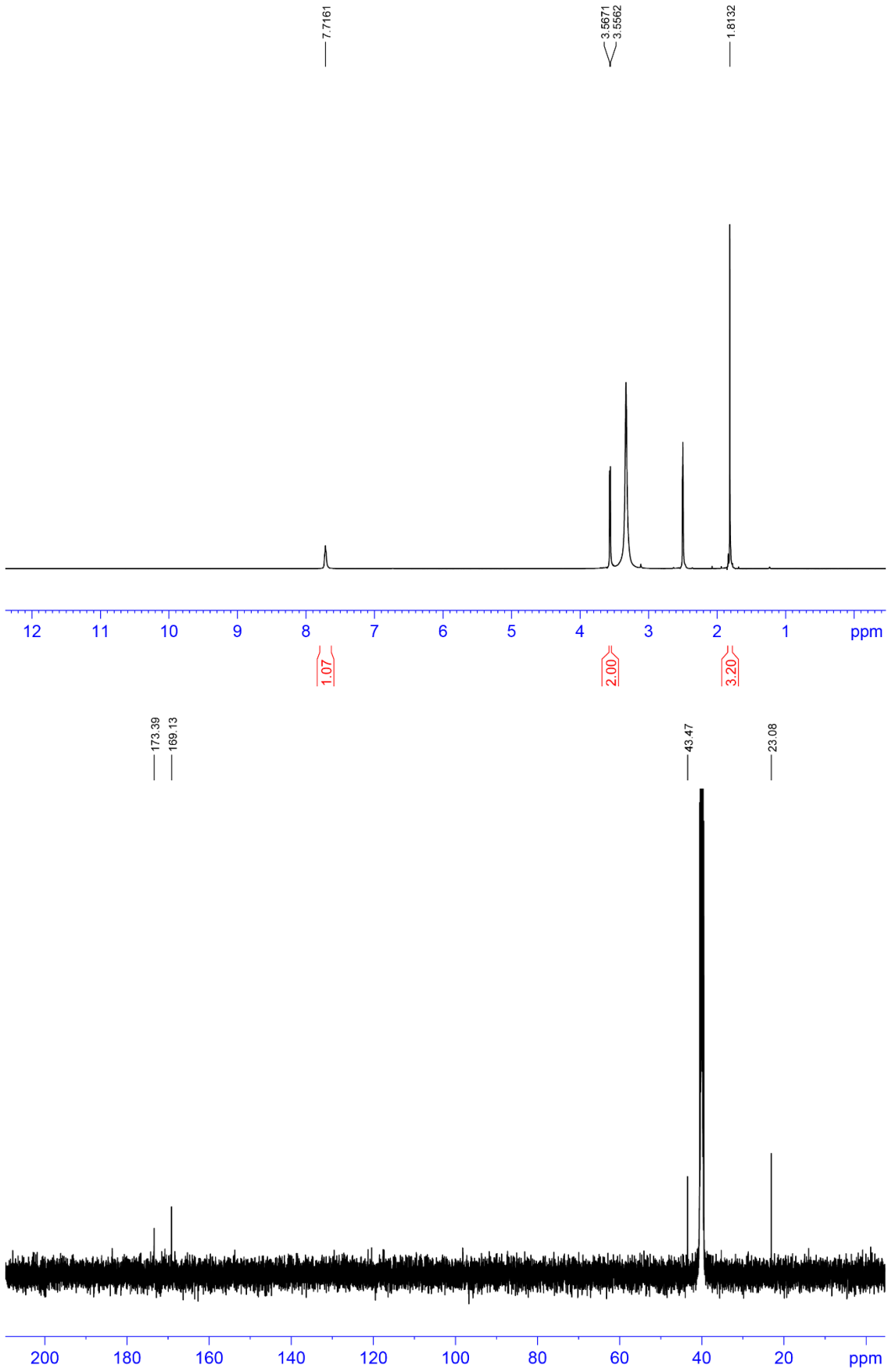

Figure A3.12. ^{1}H and ^{13}C NMR spectra for **3.4**.

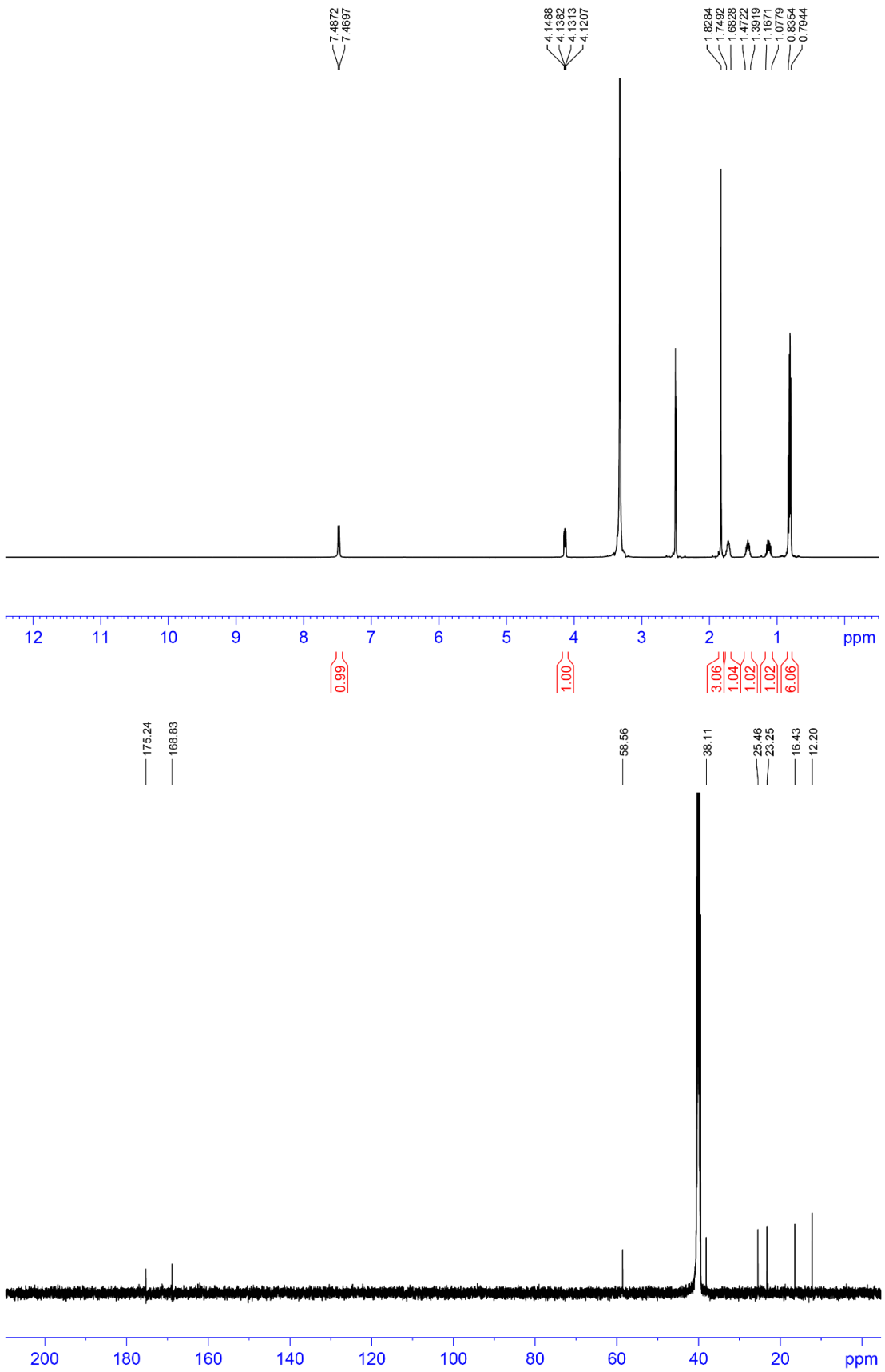

Figure A3.13. ^{1}H and ^{13}C NMR spectra for **3.5**.

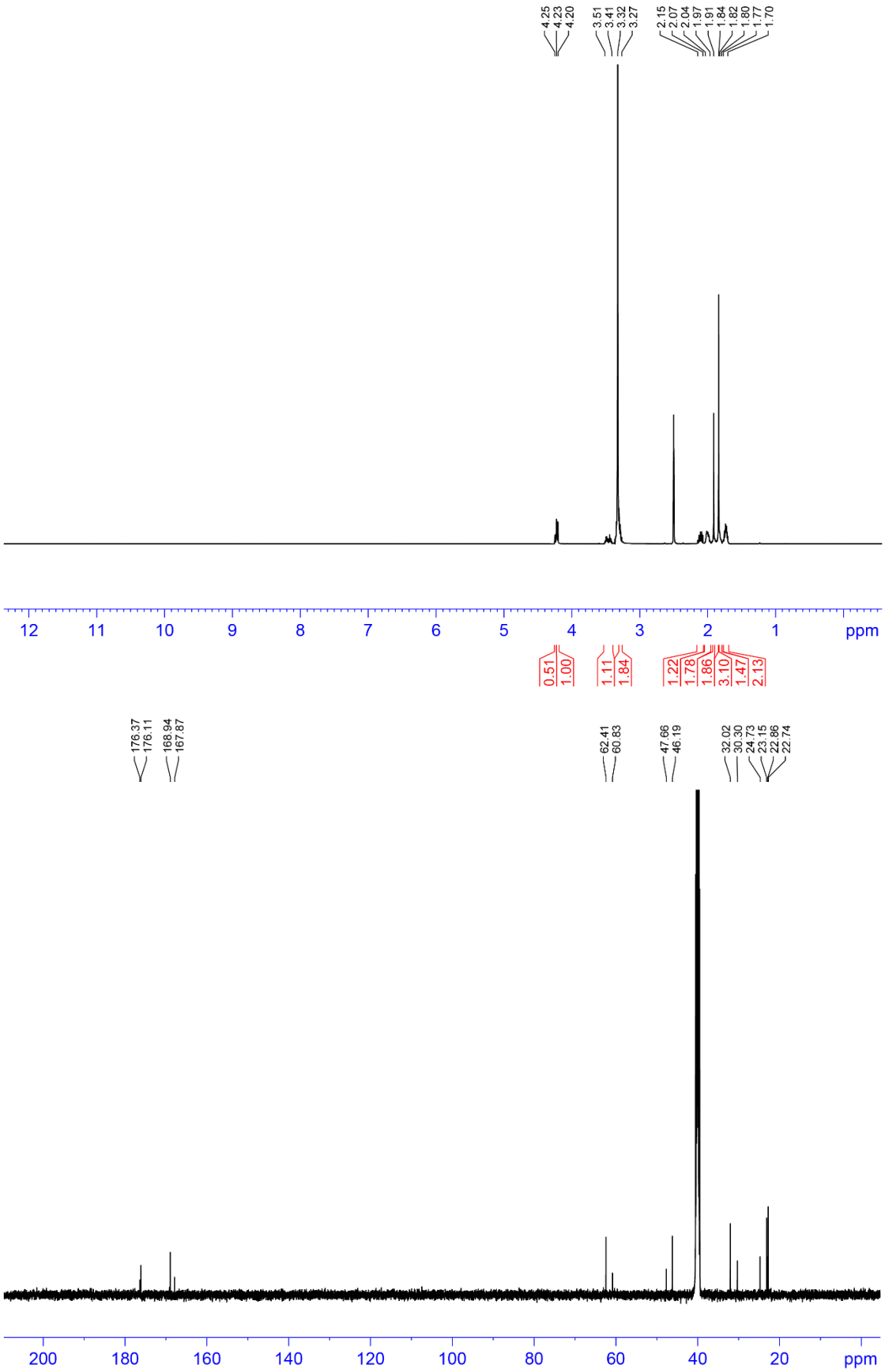

Figure A3.14. ^{1}H and ^{13}C NMR spectra for **3.6**.

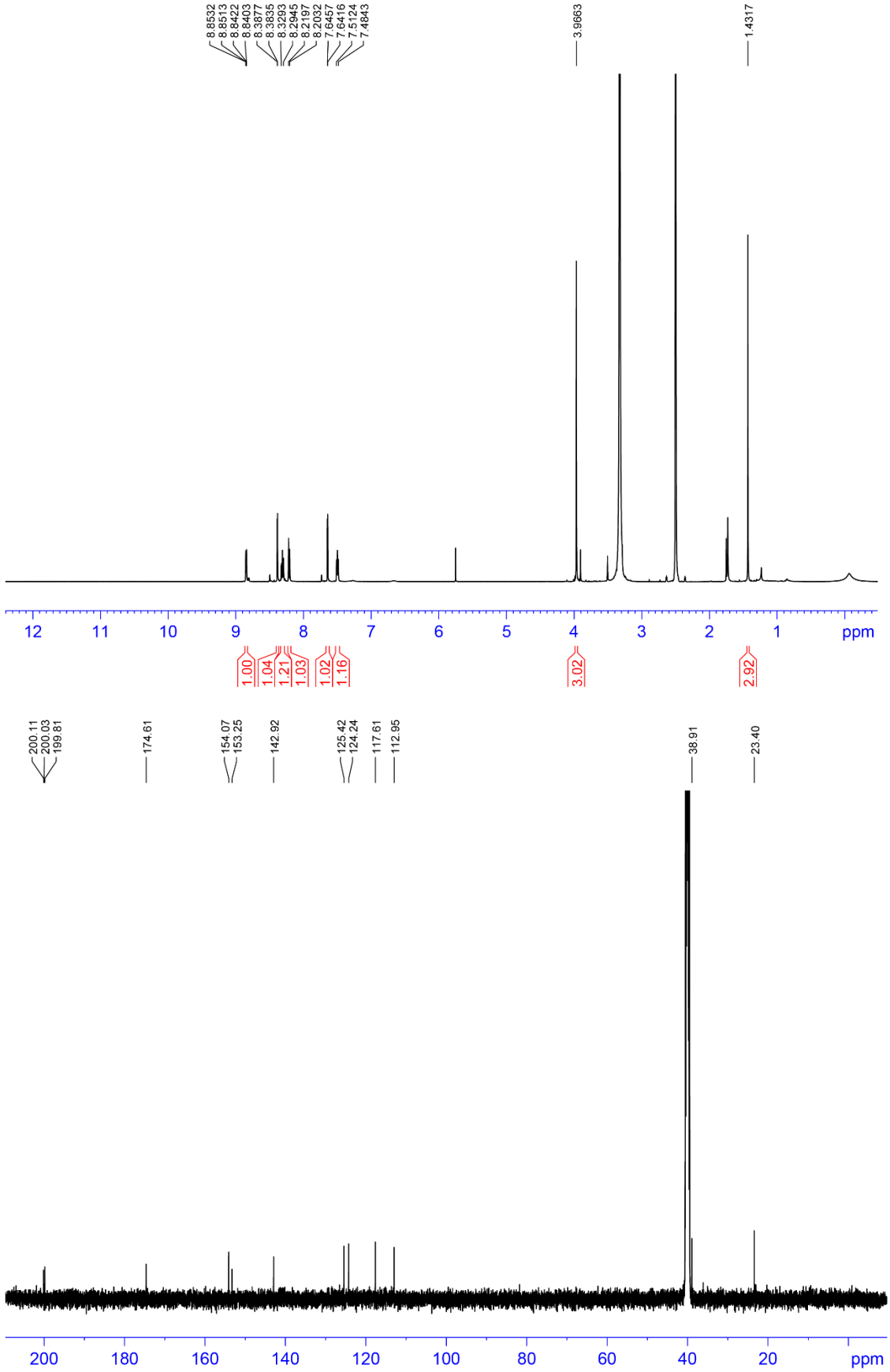

Figure A3.15. ^{1}H and ^{13}C NMR spectra for **3.7**.

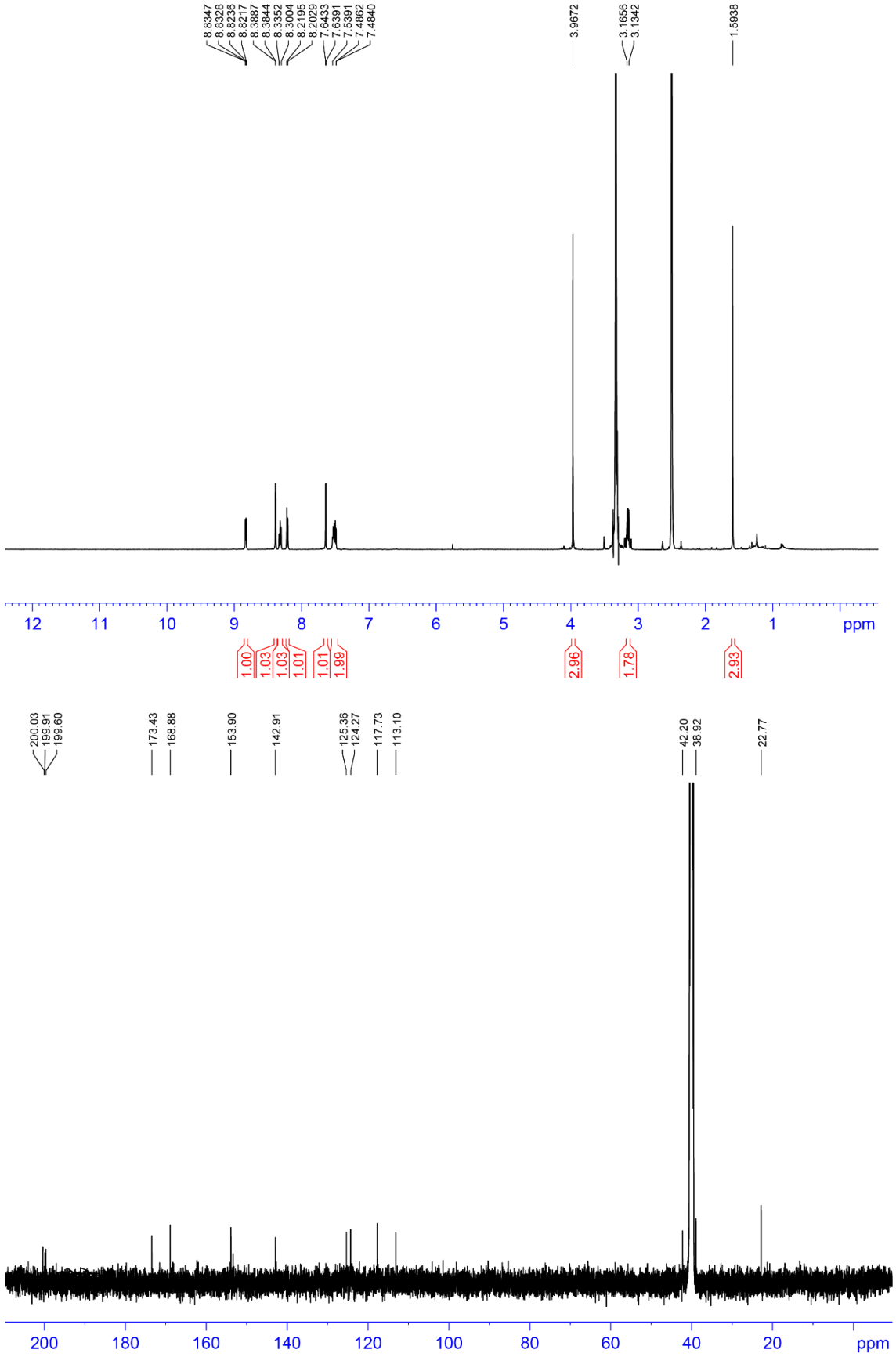

Figure A3.16. ^{1}H and ^{13}C NMR spectra for **3.8**.

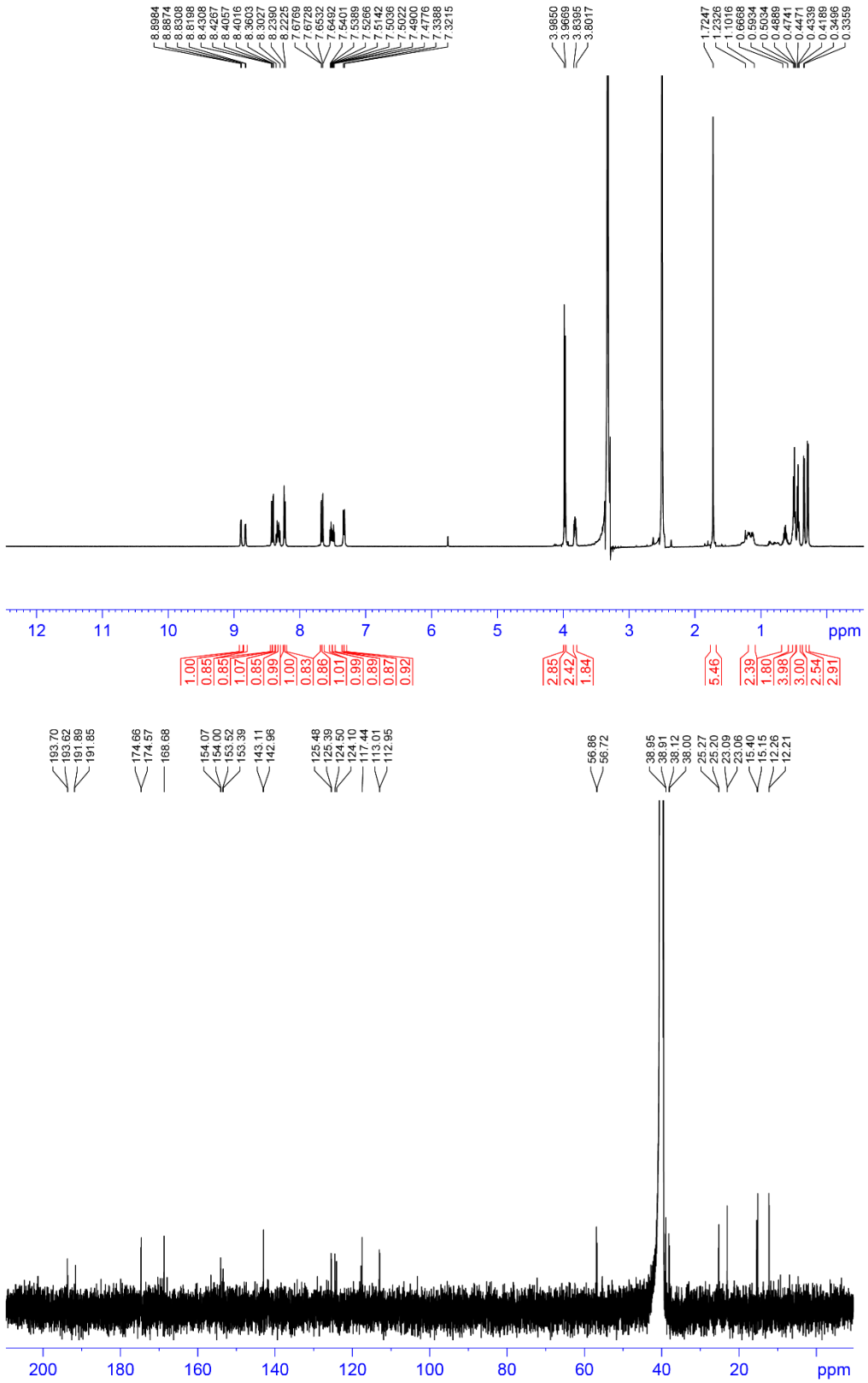

Figure A3.17. ^{1}H and ^{13}C NMR spectra for **3.9**.

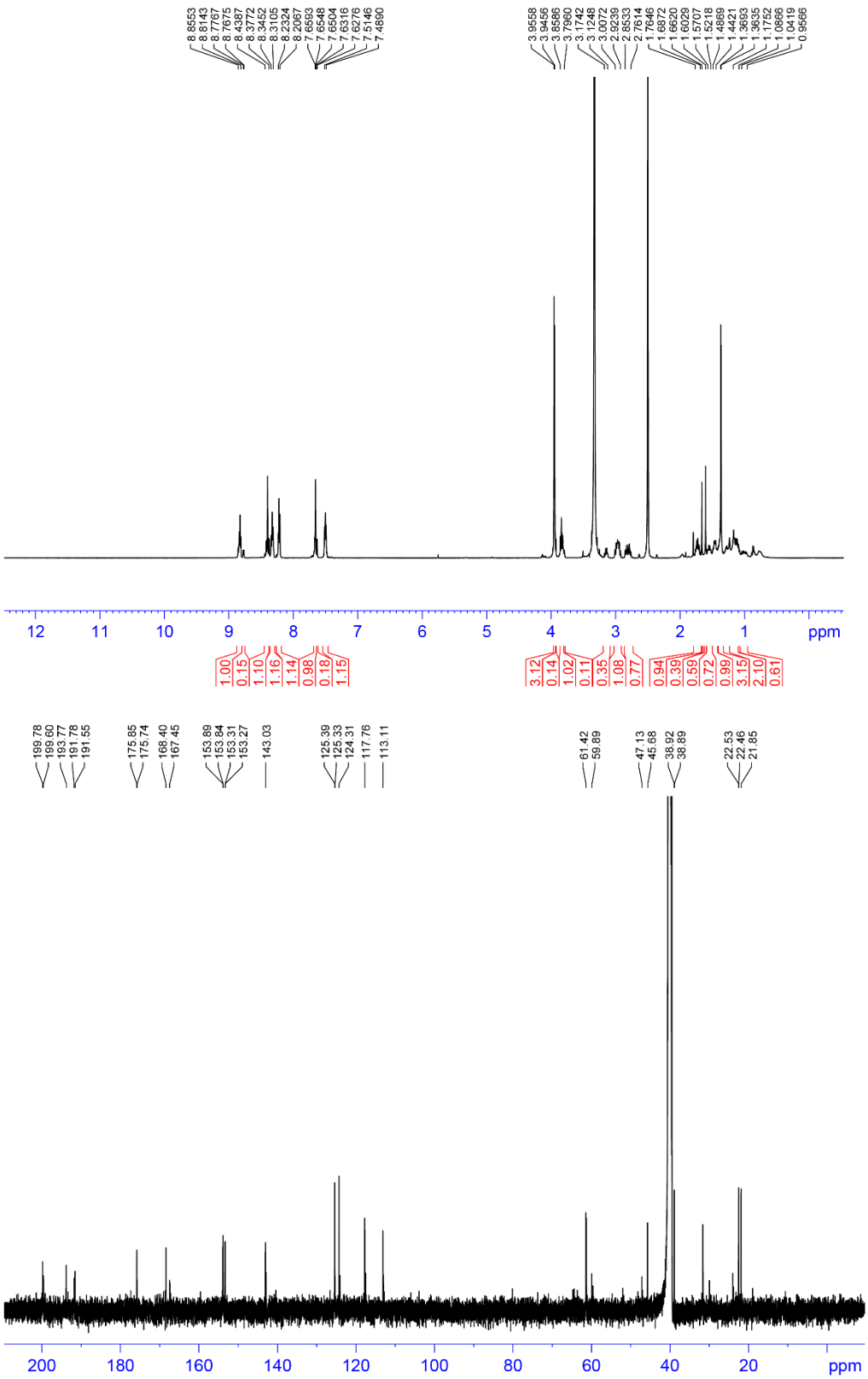

Figure A3.18. ^{1}H and ^{13}C NMR spectra for **3.10**.

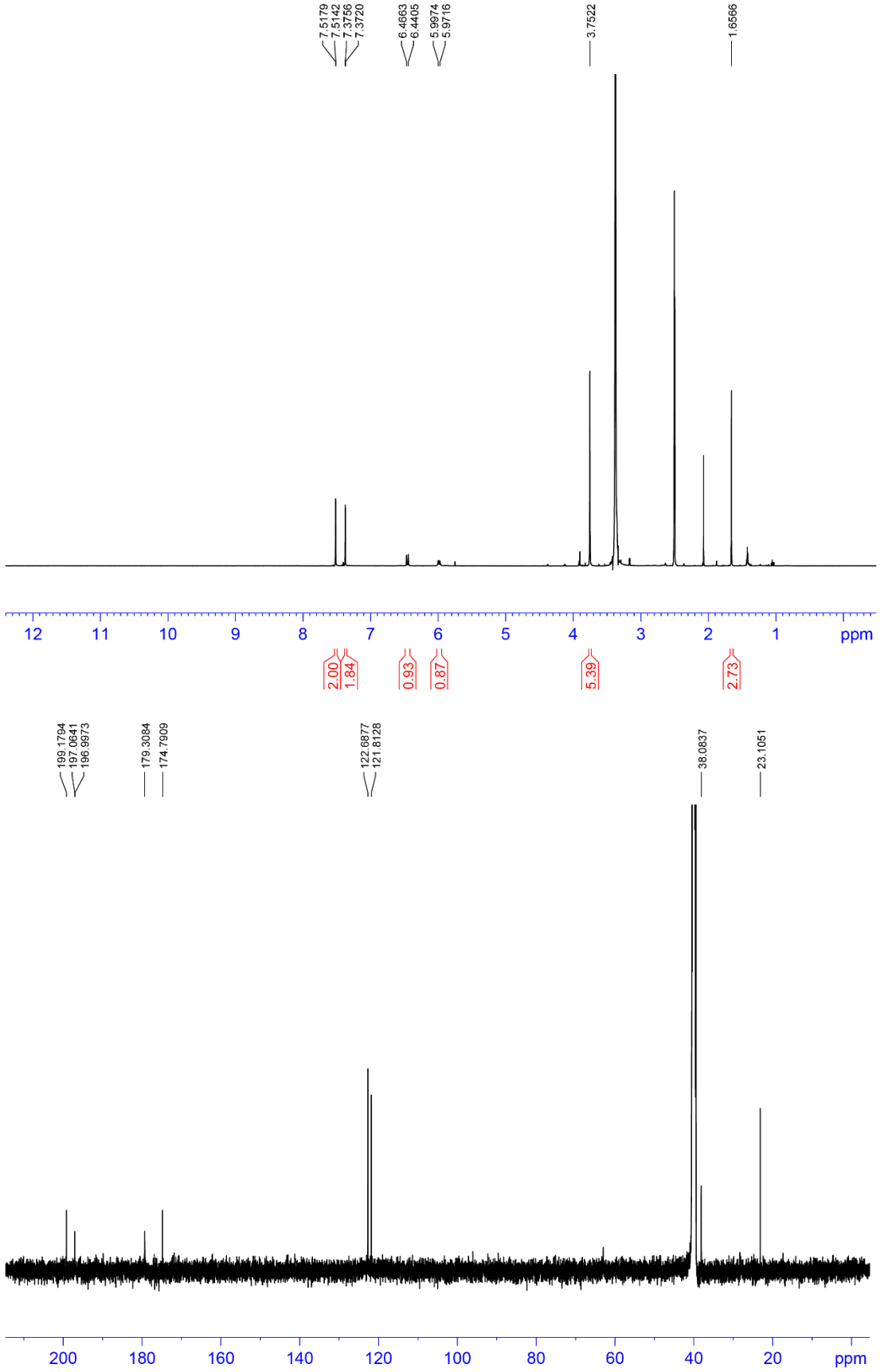

Figure A3.19. ^{1}H and ^{13}C NMR spectra for **3.11**.

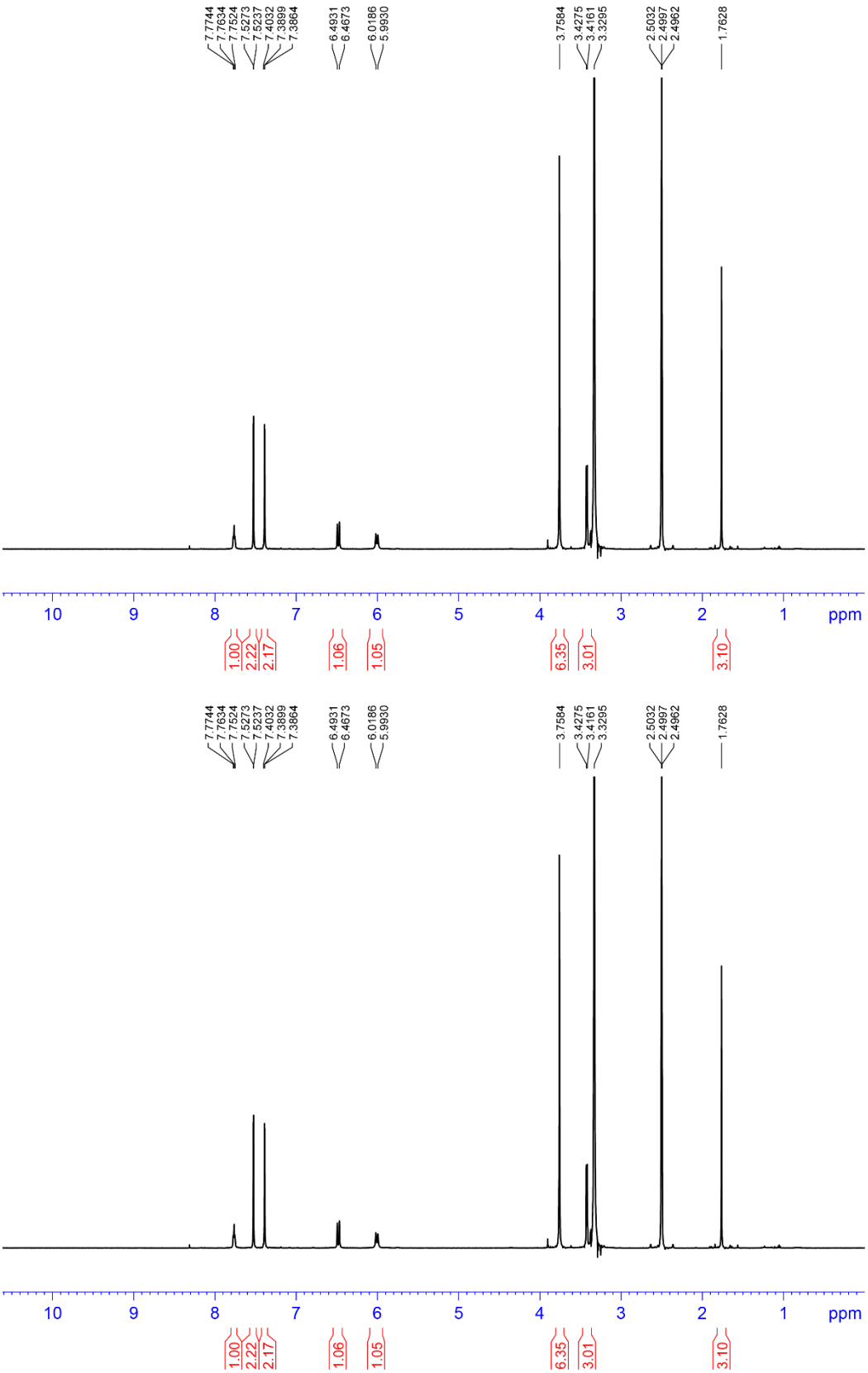

Figure A3.20. ^{1}H and ^{13}C NMR spectra for **3.12**.

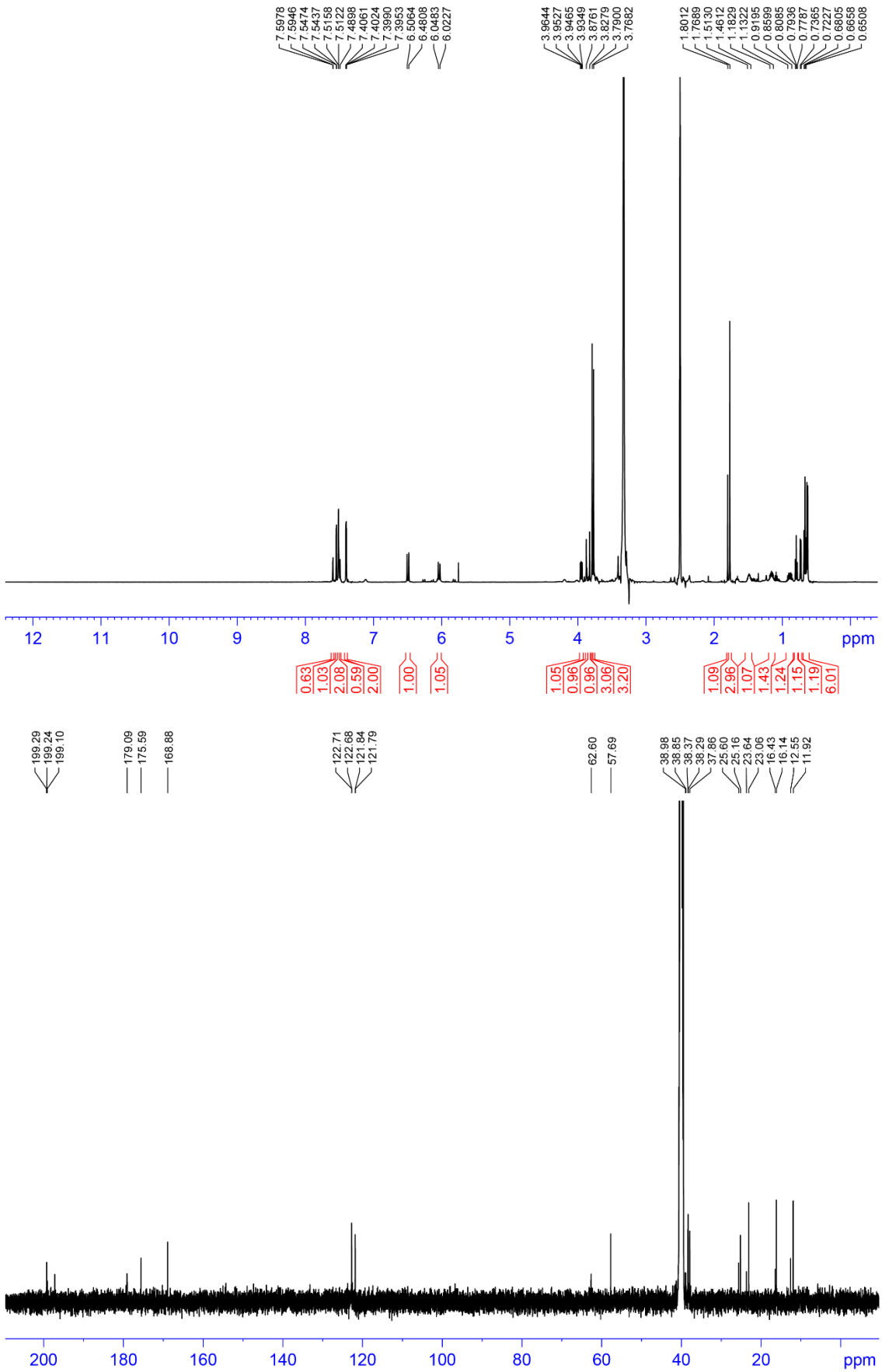

Figure A3.21. ^{1}H and ^{13}C NMR spectra for **3.13**.

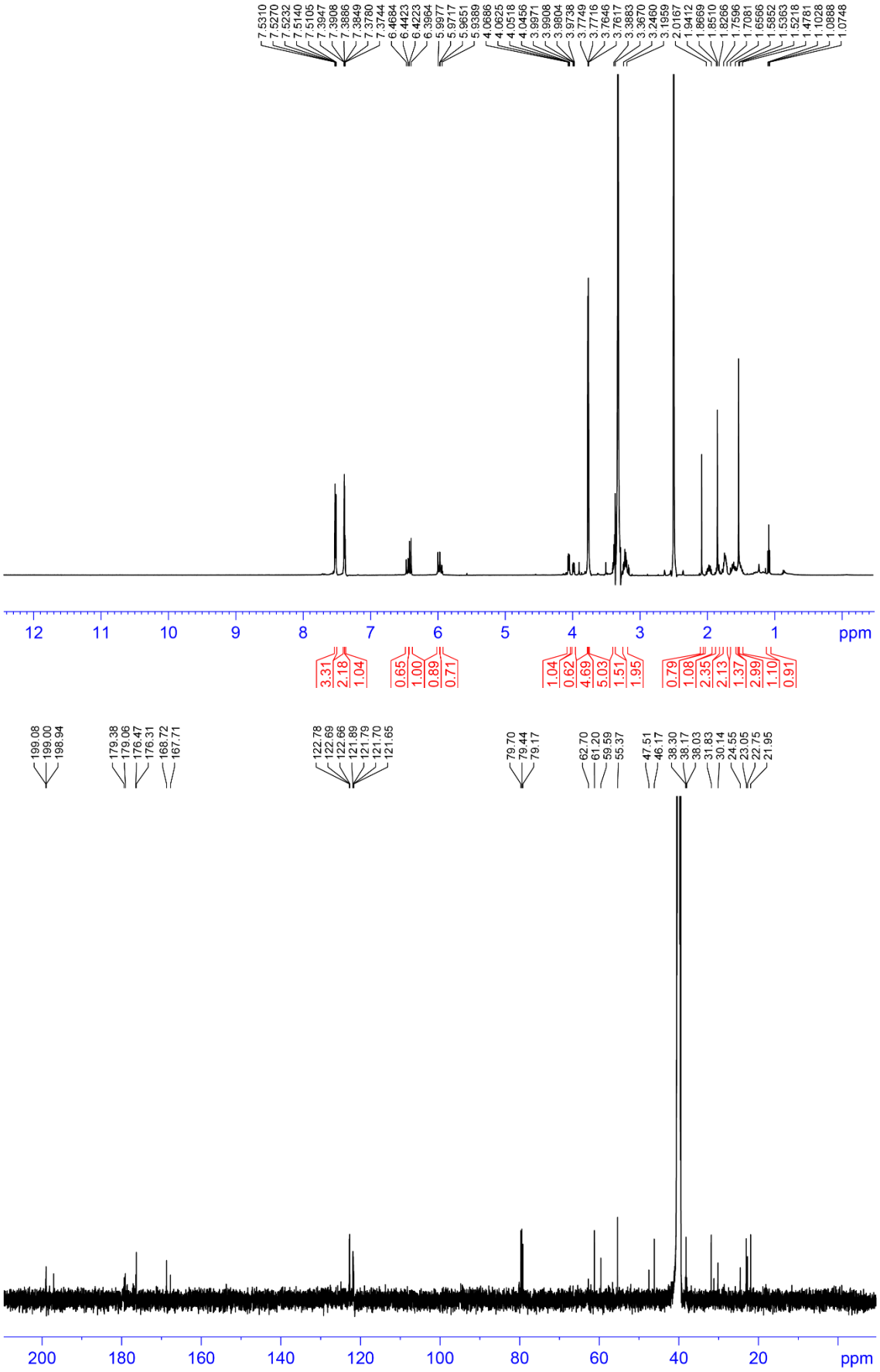

Figure A3.22. ^{1}H and ^{13}C NMR spectra for **3.14**.

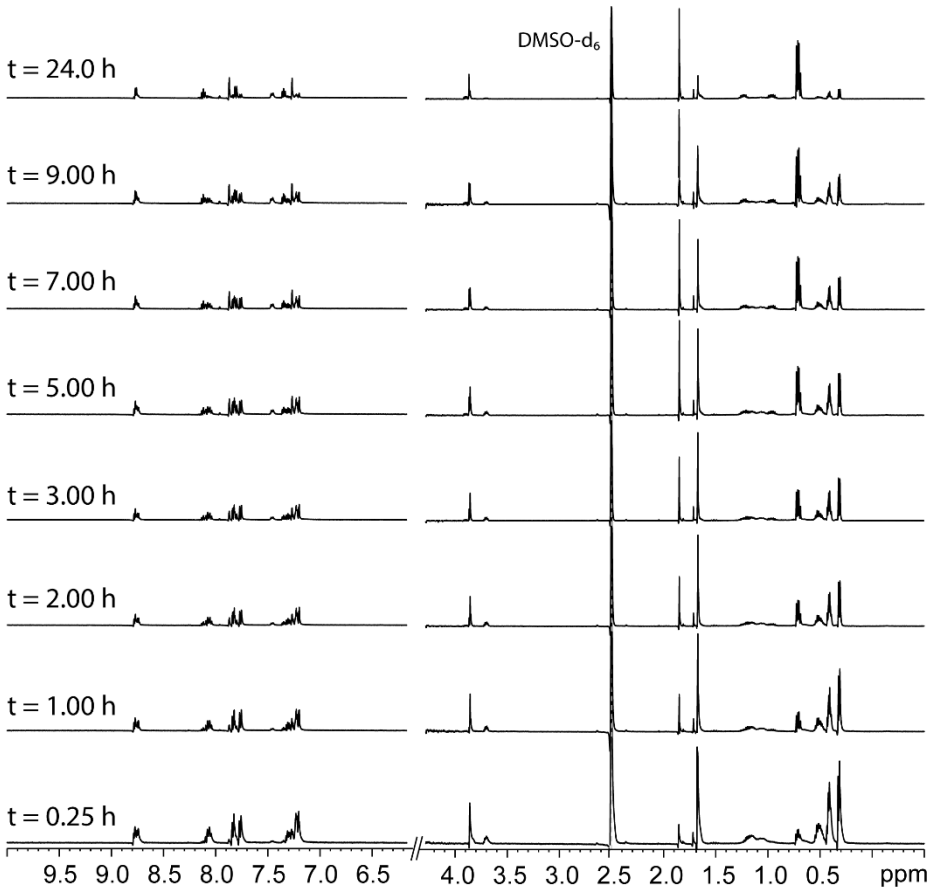

Figure A3.23. Selected ^{1}H NMR spectra (500.13 MHz) recorded for a solution of **3.9** in a mixture of water (76%), DMSO-d_6 (20%), and D_2O (4%) over a period of 24 h at 25.0 ± 0.1 °C.

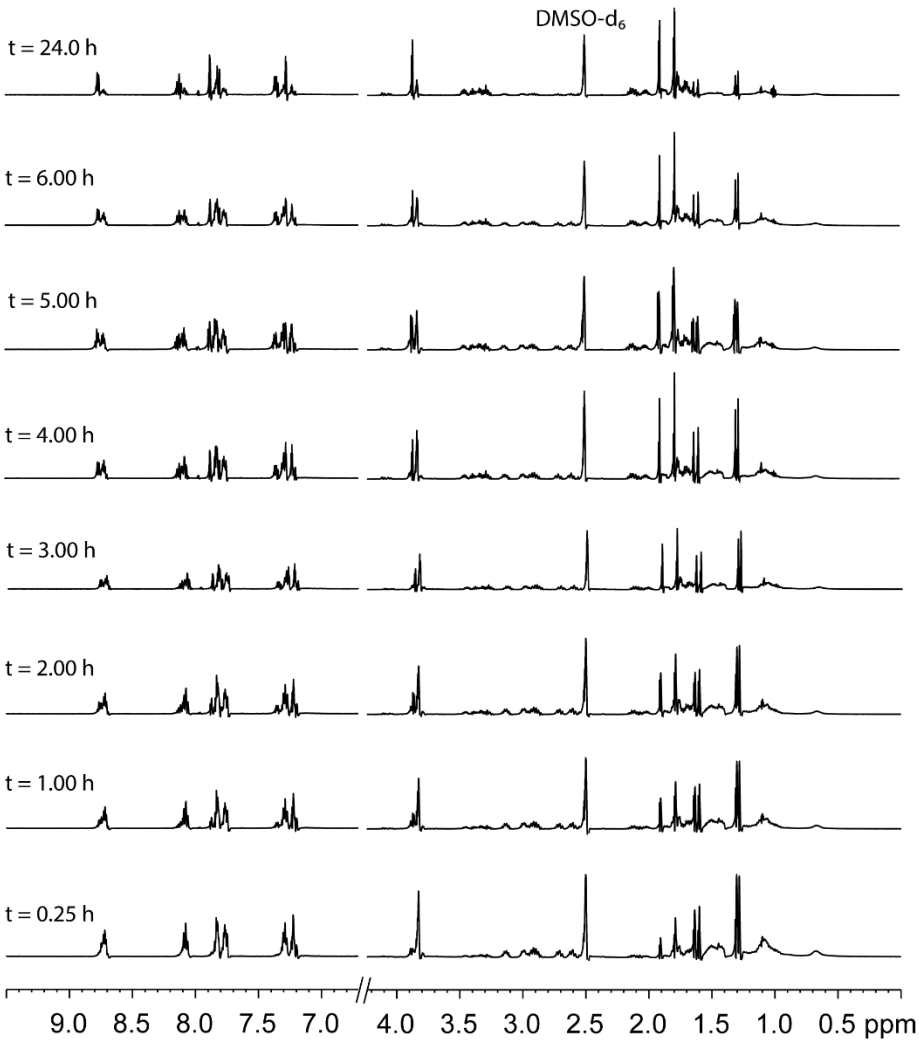

Figure A3.24. Selected ^{1}H NMR spectra (500.13 MHz) recorded for a solution of **3.10** in a mixture of water (76%), DMSO-d_6 (20%), and D_2O (4%) over a period of 24 h at 25.0 ± 0.1 °C.

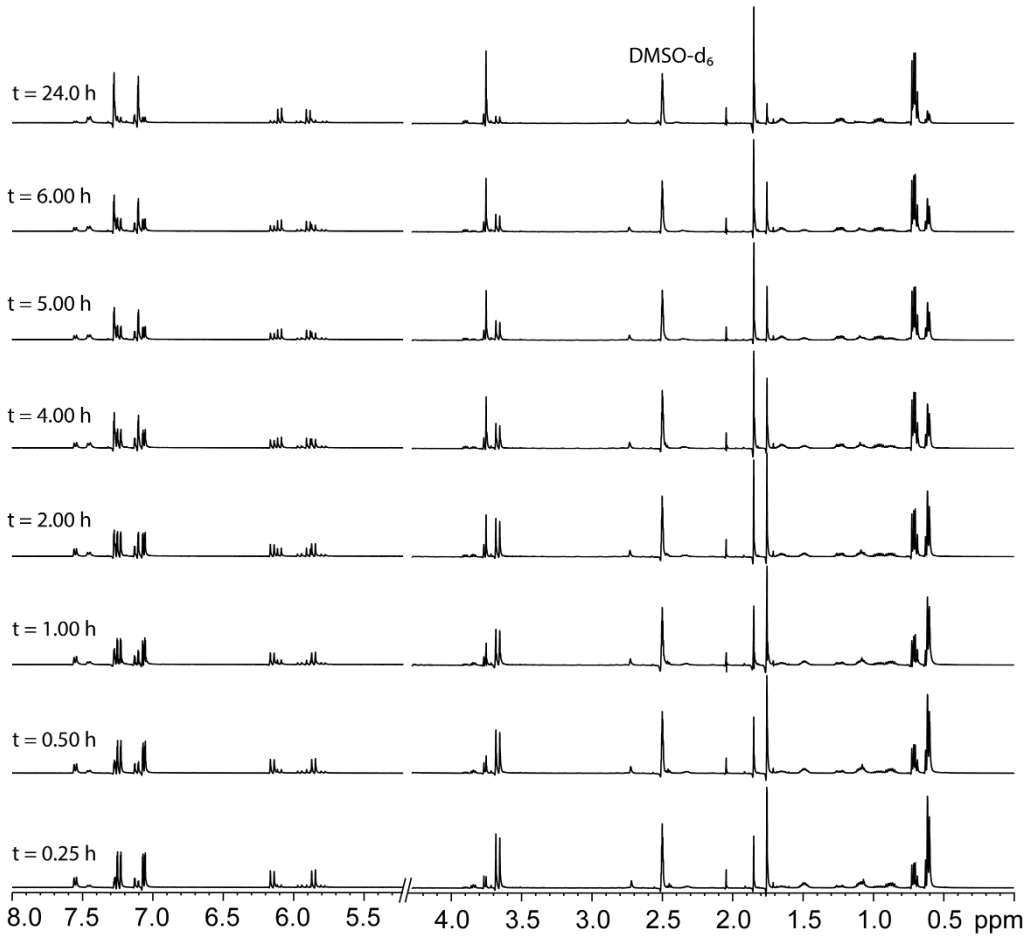

Figure A3.25. Selected ^{1}H NMR spectra (500.13 MHz) recorded for a solution of **3.13** in a mixture of water (76%), DMSO-d_6 (20%), and D_2O (4%) over a period of 24 h at 25.0 ± 0.1 °C.

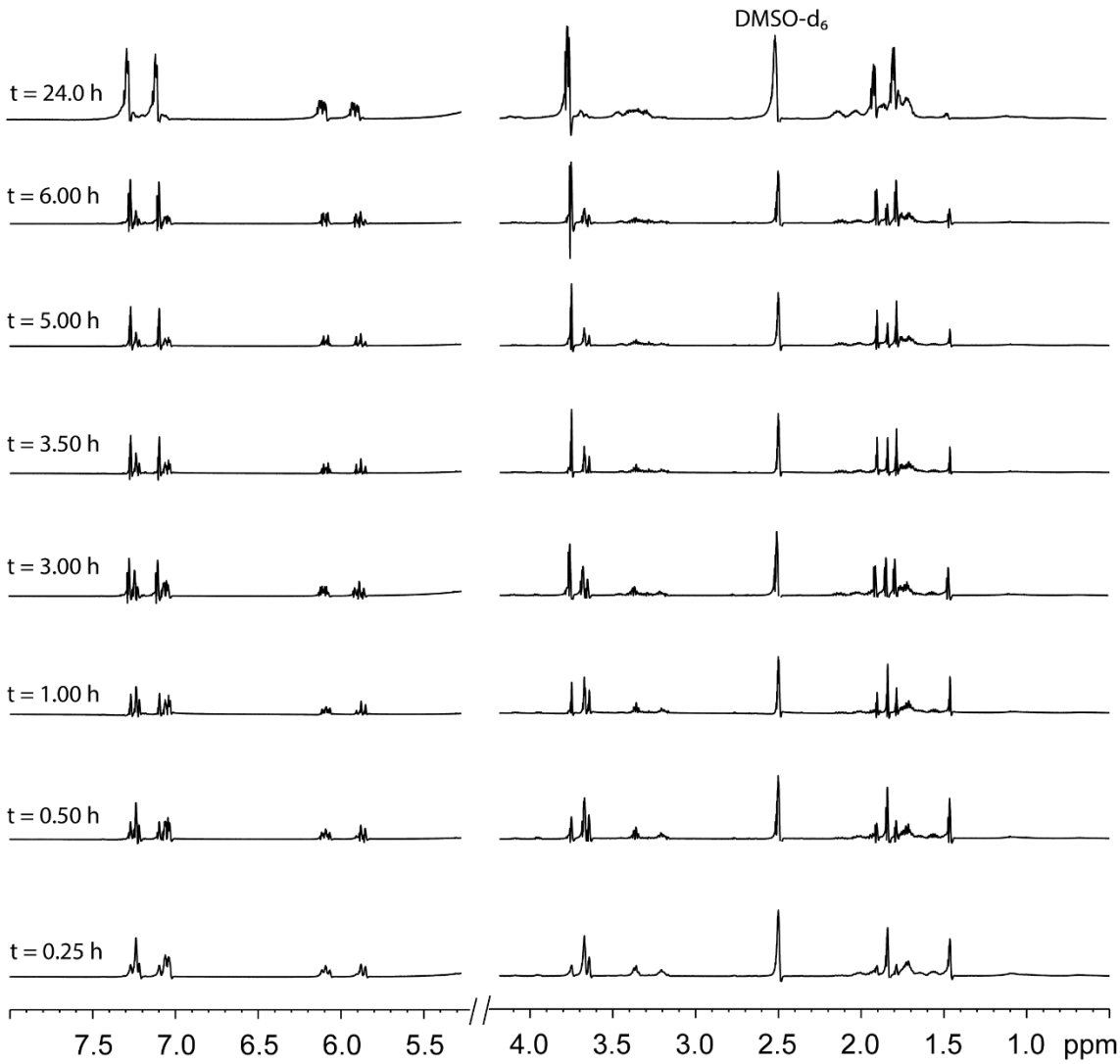

Figure A3.26. Selected ^{1}H NMR spectra (500.13 MHz) recorded for a solution of **3.14** in a mixture of water (76%), DMSO-d_6 (20%), and D_2O (4%) over a period of 24 h at 25.0 ± 0.1 °C.

3.3. High-Resolution Mass Spectra

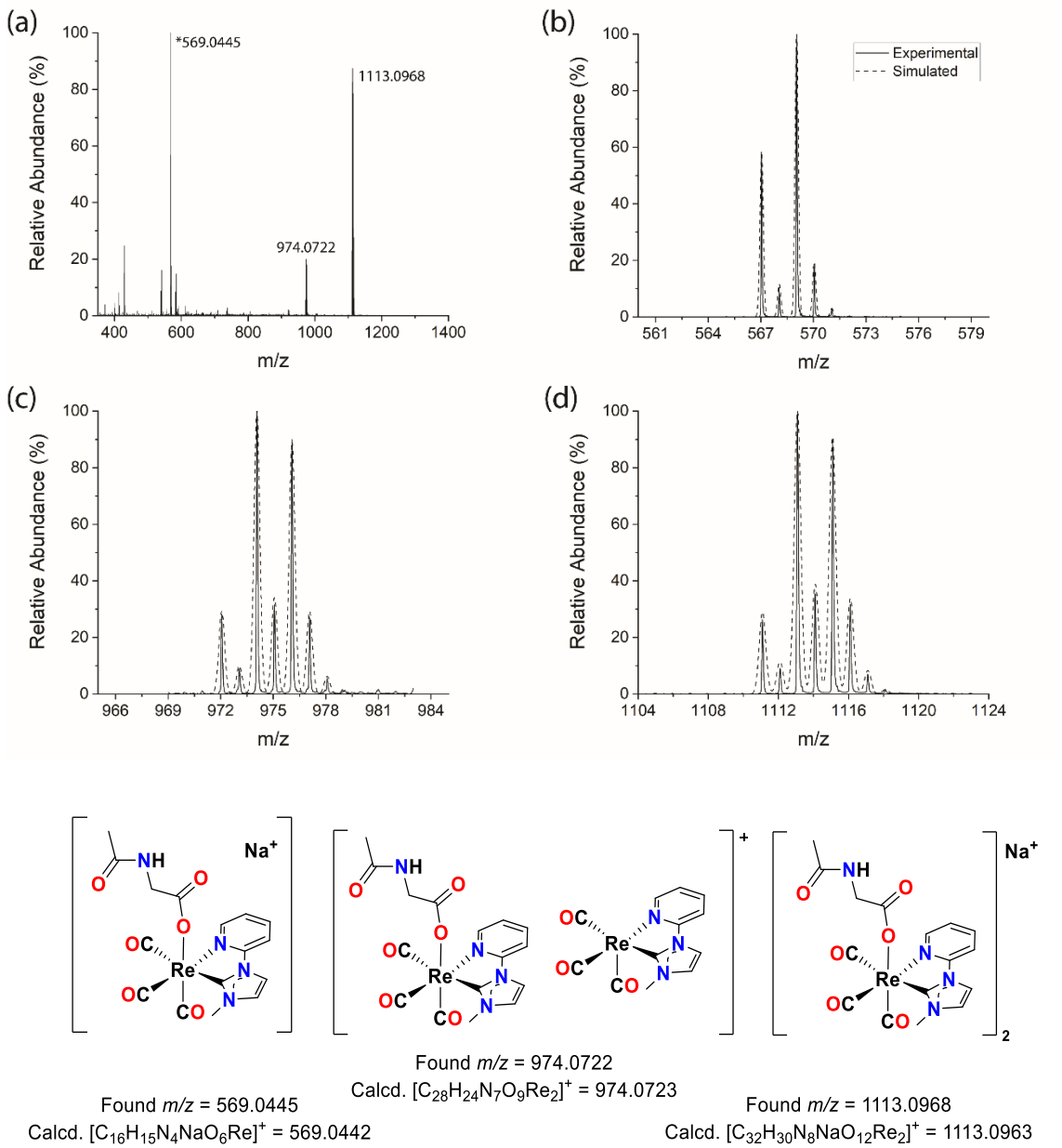

Figure A3.23. (a) HRMS spectrum of a freshly prepared solution of **3.8** in methanol. Each of the main signals from the HRMS spectrum is plotted together with the simulated isotopic distribution: (b) expanded signals at 569.0445, (c) expanded signals at 974.0722, and (d) expanded signals at 1113.0968. Lower panel, proposed structures of cations corresponding to these masses.

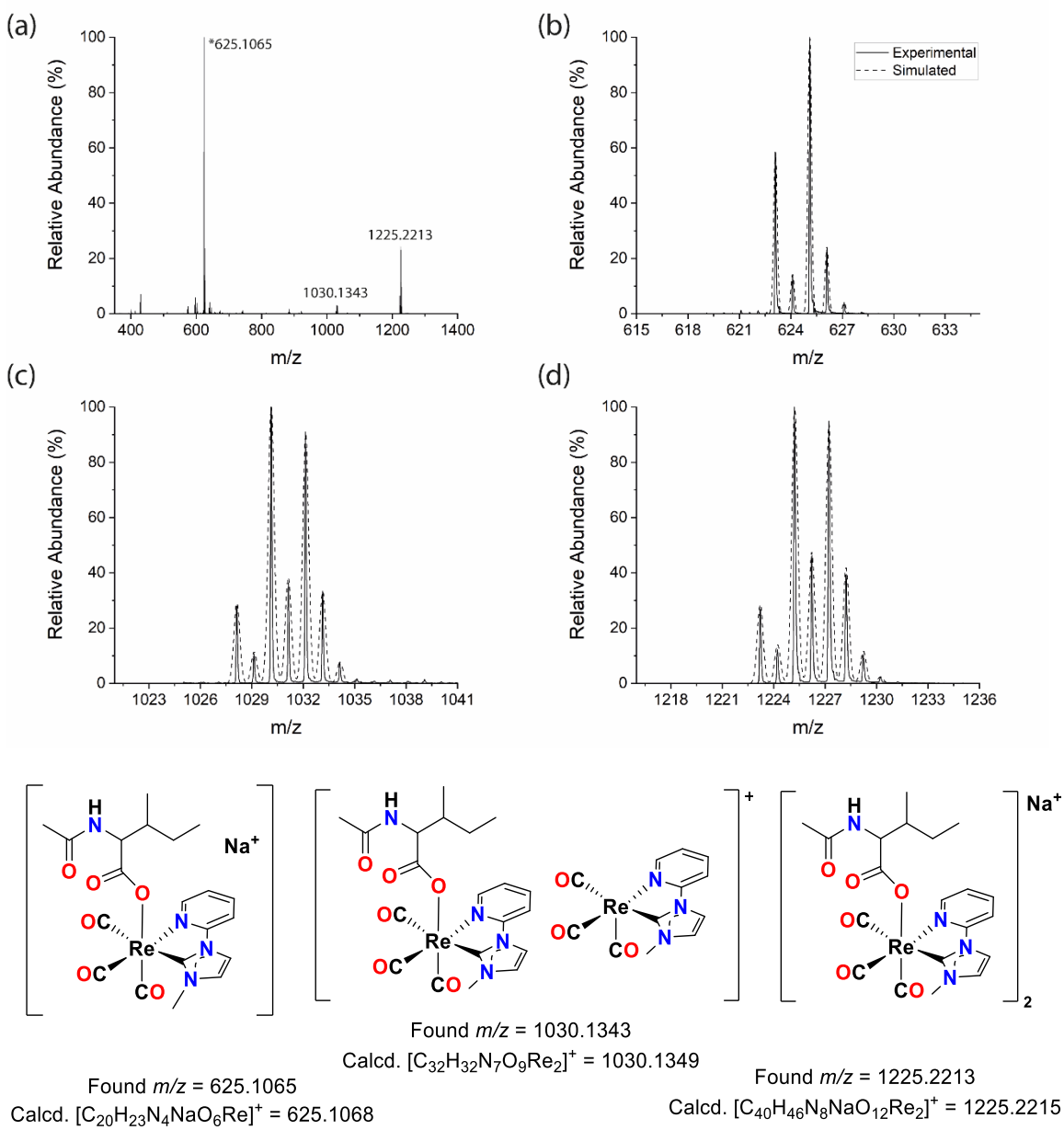

Figure A3.24. (a) HRMS spectrum of a freshly prepared solution of **3.9** in methanol. Each of the main signals from the HRMS spectrum is plotted together with the simulated isotopic distribution: (b) expanded signals at 625.1065, (c) expanded signals at 1030.1343, and (d) expanded signals at 1225.2213. Lower panel, proposed structures of cations corresponding to these masses.

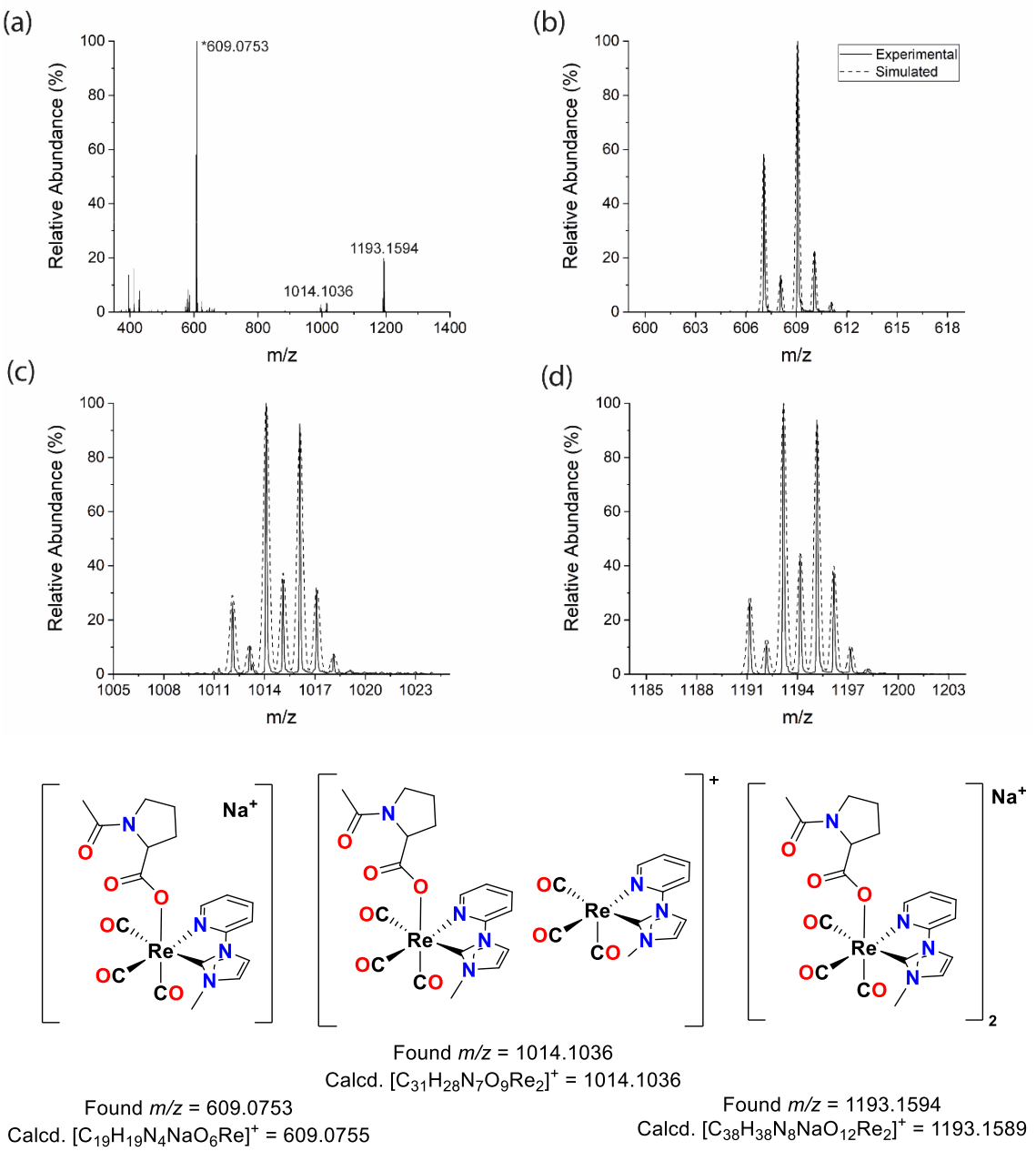

Figure A3.25. (a) HRMS spectrum of a freshly prepared solution of **3.10** in methanol. Each of the main signals from the HRMS spectrum is plotted together with the simulated isotopic distribution: (b) expanded signals at 609.0753, (c) expanded signals at 1014.1036, and (d) expanded signals at 1193.1594. Lower panel, proposed structures of cations corresponding to these masses.

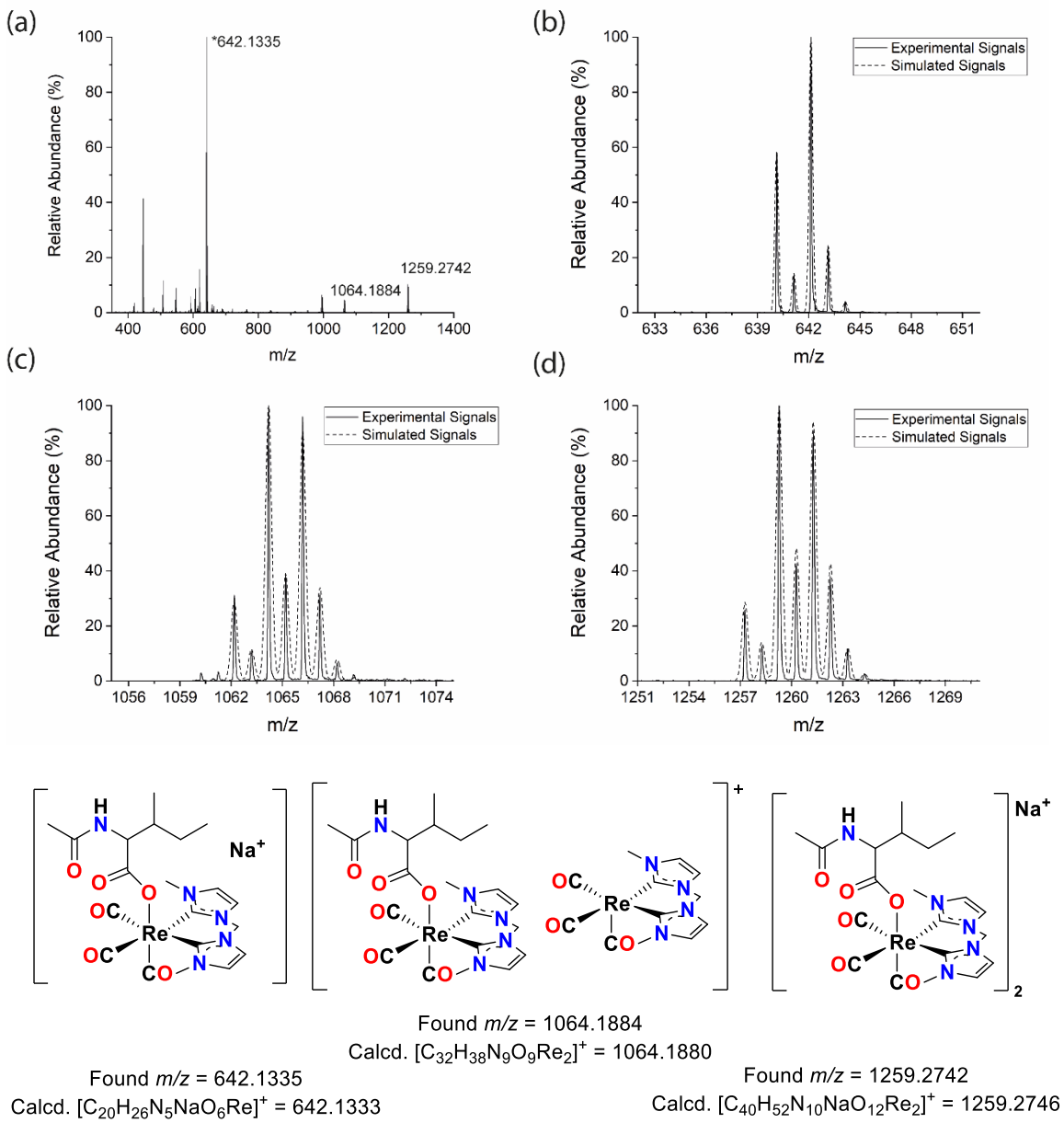

Figure A3.30. (a) HRMS spectrum of a freshly prepared solution of **3.13** in methanol. Each of the main signals from the HRMS spectrum is plotted together with the simulated isotopic distribution: (b) expanded signals at 642.1335, (c) expanded signals at 1064.1884, and (d) expanded signals at 1259.2742. Lower panel, proposed structures of cations corresponding to these masses.

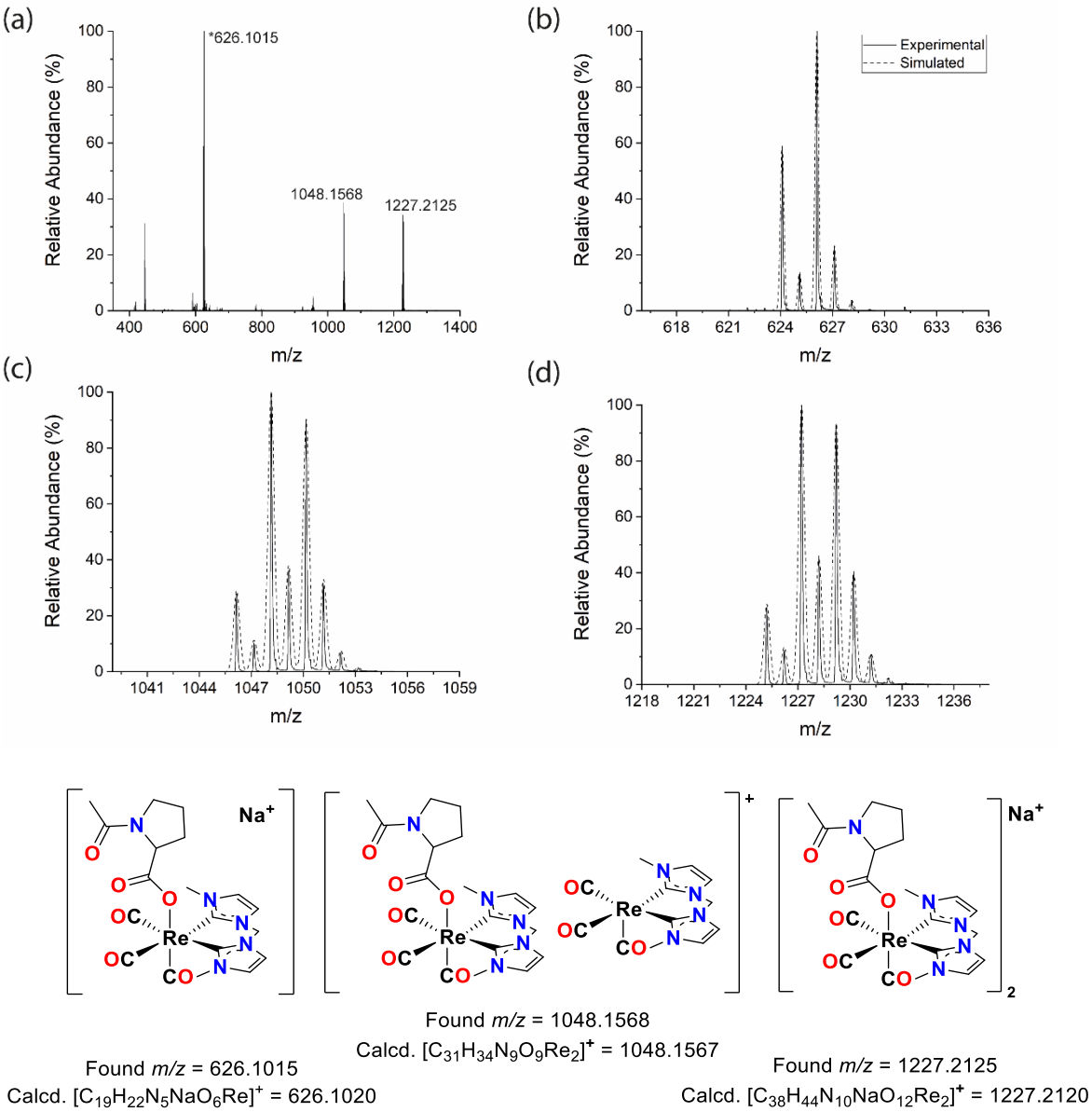

Figure A3.31. (a) HRMS spectrum of a freshly prepared solution of **3.14** in methanol. Each of the main signals from the HRMS spectrum is plotted together with the simulated isotopic distribution: (b) expanded signals at 626.1015, (c) expanded signals at 1048.1568, and (d) expanded signals at 1227.2125. Lower panel, proposed structures of cations corresponding to these masses.

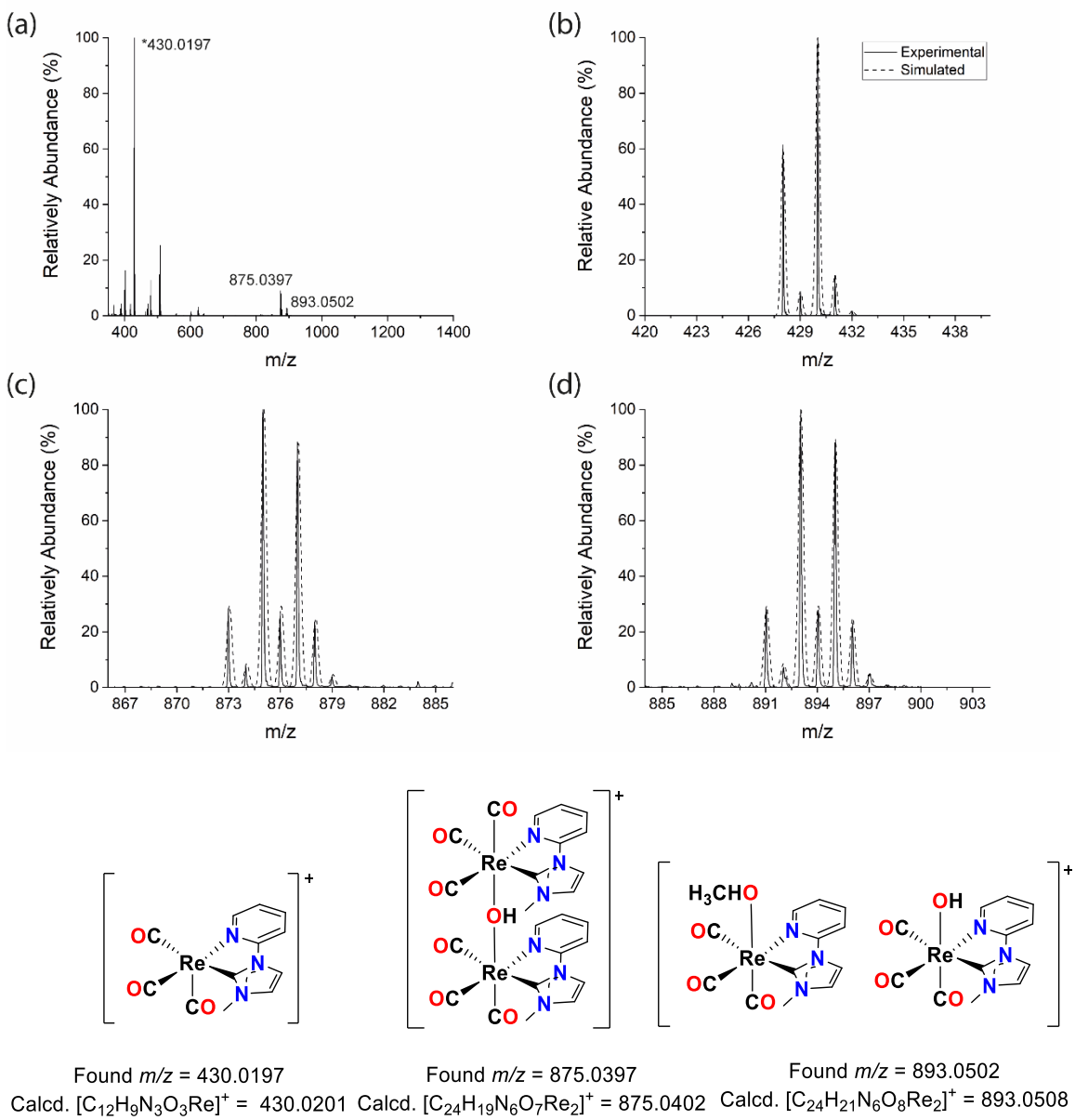

Figure A3.32. HRMS spectra of **3.9** from ^{1}H NMR WATERGATE sample after 24 h at 25.0 ± 0.1 ºC. (a) High-resolution mass spectrum of compound **3.9** after being subjected to the ^{1}H NMR time-course study for 24 h at 25.0 ± 0.1 °C. Zoom scans of the main signals at (b) 430.0197, (c) 875.0397 and (d) 893.0502 are plotted together with the simulated spectra for the formulas $[C_{12}H_9N_3O_3Re]^+$ (**3.17**), $[C_{24}H_{19}N_6O_7Re_2]^+$, $[C_{24}H_{21}N_6O_8Re_2]^+$, respectively. The structures of the compounds corresponding to these formulae are shown in the lower panel.

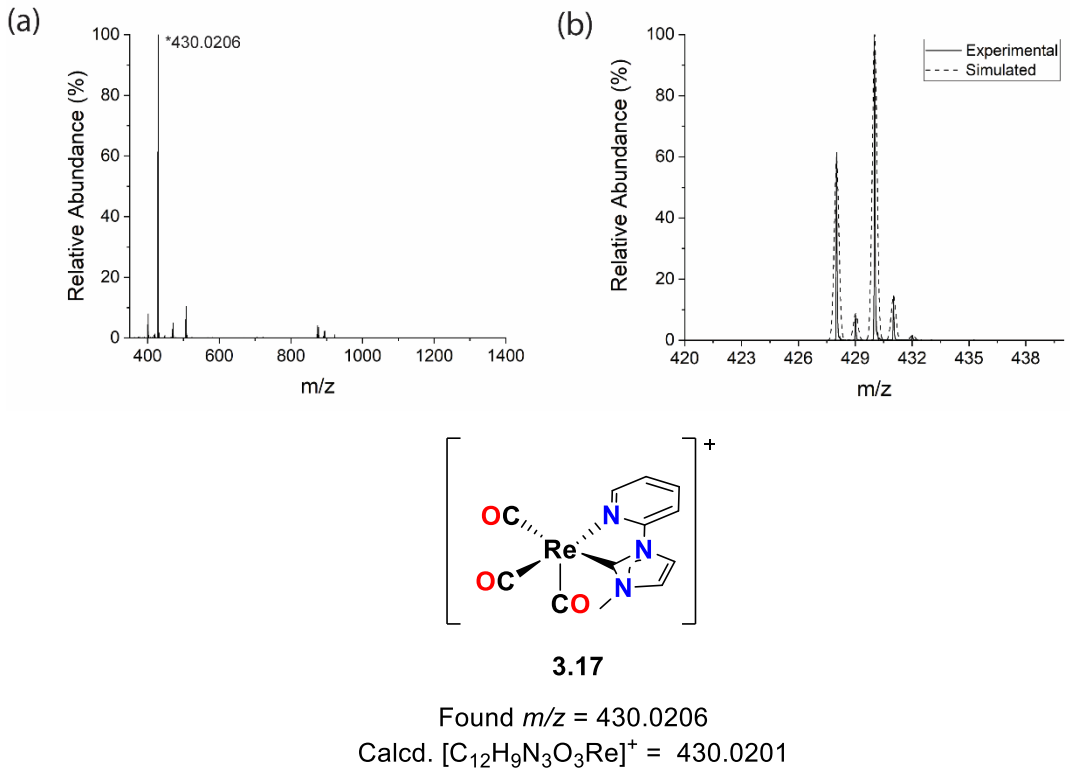

Figure A3.33. HRMS spectra of **3.10** from ^{1}H NMR WATERGATE sample after 24 h at 25.0 ± 0.1 ºC. (a) High-resolution mass spectrum of compound **3.10** after being subjected to the ^{1}H NMR time-course study for 24 h at 25.0 ± 0.1 °C. Zoom scans of the main signals at (b) 430.0206 is plotted together with the simulated spectra for the formulas $[C_{12}H_9N_3O_3Re]^+$ (**3.17**). The structure of the compound corresponding to this formula is shown in the lower panel.

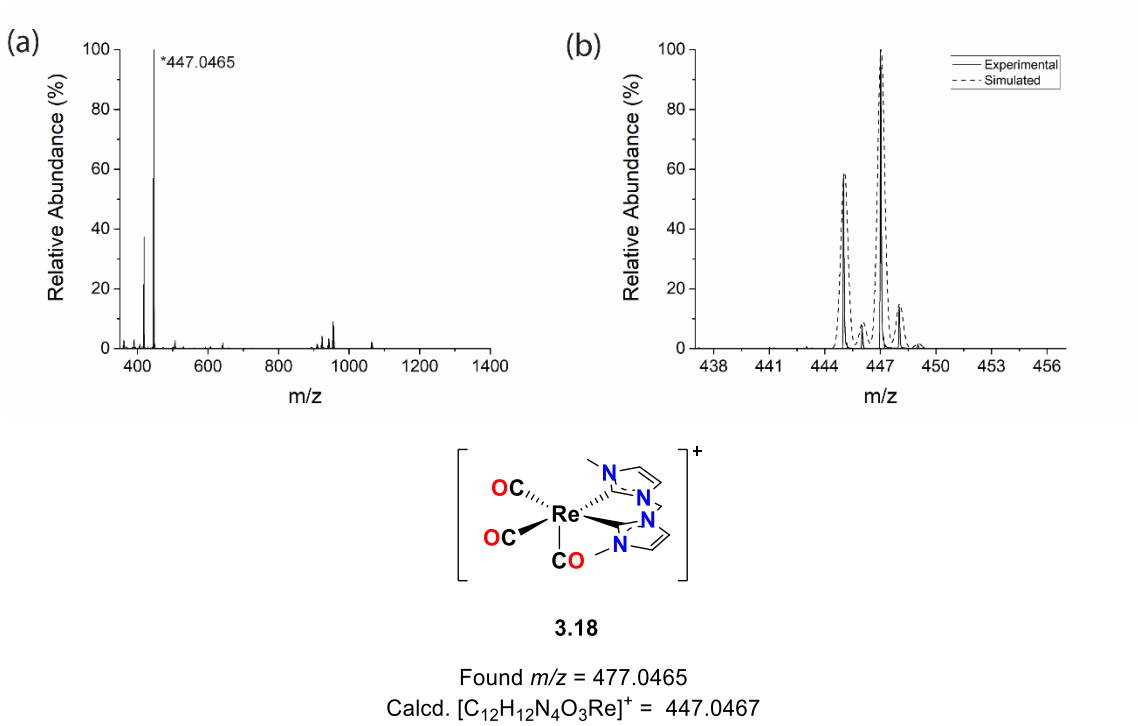

Figure A3.34. HRMS spectra of **3.13** from ^{1}H NMR WATERGATE sample after 24 h at 25.0 ± 0.1 ºC. (a) High-resolution mass spectrum of compound **3.13** after being subjected to the ^{1}H NMR time-course study for 24 h at 25.0 ± 0.1 °C. Zoom scans of the main signals at (b) 447.0465 is plotted together with the simulated spectra for the formulas $[C_{12}H_{12}N_4O_3Re]^+$ (**18**). The structure of the compound corresponding to this formula is shown in the lower panel.

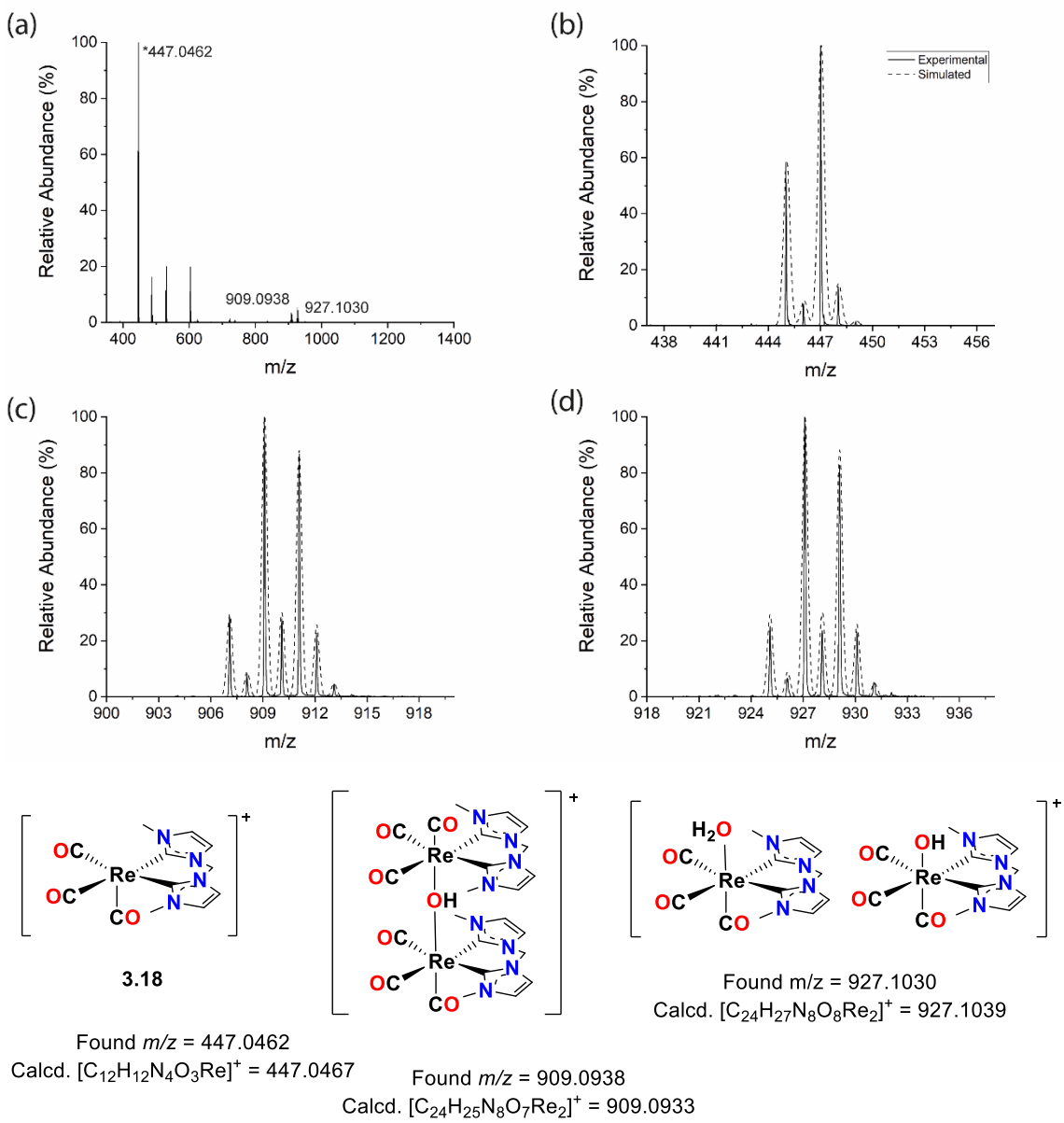

Figure A3.26. HRMS spectra of **3.14** from ^{1}H NMR WATERGATE sample after 24 h at 25.0 ± 0.1 ºC. (a) High-resolution mass spectrum of compound **3.14** after being subjected to the ^{1}H NMR time-course study for 24 h at 25.0 ± 0.1 °C. Zoom scans of the main signals at (b) 447.0462, (c) 909.0938 and (d) 927.1030 are plotted together with the simulated spectra for the formulas $[C_{12}H_{12}N_4O_3Re]^+$ (**3.18**), $[C_{24}H_{25}N_8O_7Re_2]^+$, $[C_{24}H_{27}N_8O_8Re_2]^+$, respectively. The structures of the compounds corresponding to these formulae are shown in the lower panel.

3.4. Computational Studies

Table A3.1. Re-O bond dissociation energies (kcal mol^{-1}), Re-O bond length (Å) and QTAIM bonding parameter (a.u.) for $[Re(CO)_3LH_2O]^+$.

	BDE ΔG^{298K}	Bond Length	ρ	2ρ	H	G	V	Laplacian Bond Order
L^1	16.1	2.352	0.0461	0.2301	-0.0029	0.0604	-0.0634	0.079826
L^2	15.0	2.362	0.0449	0.2281	-0.0025	0.0595	-0.0621	0.073491
L^{2i}	12.8	2.358	0.0444	0.2295	-0.002	0.0594	-0.0614	0.079015

Table A3.2. Re-O bond dissociation energies (kcal mol^{-1}), Re-O bond length (Å) and QTAIM bonding parameter (a.u.) for complexes **3.7**-**3.14**.

	BDE ΔG^{298K}_{solv}	Bond Length	ρ	2ρ	H	G	V	Laplacian Bond Order
3.7	25.9	2.138	0.0849	0.3515	-0.0198	0.1077	-0.1274	0.192863
3.8	22.6	2.163	0.0800	0.3284	-0.0177	0.0998	-0.1170	0.170943
3.9	23.0	2.139	0.0847	0.3503	-0.0196	0.1072	-0.1268	0.191173
3.10	27.1	2.144	0.0826	0.3490	-0.0182	0.1056	-0.1238	0.186384
3.11	22.9	2.161	0.0804	0.3327	-0.0176	0.1001	-0.1185	0.175456
3.12	19.71	2.176	0.0769	0.3221	-0.0159	0.0964	-0.1124	0.168519
3.13	20.09	2.173	0.0772	0.3242	-0.0159	0.0969	-0.1129	0.162441
3.14	24.17	2.178	0.0762	0.3223	-0.0155	0.0961	-0.1115	0.169363
3.11i	21.99	2.163	0.0784	0.3349	-0.0160	0.0997	-0.1158	0.176933
3.12i	18.74	2.184	0.0744	0.3176	-0.0144	0.0938	-0.1083	0.165843
3.13i	17.76	2.172	0.0762	0.3279	-0.0149	0.0969	-0.1120	0.167466
3.14i	24.11	2.176	0.0756	0.3253	-0.0148	0.0961	-0.1109	0.169424

(a)

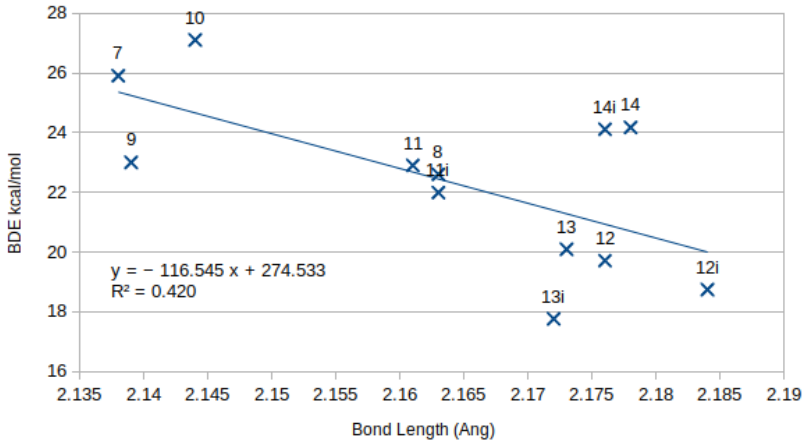

(b)

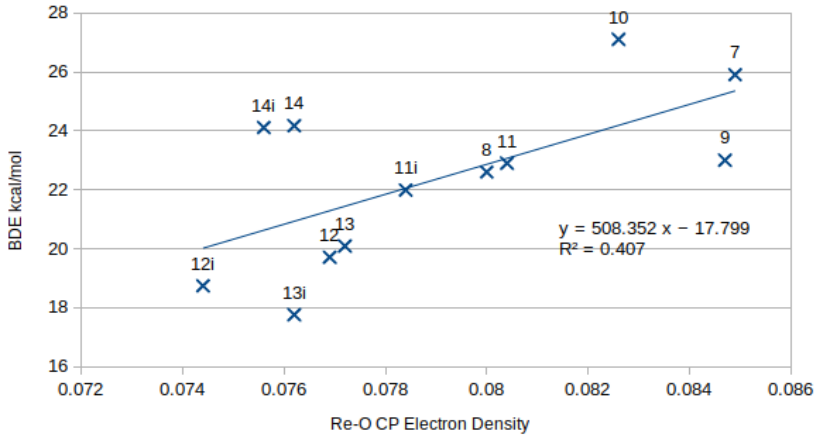

(c)

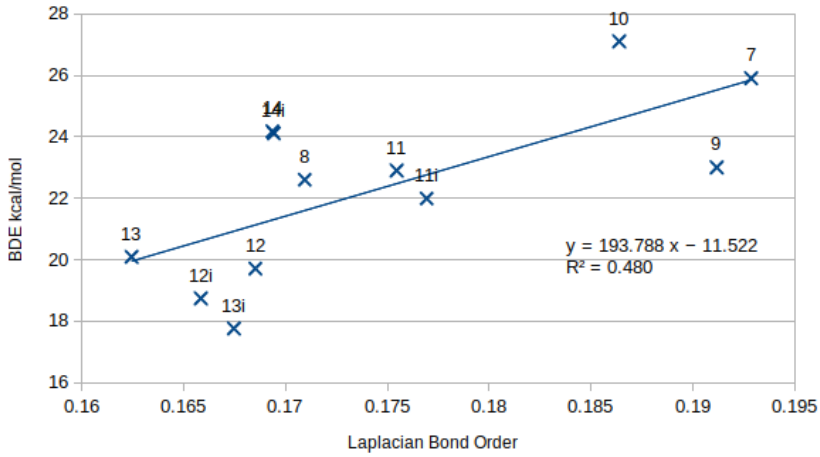

Figure A3.27. (a) Relationship between Bond Dissociation Energy and Re-O bond length, (b) critical point electron density and (c) Laplacian Bond Order for complexes **3.17-3.14**.

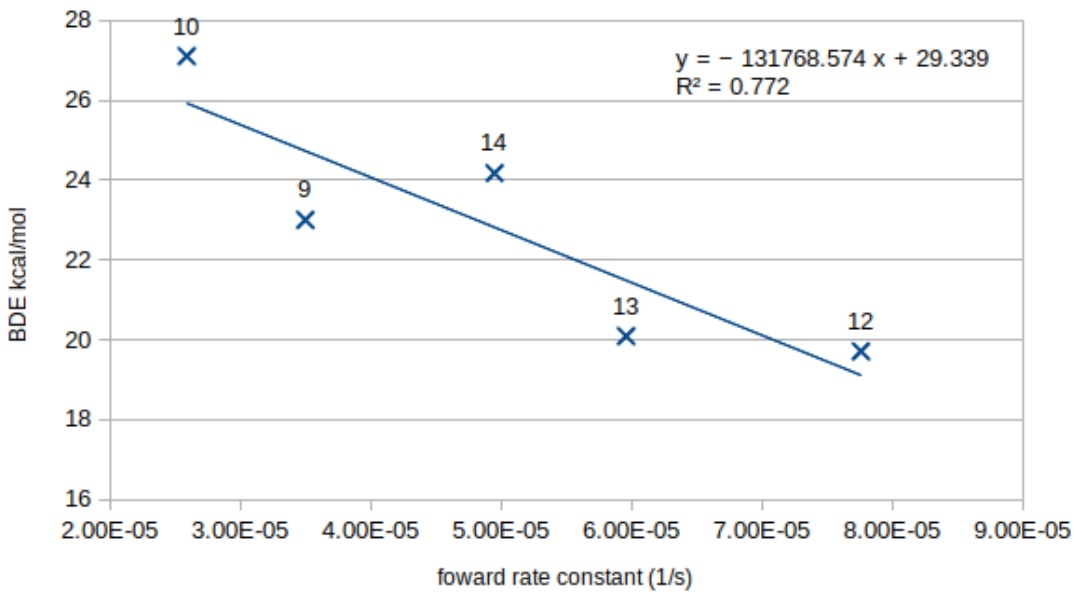

Figure A3.28. Re-O bond dissociation energy as a function of observed forward rate constant.

3.5. Ligand Exchange Studies

^{1}H NMR WATERGATE study of compound **3.9**, **3.10**, **3.12**, **3.13** and **3.14** with H_2O to give a cationic water adduct complex e.g. [**3.12**H_2O]$^+$ + *N*-acetylGly$^-$.

NMR experiments. A solution of each complex with a known concentration (0.00337 M) was prepared in 0.50 mL of a solvent mixture consisting of 0.380 mL H_2O, 0.100 mL DMSO-d_6, and 0.020 mL D_2O. The reaction was monitored by 500 Hz ^{1}H NMR spectroscopy.

Data analysis. The kinetic analysis was performed by calculating the relative concentration of the species present at each time point, based on the relative integrals for each proton resonance (e.g., carbene backbone proton signal) in the ^{1}H NMR spectra (see Figure 3.7). A pseudo-first order model was used to fit the data, in which the complex reacts with one mol equivalent of H_2O to form the cationic product (e.g. [**3.12**H_2O]$^+$).

The kinetic model is provided below, and the forward and reverse rate constants (k_1 and k_{-1}) were determined using a non-linear optimisation procedure of Scientist® (Version 3.0, MicroMath, Inc.).

$$\text{Re-}N\text{-acetyl amino acid} + H_2O \underset{k_{-1}}{\overset{k_1}{\rightleftharpoons}} [\text{Re-}H_2O]^+ + N\text{-acetyl amino acid}^- \quad (H_2O \text{ in large excess}) \tag{1}$$

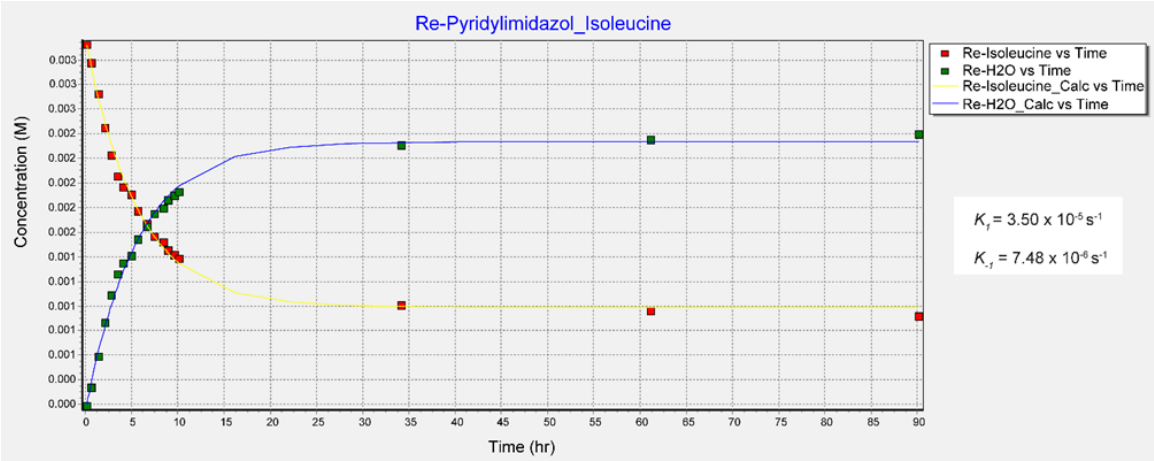

Figure A3.29. A plot of the time dependence of species (**3.9** and **3.15**) observed in the reaction of **3.9** with H_2O according to Equation (1). Concentrations derived from the integration of a pyridyl group proton. The curves are best fits using the model shown in Scheme A3.1. The pseudo-first order rate constants for the forward k_1 and reverse reaction k_{-1} are 3.50×10^{-5} s^{-1} ± 0.004 and 7.48×10^{-6} s^{-1} ± 0.004, respectively.

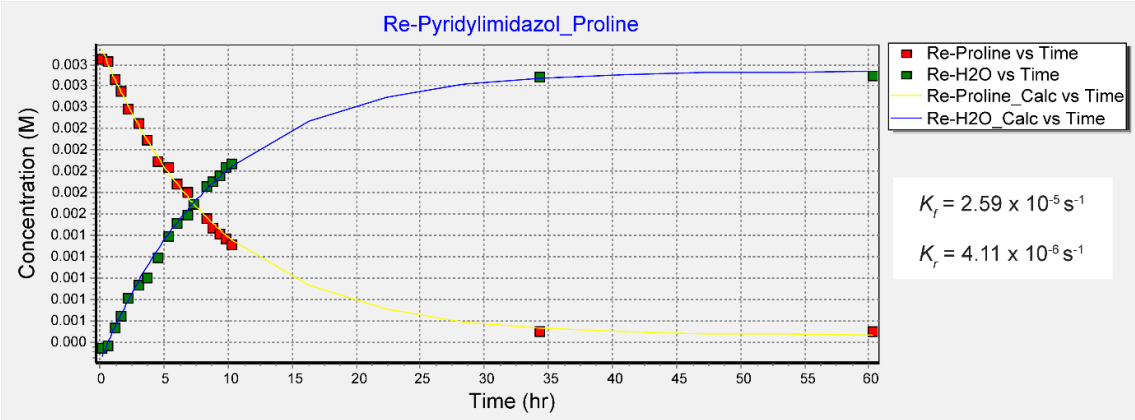

Figure A3.30. A plot of the time dependence of species (**3.10** and **3.15**) observed in the reaction of **3.10** with H_2O according to Equation (1). Concentrations derived from the integration of a pyridyl group proton. The curves are best fits using the model shown in Scheme A3.1. The pseudo-first order rate constants for the forward k_1 and reverse reaction k_{-1} are 2.59×10^{-5} s^{-1} ± 0.003 and 4.11×10^{-6} s^{-1} ± 0.003, respectively.

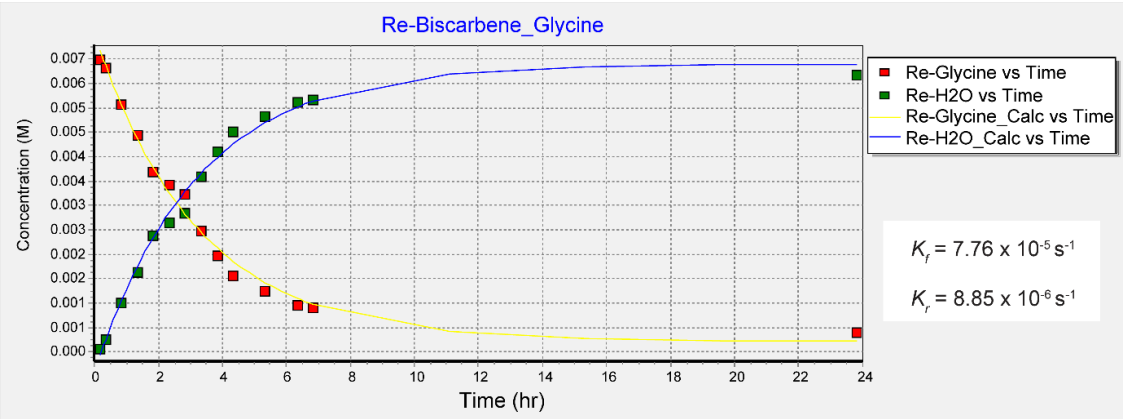

Figure A3.40. A plot of the time dependence of species (**3.12** and **3.16**) observed in the reaction of **3.12** with H_2O according to Equation (1). Concentrations derived from the integration of a carbene proton. The curves are best fits using the model shown in Scheme A3.1. The pseudo-first order rate constants for the forward k_1 and reverse reaction k_{-1} are 7.76×10^{-5} s^{-1} ± 0.044 and 8.85×10^{-6} s^{-1} ± 0.044, respectively.

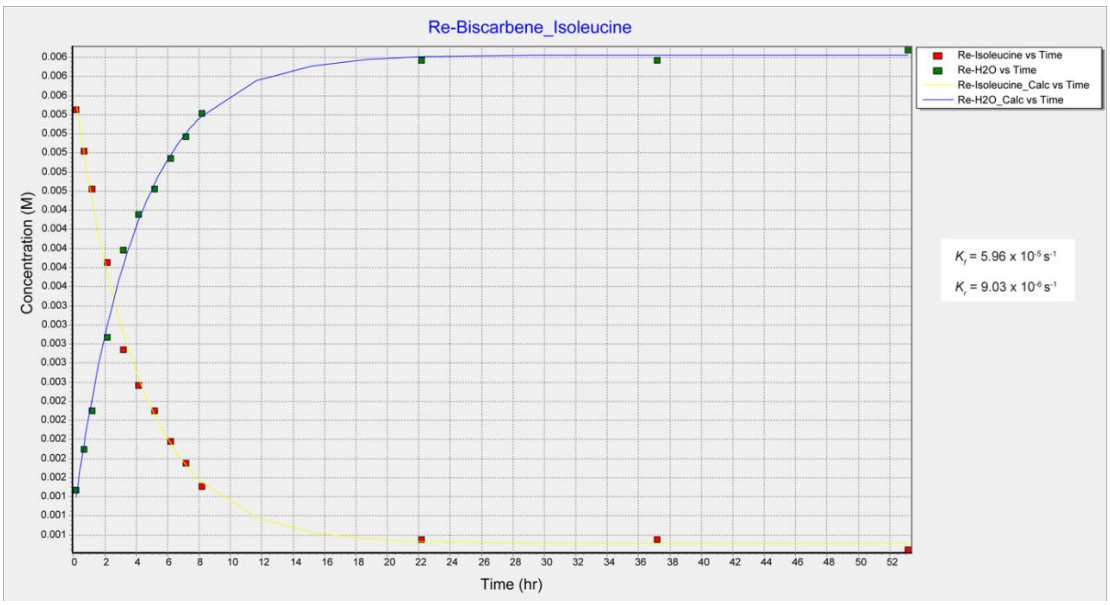

Figure A3.41. A plot of the time dependence of species (**3.13** and **3.16**) observed in the reaction of **3.13** with H_2O according to Equation (1). Concentrations derived from the integration of a carbene proton. The curves are best fits using the model shown in Scheme A3.1. The pseudo-first order rate constants for the forward k_1 and reverse reaction k_{-1} are 5.96×10^{-5} s^{-1} ± 0.007 and 9.03×10^{-6} s^{-1}± 0.007, respectively.

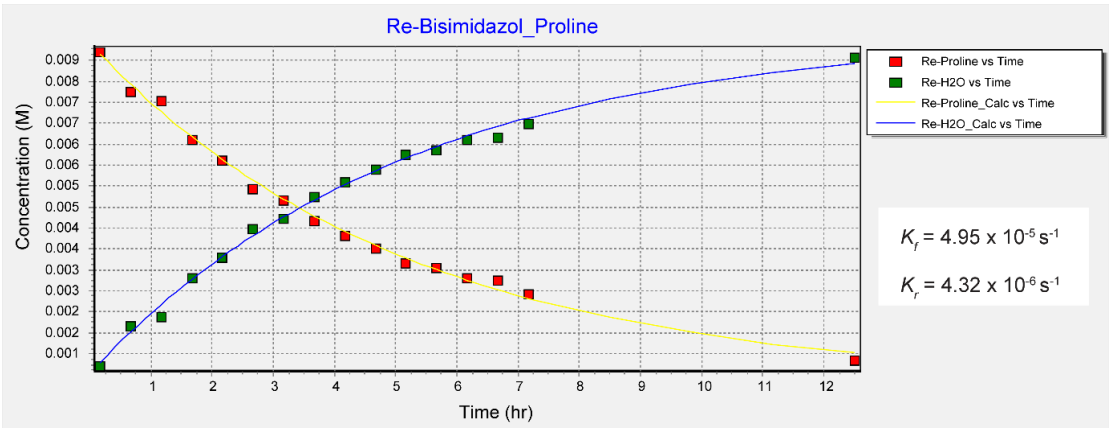

Figure A3.42. A plot of the time dependence of species (**3.14** and **3.16**) observed in the reaction of **3.14** with H_2O according to Equation (1). Concentrations derived from the integration of a carbene proton. The curves are best fits using the model shown in Scheme A3.1. The pseudo-first order rate constants for the forward k_1 and reverse reaction k_{-1} are 4.95×10^{-5} s^{-1} ± 0.027 and 4.32×10^{-6} s^{-1} ± 0.027, respectively.

Scheme A3.1. Scientist® model: Reaction of Re(I) complexes with H_2O

```
// MicroMath Scientist Model File

IndVars: T

DepVars: A, P

Params: AO, PO, KF, KR

A = (KR*(AO+PO)+(KF*AO-KR*PO)*EXP((-(KF+KR))*T))/(KF+KR)

P = (KF*(AO+PO)-(KF*AO-KR*PO)*EXP((-(KF+KR))*T))/(KF+KR)

// Representative initial conditions

T=30 min, AO=0. 0.00711 M, PO=0 M
```

KF=*Kf*

KR=*Kr*

T=first time point

AO=initial concentration of Re-Glycine

PO=initial concentration of Re-H_2O

3.6. Photophysical Studies

Table A3.3. UV-visible absorption and fluorescence spectroscopic data for compounds: starting Re(I) complex (**3.1**-**3.2**), Re(I) pyridyl-imidazolium complex (**3.9**-**3.10**), and Re(I) *bis*-imidazolium complex (**3.13**-**3.14**). All complexes were recorded at 10 μM in methanol solution.

Compound	λ_{max}/nm (ε/$M^{-1}cm^{-1}$)	Photoluminescence λ_{max}/nm
3.1	337 (7483), 271sh (11257)	385
3.2	312 (7096), 352sh (1765)	391
3.9	339 (5198), 271sh (8016)	380, 495
3.10	338 (5378), 270sh (8248)	393, 500
3.13	308 (11050), 350sh (2309)	388
3.14	309 (6361), 346sh (1675)	391

Appendix 4 : For Chapter 4

4.1. Ligand Exchange Studies

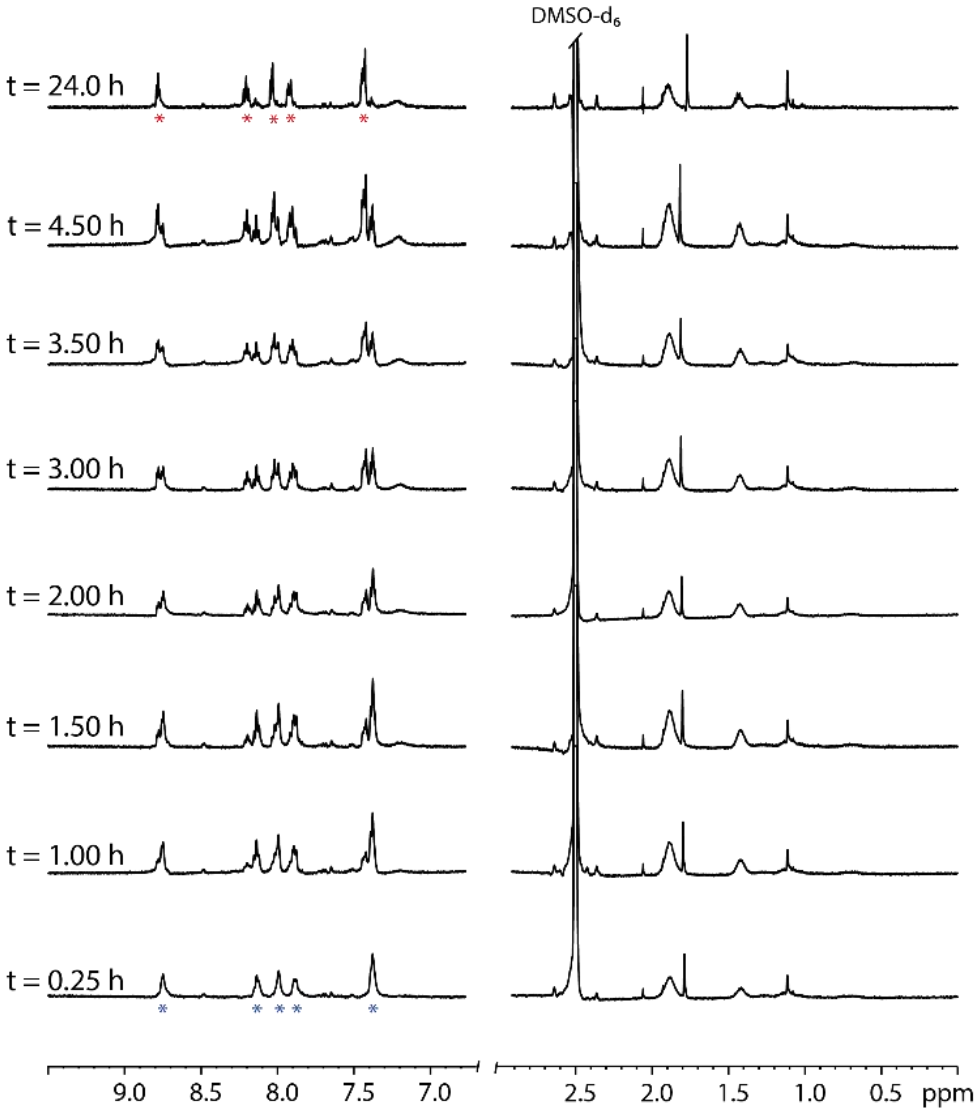

Figure A4.1. ^{1}H NMR spectra (500 MHz) recorded for a solution of **4.30** in water over a period of 24 h at 25.0 ± 0.1 °C showing the dissociation of chloride ligand for a water molecule.

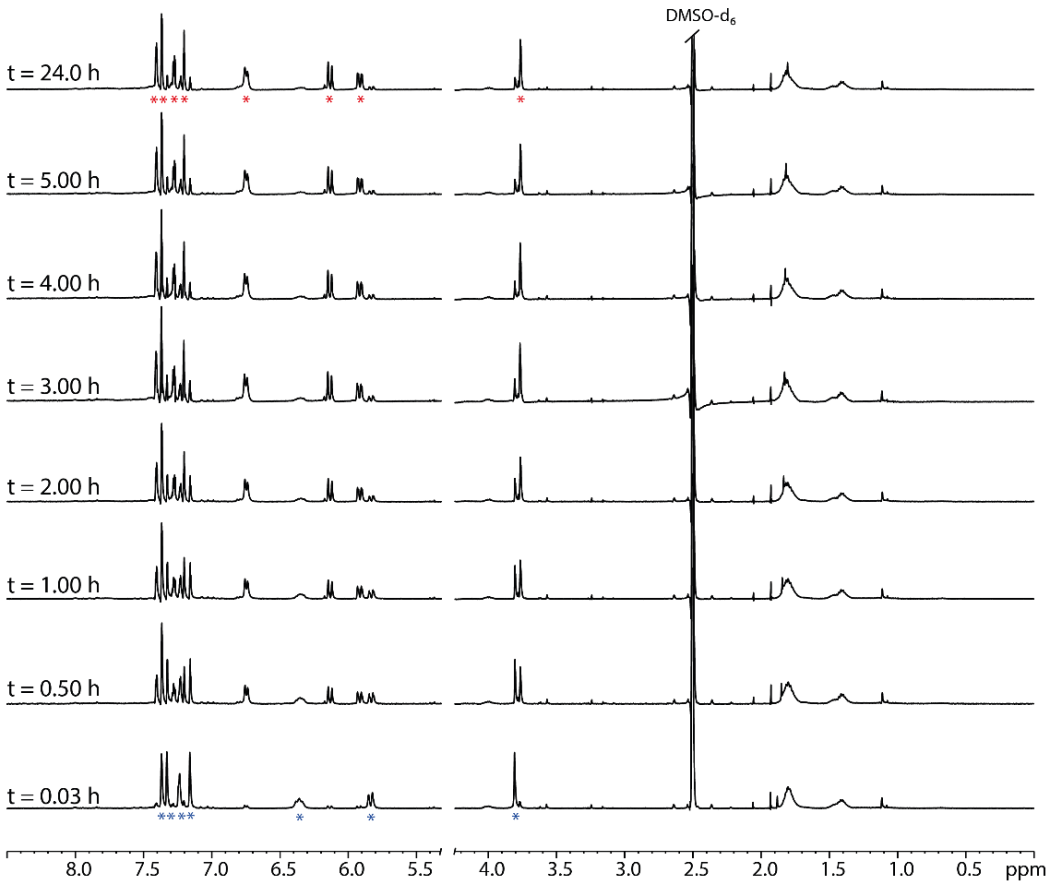

Figure A4.2. ^{1}H NMR spectra (500 MHz) recorded for a solution of **4.31** in water over a period of 24 h at 25.0 ± 0.1 °C showing the dissociation of chloride ligand for a water molecule.

NMR experiments. A solution of each complex with a known concentration (0.00172 M) was prepared in 0.50 mL of a solvent mixture consisting of 0.280 mL H_2O, 0.200 mL DMSO-d_6, and 0.020 mL D_2O. The reaction was monitored by 500 Hz ^{1}H NMR spectroscopy.

^{1}H NMR WATERGATE study of compound **4.30** and **4.31** with H_2O to give a cationic aqua complex e.g. [**4.30**H_2O]$^+$ + Cl^-.

Data analysis. The kinetic analysis was performed by calculating the relative concentration of the species present at each time point, based on the relative integrals for each proton resonance (e.g. carbene backbone proton signal) in the ^{1}H NMR spectra (see Figure A4.1 and Figure A4.2). A pseudo-first-order model was used to fit the data, in which the complex reacts with one mole equivalent of H_2O to form the cationic product (e.g. [**4.30**$(H_2O)_2$]$^+$).

The kinetic model is provided below, and the forward and reverse rate constants (k_1 and k_{-1}) were determined using a non-linear optimisation procedure of Scientist® (Version 3.0, MicroMath, Inc.).

$$Re_2Cl_2 + 2H_2O \underset{k_{-1}}{\overset{k_1}{\rightleftharpoons}} [Re_2(H_2O)_2]^{2+} + 2Cl^- \quad (H_2O \text{ in large excess}) \tag{1}$$

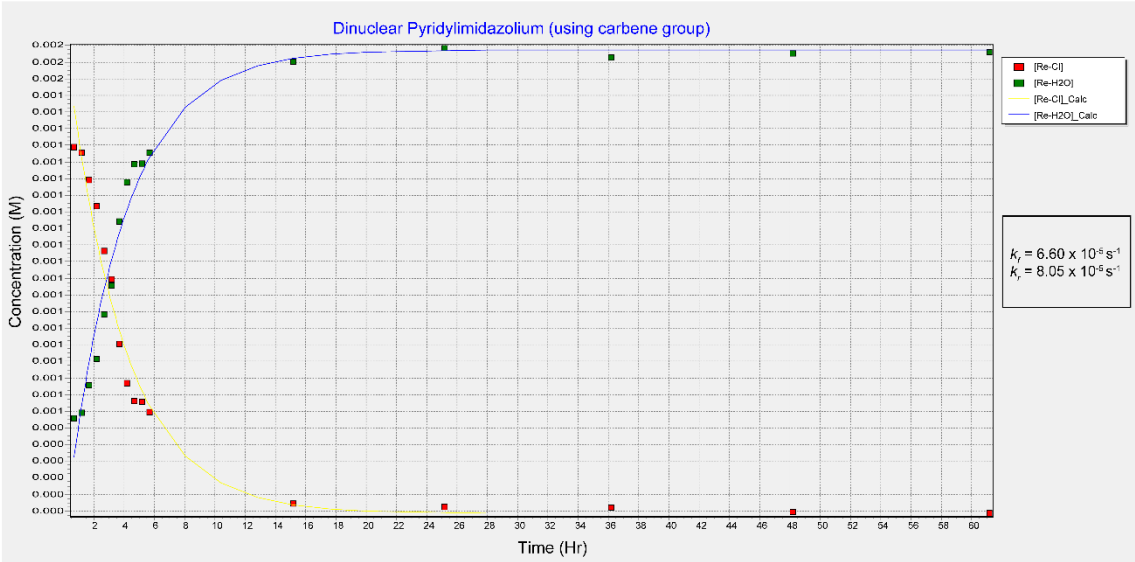

Figure A4.3. Plot of the time dependence of species (**4.30**Cl_2 and [**4.30**$(H_2O)_2]^+$) observed in the reaction of **4.30** with H_2O according to Equation (1). Concentrations derived from the integration of a carbene group proton. The curves are best fits using the model shown in Scheme A4.1. The pseudo-first order rate constants for the forward k_1 and reverse reaction k_{-1} are 6.60×10^{-5} s^{-1} ± 0.004 and 8.05×10^{-5} s^{-1} ± 0.004, respectively.

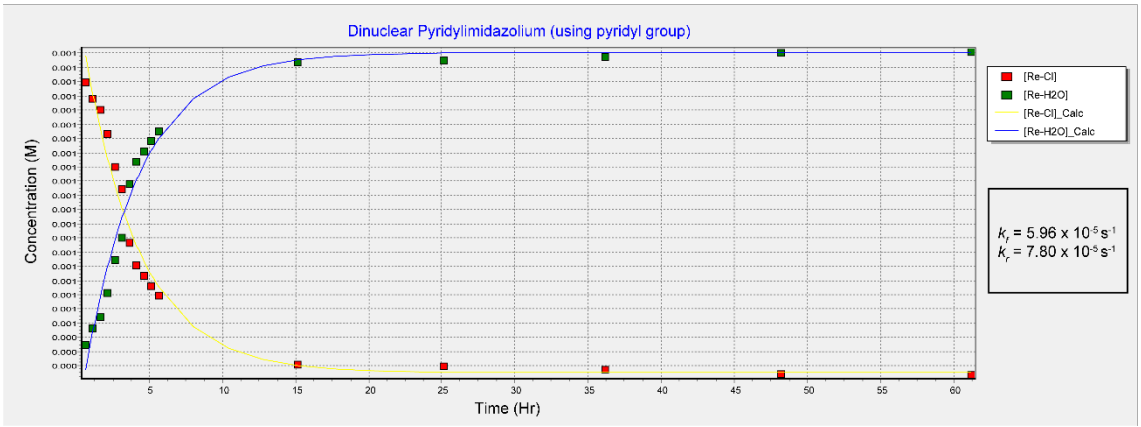

Figure A4.4. Plot of the time dependence of species (**4.30**Cl_2 and [**4.30**$(H_2O)_2]^+$) observed in the reaction of **4.30** with H_2O according to Equation (1). Concentrations derived from the integration of a pyridyl group proton. The curves are best fits using the model shown in Scheme A4.1. The pseudo-first order rate constants for the forward k_1 and reverse reaction k_{-1} are 5.96×10^{-5} s^{-1} ± 0.001 and 7.80×10^{-5} s^{-1} ± 0.001, respectively.

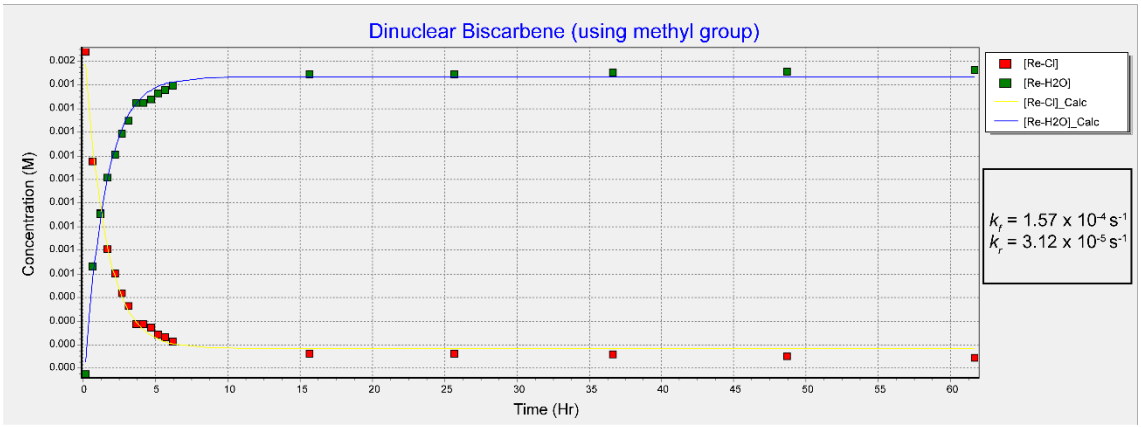

Figure A4.5. Plot of the time dependence of species (**4.31**Cl_2 and [**4.31**$(H_2O)_2]^+$) observed in the reaction of **4.31** with H_2O according to Equation (1). Concentrations derived from the integration of a methyl group proton. The curves are best fits using the model shown in Scheme A4.1. The pseudo-first order rate constants for the forward k_1 and reverse reaction k_{-1} are 1.57×10^{-4} $s^{-1} \pm 0.004$ and 3.12×10^{-5} $s^{-1} \pm 0.004$, respectively.

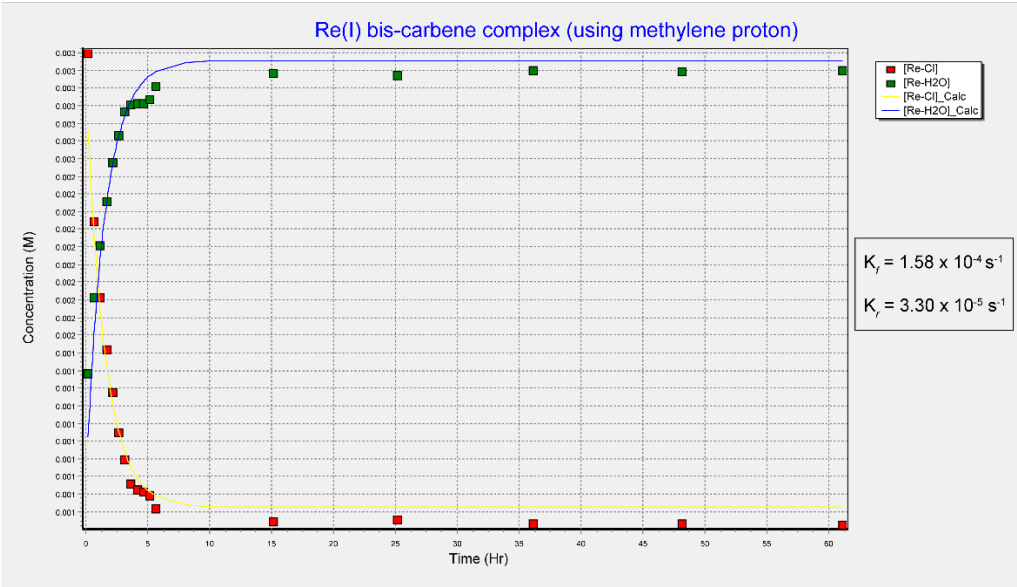

Figure A4.6. Plot of the time dependence of species (**4.31**Cl_2 and [**4.31**$(H_2O)_2]^+$) observed in the reaction of **4.31** with H_2O according to Equation (1). Concentrations derived from the integration of a methylene group proton. The curves are best fits using the model shown in Scheme A4.1. The pseudo-first order rate constants for the forward k_1 and reverse reaction k_{-1} are 1.58×10^{-4} $s^{-1} \pm 0.002$ and 3.30×10^{-5} $s^{-1} \pm 0.002$, respectively.

Scheme A4.1: Scientist® model: Reaction of Re(I) complexes with H_2O

// MicroMath Scientist Model File

IndVars: T

DepVars: A, P

Params: AO, PO, KF, KR

A = (KR*(AO+PO)+(KF*AO-KR*PO)*EXP((-(KF+KR))*T))/(KF+KR)

P = (KF*(AO+PO)-(KF*AO-KR*PO)*EXP((-(KF+KR))*T))/(KF+KR)

// Representative initial conditions

T=30 min, AO=0. 0.00178 M, PO=0 M

KF=*Kf*

KR=*Kr*

T=first time point

AO=initial concentration of Re-Glycine

PO=initial concentration of Re-H_2O

4.2. Photophysical Studies

Table A4.1. UV-visible absorption and fluorescence spectroscopic data for compounds: **4.30**, **4.31**, and **4.35** in 10% dimethyl sulfoxide and 90% methanol solutions (10 µM).

Compound (Solvent)	λ_{max}/nm (ε/M^{-1} cm^{-1})	Photoluminescence λ_{max}/nm
4.30	334 (9129)	383
4.31	312 (11795)	393
4.35	340 (10550)	391
4.36	309 (7420)	-

4.3. NMR Spectra

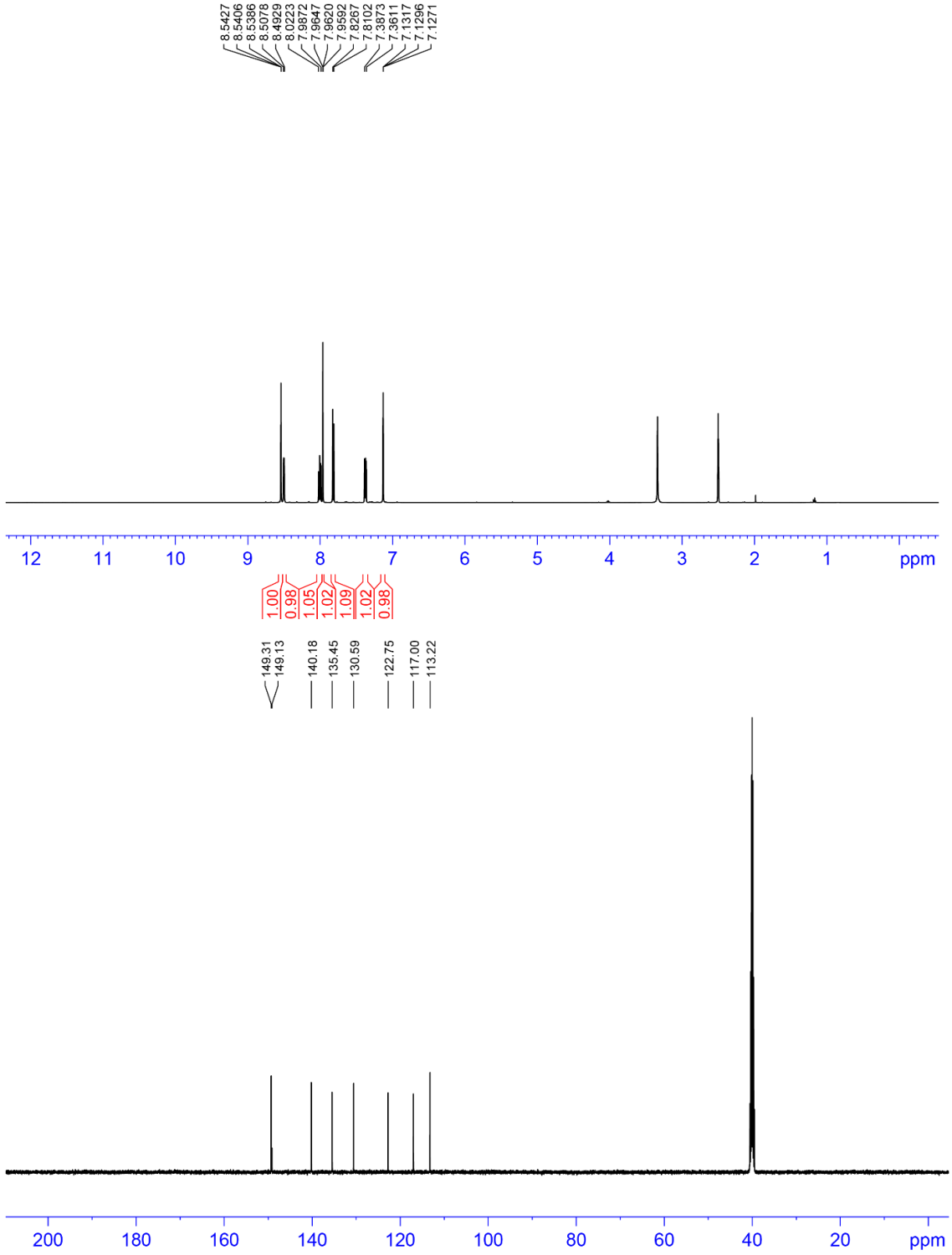

Figure A4.7. ^{1}H and ^{13}C NMR spectra for **4.25**.

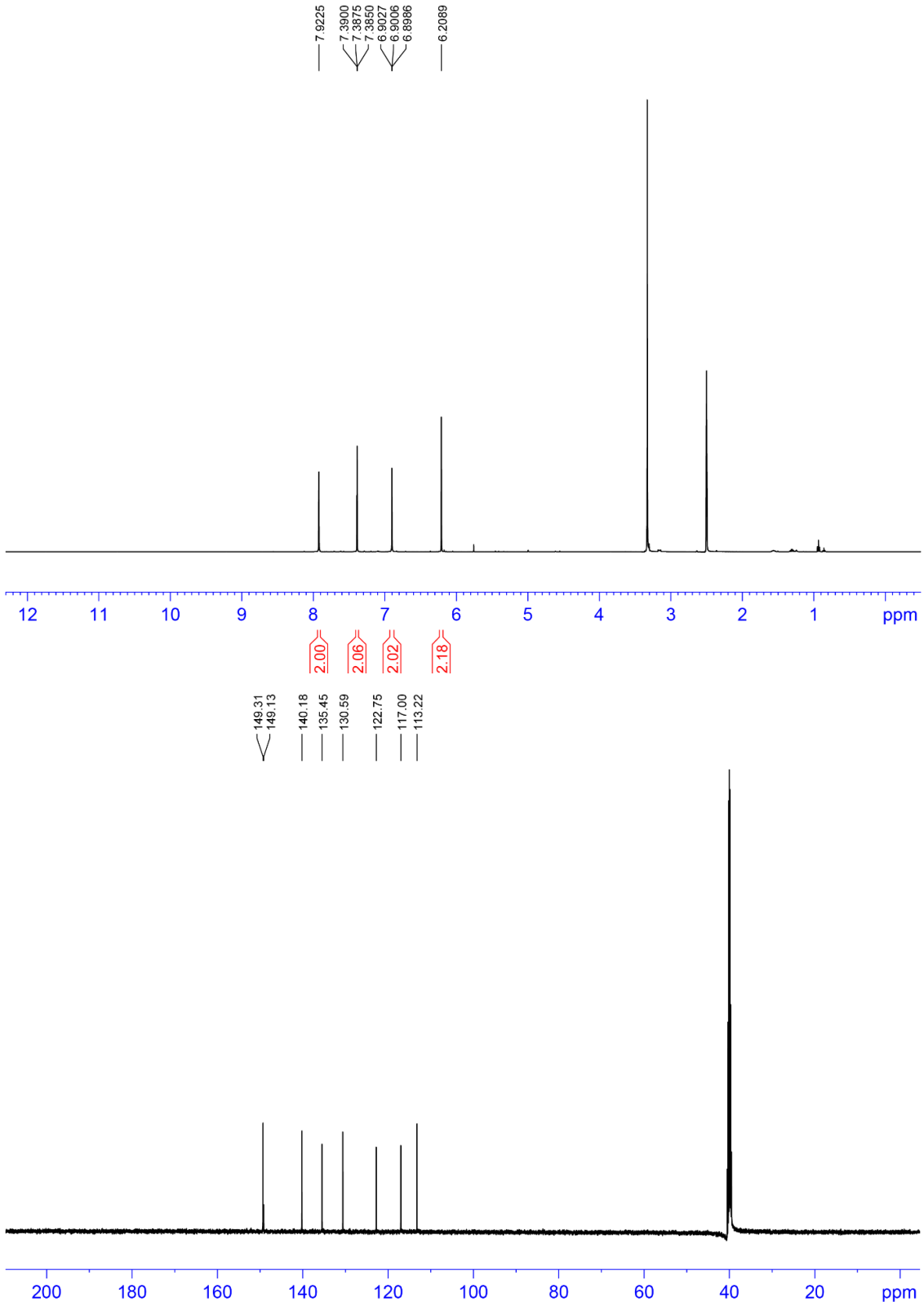

Figure A4.8. ^{1}H and ^{13}C NMR spectra for **4.26**.

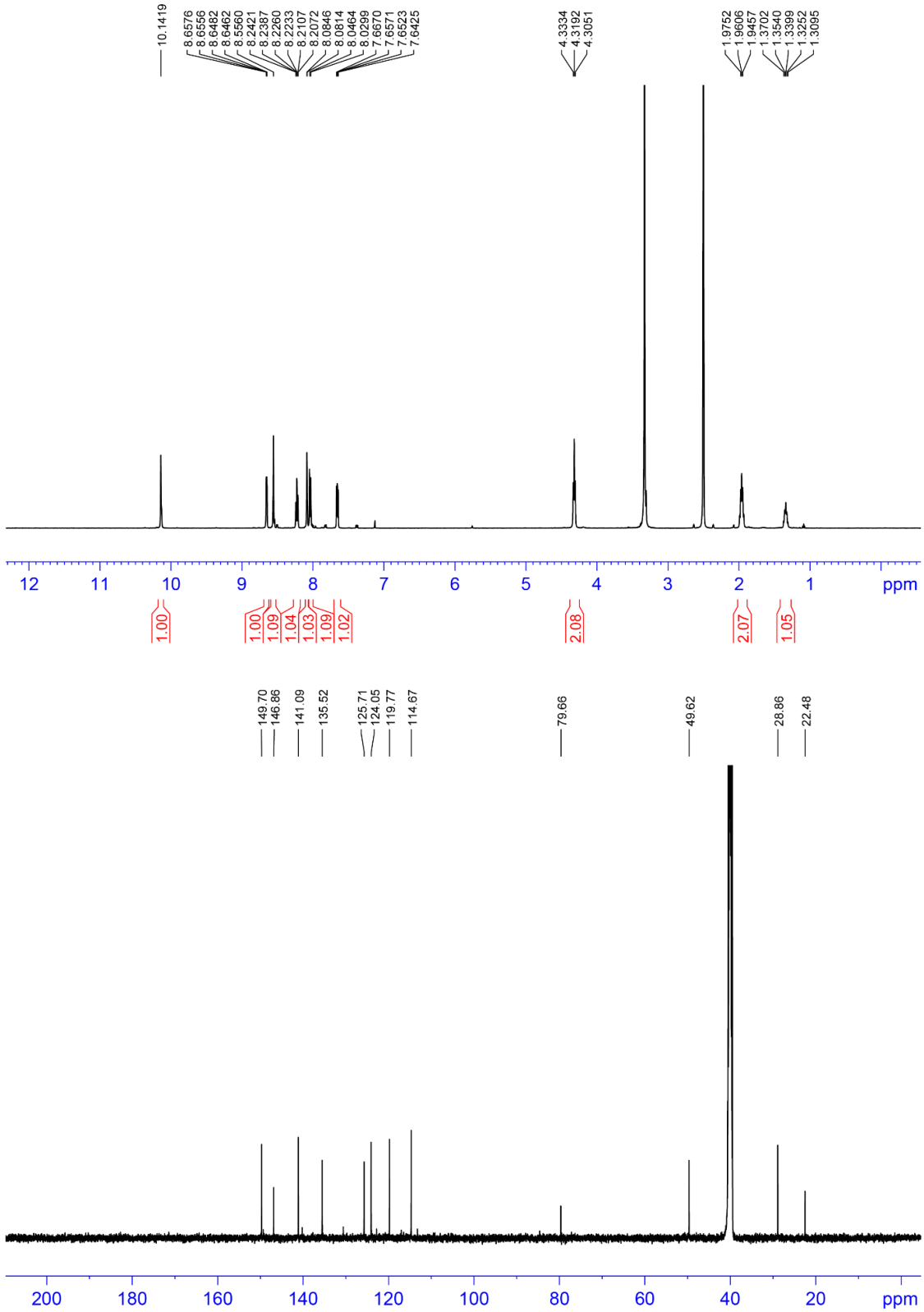

Figure A4.9. ^{1}H and ^{13}C NMR spectra for **4.28**.

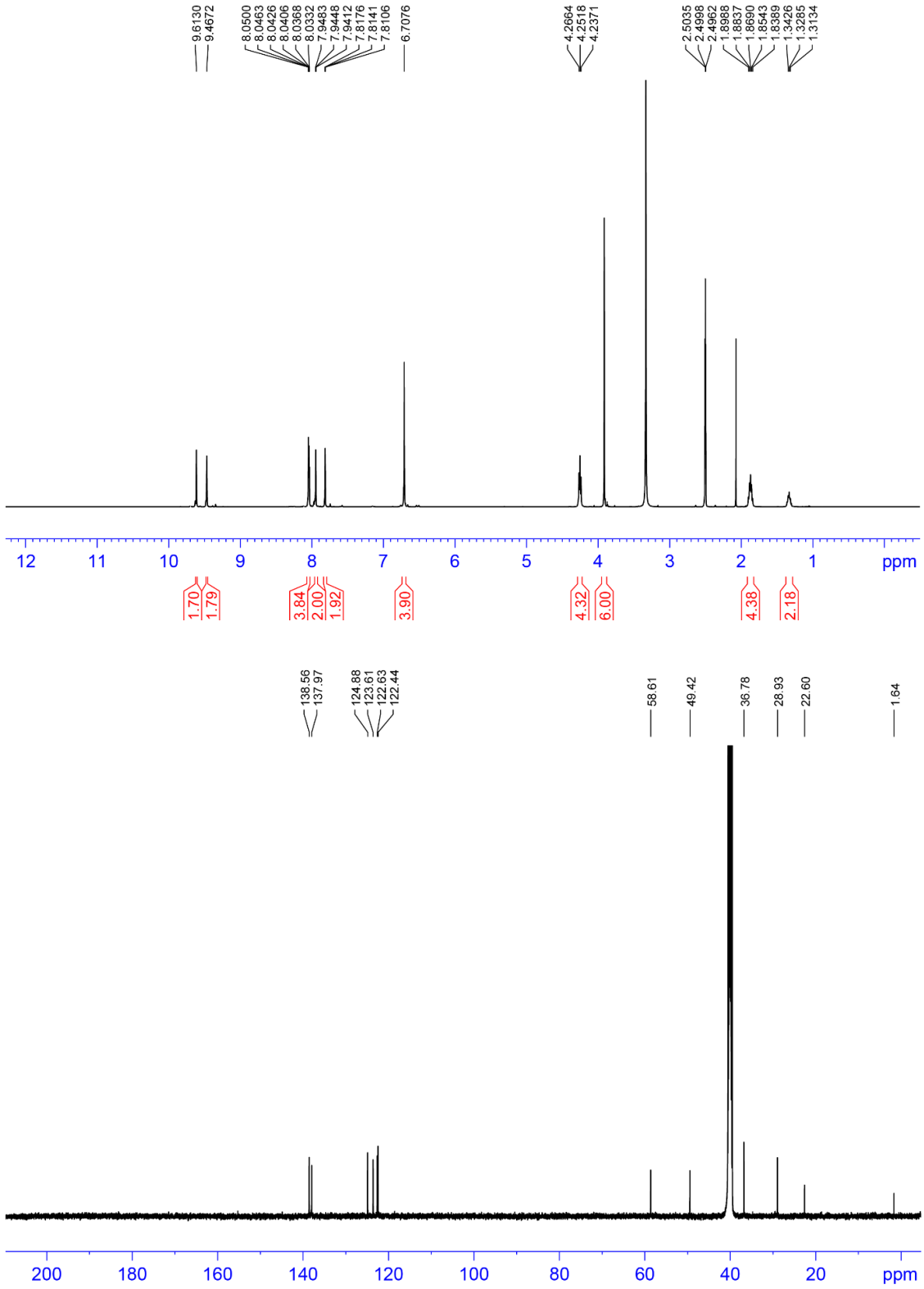

Figure A4.10. ^{1}H and ^{13}C NMR spectra for **4.29**.

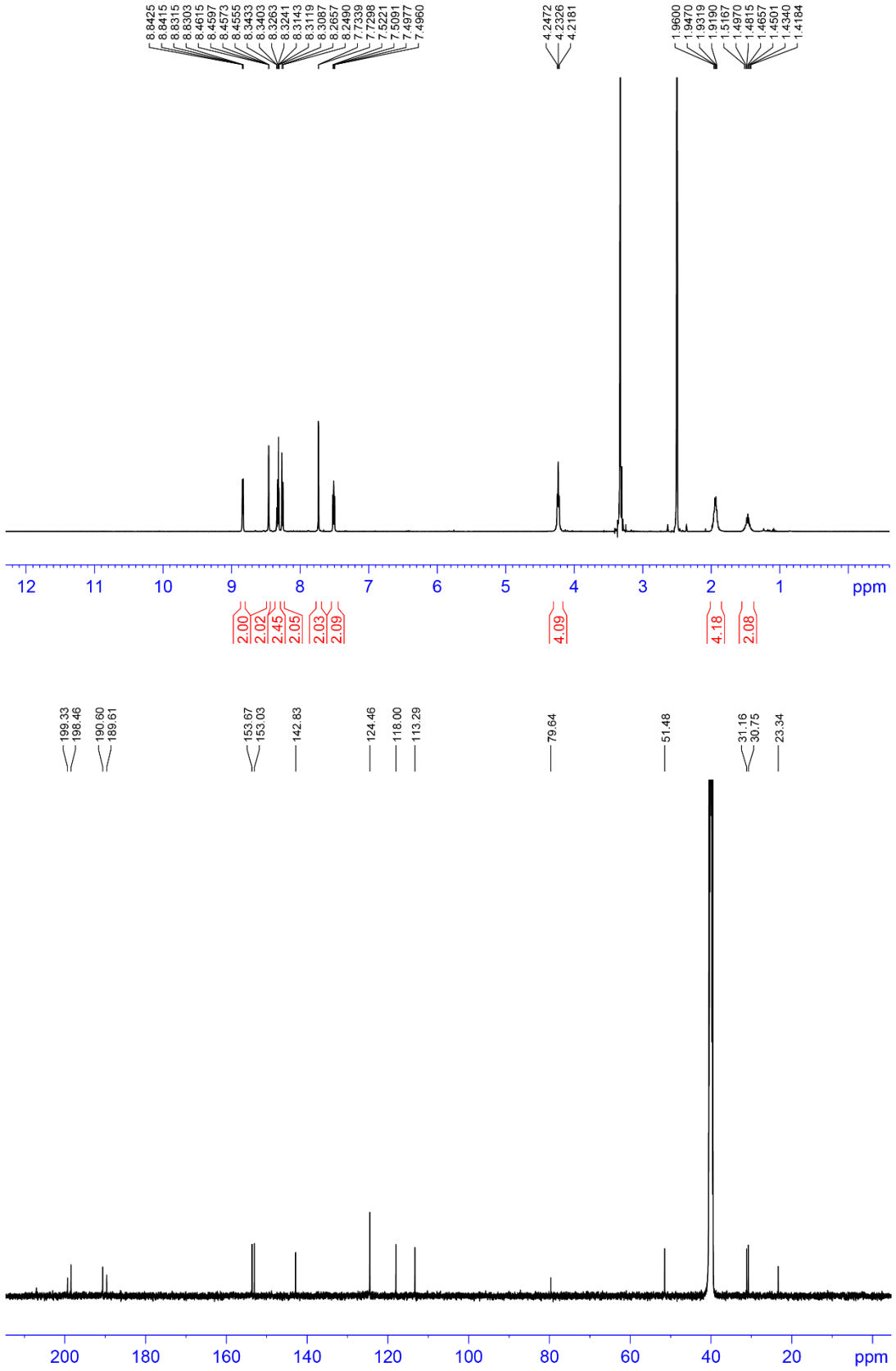

Figure A4.11. ^{1}H and ^{13}C NMR spectra for **4.30**.

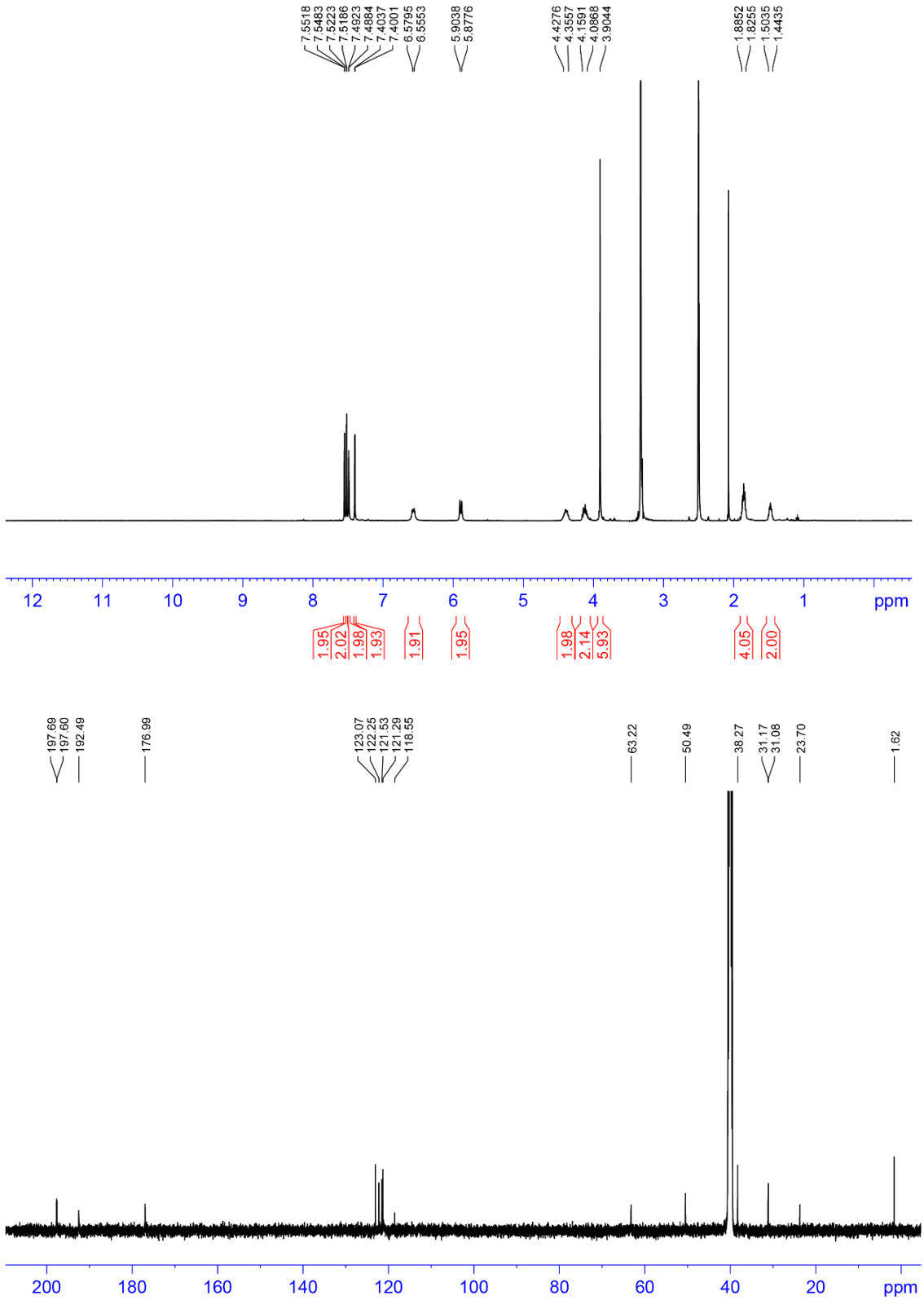

Figure A4.12. ^{1}H and ^{13}C NMR spectra for **4.31**.

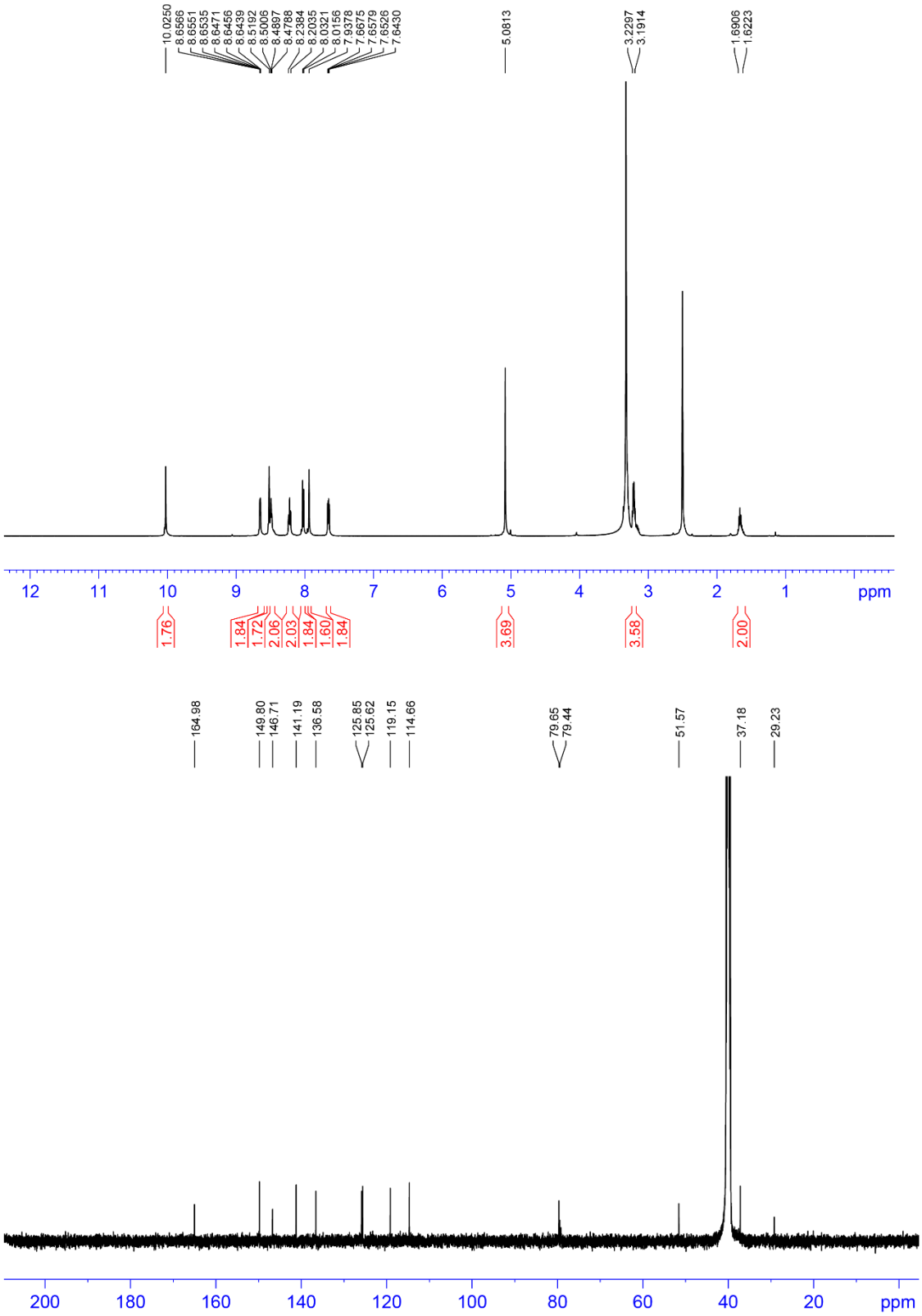

Figure A4.13. ^{1}H and ^{13}C NMR spectra for **4.33**.

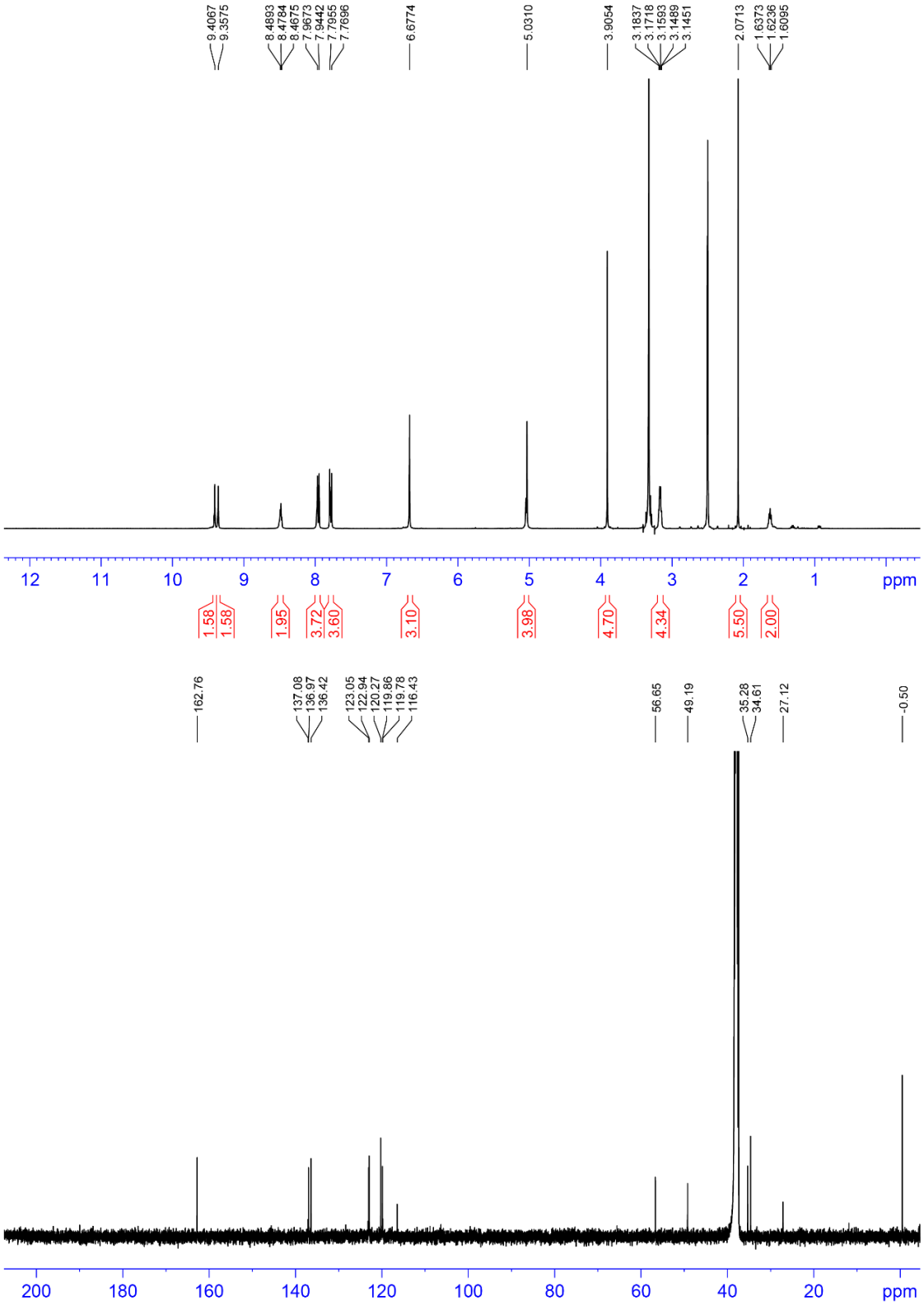

Figure A4.14. ^{1}H and ^{13}C NMR spectra for **4.34**.

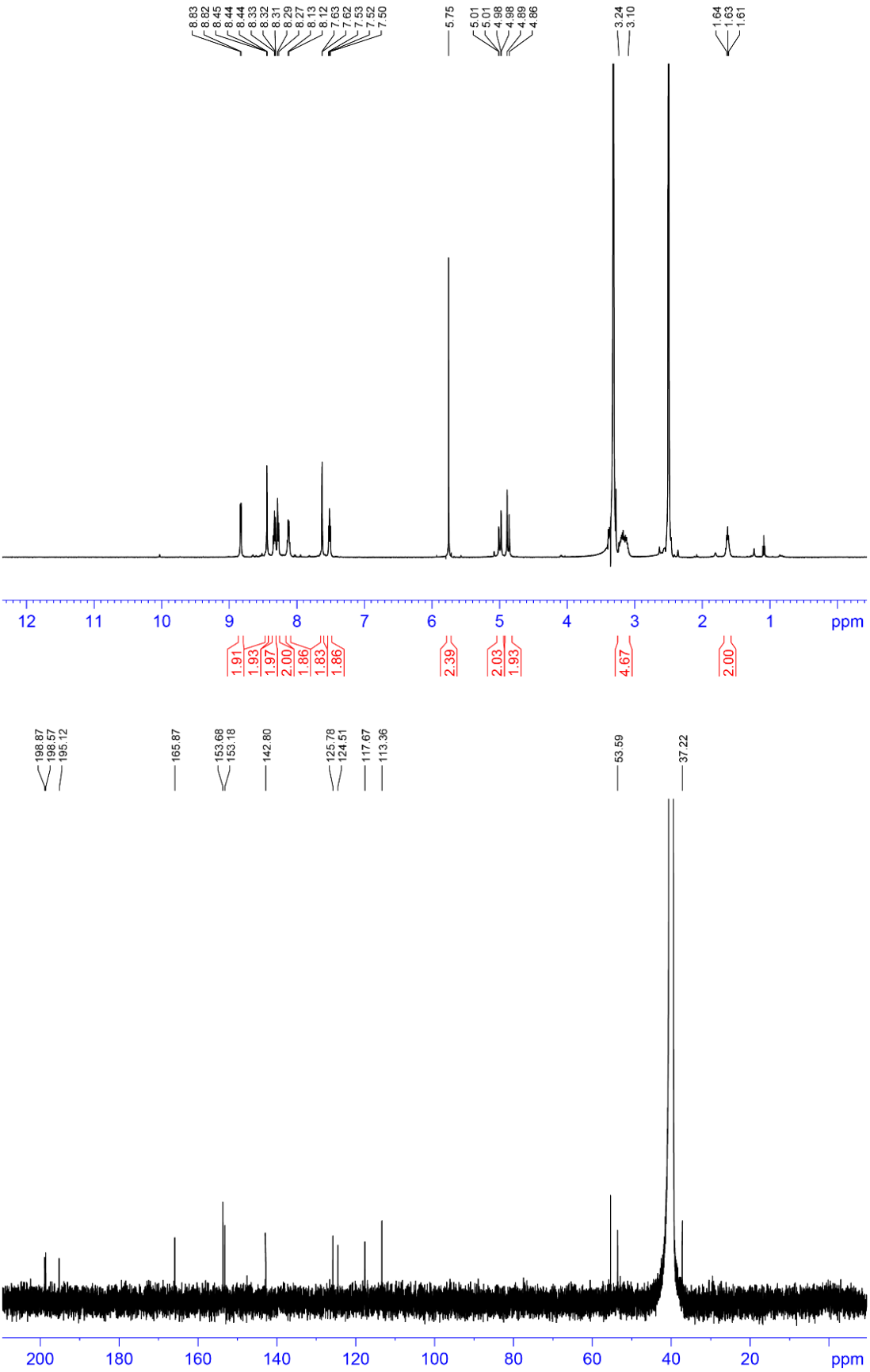

Figure A4.15. ^{1}H and ^{13}C NMR spectra for **4.35**.

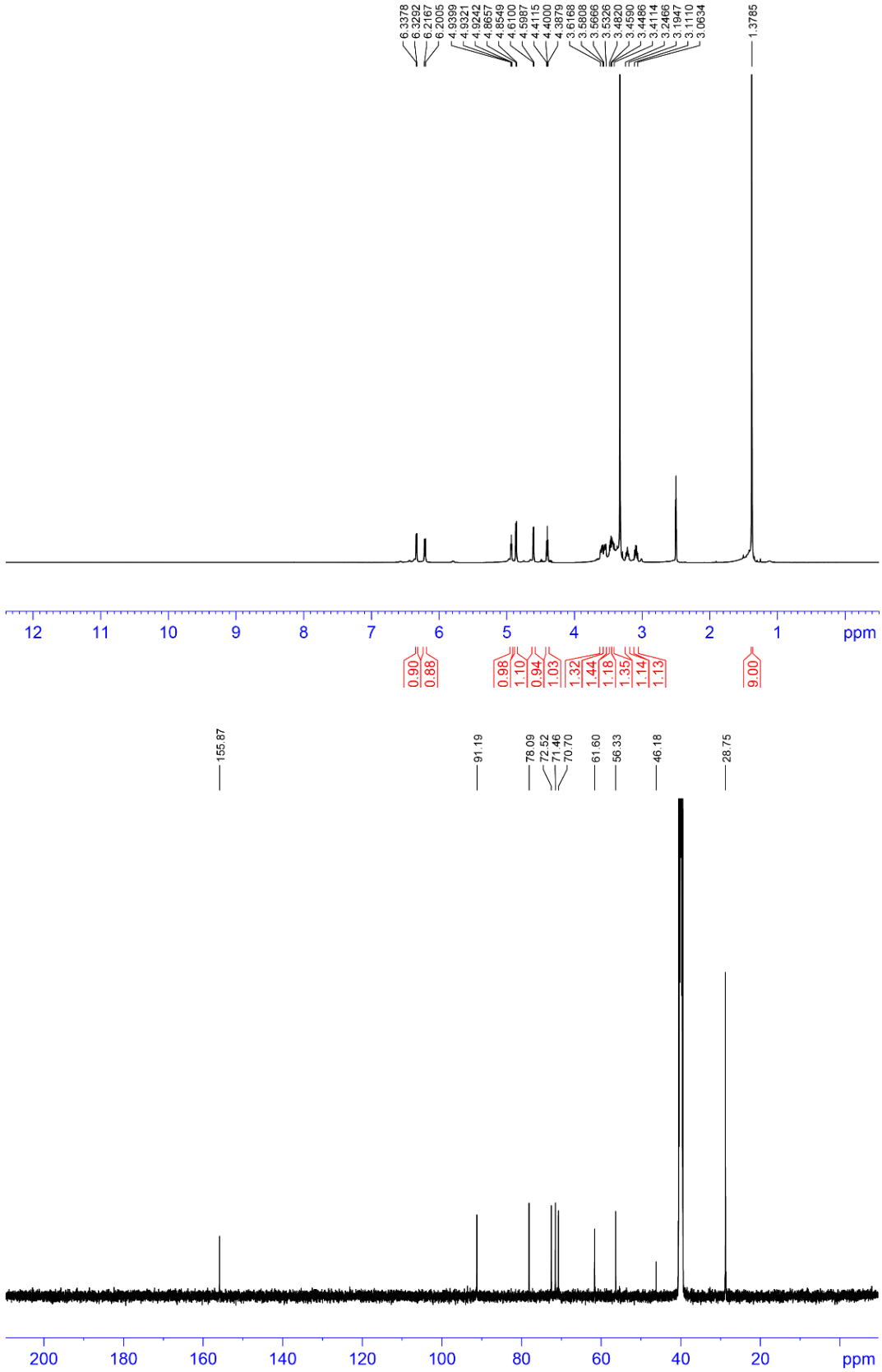

Figure A4.16. ^{1}H and ^{13}C NMR spectra for **4.43**.

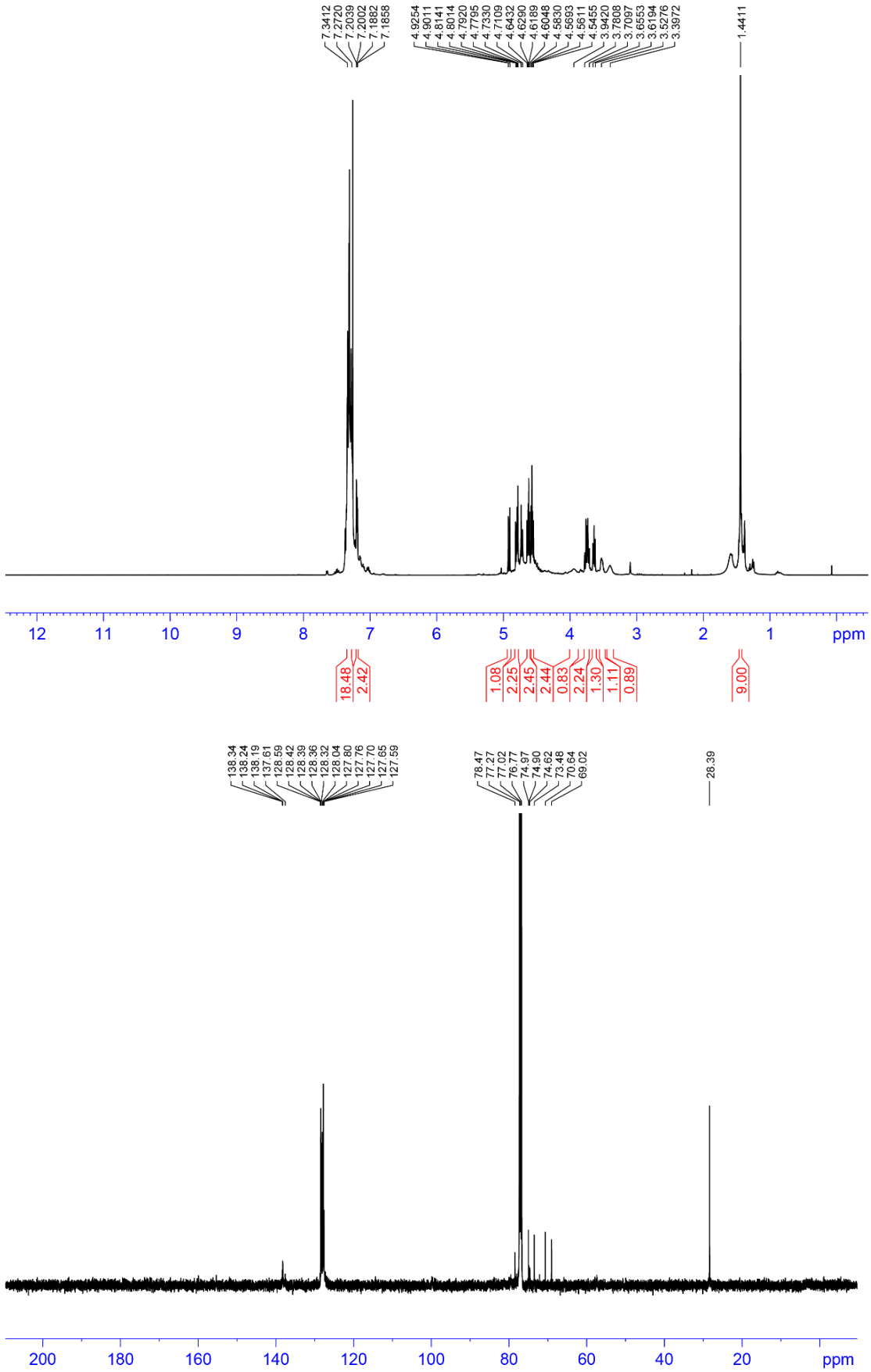

Figure A4.17. ^{1}H and ^{13}C NMR spectra for **4.44**.

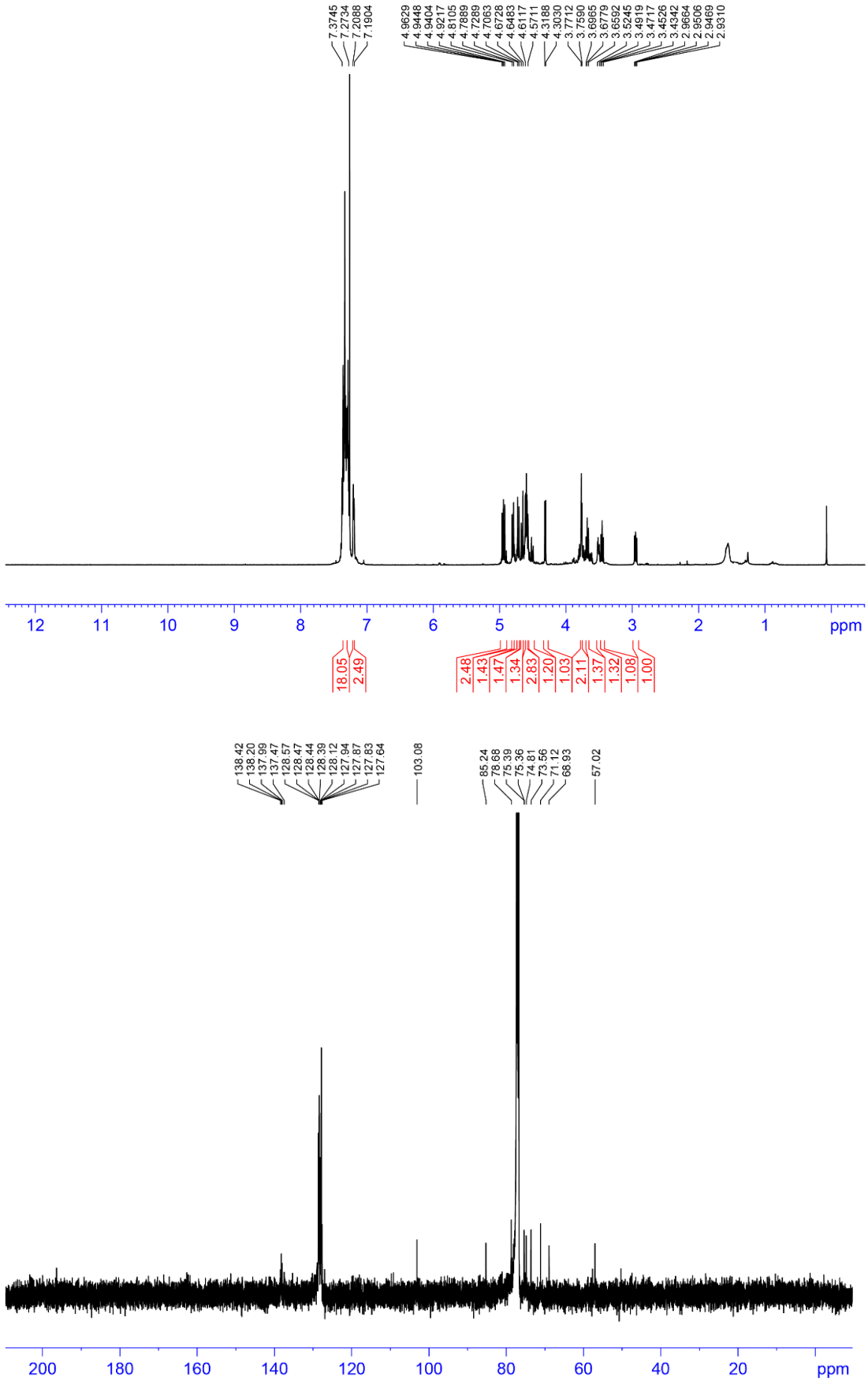

Figure A4.18. ^{1}H and ^{13}C NMR spectra for **4.45**.

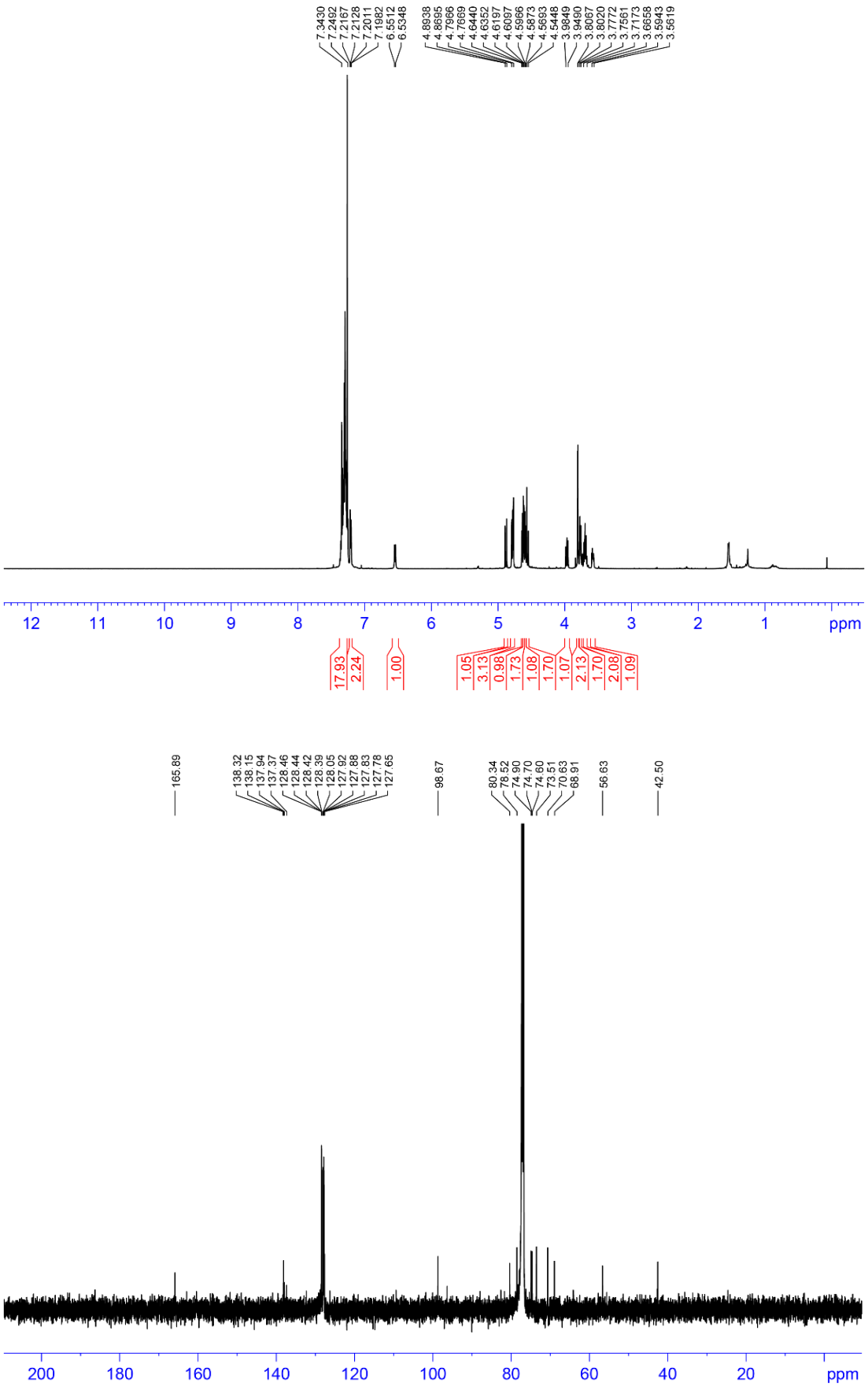

Figure A4.19. ^{1}H and ^{13}C NMR spectra for **4.46**.

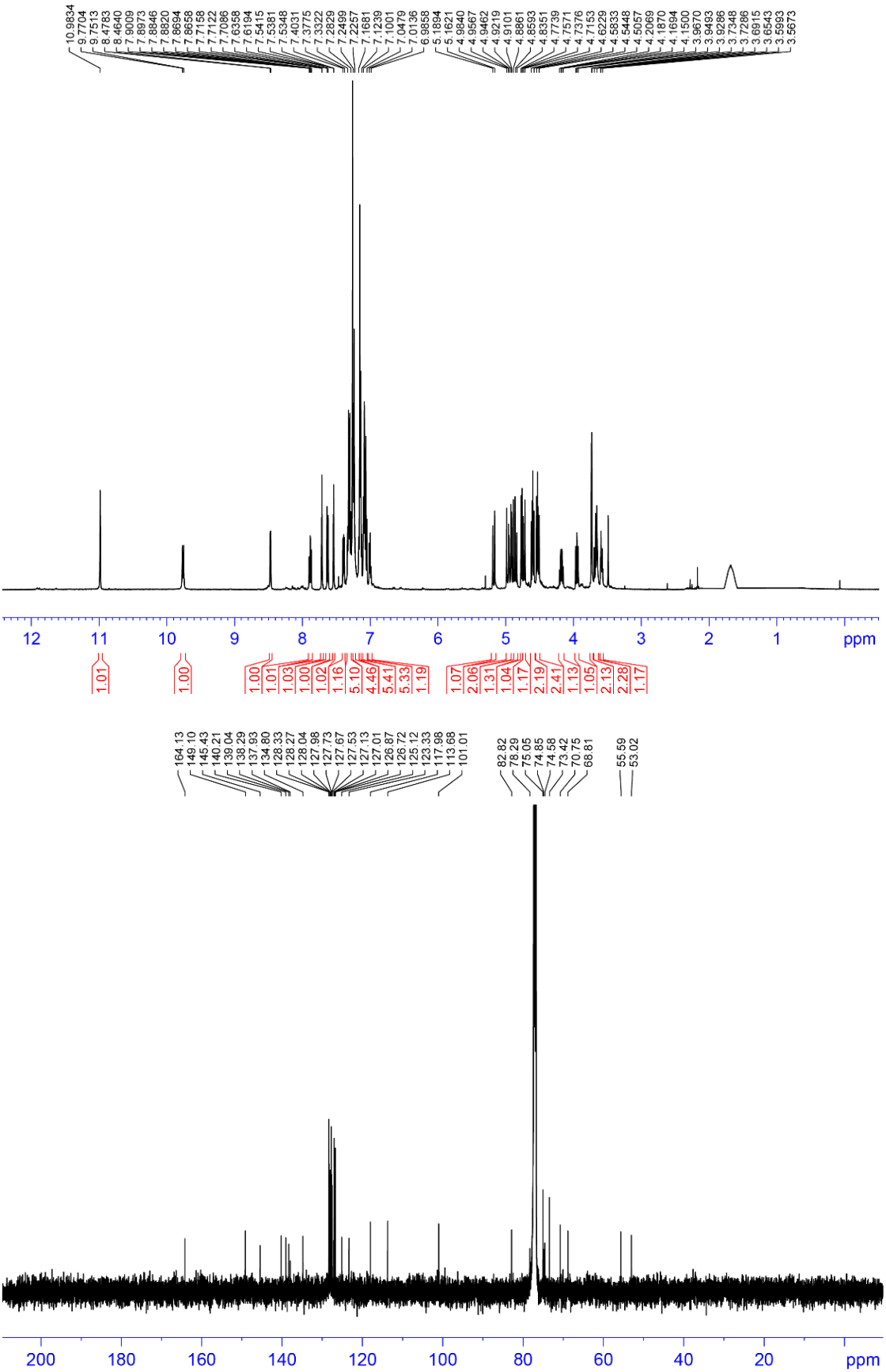

Figure A4.20. ^{1}H and ^{13}C NMR spectra for **4.47**.

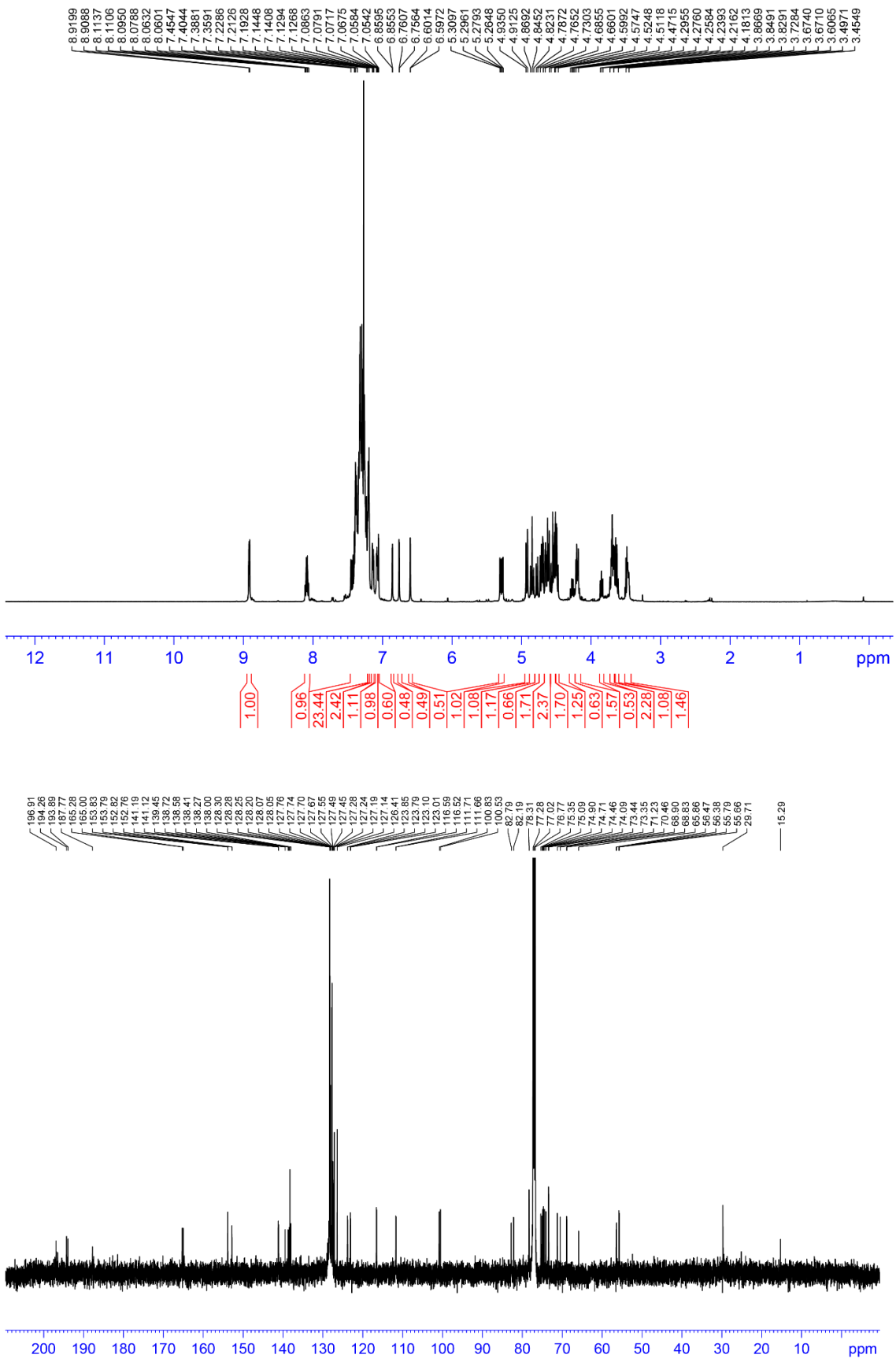

Figure A4.21. ^{1}H and ^{13}C NMR spectra for **4.48**.

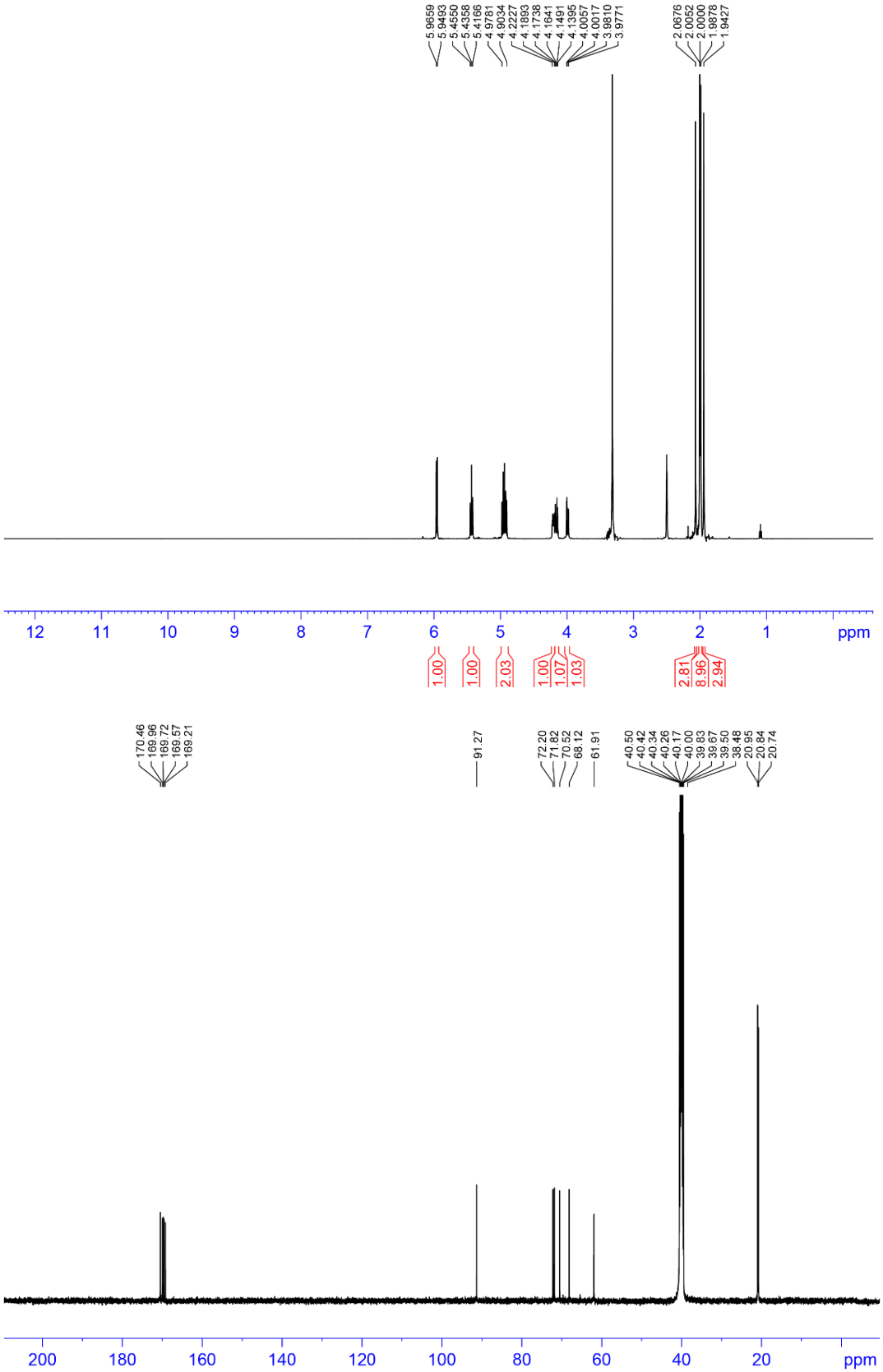

Figure A4.22. ^{1}H and ^{13}C NMR spectra for **4.50**.

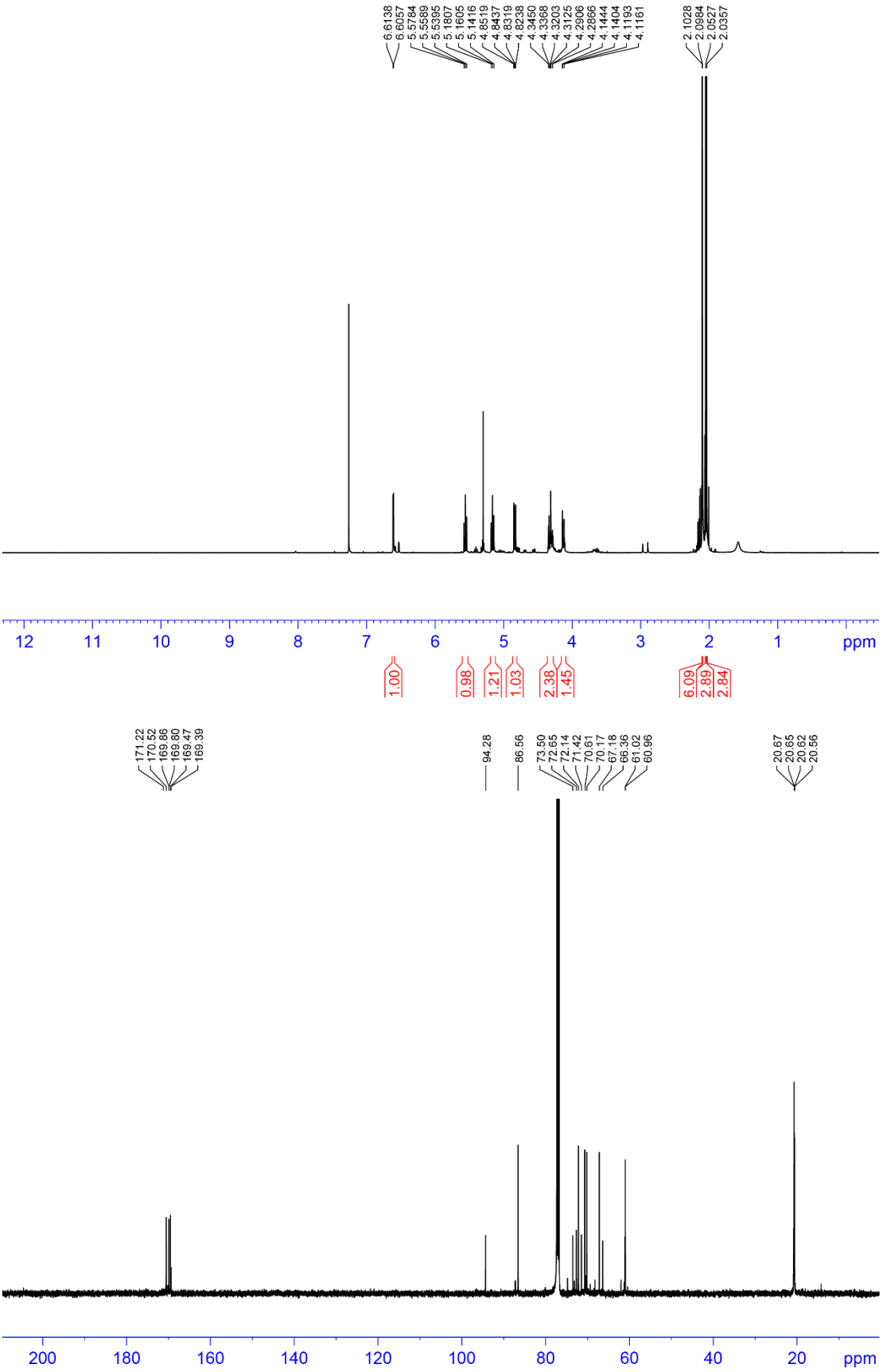

Figure A4.23. ^{1}H and ^{13}C NMR spectra for **4.51**.

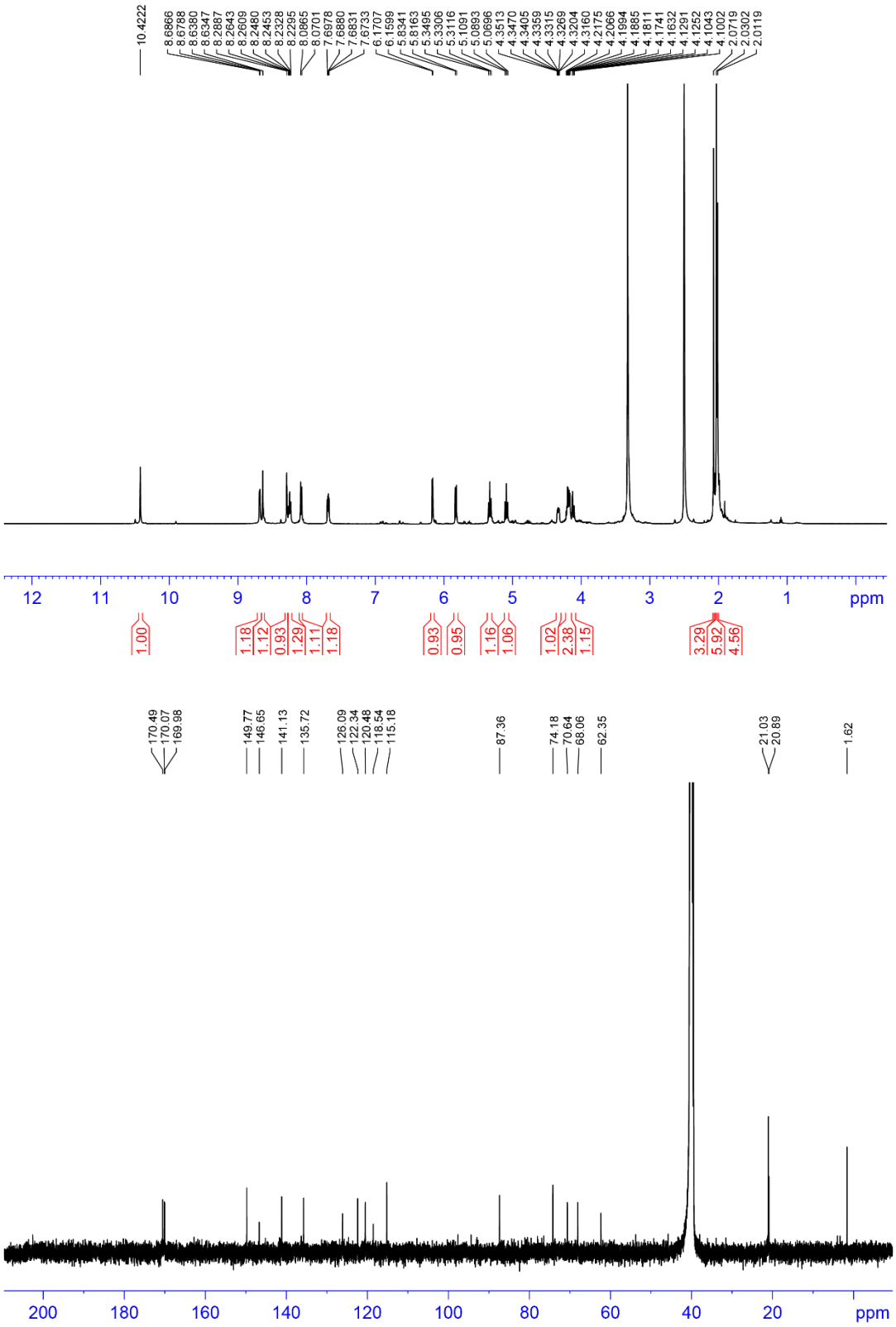

Figure A4.24. ^{1}H and ^{13}C NMR spectra for **4.52**.

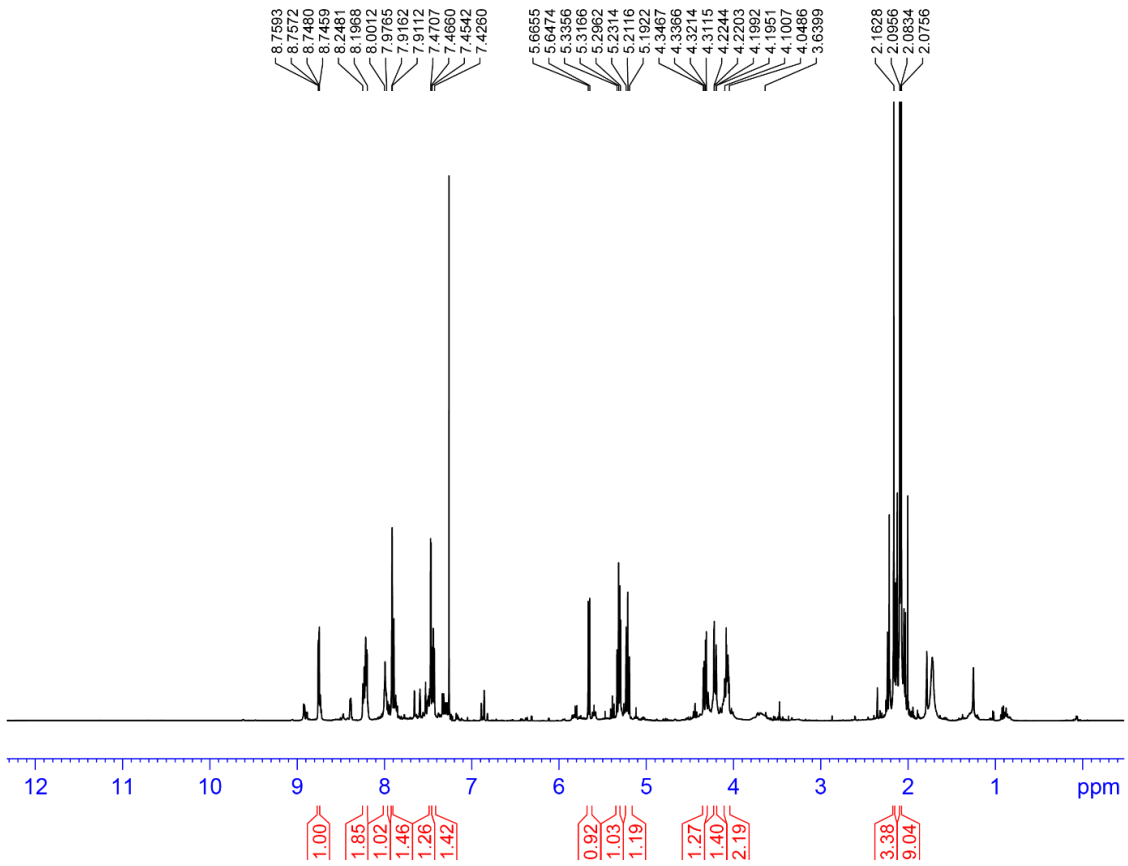

Figure A4.25. ^{1}H spectrum for **4.54**.

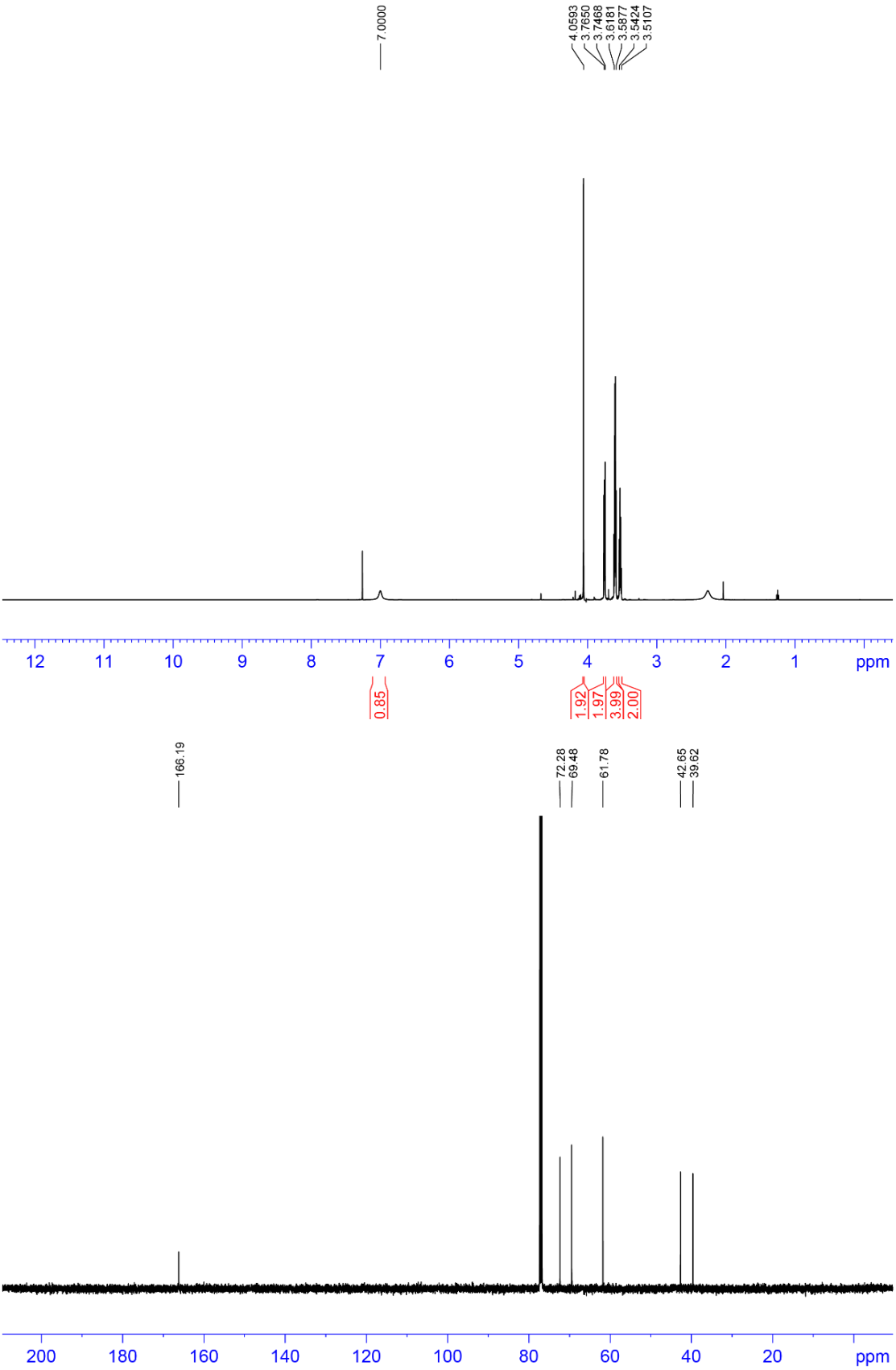

Figure A4.26. ^{1}H and ^{13}C NMR spectra for **4.60**.

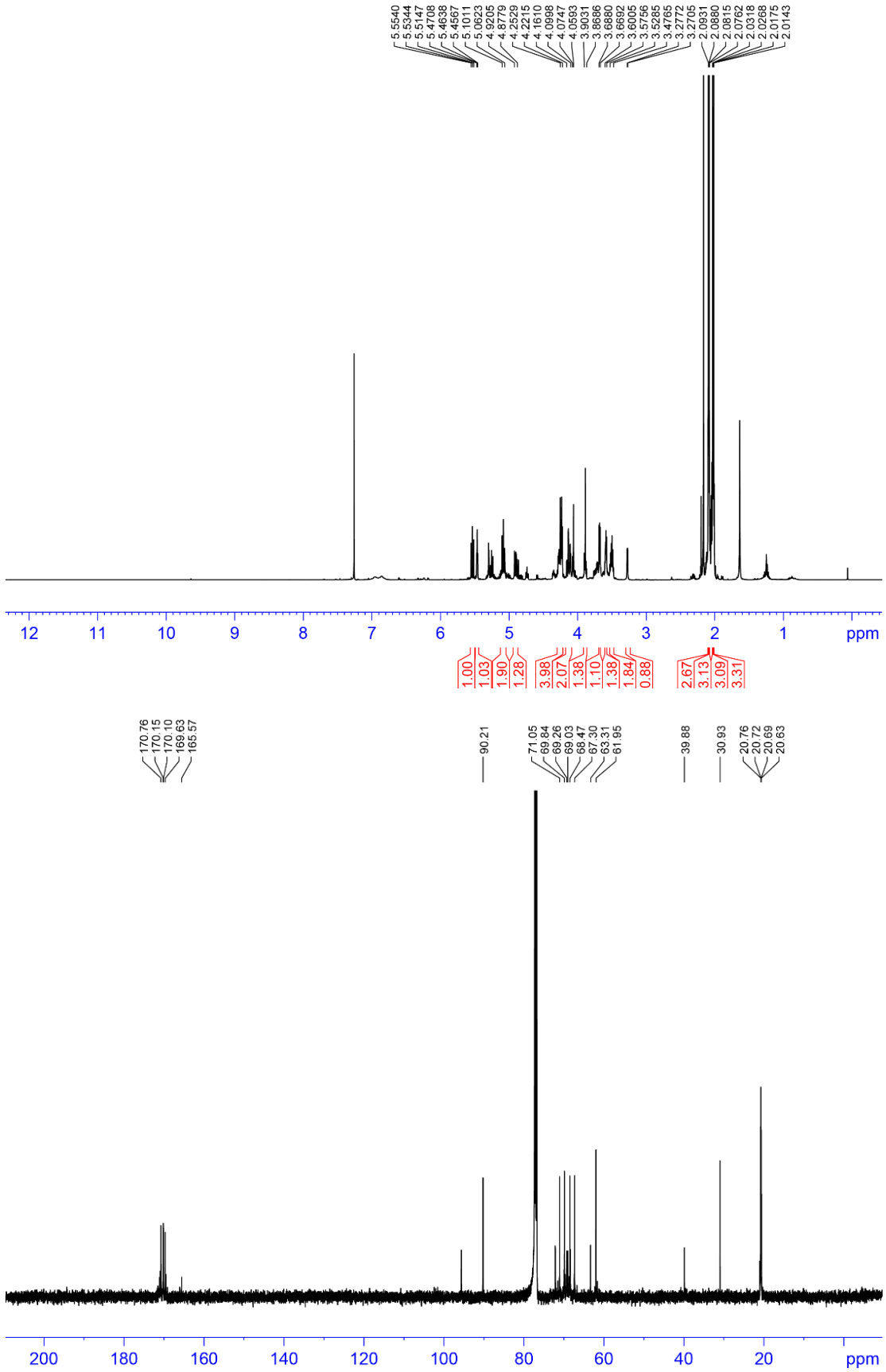

Figure A4.27. ^{1}H and ^{13}C NMR spectra for **4.61**.

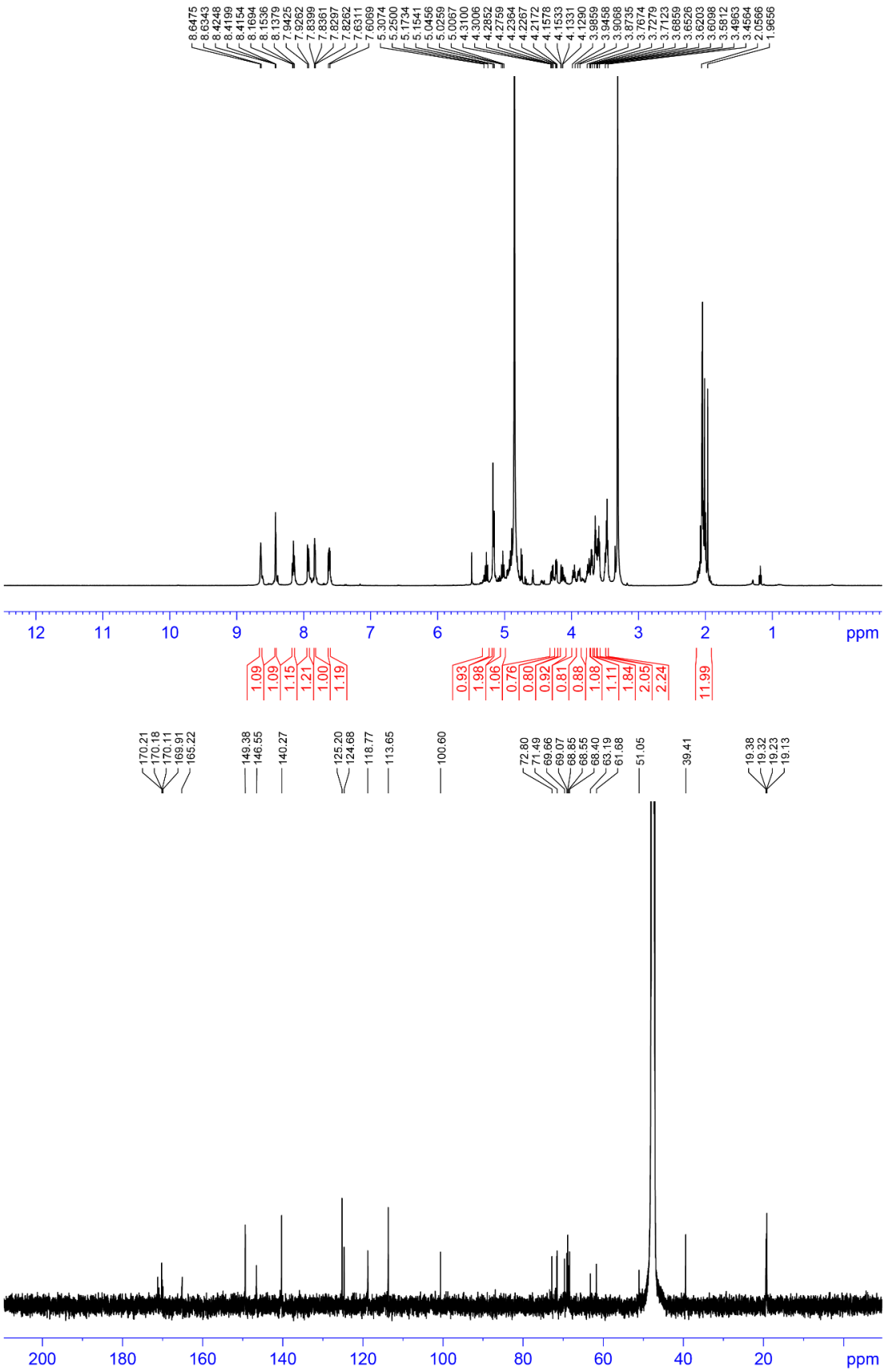

Figure A4.28. ^{1}H and ^{13}C NMR spectra for **4.62**.

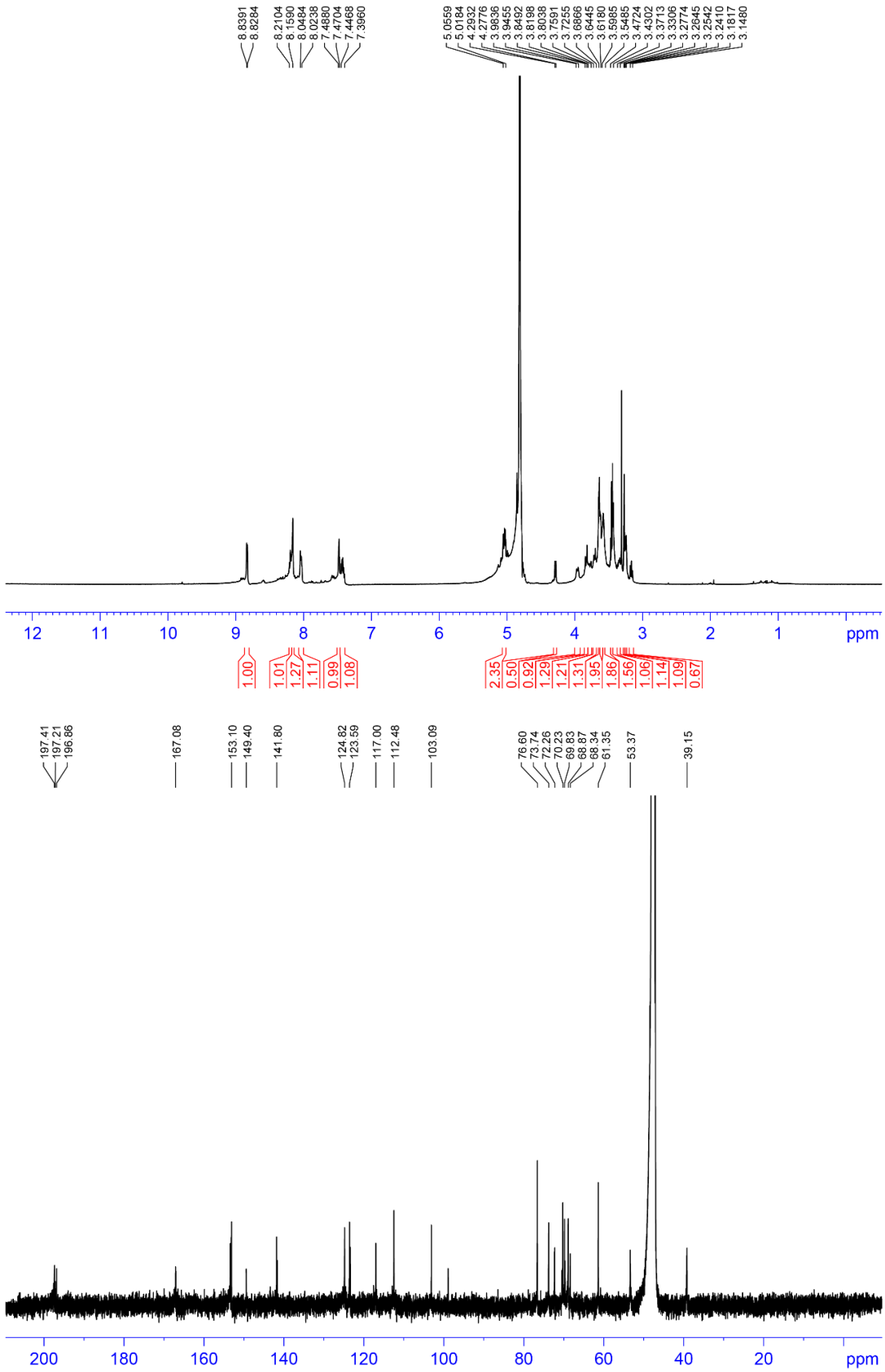

Figure A4.29. ^{1}H and ^{13}C NMR spectra for **4.63**.

4.4. Mass Spectrum

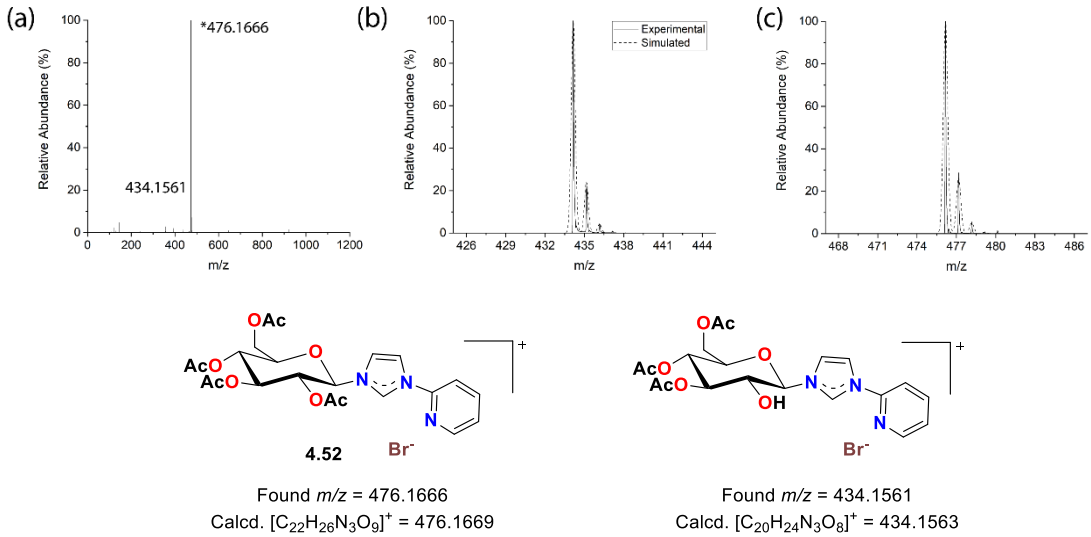

Figure A4.30. (a) HRMS spectrum of a freshly prepared solution of **4.52** in methanol. Zoom scans of the main signals at (b) m/z = 434.1561, (c) m/z = 476.1666 are plotted together with the simulated spectra for the formulas $[C_{22}H_{26}N_3O_9]^+$ (**4.52**), and $[C_{20}H_{24}N_3O_8]^+$, respectively. The structures of the compounds corresponding to these formulae are shown in the lower panel.